

European Co-operation in the Field of Scientific and
Technical Research



COST 327

Motorcycle Safety Helmets

Final Report of the Action



European Commission
Directorate General for Energy and Transport

Legal notice

Neither the European Commission nor any person acting on behalf of the Commission is responsible for the use, which might be made of the following information.

The views expressed in this publication do not necessarily reflect the views of the European Commission.

A great deal of additional information on COST Transport is available on the World Wide Web. It can be accessed through the CORDIS server at the following address:
<http://www.cordis.lu/cost-transport/home.html>

Cataloguing data can be found at the end of this publication.

Luxembourg: Office for Official Publications of the European Communities, 2001.

ISBN xx-xxx-xxxx-x

© European Communities 2001

Printed in Belgium

Key Authors:

<i>Bryan</i>	CHINN, TRL Limited, U.K.
<i>Bertrand</i>	CANAPLE, University of Valenciennes
<i>Siegfried</i>	DERLER, EMPA, Switzerland
<i>David</i>	DOYLE, Southern General Hospital, Glasgow.
<i>Dietmar</i>	OTTE, University of Hannover
<i>Erich</i>	SCHULLER, University of Munich
<i>Remy</i>	WILLINGER, University of Louis Pasteur, Strasbourg

The COST 327 Management Committee, together with the Chairman, Steve Gillingham, would like to thank all the members of the Action, in particular the authors of this report and earlier publications, for their valued contributions without which the success of this research would not have been possible. In addition, the Committee would like to acknowledge the support provided by Andrew Stimpson, Martin Kemp and René Bastiaans of the European Commission, and the kind assistance of Mary Legg, who compiled the report.

Editor-in-Chief: Dr Bryan Chinn

United Kingdom



Department for Transport, (DfT) Zone 2/06 Great Minster House,
76 Marsham Street, London SW1P 4DR. ☎ +44 20 7944 3000.
www.dft.gov.uk



Southern General Hospital, Department of Neuropathology, 1345
Govan Road, Glasgow G51 4TF. ☎ +44 141 201 1100.
www.show.scot.nhs.uk



TRL Limited, Old Wokingham Road, Crowthorne, Berkshire,
RG45 6AU. ☎ +44 1344 773131. www.trl.co.uk

France



INRETS Case 24, F69675, Bron Cedex. ☎ +33(0)1 47 407000
www.inrets.fr



Institut de Mecanique des Fluides Laboratoire de Biomecanique,
Rue Boussingault, 2, F-67083 Strasbourg Cedex. ☎ +33 3 88 41
65 65. www.intelus.u-strasbg.fr



Laboratoire de Genie Mecanique Le Mont Houy, BP 311, 59304
Valenciennes. ☎ +33 3 27 51 12 34. www.univ-valenciennes.fr

Germany



Accident Research Unit, University of Hannover, Carl-Neuberg-
Strasse 1, 30625 Hannover. ☎ +49 0511 532-0.
www.mh-hannover.de



Institut für Rechtsmedizin, Ludwig-Maximilians-Universität,
Frauenlobstrasse 7a, D-80337 München. ☎ +49 89 5160 5111.
www.lmu.de

Hungary



AUTOKUT, PF 25, XI Csoka u.9, H-1502 Budapest.

Italy



AGV spa Zona Industriale D5, I-15047 Spinetta (Alessandria).
☎ +39 01 31 213211



Dipartimento di Ingegneria Aerospaziale, Politecnico di Milano
Via Lambruschini 15, Milano. ☎ +39 02 23991. www.polimi.it

Netherlands



Technische Universiteit Eindhoven, Department of Biomedical
Engineering, Den Dolech 2, 5600 MB Eindhoven.
☎ +31 40 247 9111. www.tue.nl

Sweden



Göteborg University, SE 40530 Göteborg.
☎ +46 31773 1004. www.gu.se

Switzerland



EMPA, Lerchenfeldstrasse 5, CH-9014 St. Gallen. ☎ +41 71 274
74 74. www.empa.ch

Table of Contents

EXECUTIVE SUMMARY.....	i
CHAPTER 1. INTRODUCTION.....	1
CHAPTER 2. LITERATURE REVIEW.....	5
2.1. Introduction.....	5
2.2. Accidents and injury mechanisms.....	5
2.2.1. References.....	6
2.3. Biomechanics of head injury.....	6
2.3.1. References.....	7
2.4. Mathematical modelling of the human head and neck.....	8
2.4.1. References.....	9
2.5. Motorcycle helmets: performance and current Standards.....	9
2.5.1. References.....	10
CHAPTER 3. ACCIDENT INVESTIGATION.....	11
3.1. Introduction.....	11
3.2. Description of the COST 327 database.....	11
3.3. Accident sampling areas.....	12
3.3.1. Accident Research Unit - Medical University Hannover / Germany.....	12
3.3.2. Department of Neuropathology, Glasgow/UK.....	13
3.3.3. Institute for Legal Medicine, Munich University / Germany.....	14
3.3.4. Road Accident Investigation Teams (RAIT), Finland.....	14
3.4. Analysis technique and definitions.....	15
3.4.1. Injury severity.....	15
3.4.2. Impact speed determination.....	16
3.4.3. Head impact speed.....	16
3.4.4. Head and body impact angle.....	16
3.4.5. Collision types.....	17
3.4.6. Definition for mechanisms.....	17
3.4.7. Replication process.....	18
3.5. Linkage of COST databank to national statistics.....	18
3.6. Results of the analysis of the COST accident database.....	20
3.6.1. Effect of age.....	20
3.6.2. Helmet mass distribution and loss.....	21
3.6.3. Injury distribution.....	22
3.6.4. Head injury severity and related factors.....	23

3.6.5. Collision configuration	31
3.6.6. Neck injury.....	34
3.7. Head and neck injury mechanisms	37
3.8. Effect of climatic conditions on accident risk.....	44
3.8.1. Introduction.....	44
3.8.2. Analysis.....	45
3.8.3. Comparison of climate conditions in the different countries.....	46
3.8.4. Climate conditions in accidents	46
3.8.5. Visor condition and accident risk.	51
3.8.6. Analysis and results	52
3.9. Conclusions.....	56
CHAPTER 4. HEADFORM ASSESSMENT	59
4.1. Introduction.....	59
4.2. Characteristics of existing headforms.....	59
4.2.1. Wooden headform.....	59
4.2.2. Aluminium headform.....	59
4.2.3. Hybrid II dummy head.....	60
4.2.4. Hybrid III dummy head	60
4.2.5. Bimass head form	60
4.3. Impact response	62
4.3.1. Introduction.....	62
4.3.2. Rotational acceleration.....	69
4.3.3. Bimass response.....	75
4.3.4 Bimass and Hybrid II headforms compared	76
4.4. Headform selection	79
4.5. Conclusions.....	79
CHAPTER 5. RECONSTRUCTION OF ACCIDENTS AND HELMET DAMAGE BY EXPERIMENT AND SIMULATION.....	81
5.1. Introduction.....	81
5.2. MADYMO simulation.....	81
5.2.1. Introduction.....	81
5.2.2. Materials and methods	82
5.2.3. The motorcycle	82
5.2.4. The car	87
5.2.5. The rider.....	90

5.2.6. Contact points	91
5.2.7. Neck models	92
5.2.8. Results and discussion	94
5.3. Computer simulation of accidents	96
5.3.1. Selection of cases	96
5.3.2. Simulation of cases	97
5.3.3. Discussion	102
5.4. Replication of accident helmet damage	102
5.4.1. Introduction	102
5.4.2. Accident databases	102
5.4.3. Selection process	103
5.4.4. Experimental method	104
5.4.5. Analysis and processing of results	105
5.4.6. Replication of a full scale test (10P)	106
5.4.7. Analysis of Hannover and Finland accident cases	109
5.5. Analysis of replication data	109
5.6. Conclusions	113
Appendix 5I. Motorcycle accident replication results (2 examples)	115
CHAPTER 6. FINITE ELEMENT MODELLING AND SIMULATION OF HELMET, HEAD AND NECK	117
6.1. Introduction	117
6.2. Head modelling	117
6.2.1. Model development	117
6.2.2. Material properties	119
6.2.3. Model validation	120
6.3. Development of the finite element model of the neck	124
6.3.1. Description of the model	124
6.3.2. Characteristics of the elements	124
6.3.3. Results	125
6.4. Helmet modelling	128
6.4.1. Helmet profile measurements	128
6.4.2. Helmet modeling and validation	129
6.5. An analysis of head and head impact parameters	130
6.5.1. Method	130
6.5.2. Results	130

6.6. Numerical simulation of accidents.....	133
6.6.1. Method.....	133
6.6.2. Head impact simulation.....	134
6.6.3. Results.....	137
6.7. Conclusions.....	139
CHAPTER 7. TOLERANCE OF THE HEAD AND NECK TO INJURY.....	143
7.1. Introduction.....	143
7.2. Principles of head injury severity prediction, probability, tolerance.....	143
7.3. Estimated head impact speed and head injury severity.....	146
7.4. Experimental replication and head injury severity.....	147
7.4.1. Headform impact speed.....	147
7.4.2. Linear headform acceleration.....	148
7.4.3. Head Injury Criterion (HIC).....	149
7.4.4. Rotational impact velocity.....	150
7.4.5. Rotational headform acceleration.....	151
7.4.6. Generalised Head Acceleration Model for Brain Injury Threshold (GAMBIT)	153
7.4.7. External forces (normal and tangential).....	154
7.5. Numerical replication and head injury severity.....	155
7.5.1. Linear acceleration of Bimass headform.....	155
7.5.2. Rotational acceleration of Bimass headform.....	158
7.5.3. Finite element replication.....	161
7.6. Neck injury severity.....	163
7.7. Risk of AIS ≥ 3 head injury estimated by logistic regression.....	165
7.8. Conclusions.....	172
CHAPTER 8. DEVELOPMENT OF TEST PROCEDURES.....	175
8.1. Introduction.....	175
8.2. Oblique impact tests.....	177
8.2.1. Introduction.....	177
8.2.2. Equipment.....	177
8.2.3. Test procedure.....	178
8.2.4. Results and discussion.....	179
8.3. Dummy drop tests.....	186
8.3.1. Introduction.....	186
8.3.2. Equipment.....	186

8.3.3. Test programme and procedure.....	187
8.3.4. Oblique impact tests using a dummy: results and discussion	190
8.3.5. Dummy drop tests onto a flat anvil: results and discussion	194
8.4. Mechanical helmet tests	201
8.4.1. Chin-strap effectiveness test	201
8.4.2. Friction test.....	206
8.5. Helmet physiology	209
8.5.1. Introduction	209
8.5.2. Development of a sweating thermal headform	210
8.5.3. Interpretation of the measured data.....	212
8.5.4. Test procedure	213
8.5.5. Results and discussion	214
8.6. Motorcycle aerodynamic noise	219
8.6.1. Recommended test methods for measuring helmet noise.....	221
8.7. Conclusions	224
CHAPTER 9. CONCLUSIONS.....	227
CHAPTER 10. HELMET TEST SPECIFICATION	233
CHAPTER 11. RECOMMENDATIONS	235
11.1. Accident investigation.....	235
11.2. Numerical modelling.....	235
11.3. Test procedures	235
11.4. Advanced Helmets	235
11.5. Implementation	236
CHAPTER 12. BENEFITS TO DIFFERENT USERS.....	237
12.1. Biomechanics experts.....	237
12.2. Dummy developers	237
12.3. Crashworthiness experts.....	237
12.4. Helmet manufacturers	238
12.5. Standards authorities	238
12.6. End users	238
12.6.1. Motorcyclists.....	238
12.6.2. Other users of protective helmets.....	238
12.7. National Governments	238
CHAPTER 13. BIBLIOGRAPHY	239
13.1. Literature Review references	239

13.2. Chapter references	258
13.3. Publications resulting from the Action	263
CHAPTER 14. MEDICAL TERMINOLOGY	265

EXECUTIVE SUMMARY

Motorcyclists are among the most vulnerable of road users. Analysis has shown that there are typically 4,700 motorcycle fatalities throughout Europe each year and this represents some 16% of the total road-user fatalities, the second largest group after car occupants. It was, therefore, considered important that road safety practitioners in Europe have a good understanding of this problem to decide on future developments in this critical area.

Head injuries cause some three-quarters of all fatalities to motorcyclists, while about one quarter of all injured riders suffer a head injury. COST 327 was formed to investigate in detail, motorcyclists' head and neck injuries.

The COST 327 action was established with seven research topics, with a timetable and four main objectives, all to be achieved using a wide range of European experience to determine or modify national approaches.

It is important to note that during the course of the project it was estimated that fatal and serious head injuries could be reduced by at least 20% per annum across the EC with an achievable improvement in helmet performance. Thus, 1000 lives could be saved each year

Topics:

1. Literature review
2. Accident data collection
3. Headform assessment
4. Reconstruction of helmet accident damage
5. Mathematical model of the skull, brain, neck, and helmet
6. Human tolerance to injury
7. Development of test procedures

Objectives:

1. The first was to establish the distribution and severity of injuries experienced by motorcyclists, concentrating on the head and neck.
2. The second was to determine the most significant head and neck injury mechanisms.
3. Thirdly, the tolerance of the human head, brain and neck to these injuries and injury mechanisms was to be established.
4. The overall findings were to be used to propose a specification for the future testing of motorcycle helmets in Europe.

A Working Group with a chairman, was appointed for each of the topics and the main findings of each of these groups are given below. However, it should be noted that the project was designed so that the group activities were strongly interrelated, to obtain the most productive and effective outcome.

Literature Review

In total there are some 8.6 million motorcycles (not counting mopeds) in the 15 European countries and approximately 5 thousand fatalities annually, accounting for a substantial proportion (16%) of total road fatalities. Various injury criteria, for the head, have been

proposed in the past. The most commonly acknowledged and widely applied head injury criterion is the HIC, which is based on the assumption that the linear acceleration of the head is a valid indicator of head injury thresholds. This criterion has enabled vehicle safety to be improved. Nevertheless, it has shortcomings and does not take into account rotational acceleration, head kinematics and direction of impact. Future research should be directed to the derivation of a criterion that overcomes these criticisms.

Finite element modelling is the only method that can predict intra-cerebral parameters such as pressure, principal strains and stresses, as well as relative displacement of the principal head components. However, a lack of material characteristics and validation against accident injury mechanisms was identified as two main problems of FE head models. It was also found that further research was needed to assess the influence of the human body, especially the thorax, on the outcome for the head in an accident and models needed to be developed so that this influence was reproduced.

Performance of current helmets was found effective although it was clear that substantial improvements were possible. Improved Standards were identified as the means of improvement to helmets. Efficient energy absorption with the optimum impulse, minimum tendency to induce rotational motion and a comprehensive evaluation of the whole helmet including the chin guard of a full faced helmet are features for which standards should require tests.

Accident data collection

Detailed accident data was collected over a two-year period from July 1996 until June 1998 in Finland, Germany and the United Kingdom. Two hundred and fifty three cases were completed and were used to compile the COST 327 accident database. The COST database comprised accidents that were selected according to the following criteria:

- motorised two-wheelers
- full or open faced helmet was worn
- Casualty sustained head/neck injuries Abbreviated Injury Scale (AIS) 1 and above or known head/helmet contact occurred but without head injuries.

It should be noted that these accidents were a sub-set of a larger database in each country.

The database was analysed in detail to determine the accident mechanisms and the injury mechanisms to the head and neck. It was found that the object most frequently struck by the motorcycle was a car, 53.9%. The second most frequent was the road or roadside furniture resulting from single vehicle loss of control. However, impacts to a HGV, 9%, were the type most likely to be severe or fatal.

Sixty seven percent of casualties sustained a head injury and 27% a neck injury. Also, notable were the 57% with a thorax injury and 73% with leg injuries. Injuries were classified according to the Maximum Abbreviated Injury Scale (MAIS) and it was found that as the MAIS increased so did the proportion with head injuries, from 38% for MAIS 1 to 81% for MAIS 3 and greater.

Location of helmet damage and speed of head impact were considered critical to the understanding of head injury causes. Helmet damage was distributed evenly with 26.9% lateral right, 26.3% lateral left, 23.6% frontal and 21.0% to the rear. Impacts to the crown at 2.2% were less frequent. It was found that head injury severity increased with head impact speed quite dramatically. The median was 18km/h for AIS 1, 50km/h for AIS 2-4 and 57km/h for AIS 5/6.

Head impact energy is proportional to head impact speed, which, in turn, indicates to what extent helmets need to be improved to give a corresponding reduction in injury severity. This was calculated and it was estimated that an increase in helmet energy absorbing characteristics of some 30% would reduce 50% of the AIS 5/6 casualties to AIS 2-4. Further analysis showed that an increase in energy absorption of some 24% would reduce 20% of the AIS5/6 casualties to AIS 2-4.

The median speed at which brain injury occurred was assumed to be indicative of the sensitivity of the brain to a given impact severity at different locations. The median speed for concussion at 43km/h was lower than that for brain injury, 60km/h. Injury to the brain was not particularly sensitive to the impact location as shown by the median speed. This was just below 60km/h for the rear, upper and lateral regions and just above 60km/h for the chinguard and forehead. Concussion was considered separately from other brain injuries because the location of the injury cannot be determined and was assumed to be diffused.

Head injuries, and brain injuries in particular, were analysed and related to the direction and location of force. It was found that 31% were attributed to a direct force, 58% to an indirect force and 11% specifically to an indirect force directly opposite to the injury location, "contre coup". Fractures to the base of the skull and injuries to the brain stem were usually from an indirect force whereas vault fractures and extracranial tissue injuries were usually from a direct force.

Direction of force indicates to what extent the motion was likely to have been rotational or linear. When head injuries of AIS2 or greater were considered, rotational motion was found to be the cause of over 60% of the injuries and linear motion attributed to 30%. This is consistent with an analysis of body impact angle. This showed that 68% of impacts occurred at an angle of 30 degrees or less to a line vertically through the body whereas 32% were at an angle greater than 60 degrees.

Neck fractures were found to occur predominantly with impacts to the face, body angle less than 15° and impacts where the rider was falling onto the upper area of the head, body angle greater than 60°. Eighty percent of AIS 1 neck injuries occurred at speeds of up to 60km/h and 80% of injuries AIS 2 or greater occurred at speeds above 45km. Severe neck injuries, AIS 4 and greater, were always associated with severe head injuries. Analysis showed that there was a 30% probability of an AIS4 or greater neck injury for head injuries of AIS 5/6.

The effect of climatic conditions on accident risk was investigated as part of the extension to COST327. It is believed that extreme climatic conditions such as very low or very high temperatures may cause physiological problems for riders and lead to an increase in accident risk. The COST database was analysed but trends were difficult to identify because this was a retrospective study and climatic data was available for the area only and not for each accident site. However, of the 111 accidents investigated, climatic conditions were estimated to have been the prime cause of 10 accidents, 9%. Of these, 6 (5%) occurred when the temperature was low, less than 10°C combined with high humidity, greater than 80%. Thus, the tentative link between high humidity at low temperature and accident risk should be investigated further.

Headform assessment

Headforms are used in all Standards as the means of assessing helmet impact performance. However, a rigid headform does not represent a human head except by mass and is not connected to a body mass. It was, therefore, necessary to investigate the behaviour of the

existing devices, identify shortcomings and explore a novel headform proposed by Strasbourg University. TRL undertook extensive testing of rigid aluminium and wooden headforms and a Hybrid II and Hybrid III dummy headform. All headforms were fitted with a nine-accelerometer array so that linear and rotational motion may be calculated and the target anvil was instrumented to record helmet contact force. Each headform was assessed with a variety of helmets, onto flat and oblique anvils at different velocities and different helmet impact locations. Tests were sufficiently numerous for the results to be analysed statistically. Development of a Bimass headform designed by Strasbourg University was also part of the research. This device comprised a dummy headform with a mass attached to the inside by a damped spring system carefully designed to represent the dynamic characteristics of a human brain. The headform was fitted with accelerometers so that the linear and rotational acceleration of both the brain and skull mass may be separately calculated and compared. This device was tested by EMPA of Switzerland in a variety of impacts and by TRL in drop tests designed to represent specific COST 327 accident cases.

Analysis of rigid and dummy headform tests onto a flat anvil showed that the peak linear acceleration of the wooden headform averaged 17% greater and the aluminium headform 8% greater than that for the Hybrid II at the same velocity. From the same tests the Head Injury Criterion, HIC, with the aluminium headform was found to be greater than the Hybrid II by 13% overall, although the variation between helmet types was large.

Rotational acceleration was identified by the accident analysis to be a principal cause of head injury. When measured in the oblique impact tests it was found that the Hybrid II experienced a peak rotational acceleration at a given impact velocity considerably greater than for either the aluminium or wooden headform. However, the Hybrid II gave the smallest standard deviations. These results were attributed to the much better grip of the Hybrid II and hence lower slippage between helmet and headform. It should also be noted that, for the Hybrid II, the force measured tangential to the helmet correlated well with the rotational acceleration measured at the centre of the headform.

The results of the Bimass as developed in a Hybrid III headform showed that the risk of injuries related to the skull-brain motion could be predicted. This was considered a substantial and important improvement over a conventional headform.

Overall, the research showed that that the dummy headform gave the best repeatability and the Bimass gave the most realistic injury prediction. However, only the rigid headforms are available in a range of sizes. It was thus concluded that helmets of the appropriate size should be tested using a Bimass dummy headform and a rigid headform should be used to evaluate other sizes. This research provided a vital input to the Test Procedures Working Group

Reconstruction of helmet damage

Of vital importance to the efficacy of a helmet is the link between the measurements prescribed by Standards and the tolerance of the human head to injury in an equivalent impact. Criteria exist for human tolerance to rapid linear motion and it was clearly identified by the Accident Investigation Working Group that rapid rotational motion was responsible for over 60% of the head injuries. The main objective of the Reconstruction Working Group was to provide the Head and Neck Tolerance Working Group with "state of the art" data on the relationship between test measurements and human injury. This was achieved mainly through the replication of damage observed on the accident helmet.

Part of the accident investigation task was to collect the accident helmet whenever possible. This was then sent to TRL who examined the damage carefully and assessed the accident report. A new helmet, equivalent to the accident helmet, was drop tested, at different speeds and angles onto a target, car wheel or specimen of road surface for example, similar to what was struck during the accident until the damage matched that of the accident helmet. The headform used was from a Hybrid II dummy and was fitted with a nine-accelerometer array so that the rotational and linear motion of the headform in three axes could be calculated. Thus linear and rotational, acceleration, velocity and displacement, against time, for each of three axes and resultants were available. In addition, the target was mounted on a transducer to give external force normal and tangential to the helmet surface. Much of this data was given to the Computer Simulation Working Group, see below.

This technique of replicating helmet damage was perfected by TRL, UK who replicated 21 COST cases. Five of these were also replicated using the Bimass headform to provide a comparison of the output of a conventional dummy headform with that of the Bimass (Chapter 4). The results of the tests were compared with the AIS values of the head injury and the correlation was examined. The replication tests showed that the limit for rotational motion should be a peak acceleration of 5,000rad/s/s and a rotational velocity of 40rad/s.

Linear motion was examined and it was found that a HIC of 1000, as used by the automotive industry, might be appropriate. Peak linear acceleration should be less than 250g. Gambit is a formula that combines the peak linear acceleration and the peak rotational acceleration and it was considered that this be further analysed by the Head and Neck Tolerance Working Group.

Also part of the research was the construction, by Valenciennes University, France of a lumped mass computer model of a motorcycle with dummy rider and a moving car. The model was used to simulate various accident cases to understand the rider dynamics during an accident and to assess the influence of the neck on the potential for head injury. The computer model comprised a Hybrid III dummy rider, a Norton Commander motorcycle and a moving Ford Mondeo developed in MADYMO. Much care was taken to ensure that the characteristics of the components of the dummy, the motorcycle and the car were accurately determined. This necessitated for example, crush testing the wheels and forks of the motorcycle and the metal panels and sill of the car. Also examined were the suspension characteristics of the vehicles and the physical properties. The dummy and helmet material characteristics were similarly determined.

The above model was successfully used to simulate motorcycle accidents of the type similar to the configuration of the full-scale impact test, 50km/h at 90° into the side of a stationary car, against which the model was validated. For example, in an accident where a motorcycle collided with the rear of a stationary van at 20km/h the rider sustained only minor leg abrasions from contact with the road. The peak linear acceleration predicted by the simulation, 70g, was similar to the 107g measured in the helmet damage replication tests. The rotational acceleration 8000 rad/s/s for the simulation was greater than the 5026 rad/s/s measured in the helmet damage replication tests but of the same order of magnitude.

The influence of the neck on the kinematics of the head in an accident is an important factor when considering the relationship between the output from drop tests and the motion of a rider in an accident. This was investigated in the computer model using a neck developed to study the kinematic motion in slow speed rear car impacts as a replacement

for the Hybrid III neck. The results showed that although the linear acceleration was similar, the rotational acceleration was somewhat greater for the modified neck, 9,000rad/s/s, compared with 6,000rad/s for the standard neck. The stiffer the neck the more it will tend to resist rotational motion. This substantiates the belief that the Hybrid III neck is stiffer than a human neck and will lead to predictions of rotational acceleration that are too low. The effect of a dummy neck was further investigated by the Test Procedures Working Group, see below.

Mathematical model of the skull, brain, neck, and helmet.

It was essential that the link between accident impact mechanisms and the injury outcome be investigated for a range of circumstances far greater than was possible with experimental methods. Finite element simulation was identified in the literature review as the most appropriate method and a unique "state of the art" FE model of the skull, brain, neck and helmet was constructed and validated. Strasbourg University was responsible for the construction of all but the neck, which was completed by Polytecnico Milano.

The skull model was meshed using data obtained by digitising, in detail, the inner and outer profiles of a human skull. The model is unique in the extent to which the various parts of the head and brain are defined. Of particular note is the representation of the subarachnoid space between the brain and skull with brick elements, which in this model were used to simulate the cerebral-spinal fluid. Overall, the head model comprised 11939 nodes and 13208 elements divided in 10395 bricks and 2813 shells and it had total mass of 6.7 kg.

The head model was successfully calibrated against the well-known Nahum cadaver data and was shown to give accurate predictions at all the five sites within the brain as examined by Nahum. Impact force, pressure at the impact site and opposite to it and the distribution of von Mises stresses were simulated sufficiently accurately to give confidence that the model may be used, as intended, for the investigation of head injury mechanisms over a wide range of input parameters.

The helmet model was developed by meshing from three-dimensional data, supplied by TRL, of the outer profile of a glass fibre helmet. The model was calibrated against data from impact tests of the helmet on a headform, supplied by TRL and Strasbourg University.

The neck model was developed by Polytecnico Milano, first as a multi-body lumped mass model and then as a finite element model, in PAM CRASH. It was linked, with the model of the skull brain and helmet by Strasbourg University. The neck comprised eight rigid vertebrae, six non-linear viscoelastic intervertebral discs, 34 non-linear viscoelastic ligaments, 17 nonlinear facet joints and 13 pairs of muscles. The model was successfully calibrated against published human volunteer data obtained from sled tests. Particularly good agreement was obtained for the head acceleration and neck rotation. It should be noted that the inclusion of non-linear visco-elastic ligaments was essential to obtain good agreement of the head rotation with time.

A copy of the model was transferred to TRL who analysed the head impact parameters of the finite element model of the skull and brain. This was important to understand the behaviour of the model and thus have confidence in the results of the accident simulation described below. The head model was struck with an impactor at two velocities over a wide range of values for the parameters of the brain. Also the impactor mass and stiffness were varied.

The results of the parameter study showed that:

1. The brain bulk modulus has a significant influence on the peak pressure and von Mises stress of the brain, although large changes in the bulk modulus of the brain are needed to arouse significant changes in these model responses,
2. The short time shear modulus of the brain has a significant impact on the peak von Mises stress of the model, but an insignificant influence on the peak pressure,
3. In general, Young's modulus of the CSF has an insignificant influence on the peak pressure and von Mises stress of the brain in the head model,
4. The peak von Mises stress of the brain was about five orders of magnitude more sensitive to a unit change (KPa) in the brain short time shear modulus than it is to a unit change (KPa) in the bulk modulus of the brain,
5. Both the mass and stiffness of an impactor have an important impact on the peak pressure and von Mises stress in the brain,
6. Both the peak pressure and von Mises stress of the brain are around a thousand times as sensitive to a unit change (Kg) in the mass of an impactor striking the forehead, as they are to a unit change (KPa) in the stiffness of the impactor.

An FE mesh of a motorcycle helmet was added to the model, which was then used to simulate 13 motorcycle accidents selected from the COST 327 Action database. The damage to the accident helmets had been replicated by drop tests at TRL during which rotational and linear acceleration and external forces were measured. The output from the model was compared with the head injuries recorded for each case. It was concluded that AIS does not correlate well with the conventional test criteria such as acceleration, HIC and GAMBIT.

However, Southern General Hospital, Glasgow had provided details of the brain injuries, for the serious and fatal casualties. This data was determined from a neuropathological study of the brain. For the fatal cases the brain was sliced and examined under a microscope. The serious cases were analysed from CAT scans. This presented a unique opportunity to compare the output from the model directly with the brain injuries that occurred during the accident under the same kinematic conditions. When the results were examined, the four distinct groups emerged: uninjured, concussion, sub-dural haematoma and skull fracture.

The accident simulation was very encouraging and lead to the following tentative proposals for injury criteria as follows:

- 1) Intra-cerebral von Mises stress of 10kpa for short duration concussion
- 2) Intra-cerebral von Mises stress of 20kpa for long duration concussion
- 3) Strain energy in the cerebro-spinal fluid of approximately 4J for sub-dural haematoma
- 4) Skull fracture was identified but not assessed in this study but should be included in future research.

The Computer Simulation Working Group believes, with good supporting evidence, that this overall model represents the state of the art for a finite element model of the skull, brain, neck and helmet.

Human tolerance to injury

Critical to the success of the whole project is the clear identification of the tolerance of the human head to impact parameters, which is essential if future Standards are to be

improved. The prime objective of the Human Tolerance Working Group, led by Munich University, was to examine, statistically, data produced by the preceding groups. Data was analysed to determine the probability of injury severity against, impact speed, linear acceleration, head injury criterion, rotational acceleration, rotational velocity, GAMBIT, external force (normal and tangential) and liner deformation.

The correlation was examined using ALL of the data available from accident investigation, headform drop tests to replicate the helmet damage, including those using the Bimass headform and computer simulation. Correlation of injury was by AIS given in the accident case analysis, by specific brain injury as given in the neuropathological analysis and by values of the brain parameters as given by the FE model.

Injury severity was correctly predicted in 25% of cases using the speed estimated from accident reconstruction and 24% of cases using speed measured in the damage replication drop tests. The human tolerance values were AIS 2 at 30km/h for the accident reconstruction and AIS 2 at 30km/h and AIS3 at 40km/h for the helmet damage replication. Speed and injury correlated better in the helmet damage replication tests than in the accident reconstruction.

Resultant linear headform acceleration gave a better correlation and the AIS was accurately predicted for 29% of cases. Injury severity of AIS 2 at was predicted to occur at 180g and AIS 3 at 220g. However, the most accurate estimate and the best correlation was with HIC for which 33% of cases were accurately predicted with a correlation coefficient of 0.8. In addition, injury severity of AIS 2 was predicted for HIC 1000 and AIS 3 at 1500, which is consistent with previous research.

Analysis against GAMBIT showed that the human tolerance was AIS 2 for a GAMBIT of 1 but the correlation was very poor and only 10% of cases were accurately predicted. Rotational acceleration was much better with 25% of cases accurately predicted and injury severity of AIS 2 at 8000 rad/s/s and AIS 3 at 19,000 rad/s/s.

The replication of helmet damage and FE numerical analysis of cases using the Bimass headform were separately analysed for a range of variables. Of these, the skull-brain relative linear acceleration analysis accurately predicted the injury in 50% of the accident cases. Skull-brain relative rotational acceleration, brain rotational acceleration and skull linear acceleration all accurately predicted the injury in 44% of cases. The Bimass relative measures provided the second best correlation coefficients.

The corresponding human tolerance values were calculated as follows:

	AIS 2	AIS3
Skull-brain relative linear acceleration	80 G	150 g (50%)
Skull-brain relative rotational acceleration	35,000rad/s ²	65,000rad/s ² (44%)
Brain rotational acceleration	36,000rad/s ²	70,000rad/s ²
Skull linear acceleration	160g	280g

It should be noted that the values in the above table cannot be related to measurements from a solid headform and should not be compared when considering tolerance to injury.

Development of test procedures

This was the last step needed to determine a new Standard for Europe. This research explored the relationship between rotational motion measured at the centre of the headform and forces measured at the helmet surface. This was examined both for a headform alone and for a whole dummy in an attempt to correlate research test methods with those prescribed by Standards.

It was clear from the conclusions of three Working Groups that rotational motion is a substantial cause of injury and should be evaluated when helmets are tested. However, although measurement at the centre of the headform is a direct means of assessment, this requires a nine-accelerometer array and a computer programme to analyse the results. In theory, measurement of force tangential to the helmet surface should give an accurate indication of the potential to induce rotational motion. This was investigated.

A Hybrid II headform was drop tested onto an oblique abrasive anvil at impact velocities of 6.0 m/s, 7.5 m/s, 8.5 m/s, 10.0 m/s and 12.0 m/s, using four different helmet types. The mean values of peak rotational acceleration varied between about 2500 rad/s² and 8500 rad/s² and the rotational velocity varied between about 20 rad/s and 41 rad/s. The mean tangential force varied from about 800 N to about 2500 N and the anvil tangential impulse varied between about 9 Ns and 20 Ns.

It was found that the correlation between peak rotational acceleration and peak tangential force was significantly linear ($r = 0.97$), and similarly between peak rotational velocity and anvil tangential impulse ($r = 0.95$). A significant linear correlation ($r = 0.91$) between peak linear acceleration and rotational acceleration was also measured. It was thus established that measurement of force is a reliable method. In addition, the oblique impact test is a suitable method with which to determine the differences in rotational acceleration and thus performance of different helmet types that may be caused for example, by different shell materials, liner density and helmet shape.

Part of the research was to establish the influence of the neck on the outcome in drop tests. A helmeted Hybrid III dummy was drop tested in 31 tests, onto a flat anvil at three different impact velocities (4.4 m/s, 5.2 m/s and 6.0 m/s) at the helmet impact points and body impact angles R/0°, B/30° and P/90°. Mean peak linear accelerations measured were between about 85g and 165g depending on the impact velocity and the helmet impact point. Mean peak force normal to the anvil varied between about 6500 N and 15600 N. It should be noted that the test repeatability was very good.

The helmeted Hybrid III dummy was also drop tested in 18 tests, onto an oblique abrasive at 4.4 m/s, 5.2 m/s and 6 m/s. The mean peak rotational accelerations were low and varied between about 1900 rad/s² and 3100 rad/s². The mean peak linear acceleration values ranged from about 27g to 41g and the mean peak tangential forces varied between about 700 N and 1100 N depending on the impact velocity.

Results from the headform tests and dummy tests were compared. It was found that although the results for a given set of conditions were similar, in general the headform test needed to be at a slightly greater velocity to give the same results. More specifically dummy impacts at 5.2 m/s corresponded approximately to headform impacts at 6 m/s. Dummy measurements at 6 m/s gave results that were between headform measurements at 6 m/s and at 7.5 m/s. The linear relationship between peak rotational acceleration and peak tangential force in the dummy tests was significant ($r = 0.90$) and was very similar to that obtained in detached headform tests (0.97). It was concluded from these tests that a good replacement for dummy tests onto the oblique abrasive anvil are headform drop tests

at a slightly greater velocity. However, this does not imply that the dummy tests accurately replicate a human rider in an accident.

The COST 327 Action was extended to investigate physiological effects on accident occurrence. However, such effects need to be assessed in Standards if improvements are to be sought. A novel sweating thermal headform prototype was developed by EMPA of Switzerland to assess the physiological and ergonomic properties of motorcycle helmets, including the simulation of sweat. A comparative helmet ventilation test series showed that there are large differences in the effectiveness of the ventilation openings of different helmet types and also for the same helmet between the different openings. Generally, helmet ventilation systems need substantial improvement. The experiments have demonstrated the need for an objective test method to assess the physiological properties of helmets and, in particular, to quantify the efficiency of ventilation systems. The temperatures measured on the sweating thermal headform with the vents set to the open and closed positions may provide the physiological criteria for future helmet Standards.

A review of literature showed that noise generated by motorcycle helmets can cause premature deafness. Measuring noise as part of a motorcycle helmet Standard is recommended and a two part test is proposed. Part A measures the noise level at the ear and part B assesses the sound attenuation over a range of frequencies.

In conclusion, a specification for a new European Standard was prepared from the findings above. If this is implemented, COST 327 confidently expects an improvement to motorcycle helmets that will reduce casualties with fatal and serious head injuries by at least 20% per annum across the EC. Thus, 1000 lives could be saved each year.

CHAPTER 1. INTRODUCTION

Motorcyclists are among the most vulnerable of road users. Analysis has shown that there are typically 4,700 motorcyclist fatalities throughout Europe each year and this represents some 16% of the total road-user fatalities, the second largest group after car occupants. It is, therefore, important that road safety practitioners in Europe have a good understanding of this problem to decide on future developments in this critical area.

It was known that head injuries cause some three-quarters of all fatalities to motorcyclists, while about one quarter of all injured riders suffer a head injury. COST 327 was formed to investigate in detail, motorcyclist head and neck injuries.

The COST 327 action was established with four main objectives, to be achieved using a wide range of European experience to determine or modify national approaches.

The first was to establish the distribution and severity of injuries experienced by motorcyclists, concentrating on the head and neck.

The second was to determine the most significant head and neck injury mechanisms.

Thirdly, the tolerance of the human head, brain and neck to these injuries and injury mechanisms was to be established.

The overall findings were to be used to propose a specification for the future testing of motorcycle helmets in Europe. It is important to note that during the course of the project it was estimated that fatal and serious head injuries could be reduced by at least 20% per annum across the EC if the proposed specification is implemented. Thus, around 1000 lives could be saved each year

Seven topics were identified as essential to achieving these objectives:

- Literature review
- Accident data collection
- Headform assessment
- Reconstruction of helmet accident damage
- Mathematical model of the skull, brain, neck, and helmet
- Human tolerance to injury
- Development of test procedures

A timetable based upon four and a half years was agreed for the overall project and a Working Group with a chairman was appointed for each of the above topics. The project was structured such that the findings of any one group would be needed by other groups, in the belief that that this was the best way to achieve the objectives. This final report describes the work of each of the groups and the their interdependency.

The literature review was necessary to understand the findings of existing research and to identify gaps in knowledge. Of critical importance was the need for more detailed accident information, particularly relating to the head and neck injury causes and mechanisms.

Thus, the need for a COST 327 accident database and analysis was identified.

Accident data was collected mainly by Southern General Hospital, Glasgow, UK, Medical School Hannover and Munich University, Germany and also by the Road Accident Investigation Team (RAIT) Finland but this data was provided toward the end of the project. The COST database was assembled by the Medical School Hannover. Details of the accident data collection and analysis are given in Chapter 3.

Collecting and analysing accident data was a vital part of the project and one on which all other groups depended. The research findings are thus presented in some detail.

Part of the research was to formulate a specification for the future testing of helmets sold in Europe. Identifying the characteristics of existing test headforms and exploring the possible benefits of new ideas for headforms was an important part of the research of the Headforms Working Group. Of particular importance was the development of a Bimass headform by Strasbourg University. This device was constructed with a mass representing the brain fitted inside a dummy headform to which it was attached with a damped spring system. This was designed to provide the headform with a response more human like than a conventional rigid headform. A full description of the mathematics, construction and of the finite element modelling that was used in the development of the Bimass is given in chapter four. Also given are details of the tests and results on conventional headforms. Each of these was fitted with a nine-accelerometer array so that rotational and linear acceleration could be measured. Tests were sufficiently numerous for the results to be analysed statistically and the chapter concludes with recommendations for the use of headforms in a new European standard.

Of vital importance to the efficacy of a helmet is the link between the measurements prescribed by Standards and the tolerance of the human head to injury in an equivalent impact. Criteria exist for human tolerance to rapid linear motion and, although, it is known that rapid rotational motion is equally, if not more, injurious a criterion has yet to be established. The main objective of the Reconstruction Working Group was to provide the Head and Neck Tolerance Working Group with "state of the art" data on the relationship between test measurements and human injury.

This was achieved mainly through the replication of damage observed on the accident helmet. A new helmet, equivalent to the accident helmet, was drop tested, at different speeds and angles onto a target, car wheel or specimen of road surface similar to that struck during the accident, until the damage matched that of the accident helmet. This technique was perfected by the Transport Research Laboratory (TRL) UK and was applied to a selected number of cases with the Bimass headform.

Also part of the research was the construction, by Valenciennes University, France of a lumped mass computer model of a motorcycle with dummy rider and a moving car. The model was used to simulate various accident cases to understand the rider dynamics during an accident and to assess the influence of the neck on the potential for head injury. The reconstruction research is described in chapter five.

It was essential that the link between accident impact mechanisms and the injury outcome be investigated for a range of circumstances far greater than was possible with experimental methods. Finite element simulation was identified in the literature review as the most appropriate method and chapter six describes the construction and validation of a unique and "state of the art" FE model of the skull, brain, neck and helmet. Strasbourg University was responsible for the construction of all but the neck, which was completed by Polytecnico Milano. During the course of the project, a copy of the head and brain model was supplied to TRL who analysed head parameters. TRL supplied extensive data

from the replication process and this was used as part of the validation procedure. It was also used in the investigation of accident cases using the FE model. A full description of the research of the Computer Simulation Working Group is given in chapter six.

Critical to the success of the whole project is the clear identification of the tolerance of the human head to impact parameters, which is essential if future Standards are to be improved. The prime objective of the Head and Neck Tolerance Working Group, lead by Munich University, was to examine statistically, data produced by the preceding Working Groups. Chapter seven provides details of this extensive analysis. This leads to chapter eight, test methods, which is the last part of the process to determine a new Standard for Europe. This research has explored the relationship between rotational motion measured at the centre of the headform and forces measured at the helmet surface. This was examined both for a headform alone and for a whole dummy in an attempt to correlate research test methods with those prescribed by Standards.

Toward the end of the project, an extension was granted to investigate the effect of physiological parameters on motorcycle riders. The accident data was analysed to examine the effect of climate on accident risk, see chapter three. The Test Procedures Working Group examined how best to measure physiological parameters using a revolutionary new headform developed by EMPA of Switzerland who lead the test procedures research.

It was believed that motorcyclists can suffer premature deafness from the noise generated by the helmet. Literature was reviewed and reported on.

Finally, the report gives a specification for a new helmet standard that, if implemented, is expected to result in helmets that offer substantially better protection than the helmets currently on the market.

CHAPTER 2. LITERATURE REVIEW

2.1. INTRODUCTION

It is well known that motorcycling carries a very high accident risk and yet almost the only protection afforded to a motorcyclist is the helmet he wears. In spite of the high wearing rate in most European countries, head injuries are still the cause of the vast majority of fatal and serious injuries to motorcyclists. COST 327 action committee was convened to investigate means whereby helmets can be improved and thus provide better protection. However, in order to improve the protection afforded by helmets, it is first necessary to gain a proper understanding of the ways in which motorcycle accidents happen, and in particular the ways in which head and neck injuries occur. Nevertheless, whilst some improvement to helmets may be possible from a better understanding of injury mechanisms and helmet construction, the process will only be truly successful if human tolerance to head injury is further investigated and better understood.

The purpose of any literature review is to provide researchers with detailed information on what has previously been achieved so that the research does not duplicate, unnecessarily, what has gone before. The COST 327 review was no exception and is summarised below under the appropriate headings.

The review concludes with a list of the 305 references used in its compilation. These are given below each section by author and date.

2.2. ACCIDENTS AND INJURY MECHANISMS

Casualty rates, accident causes and configurations, injury mechanisms, head injury patterns and skull and neck injuries are reviewed. The main conclusion was that, in total, there are some 8.6 million motorcycles (not counting mopeds) in the 15 European countries, and approximately 5 thousand fatalities annually, accounting for a substantial proportion (9%) of total road fatalities. In Europe, motorcycling tends to be a minority mode and yet the risk of injury is considerably higher than for car users and by a factor of ten per kilometre travelled.

The majority of collisions, particularly those causing head injury, are head-on impacts, where the motorcycle is at roughly 90 degrees to the front or side of the target vehicle, and the rider is thrown forward over the handlebars into the side, front or rear of the vehicle. Although the majority of these collisions are with cars, the head hitting the road or roadside furniture causes most serious head injuries. Most motorcycle collisions take place at relatively low speeds of around 30 km/h. Skull fractures occur at speeds of 30 km/h upwards but brain injuries can be sustained at relative speeds as low as 11 km/h. Therefore, there is some hope that better protection might be afforded. At the moment, progress in research is hampered by inadequate accident data, especially on accident configurations, so more effort needs to be put into this area of investigation.

Most head injuries are sustained at the front of the head, with more than two thirds of skull fractures involving chin impact. The type and severity of these injuries depends upon the speed and angle of impact. A high proportion of fatalities with head injuries sustained base of the skull fractures, almost always caused by direct impact, through the chin guard, to the facial skull, and in turn through to the skull base. Thus the chin guard is an area of the helmet that requires particular attention.

2.2.1. References

Chinn, Hopes and Finnis (1989), Dowdell et al (1988), EEVC(1993), Engel (1992), Fuller and Snider (1987), Gennarelli (1985), Gilchrist and Mills (1987), Grandel (1987), Harms (1981), Harms (1984), Harms (1989), Harms (1993), Hight et al (1986), Hurt and Thom (1992), Hurt et al (1981), Hurt et al (1986), Kalbe et al (1981), Kranz (1985), Langweider (1977), Langweider et al (1986), Larder (1984), Onser (1983), Otte (1980), Otte (1989), Otte (1991), Otte and Felten(1991), Otte et al (1981), Otte et al (1982), Otte et al (1984), Pedder et al (1979), Pedder et al (1982), Ramet et al (1981), Sporner et al (1987), Sporner et al (1989), Sporner et al (1990), Vallée et al. (1981), Whitaker (1980), Wismans et al (1992).

2.3. BIOMECHANICS OF HEAD INJURY

The biomechanics of head injury was reviewed with particular reference to the different types and mechanisms of brain injury and it should be noted that injuries from a wide variety of causes were described and discussed. Head injury tolerance and associated criteria were also included and the findings are given below.

Defining the causes of head injury is not an easy task because several different types of head injury can originate from the same accident. Certain head injuries, for example extensive axonal damage and subdural haematoma, have more severe consequences than others and will, therefore, determine the overall outcome.

The various forces to the head during an accident tend to combine in two different ways. First, the individual effects of simultaneous forces can influence each other as occurs with an oblique force, which induces both linear and rotational acceleration. The two types of force combined result in deformations of the brain that differ considerably from the effects seen from the individual forces. Second, the effects of subsequent forces can accumulate. For example, when the brain is first pushed toward the skull base and then forced to slide against it, the effects of the contact between the cortical tissues and the highly irregular skull base will be much more severe than in either of the individual cases. Therefore, knowledge of the complete loading sequence of the head in the most common accidents is a pre-requisite for a clear understanding of the causes of head injury.

Injuries from an impact can occur at, or remote from, the site of contact. The effects of the impact at the site of contact are fairly well understood and are known to cause deformation, fracture and penetration of the skull (mainly the vault), whereas the effects remote from an impact are still not clearly understood. Remote effects are thought to be the cause of basilar skull fractures by means of skull distortion in vault impact, by transmission of the impact force through the mandible in facial impacts, and by hyper motions of the head from an impact. However, there is no detailed information available on the overall deformation of the skull in an impact, on the impact force transmitted by the mandible and on the extent of the effects of the hyper motions of the head. Further research in this area is necessary.

The response of the brain to loading of the skull may be frequency dependent and this may explain the differences in injuries found after long duration (low frequency) and short duration (high frequency) impacts. However, the response of the brain to a load on the skull remains largely unknown.

The theory that translational acceleration was not injurious to the brain, but that brain injury was caused by shear strains produced by rotational acceleration was first postulated by Holbourn in 1943. Subsequent research showed that rotational and linear acceleration

almost always occurred together in an accident and both cause injury. A detailed analysis of the effect of rotational motion has shown that in one set of tests a rotational acceleration of $4,500 \text{ rads}^{-2}$ proved fatal whereas in other experiments a value of $16,000 \text{ rads}^{-2}$ caused no injury. However, duration is thought to be critical to the outcome and research should be directed to finding the threshold of injury from rotational motion.

Various injury criteria, for the head, have been proposed in the past. The most commonly acknowledged and widely applied calculation of injury parameters is the head injury criterion (HIC), which is based on the assumption that the linear acceleration of the head is a valid indicator of head injury thresholds. The literature suggested that HIC 1000, used as a pass/fail criterion in the automotive industry, corresponds to a probability of death of some 10% and HIC 2000 of some 50%. The HIC has enabled vehicle safety to be improved. Nevertheless, it has shortcomings and does not take into account rotational acceleration, head kinematics and direction of impact. Future research should be directed to the derivation of a criterion that overcomes the criticisms.

Peak linear acceleration is widely used in potential head injury assessment. Fatal injuries are estimated to have occurred at 200g and above which is consistent with Newman (1986) who suggested that 200g-250g corresponds to AIS4, 250g-300g to AIS5 and greater than 300g to AIS6.

The greatest gaps in head injury research are the knowledge of the kinematics of the head in an accident, the resulting behaviour of the intracranial structures, and the quantification of the potential for injury from rotational motion.

2.3.1. References

Abel et al. (1978), Adams (1975), Adams and Doyle et al. (1986), Adams and Mitchell et al. (1977), Adams et al. (1977), Adams et al. (1980), Adams et al. (1982a), Alem et al. (1984), Aoki and Masuzawa (1984), Bakay and Glasauer (1980), Beusenberg (1991), Brit et al. (1980), Capra and Anderson (1984), Chamouard et al (1986), Chapman (1985), Chapon et al. (1985), Clark (1974), Clemens and Burow (1972), Cooper (1982), Courville (1942), Denny-Brown (1945), Denny-Brown and Russell (1941), Douglass et al. (1968), Eiband (1959), Fruin et al. (1984), Gadd (1966), Gardner et al. (1986), Gennarelli (1985), Gennarelli (1987), Gennarelli and Thibault (1982), Gennarelli et al. (1971), Gennarelli et al (1972), Gennarelli et al. (1982b), Gennarelli et al. (1979), Gennarelli et al (1987), Gosch et al. (1969), Gosch et al. (1970), Got et al. (1983), Grecevik and Jacob (1965), Gurdjian (1966), Gurdjian (1975), Gurdjian and Gurdjian 1976, Gurdjian and Lissner (1961), Gurdjian et al. (1949), Gurdjian et al. (1950), Gurdjian et al. (1953), Gurdjian et al. (1955), Gurdjian et al. (1961), Harvey and Jones (1980), Hirakawa et al. (1972), Hodgson and Patrick (1968), Hodgson and Thomas (1972), Hodgson and Thomas (1979), Hodgson et al. (1970), Hodgson et al. (1983), Holbourn (1943), Holbourn (1945), Hopes and Chinn (1989), Hopes and Chinn (1990), Huelke et al. (1988), Hurt et al. (1981), Hurt et al. (1986), Kessler (1987), Komatsu et al. (1979), Lau et al. (1987), Lee et al. (1987), Leestma et al. (1983), Lindenberg and Freytag (1957), Lindenberg and Freytag (1960), Lindenberg and Freytag (1970), Lissner and Gurdjian (1961), Lissner et al. (1960), Löwenhielm (1974a), Löwenhielm (1974b), Löwenhielm (1975), Luna et al. (1981), McElhaney et al. (1972), Melvin and Evans (1971), Miller and Jennett (1968), Nahum et al. (1968), Nahum et al (1977), Nevin (1967), Newman (1980), Newman (1986), Nusholtz et al. (1979a), Nusholtz et al. (1979b), Nusholtz et al. (1984), O'Connell (1934), Oka et al. 1985), Olsson et al. (1971), Ommaya (1966), Ommaya and Corrao (1968), Ommaya and Gennarelli (1974),

Ommaya et al. (1964), Ommaya et al. (1969), Oppenheimer (1968), Patrick et al. (1963), Peerless and Rewcastle (1967), Pincemillé et al (1989), Prasad et al. (1985), Pudenz and Shelden (1946), Ryan et al (1989), Sellier and Unterharnscheidt (1963), Shatsky et al. (1974a), Shatsky et al. (1974b), Shelden et al. (1944), Simpson et al. (1989), Skold and Voight 1977), Slattenschek and Tauffkirchen (1970), Smith and Dehner (1969), Strich (1956), Strich (1961), Strich (1969), Strich (1970), Symonds (1962), Thom and Hurt (1993), Thomas et al. (1973), Tomlinson (1970), Trotter (1924), Unterharnscheidt and Higgins (1969), Versace (1971), Viano (1988), Viano (1995), Voigt and Löwenhielm (1974), Voight and Skold (1974), Walker (1973), Zimmerman and Bilaniuk (1978).

2.4. MATHEMATICAL MODELLING OF THE HUMAN HEAD AND NECK

Mathematical modelling of the head and the neck is a difficult and diverse subject and is discussed at length with the head and neck reviewed separately. Of particular importance is the review of physical and mechanical properties of tissues. Values chosen by some modellers have caused considerable difficulty and, therefore, a table of values used in a wide range of models is provided.

Among the conclusions of the section on head modelling is that all the discrete models (lumped mass) have the same severe limitations. Neither the location nor the severity of the head injuries can be predicted and the type of injury is only inferred from the measurements on the assumption that if certain values for the parameters are exceeded then a certain range of injuries may be predicted. None of the models was properly validated against experimental data such as that obtained from cadavers or other biomechanical experiments.

Finite element modelling is the only method that can predict intra- cerebral parameters such as pressure, principal strains and stresses, as well as relative displacement of the principal head components. The variation in total skull thickness is well reproduced in some models and 'sandwich' elements have been used to estimate skull deformation correctly. Different anatomical head characteristics such as the foramen magnum, the falx cerebri, and the tentorium have also been incorporated in the more recent models

The neck joint boundaries have been neglected. Further research is needed to assess the influence of the human body, especially the thorax, on the outcome for the head in an accident and models need to be developed so that this influence is reproduced.

The neck is described anatomically, some examples of typical neck injuries are given and lumped-mass and finite element models of the neck are compared. The principal findings are as follows. Mathematical modelling of the neck has the potential to provide a detailed description of the dynamics of the neck. Injury potential is also likely to be accurately predicted when the limit of the tissue tolerance is exceeded.

The majority of neck models developed over the last 20 years have considered the vertebrae to be rigid bodies linked together by deformable elements, often modelled as beams or massless springs. The importance of describing the actual geometry of the vertebrae and the global lordosis of the neck was emphasised by several authors. This was particularly so, when the head was subjected to compressive loading. An accurate description of the anatomy of the ligaments and muscles and their disposition around the bones was also found to be very important and especially so, when large displacements and rotations are likely to occur. In long duration impacts, it was demonstrated that the muscular contraction changes the global dynamics of the head-neck system.

The more recent three-dimensional models demonstrated, in most cases, good agreement with experimental tests. Where discrepancies did occur, these were eventually attributed to the inadequate description of the materials used in the model and/or to the poor anatomical definition of the structural components.

Of great importance are the mechanical properties of neck tissue. The neck structural components are the vertebrae, made of cortical and spongy bone; the almost incompressible discs, that consist mainly of water (nucleus pulposus) and fibrous tissue (annulus fibrosus), and the ligaments and muscles, that consist of fibrous connective tissue. All of these materials have been studied in the past 20 years and their mechanical characteristics are available from the literature. It should be noted that, in most cases, the studies have not been conducted specifically on the cervical tissues. An extrapolation is, therefore, necessary to model the materials of interest.

Bone tissue elasticity of the vertebrae was demonstrated to have a considerable influence on the mechanical behaviour of the neck. The review strongly recommends, therefore, that this characteristic is included in future neck models; techniques offered by finite element procedures make this readily possible.

2.4.1. References

Alem et al. (1978), Anderson 1985; Lighthall 1988), Anzelius (1943), Bandak et al. (1994), Belytschko and Privityzer (1979), Belytschko et al. 1976), Brinn and Staffeld (1970), Bycroft (1970), Cheng et al. (1990), Chu and Lee (1991), Chu et al. (1994), Deng and Goldsmith (1987), Dimasi et al. (1991), Douglass et al. (1968), Engin (1969), Ewing et al. (1972), Ewing et al. (1977), Fan (1971), Gross (1958), Haynes and Lissner (1962), Hodgson and Patrick (1968), Hodgson and Thomas (1971), Hodgson et al. (1967), Hosey and Liu (1982), Hosey et al. (1982), Huston and Advani (1976), Khalil and Hubbard (1977), Khalil and Viano (1982), King, Nakhla and Mital (1978), Krabbel et al. (1994), Kuijpers (1996), Lau and Viano (1986), Lighthall 1988), Lee (1973), Lee and Advani, (1970), Low and Stalnaker (1987), McElhaney et al. (1971), McElhaney et al. (1973), McKenzie and Williams (1971), Margulies (1985), Margulies et al. (1985), Margulies and Thibault (1989), Mendis (1992), Merrill (1981), Merrill, Goldsmith and Deng (1984), Nahum (1977), Nahum and Smith (1976), Nahum et al. (1977), Nitsche (n.d.), Nusholtz et al. (1984), Pluche (1985), Pluche and King (1985), Rade (1993), Rojanavanich and Stalnaker (1991), Ruan et al. (1991), Ruan et al. (1992), Ruan et al. (1993), Sances & Myklebust. (1982), Shuck (1970), Shuck and Advani (1972), Shugar (1977), Slattenschek and Tauffkirchen (1970), Stalnaker et al. (1971a), Stalnaker et al. (1971b), Stalnaker et al. (1977), Stalnaker et al. (1985), Stalnaker et al. (1987), Suh (1977), Tien and Huston (1987), Ueno (1995), Ueno and Melvin (1995), Viano (1988), Viano (1989), Viano and Lau (1988), Viano et al. (1986), Viano et al. (1989), Vicentini (1995), , Vicentini and Giavotto (1995), Ward (1975), Williams and Belytschko (1983), Willinger et al. (1991), Willinger et al. (1992), Willinger et al. (1995), Willinger et al. (1995b), Yoganandan et al. (1990), Yoganandan et al. (1991).

2.5. MOTORCYCLE HELMETS: PERFORMANCE AND CURRENT STANDARDS

Current helmets and how they perform is linked very closely to the requirements of existing Standards. The benefits and problems with current helmets and ways in which helmets may be improved are described and discussed. Current standards are also reviewed and the main requirements of the leading standards from around the world are tabulated for ease of reference. It was found that wearing a helmet reduces the risk of a

fatality by about a half and the frequency and severity of head injuries with their considerable associated costs are also reduced. There is no evidence that wearing a helmet increases the risk of neck injury, although head injuries may be slightly more frequent with full-face than with open-face helmets. However, full-face helmets offer better protection than open-face helmets for the face and chin area.

Helmets could be improved: current designs are too stiff and too resilient and energy is absorbed efficiently only at values of HIC well above those which are survivable. Helmet shells and helmet liners should absorb energy efficiently from HIC of about 1000 upwards. Rotational acceleration is also an important cause of injury and helmet design should ensure that the potential for rotation is minimised. Work should also be done to reduce the problems of noise and heat subjected to the rider by the helmet.

The route for helmet improvement is through improved standards. Efficient energy absorption with the optimum impulse, minimum tendency to induce rotational motion and a comprehensive evaluation of the whole helmet including the chin guard of a full faced helmet are features for which standards should require tests. Currently only the British Standard 6658 includes tests for rotation and the chin guard, and only Regulation 22-04 requires an assessment against HIC (time dependent criterion). Although ECE Regulation 22-04 (recently amended from -03) is widely used, it does not require tests for rotation or the chin guard. It was also found that penetration is a very infrequent cause of injury and it is recommended that Standards follow the example of Regulation 22-04, which does not require a test for penetration.

2.5.1. References

Aldman and Thomgren (1979), American National Standard Inst. (1991), ARU, (1994), Australian Standard AS 1698 (1988), Australian Standard AS 2512 (1984), British Standard Institution BS 6658 (1985), de Wolf (1986), Department of Public Safety and Texas Department of Health (1988), ECE R22-04, (amended from R22-03) EEVC (1993), Federal Motor Vehicle Safety Standard MVSS 218 (1973), Hopes and Chinn (1989), Hurt et al (1981), ISO Recommendation 1511 (1970), JSA JIS T 8133 (1982), Laboratoire de l'Union Technique de l'Automobile du Motorcycle et du Cycle (unpublished), McSwain and Belles, (1990), McSwain et al, (1985), Mohan et al (1984), Noël (1979), Otte and Felten (1991), Otte and Suren (1985), Otte et al (1984), Patel and Mohan (1993), Pedder et al (1979), Schuller and Beier (1981), Schuller et al (1985), Shankar et al, (1992), Shaper et al (1984), SNELL-Standard (1985), Snell Memorial Foundation (1990), Stöcker and Löffelholz (1984), Tangorra and George, (1991), United Nations ECE 22/04 (1995), Vaughan (1977), Vallée et al. (1984), Walz et al (1976), Whitaker (1980), Yetram, Godfrey and Chinn (1994).

CHAPTER 3. ACCIDENT INVESTIGATION

3.1. INTRODUCTION

This chapter was prepared by the Accident Investigation Working Group and describes the patterns of injury for helmeted motorcyclists. Four different research groups were responsible for the data collection: the Universities of Hannover and Munich in Germany, Glasgow in the United Kingdom and VALT, operated by insurance companies, in Finland. The data was collected from in-depth investigations by teams comprising technical and medical experts who concentrated on the causes of head and neck injury.

The accident data recording began in July 1995 using forms developed especially for the COST 327 database. The forms were then sent to Hannover where the data were coded and entered onto the COST database. Each organisation completed an original case file for its own use and the COST data file sent to Hannover was a summary of the original file together with special information such as computed vehicle speed and identification of the helmet impact location and direction. Each case was discussed in detail within the Accident Investigation expert group of COST 327 during Working Group meetings. The task of these expert discussions was to determine the injury mechanisms, magnitude and direction of forces to the head and to select cases for replication by the Reconstruction Working Group. There were also links to other Working Groups especially to the Head and Neck Tolerance Working Group.

This chapter describes the structure of the database and the analysis of 253 accident cases that were collected within a three year period from July 1995 until June 1998 in Finland, Germany and the United Kingdom and entered in the COST 327 database at Hannover.

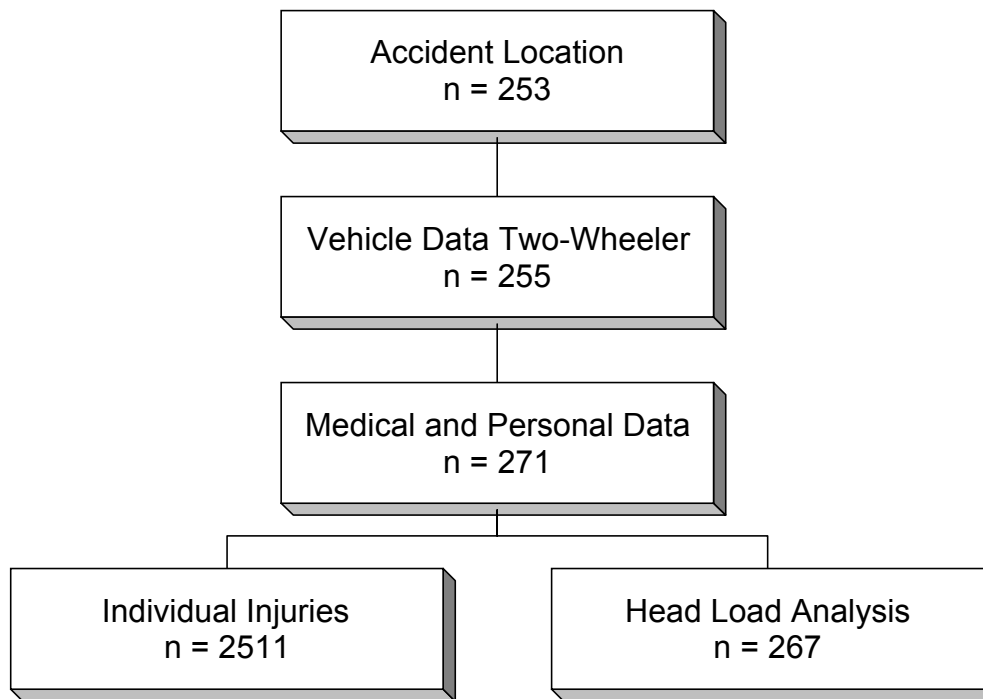
The following criteria were used for selecting accidents for inclusion in the COST 327 database:

- two-wheel motor vehicles
- helmet, full face (integral) or open face (jet), worn
- head and or neck injuries of AIS 1 and above
- known head/helmet contact but without head injuries

3.2. DESCRIPTION OF THE COST 327 DATABASE

The COST database was stored using SIR (Scientific Information Retrieval). SIR is a comprehensive database management and application development system with facilities to organise and store data, to process and manage the data and to produce statistical and other outputs. DBMS (Data Base Management System) is the main SIR module and provides a relational database and application development system.

The COST 327 data bank comprises six record types at four different hierarchical-levels as described in the following flow chart. Each record type may have one or more variables defined as keys, which are used to identify each individual record. The description of the database and all record types is known as the database schema.



It was necessary, for the analysis, to have as much information as possible on the head impact. In particular, the injuries, the damage to the helmet, the type of target and contact location, and the vehicle damage and impact location when relevant. Thus, with this information, it was possible to obtain detailed and high quality analyses of the head injury mechanisms.

The database comprises the following number of accidents from each investigation area:

Area	Country	
Hannover	Germany	n = 111
Munich	Germany	n = 55
Glasgow	United Kingdom	n = 52
<u>Finland</u>	<u>Finland</u>	<u>n = 35</u>
Total COST 327 database		n = 253

It should be noted that in all cases the casualties were complying with the appropriate national law for helmet wearing. It should also be noted that the data collected on accidents contains mainly information generally accessible at the scene. However, it also contains personal information relating to the casualties and witnesses and this is recorded strictly under the requirements of all countries' Data Privacy Laws. For example names are not stored in the database, it is not possible to identify any person retrospectively and information is never given to third parties.

3.3. ACCIDENT SAMPLING AREAS

The four different investigation areas within COST 327 are described below.

3.3.1. Accident Research Unit - Medical University Hannover / Germany

The Hannover Accident Research Unit (ARU) has been operational since 1973. It is based at the Medical University of Hannover and is directly funded by the Federal Highway Research Institute (Bundesanstalt für Straßenwesen, Bergisch-Gladbach). About 1000 accidents, to all

categories of road user, are investigated annually and detailed accident and injury information is recorded and entered into a database. Since 1985 the accidents have been selected for investigation using a statistical sampling procedure to ensure that the database is representative and can be related to national statistics (Otte, 1994a). It should be noted that the accidents are investigated by teams working two six-hour shifts during a 24 hour period. The cases for the COST database are a sub-sample of the overall database based upon the criteria defined below.

The investigation area extends from the urban to the rural regions of Hannover with a radius of approximately 60 km. About 1.2 million people live in this region and it covers 2,289 square kilometres of which about 10% are defined as urban. This is typical of the Federal Republic of Germany, thus Hannover may be considered representative.

The comparison of the accidents in the official statistics with those documented by the team shows that they correspond to each other in respect of a multitude of variables although, a weighting is necessarily applied to the following variables:

- Injury severity (minor, severe, fatal)
- Accident location (rural, urban)
- Time of the accident investigation period.

Apart from the primary data sampling at the site of the accident with the use of pre-prepared check-lists, there are also police reports, medical reports from the hospitals, X-ray photos of the injuries, and questionnaires sent to persons involved in the accidents. These are archived and the information is used to complete the database records.

The data collected on accidents contain largely information generally accessible, regarding the site of accidents, environmental conditions and technical data on vehicles. But it also contains personal information that is recorded under the requirements of the German Data Privacy Laws. For example, names are not stored in the database and it is not possible to identify any person retrospectively. During the accident evaluation, names and addresses of involved persons are needed and these are deleted later.

3.3.2. Department of Neuropathology, Glasgow/UK

The Motorcycle Accident Injury Study at the Southern General Hospital in Glasgow started in 1984. It is carried out with the co-operation of the Department of Neuropathology, the Department of Transport Vehicle Inspectorate, Strathclyde Police and the Crown Office (Scotland).

The investigation area is the Strathclyde Police region. Within this region there are densely populated urban areas, for example, central Glasgow which has a population of 24,031 in an area of 2.5 sq. miles and also relatively sparsely populated rural areas (Dumbarton, Argyll & Bute division) with a population of 145,900 dispersed over an area of 2,900 sq miles. The Strathclyde Police region as a whole has an area of 5,500 sq miles, and a population of 2,306,000.

All reported accidents involving motorcycles in the Strathclyde region are passed to the Department of Neuropathology from Strathclyde Police. The Department investigates any motorcycle accident for which the following criteria apply:

A rider or pillion passenger who has sustained a head injury

A rider or pillion passenger who has sustained an injury rated AIS level 2 or above (Abbreviated Injury Scale 90)

A rider or pillion passenger who has spent 24 hours or more in hospital.

Three sets of forms are completed for each case:

Accident and Vehicle Data Forms - these are completed by the Vehicle Inspectorate, from information gained from questionnaires, examination of vehicles involved and examination of the accident locus. Wherever possible the Vehicle Inspectorate will also obtain photographs of the case vehicles, accident locus, helmet and clothing.

Injury Data Forms - are completed by the Department of Neuropathology, with data from questionnaires and medical records or post mortem reports, obtained from hospitals and Procurators Fiscal.

Brain injury diagrams are completed in the Department of Neuropathology from examination of the brain in fatal cases or from neuro-radiology in serious cases.

Occupant names are removed and case numbers assigned as soon possible, to ensure confidentiality. The cases are then reviewed to determine accident cause, mechanism, and the contact points, to clarify injury mechanisms. The COST-cases are a sub-sample of this overall sample.

3.3.3. Institute for Legal Medicine, Munich University / Germany

IFR activities include biomechanical analysis and assessment of forensic traffic accident cases commonly based on autopsy data, police reports, technical expert investigations, and special investigations using IFR staff. More than 2,000 autopsy cases are currently investigated each year of which one-third represent all kinds of fatal traffic accidents including a considerable number of motorcycle accidents. Additionally, some non-fatal motorcycle cases are also investigated, for which injury data are derived from clinical files.

The selection of the IFR-cases is not as strictly related to a defined sampling procedure as in the Hannover and Glasgow studies. It is determined more by criminal or liability relevance, for example, to determine the seating positions and seat-belt use for vehicle occupants and helmet use for motorcyclists. Usually, police and/or prosecutors decide whether or not forensic investigation is needed and, for some cases, insurance companies request analysis of the accident as evidence of liability. For this COST 327 project only, those motorcycle accidents where a helmet was worn, were selected.

The area from which IFR cases are selected for forensic investigation is the City of Munich and the surrounding area of Southern Bavaria, enclosing a region with population of approximately 3 million. Additionally, a few cases come from other states or countries, for example Austria and Luxembourg.

For IFR autopsy cases, detailed injury data is available and, if relevant, a neuropathological analysis of the head injuries is obtained. Clinical files of the non-fatal cases comprise an injury description and documentation by means of x-rays, CT-and/or NMR-scans.

3.3.4. Road Accident Investigation Teams (RAIT), Finland

The data compiled on motorcycle accidents in Finland are based on the database of the Traffic Safety Committee of Insurance Companies (VALT), which is an organisation run by the Finnish insurance industry. This database includes information from all the fatal road accidents.

In Finland there are about 3.45 million motor vehicles registered, out of which 72,000 are motorcycles and almost 100,000 are mopeds. Of the total area of 338,000 square kilometres, 61.8 billion passenger kilometres are covered by these vehicles annually, 0.9 billion kilometres of which are by motorised two-wheelers. In 1998 of all the 6,887 accidents involving personal injuries, 365 cases were fatal to at least one of the casualties. Respectively, there were 9,083 injuries and 398 fatalities in these accidents.

All of the fatal cases were investigated by special voluntary-based Road Accident Investigation Teams (RAIT) led by a representative of the police and consisting of experts in vehicle engineering, road engineering and medicine. If necessary, the team was helped by a member with expertise of behavioural sciences. On average, the team arrives at the site in one or two hours after it has been notified by the local police.

The examination process of the fatal accidents concentrates on the pre-crash phase by collecting data from all the participants, vehicles, road and its surroundings. If possible, the team reconstructs the accident on the site. The database of VALT has been built up by storing the data collected by the RAIT's into a computer file. It consists of four categories: accidents, participants, occupants and risk factors. The oldest data from this database are for the year 1971.

Annually, the Finnish road accident statistics include 10 to 15 cases that are fatal either to motorcycle drivers or pillion passengers. Because of a relatively short driving season, most of these accidents take place during a period of a few months beginning at the end of May and lasting up to mid-October.

The data, for the purposes of this research project, were selected from the database of VALT. COST 327 began in July 1995, therefore, the Finnish data was also taken from the years 1995-1998. The information from the database was obtained from the RAIT final reports and transferred to the COST 327 forms as completely as possible. However, because of the variation in the availability and the accuracy of some details (especially photographs and drawings), it was not possible to provide all of the information needed. The impact points and impact angles were estimated whenever it was possible.

The data describing the condition of the helmets, their types and impact points were not often available from the reports. A pilot project aimed at creating a method of collecting information that is more detailed, began in the Helsinki area in 1998 and this has been expanded to the whole country since spring 1999.

3.4. ANALYSIS TECHNIQUE AND DEFINITIONS

3.4.1. Injury severity

The Abbreviated Injury Scale (AIS 90) developed by the Association for Automotive Medicine was used. This AIS-scale was developed to provide researchers with a simple numerical method for ranking and comparing injuries by severity, and to standardise the terminology used to describe injuries.

The Abbreviated Injury Scale (AIS) is a consensus derived, anatomically based system that classifies individual injury by body region on a 6-point ordinal severity scale ranging from AIS 1 (minor) to AIS 6 (currently untreatable). The AIS does not assess the combined effects of multiple injuries.

The Maximum AIS (MAIS), which is the highest single AIS code for a patient with multiple injuries, has been used by investigators to describe overall severity. In the tables in this report grades have been combined as follows: AIS 1, slight/minor, AIS 2-4 serious/severe, AIS 5/6 very severe and fatal. This classification enabled the results to be compared with national statistics.

It has been established (Otte, 1995) that MAIS 1 corresponds to 88% minor, MAIS 2 to 4 to 80% serious, and MAIS 5/6 with 75% fatal as classified in the official national statistics

3.4.2. Impact speed determination

The accident case file contains information on vehicle deformation, contact location, skid marks, injuries, pre-impact and collision speeds and the driver behaviour. Each of these is necessary for scientific analysis of the accident and injury causes and mechanisms for which information on the impact speeds is essential.

The collision speed, however, can be evaluated only by a mathematical impact analysis using the basic principles of physics. Evidence of the vehicle movement and deformation pattern and the statements relating to the driving behaviour prior to the collision, must be taken into consideration.

The accuracy of the results depends upon the skill of the accident investigation team in collecting the data required for the mathematical accident reconstruction for which the following information must be available: accurate scale drawings, extensive photographic documentation of the vehicle deformation and accident traces, for example skid and scrape marks. The use of photogrammetric procedures provides for a high quality of measuring precision for trace reproduction. The extent of the vehicle damage is used for the assessment of impact directions and the collision angle as well as the energy absorption during the impact.

3.4.3. Head impact speed

The head impact speed was evaluated from the calculated speed of the motorcycle, an analysis of the body kinematics during the accident, the position of the body at the point of impact against the road surface and/or vehicle parts or other obstacles.

3.4.4. Head and body impact angle

3.4.4.1 Body Impact Angle

The body impact angle was determined for every case, and is defined as the angle between the body longitudinal axis and the surface of the impacted obstacle.

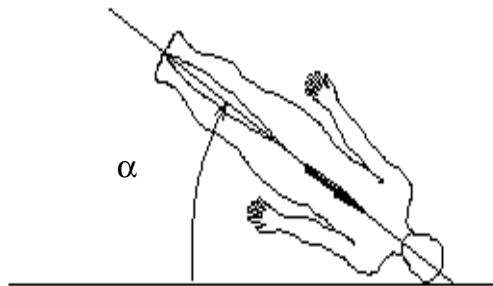


Figure 3.1. Body impact angle

3.4.4.2 Head Impact angle

The head impact angles were classified in accordance with the following co-ordinate system. ZX and XY together describe the position of the head related to the direction of force to the head. These angles were estimated for every head impact and assigned to every head injury.

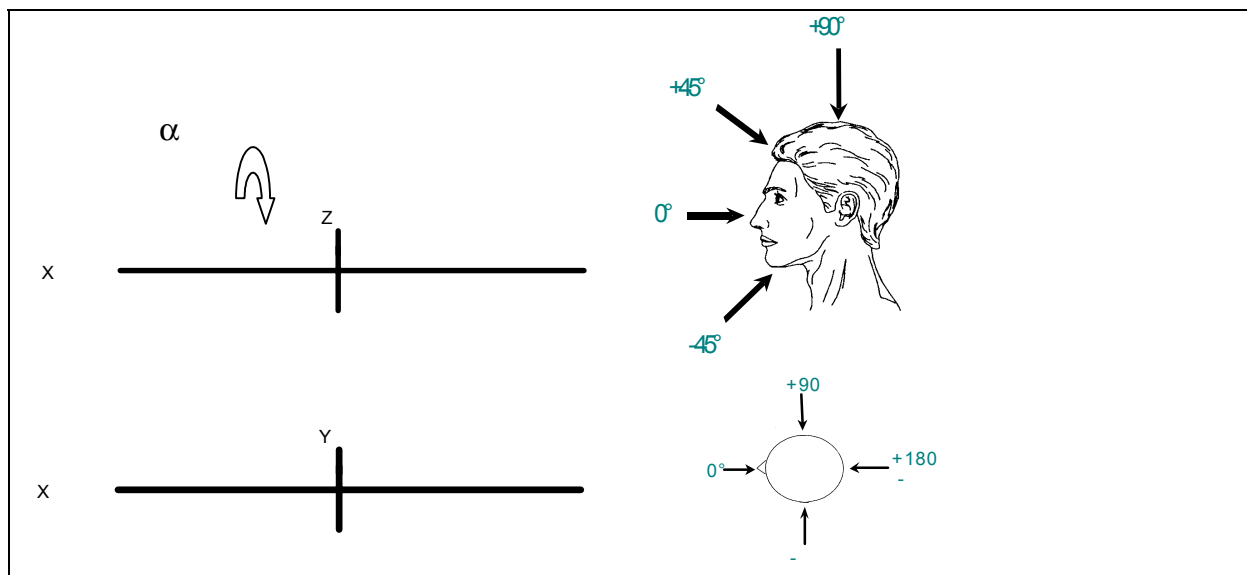


Figure 3.2. Head impact angle

The angle ZX is defined by a horizontal axis through the head and the impact direction. A horizontal impact is a 0 degree-impact, it can be frontal, rear or a side impact. A vertical impact to the top of the head is a 90 degree-impact. For impacts at an angle from the top, the angle ZX can be from 1 degree up to 89 degree. Impacts with a head impact angle ZX of plus 46 degrees or more are defined as impacts from the top, angles of minus 46 degrees or less are impacts from the bottom.

The angle XY describes the direction of the impact in the view from the top. A frontal impact is characterised by 0 degree, from the back it is ± 180 degrees. The lateral right side is marked by positive XY angles, at the left side they are negative between minus 1 and minus 179 degrees.

3.4.5. Collision types

For COST 327, "collision types" were defined according to the classification developed by Koch (1986) and Otte et al (1994) plus a further collision type for obstacle collisions; this gave a representative selection.

3.4.6. Definition for mechanisms

The head injury mechanisms were divided into consequences of force transmission:

- direct impact
- indirect impact
- contre coup (injuries on the opposite impact side)

The load mechanisms were classified as

- compression
- direct force transmission
- inertial load
- penetration

The results of mechanisms were considered as

- translation

- rotation around the z-axis
- rotation around the y-axis
- rotation around the x-axis

3.4.7. Replication process

All cases were discussed in the Accident Investigation Working Group and some were selected for replication, which consisted of drop testing to simulate real head impact conditions.

3.5. LINKAGE OF COST DATABANK TO NATIONAL STATISTICS

The COST databank consists of a number of cases, compiled by the investigators local to the defined areas of UK, Germany and Finland. Detailed results are summarised in the Working Group report "Accident Description and Analysis of Motorcycle Safety Helmets" (March 1999).

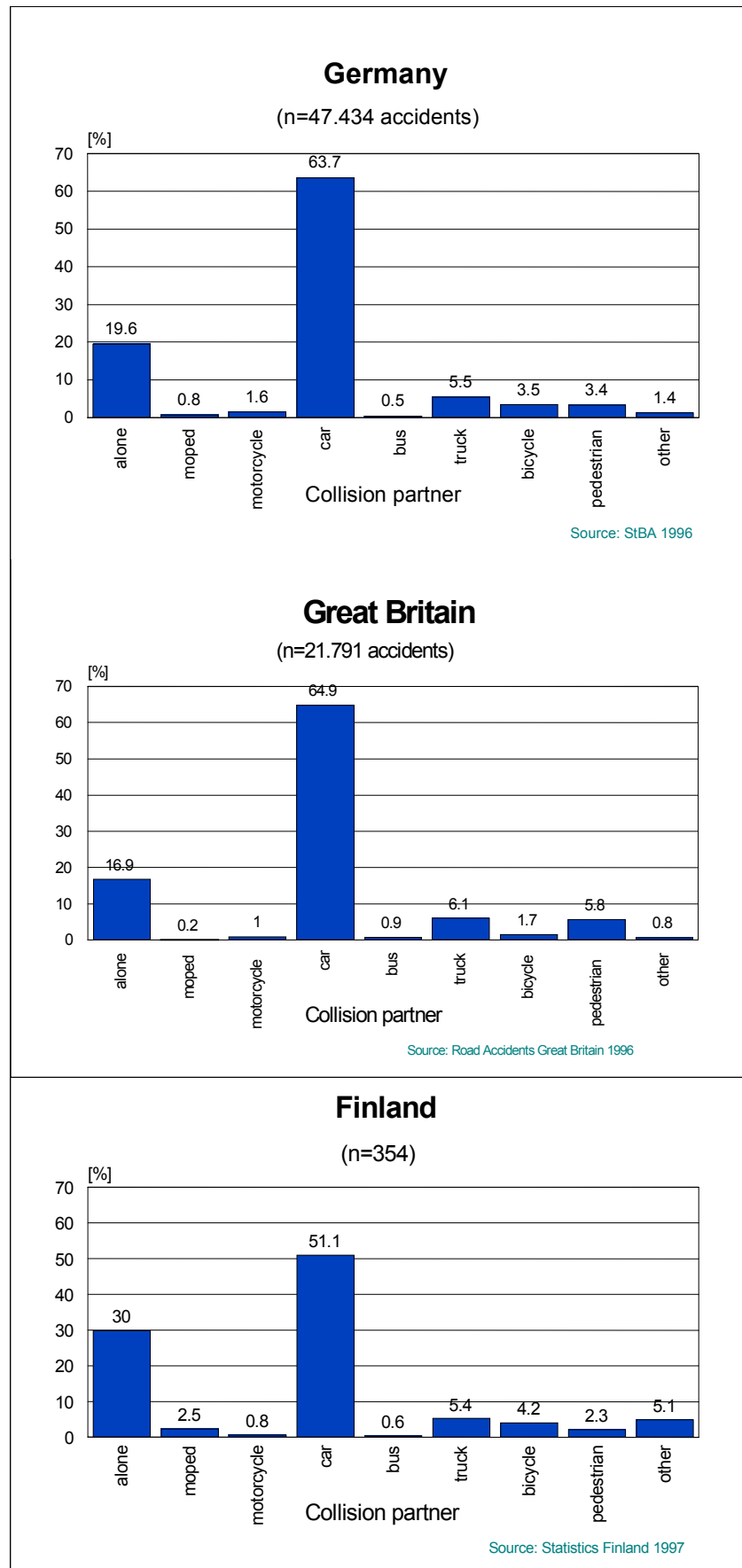
The COST accident data for each of the groups compared favourably with the corresponding national statistics for motorcycle accidents. Results of this comparison are given in Table 3.1, which shows that 53.9% are collisions with cars, compared with 63.7% for Germany, 64.9% for UK and 51.1% for Finland, figure 3.3. Nearly one fifth of the accidents belong to the "single vehicle" category where the collision is with the road or roadside furniture such as a tree or lamppost etc.

Collisions with a 'truck', HGV, were generally severe and appear to be more frequent, 9% in the COST Database compared with 5,5% for Germany, 6,1% for the UK and 5,4% for Finland for the national statistics.

Table 3.1 Accident severity related to the other vehicle.

Collision partner	Total		Severity of accident					
	n	%	slight		severe		fatal	
			n	%	n	%	n	%
alone (object, road, etc.)	66	26.9	19	35.2	15	27.8	32	27.6
truck	22	9.0	3	17.6	3	17.6	16	13.8
car	132	53.9	41	33.3	34	27.7	57	49.1
powered two-wheeler	2	0.8	-	-	1	50.0	1	0.9
bicycle	3	1.2	2	66.7	1	33.3	-	-
pedestrian	5	2.0	2	40.0	2	40.0	1	0.9
others	15	6.1	4	44.5	2	22.2	9	7.8
Total	245	100.0	71	29.0	58	23.7	116	47.3

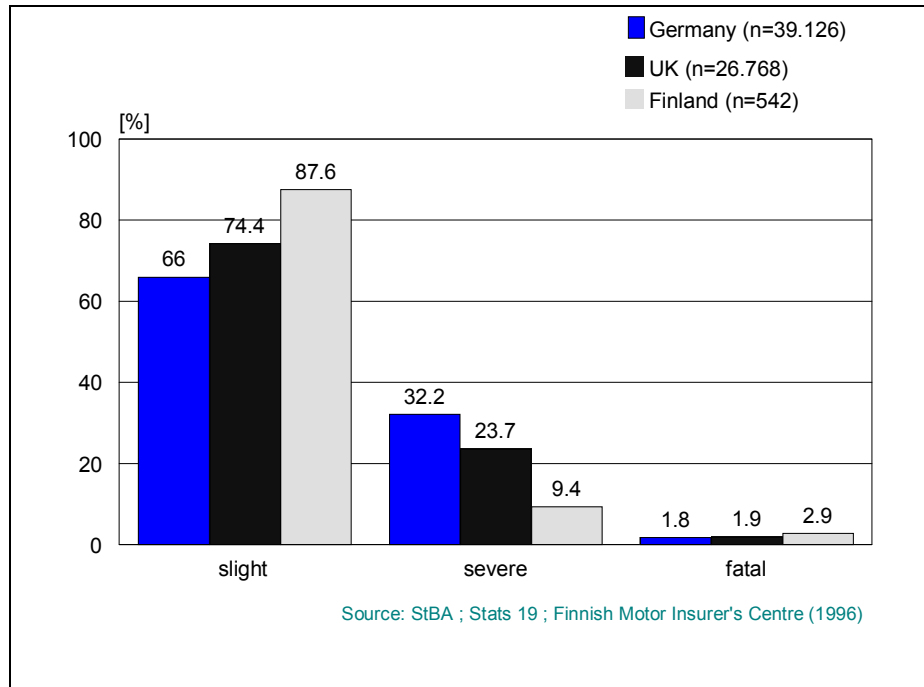
Source: COST database. (100%=all accidents;)



(100% all accidents with motorcycles)

Figure 3.3. Collision partners of motorcycles in different countries

Of more relevance in this study is the comparison of injury severity of documented cases in the different countries. In the COST study, 16% of those admitted to hospital sustained a head injury of AIS 2-4 and just fewer than 20% sustained a head injury. In the UK 74.4% of casualties were categorised as slight, compared with 66% in Germany and 87.6% in Finland, figure 3.4. Fatal motorcyclist casualties were between 1.8% to 2.9% and thus similar in all of the countries.



(100%= all injured persons in accidents with motorcycles)

Figure 3.4. Comparison of injury severity of accidents in different countries - total

3.6. RESULTS OF THE ANALYSIS OF THE COST ACCIDENT DATABASE

3.6.1. Effect of age

Accident and injury severity are known to be age related and the frequency distribution by age is given in figure 3.5. For all accidents, there are far more for young than for older riders with 60% of casualties in the 18 to 35 age group. However, it is surprising that the majority are in the 26 to 30 age group and that the 31 to 35 age group, 17%, is only slightly smaller than the 18 to 25 age group, 20%. This contrasts with previous studies for which the 18 to 25 group was by far the largest of all categories. The maximum in the overall distribution 22.6% in the age group 26 to 30 is not seen as maximum in the severe cases AIS 2+.

Trends within each area are similar to each other but there are some notable differences. In the under 18 age group, the proportion from Glasgow, 2%, was very small compared with 11% from Munich and 5% from Hannover. For the 18 to 25 group, Hannover and Glasgow were similar at 23% and 22% whereas for the 26 to 30 age group Hannover was 27% whereas Glasgow was 18%. In the 31 to 35 group Glasgow and Munich were similar, 24%, but Hannover was much less at 14%. Variations in other groups can be seen but some of the differences may be exaggerated because of the small number of cases in a particular age group.

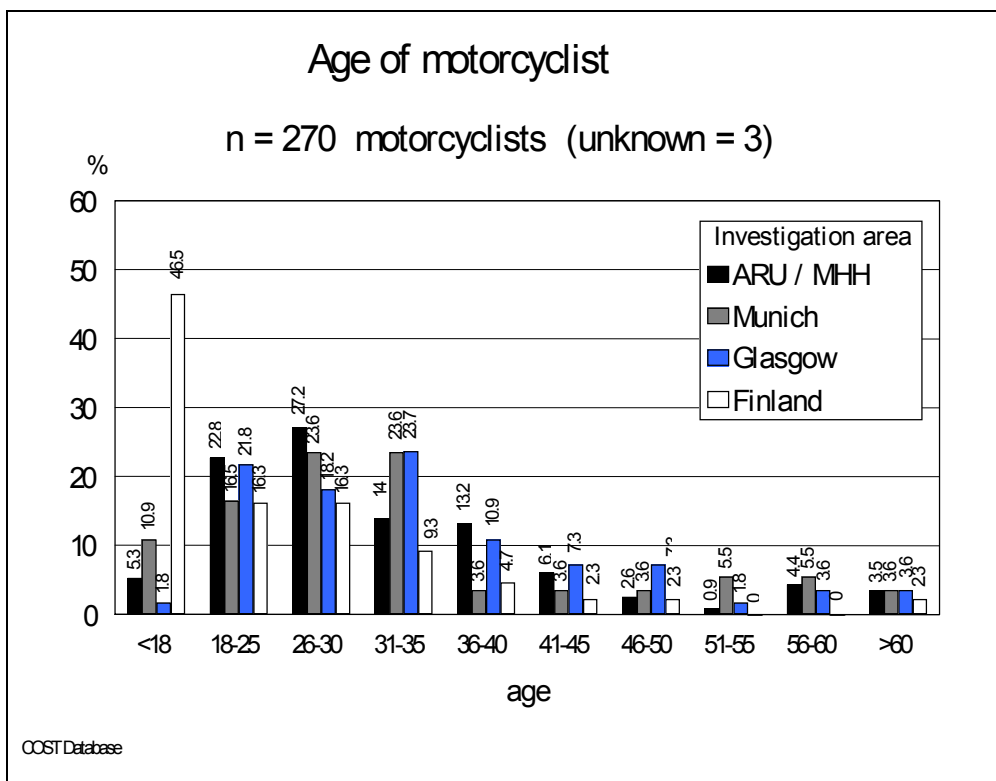
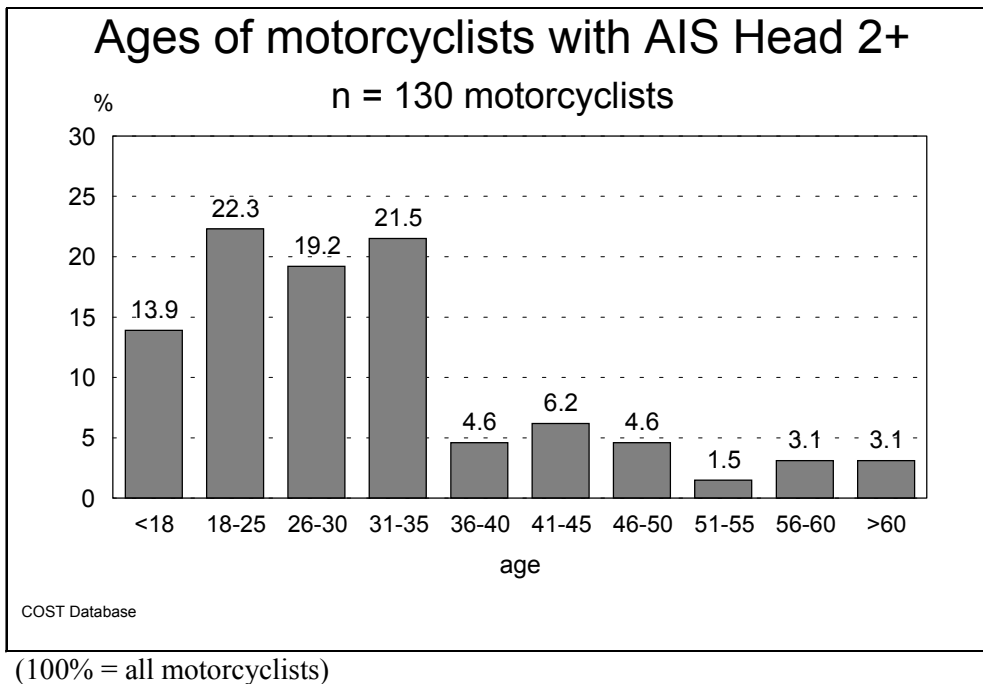


Figure 3.5. Source: COST database; Motorcycle casualties by age distribution

3.6.2. Helmet mass distribution and loss

Table 3.2 below shows helmets grouped by mass and it is interesting to note that the range of mass, 0.780 kg to 1.650 kg, is more than two to one. However, a large majority, 59%,

(unknown excluded) lay in a narrow band between 1 kg and 1.2 kg. Mass did not affect the injury outcome there was no evidence of a greater risk of injury when wearing an open faced helmet.

Table 3.2 Distribution of helmet mass of the motorcyclists (total registered)

Mass of helmets [g]	N	%	% (known)	portion AIS Head 2+ %
780g - 930g	4	1.6	4.4	50.0
1000g - 1200g	53	19.6	58.9	83.0
1240g - 1425g	17	6.5	18.9	17.6
1450g - 1650g	14	5.2	15.5	-
Unknown	181	66.8	-	40.9

Source: COST database; shadowed fields: all motorcyclists with AIS Head 2+ (n=123), portion 100% of each weight group

Table 3.3 Type of helmet

Type of helmet	N	% (known)	portion AIS Head 2+ %
helmet (not further specified):	12	4.9	58.3
full face helmet	209	85.3	45.9
open face helmet	24	9.8	37.5

Source: COST database; (unknown n=25, 1 motorcyclist without helmet); shadowed fields: all motorcyclists with AIS Head 2+ (n=112), portion 100% of each type

The vast majority, 85.3%, were full faced and this would partly explain the mass grouping noted above, although, type of helmet was recorded for all but three cases whereas mass was not.

Table 3.4 Loss of helmets

Loss of helmets:		(unknown n = 38)
no	n = 199	85.8%
yes (not further specified):	n = 7	3.0%
yes, before first impact	n = 3	1.3%
yes, after first impact	n = 19	8.2%
yes, after second impact	n = 4	1.7%

Source: COST database; (100% = all motorcyclists)

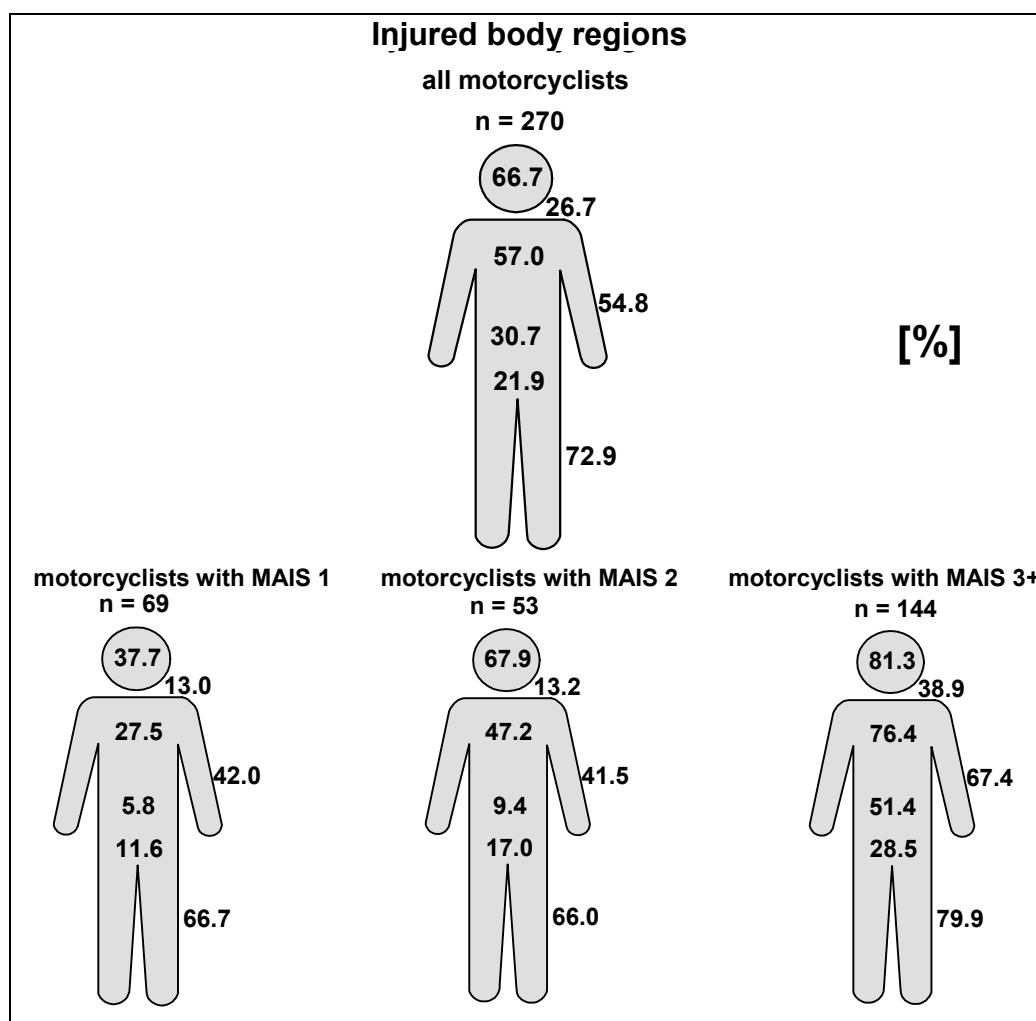
It is encouraging that the loss of a helmet prior to impact was low at 1.3 % by comparison with the 12.9 % loss during the impact sequence. Thus, there is a need for improvement of retention during an impact.

3.6.3. Injury distribution

It is important to note that the sample of cases for Munich was restricted to severe and fatal cases whereas the cases of Finland included fatal cases only. Hannover was randomly selected whereas Glasgow cases involved an injury or a head impact. COST 327 was based

upon a selection from each area that satisfied the criteria that a head impact, although not necessarily a head injury, had occurred. For the COST database, there were 66.7% with a head injury and 26.7% with a neck injury; figure 3.6 below illustrates this distribution. Also notable were the 57.0% with a thorax injury and 72.9% with leg injuries. It is not surprising that, when the injuries were classified, as the MAIS increased, so did the proportion with head injuries, from 38% for MAIS 1 to 81% for MAIS 3 and greater.

The overall pattern for the COST 327 database shows that risk of sustaining a head injury increases as MAIS increases, a similar pattern to that for the abdomen. The motorcyclists with severe head injury severity often have suffered additional injuries to thorax, arms and legs.



Source: COST database

Figure 3.6. Injured body regions of motorcyclists (100% = all motorcyclists)

3.6.4. Head injury severity and related factors

3.6.4.1 Helmet damage and head injuries

Table 3.5 gives the location and extent of the damage observed on the accident helmet. For ease of identification, the helmet is divided into 17 areas and each area has a unique two-digit number. The first digit indicates the side of the helmet, one for right and two for left as per normal body convention, and three for the crown; the second digit indicates vertical and horizontal position. Frontal, lateral, and rear are used to augment the numbers and further clarify the position.

Location of damage is distributed fairly evenly with 26.9% lateral right, 26.3% lateral left, 23.6% frontal and 21.0% to the rear, slightly fewer than the other regions. Other locations of importance, and frequently damaged, were the chin guard, 15.4% (sections 18 and 28), and the right upper temporal fossa region, 9.6% (sections 13 and 14) and left, 8.8%, (sections 23 and 24), 18.4% total. The lower temporal fossa (sections 15, 16, 25 and 26) was the next most frequently impacted region, 15.1% total for both sides. The crown, section 35, received with only 2.2% of the impacts.

Not surprisingly, laceration (sliding mark) was the most frequent type of damage followed by deformation and then cracks; frequency of occurrence for each type of damage was largely consistent with the overall frequency as discussed above. However, the area most likely to be cracked was the chin guard and the area in the region of the visor attachment. This may indicate that the impacts to these areas were severe or that these parts of the helmets are weaker than other areas. It is likely that the visor area is slightly weaker and that the impacts to the chin guard are particularly severe. Helmet standards should include tests that reflect these findings, particularly in relation to the chin guard and the temporal fossa region, which is known to be particularly vulnerable to skull injury.

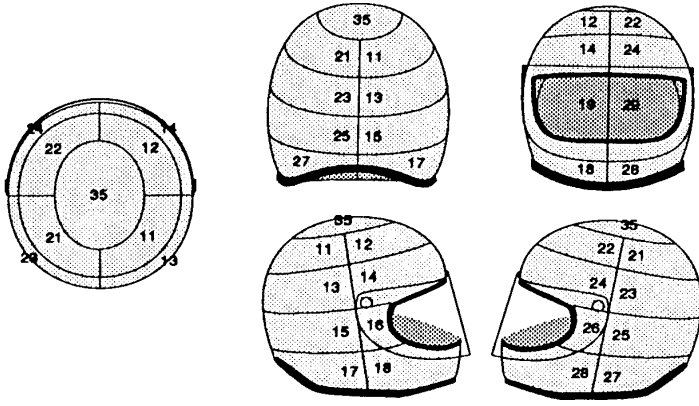
Whether or not injuries occur at the location of impact is often debated particularly in relation to brain injuries, hence the suggestion, although disputed by some researchers, that “coup” and “contra coup” injuries occur. Table 3.5 indicates the location of damage on the helmet. There is some notable correlation between the damage and head injury region but also some possible exceptions. Both are important in understanding how head injuries occur, how helmet design may affect injuries and, in turn, how the design may be changed to improve protection.

It is clear that injuries to the side of the head (lateral injuries) and injuries to the rear correlate exactly with the damage location. However, injuries to the face, upper and lower, occur not only with frontal impacts as may be expected, but also with lateral impacts. The reason for this is not clear but it is possible that loads to the side of the helmet are transmitted to the face. Damage to the upper part of the helmet seems to be evenly distributed around the helmet and probably correlates with the injury location.

3.6.4.2 Helmet target shape and head injury

Table 3.6 below gives the distribution of accidents by injury and shape of object struck.

A round object was the most frequently struck, 79%, and the severity of injury was fairly evenly distributed. An edge object, for example a kerbstone, was the least likely to be struck, 4%, but the most likely to cause a severe, AIS 5, injury. A flat object was struck in 9% of cases but was the least likely to cause an injury.

Table 3.5 Location of the external damage to the helmet


Location on helmet	Total		Type of damage							
			deformation		laceration		crack		other	
	n	%	N	%	n	%	n	%	n	%
Crown Section 35	17	2.2	3	17.6	12	70.6	2	11.8	-	-
Lateral right Sections 11 to 19	212	26.9	39	18.4	151	71.2	20	9.4	2	0.9
Lateral left Sections 21 to 29	207	26.3	44	21.3	123	59.4	40	19.3	0	0.0
Frontal Even sections 12 to 28 (excluding 20) plus 19 and 39	186	23.6	28	15.1	115	61.8	41	22.0	2	1.1
Rear Odd sections from 11 to 27 (excluding 17 and 19) plus 16	166	21.0	24	14.5	129	77.7	11	6.6	2	1.2
Total	788	100	138	17.5	530	67.3	114	14.5	6	0.8

Source: COST database; (100%= all damages of each sector)

**Table 3.6 Head injury severity related to impact target shape.
(100%=all head injuries)**

	shape of impact objects									
	total		round		edge		flat		no information	
AIS Head	n	%	n	%	n	%	n	%	n	%
uninjured	80	32.0	61	30.5	2	20.0	9	39.1	8	47.1
AIS 1	47	18.8	37	18.5	1	10.0	6	26.1	3	17.6
AIS 2	27	10.8	25	12.5	-	-	1	4.3	1	5.9
AIS 3	20	8.0	13	6.5	1	10.0	2	8.7	4	23.5
AIS 4	18	7.2	14	7.0	2	20.0	2	8.7	-	-
AIS 5	30	12.0	25	12.5	4	40.0	1	4.3	-	-
AIS 6	28	11.2	25	12.5	-	-	2	8.7	1	5.9
Total	250	100	200	100	10	100	23	100	17	100

3.6.4.3 Head injury type, and severity, and impact speed

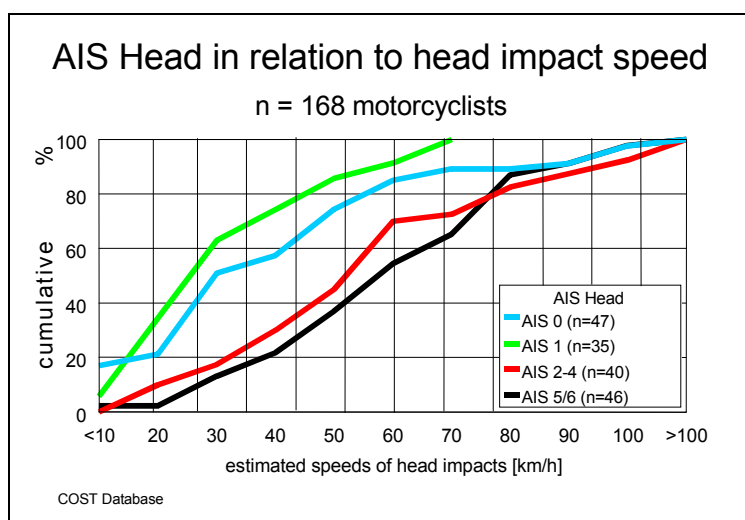
Within the COST 327 database, 180 of the motorcyclists sustained a head injury and 87 suffered no head injury at all (excluding the unknown). Thirty-three percent of the riders and passengers suffered an impact to the helmet/head but were protected by the helmet and did not sustain a head injury. Of those suffering a head injury, 28.9% sustained only a minor (AIS 1) and 16.7% a moderate (AIS 2) head injury; 15.6% of the motorcyclists sustained a head injury of AIS 6 and almost the same proportion (16.7%) sustained a critical head injury (AIS 5); 11.1% suffered AIS 3 and the same proportion suffered AIS 4 head injuries.

Of particular interest was the relationship between head impact speed and head injury (figure 3.7). Not surprisingly (Table 3.7) the majority of low speed impacts were associated with minor head injury (< 10 km/h and AIS 0 = 72.7%) and the higher the impact speed, the more likely it became that the head injury was critical or fatal. For example, between 61 and 70 km/h, 36.4% were AIS 6 and between 71 and 80 km/h, 57.1% were AIS 5. Even very high speed head impacts were not always associated with severe head injury. This is evident from Table 3.7 where, in five cases, an impact with the road surface occurred at a speed exceeding 80 km/h without head injury. In addition, two cases with impact speeds exceeding 100 km/h resulted in head injury of only AIS 3.

Table 3.7 AIS Head in relation to head impact speed

AIS Head	Total		AIS 0		AIS 1		AIS 2		AIS 3		AIS 4		AIS 5		AIS 6	
	n	%	n	%	n	%	n	%	n	%	n	%	n	%	n	%
< 10	11	6.6	8	72.7	2	18.2	-	-	-	-	-	-	1	9.1	-	-
11 - 20	16	9.5	2	12.5	10	62.5	3	18.8	-	-	1	6.2	-	-	-	-
21 - 30	32	19.0	14	43.7	10	31.3	3	9.4	-	-	-	-	2	6.2	3	9.4
31 - 40	16	9.5	3	18.8	4	25.0	3	18.8	-	-	2	12.4	3	18.8	1	6.2
41 - 50	25	14.9	8	32.0	4	16.0	5	20.0	1	4.0	-	-	2	8.0	5	20.0
51 - 60	25	14.9	5	20.0	2	8.0	5	20.0	-	-	5	20.0	3	12.0	5	20.0
61 - 70	11	6.5	2	18.2	3	27.3	1	9.1	-	-	-	-	1	9.1	4	36.4
71 - 80	14	8.3	-	-	-	-	1	7.1	1	7.1	2	14.3	8	57.2	2	14.3
81 - 90	5	3.0	1	20.0	-	-	-	-	-	-	2	40.0	1	20.0	1	20.0
91 - 100	8	4.8	3	37.5	-	-	-	-	1	12.5	1	12.5	1	12.5	2	25.0
> 100	5	3.0	1	20.0	-	-	-	-	2	40.0	1	20.0	-	-	1	20.0
Total	168	100	47	28.0	35	20.8	21	12.5	5	3.0	14	8.3	22	13.1	24	14.3

Source: COST database (100%= all motorcyclists of each speed range, 74 unknown AIS-Head or unknown head impact speed)



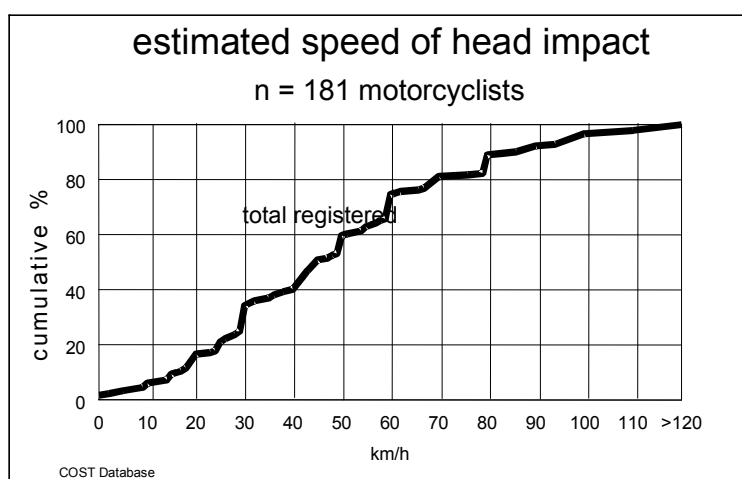
Source: COST database;

Figure 3.7. AIS Head in relation to head impact speed

Nevertheless, there was a trend for the head injury severity to increase as the head impact speed increased as shown in figure 3.7.

Figure 3.8 illustrates the cumulative frequency of estimated head impact speed for all 181 cases where the speed was known. The 50% cumulative frequency occurs at approximately 44 km/h, which appears surprisingly high when compared with the typical 20 km/h impact speed for drop tests in helmet Standards at which life threatening head accelerations are measured. Therefore, the test speed should be raised to that of the 50% cumulative frequency. However, such exceptions as shown in Table 3.7 may explain the high median of the head impact speed.

The cumulative frequency of the estimated head impact speed was determined for different regions of the head. figure 3.9 shows the analysis for the forehead, face, and side and top of the head. It is evident that impacts to the side and the top of the head occurred at higher speeds (50%, median = 59 km/h) compared with those to the face and forehead (50%, median = 49 km/h).



Source: COST database

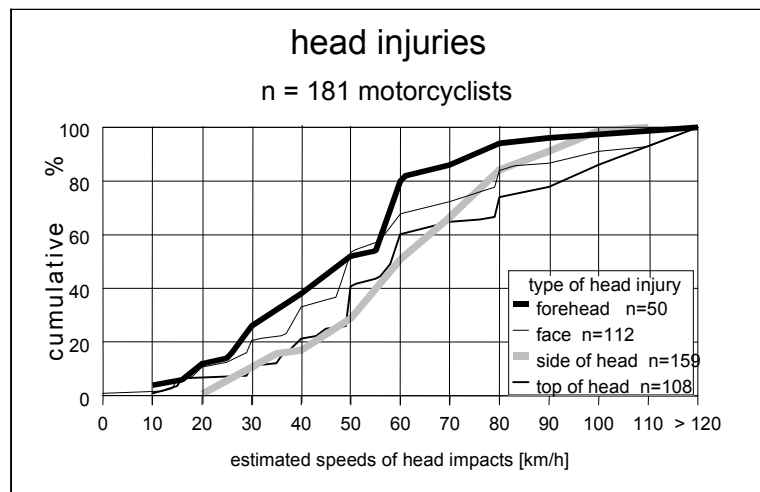
Figure 3.8. Estimated speed of head impact

Further analysis of the data illustrated in figure 3.7 showed that an increase in injury severity of AIS 2-4 to AIS 5-6 was the consequence of an increase in the median speed, 50-57 km/h equivalent to an increase in energy of some 30%. Thus, if helmets could be made to absorb 24% more energy then it is postulated that some 20% of the AIS 5-6 casualties would sustain

injuries of only AIS 2-4. This is based upon the energy difference of AIS 2-4 and AIS 5-6 at 20% cumulative speed (AIS 2-4 24km/h, AIS 5-6 34km/h). The energy at 50% cumulative speed at AIS 2-4 (50 km/h) was used as the reference to determine the percent.

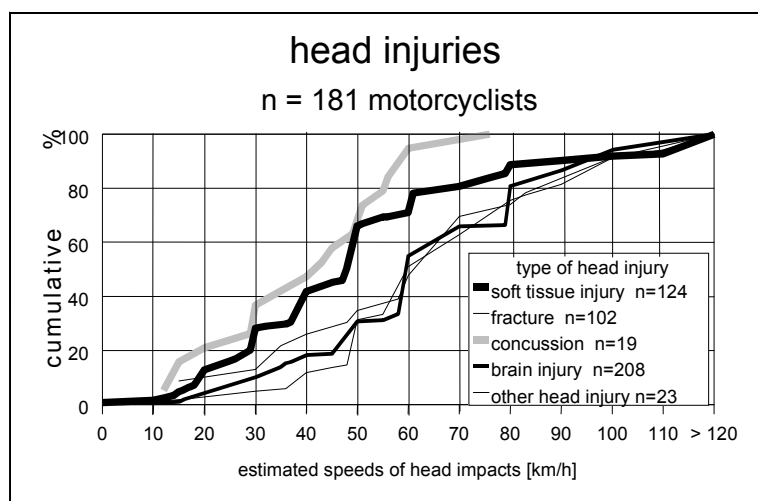
This result is somewhat surprising when the biomechanical injury tolerance of different head regions is considered. For example, the frontal bone is much stronger than the temporal bone and therefore, it may have been expected that the median impact speed would have been greater for the forehead than the side of the head. However, for this particular relationship the helmet protection may have been the decisive factor whereby less protection is provided in the facial region.

In accordance with biomechanical principles, figure 3.10 illustrates that low severity soft tissue injury and moderate concussion occurred at a head impact speed of 45 - 50 km/h (50% median). This is significantly lower than that for fractures and other more severe head injuries for which the 50%, median, was 60 km/h as is also illustrated in figure 3.10. This demonstrates that helmets can protect against skull fracture and severe brain injuries.



Source: COST database;

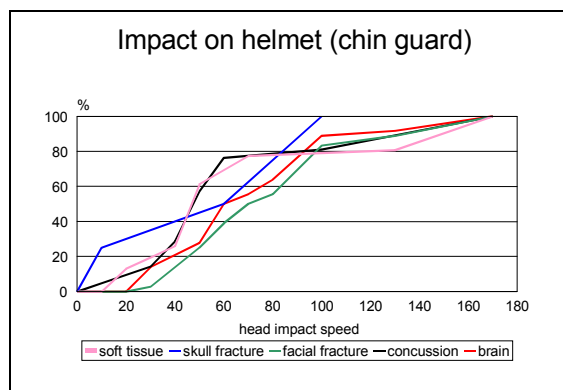
Figure 3.9. Estimated speed of head impact for each head region (100%= each head region), n=86 unknown



Source: COST database

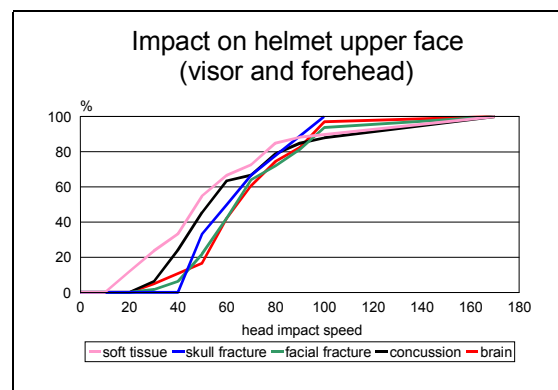
Figure 3.10. Estimated speed of head impact for each type of head injury, (100% all motorcyclists of each type) n=86 unknown

Figure 3.11 to figure 3.15 show the relationship between impact speed and four types of injury, soft tissue, skull fracture, facial fracture, concussion and brain injury, for five different locations of impact on the helmet. Of particular interest is the median speed at which brain injury occurs, which may be assumed to be indicative of the sensitivity of the brain to a given impact severity at different locations. For the face and upper head the median speed is approximately 60 km/h whereas for the head lateral and head rear, the median speed is approximately 50 km/h. This indicates that the rear and lateral regions are similarly susceptible to injury. It was also noticed that the median speed for concussion was always lower than that for brain injury, which is entirely consistent with what may be expected.



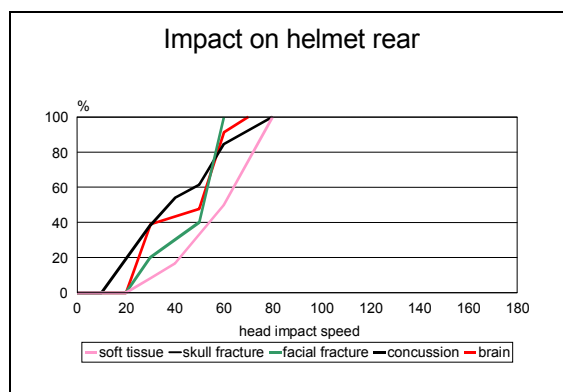
Source: COST database

Figure 3.11. Cumulative speed of head impact for each type of head injury, impact on lower face of helmet (100%=all motorcyclists of each type)



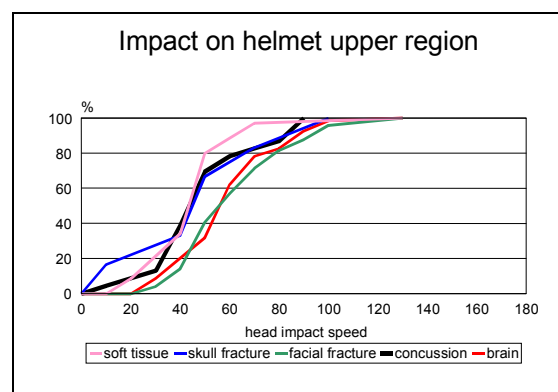
Source: COST database

Figure 3.12. Cumulative speed of head impact for each type of head injury, impact on upper face area of helmet, (100%=all motorcyclists of each type)



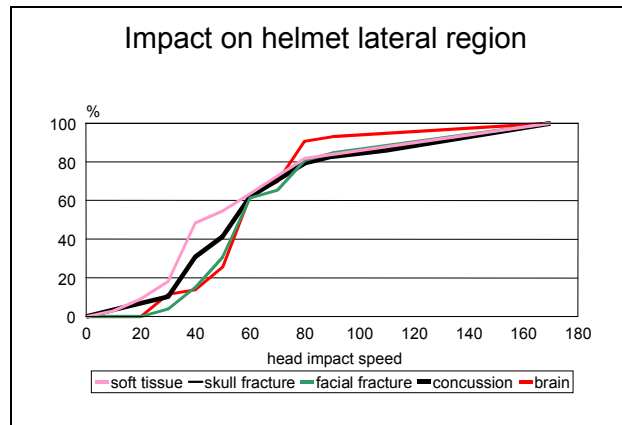
Source: COST database

Figure 3.13. Cumulative speed of head impact for each type of head injury, impact on rear head area of helmet. (100%=all motorcyclists of each type)



Source: COST database

Figure 3.14. Cumulative speed of head impact for each type of head injury, impact on upper head area of helmet. (100%=all motorcyclists of each type)



Source: COST database;

Figure 3.15. Cumulative speed of head impact for each type of head injury, impact on lateral head area of helmet, (100%=all motorcyclists of each type)

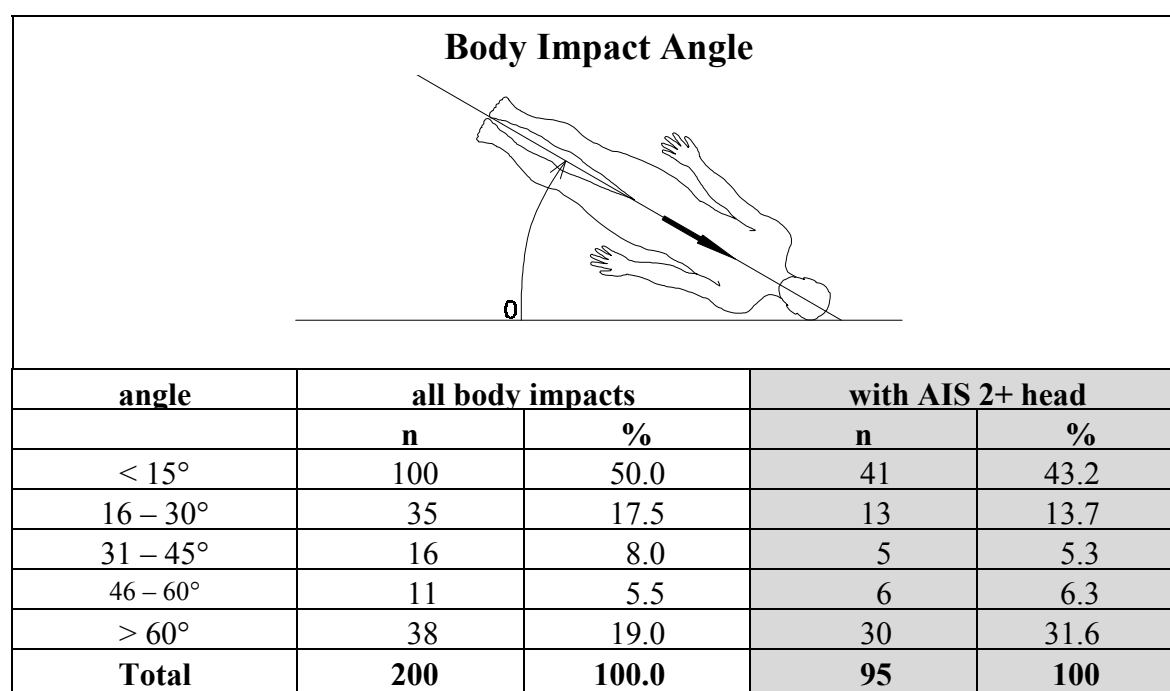
3.6.4.4 Head injury type and head impact angle

Determining the impact angle of the body and the head was an important part of the reconstruction of the accident. The body impact angle was determined for every head impact and it was found that 43% of AIS 2+ injured motorcyclists impacted with a shallow body angle of less than 15 degree, nearly parallel to the opponent, such as road surface (figure 3.16). A further 17.5% (13.7% of AIS 2+) collided at an angle of the body of between 16 and 30 degrees and 32.5% (43.2% AIS 2+) impacted with a body impact angle above 30 degrees. It is seen that oblique impact angle has a much higher incidence of severe injuries.

However, the body angle is not necessarily indicative of the head impact angle and this was analysed separately according to the convention given below in Table 3.8. The head impact angle needed to be known relative to three dimensions to establish the location and direction of the impact to the head. This enabled the impact to be identified as direct and likely to induce largely linear acceleration or oblique and likely to induce a substantial rotational component.

The analysis showed that 25.6% were at 0° and thus perpendicular to a line vertically through the body. 22.6 % were between 6° and 30° to this vertical and toward the top of the head whereas 10% were in this range, toward the base of the skull. However, Table 3.8 gives the analysis in the horizontal plane. This shows that most of the recorded head impacts (64.8%) were at an impact angle XY between minus 45° and plus 45° and led to a dorsal flexion of the cervical spine and rapid rotational motion. Only 12.1% occurred at the rear of the helmet within the range of 180° ± 30°. About 23.1% were side impacts.

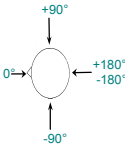
An oblique impact from the top often leads to a compression of the cervical spine when the head is in an upright position in relation to the body. Otherwise the impact results in dorsal, ventral or lateral flexion of the neck and the cervical spine in combination with a compression. 25.6% of all head impacts were frontal impacts with 0 degree, 9.1% were rear impacts with ±180 degrees.



Source: COST database; Shadowed fields: Body impact angle for head injuries with AIS Head 2+; n=36 body impact angle unknown

Figure 3.16. Body impact angles for head injuries in degrees [°]
(100% = 200 angles - all head injuries); n=70 body impact angle unknown

Table 3.8 Head impact angles XY in degrees [°]

Head Impact Angle XY											
α											
Head Impact Angle XY	0	1 - 45	46 - 90	91 - 135	136 - 179	±180	(-179) - (-136)	(-135) - (-91)	(-90) - (-46)	(-45) - (-1)	total
N	51	45	20	3	4	18	2	8	15	33	199
%	25.6	22.6	10.1	1.5	2.0	9.1	1.0	4.0	7.5	16.6	100

Source: COST database;
(100% = all head injuries); n=68 unknown

3.6.5. Collision configuration

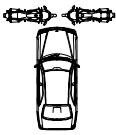
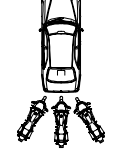
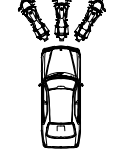
When differentiated according to collision types, Table 3.9, it is evident that 41.5% were type 7, a single vehicle accident. However, in this study there were no collisions with pedestrians or pedal cyclists. Type 4, an oblique collision of the two-wheeler with the side of a car, was the most frequent collision configuration, 28.5%. It is interesting to note that type 3, a frontal collision of a two-wheeler against the car side is over-represented in the COST database with 14.6% compared with only 5.3% for the national rate. It is also notable that serious injuries were more frequent in the COST study than is typical given that, in general, 75% of two wheeler riders are only slightly injured. In particular, for collision type 2, 58.3% were

seriously or fatally injured with MAIS 5/6 and 57.3% suffered very serious or fatal head injuries, AIS 5/6.

Too few cases in some collision types prevented statistical analysis. This arose, partly, because it was possible to determine the collision angle in only 140 of the 253 cases.

The frequency and seriousness of the injuries to different body regions were also analysed. Head injuries were particularly prevalent in type 2 where 92% of riders sustained an injury of AIS2 or greater. However, in types 3 and 4 although only 50% were seriously injured, 67% sustained serious head injuries. In oblique collisions against the motorcycle, injuries to other parts of the body, thorax, abdomen and pelvis were frequent as shown in Table 3.9. In particular, the legs were frequently injured, 75% in type 3 and 80% in type 4. In addition, 25% of these leg injuries were serious, AIS 2-4. Only 25% of two-wheeler casualties did not sustain a leg injury.

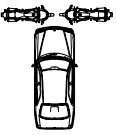
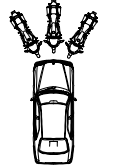
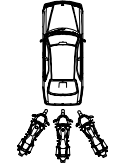
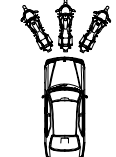
Table 3.9 Collision types in relation to the maximum injury severity

Collision types		Total n=140	Maximum Injury Severity of motorcyclists			
			Uninjured	MAIS 1	MAIS 2-4	MAIS 5/6
		100%	----- 100% -----			
type 1		1.5%	-	50.0%	50.0%	-
			100.0%	-	-	-
type 2		9.2%	-	8.3%	33.3%	58.3%
			16.7%	8.3%	16.7%	58.3%
type 3		14.6%	5.3%	42.1%	31.6%	21.1%
			52.6%	10.5%	21.1%	15.8%
type 4		28.5%	-	51.4%	29.7%	18.9%
			51.4%	18.9%	24.3%	5.4%
type 5		4.6%	-	50.0%	50.0%	-
			50.0%	50.0%	-	-
type 6		-	-	-	-	-
type 7		41.5%	1.9%	25.9%	29.6%	42.6%
			20.4%	24.1%	31.5%	24.1%

Source: COST database;

Shaded fields: Collision types in relation to the maximum head injury severity. n=271 total of which 131 were unknown.

Table 3.10 Collision types in relation to injured body regions

Collision types		Injured Body Region of motorcyclist						
total	n = 140	Head	Neck	Thorax	Arms	Abdomen	Pelvis	Legs
type 1 	uninjured	100%	100%	50.0%	50.0%	100%	100%	50.0%
	AIS 1	-	-	-	50.0%	-	-	50.0%
	AIS 2-4	-	-	50.0%	-	-	-	-
	AIS 5/6	-	-	-	-	-	-	-
type 2 	uninjured	14.3%	71.4%	21.4%	21.4%	42.9%	57.1%	28.6%
	AIS 1	14.3%	-	7.1%	28.6%	14.3%	14.3%	28.6%
	AIS 2-4	14.3%	-	42.9%	50.0%	28.6%	28.6%	42.9%
	AIS 5/6	57.1%	28.6%	28.6%	-	14.3%	-	-
type 3 	uninjured	55.0%	85.0%	60.0%	55.0%	85.0%	85.0%	25.0%
	AIS 1	10.0%	5.0%	15.0%	25.0%	-	10.0%	50.0%
	AIS 2-4	20.0%	10.0%	15.0%	20.0%	15.0%	5.0%	25.0%
	AIS 5/6	15.0%	-	10.0%	-	-	-	-
type 4 	uninjured	52.5%	77.5%	60.0%	27.5%	80.0%	77.5%	20.0%
	AIS 1	17.5%	12.5%	12.5%	47.5%	7.5%	15.0%	50.0%
	AIS 2-4	25.0%	7.5%	12.5%	25.0%	12.5%	7.5%	30.0%
	AIS 5/6	5.0%	2.5%	15.0%	-	-	-	-
type 5 	uninjured	50.0%	66.7%	66.7%	66.7%	83.3%	83.3%	50.0%
	AIS 1	50.0%	33.3%	16.7%	33.3%	16.7%	-	16.7%
	AIS 2-4	-	-	16.7%	-	-	16.7%	33.3%
	AIS 5/6	-	-	-	-	-	-	-
type 6 	uninjured	-	-	-	-	-	-	-
	AIS 1	-	-	-	-	-	-	-
	AIS 2-4	-	-	-	-	-	-	-
	AIS 5/6	-	-	-	-	-	-	-
type 7 	uninjured	24.1%	79.3%	54.2%	45.8%	70.2%	84.5%	25.4%
	AIS 1	22.4%	6.9%	15.3%	32.2%	5.3%	6.9%	40.7%
	AIS 2-4	31.0%	3.4%	11.9%	20.3%	15.8%	6.9%	33.9%
	AIS 5/6	22.4%	10.3%	18.6%	1.7%	8.8%	1.7%	-

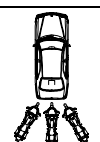
Source: COST database; (100% = all motorcyclists without unknown; for n=2 motorcyclists the injured body region was unknown)

Objects that the head struck were recorded in detail and given in Table 3.11. It was possible to analyse 270 head injuries from 140 motorcyclists in relation to the defined collision types; 26.5% of the head injuries occurred as a result of impacting the road. An impact of the head on the road was particularly frequent when the two wheeler struck the car side, collision types 3 / 4, but infrequent in collisions with the car front, types 1, 2 and 6, where 67% of the head injuries were caused by the vehicle structure.

Although 60% of all injuries were from the first impact, which was with the opposing vehicle, approximately 64% of the subsequent collisions were with the road. Only 2.3% of all motorcyclists have more than two collisions.

Table 3.11 Collision types in relation to injury causing parts

A number of n=208 head injuries could not be assigned to these 7 collision types; total number of head injuries n=560

Collision types		Total	Injury causing parts of all head impacts													
			own vehicle							opposite vehicle					unknown	
			own action	rolled over	road surface	field, meadow	post, kerbstone, tree, fence	guard-rail	front of vehicle, windscreen	pillar	roof frontal	side of vehicle	rear end	own vehicle	own helmet	unknown
	Total	N=260	4	9	69	2	59	27	52	4	4	8	5	2	12	3
	%	100%	1.5	3.5	26.5	0.8	22.7	10.4	20.0	1.5	1.5	3.1	1.9	0.8	4.6	1.2
			-----100%-----													
type 1			-	-	-	-	-	-	-	-	-	-	-	-	-	-
type 2		20.8	-	13.0	7.4	-	-	-	70.4	7.4	1.9	-	-	-	-	-
type 3		9.6	-	-	36.0	-	-	-	12.0	-	12.0	32.0	4.0	-	4.0	-
type 4		19.6	-	3.9	52.9	3.9	3.9	-	21.6	-	-	-	3.9	-	7.9	2.0
type 5		1.2	-	-	66.7	-	-	-	-	-	-	-	33.3	-	-	-
type 6		-	-	-	-	-	-	-	-	-	-	-	-	-	-	-
type 7		48.8	3.2	-	21.3	-	44.8	21.3	-	-	-	-	0.8	1.6	5.5	1.6

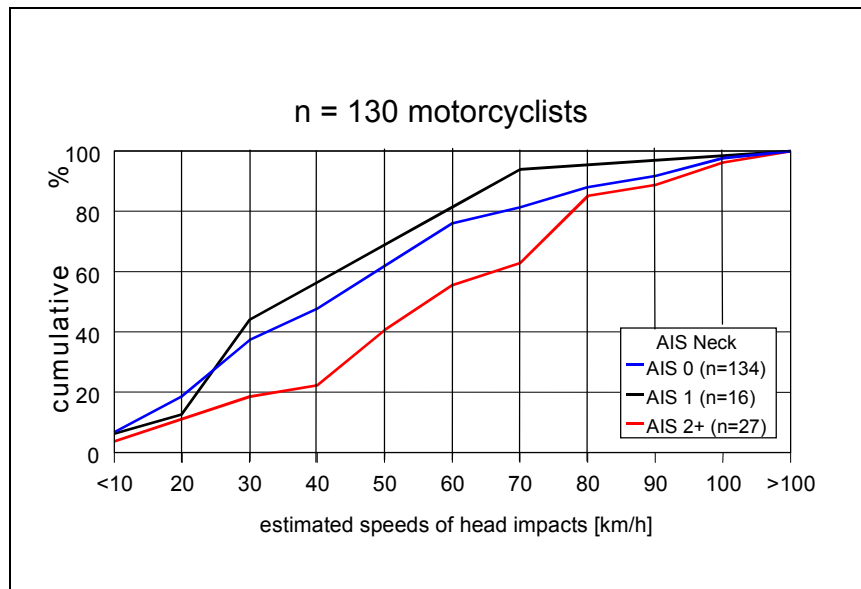
Source: COST database; Collision types in relation to injury causing parts (100% = all injuries of the head without unknown collision types; n=208)

3.6.6. Neck injury

Figure 3.17 presents the distribution of neck injury severity related to head impact speed. Excluding the 83 cases with unknown head impact speed the relative frequency of neck injury is still consistent with the overall distribution of neck injury severity, for which the vast majority of the riders and pillions sustained no neck injury, 74.8% or only a minor neck

injury, AIS 1, 10.1%. There is no evidence that high head impact speed is necessarily associated with severe neck injury.

Eighty per cent of all neck injuries of AIS 1, so called whiplash, occurred at a speed up to 60 km/h, while 80% of all severe neck injuries of AIS 2 and greater occurred above 45 km/h, see figure 3.17.



Source: COST database; (100%=all motorcyclists of each speed range, 1 unknown AIS-Neck and 83 unknown Speed head impact)

Figure 3.17. AIS Neck in relation head impact speed

Except in two cases where the neck injury was AIS 6 and the head was AIS 0, not injured, Table 3.12 shows that severe neck injuries, AIS 4 and greater, occurred only in combination with severe head injuries, AIS 4 and greater. When the head injury did not exceed AIS 3 in the vast majority, 82% of cases, the neck was not injured, AIS 0, and in only 5% of cases a neck injury AIS 2 or AIS 3 occurred; neck injuries greater than AIS 3 did not occur with head injuries of up to and including AIS 3.

In cases with fatal head injury, 25% of the motorcyclists also sustained a fatal neck injury and a further 14% sustained a critical neck injury, AIS 5. However, for half of the fatalities, the neck injury was minor, AIS 1, or the neck was not injured, AIS 0.

Critical head injury, AIS 5, was associated with 24.1% AIS 5 neck injury and 6.9% AIS 6 fatal neck injury. Twenty-five percent of those with a fatal, AIS 6, head injury sustained a fatal, AIS 6, neck injury. However, 56% of the casualties with an AIS 5 or AIS 6 head injury and 60% with an AIS 4 head injury did not sustain a neck injury. AIS 2 and AIS 3 neck injuries were very infrequent with AIS 5 and AIS 6 head injuries.

Table 3.12 AIS Head in relation to AIS Neck (100%=all motorcyclists)

	AIS Head															
	Total		AIS 0		AIS 1		AIS 2		AIS 3		AIS 4		AIS 5		AIS 6	
	n	%	n	%	n	%	n	%	n	%	n	%	n	%	n	%
AIS Neck																
AIS 0	199	74.8	75	86.2	45	86.5	26	86.7	9	45.0	12	60.0	18	62.1	14	50.0
AIS 1	27	10.2	9	10.3	5	9.6	3	10.0	6	30.0	2	10.0	1	3.4	1	3.6
AIS 2	9	3.4	1	1.1	1	1.9	1	3.3	3	15.0	2	10.0	-	-	1	3.6
AIS 3	5	1.9	-	-	1	1.9	-	-	2	10.0	1	5.0	-	-	1	3.6
AIS 4	1	0.4	-	-	-	-	-	-	-	-	-	-	1	3.4	-	-
AIS 5	13	4.9	-	-	-	-	-	-	-	-	2	10.0	7	24.1	4	14.3
AIS 6	12	4.5	2	2.3	-	-	-	-	-	-	1	5.0	2	6.9	7	25.0
Total	266	100	87	100	52	100	30	100	20	100	20	100	29	100	28	100

Source: COST database; 1 unknown AIS Neck, 3 unknown AIS Head)

Table 3.13 gives the location of the injury for a single fracture of the cervical spine and Table 3.14 gives the location when two fractures occurred.

Table 3.13 Cervical spine fractures.

Location of injury	n	%
C1	6	18.8
C2	5	15.15
C3	3	9.09
C4	5	15.15
C5	2	6.06
C6	2	6.06
C7	3	8.3
dens	1	3.03
n.f.s	6	18.8
Total	36	100

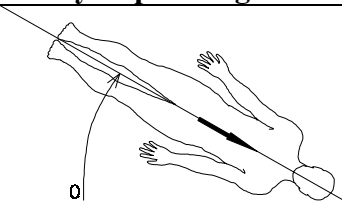
Table 3.14 Multiple cervical spine fractures.

Location of injury major combined fractures	n	%
C1 + C2	4	33.3
C3 + C4	3	25.0
C4 + C5	1	8.3
C6 + C7	2	16.7
C1 + C7	1	8.3
C2 + C5	1	8.3
Total	12	100

The distribution of body impact angle was determined for 97 neck injuries, see Table 3.15. The neck injury types are classified as follows: cervical spine strain, so called Distortion, AIS 1, cervical fractures AIS 2 and greater, soft tissue injury, and other injury, for example, ligament and spinal cord rupture; 51.5% of the neck injuries were fractures to the vertebrae, 23.7% were soft tissue injuries, 8.2% cervical strain injury and 16.5% other neck injuries

The impact conditions were critical for the occurrence of a fracture of the cervical spine. In particular, if a relatively large angle occurred between the body longitudinal axis and the impact object then neck injury was highly likely, Table 3.14. Thus, 33% of all cervical fractures occurred at impact angles between body and object of over 60°. However, injuries to soft parts and also the cervical spine strains occurred at angles of up to 30°. Skull fractures were particularly frequent when the head, obviously in horizontal plane, impacted primarily in the area of the middle face or back of the head, when hyperflexion or hyperextension of bending movements were induced.

Table 3.15 Body impact angle in relation to neck injury location

Body impact angle										
										
	total		location of neck injuries							
			cervical spine strain		cervical spine fracture		soft tissue injury		other	
Body impact angle [°]	n	%	n	%	n	%	n	%	n	%
< 15	39	40.2	4	50.0	21	42.0	4	17.4	10	62.5
16 - 30	12	12.4	3	37.5	-	-	9	39.1	-	-
31 - 45	5	5.2	-	-	3	6.0	1	4.3	1	6.2
46 - 60	9	9.3	-	-	4	8.0	5	21.7	-	-
> 60	32	33.0	1	12.5	22	44.0	4	17.4	5	31.3
			<-----100%----->							
total	97	100	8	8.2	50	51.5	23	23.7	16	16.5

Source: COST database; (100%=each neck injury location; 33 unknown body impact angle)

3.7. HEAD AND NECK INJURY MECHANISMS

A special additional COST 327 study “Data Gathering Analysis Study on Motorcycle Safety Helmets” (September 1999), was commissioned to determine the detailed injury mechanisms for head and neck injuries. This study was needed because it was not possible simply to interrogate the COST 327 database for this analysis because the data was recorded as coded values for discrete variables. Therefore, it would not have been possible, for example, to determine information such as body trajectory during the impact, the direction of the impact force to the head and the head impact speed related to the mechanisms that caused the skull and brain injuries.

This task needed very detailed accident reconstruction with a multi-disciplinary assessment to relate medical information with the physical parameters describing the linear and rotational motion of the head and the type and direction of the forces. It was decided that the study should be confined to cases where the head injury was AIS 2 and greater because much more detail was available in these cases. The database contained n=128 cases of motorcyclists with head injuries AIS 2 and greater but of these only n=81 cases were sufficiently comprehensive for a detailed analysis as indicated in Table 3.16.

Table 3.16 Head injury severity

	COST database			
	total number		cases for special study	
AIS Head	n	%	n	%
uninjured	87	32.6	-	-
AIS 1	52	19.5	-	-
AIS 2	30	11.2	8	9.9
AIS 3	20	7.5	14	17.3
AIS 4	20	7.5	11	13.6
AIS 5	30	11.2	23	28.4
AIS 6	28	10.5	25	30.8
Total	267	100.0	81	100.0

Head injury severity grades of COST database and gathering study
(n=3 AIS unknown in COST database)

A mechanism was determined for each injury even when a casualty sustained multiple injuries and for the 81 cases 409 injuries were analysed. The forces were divided into direct, indirect or contracoup and the results are given in Table 3.17.

The study has shown that 57.5% of the forces transmitted to the head were indirect 31.3% were direct and 11.3% were considered to be contracoup, Table 3.17.

Table 3.17 Force related to injury location

	Absolute Frequency	Relative Frequency
Impact force direct	128	31.3 %
Impact force indirect	235	57.5 %
Contre Coup	46	11.3 %
Total	409	100.0 %

Most of the contusions, laceration wounds, comminuted fractures and teeth defects were correlated to direct impact force transmission, Table 3.18. The complicated middle face fracture, Le Fort III, also occurred from a direct force. A so-called "concussion" which is defined as unconsciousness was always caused by an indirect impact force. Brain ruptures

or vascular separation and subarachnoid bleeding, brain oedema, were caused mostly by an indirect force.

Table 3.18 Type of injury and force.

	Total	Impact force direct	Impact force indirect	Contre Coup
Type of injury		<-----100%----->		
Total	n = 409	31.3%	57.5%	11.2%
Injury NFS	0.5%	50.0%	50.0%	-
soft tissue				
Contusion	2.9%	91.7%	8.3%	-
Haematoma	1.7%	71.4%	28.6%	-
Abrasion	13.4%	87.3%	12.7%	-
Laceration	0.5%	50.0%	50.0%	-
skull				
Luxation	0.2%	-	100.0%	-
Fracture	22.5%	50.0%	50.0%	-
Ring fracture	0.5%	50.0%	50.0%	-
Comminuted fracture	0.2%	100.0%	-	-
Teeth defect	0.2%	100.0%	-	-
brain				
Concussion	0.5%	-	100.0%	-
Contusion	10.3%	7.1%	66.7%	26.2%
Haematoma (subdural)	12.0%	2.0%	69.4%	28.6%
Haematoma (epidural)	2.2%	11.1%	66.7%	22.2%
Brain oedema	2.4%	10.0%	90.0%	-
Subarachnoid bleeding	15.9%	1.5%	78.5%	20.0%
Intracerebr. bleeding	4.6%	15.8%	73.7%	10.5%
Ventricle bleeding	0.7%	-	100.0%	-
Rupture	8.1%	6.1%	81.8%	12.1%
Vascular separation	0.2%	-	100.0%	-
Anisocoria	0.2%	100.0%	-	-

Table 3.18 presents the location of injury related to the type of force. This table indicates that most of the injuries to the middle face structure are correlated with a direct impact force whereas most of the brain injuries and even some skull fractures in the upper region of the head were caused by an indirect force.

Table 3.19 Location of injury and consequences of transmission

Location of injury	Total	Impact force direct	Impact force indirect	Contre Coup
	<-----100%----->			
Total	n = 409	31.3%	57.5%	11.2%
head injury NFS	2.4%	80.0%	20.0%	-
scalp	2.2%	88.9%	11.1%	-
vault	5.1%	85.7%	14.3%	-
bony occiput	0.7%	66.7%	33.3%	-
base of skull	11.2%	8.7%	91.3%	-
forehead	1.0%	100.0%	-	-
orbit	1.0%	100.0%	-	-
face NFS	4.6%	100.0%	-	-
frontal sinus	0.5%	100.0%	-	-
middle part of face	1.2%	100.0%	-	-
eye	1.2%	60.0%	40.0%	-
eyelid	1.2%	100.0%	-	-
ear	0.5%	100.0%	-	-
ear drum	0.2%	-	100.0%	-
nose	1.7%	100.0%	-	-
nasal bone	1.2%	100.0%	-	-
lower part of face	0.2%	100.0%	-	-
cheek	0.2%	100.0%	-	-
upper jaw	0.7%	100.0%	-	-
lower jaw	2.0%	87.5%	12.5%	-
teeth	0.2%	100.0%	-	-
lip	1.0%	100.0%	-	-
chin	1.2%	80.0%	20.0%	-
Brain NFS	42.5%	5.2%	72.4%	22.4%
cerebrum	2.7%	9.1%	81.8%	9.1%
cerebellum	3.9%	-	81.2%	18.8%
Tentorium cerebelli	0.5%	-	100.0%	-
brain stem	6.8%	3.6%	85.7%	10.7%
ventricle	0.7%	-	100.0%	-
brain basilar artery	0.2%	-	100.0%	-
Neck cervical vertebra	0.7%	-	100.0%	-

(NFS = not further specified)

The location of each of the 409 injuries was related to the type of force that caused the injury and the results are given in Table 3.19. The direct impacts were distributed evenly over the entire head, with the greatest numbers of fractures, 4.4%, located at the vault. One hundred and seventy six, 75%, of the indirect impacts were located at the brain and brain stem and 42, 18%, were fractures of the base of the skull. The contre coup injuries were located only at the brain or brain stem.

Skin and soft tissue injuries, with only few exceptions, were caused by direct impact. Fractures of the vault were caused mainly in direct impacts, 86%, with a few, 14.3%,

caused by indirect impacts. Conversely, 91% of fractures of the base of the skull, 82% of the cerebrum lesions and 81% of the cerebellum lesions were caused by indirect impacts. Contracoup impacts were responsible for 9% of cerebral lesions and 19% of cerebella lesions.

Thirty-four percent of the injuries were located on the right side of head, 30% on the left side and 21% were to the front; occipital injuries were infrequent.

Risk of injury with increasing speed of head impact did not differ greatly with the three types of force as is shown figure 3.18. In only four cases was the impact speed less than 30 km/h and, therefore, statistically, each of the curves begins at above 30km/h.

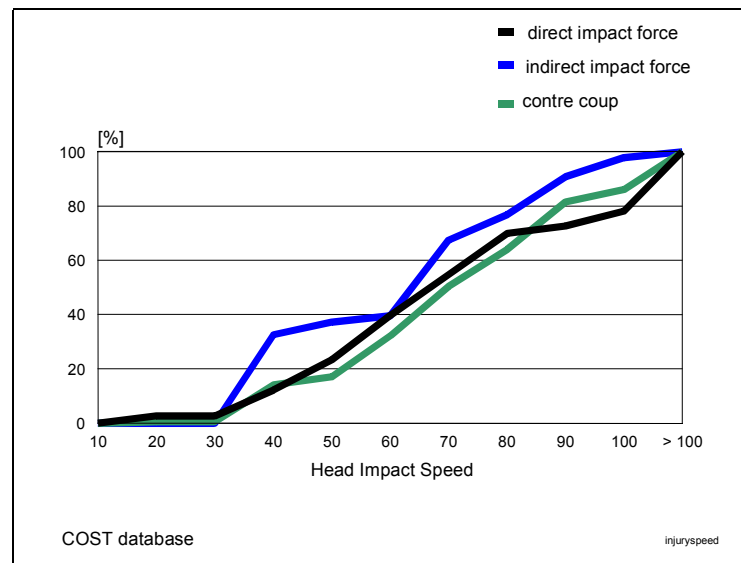


Figure 3.18. Consequences of force transmission related to head impact speed

Figure 3.19 demonstrates brain injury risk for the cerebrum in relation to head impact speed and figure 3.20 shows similar curves for other parts of the brain, cerebellum, brain stem, cerebral ventricle and blood vessels. It can be seen that injuries to these other parts often tend to occur at high speeds.

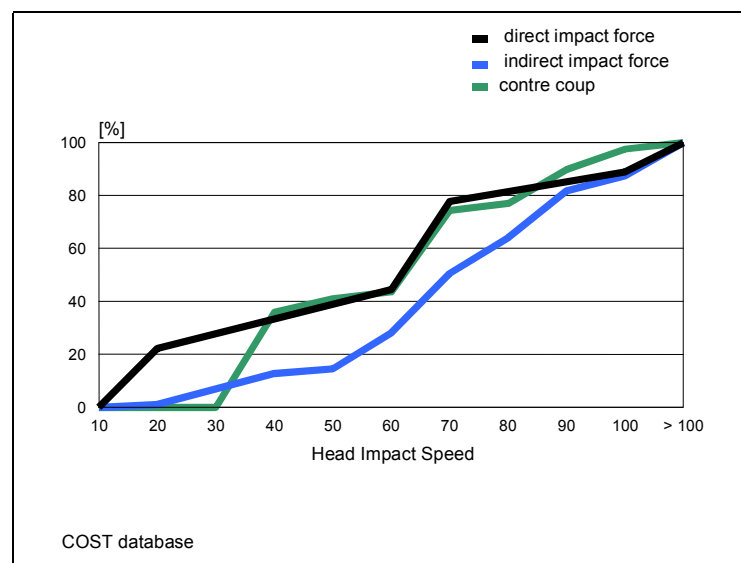


Figure 3.19. Brain injury risk for injuries of cerebrum

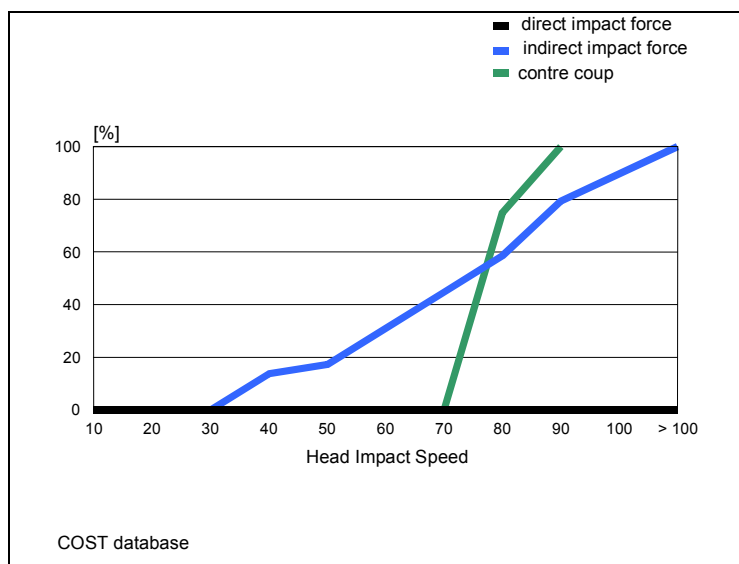


Figure 3.20. Brain injury risk for injuries without cerebrum

The mechanisms were analysed for the tendency to occur in translation and rotation about the x, y and z-axes. It can be seen from figure 3.21 and table 3.20 that 30% of the injuries AIS 2 and greater were caused by translation, 23% by rotation in the y axis and 27% resulted from a combination of linear and rotational motion.

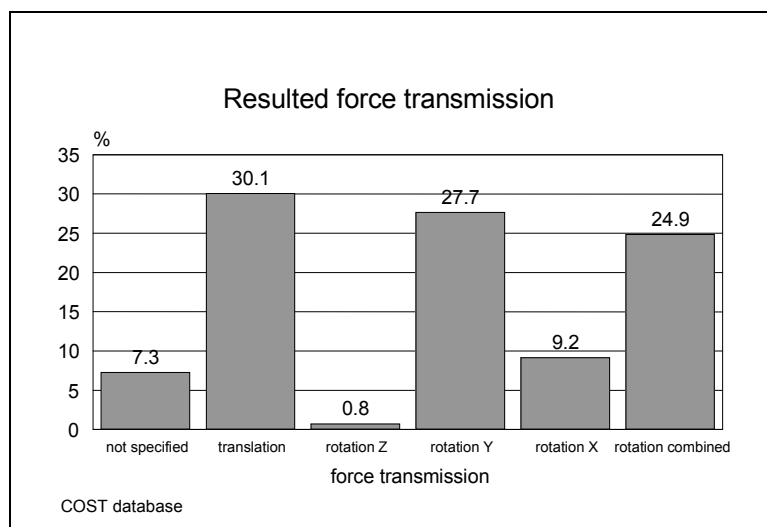


Figure 3.21. Resulted force transmission

Neck injury - cervical spine fracture, was examined in relation to three force mechanisms: direct transmission, compression and inertial loading without impact. Table 3.21 gives the results for single fractures and Table 3.22 for multiple fractures and in both sets, by far the dominant mechanism was direct impact. This is further evidence that the helmet does not increase the risk of injury to the neck.

Table 3.20 Results of force transmission related to head injury type

Location of injury	total	not specified	trans- lation	rotation around			combined
				Z Axis	Y Axis	X Axis	
		<-----100%----->					
Total	n = 409	7.3%	30.1%	0.8%	27.7%	9.2%	24.9%
head injury NFS	2.4%	33.3%	33.3%	-	11.1%	-	22.2%
scalp	2.4%	-	22.2%	11.1%	33.3%	-	33.3%
vault	5.5%	14.3%	42.9%	-	14.3%	9.5%	19.0%
bony occiput	0.8%	-	33.3%	-	33.3%	-	33.3%
base of skull	11.8%	8.9%	33.3%	-	24.4%	11.1%	22.2%
forehead	1.0%	-	50.0%	-	25.0%	-	25.0%
orbit	1.0%	-	-	-	50.0%	-	50.0%
face NFS	3.7%	14.3%	35.7%	-	28.6%	-	21.4%
middle part of face	1.0%	-	-	-	100.0%	-	-
frontal sinus	0.5%	-	100.0%	-	-	-	-
eye	1.0%	-	50.0%	-	25.0%	-	25.0%
eyelid	1.3%	-	20.0%	-	20.0%	-	60.0%
ear	0.3%	-	-	-	-	-	100.0%
nose	1.8%	-	57.1%	-	14.3%	-	28.6%
nasal bone	1.3%	-	20.0%	-	60.0%	-	20.0%
lower part of face	0.3%	-	-	-	100.0%	-	-
cheek	0.3%	-	100.0%	-	-	-	-
upper jaw	0.8%	-	-	-	66.7%	-	33.3%
lower jaw	2.1%	-	-	-	50.0%	-	50.0%
teeth	0.3%	-	-	-	-	-	100.0%
lip	0.5%	-	50.0%	-	50.0%	-	-
chin	1.3%	-	40.0%	-	-	-	60.0%
brain NFS	43.5%	7.8%	1.3%	1.2%	23.5%	12.7%	23.5%
cerebrum	2.6%	10.0%	30.0%	-	20.0%	-	40.0%
cerebellum	3.4%	-	30.8%	-	46.2%	7.7%	15.4%
tentorium cerebelli	0.5%	-	-	-	-	-	100.0%
brain stem	6.8%	3.8%	11.5%	-	53.8%	15.4%	15.4%
ventricle	0.8%	33.3%	66.7%	-	-	-	-
brain basilar artery	0.3%	-	-	-	-	100.0%	-
neck cervical vertebra	0.8%	-	-	-	33.3%	33.3%	33.3%

(NFS = not further specified)

Table 3.21 Cervical spine fracture related to force mechanism.

Location of injury	Mechanisms of force			
	No.	Direct force transmission	Compression	Isol. inertial load
C1	6	4	1	1
C2	5	4	-	1
C3	3	1	-	2
C4	5	3	-	2
C5	2	2	-	-
C6	2	2	-	-
C7	3	2	1	-
dens	1	1	-	-
n.f.s	6	5	1	-
Total	33	24 (72.7%)	3 (9.1%)	6 (18.2%)

Table 3.22 Multiple cervical spine fractures related to force mechanism.

Location of Injury major combined fractures	Mechanisms of force			
	No.	Direct force transmission	Compression	Isol. inertial load
C1 + C2	4	3	-	1
C3 + C4	3	1	-	2
C4 + C5	1	1	-	-
C6 + C7	2	2	-	-
C1 + C7	1	-	1	-
C2 + C5	1	1	-	-
Total	12	8 (67%)	1 (8%)	3 (25%)

3.8. EFFECT OF CLIMATIC CONDITIONS ON ACCIDENT RISK

3.8.1. Introduction

This section is a description of the effect of climatic conditions on accident risk and is included as part of the extension to COST 327. The data used for analysis were collected by the research groups at the University of Hannover, the Central Organisation for Traffic Safety in Finland, and Glasgow Southern General Hospital.

The data used was a sub-set of the COST 327 database and was collated on a form devised specifically for the purpose of examining the data to study the possible adverse effect of climatic conditions on the potential for increasing the risk of a motorcycle accident. It should be noted that the most appropriate method would have been to study the direct

consequences of unfavourable physiological conditions such as sweating from excess body temperature and extreme cold. However, because this was a retrospective study such data was not available. Thus, the study was based upon an analysis of accidents and the prevailing weather conditions. One hundred and forty six (146) cases, 111 from Hannover and 35 from Finland were analysed.

3.8.2. Analysis

The climatic conditions obtained in relation to the occurrence of the accidents was as follows:

- temperature
- humidity
- air pressure
- wind speed

For the Hannover cases, the monthly reports of the German Meteorological Service at Langenhagen airport was used. For the Finnish cases, only temperature could be collected for Helsinki and the Lapland area.

It is difficult to analyse the influence of climatic conditions retrospectively because although weather conditions are an indication of potential problems for the rider it is not possible to be certain that adverse conditions were a principal cause. The following diagram is an attempt to identify the link between poor physiological conditions, human factors and the consequences.

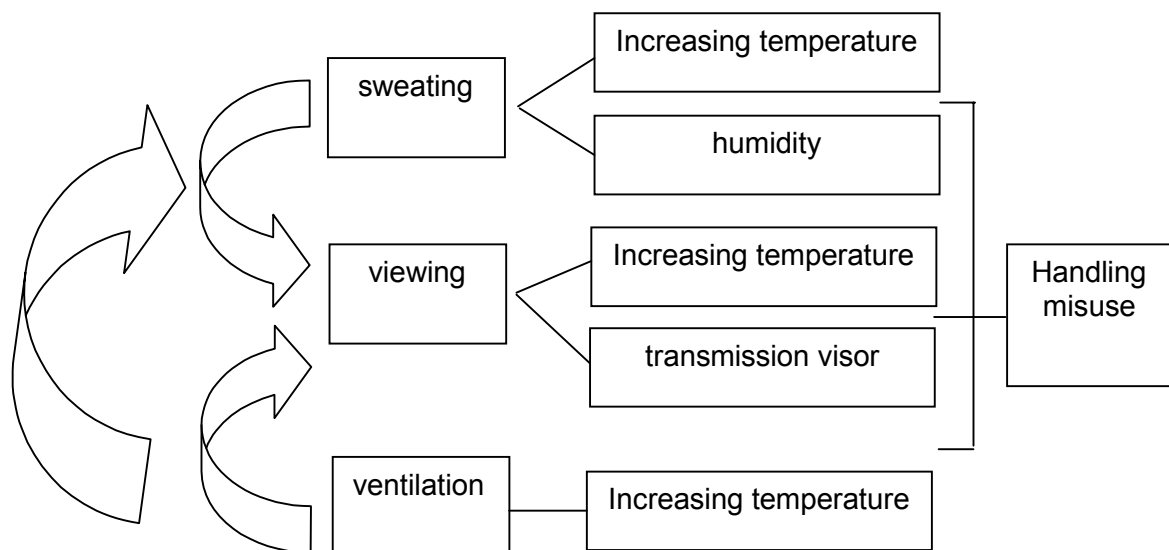


Figure 3.22. Identification of links between human factors

This study has investigated the effect of climatic conditions on the likely conditions within the helmet and on road conditions and, in turn, on the accident risk. Loss of control, in particular, was studied.

Table 3.23 Head injury severity

	COST 327 database					
	Total number COST database		Basis of gathering study		Climate study<	
AIS Head	n	%	n	%	n	%
Uninjured	87	32.6	-	-	64	40.8
AIS 1	52	19.5	-	-	37	23.6
AIS 2	30	11.2	8	9.9	22	14.0
AIS 3	20	7.5	14	17.3	7	4.5
AIS 4	20	7.5	11	13.6	11	7.0
AIS 5	30	11.2	23	28.4	10	6.4
AIS 6	28	10.5	25	30.8	6	3.8
Total	267	100.0	81	100.0	157	100.0

3.8.3. Comparison of climate conditions in the different countries

For the countries within the study, the distribution of the mean monthly temperature is shown in figure 3.24. For Finland, sub-zero temperatures occur from December until March for the Helsinki area and from November until April for the Lapland area. The highest mean temperature for the summer period in Finland is less than 20°C compared with 20°C for Hannover. Figure 3.24 below shows the average temperatures in the years 1996 to 1999.

3.8.4. Climate conditions in accidents

The weather conditions in most of the accidents was good because, in general, motorcyclists do not travel in very bad weather conditions such as when there is snow and ice on the road. Wind speed and air pressure were studied but found to have little influence on the accidents and the analysis has been excluded from this section.

The distribution of temperature for all of the cases from Germany (Hannover) and Finland that were analysed is shown in figure 3.23. The overall mean value was 16°C for the accident cases whereas the mean annual value for Hannover was 9.4 °C, for Helsinki 5.7 °C and for Lapland -0.75 °C. This illustrates that the accidents tended not to occur in very cold weather.

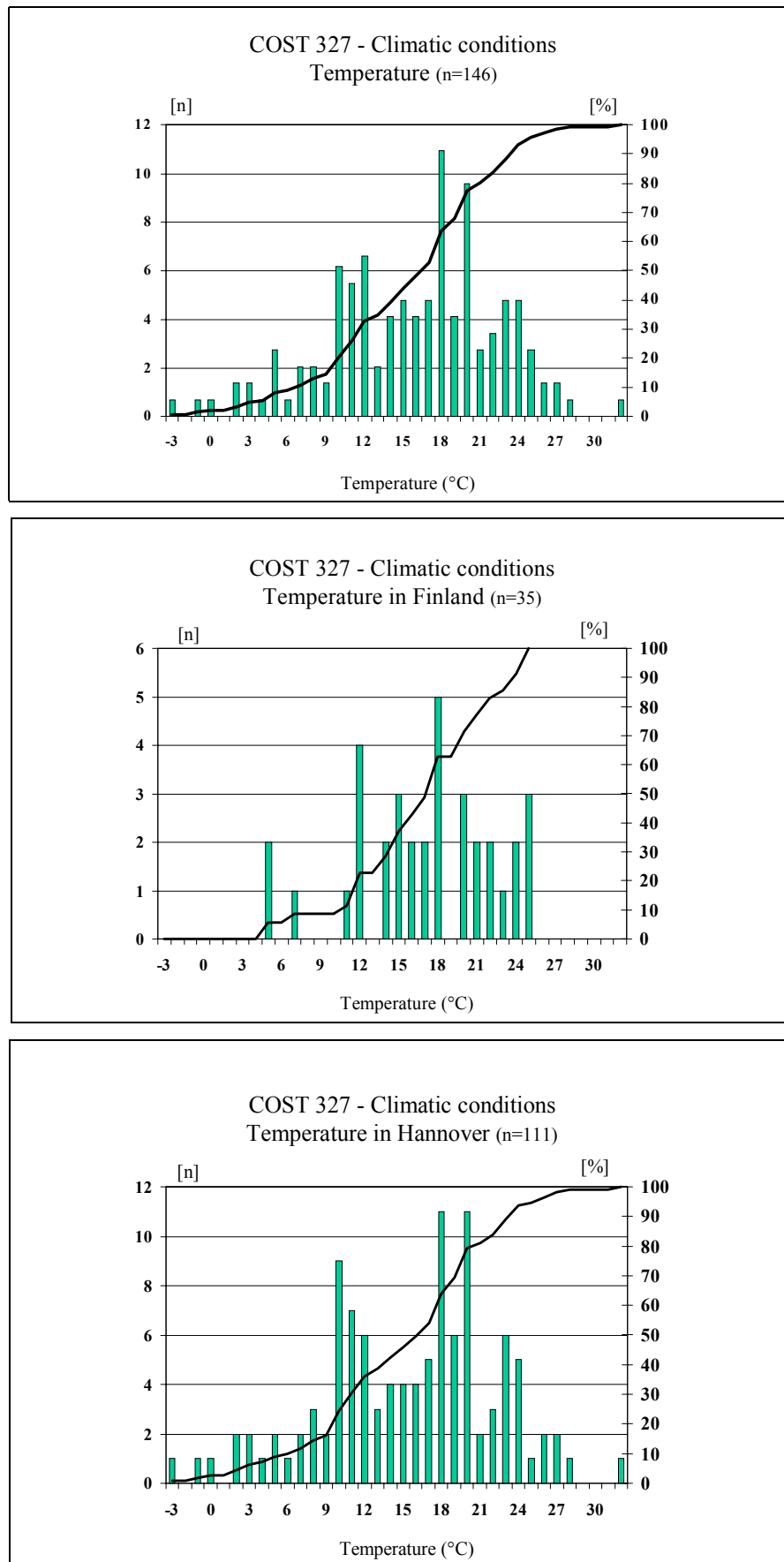


Figure 3.23. Distribution of temperature of COST cases (100% all accidents with motorcycles)

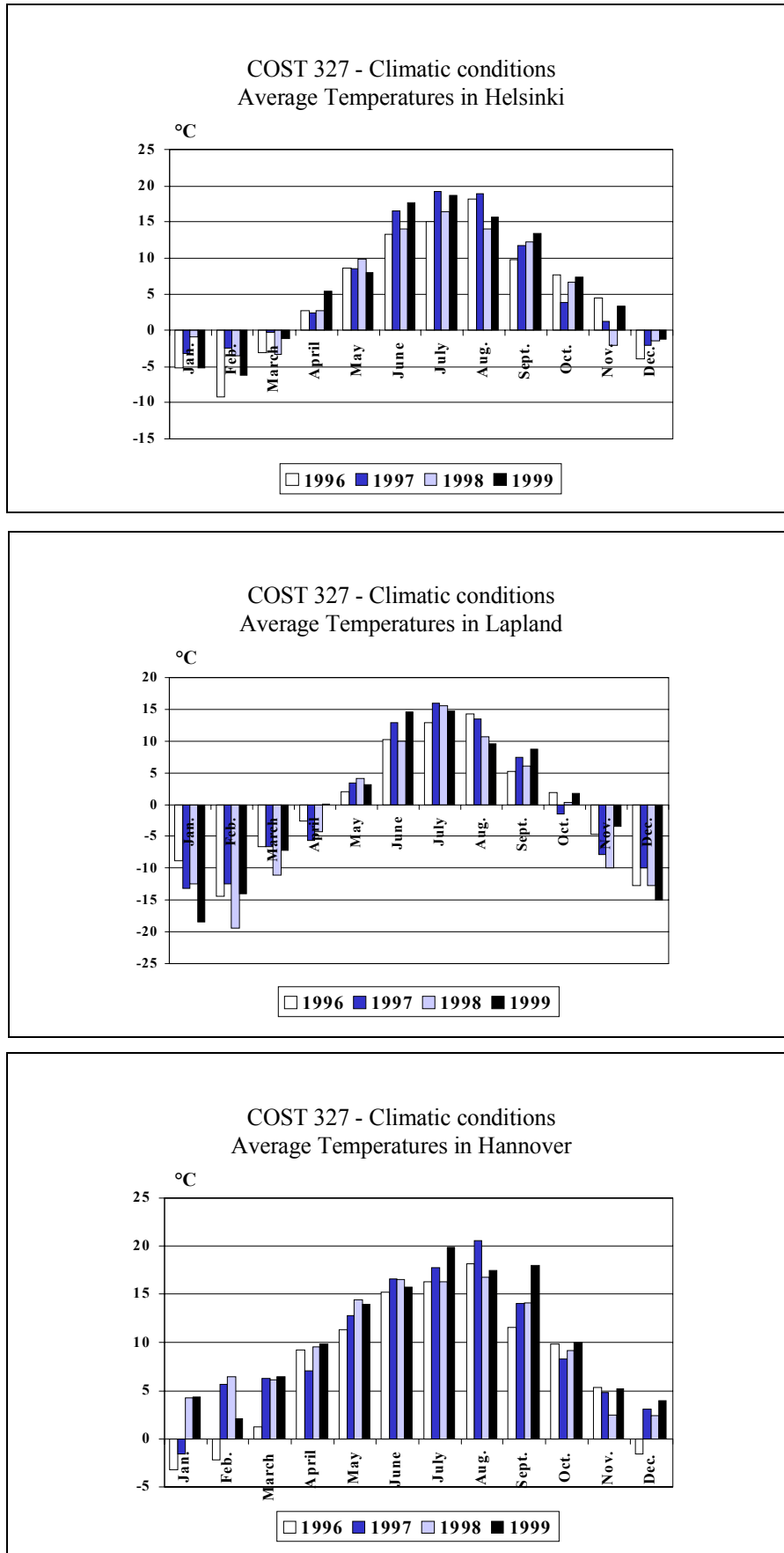
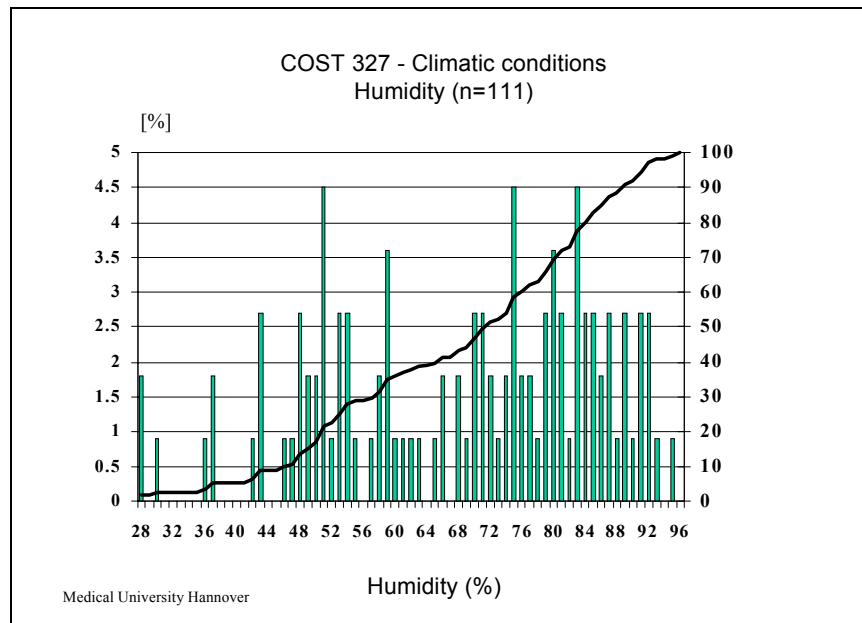


Figure 3.24. Official average temperatures.

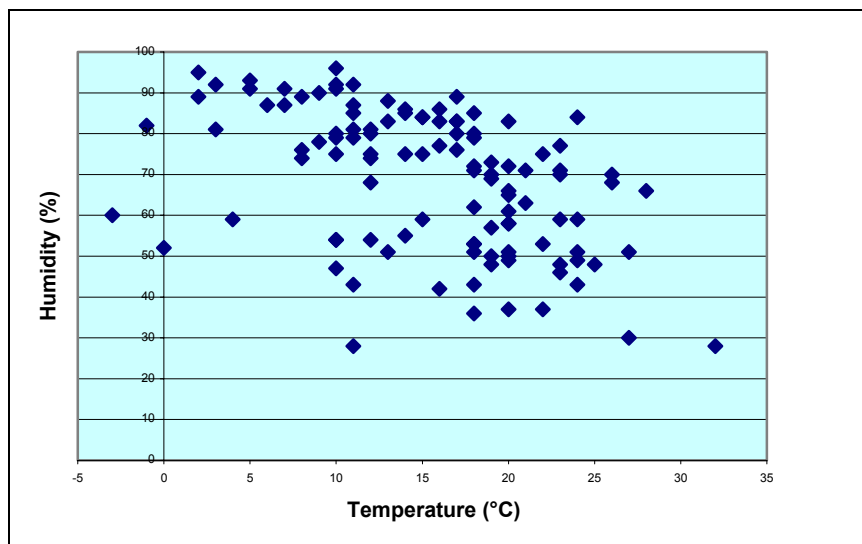
The distribution of humidity for the accident cases of Germany (Hannover) only is shown in figure 3.25. The mean value lies at 69% whereas the mean annual value for Hannover is a humidity of 76%.



100% all accidents with motorcycles; n=35 unknown)

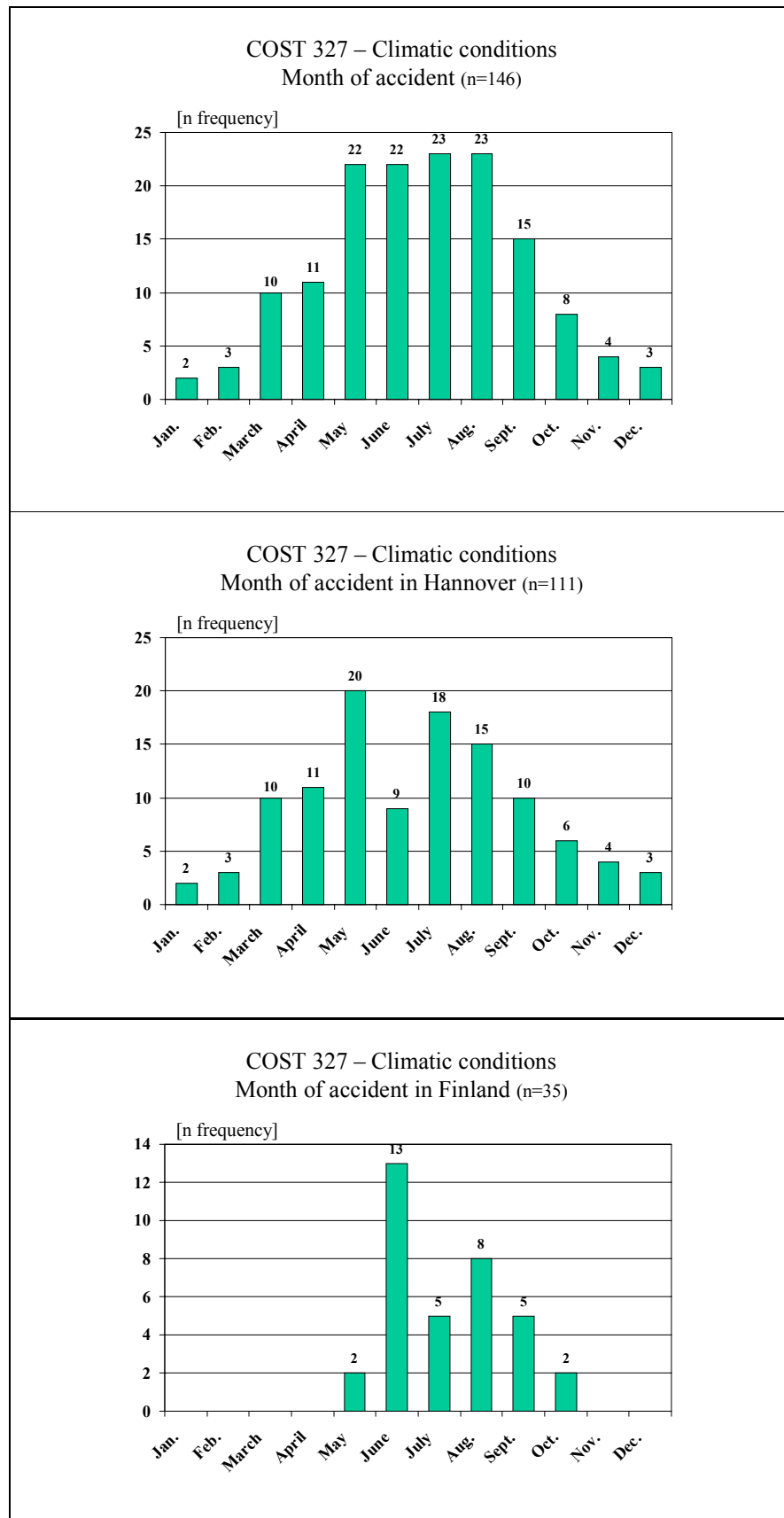
Figure 3.25. Distribution of humidity

It was found that there was a relationship between humidity and temperature at the time of the accidents as may be expected.



100% all accidents with motorcycles; n=35 unknown

Figure 3.26. Distribution of humidity and temperature



100% all accidents with motorcycles

Figure 3.27. Monthly reported motorcycle accidents in different areas

3.8.5. Visor condition and accident risk.

Tables 3.24 and 3.25 give a general comparison between the weather and visor conditions.

Table 3.24 Visor and weather condition compared.

	Total	Precipitation						
		Yes n.f.s.	None	Rainfall	Hail	Snow	Freezing rain	unknown
Total	146	1	136	9	-	-	-	-
Condition of visor								
Not applicable	27	-	23	4	-	-	-	-
Good	27	-	27	-	-	-	-	-
Scratched	39	-	34	5	-	-	-	-
Cloudy	1	-	1	-	-	-	-	-
unknown	52	1	51	-	-	-	-	-
Total	100%	-	100%	100.0%	-	-	-	-
Condition of visor								
Not applicable	28.7%	-	27.1%	44.4%	-	-	-	-
Good	28.7%	-	31.8%	-	-	-	-	-
Scratched	41.5%	-	40.0%	55.6%	-	-	-	-
Cloudy	1.1%	-	1.2%	-	-	-	-	-
Total	100.0%	0.7%	93.2%	6.2%	-	-	-	-
Condition of Visor								
Not applicable	100.0%	-	85.2%	14.8%	-	-	-	-
Good	100.0%	-	100.0%	-	-	-	-	-
Scratched	100.0%	-	87.2%	12.8%	-	-	-	-
Cloudy	100.0%	-	100.0%	-	-	-	-	-
Unknown	100.0%	1.9%	98.1%	-	-	-	-	-

A substantial number of helmets were fitted with visors in poor condition; excluding the unknown, 41.5% were scratched. A combination of a scratched visor and rainfall was considered to be the condition in which an accident was most probable and this occurred in 55.6% of cases. It should be noted that in 28.7% of all cases the helmet was not fitted with a visor ("not applicable" in the Tables 3.24 and 3.25).

Table 3.25 Visor condition and rainfall.

	Total	Precipitation rate				
		No rain	Light	Medium	Heavy	Unknown
Total	146	136	5	5	-	-
Condition of visor						
Not applicable	27	23	3	1	-	-
Good	27	27	-	-	-	-
Scratched	39	34	1	4	-	-
Cloudy	1	1	-	-	-	-
Unknown	52	51	1	-	-	-
Total	100.0%	100/0%	100.0%	100.0%	-	-
Condition of visor						
Not applicable	28.7%	27.1%	75.0%	20.0%	-	-
Good	28.7%	31.8%	-	-	-	-
Scratched	41.5%	40.0%	25.0%	80.0%	-	-
Cloudy	1.1%	1.2%	-	-	-	-
Total	100.0%	93.2%	3.4%	3.4%	-	-
Condition of Visor						
Not applicable	100.0%	85.25	11.15	3.7%	-	-
Good	100.0%	100.0%	-	-	-	-
Scratched	100.0%	87.25	2.6%	10.3%	-	-
Cloudy	100.0%	100.0%	-	-	-	-
Unknown	100.0%	98.1%	1.9%	-	-	-

3.8.6. Analysis and results

3.8.6.1 Cases influenced by climatic conditions

Fifteen cases, six from Finland and 19 from Hannover, Germany, were identified in which climatic conditions were considered a contributory cause. These cases are listed below together with the cause.

- 15 (UPK 28/95) road was poorly lit, motorcyclist travelling too fast
- 18 (OPK 43/96) cloudy dim night
- 20 (HPK 86/95) tinted visor, darkness
- 30 (POPK 6/98) tinted, scratched visor, darkness
- 34 (PIPK 12/98) darkness
- 35 (PIPK 13/98) possibly glare, motorcyclist overlooked the turning camper van

114202	possibly wetness caused loss of handling
114658	fog approximately 100 m caused reduction of view, too fast
114865	wetness and mud on the road
115475	heavy rain, car began to slide, motorcyclist lost the handling of his motorcycle
115796	probably reduction of view due to rain
115995	possibly reduction of view due to rain, sliding motorcycle caused by wet road?
116134	loss of handling due to wetness
116216	possible glare
116267	integral helmet without visor, possible reduction of view due to rain

3.8.6.2 Analysis of the 146 cases.

In most of the cases, 88 %, the road was dry and in 93%, there was no precipitation. It was raining in 7% of cases. Seventy-one percent of all the accidents occurred in daylight, 20 % at night and 9% at half-light (dusk/dawn). The weather conditions caused loss of handling in two of the 146 cases, 1.4%, and speed of the motorcycle inappropriate to the road conditions was the cause of nine accidents 6.2%.

Poor visibility caused 7, 4.8%, of accidents: four from heavy rain, two from fog and one from glare from the sun. Extreme physiological conditions were investigated as a possible cause. Two cases were found: one with high temperature and high humidity and one with very low temperature and snow. In addition, there were three cases where the temperature was high and the riders were wearing leather clothes. It is possible, though not confirmed, that these conditions were uncomfortable and contributed to the accident.

Two cases have been included below to clarify the analysis.

Case 35 (PIPK 13/98) Finland

Course of events during accident:

The driver of a motorcycle (Yamaha) rode along a rural road exceeding the speed limit. From the opposite direction, a camper van drove on the street. He was starting to turn without noticing the approaching motorcycle. The motorcyclist was killed in this accident.

Photo of helmet:



Climatic condition:

The weather was half-clouded with a temperature of 18°C. The road surface was dry. The motorcyclist failed to notice the turning camper due to glare from the sun.

Collision situation:

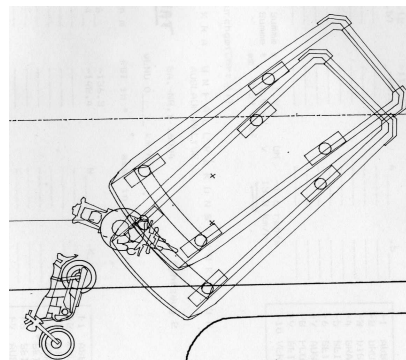


Photo of motorcycle:



Photo of opposite vehicle:



Case 14.658 Germany / Hannover

Course of events during accident:

A motorcycle (Honda CB 500) driver wanted to pass a passenger car, which was slowly driving at the end of a traffic jam. The weather condition was not good, the sight distance was approx. 100m due to fog and the road surface was wet. The motorcyclist failed to notice a truck (IVECO MAG) which was driving on the opposite site of the road. The motorcycle collided frontal with the front parts of the truck. The Honda driver was severely injured in this accident (AIS 5).

Photo of helmet:

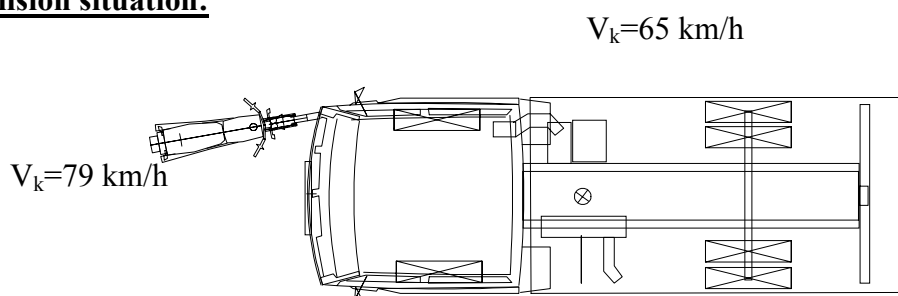


Climatic condition:

The driver of the motorcycle tried to overtake some cars despite the reduction of visibility caused by the fog. He didn't notice the oncoming truck and collided with it. An influence on climate related to high humidity can be assumed.



Collision situation:



3.9. CONCLUSIONS

1. The COST 327 action has provided the first European database compiled from a detailed study of motorcycle accidents. Cases were drawn from Glasgow UK, Hannover and Munich, Germany and Helsinki and Lapland, Finland. From the national statistics of these countries, it was found that, overall, only 20% of riders admitted to hospital suffered a head injury. This indicated that current helmets offer good protection. However, 16%, overall, sustained a head injury of AIS 2-4 and this indicated that improvements to helmets would offer a worthwhile saving in injuries.

2. Analysis of the COST database showed that 66.7% of the casualties sustained a head injury and 26.7% a neck injury. Fifty seven percent sustained a thorax injury and 72.9% leg injuries. When the injuries were analysed by MAIS it was found that the proportion with a head injury increased from 38% for MAIS 1 to 81% for MAIS 3 and greater. It was thus concluded that the risk of sustaining a head injury increased as the MAIS increased.

3. Location of helmet damage was distributed evenly with 26.9% lateral right, 26.3% lateral left, 23.6% frontal and 21.0% to the rear. Other frequently damaged locations were the forehead 16.1% and the chinguard, 15.4%. Impacts to the crown at 2.2% were less frequent.

4. It was found that head injury severity increased with head impact speed quite remarkably. The median was 18km/h for AIS 1, 50km/h for AIS 2-4 and 57km/h for AIS 5/6. Thus, it was estimated that an increase in helmet energy absorbing characteristics of some 30% would reduce 50% of the AIS 5/6 casualties to AIS 2-4. Further analysis showed that 20% of AIS 5-6 casualties could be reduced to AIS 2-4 if the energy absorbed by the helmet could be increased by some 24%.

5 Of particular interest was the median speed at which brain injury occurred, which may be assumed to be indicative of the sensitivity of the brain to a given impact severity at different locations. The median speed for concussion (considered separately to other brain injury types) at 43km/h was lower than that for brain injury, 60km/h. Injury to the brain was not particularly sensitive to the impact location, as shown by the median speed. This was just below 60km/h for the rear, upper and lateral regions and just above 60km/h for the chinguard and forehead.

6. Mass of a helmet did not affect the type or severity of an injury. Open-faced helmets were as protective as full-faced helmets except when the impact was to the face.

7. Angle of body impact was investigated and it was calculated that 68% occurred at an angle of 30 degree or less to a line vertically through the body and thus with the potential to induce substantial rotational motion to the head. Thirty two percent were at an angle greater than 60 degree. This is consistent with a separate analysis that showed that rotational motion contributed to head injury in over 60% of casualties.

8. Neck fractures were found to occur primarily with impacts to the face whilst bending moments from low severity head impacts tended to be the main cause of neck strain, AIS 1. Eighty percent of AIS 1 neck injuries occurred at speeds of up to 60km/h and 80% of injuries AIS 2 or greater occurred at speeds above 45km. Severe neck injuries, AIS 4 and greater, were always associated with severe head injuries. Analysis showed that there was a 30% probability of an AIS4 or greater neck injury for head injuries of AIS 5/6.

9. The effect of climatic conditions on accident risk was investigated as part of the extension to COST327. Trends were difficult to identify because this was a retrospective study and only regional climatic data was available and not for the location of each

accident. However, of the 111 accidents investigated, climatic conditions were estimated to have been the prime cause of 10 accidents, 9%. Of these, 6 (5%) occurred when the temperature was low, less than 10°C and at high humidity, greater than 80%. Thus, the tentative link between high humidity at low temperature and accident risk should be further investigated.

CHAPTER 4. HEADFORM ASSESSMENT

4.1. INTRODUCTION

A helmet is a very effective device to protect the head of a motorcyclist against severe head injuries. Helmets currently sold within the European Community must comply with the requirements of a Standard such as UNECE Regulation 22 for which helmets need to be tested dynamically using a headform. The protection afforded by the helmet is judged by the results of these tests, which, in turn depend critically upon the choice of the headform and associated instrumentation. Standards specify the use of headforms made of a rigid material, usually metal, as in Reg. 22, but sometimes wood as in BS 6658. These headforms resemble the human head only in mass and shape and, therefore, may not be the best tool for evaluating helmets; a typical dummy head is similarly constructed but is covered with a plastic material to represent flesh.

The purpose of the research undertaken by the Headforms Working Group was to investigate the performance of these existing headforms and then compare the results with those from a novel, more human like, device. This novel device known as the Bimass headform represents the skull and brain with two masses connected by damped springs and carefully constructed to give the correct modal frequency response. The Bimass described here is the version based upon a Hybrid III headform developed by Strasbourg University which was granted a study contract by the EC. Included in this development was the construction of a FE model of the new headform, which was used to assist with the physical model development. It was also used in accident reconstruction in parallel with the physical headform. Experimental tests can be time consuming and the FE model provided a convenient and inexpensive means of examining a wide range of impacts. The original version of the Bimass was based upon an Onser dummy and was evaluated as part of the Working Group research. The tests and results are fully described in the final report of the Working Group on Headforms.

A detailed description of all of the headforms used in the tests including details of the construction and performance of the Bimass headform is given in section 4.2. The results of the wide range of tests are given in section 4.3. A discussion of the selection of headforms is given in section 4.4 and the conclusions are in section 4.5.

4.2. CHARACTERISTICS OF EXISTING HEADFORMS

Rigid headforms are generally used in standard tests to approve helmets. They may be made of wood or of aluminium. Crash dummy heads (with or without modification) may also be used to assess the protection afforded by safety helmets.

4.2.1. Wooden headform

Wooden headforms are normally used for shock absorption and penetration tests with fixed headform and helmet assembly. Shape and sizes may correspond to EN 960 (see also section 2.2).

4.2.2. Aluminium headform

This kind of headform is mainly used for the falling headform test method. EN 960 'Headforms for use in the testing of protective helmets' of December 1994 describes the details of the commonly used headforms in Europe. There are significant differences between

those and the headforms used for the testing of helmets for drivers of motorcycles in northern America.

Main properties of the EN 960 headform:

Material: Magnesium/Zirconium binary alloy with 0.3 to 0.8 per cent Zirconium.
Density 1.79 kg/dm³

Resonance frequency of the headform not below 3000 Hz

Size: 15 sizes (A to Q) are defined, starting with a circumference of 500 mm up to 640 mm with intervals of 10 mm.

Mass: Only 5 sizes are designed for shock absorption tests and for these sizes only, the masses are defined:

Letter Code	Circumference in mm	Mass in kg
A	500	3.1 ± 0.10
E	540	4.1 ± 0.12
J	570	4.7 ± 0.14
M	600	5.6 ± 0.16
O	620	6.1 ± 0.18

Shape and geometry: In contrast to other helmet standards EN 960 defines not only the shape of the upper part of the head, but also gives figures for the lower head, including the chin.

A point G is defined for the mounting of the accelerometers. This point should lie near the centre of gravity.

4.2.3. Hybrid II dummy head

The Hybrid II dummy was developed by General Motors in 1972 to assess the integrity of the lap/shoulder belt systems. The Hybrid II dummy exists only in the 50th percentile size, and is fully specified in the PART 572 of FMVSS 208. The Hybrid II dummy is considered to have a limited impact response biofidelity, and is used to test the resistance of protection devices rather than assessing injury protection level.

4.2.4. Hybrid III dummy head

The Hybrid III is the result of a research programme performed in the early 1970's aimed to develop a biofidelic anthropometric and anthropomorphic test device. The Hybrid III dummy was designed by General Motors and first presented in 1977. The first version of the Hybrid III dummy represented the 50th percentile of the male adult, and more recently it has been completed with a small female (5th percentile female.) and a large male (95th percentile male).

4.2.5. Bimass head form

The experimental analysis of the in vivo human head's dynamic response revealed a natural frequency at about 120 Hz accompanied by a "decoupling" of about 1 kg mass (figure 4.1). This leads to the hypothesis that there is "decoupling" of the brain with respect to the skull. In vitro epidemiological studies have revealed focal contusions, which appears to confirm the

hypothesis of "decoupling". These studies form the basis of a lumped model, which distinguishes between the brain mass and other masses present such as the frontal bone and the rest of the skull. This work was conducted by the University of Strasbourg.

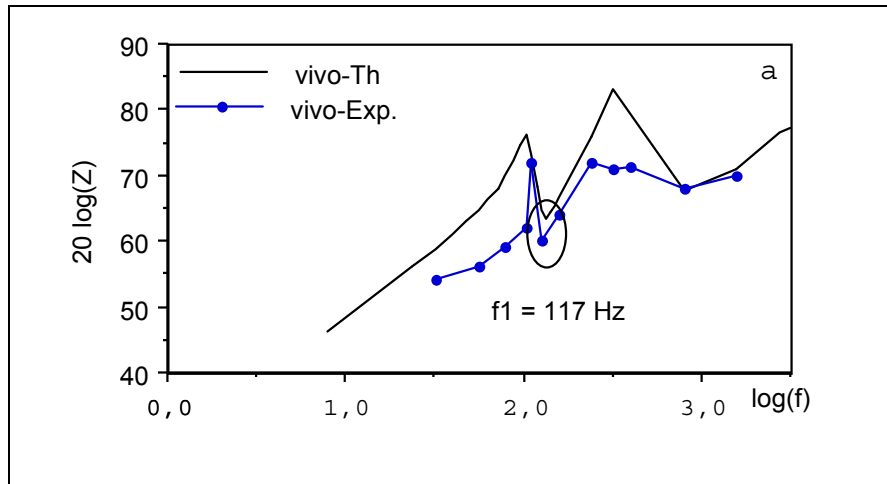


Figure 4.1. In vivo head mechanical impedance

This was achieved by reducing the mass of a Hybrid III dummy head and attaching a component in the centre, equivalent to the removed mass, to represent the brain. The two masses were linked by means of a plastic element with geometrical and mechanical properties to give a natural frequency of the head at 150 Hz.

In order to complete the design rapidly, a finite element (FE) model of the new dummy head was developed, (figure 4.2) and tested in the frequency and temporal domains. The FE model was also a fundamental part of the theoretical accident reconstruction used in parallel with the human head FE modelling (see section 3.4). Instrumentation was added to the physical head to record and analyse multi-directional impacts so that 3D translation and rotation of the "skull" could be recorded as well as the 3D motion of the "brain" within the "skull". This was achieved by fitting each body with four three-axial accelerometers.

The outputs of this physical head model are the skull acceleration, the brain acceleration and the brain-skull relative acceleration. Each one of these parameters can be related to a specific head injury mechanism. Skull acceleration can be related to skull deformation and related lesions such as extradural haematoma and skull fracture. The brain-skull relative motion is indicative of subdural haematoma and focal cerebral contusions and, finally, linear brain acceleration remains the main indicator of intracerebral contusions and haematoma.

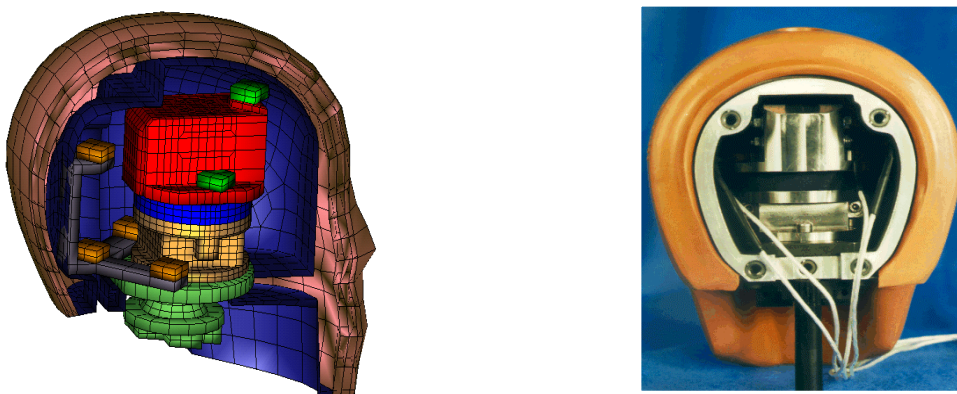


Figure 4.2. Numerical and physical model of the Bimass 150 dummy head prototype.

The prototype headform was validated using modal analysis on the frequency response measured in the horizontal plane in a variety of directions. This response conformed to expected results both in terms of the natural frequencies and modal shapes. A de-coupling of a mass of about 1 kg occurred at the natural frequency of 140 - 150 Hz, with a damping of 10%. This validated the Bimass against the human head in the 10 - 500 Hz frequency range.

In the temporal domain, the prototype was first subjected to non-helmeted direct impacts on a flat anvil at a 2 m/s speed. Figure 4.3 below shows the linear skull and brain acceleration amplitude for two parietal impacts and the theoretical result obtained by simulating this impact with the dummy FE model. In the temporal domain, the physical model has good reproducibility and its response agrees with that of the FE model. Results from the Bimass were compared with those from a conventional Hybrid II headform and it was found that the Bimass gave greater values of acceleration. It was concluded that the headforms are too different for comparison to be productive.

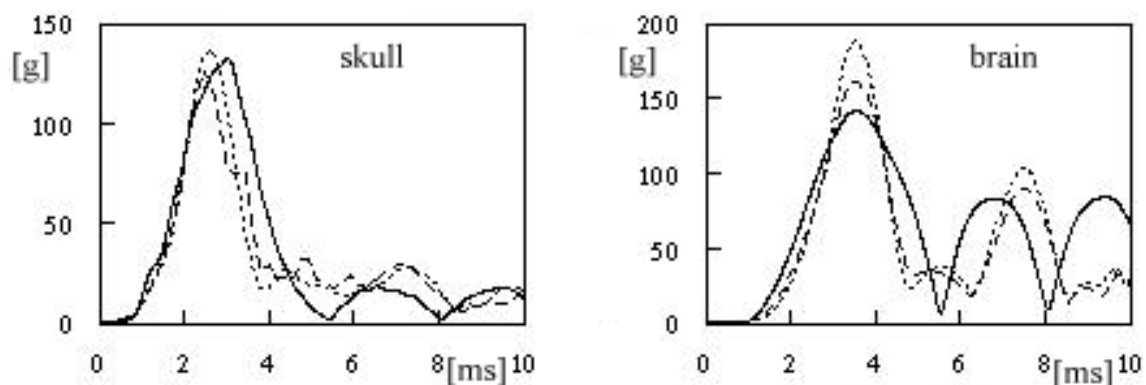


Figure 4.3. Non helmeted Bimass 150 parietal impact on a flat anvil at 2 m/s. Graphics show the linear skull and brain acceleration amplitude for two experiments (dotted lines) and for the FEM simulation (solid line).

4.3. IMPACT RESPONSE

4.3.1. Introduction

There are currently a number of headforms used to test crash helmets throughout the world. This can cause uncertainties when results obtained using different headforms are compared with each other. The aim of this study was to compare the results from drop tests on the four most common headforms used at TRL; a wooden headform to BSI specification, a Hybrid II, a Hybrid III and an aluminium headform used in Regulation 22. The headforms were tested both for rotational and linear acceleration by conducting drop tests onto an oblique anvil and a flat anvil respectively. The test procedures are described in detail below. These results were compared with equivalent tests from the prototype Bimass headform performed at EMPA, see section 4.3.3.

4.3.1.1 Aims

4.3.1.1.1 Tests for linear acceleration

The aims of the linear impact tests onto a flat anvil were as follows:-

1. To establish the differences in linear acceleration levels recorded by different headforms during impact at a given velocity.
2. To investigate which of the following headform parameters; mass, kinetic energy (i.e. the variation between headforms at the same velocity), surface (e.g. skin covering on the Hybrid headforms) and helmet construction have most effect on the measured acceleration.
3. To assess the importance of the impact site on the helmet.

4.3.1.1.2 Tests for rotational acceleration

The aims of the rotational impact tests onto an oblique anvil were as follows:-

1. To establish the differences in rotational acceleration levels recorded by different headforms during impact at two velocities (i.e. 5m/s and 10m/s).
2. To investigate the effects of headform inertia, helmet inertia and friction between the headform and the helmet and to ascertain which of these is the most significant.
3. To find which headform yields the most consistent results. In the past, at TRL, a large amount of variability has been observed when the wooden headform has been used in oblique impact tests. It was hoped that the work described in this report would confirm or refute this.
4. To find which headform is the most suitable for oblique impact tests and to determine the reasons why.

4.3.1.2 Equipment

Table 4.1 below, shows the masses and moments of inertia of the headforms considered here and Table 4.2 shows the masses and moments of inertia of the different helmets used. The headforms and helmets were weighed on a Mettler optical balance while their moments of inertia about the vertical axis (z-axis) were measured using a torsional pendulum facility. The z-axis for the headforms is the standard anatomical z-axis which passes through the centre of gravity of the head. The z-axis for each helmet is the same as that for the Hybrid III headform when placed on the headform so that it complies with the peripheral vision requirements of BS6658.

Table 4.1 Headform Specifications

	Wooden	Aluminium	Hybrid II	Hybrid III	Bimass
Size	L, 590 mm	J, 570 mm	J, 570mm	J, 570 mm	J, 570mm
Mass [kg]	5.07	4.94	4.27	4.81	5.61
Moment of inertia about Z axis [kg.mm ²]	17,200	19,100	14,700	19,200	17,670
Accelerometers	Nine accelerometer array				

It can be seen in Table 4.1 that the moment of inertia for the Hybrid III headform is about 30% higher than that of the Hybrid II. This difference is due to the fact that the mass in the Hybrid III is concentrated more towards the perimeter of the headform than in the case of the Hybrid II. It should be noted that the Bimass (see 4.3.3) is included here for completeness.

Four helmet types were used, two open faced and two full-faced each in thermoplastic glass fibre reinforced plastic (grfp). The wooden headform required the use of a larger, size 3, helmet while size 2 helmets were used on the other headforms.

Table 4.2 Helmet Specifications

Model	New Ace		Nimrod		Spectra		Wasp	
Type	Full-face		Full-face		Open face		Open face E	
Material	GFRP		Thermoplastic		GFRP		Thermo-plastic	
Size	Size 2	Size 3	Size 2	Size 3	Size 2	Size 3	Size 2	Size 3
Mass [kg]	1.60	1.65	1.35	1.48	1.27	1.29	1.01	1.14
Moment of inertia about Z axis [kg.mm²]	22,36	23,176	19,179	20,413	14,760	14,916	10,635	12,941

4.3.1.3 Procedure

4.3.1.3.1 Tests

The headforms were tested for both rotational and linear acceleration. The tests selected were based on the shock absorption and oblique impact tests outlined in BS 6658:1985 and the same impact velocities were incorporated here. Thus most of the oblique impact tests were conducted at an impact velocity of 10m/s and a few were conducted at a quarter of the kinetic energy (i.e. 5m/s) for comparison purposes. It was decided to base the experimental work on BS 6658:1985 because the outcome of this work may influence the design of future helmet test standards.

4.3.1.3.2. Method

Linear acceleration was measured by dropping the helmeted headform onto a flat anvil with an impact velocity of 7.5 m.s⁻¹. This is equivalent to the shock absorption test in BS 6658: 1985 for a type A helmet. The anvil was a Kistler type 9293 force transducer set to measure the normal force during impact. Each helmet was positioned for an impact to the forehead region, figure 4.5. It was found, afterwards, that the results from impacts at this particular site were sensitive to the curvature of the helmet, thus a number of further comparative tests were conducted using the rear of the helmet.

Rotational accelerations were measured by using the oblique impact test procedure given in BS 6658: 1985. The apparatus used for this test method is shown in figure 4.4. In the TRL helmet impact facility the helmeted headform is not guided after being released from a pre-selected height but is allowed to fall freely under gravity. Each helmeted headform was dropped onto an anvil inclined at 15° to the vertical with an impact velocity of 10 m.s⁻¹. A few tests with each helmet type were also conducted at 5 m.s⁻¹. The anvil was a Kistler type 9255 force transducer allowing the measurement of both normal and tangential force. An abrasive sheet of grade 80 aluminium oxide was attached to the anvil's impact surface. Each helmet was impacted twice, once on the left and once on the right side.

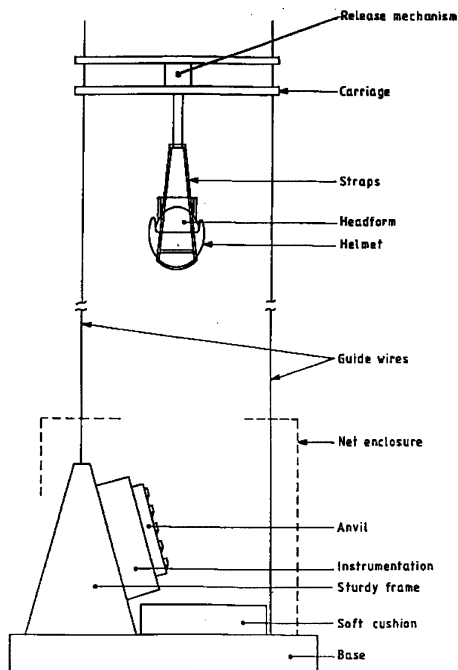


**Figure 4.4. Helmet impact location.
Linear impacts**

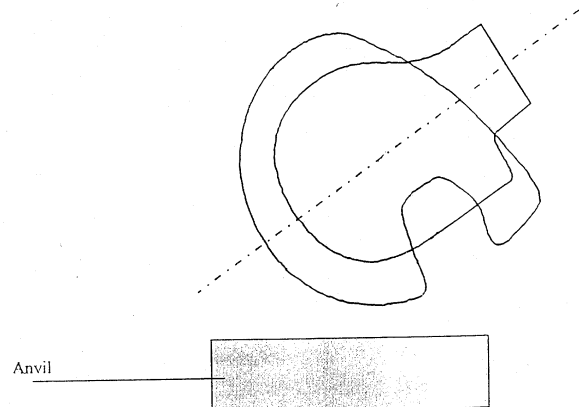


**Figure 4.5. Apparatus for the oblique linear
impact test**

Table 4.3 Mean performance of headform/helmet combination

	Peak Normal [N]			Peak Linear [g]			HIC		
	Wood	Al	Hybrid II	Wood	Al	Hybrid II	Wood	Al	Hybrid II
New Ace	12742	10729	8829	217	189	185	1916	1549	1396
Nimrod	12182	10699	8250	206	178	176	1765	1657	1423
Spectra	13192	9995	8901	251	194	208	2477	1574	1741
Wasp	12119	11781	9449	224	272	216	1986	1977	1739
Overall	12552	10825	8739	225	208	192	2053	1736	1542

The results are shown in Table 4.3. In general, the wooden headform experienced greater peak accelerations and normal forces and higher HICs than the Hybrid II and aluminium headforms. The results were reasonably consistent for a given helmet and headform combination except for some of the results obtained with the Wasp helmet. Two of the tests on the Wasp helmet using the Hybrid II headform gave high forces and accelerations. The precise reasons for this are unclear but the most likely cause is the interaction between the anvil and a press-stud on the front of the Wasp helmet during impact. In the first of these three tests, which produced a lower acceleration and anvil force than in the latter two, it was noticed that the damage to this stud was more severe indicating that it had

absorbed some of the impact energy. Table 4.3 shows the average performance with each helmet type and the overall mean results. Peak linear acceleration was 17 % higher for the wooden headform than the Hybrid II for all helmet types except the Spectra for which the wooden headform experienced accelerations 21 % greater. This correlates well with the difference in mass between the two headforms, the wooden head is 19 % heavier than the Hybrid II and so has a correspondingly higher kinetic energy at impact which must be absorbed by the helmet.

The peak acceleration, normal force and HIC values for the aluminium headform lie between those of the wooden and Hybrid II headforms. This is to be expected because the mass of the aluminium headform is between those of the other two headforms (Table 4.1).

The median headform force versus displacement curves for the three tests on each helmet type were plotted and examined. Figure 4.6 shows the Spectra helmet as an example. The graphs showed that the wooden headform experienced a higher peak force but less displacement, i.e. there is less liner crush. The differences in the peak forces experienced by the three different types of headform are closely related to their different masses. More displacement, of the order of several millimetres, is generally seen to occur with the Hybrid II and aluminium headforms than with the wooden headform. The reasons for this are because the wooden headform was a larger size than the other two and, therefore, required a larger helmet. To accommodate this, the liner for the larger helmet (size 3) was only 32mm thick compared with 40mm for the size 2 helmets used with the Hybrid II and aluminium headforms. This meant that for the wooden headform, the inside diameter of the liner is larger which results in a greater surface area over which to distribute the force. Furthermore, the thinner liner will appear to be stiffer because its density will increase at a greater rate with increasing displacement and this will result in a lower total displacement.

The greater mass of the wooden headform would normally be expected to result in a higher deflection compared with the Hybrid II but it seems that this may be counteracted by the larger surface area of the wooden head distributing the force so that the wooden headform has less deflection. From this, it could be expected that a wooden headform r, of a similar size to the Hybrid II and aluminium headforms, should give closer results.

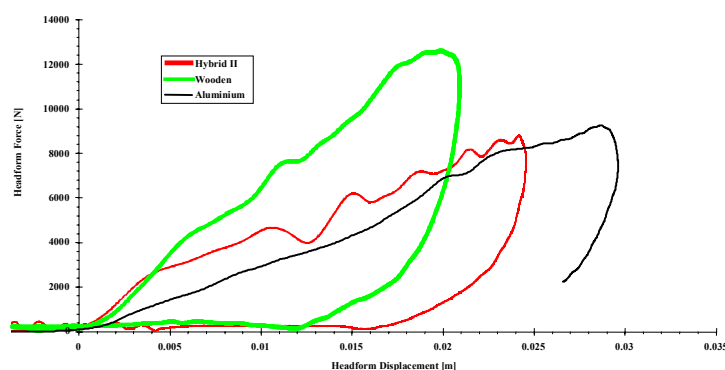


Figure 4.6. Headform force v. displacement. Spectra helmet

An additional factor in the different displacements may have been the covering of the Hybrid II headform. It is possible that compression of this covering could result in greater displacements of the headform by 2 to 3mm. However, a comparison of the Hybrid II and

aluminium headform results shows that this effect is not significant since the displacement of the Hybrid II is generally not more than that of the aluminium headform.

An example of the time histories of the median accelerations is shown, for the Spectra helmet, in figure 4.7. The initial part of the three curves for a particular helmet is similar up to an acceleration of about 500ms^{-2} (51g). Beyond this point, the Hybrid II and aluminium headforms experience a lower rate of acceleration increase and peak between 0.5 and 2 ms later than the wooden headform reaches peak acceleration. In general, the acceleration pulses for the Hybrid II and aluminium headforms tend to be between 0.5 and 4ms longer than those for the wooden headform. Since the Hybrid II and aluminium headforms compress the liner further, it should be expected that the peaks in the acceleration occur later and that it takes longer to complete the pulse.

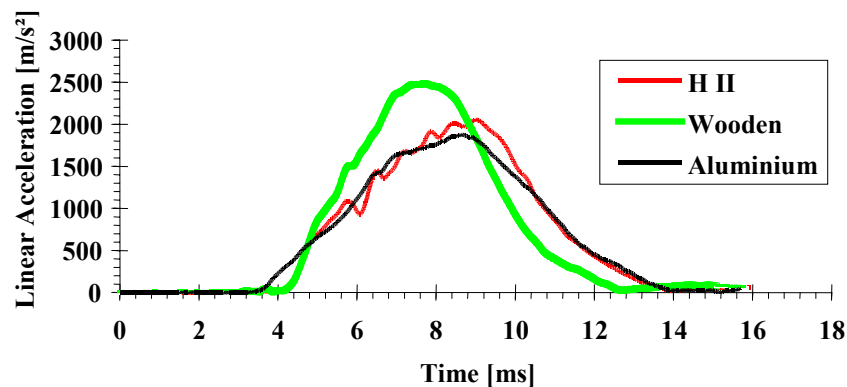


Figure 4.7. Linear acceleration. Spectra helmet

Figure 4.8 shows all three forces versus displacement results for the aluminium headform when tested inside a Nimrod helmet. It can be seen that there is a considerable degree of scatter in the results. Initially, it was thought that the large amount of scatter in the aluminium headform results, seen in figure 4.8, might be due to the choice of impact site at the front of the helmet. As a consequence of the curvature of the helmet and because of the closeness of the front of the helmet to the facial opening, it is believed that the dynamic mechanical properties in this area might be particularly sensitive to the exact location of the point of impact.

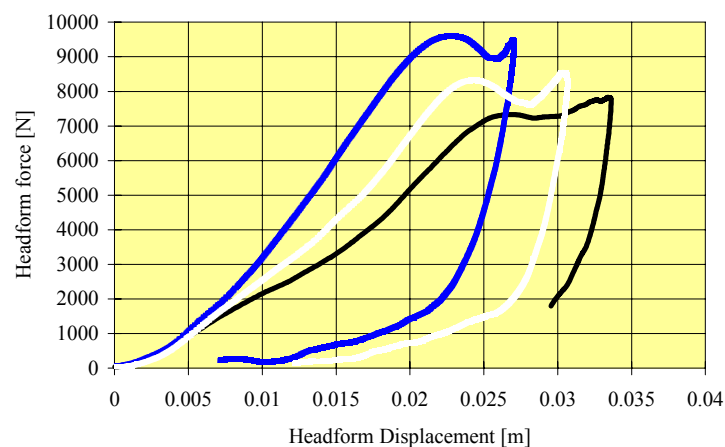


Figure 4.8. Headform force v displacement for the aluminium headform in three different tests using a Nimrod helmet

Further comparative drop tests were conducted with the three headform types using the rear of a Spectra helmet, which should be less sensitive to the position of the impact point. However, a similar degree of scatter was also seen in these results. Unfortunately, a considerable amount of 'ringing' was recorded with the wooden headform in these tests which made the results invalid. The aluminium and Hybrid II results were more consistent in terms of peak force but there was still 2 or 3mm variation in the displacement. Nevertheless, the rear of the helmet is probably a more suitable impact site for use in future work.

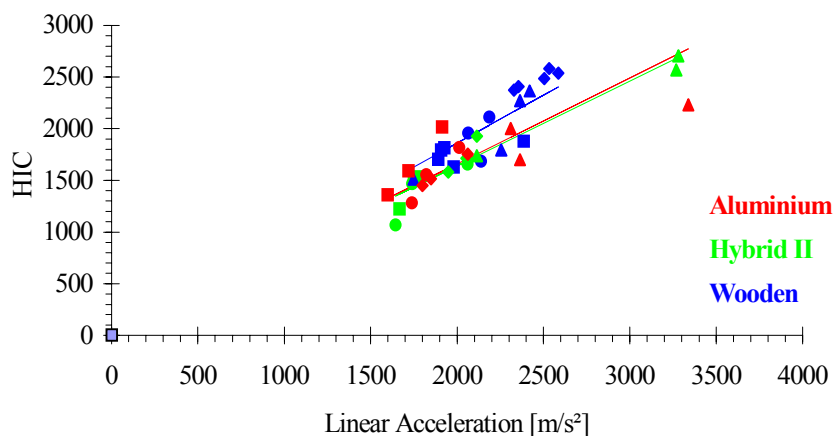


Figure 4.9. HIC v linear acceleration for all helmet types.

Figure 4.9 shows plots of HIC versus acceleration for all the flat anvil tests. The points for the Hybrid II and aluminium headforms are reasonably close to each other and below those for the wooden headform. In general, the wooden headform experiences higher accelerations and consequently produces higher HIC values because of its greater mass and larger surface area.

Peak linear acceleration is plotted against normal anvil force in figure 4.10. The grouping between individual helmet types is close with each headform except for those results obtained with the Wasp helmet. Visual inspection of the graph reveals that the wooden headform gives the least amount of scatter in these results. However, the Hybrid II results appear to be consistent if one ignores the two outlying Wasp results which were discussed earlier. Unfortunately, the Hybrid III headform was not available during the linear impact testing phase.

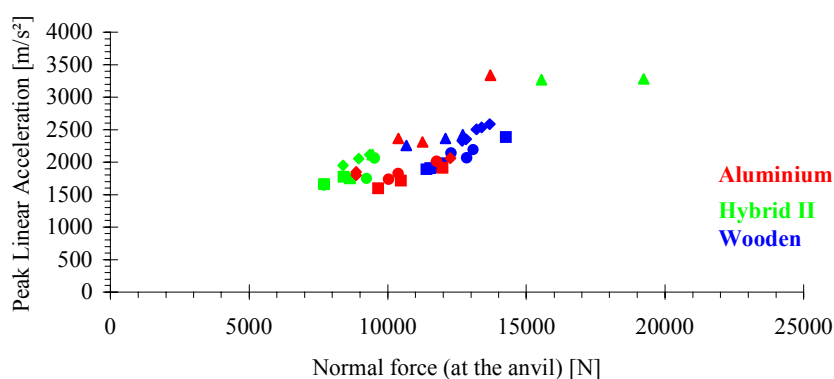


Figure 4.10. Peak linear acceleration v normal force. All helmet types

4.3.2. Rotational acceleration

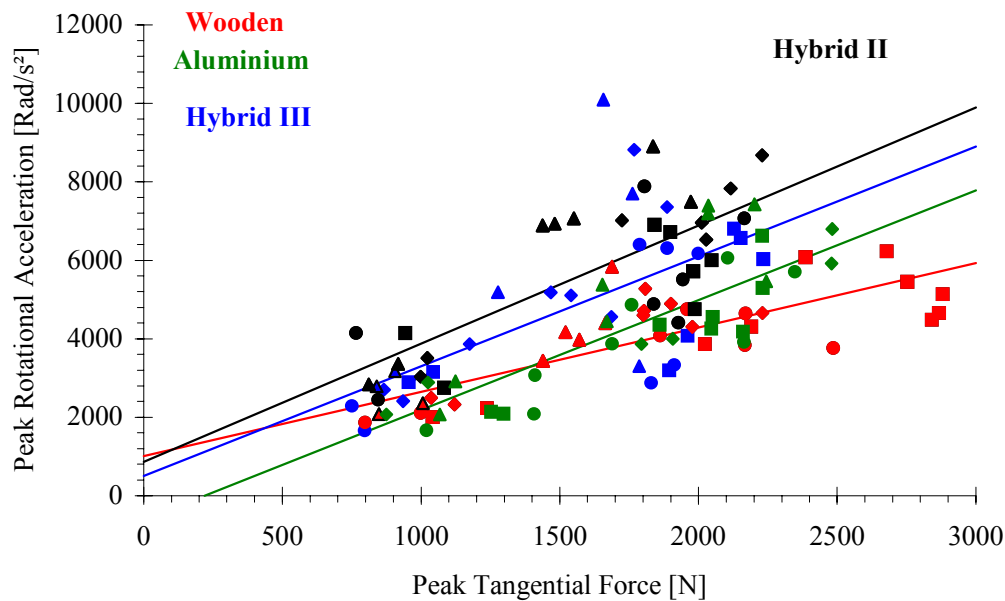


Figure 4.11. Rotational acceleration versus tangential force. All helmet types

Oblique impacts were performed at velocities of 10 m.s^{-1} and 5 m.s^{-1} . Oblique impact tests were also conducted using a Hybrid III headform. A summary of the results is given in Tables 4.4 and 4.5 which show average peak rotational accelerations and tangential forces respectively.

Although the overall average tangential forces agree within $\pm 10\%$, the peak rotational accelerations for the Hybrid II and Hybrid III are considerably higher than those for the wooden and aluminium headforms. This is in some part due to the lower moment of inertia of the Hybrid II headform, but the main reason is that the friction between the headform and the interior of the helmet is greater for the Hybrid II and III than for the other headforms. In the series of impact tests using the aluminium headform described in this report, it was found that this headform tended to slip several centimetres out of position after each impact. In contrast, very little relative movement is observed between the Hybrid II headform and the helmet during impact and, after impact, the Hybrid II appeared to still be in its original position inside the helmet.

Included in Tables 4.4b and 4.5b are the standard deviations from the means of the helmet results considered here. They give an indication of the degree of scatter in the data. In Table 4.4b, the results for the Hybrid III headform have the largest standard deviations revealing that the amount of scatter for these tests is greater than for those with the Hybrid II and wooden headforms (overall standard deviation = 13%). Table 4.5b indicates that there is a smaller amount of scatter in the measured tangential forces with the Hybrid II headform producing the most consistent results (overall standard deviation = 7.6%).

Peak rotational acceleration against peak tangential force at the anvil is plotted in figure 4.11 for all of the oblique impact test results. On the assumption that tangential force is linearly related to rotational acceleration, least squares regression lines have been also plotted for the four headform types.

In figure 4.11, it can be seen that the regression lines for the Hybrid II, Hybrid III and aluminium headforms are more or less parallel. The Hybrid II headform tends to have the highest rotational acceleration for a given tangential force because it has the lowest moment of inertia (see Table 4.1). The Hybrid III and aluminium headforms have similar moments of inertia but the line for the Hybrid III lies above that for the aluminium because there is more frictional coupling between the headform and the helmet with the Hybrid III than with the aluminium headform. The relatively low correlation coefficient of 0.62 for the Hybrid III results is an indication of the large amount of scatter in them although the reasons for this scatter are uncertain.

The amount of slippage between the wooden headform and the helmet, which occurred during impact is even more pronounced than with the aluminium headform and consequently the rotational accelerations tend to be lower. This in part accounts for the different gradient of the regression line for the wooden headform. Another factor, which may have affected the gradient of this line, is that the wooden headform is a larger size than the other headforms and the helmets fitted to it had slightly larger moments of inertia than those fitted to the other headforms (see Table 4.1).

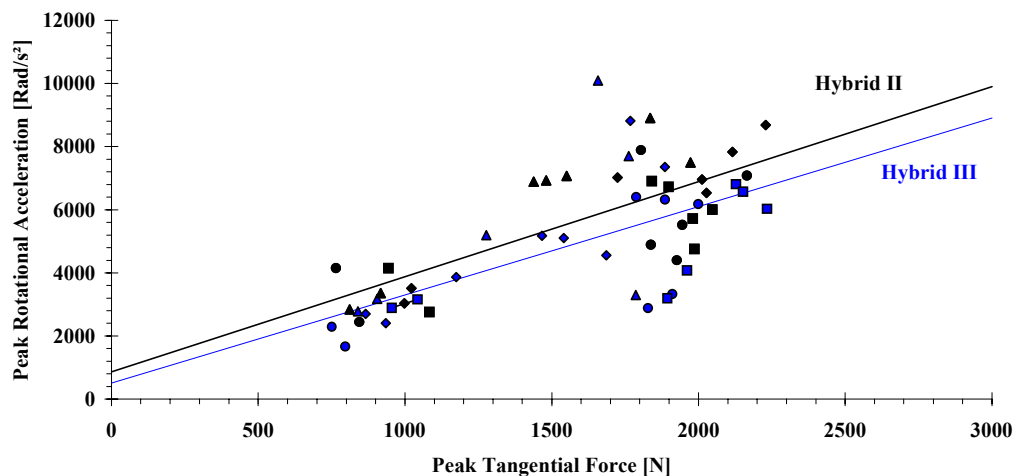


Figure 4.12. Rotational acceleration v tangential force. Hybrid II and III headforms

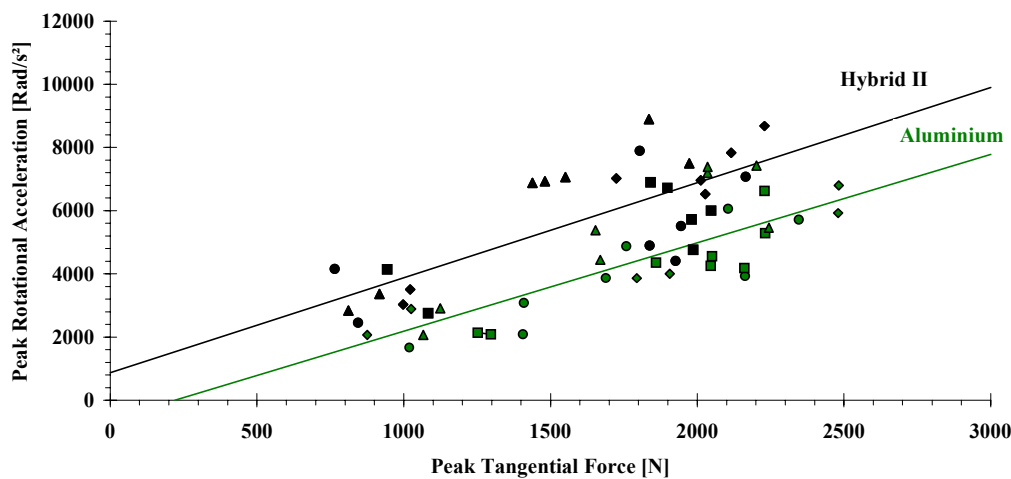


Figure 4.13. Rotational acceleration v tangential force. Hybrid II and Al Headform

For clarity, the results have been plotted separately for each headform in comparison with those for the Hybrid II in figures 4.12 to 4.14. Figure 4.12 shows that there is good agreement between the Hybrid II and Hybrid III results at both 5m/s and 10m/s. This is to be expected because of the similar structure of these headforms.

Figure 4.14 shows that, at 10m/s, the range of tangential force over which the wooden headform results for all helmet types are scattered, is larger than that of the other headforms even though the consistency for a particular helmet type is reasonably good (Table 4.5b). It would appear that the rotational acceleration recorded by the wooden headform is influenced by the inertia of the helmets fitted onto it more than is the case with the other headforms. In figure 4.14, it can be seen that the results for the full face helmets, which have higher moments of inertia (Table 4.2), give higher rotational accelerations and higher tangential forces.

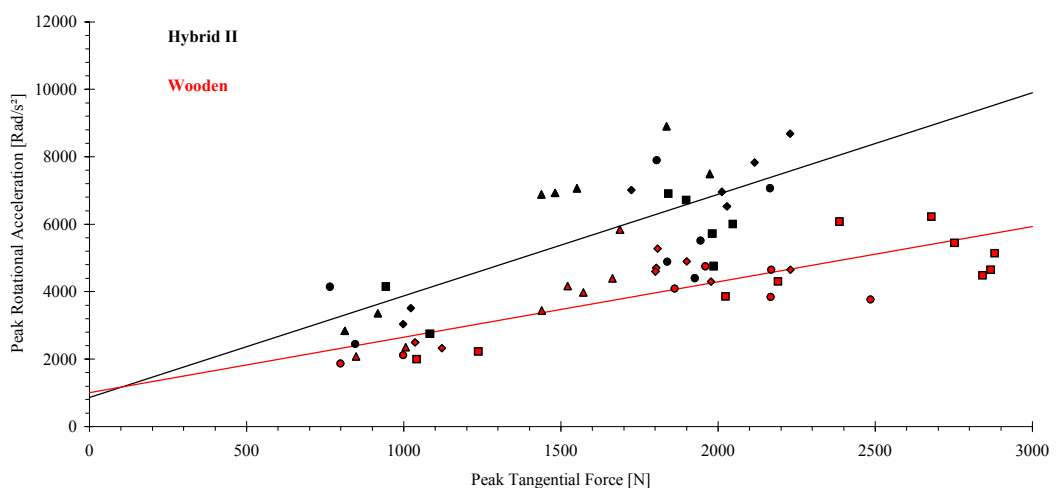


Figure 4.14. Rotational acceleration v tangential force. Hybrid II and wooden headform

The aluminium headform results, displayed in figure 4.13, also show a large amount of scatter over a wide range of tangential force. It is this wide spread of results for both the aluminium and wooden headforms, which produces the higher correlation coefficients of 0.84 and 0.81. The Hybrid II results at 10m/s are concentrated over a smaller range of tangential force and so the regression line is not quite such a good fit to the data as indicated by the lower correlation coefficient of 0.76. Overall, when both tangential force and rotational acceleration are considered, the Hybrid II headform would seem to yield the most consistent results as indicated by the relatively low standard deviations in Tables 4.4 and 4.5.

Table 4.4a Average peak rotational accelerations (rad. s⁻²) for oblique drops at 5m/s

	Hybrid II	Hybrid III	Aluminium	Wooden
New Ace	3293	1970	1872	1983
Nimrod	3452	3024	2116	2120
Spectra	3273	3284	2476	2411
Wasp	3099	2981	2492	2117
Overall	3279	2815	2239	2157

Table 4.4b Average peak rotational accelerations, R (rad.s⁻²) for oblique drops at 10m/s {s.d = standard deviation}

	Hybrid II		Hybrid III		Aluminium		Wooden	
	R	s.d.	R	s.d.	R	s.d.	R	s.d.
New Ace	5948	1322 (22%)	5013	1572 (31%)	4578	1059 (23%)	4214	408 (10%)
Nimrod	6022	769 (13%)	5336	1439 (27%)	4880	865 (18%)	5026	795 (16%)
Spectra	7402	765 (10%)	5570	2046 (37%)	5625	1475 (26%)	4798	311 (6.5%)
Wasp	7455	754 (10%)	6570	2562 (39%)	6216	1169 (19%)	4362	801 (18%)
Overall	6707	903 (13%)	5622	1905 (34%)	5325	1142 (21%)	4600	579 (13%)

Table 4.5a Average peak tangential forces (N) for oblique drops at 5m/s

	Hybrid II	Hybrid III	Aluminium	Wooden
New Ace	806	774	1213	899
Nimrod	1013	999	1275	1139
Spectra	1010	1021	950	1079
Wasp	865	873	1096	909
Overall	924	917	1133	1007

**Table 4.5b Average peak tangential forces, T (N) for oblique drops at 10m/s
{s.d. = standard deviation}**

	Hybrid II		Hybrid III		Aluminium		Wooden	
	T	s.d.	T	s.d.	T	s.d.	T	s.d.
New Ace	1937	126 (6.5%)	1883	73 (3.9%)	1913	320 (17%)	2129	215 (10%)
Nimrod	1951	72 (3.7%)	2074	126 (6.1%)	2096	130 (6.2%)	2577	312 (12%)
Spectra	2022	168 (8.3%)	1547	307 (20%)	2349	501 (21%)	2007	255 (13%)
Wasp	1656	211 (13%)	1621	204 (13%)	1974	234 (12%)	1577	92 (5.8%)
Overall	1892	144 (7.6%)	1781	178 (10%)	2083	296 (14%)	2082	219 (10%)

4.3.2.1 Frictional effects

Examples showing the variation of rotational acceleration and tangential force with time are given in figures 4.11. The wooden headform takes between 1.5 and 2.5ms longer to reach peak rotational acceleration than the Hybrid II headform but the tangential force traces for the Hybrid II and wooden headforms are of similar shape and duration. The rotational acceleration traces of the wooden headform decay at a slower rate after the peak and in some cases, there also appears to be a second less pronounced peak as the force reduces.

These initial comparative tests on the Hybrid II and wooden headforms were conducted by a previous researcher while tests on the aluminium headform were completed over a year later using TRL's new helmet impact test facility. Results for the aluminium headform are shown in black in figure 4.11. It can be seen that these results agree most closely with those of the wooden headform except in the case of the Wasp helmet. For a given tangential force, the rotational accelerations experienced by the aluminium headform were lower than those produced with the Hybrid II headform (see also figure 4.11). The same is true of the wooden headform which also gives rotational accelerations lower than those of the Hybrid II.

The larger masses of the wooden and aluminium headforms account for the higher tangential forces produced upon impact with the anvil at a given velocity. These larger tangential forces might, at first sight, be expected to produce higher rotational accelerations but the effect is more than compensated for by the fact that the wooden and aluminium headforms also have larger moments of inertia. This is one reason why the aluminium and wooden headforms experience rotational accelerations lower than the Hybrid II. However, the predominant cause is believed to be the differences in the surface friction between the helmet and the headforms.

Mellor (1995) has suggested that the smooth surface of the wooden headform could explain the difference in the performance between it and the Hybrid II. Calculations from film analysis of the original tests showed that the wooden headform slips inside the helmet substantially more than the Hybrid II. The Hybrid II has a maximum slip between headform and helmet of approximately 3°. The wooden helmet shows a slip of 10°. To examine this further, it is possible to calculate the dynamic friction between the headform and the helmet.

Friction can be calculated from:

$$\mu = T/N$$

where μ is the coefficient of friction, T and N are the tangential and normal forces experienced by the headform. The forces can be calculated from the rotational and linear accelerations of the headform.

The normal force can be found from:

$$\mathbf{N} = \mathbf{ma}$$

where m is the headform mass and a is the acceleration of the headform.

Tangential force can be found using:

$$\mathbf{T} = \mathbf{Ia/X}$$

Where I is the mass moment of inertia of the headform about the Z axis, a is the angular acceleration and X is the distance between the point of application of the force, i.e the surface of the headform, to the centre of mass of the headform.

Using this method, graphs for the Nimrod and Spectra helmets were produced. The traces for the Hybrid II headform show that once impact has occurred the dynamic coefficient of friction rises steadily from about 0.1 up to a peak between 0.5 and 0.6 before falling. This rise coincides with the rising force. The wooden headform gives a different graph. The friction begins at between 0.1 and 0.2 it then rises at a much slower rate than the Hybrid II and is still around 0.2 when the force on the headform is at its peak. As the force decays, the friction continues to rise until there is a sharp increase to a high level at the end of the impact.

These results can be used to explain many of the differences between the two headforms. A higher level of friction between the headform and the helmet will permit more of the force to be transmitted between the two. For the Hybrid II the highest friction coincides with the highest force and so, when the force is at its peak, there is a high transmission of this force to the headform resulting in high acceleration. In the case of the wooden headform the level of friction is much lower during the peak force and so less of the force is transmitted and the peak acceleration is much lower than that experienced by the Hybrid II. Instead the head will slip relative to the helmet as shown by Mellor (1995).

The sudden rise in the friction for the wooden headform as the force decays is probably due to the head suddenly reaching the limit of slip at which point it becomes wedged against the sides of the helmet and cannot slip further. Because the forces acting on the helmet at this point are low compared with the peak, this high level of friction does not produce large peak acceleration. Instead, the lower forces which are transmitted with greater efficiency result in the slight secondary acceleration peak sometimes seen and the slower decay of the acceleration pulse.

Comparison of rotational acceleration with tangential force in figures 4.11 to 4.14 reveals that the wooden headform motion lags the tangential force input whereas, in the case of the Hybrid II headform, the two are more or less in phase. This is a further indication that the wooden headform slips for a short period of between one and two milliseconds before locking into place and then rotating with the helmet. No such effect would appear to occur with the Hybrid II headform. It is believed that the rotational behaviour of the Hybrid III headform is similar to that of the Hybrid II because they each have the same skin covering.

Although tests using the aluminium headform were not filmed, it is believed that a similar amount of slippage occurs during impact with this type of headform as with the wooden headform, again because of the low level of friction between the surface of the headform and the helmet. It was observed, after each impact, that the aluminium headform had been appreciably displaced, something which does not occur with the Hybrid II headform. Thus

the aluminium headform results are closer to the wooden headform results than those of the Hybrid II.

4.3.3. Bimass response

More interesting was the prototype Bimass response during impacts when fitted with a helmet. EMPA of St Gallen, Switzerland were responsible for these tests as part of the collaboration between the Headforms and Test Procedures Working Groups. Brain translational and rotational acceleration and brain-skull relative acceleration were measured and recorded. Figure 4.15 gives the dummy response for a frontal impact on a flat anvil at a speed of 5.95 m/s. These recordings illustrate results for the brain and skull-brain dynamics that are typical when using the new dummy head prototype.

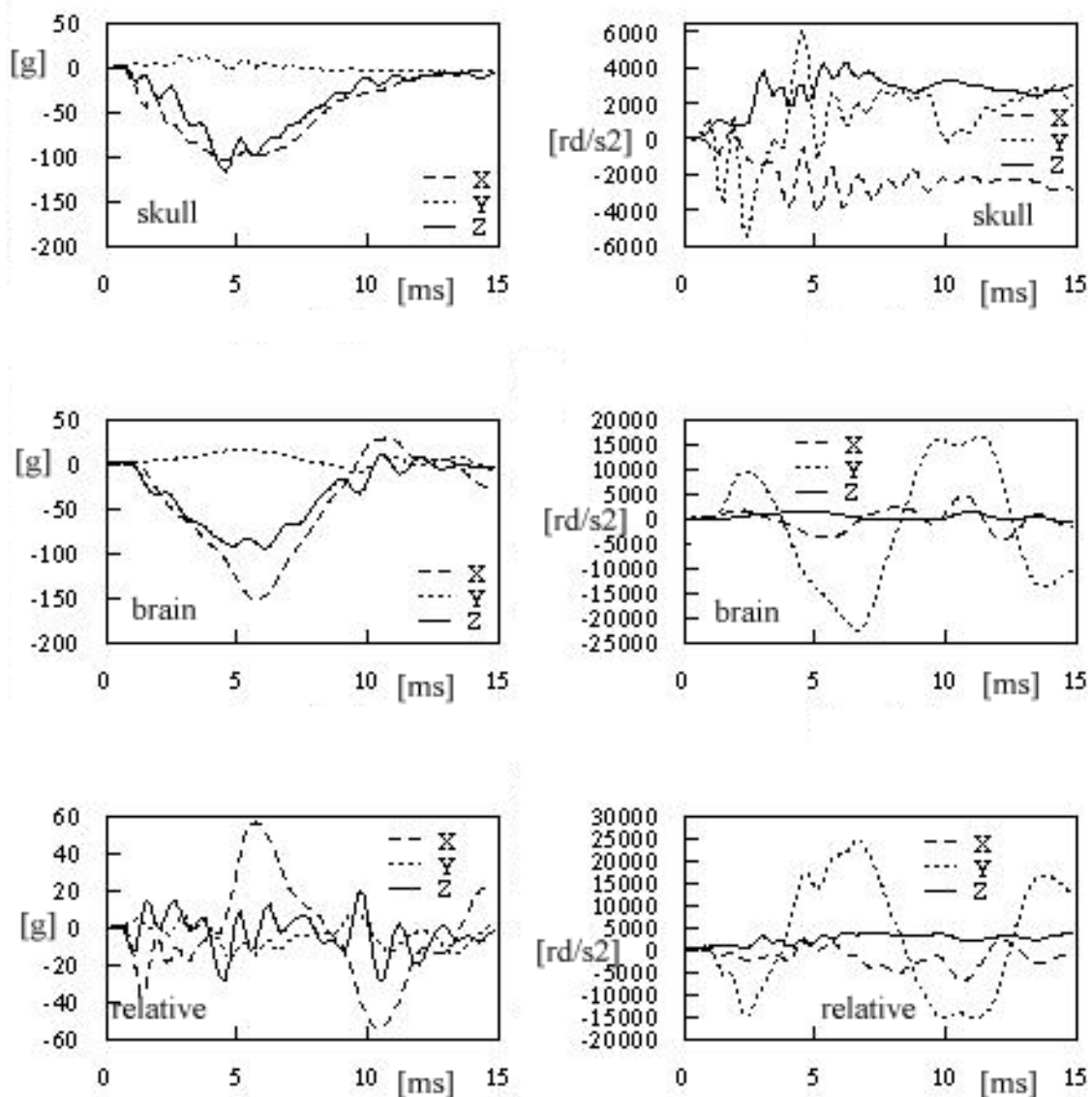


Figure 4.15. Helmeted Bimass 150 frontal impact on a flat anvil at 5.95 m/s. Graphics show the three components of the linear and angular acceleration of skull and brain as well as the relative accelerations.

4.3.4 Bimass and Hybrid II headforms compared

4.3.4.1 Tests

The Bimass headform was compared with the Hybrid II in two series of tests. Three tests using a flat, a kerbstone and an oblique anvil and five of the TRL replication tests as described in Chapter 5. Table 4.6 below gives the test details and Table 4.7 gives the results for the tests .

Tests using the Bimass headform were initially performed using the same impact conditions as the best single replication using the Hybrid II headform; helmets of the same type and model were used where possible. However, the instrumented Bimass at 5.45kg was 0.95kg heavier than the instrumented Hybrid II and thus the Bimass impacts were repeated at a lower velocity to give the equivalent energy. Moreover, the Bimass headform was not fitted with a neck and was thus secured into the helmet with polystyrene between the headform and chin strap.

Table 4.6 Test configurations

Description/Case	Site	Anvil	Conditioning	Test velocity
Standard 1	Front	Kerb	Hot	7.5m/s
				10m/s
Standard 2	Crown	Flat	Cold	7.5m/s
				10m/s
Standard 3	Side	15° oblique abrasive	Ambient	8.5m/s
Replication G345	Side	45° asphalt	Ambient	6.8m/s
Replication G197	Crown	30° concrete	Ambient	9m/s
Replication G372	Front	30° concrete	Ambient	12m/s
Replication G196	Side	30° concrete	Ambient	7.5m/s
Replication G411	Side	45° lamp post	Ambient	9.6m/s

The Bimass output was not directly comparable to that of the Hybrid II and nor was it intended to be. However, given that the biomes performance is not well known it was decided to compare the results for interest and understanding. Thus the following two sections give a comparison of the outputs and potential correlation.

4.3.4.2 Results: linear acceleration

The test data from the ‘high speed’ tests show that the peak linear acceleration of the Bimass headform skull was proportional to that measured using the Hybrid II for the same impact conditions. A linear regression analysis gave an r^2 value of 0.57 for the relationship $1.06 \times \text{Hybrid II acceleration} = \text{Bimass acceleration}$.

However, it was noted that for case G411, the linear acceleration for the Bimass headform was almost 80% higher than the 274g recorded using the Hybrid II headform. This replication was performed at high speed (normal impact speed = 6.8m/s) onto an aggressive lamp post anvil. It is likely therefore that the increased mass and consequently energy of the Bimass headform was in excess of that which could be absorbed by the helmet for these impact conditions. Indeed, repeating the regression analysis with this data

set removed (nine data sets) demonstrated an improved correlation with a r^2 of 0.69. In this case, the relationship between Hybrid II and Bimass linear acceleration was 0.91:1 i.e. Bimass acceleration was 10% lower than the Hybrid II.

This was not an unexpected result because the force versus displacement characteristic of the helmet liner remain the same and thus the same force for an increased mass will be achieved at a lower deceleration ($F=ma$). However, this applies only up to the thickness at which the liner material ceases to absorb energy 'bottoms-out'. Overall the Bimass brain linear acceleration was approximately 10% higher than the equivalent Hybrid II skull results.

4.3.4.3 Results: rotational acceleration.

The force generated at the helmet surface comprises components normal and tangential to the helmet surface. The tangential force is related to the normal force by the coefficient of friction between the helmet and impact surface. In this study, the coefficient of friction and the normal impact force generated by a particular helmet for a particular impact energy was similar for 'low-speed' replications (excluding G411). The difference between the generated rotational accelerations was considered to be, at least in part, a function of the inertial properties of the headforms used.

As for the linear acceleration, the most significant correlation between Bimass and Hybrid II skull data was achieved for impacts in which the energy rather than the velocity were equivalent (excluding G411). The r^2 of 0.75 (8 data sets) indicates much better correlation than the r^2 of 0.35 for the tests at the same velocity. In general the relationship between the peak rotational acceleration of the Hybrid II headform and the Bimass (skull) was approximately 2:1 when test at the same energy were compared.

Table 4.7 Results of test to compare the Bimass with the Hybrid II headform

Description/case	Configuration		Bimass data					Hybrid II data		
	Velocity	Anvil	Test	Skull peak linear	Skull peak rotational acc.	Brain peak linear	Brain peak rotational acc.	Test	Peak linear	Peak rotational acceleration
	[m/s]			[g]	[rad/s ²]	[g]	[rad/s ²]		[g]	[rad/s ²]
Crown/Cold	7.5	Flat	a04fu	368.6	-	339.0	-	b02jv	381.8	-
Front/Hot	7.5	Kerb	c04fu	143.9	-	150.5	-	g02jv	160.4	-
Side/Ambient	8.5	15°	d01fu	57.4	2239.7	56.4	10421.0	b01jv	67.9	4143.3
G345 (1)	6.8	45°	a14gs	243	40597	221	41376	b14jr	222	24945
	6.2 ₁	45°	b14gs	178	57944	272	49610			
G197 (1)	9	30°	a15gs	118	31885	181	50244	b20cr	167	8341
	8.2 ₁	30°	b16gs	237	41000	168	28531			
G197 (2)	8	30°	c15gs	152	26062	168	30557	a20cr	123	3441
	7.3 ₁	30°	a16gs	102	17814	121	25337			
G372	12	30°	a03is	162	38098	153	52018	e01cs	206	10284
	10.9 ₁	30°	b03is	287	43215	200	43884			
G196	7.5	30°	a07is	86	14313	154	20617	b05lq	106	4056
	6.2 ₁	30°	c07is	64	20868	265	59670			
H14.130	6.5	45°	a08is	128	32263	396	99054	a06hs	224	9088
	5.9 ₁	45°	b08is	106	31618	285	84096			
G411	10	45°	b01fu	594	30967	346	60288	a02ir	274	14715

1 Test performed at lower speed to account for additional Bimass headform mass.

4.4. HEADFORM SELECTION

The selection of headforms to be used in impact tests, aimed to evaluate the safety performances of helmets, can be made according to three main criteria: the anthropometric characteristics, the capability to predict realistic injuries and the repeatability of test results.

The anthropometry of rigid headforms is defined according to an ISO standard, which is universally accepted. The rigid headforms exist in five different sizes, which cover the variation range of motorcyclists' helmets. The dummy heads exist in limited sizes: the Hybrid II head is available only in one size (50th percentile) and the Hybrid III head in three sizes (95th, 50th and 5th percentiles).

All headforms can be fitted with a nine accelerometer array allowing the determination of the complete head kinematics, but the head kinematics are controlled by the characteristics of the neck, and only dummy heads can be attached to a neck. The impact response of the helmet is also partly controlled by the stiffness of the headform used in the test. Aluminium and wood headforms are considered as rigid, whereas the dummy headforms have an aluminium skull covered by a deformable flesh. The design of the Hybrid III head is aimed to have a biofidelic response based on cadaver test results.

The Bimass headform is able to determine the relative motion between the brain and the skull. This mechanism is considered important to predict the risk of internal head injuries. The results of an extensive programme of impact tests with three different helmets indicate that the Hybrid II headform has the best repeatability and response and because the dummy heads are built with the same technology it is expected that Hybrid III head will have the same level of repeatability.

4.5. CONCLUSIONS

1. Different headforms, wooden, metal Hybrid II and III, and Bimass, were evaluated for use in impact tests to assess the safety performance of helmets. The helmets could be selected according to three main criteria:

- the anthropometric characteristics
- a capability to predict injuries
- repeatability of the test results.

2. The anthropometry of rigid headforms is defined according to an ISO Standard and these headforms are available in five sizes. The Hybrid II headform is available in only 50th percentile and Hybrid III in only 50th, 5th and 95th percentile.

3. All headforms tested can be fitted with a nine accelerometer array so that the complete kinematics may be determined but the head motion is influenced by the neck and only a dummy head can be fitted with a neck.

4. In a wide range of tests with rigid and dummy headforms it was shown that the peak linear acceleration of the wooden headform averaged 17% greater than that for the Hybrid II at the same velocity.

5. HIC showed a wide variation between helmet types but the overall trend was for HIC to be greater when the headform mass was greater. Thus, the wooden headform averaged from 24% to 42% greater than the Hybrid II headform, depending upon the helmet type.

6. The Hybrid II experienced a peak rotational acceleration at a given impact velocity considerably greater than for either the aluminium or wooden headform but the Hybrid II gave the smallest standard deviations. These results were attributed to the much better grip of the Hybrid II and hence lower slippage between helmet and headform.

7. When compared with tests at the same energy the Bimass gave some correlation with the Hybrid II headform, 0.69 for peak linear skull acceleration and 0.75 for peak rotational skull acceleration. It should be noted that these correlations are an indication of the performance of the two devices and are not intended to be used for direct comparison of results.

8. The Bimass, as developed in a Hybrid III headform, allows the risk of injuries related to the relative motion between the brain and skull to be predicted. This offers a substantial and important improvement over a conventional headform

9. The overall conclusion was that the dummy headform gave the best repeatability, the Bimass gave the most realistic injury prediction. Thus, helmets of the appropriate size should be tested using a Bimass dummy headform and a rigid headform should be used to evaluate other sizes, as rigid headforms are available in a greater range of sizes.

CHAPTER 5. RECONSTRUCTION OF ACCIDENTS AND HELMET DAMAGE BY EXPERIMENT AND SIMULATION

5.1. INTRODUCTION

The reconstruction task was linked very closely to the Accident Investigation Working Group, which is responsible for data collection in Glasgow, Hannover and Munich. A very important part of the investigation was to collect and examine the helmets and to record the extent and location of the damage. Also recorded is an estimate of the direction of the impact force to the head and an estimate of the motorcyclist's trajectory during the accident. Detailed injury information is recorded and for the serious and fatal cases, this includes neuropathological data for the brain injuries. The Accident Investigation Working Group used such information, together with an extensive range of other data, to determine which accidents were likely to be suitable for replication. This information was then given to the Reconstruction Working Group.

The purpose of reconstruction was to examine the accident case file and the helmet, and then to attempt to reproduce the same damage, by drop testing equivalent new helmets. The test method used was to drop a helmeted headform at different velocities onto a surface similar to what was impacted during the accident and at the angle identified by the accident data collection team. The headform was equipped with extensive instrumentation such that both the linear and rotational acceleration was recorded. These measurements were compared with the type and severity of head injuries that were identified by clinical experts and, in particular, the neuropathological analysis provided detailed brain injuries for the fatal and serious cases.

The COST 327 task of reconstruction began in April 1996 and a Working Group was convened to determine the overall way to proceed. It was agreed that the proposed method of replication was the correct way to proceed for the examination of a large number of cases. Nevertheless, there were concerns that the use of a headform alone may, in some cases, not adequately represent the correct dynamics of the accident particularly the head effective mass, which it was thought may be influenced by the thorax mass. It was agreed that the replication process should be supported by an investigation of the effects of the overall dummy mass and the thorax mass, on the outcome for head injury potential in a range of impact conditions.

5.2. MADYMO SIMULATION

5.2.1. Introduction

Statistical studies have assessed the different types of collisions involving motorcycles and established the body parts of the rider which are most frequently exposed to high levels of injury. Zellner et al. (1991), have been working on possible solutions which can be applied to current motorcycles based on these findings. However, to validate these solutions there is a need to represent the rider's behaviour during impacts using a simple and economic tool. Currently, full-scale track tests are very expensive and require a large number of tests if they are to represent a range of typical impact types.

The main solution, in terms of repeatability, is a mathematical model of whole body motion in the impact system. Fortran programming has been used in earlier work by J. Happian-Smith et al. (1994), but more sophisticated multi-body dynamics software is now

used - the most widely used (in Europe) being TNO's software, Madymo-3D™. The software has incorporated ready-to-use hybrid dummies with appropriate articulation characteristics deduced from experimental testing.

To understand the kinematic behaviour of the model during the accident simulation, a simple representation of the elements, which are directly involved in the impact, are modelled dynamically. This allows an exceedingly complex impact to be understood. Part of this complexity is because of the similarity between the masses of the motorcycle and the dummy.

Despite their limitations, numerical models are extremely useful. They are much more sensitive and repeatable than track tests, much cheaper to run than FE models and they enable statistical studies to be carried out very economically.

5.2.2. Materials and methods

The purpose of the computer model was to identify the forces sustained by the head and the associated kinematics. The model was validated against a recent Transport Research Laboratory full-scale side-impact test of a Norton Commander travelling at 50km/h at 90° into the side of a stationary Ford Mondeo, for which impact loads on the dummy's head were available. The purpose was to obtain a generic model of a motorcycle impact which, when correctly validated, could be used to simulate accidents, of similar impact configuration, selected from the COST database.

There were three main physical components to this simulation: the motorcycle, the dummy rider and the target vehicle for which appropriate physical properties of the various interacting elements were required. This data was obtained from the literature, a biomechanical database, laboratory testing and numerical calculations with appropriate software. A three dimensional Cartesian co-ordinate system was used to locate the body segments with respect to each other and this was based upon the ISO standard.

5.2.3. The motorcycle

The motorcycle used was a Norton Commander, a large touring motorcycle with full fairing. The model of the motorcycle consisted of six rigid components, connected by five compliant joints, representing the frame, headstock, upper front fork, lower front fork, front wheel and rear wheel respectively. The frame has six degrees of freedom, being free to translate and rotate relative to all three global Cartesian axes. A rotational joint between the motorcycle frame and the headstock represented the motorcycle steering and similarly a rotational joint between the headstock and the upper front forks represented the front fork bending system. A translational joint in combination with a Kelvin element represented the suspension movement of the upper and lower front fork relative to one another. The wheels were connected to the front fork assembly by means of two rotational joints. In total, the system had eleven degrees of freedom. A representation of the motorcycle model complete with the lumped mass and joint positions is shown in figure 5.1.

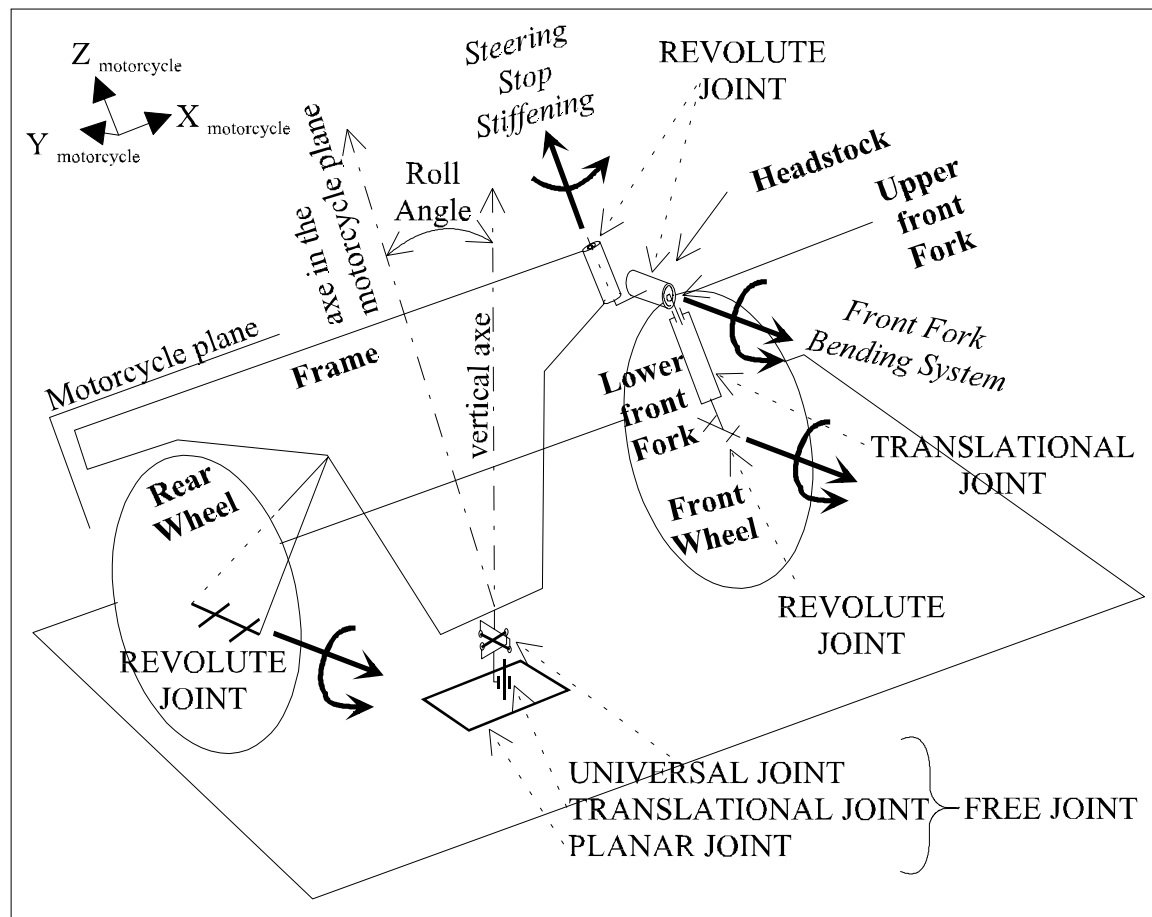


Figure 5.1. Motorcycle multibody model.

The principal dimensions of the motorcycle, the mass, centre of gravity and moments of inertia about the component's principal axes were all measured experimentally (McDonough 1993). The results are presented in Table 5.1 below.

Table 5.1 Motorcycle components mass and inertia

Body	Mass (Kg)	Ixx (Kg.m ²)	Iyy (Kg.m ²)	Izz (Kg.m ²)
Frame	197.4	59.4	19.6	39.8
Headstock	0.75	0.2	0.2	0.2
Upper front fork	3	0.001	0.028	0.028
Lower front fork	3	0.001	0.028	0.028
Front wheel	13.3	0.2889	0.5104	0.2889
Rear wheel	13.3	0.2889	0.5104	0.2889

The fundamental shape of the motorcycle was defined using planes and ellipsoids which, enabled the contact points to be determined. The geometrical model is presented on the following figure:

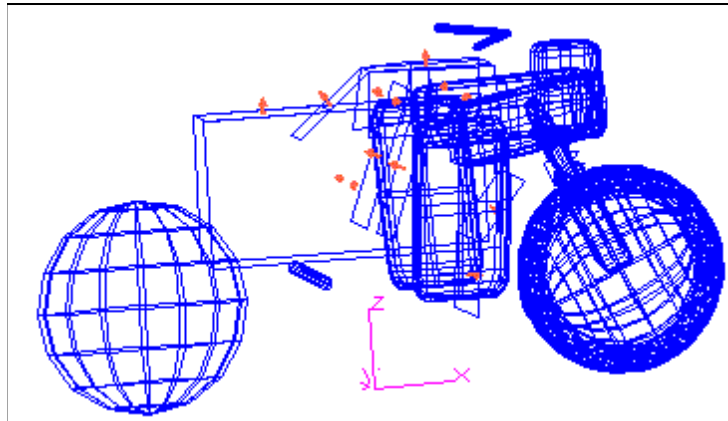


Figure 5.2. Motorcycle geometrical model

In addition to physical dimensions, mechanical properties were defined.

Stiffness values for the upper front-fork system were established through test work performed by Dr Happian-Smith during his PhD at Brunel University (1988). By comparing these values with those given in McDonough(1993), it is not possible to say whether or not they are acceptable unless a parametric study is carried out. Nevertheless, these values have been used in some model cases where acceptable results have been obtained. Moreover, damping and force/deflection characteristics of various interacting elements of the motorcycle during the impact, like the front wheels, the headlamp and the fairings have been obtained through quasi-static tests performed by the TRL.

The motorcycle steering operation was measured and the resulting steering stiffness can be seen from the following figure:

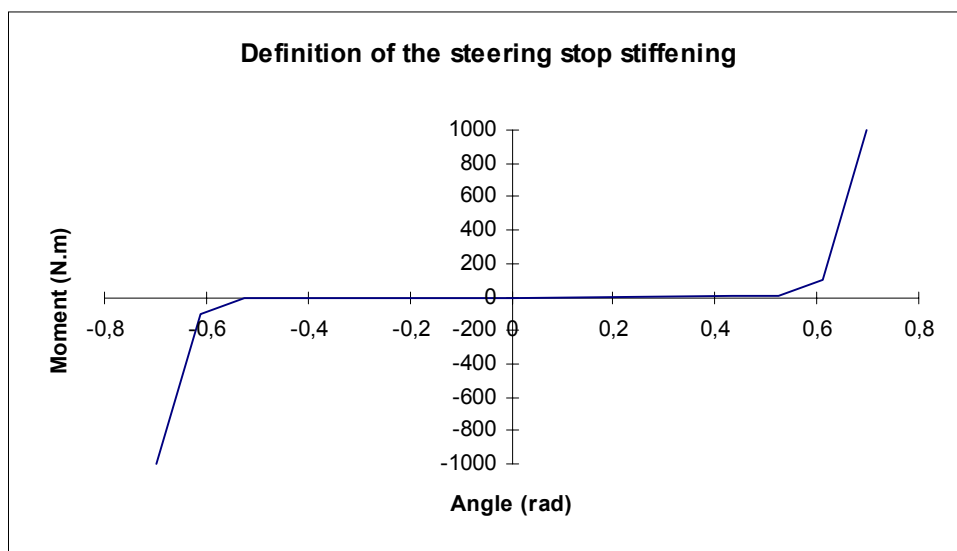


Figure 5.3. Steering stop stiffness

The angular damping of the steering systems was defined as 5Ns/m and the front fork bending system was calculated to be 200Ns/m as shown in figure 5.4 below.

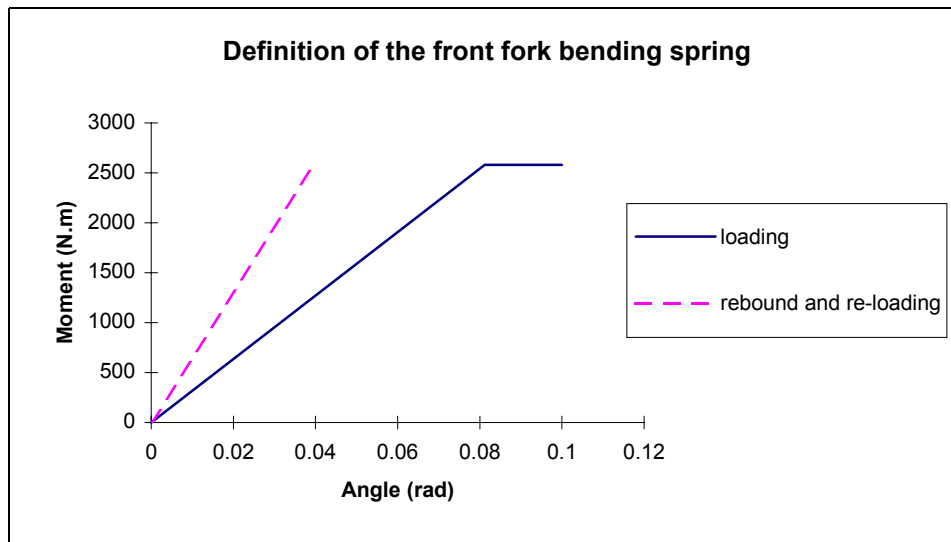


Figure 5.4. Characteristics of the front fork bending

The behaviour of the front fork is managed by a Kelvin element, which is a massless, uniaxial element that calculates the forces produced by a spring in parallel with a damper. The non-linear force elongation characteristics of the spring were experimentally defined as shown in figure 5.5. The downward damping of the front fork was defined at 60Ns/m whereas the upward damping of the front fork is defined at 90Ns/m. An initial 0.030m compression of the element was defined to take the rider mass into account.

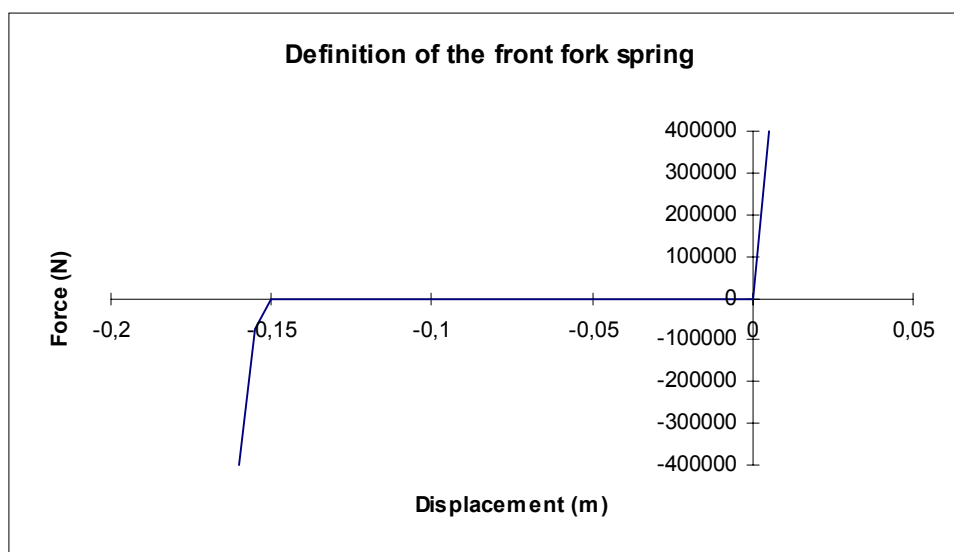


Figure 5.5. Front fork characteristic

The first point of contact in a head on crash into an obstacle is the front wheel. To model the motorcycle impact accurately it was important to know the front wheel assembly crush characteristics. A complete front wheel assembly was crushed across its diameter and the force -deflection characteristics are given in figure 5.6 below.

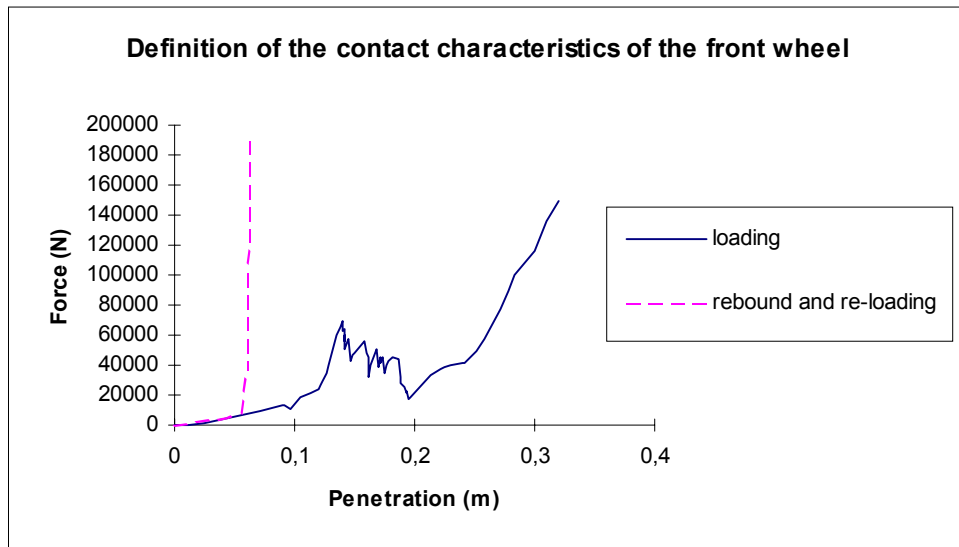


Figure 5.6. Front wheel characteristic

It was also necessary to measure the stiffness of the motorcycle components at the point of contact between the dummy and the motorcycle. Initially the feet are in contact with the footrest and the pelvis is in contact with the seat. The stiffness of these components was defined by the following characteristics:

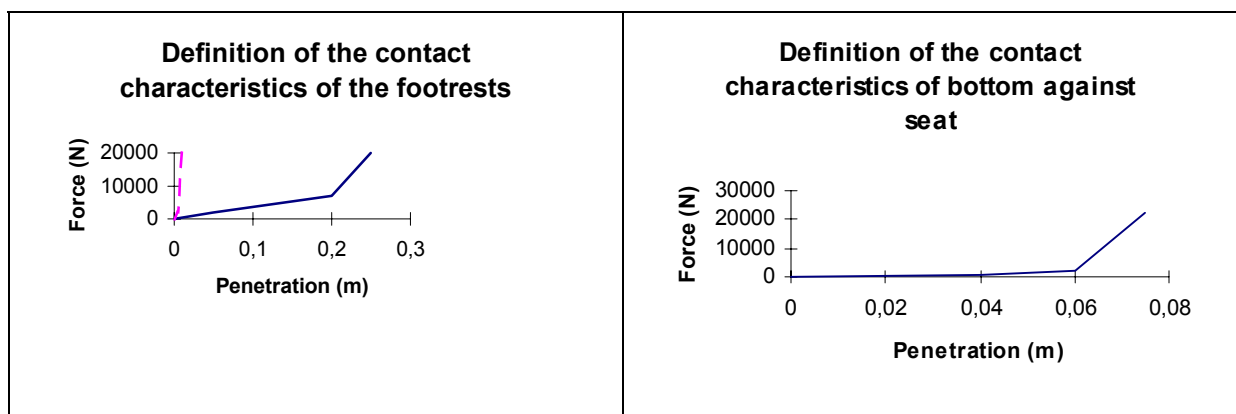


Figure 5.7. Characteristics of contact of the motorcycle with the dummy

The forces and moments acting on the motorcycle centre of gravity were used to evaluate its translational and rotational motion. These forces are:

- the gravitational force acting on the motorcycle
- the front wheel load when it impacts the lower front section of the car's frame
- the loading in the front forks, including moments due to their rotation about the headstock
- the action of the rear-wheel on the road (the rear suspension system was initially considered to have a negligible effect on the global motion of the motorcycle)

- The frictional and normal forces on the motorcycle arising from the motion of the rider along the seat and onto the petrol tank.

The seat and petrol tank were modelled as non-linear spring damper systems with permanent deformation on the tank. It was found that these features were critical to the global behaviour of the model during an impact.

5.2.4. The car

The car used was Ford Mondeo, a medium-sized five-door hatchback. The kinematic model of the car consisted of five rigid components connected by four compliant joints, representing the chassis and the four wheels. The chassis had six degrees of freedom, being free to translate and rotate relative to all three global Cartesian axes. Four joints were free to rotate and translate about a single axis in combination with Kelvin elements to constrain the motion of the wheel relative to the car frame, thereby simulating the suspension movement and rotation of the wheel. This gave 14 degrees of freedom for the total motion of the car. The locations of the lumped masses and the joints are shown in figure 5.8.

The geometrical model of the Ford Mondeo is defined by planes, ellipsoids and cylinders. Each wheel was simplified to one ellipsoid and the impact reaction force is calculated perpendicular to the contact plane. Cylinders were used to represent the overall car shape.

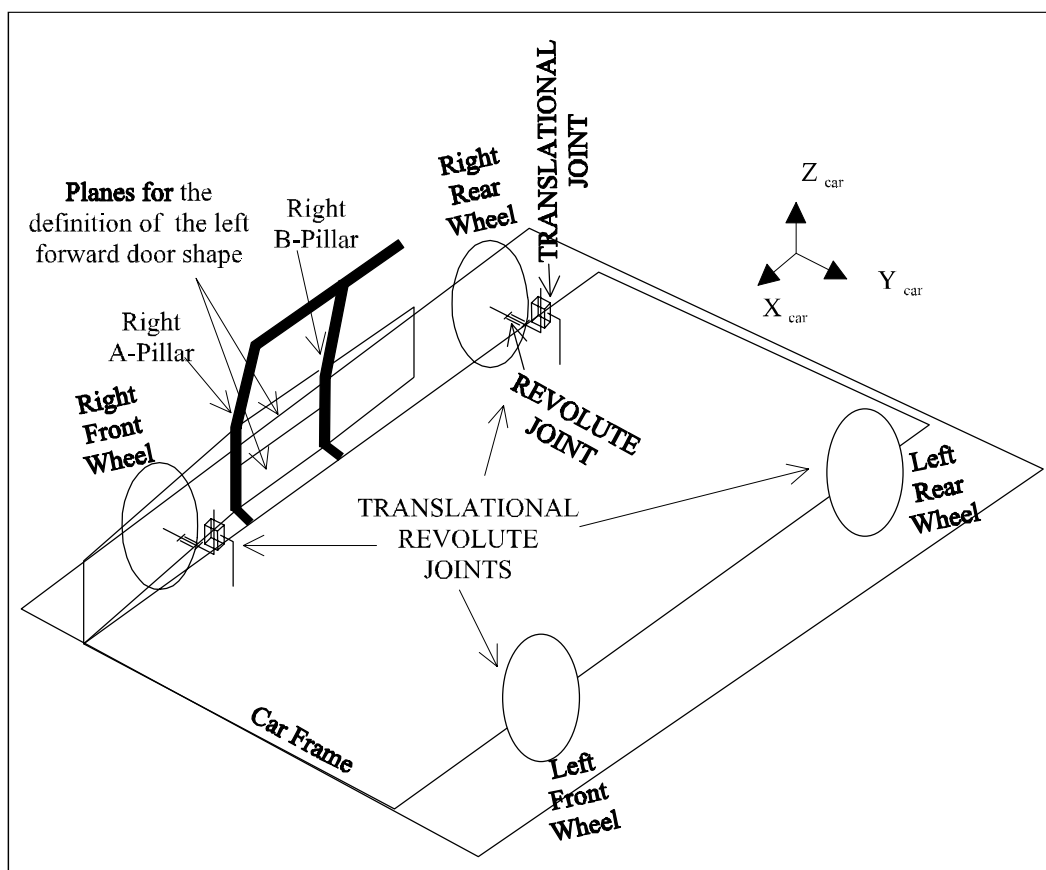


Figure 5.8. Car multibody model

Two methods were used to model the car door and its interaction with the vehicle chassis. The first one (figure 5.9), consisted of a simple representation of the car's door with two fixed planes placed on the door's frame representing the upper/lower front door and a third

plane used as the car's right front-sill. Appropriate force/deflection, damping-characteristic curves and friction coefficient values are given to the respective planes.

The second one (Model B) was designed to be more representative of the interaction and intrusion of the motorcycle into the car door structure. The door region was represented by a combination of rigid bodies interconnected by cardan and universal joints, as shown in figure 5.9. The joints were located in the areas of plastic deformation seen in the test car. The right sill was defined by six rigid bodies; the lower A-pillar by one rigid body, the lower B-pillar by two rigid bodies, the door by nine planes and the lateral reinforcing beam by three rigid bodies. The geometries of the beams' structures at these joint locations are identified from a Mondeo car frame, figures 5.10 and 5.11.

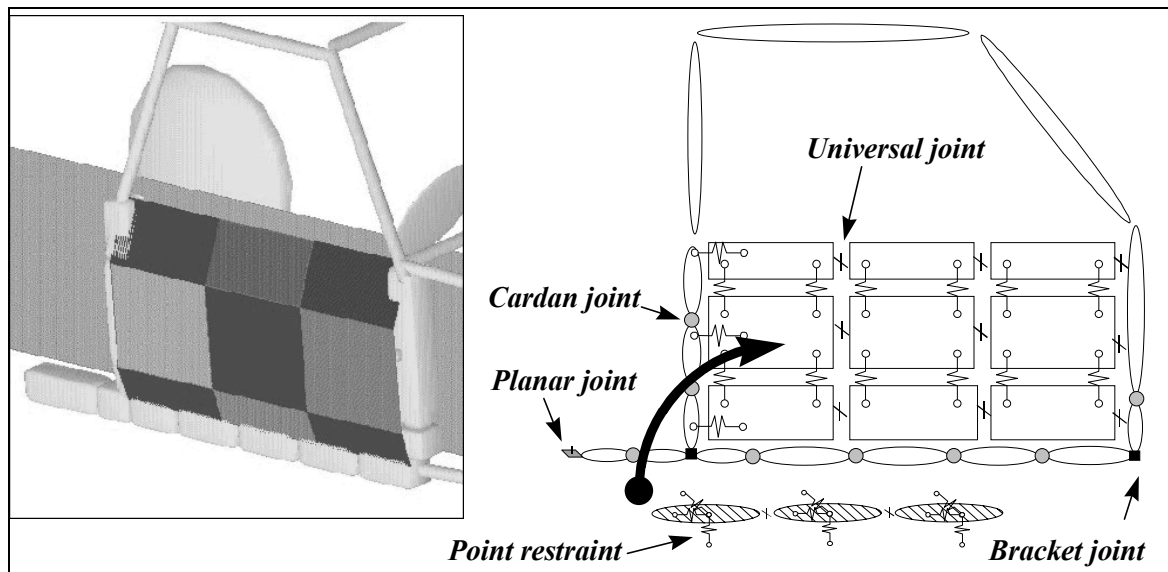


Figure 5.9. Multi-body discretisation of the right-forward door structure



Figure 5.10. Identification of beams' sections from a Mondeo car frame

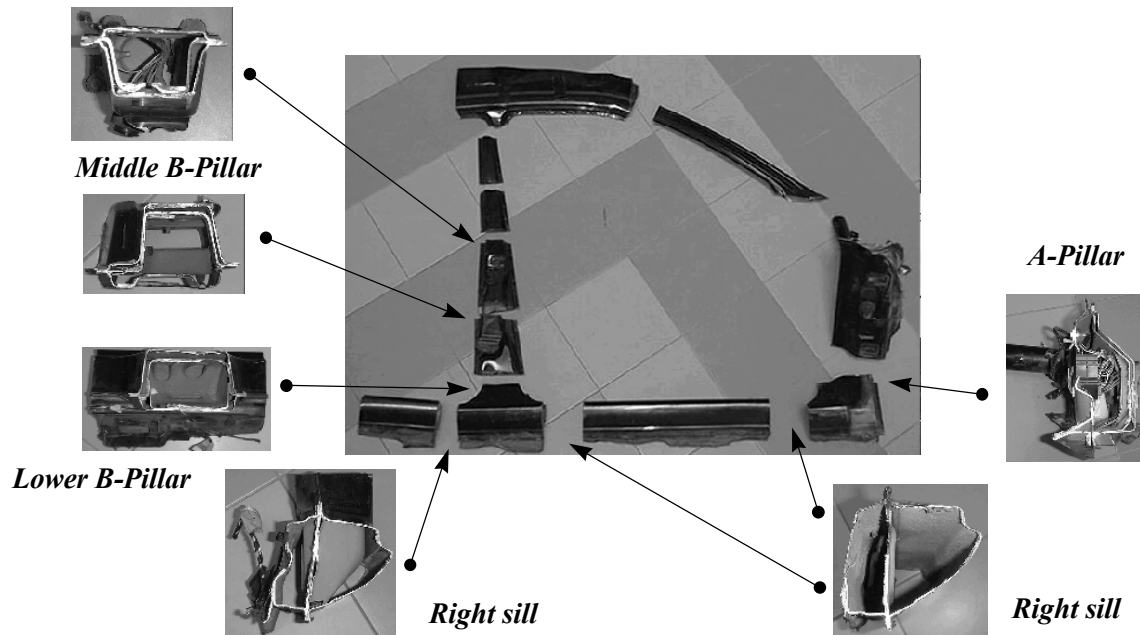


Figure 5.11. Respective geometries of the beams' sections

Approximate masses of the rigid bodies were obtained by cutting through the door frame structure and the corresponding moments of inertia calculated. Tensile tests were performed to identify the mechanical characteristics of the door material and surrounding structure. The beam sections, together with the material data, were implemented in PAM-SBE™ software where corresponding torque/angle values were calculated for the joints' characteristics, figure 5.12.

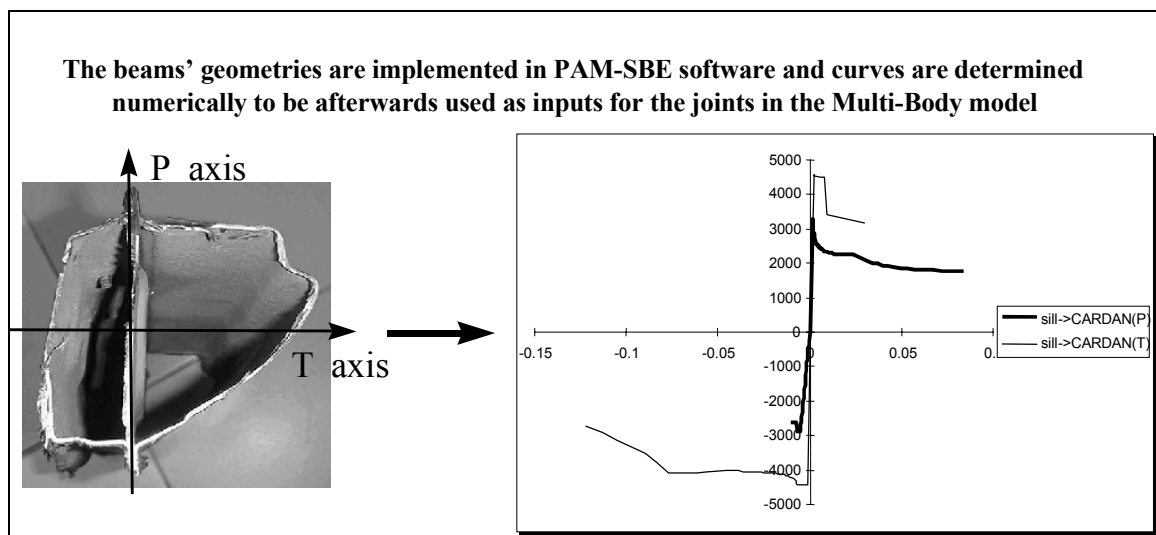


Figure 5.12. Determination of *Torque/Angle* characteristic curves

The mass of the car as a whole, unladen, was measured to be 1250kg. The moment of inertia was calculated with the formula of Burg and the Steffan method [Macinnis 1997]. The moments of inertia about the three axes of the car model were also calculated and the height and fore-aft centre were determined experimentally. The centre of gravity was measured 429mm above ground and 1.92m behind the front bumper and 12mm to the right of the car's centre-line when viewed from the rear of the car.

The car's suspension stiffness was determined quasi-statically for the front and rear struts by using a hydraulic press. These characteristic values are used to define the suspension behaviour modelled by four Kelvin elements, where an initial compression has been added. The damping for the downward and upward motions of the suspension system was arbitrarily defined.

5.2.5. The rider

A 50th percentile Hybrid III was used as the dummy model. The dummy's properties were taken from MADYMO database (TNO, 1997). The properties included joint stiffness, body segment dimensions, segment mass and associated moments of inertia. The mechanical properties of the dummy flesh effect the resulting motion of the dummy during impact. The non-standard sections of the dummy were given non-linear, velocity and deflection related stiffnesses and damping characteristics obtained from dynamic tests performed by the TRL.

It should be noted that the dummy used in the TRL motorcycle test was an MATD II which differs from the standard Hybrid III in several ways, the most important of which is the neck, which has a modified torsional response, and the legs, which are frangible.

The characteristics of the helmet and head were measured. These included the mass and moment of inertia of a dummy head, Bieffe helmet and neck and a force deflection curve to define the helmet material characteristics. The following figures provide the force displacement curve and the damping force curve used for the helmet characteristics.

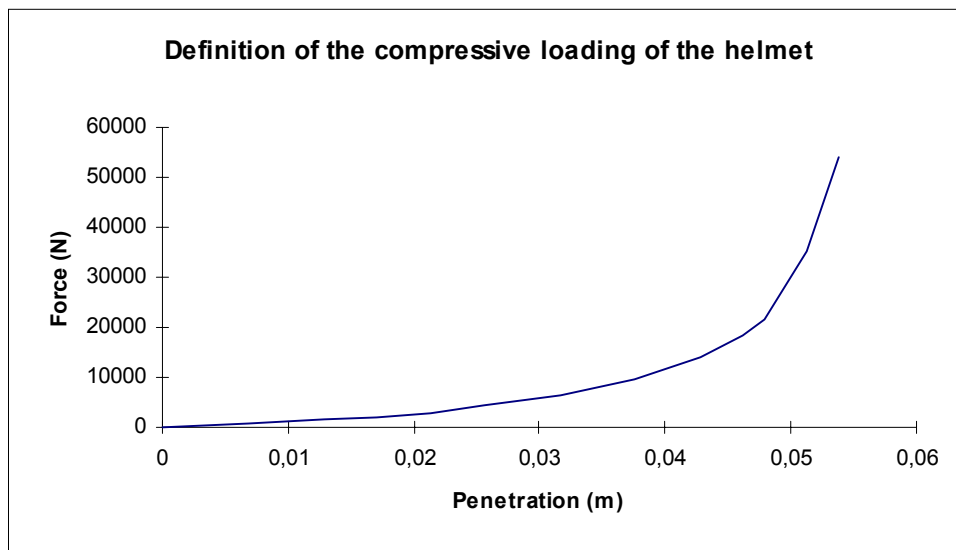


Figure 5.13. Helmet contact rigidity

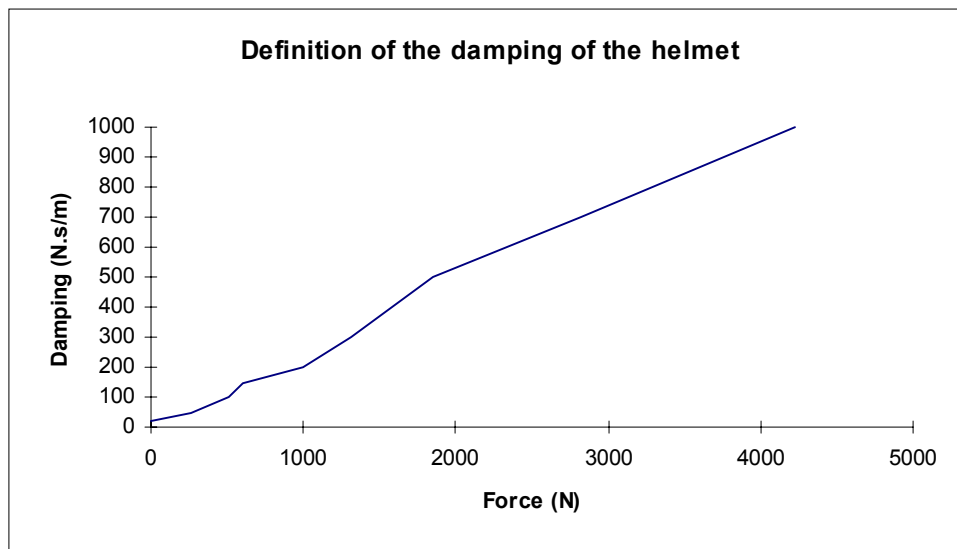


Figure 5.14. Helmet contact damping

5.2.6. Contact points

Contact points were assigned to the existing and possible dummy/motorcycle, motorcycle/target-vehicle and dummy/target-vehicle interactions as deduced from observation and analysis of the track test results. The ellipsoids, cylinders and planes, used to define the body elements of the system, were given non-linear velocity and deformation related stiffness and damping characteristics. These were derived from data obtained mainly from dynamic and quasi-static tests performed at the Transport Research Laboratory. There is a paucity of reliable damping data and so damping values were slightly adjusted so that motion from film analysis could be replicated. Adjustments were within 5% to 10 % of the energy absorbed by the compressed spring. Quasi-static tests were applied to some parts of the motorcycle to measure the force displacement characteristics. Appropriate friction coefficient values were given to the contacts depending on the interacting surface characteristics. The values were fine-tuned based on their simulation performance.

In a frontal impact, the first part of the motorcycle fairing to contact the target vehicle is the front wheel and the headlight area. The contact points between the dummy and the motorcycle are the pelvis into the rear of the petrol tank, the knees into both the side of the tank and the fairing immediately forward of the knees. Specific attention was paid to these contact points which were judged to be crucial in the resulting system's kinematics. It is of particular importance since they form part of the dummy's action of pitching. Furthermore, a careful positioning of the dummy's lower torso on the motorcycle seat was necessary to ensure that the motorcycle transmitted the vertical acceleration to the dummy realistically. The rider's knees/motorcycle's fairings force-deflection values have been closely verified and in some cases characteristic values given by Kaleps et al. (1988) have been used. Again a parametric study was needed to evaluate the model.

A third model (Model C), based on Model B (with partitioned door), was created whereby the dummy was coupled to the motorcycle to become one system. This model was necessary because, in earlier models, the dummy lower torso became incorrectly positioned on the motorcycle seat prior to impact. This was caused by abnormal oscillations of the dummy during the period up to impact point. Correct positioning of the dummy at impact point was essential for the dummy to receive the correct upward impulse

that, in turn, determined the kinematics of the flight of the dummy. The correct impulse was obtained by coupling the dummy's lower torso to the motorcycle using a breaking kinematic joint, which was activated during the simulation.

The model was validated against a full-scale impact test and the impact conditions were established through video analysis and test results. A linear velocity of 13.89 m/s, a 12.5° roll angle and an angular rotation of 2.0rad/s were established and imposed on the motorcycle model and the car was defined to be stationary. The complete model is given in the following figure.

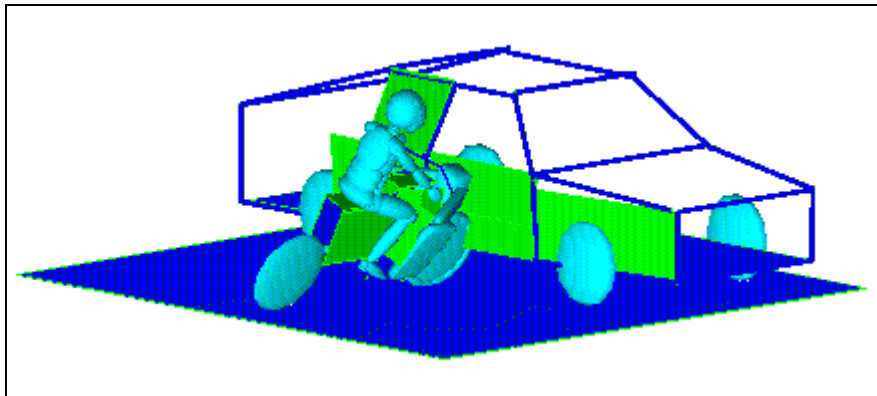


Figure 5.15. Whole multibody model

5.2.7. Neck models

In order to understand the body mass effect on the acceleration experienced by the head and the damage sustained by the helmet, two simulations with two numerical models of the neck are performed.

A two-pivot neck model has been implemented on the standard Hybrid III model of the MADYMO database. The stiffness of the Hybrid III neck depends on the bending direction. For large bending angles, the bending stiffness is substantially non-linear. To account for this, a direction-dependent non-linear bending stiffness was defined for the neck. Three flexion-torsion restraints were implemented, representing forward bending, lateral bending and rearward bending, respectively.

A neck model, specially developed to study the head/neck kinematics during low-severity rear-end collisions, has been inserted into the standard Hybrid III database. The neck consists of seven rigid segments representing the human cervical vertebrae C1 through C7. Between the rigid vertebrae, the neck incorporates soft elements representing the intervertebral disks. This design enables a trajectory and angular range of motion in the sagittal plane similar of the 50th percentile male human neck in extension. Both geometrical representation of these models can be seen in the following figure.

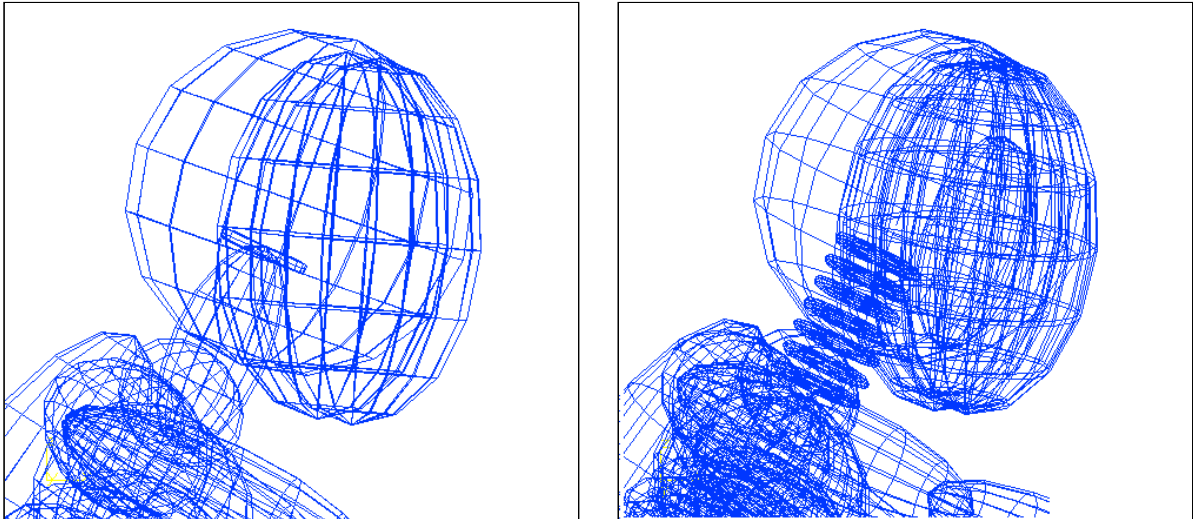


Figure 5.16. Neck models

Each neck model was used in an otherwise identical simulation to examine the differences between the two types of neck and the results are given below. Similar head linear resultant accelerations were observed but some differences in the rotational resultant acceleration can be seen. Currently it is not possible to draw conclusions as to the influence of the neck. The final objective of these two simulations is to identify the influence of effective body mass on the head kinematics. However, this was not possible within the time available.

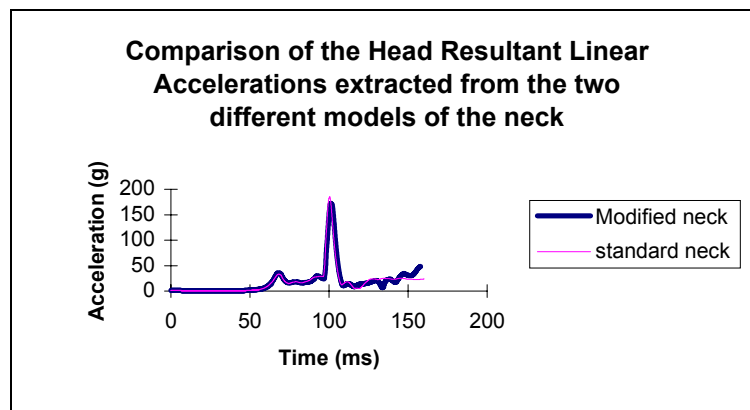


Figure 5.17. Head linear accelerations

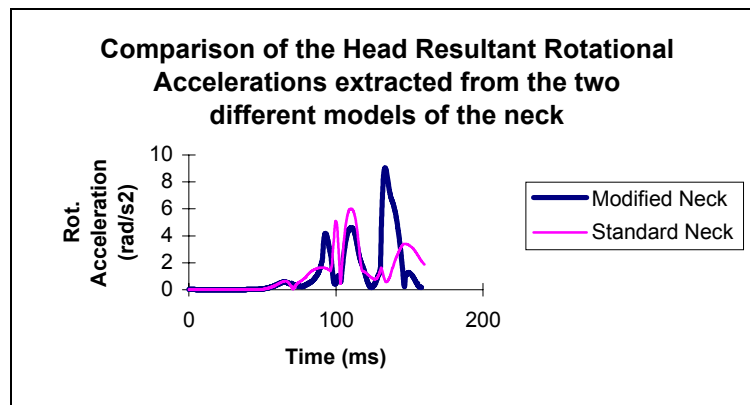


Figure 5.18. Head Rotational Accelerations

5.2.8. Results and discussion

The kinematics of the simulation can be seen in figures 5.22 and 5.23. First, the motorcycle front wheel impacted the car's right sill and the lower plane of the car's front door. The motorcycle pitched forward and the dummy femurs struck the petrol tank when the knees contacted the leg protectors. The dummy was then thrown up the motorcycle. The helmet impacted and slid across the A-pillar. At the end of the impact the car moved away from the motorcycle and, consequently, the door of the car recovered elastically and relaxes. As a rule, the motorcycle kinematics are similar but the main differences occurred when the dummy separated from the motorcycle.

For all three models (A, B & C), the deceleration of the motorcycle during the first 20ms of impact, the peak obtained for the dummy head linear acceleration and the motorcycle/car interaction kinematics closely correlated with track test data, figures 5.19 and 5.20.

Differences were noted in the rotational acceleration of the dummy's head figure 5.21. This was due to differences in the dummy's kinematics during impact. In the full-scale track test the head impacted the A-Pillar when the plane of dummy's back was almost horizontal. In the numerical models proposed, the back rotated out of position and was more upright, figure 5.22 and 5.23. The difference was shown to be due to the interaction of the dummy's lower-torso with the motorcycle's seat.

In the first two models, the dummy was initially positioned correctly on the seat (with a seat load of about 500N) but oscillated out of the stable position directly influencing the dummy's pitching mechanism. Model C eliminated this abnormal and undesired oscillating effect by linking the dummy's lower-torso to the motorcycle seat. A breaking joint was used and was activated with a positive increase in the Z-acceleration of the dummy's lower-torso. In this way, the lower-torso followed the induced Z-acceleration of the motorcycle's pitch before activating the breaking joint. However, the release mechanism produced an abrupt discontinuity in the lower-torso's Z-acceleration, figure 5.24. This again influenced the dummy's pitching motion and must be further modified to correct the disagreement.

To understand the difference in the timing of significant events, the full-scale test film was analysed and the time of events calculated. The results clearly show a good correlation to the simulation timing. For example, the period between the first contact and that between the head and the A-pillar was 105 to 110ms which was the same as for the simulation.

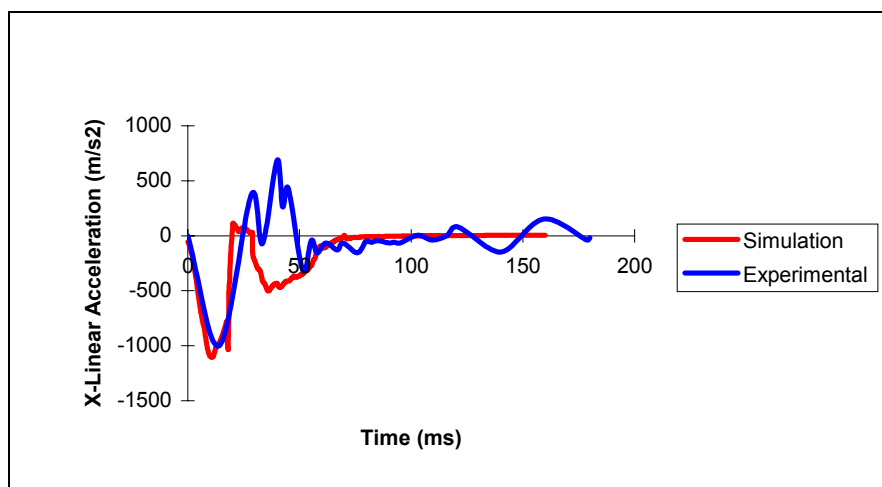


Figure 5.19. Front wheel linear acceleration

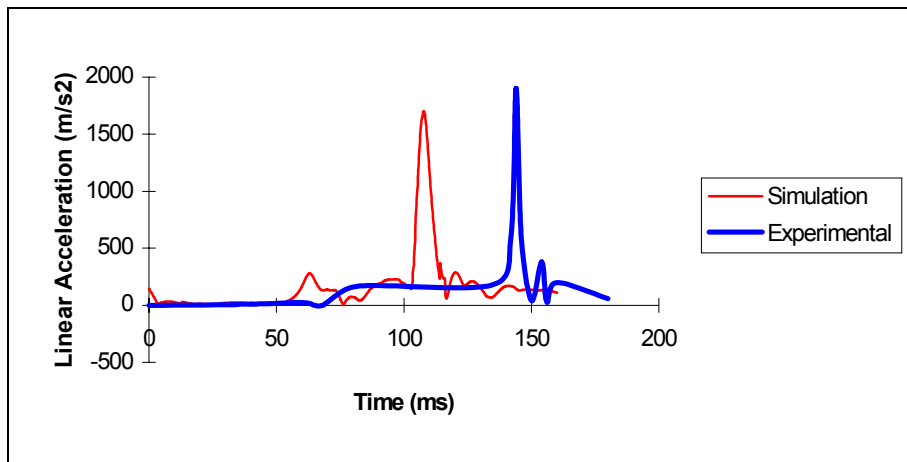


Figure 5.20. Head resultant linear acceleration

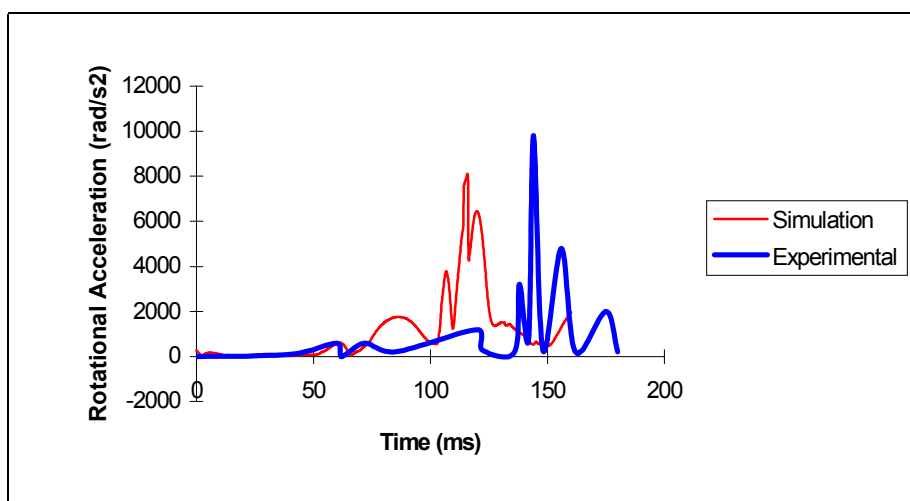


Figure 5.21. Head resultant rotational acceleration

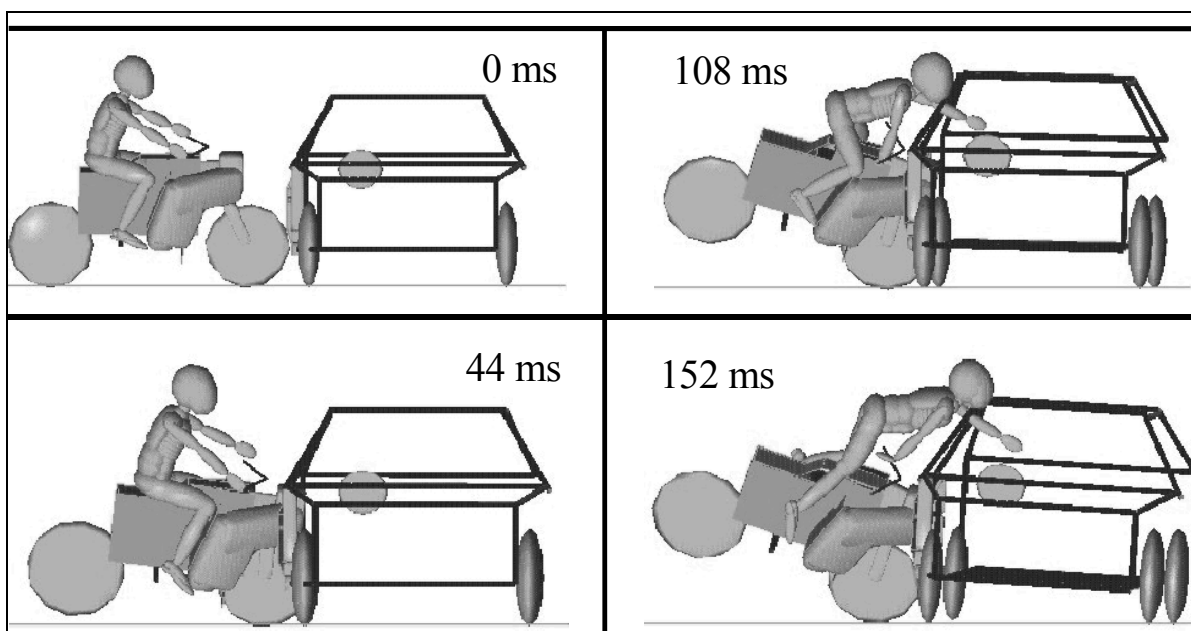


Figure 5.22. Crash simulation kinematics

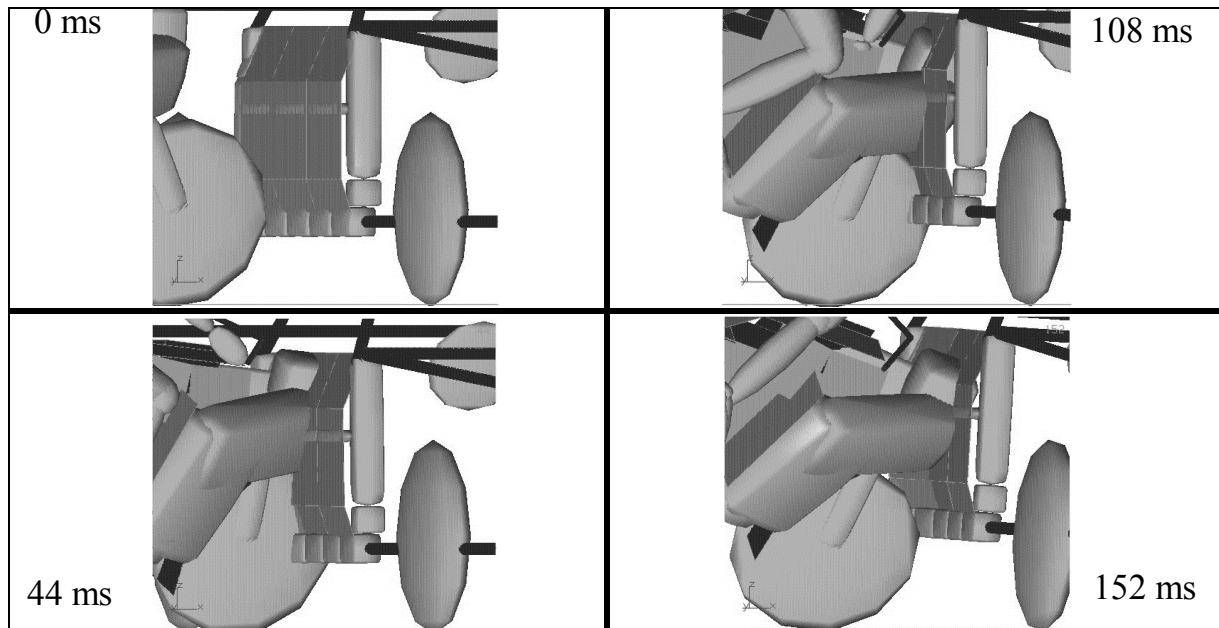


Figure 5.23. Crash simulation kinematics (perspective view)

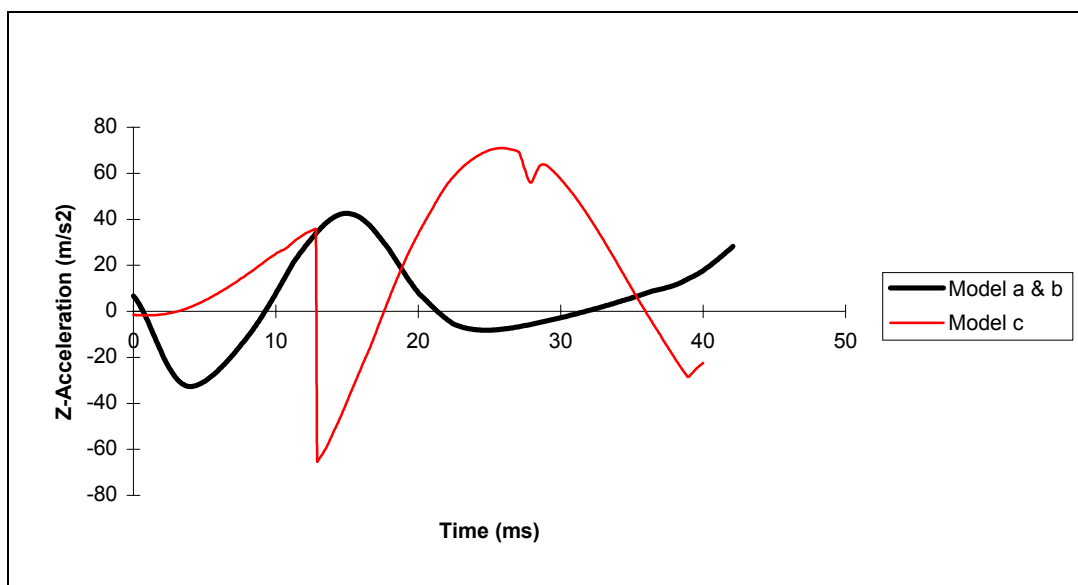


Figure 5.24. Z-Direction acceleration of lower torso

5.3. COMPUTER SIMULATION OF ACCIDENTS

5.3.1. Selection of cases

As has been described in the previous section, the computer model was calibrated against a full-scale impact of a motorcycle travelling at 50km/h and at 90° into the side of a stationary car. It was, therefore, necessary to select accidents that approximated to this configuration and for which sufficient general accident and injury data was available to ensure that the results were likely to be a true representation of the accident.

On this basis, G327, H14.057, G325 G411, H16.226, were selected and simulation conclusions for each of these are given below. Reasons for the lack of success of the other cases are also explained.

5.3.2. Simulation of cases

5.3.2.1 G327

This was an accident where a motorcycle collided with the rear of a stationary van at 20km/h. The rider sustained only minor leg abrasions from contact with the road.

The results for the force between the head and the target impacted by the head (rear of van) are given in figure 5.25 and the time histories for the resultant angular and linear accelerations are given in figures 5.26 and 5.27 below. Six frames of animation, taken from the simulation, are given in figure 5.33 at the end of the section. The peak linear acceleration, 70g, was a little lower than that measured in the helmet damage replication tests, 107g, whereas the rotational acceleration, 8000 rad/s/s, for the simulation was somewhat greater than the 5026 rad/s/s measured in the helmet damage replication tests. However, the simulation showed a very sharp peak in the time history that, if filtered, may have led to a lower value. HIC agreed more closely, 298 for the simulation and 248 for the replication test.

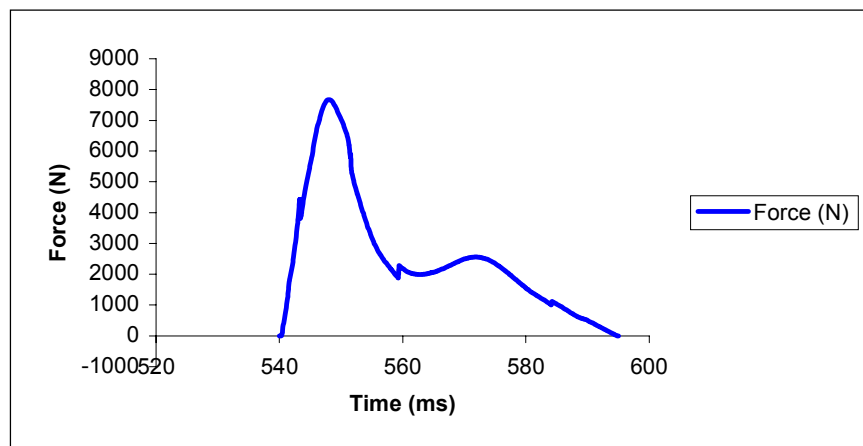


Figure 5.25. Impact forces generated on the dummy's head.

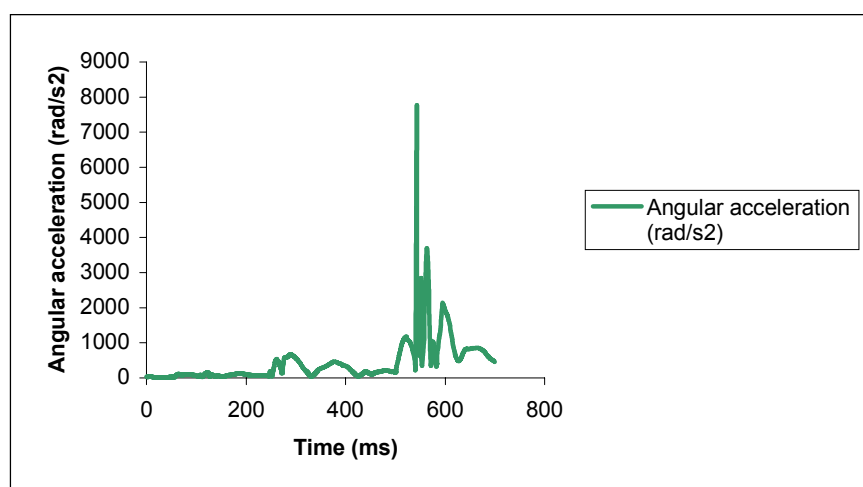


Figure 5.26. Resultant angular acceleration generated on the dummy's head.

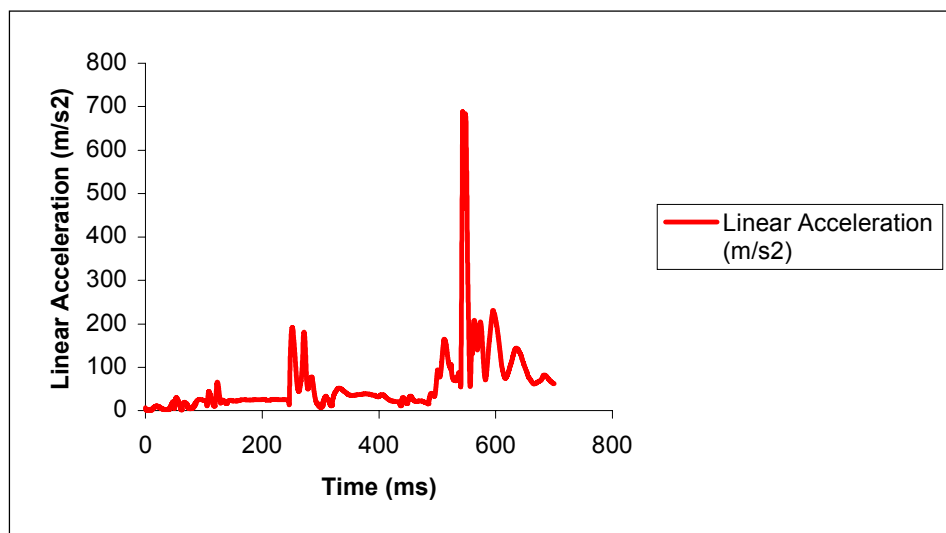


Figure 5.27. Resultant linear acceleration generated on the dummy's head.

See figure 5.33 for the simulation animation.

5.3.2.2 Case H14.057

A motorcyclist travelling at 48km/h impacted the rear of a goods vehicle travelling at 16km/h and at an angle of about 30°. These conditions were simulated although the stiffness for the rear of the goods vehicle was estimated.

The results are given below in figures 5.28, 5.29 and 5.30 and the simulation animation is given in figure 5.34 at the end of the section. The motorcyclist sustained concussion equivalent to AIS 3 which is entirely consistent with the damage replication measurements of 184g peak linear acceleration, 11,000 rad/s² peak rotational acceleration and 1227 HIC. However, the simulation gave 19g, 1000 rad/s² and 14 HIC, substantially lower values and not consistent with the injuries.

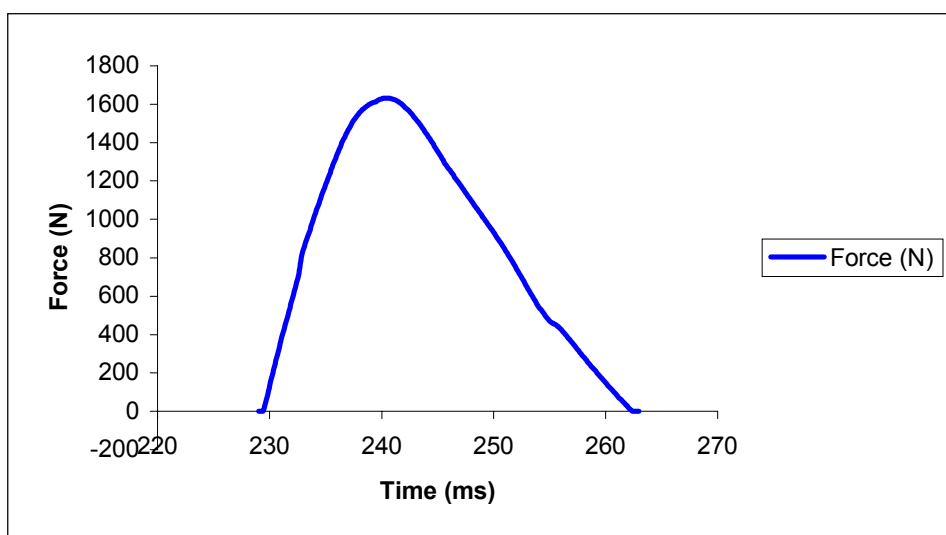


Figure 5.28. Impact forces generated on the dummy's head.

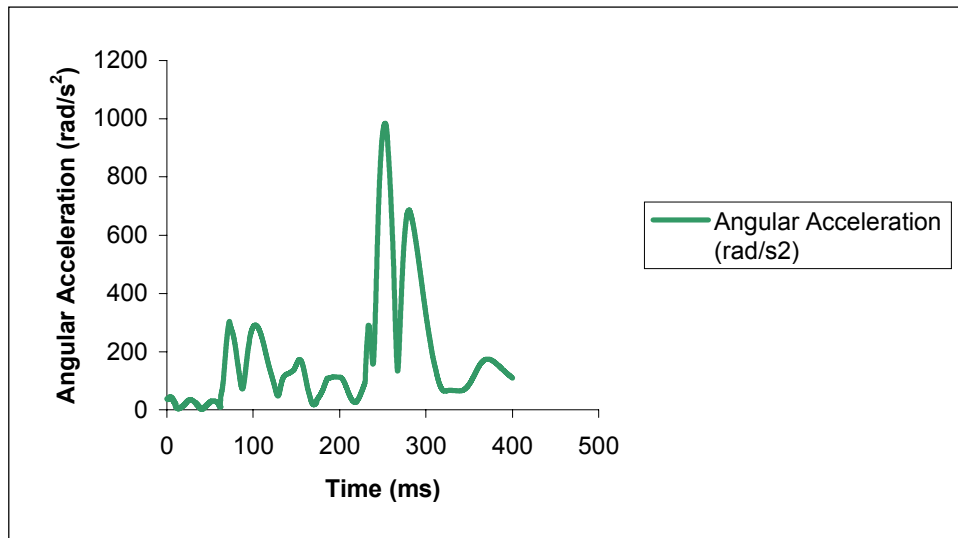


Figure 5.29. Resultant angular acceleration generated on the dummy's head.

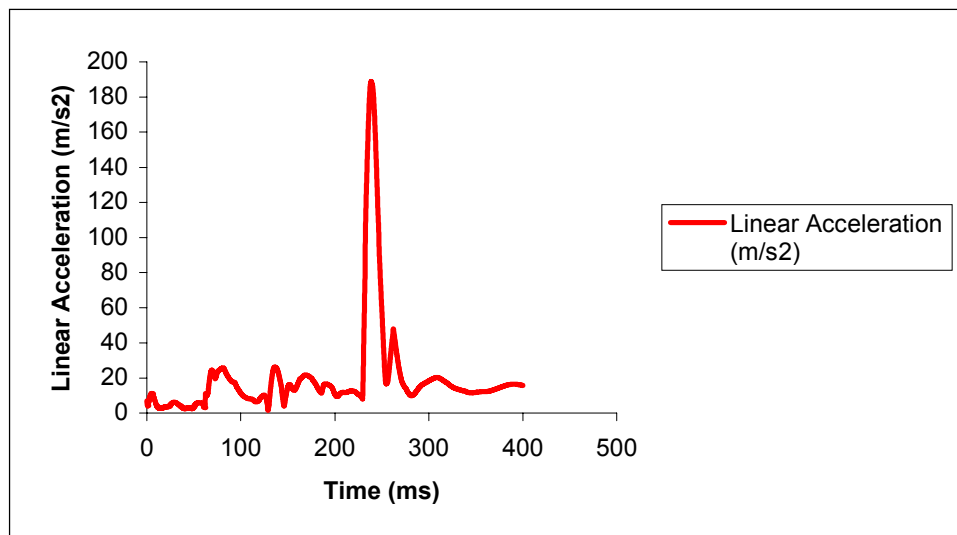


Figure 5.30. Resultant linear acceleration generated on the dummy's head.

5.3.2.4 Case G325

A small motorcycle travelling at 8km/h emerged from a side road into the path of a larger motorcycle travelling at 88km/h. This accident was simulated because it represented an unusual case, however, both motorcycles were necessarily given the same characteristics so the results should be viewed with caution. Nevertheless, the peak linear acceleration at 58g and the peak rotational acceleration at 2,2000 rad/s^2 compare favourably with those of the replication tests which were 118g and 3735 rad/s^2 for the rider emerging from the side road.

The simulation results are given below in figures 5.31 and 5.32 and the animation is given in figure 5.35.

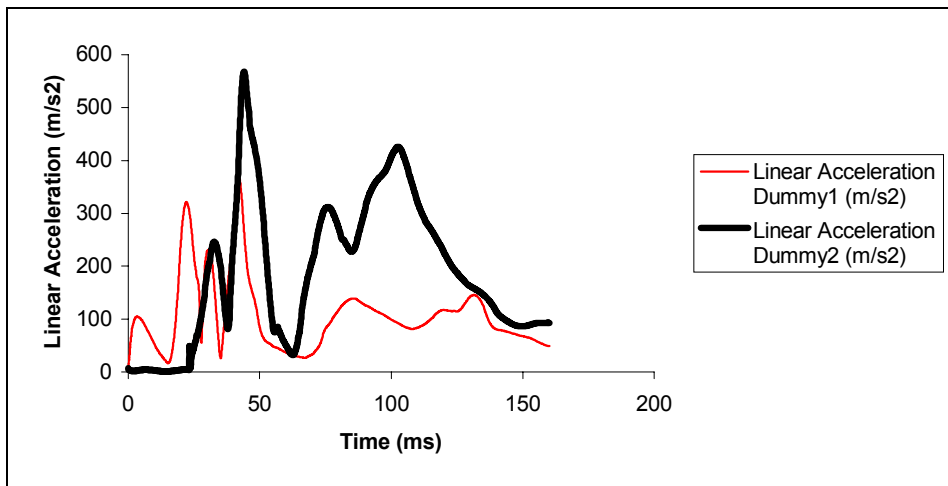


Figure 5.31. Resultant linear acceleration generated on the dummy's head.

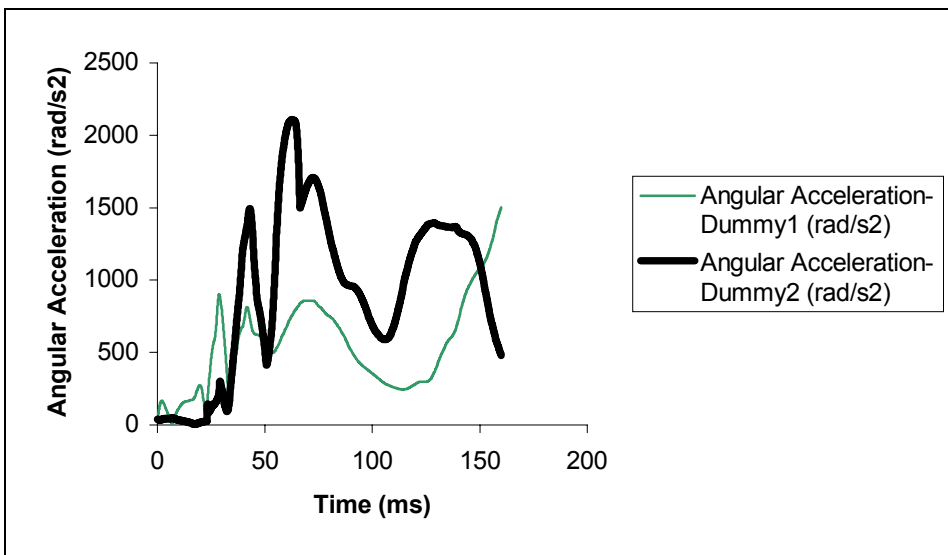


Figure 5.32. Resultant angular acceleration generated on the dummy's head.

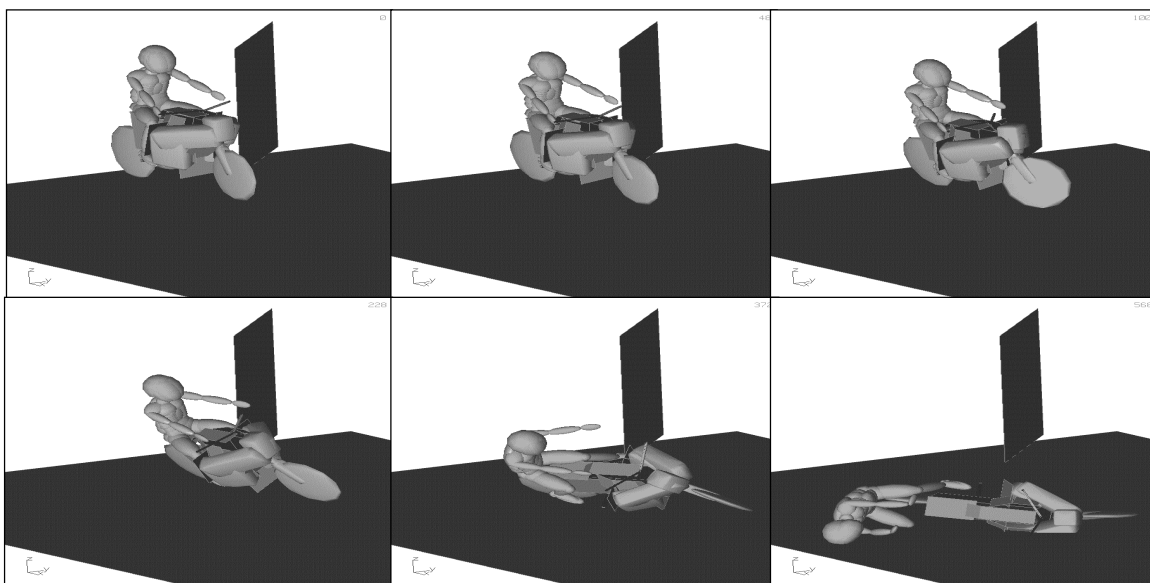


Figure 5.33. Simulation of case G327

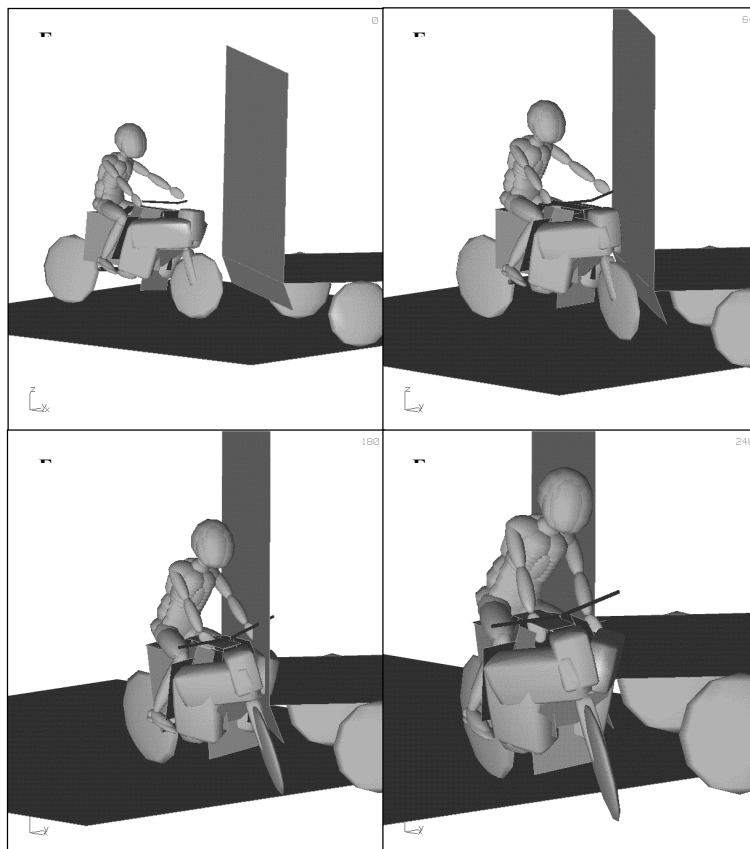


Figure 5.34. Simulation of Case H14057

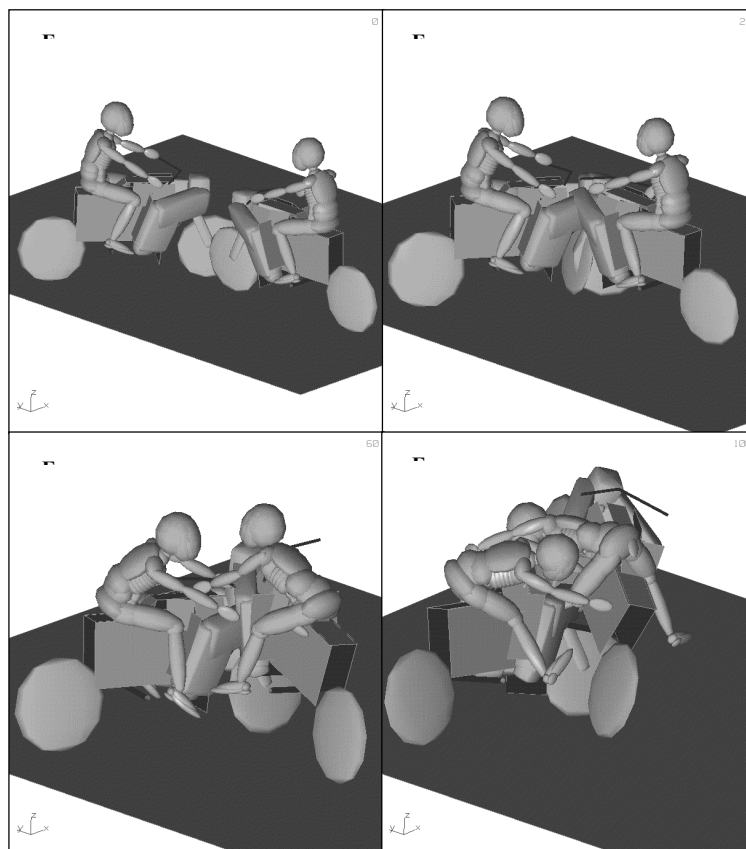


Figure 5.35. Simulation of Case G325

5.3.3. Discussion

The computer model has been successfully used to simulate accidents of the type similar to the configuration of the full-scale impact test against which the model was validated. However, accidents occur to a wide range of motorcycles in a wide range of circumstances and it is difficult to obtain information to validate the model for use across the range. Nevertheless, the model that has been developed is a sophisticated tool and there is extensive motorcycle impact test data available. Thus it is reasonable to assume that, with more research, the model could be validated against this data and a wide variety of motorcycle accident configurations and mechanisms could be investigated.

5.4. REPLICATION OF ACCIDENT HELMET DAMAGE

5.4.1. Introduction

It is believed that an increased understanding of the complex relationship between head accelerations and brain injuries sustained during head impacts could help to improve the design of safety helmets and other secondary safety systems.

Although much work is being done to model the brain during impact conditions using computational techniques, the data can only be meaningful if the dynamics of typical head impacts are known. In addition, modelling techniques must be validated with experimental data to ensure the model's accuracy.

The aim of this work was to replicate head impacts sustained during real motorcycle accidents while measuring the dynamics of the head. In this way, it is possible to correlate the documented head injuries with the associated instrumentation data.

Essentially, there were four phases to this work:

1. Compile a database to include: accident profiles, casualty injuries and helmet damage
2. Select accident cases that are appropriate for replication
3. Replicate helmet damage in the laboratory
4. Process and analyse the instrumentation data

A full scale crash test, 10P, which incorporated a Hybrid III dummy riding a GPZ 500 motorcycle into the side of a Ford Mondeo car has been replicated by the drop test method. This test is summarised at the end of this chapter.

Additionally, some cases from Hannover, were judged suitable for replication but, unfortunately, the helmets were not available. However, detailed photographs of the accident helmet were provided and it was thus decided to try and estimate the likely measurements by comparing the damage in the photographs with the damage to the accident helmets that were replicated.

5.4.2 Accident databases

5.4.2.1 Accident reports

TRL collaborates with the Southern General Hospital Neuropathology Department, Strathclyde Police Traffic Department and the Vehicle Inspectorate at Bishopriggs, to provide reports of accidents involving motorcycles. A report includes a full accident description and information regarding vehicle damage. Each report is allocated a unique case number.

The accident description details initial vehicle velocities, trajectories and relevant contact points. In addition, the final positions of the vehicles and occupants are documented. Such detail is essential to appreciate the sequence of events and the nature of the impact that is to be replicated.

5.4.2.2 Occupant injury forms

Injury information was supplied by Glasgow's Southern General Hospital, chosen because it is one of the world's leading head injury hospitals. It is sited within the Strathclyde region, which is very large geographically and provides a wide range of road conditions.

The occupant injury forms were linked to the correct accident data by means of the case number. A standard format was used that began by recording the physical attributes of the casualty, including height, weight and age. Any long term illnesses or complication resulting directly from the injuries sustained were also described together with the level of consciousness on admission, using the Glasgow Coma Scale.

Most of the form was used to record each of the casualty's injuries using the Abbreviated Injury Scale (AIS). For example, diffuse subdural haemorrhage corresponds to the AIS code 140650-4. The last digit is an indication of the injury severity ranging from 1 (minor) to 6 (currently untreatable).

The scale does not assess the consequences of injuries and does not indicate the combined effects for multiple-injury cases. For this reason, the scale cannot simply be used to measure the threat to life for any single injury although it has been shown to correlate well with the threat to life for more serious cases (AIS >3).

5.4.2.3 Helmet damage

Each accident report included a description of damage to motorcycle helmets. Detail included both cosmetic and structural damage and an indication of impact sites. The accident helmet was also supplied, which enabled TRL to conduct a more thorough analysis of the damage.

5.4.3. Selection process

TRL prepared a summary of each accident to help with the selection of suitable replications. Each summary includes the accident description, associated helmet damage and details of any head injuries sustained.

An assessment of the suitability for replication was usually made using this summary although a closer examination of the accident helmet was often required. The assessment was based on three main factors:

1. Severity and type of head injury - it is important to choose cases for replication, which have a range of head injuries.
2. Accident kinematics - it is important that the helmet impact can be replicated within the laboratory.
3. Helmet damage - damage to the helmet must be replicated in the laboratory and is related to the nature of the impact. For example, a long abrasion due to the helmet sliding along a road cannot be replicated by a single impact.

5.4.4. Experimental method

5.4.4.1 Procedure

TRL replicated the helmet damage using a purpose-built helmet drop test facility. The method allowed impact parameters - including impact speeds, angles and targets, to be controlled and quantified. By inspection of the helmet, it was possible to modify the impact parameters until the desired damage was produced.

Instrumentation was used to measure the dynamics of the impact and ultimately enabled the accelerations, likely to have been experienced by the accident casualty, to be estimated.

Analysis of the damage to the shell and liner was used to identify kinematics of the impact. Surface scratches, scuffs and paint chips often relate to the impact speed, angle and target shape. The accuracy of the replication was judged by comparing the replicated damage with the accident damage.

The test helmet was an identical make and model to the accident helmet to ensure similar performance during the impact. When this was not possible, a similar helmet was used.

5.4.4.2 The TRL helmet impact test facility

5.4.4.2.1 Drop test rig

TRL replicated helmet damage using the drop test method whereby the impact velocity was controlled by the drop height. This facility has a maximum drop height of 13m allowing a maximum impact speed of approximately 16m/s (almost 60km/h). The facility includes a guidance system to control the impact position.

5.4.4.2.2 Instrumentation and acquisition

An instrumented headform was fitted inside the test helmet during the impact. This enabled measurement of linear and rotational accelerations. A load cell was fitted to the impact anvil to measure normal and tangential forces. Data was acquired using digital recorders at the rate of 100,000 samples per second. All instrumentation conforms to SAE J211. A helmet impact produced, typically, 50ms of data.

5.4.4.2.3 Instrumented headform

Rotational acceleration is believed to contribute to brain injuries. Current BS and Snell standards are not required to measure rotational acceleration and require only a single accelerometer to measure linear acceleration along a single impact axis. In order to quantify rotational and linear accelerations TRL has modified a Hybrid II dummy headform to include a nine accelerometer array. This allowed linear and rotational acceleration to be measured in three axes.

The headform, consisting of a metal skull with flesh like skin, is well suited to this work because the rubber skin tends to fit helmets well and is able to transmit impact forces (particularly rotational) without any significant slippage between headform and the helmet. In addition, the headform has a full chin structure making it easily secured inside a test helmet.

5.4.4.2.4 Instrumented load cell

A tri-axial load cell with a platen area of 260mm x 260mm was used to measure impact loads at the anvil. The load cell has a natural frequency of 1500Hz. There is provision to fit the load cell to an angled anvil as well as to fit various target materials to the platen.

5.4.4.2.5 Anvil and targets

In order to replicate road surface impacts, various textured slabs were typically used. For other, profiled surfaces some standard drop test targets were found suitable. Standard targets available to TRL include:

- Hemisphere - 50mm.radius (BSI 6658:1985)
- Kerbstone - 125mm in length, angle of 105 (ECE regulation)
- Bar - 50mm diameter, 200mm length (SNELL SA-95)
- Steel edge - 180mm by 6.3mm (SNELL SA -95)

If the accident involved an impact onto a part of a car then the appropriate part of the car was used as the target. For example a wheel and a car door were used.

The impact very seldom occurs at 90° (perpendicular) and to enable the impacts to be at different angles, TRL constructed a range of anvils at angles of 15°, 30°, 45°, 60°, 75° and 90° to the vertical. The load transducer was fitted to the surface of these anvils.

5.4.5. Analysis and processing of results

5.4.5.1 *Helmet damage*

Analysis of helmet damage involved inspection of the exterior damage to the shell surface and interior damage to the liner. Direct measurement of the residual liner deformation, crack length, intrusion depth and the area of material loss, quantified the damage.

It was found that the exterior damage to the shell indicated the type and profile of the target whereas the severity of damage to the liner and shell structure indicated the impact angle and speed. It was, therefore, essential that the replicated damage was accurate in both of these aspects. For example, it was inappropriate to assume that helmet damage was accurately replicated if the shell damage was visually identical but measured liner deformation was more severe.

5.4.5.2 *Processing of instrumentation data*

Instrumentation data must be processed for it to become entirely meaningful. TRL uses commercially available processing software for this purpose. The processing software includes digital filters, conforming to SAE J211b channel class 1000 (1850Hz), which are used to remove noise from the data.

TRL has written specific software routines to process the data from the nine accelerometer array so that the resultant linear and rotational acceleration of the headform can be deduced.

5.4.5.3 *Co-ordinate System Convention*

5.4.5.3.1 Summary data for TRL replication studies

TRL provides a summary of the test data with each accident replication report. The summary includes the peak linear acceleration of the headform, HIC, peak rotational acceleration and rotational velocity. The co ordinate system for this data is as follows;

The impact trajectory is detailed in terms of the angle relative to the impact surface and velocity (relative between the impact surface and the helmet). The peak forces exerted on the helmet at the impact surface are detailed in terms of normal and tangential components (relative to the impact surface). The coefficient of friction is calculated, based on these results.

5.4.5.3.2 Detailed information for modelling purposes

For computer modelling purposes, the information provided in the summary was insufficient because it did not enable the impact kinematics to be defined accurately. Therefore, TRL provided the following information to the Computer Simulation Working Group.

- (i) Local co-ordinate system for the headform (x, y and z)
- (ii) Position of impact site on the helmet
- (iii) Direction of impact on the helmet (using local co-ordinate system relative to impact site)
- (iv) Local co-ordinate system for target structure (x, y and z)
- (v) Position of impact on the target structure
- (vi) Direction of impact on the target structure

5.4.6. Replication of a full scale test (10P)

The main difference between a replication test and the associated accident impact is that the latter includes the whole of the motorcyclist's body and not just an isolated head. What is not fully understood is the magnitude of the effect of body mass on the acceleration sustained by the head. For this reason it was decided to replicate a full scale crash test 10P, which incorporated a Hybrid III dummy riding a motorcycle into the side of a car, by the drop test method.

5.4.6.1 Stage 1 - Full scale impact (10P)

The test (10P) was an impact between a Kawasaki GPZ500 motorcycle travelling at 30mile/h (13.4m/s) into a stationary Ford Mondeo1.8LX hatchback car. The angle between the direction of travel of the motorcycle was perpendicular to the centre line of the car. The motorcycle impacted the front right hand side door. The test was conducted in accordance with the specifications of ISO DIS 13232.

The "rider" was a Hybrid III dummy fitted with frangible legs. Included in the dummy instrumentation was a nine-accelerometer array fitted inside the headform. The array allowed linear and rotational accelerations to be measured. High-speed cine cameras were used to film the impact. Subsequent film analysis enabled the impact angle and impact velocity of the helmeted headform to be estimated.

Examination of the helmet revealed slight shell damage with mainly surface marks. A large yellow paint mark, close to the upper edge of the visor opening, indicated the point where it struck the car. Helmet liner damage was more severe particularly at the front edge close to the visor opening where the level of residual damage suggested that it had

probably bottomed out during the impact. Two cracks in the liner running from left to right across the front of the helmet were also seen.

Damage to the top of the car door resulting from the head impact was also slight. The damage consisting of a slight dent above the door window was about 1mm depth and identified the target impact point to be used in the replication tests.

5.4.6.2 Stage 2 - Helmet damage replication

The experimental arrangement used for the replication of damage to the helmet of the full-scale test was typical of that used previously by TRL in accident replication studies.

The impact conditions of the full-scale test, 10P, were reconstructed in the laboratory as closely as possible. The type of helmet used in every test was a Bieffe B10 (size 56, small), identical to that used in the actual full-scale test. Also, the same Hybrid III headform was used in these replication tests.

To reproduce the target realistically, an undamaged section of roof rail was removed from an identical model of Ford Mondeo and used to support the top of an identical undamaged door. An original rubber seal was used between the door and frame while sandbags and wooden platforms were used at the base of the door to secure it firmly. The door frame was bolted onto a load cell which was supported by a 1000kg steel block.

The damage observed on the car indicated that the impact point between the vehicle and the helmet was at the top of the front right side door. The replication test helmet (complete with instrumented headform) was suspended above the desired impact position on the door and adjusted to the correct orientation. The angle of impact to the forehead of the helmet was determined using film analysis of the track test.

Initial drop tests were made with an impact velocity of 7.5m/s, which was the relative velocity between the head and the car at the time of impact in test 10P. Inspection of the helmets following the tests revealed that the liner damage was less severe than that which had resulted in 10P. Three further tests were therefore conducted at 10m/s and one final test at 12m/s; there were six impact tests in total with car doors being reused whenever possible.

5.4.6.3 Results

A summary of the results obtained from full-scale test 10P and 6 replication tests are given below.

Peak linear and rotational accelerations were calculated using the instrumented headform data. The HIC value was an indication of the impact severity and was calculated by analysis of the resultant linear acceleration. The peak anvil force was the maximum resultant force observed at the load cell that was used to support the door frame. Depths of indentation to the top of each door resulting from the helmeted headform impact were measured using a Vernier gauge to an accuracy of ± 0.1 mm.

Table 5.2 Summary of Results

Test	Impact velocity (m/s)	HIC	Peak resultant linear acceleration (g)	Peak resultant rotational acceleration (rad/s/s)	Peak anvil force (kN)	Door indentation (mm)
10P	7.5	254	98	14000	12.5(calculated)	1
1	7.5	1144	151	3300	3.7	1.3
2	7.5	1018	149	4300	Signal clipped	1.6
3	10	2006	229	9000	12.7	1.5
4	10	2251	219	8200	11.7	1.6
5	10	2107	204	6600	12.9	1.4
6	12	3563	275	7000	16.6	2

5.4.6.4 Findings

Permanent liner damage to helmets used in 7.5m/s replication tests was slight and did not match that of the helmet liner from 10P. Replication tests at the higher velocity of 10m/s produced damage of similar severity to that of the liner from 10P.

For equivalent levels of helmet damage, peak rotational acceleration, recorded in the full-scale test, was far greater than that in the replication tests. Conversely, the resultant linear accelerations and HIC values observed were significantly higher in the replication tests than for the full-scale test 10P.

During a full-scale impact the headform is attached to the dummy and any force acting on the head will be transmitted by the neck to the body. Resulting linear acceleration to the head will consequently be lower for the same impact force than in helmet drop tests, due to an increase in the effective mass of the headform. This can be demonstrated by force and energy considerations for the full-scale tests 10P and the 10m/s replication tests that had equivalent levels of helmet damage.

It was assumed that the same force was required to produce the same helmet damage,

$$m_e \times a = m_r \times a_r$$

where the effective mass of the helmeted dummy head in test 10P was m_e , its acceleration was a , the mass of the helmeted headform in the replication test was m_r and its acceleration a_r . Therefore;

$$m_e \times 98 = 6.5 \times 217$$

$$m_e \sim 14\text{kg}$$

Similarly, it was assumed that the same energy was required to produce the same helmet damage,

$$(m_e v_e^2)/2 = (m_r v_r^2)/2$$

$$m_e \times 7.5^2 = 6.5 \times 10^2$$

$$m_e \sim 12\text{kg}$$

The large rotational acceleration occurring in 10P can also be explained by the momentum of the dummy body, which forced the head to rotate inside the helmet. The force reaction at the impact point on the car door and the resultant neck force in the dummy act as a couple which produces a rotation of the head. In the replication drop tests, however, forces at the neck were absent and so less rotation of the head was generated.

The results of this work revealed some interesting insights into the biomechanics, which were in agreement with earlier TRL replications, which incorporated an OPAT dummy. Generally, the experiment demonstrated that helmet damage can be accurately replicated in the laboratory with good results.

The complex inertial effects of body mass acting on the head through the neck were not replicated in the laboratory and indeed it is known that the Hybrid III neck is much stiffer than a human neck. It should therefore, be noted that the differences recorded in this experiment may be greater than for a human being.

5.4.7. Analysis of Hannover and Finland accident cases

Only two helmets were available from Hannover and one from Finland and damage was replicated experimentally as described in the previous section. However, photographs of the damaged helmets were available from Hannover. These were compared with damage to helmets that were available and for which the damage had been replicated. Where the damage to the tested helmet was very close to the damage in a photograph the result was recorded for the Hannover case. However, this was attempted as an exploratory method and the results were not used in this analysis. The details are given in the Reconstruction Working Group final report.

5.5. ANALYSIS OF REPLICATION DATA

Laboratory replication of helmet damage, as described in section 5.4.7 was performed to determine the relationship between the test parameters and the injury type and severity sustained. The following were calculated from the instrumentation output:

- Resultant peak linear acceleration,
- Head Injury Criterion (HIC).
- Resultant peak rotational acceleration
- Rotational velocity
- Impact velocity
- GAMBIT

Figures 5.36, 5.37, 5.38, 5.39, 5.40 and 5.41, show the above parameters plotted against AIS for the head injury severity. It should be noted that, as may be expected, there is some scatter but the following interesting trends have emerged.

Linear acceleration: injury did not occur below 100g peak resultant linear acceleration and fatal injury occurred at values above 250g. However, injuries of AIS 5, normally considered very serious, occurred at values of approximately 200g or less.

HIC: AIS 1 to 2 usually occurred at values between 500 and 1100. AIS 5 occurred at values around 1500. Both fatal cases were at very high values of about 9000 or greater;

there was an AIS 5 at only about 200 but this was a very unusual case of a basal skull fracture that occurred on contact with a windscreen.

Rotational Acceleration: there was little evidence of injury below approximately 5000 rad/s/s, peak resultant, but a substantial risk of AIS 3 to 5 at values between 10,000 rad/s/s and 15,000 rad/s/s. An injury of AIS 1 or 2 was highly likely at values between 5000rad/s/s and 10,000 rad/s/s. Fatal injury occurred at values above 30,000rad/s/s.

Rotational Velocity: the trends were not obvious but it was clear that injury is highly likely at values above 40rad/s. Indeed there was a fatality at just below 70rad/s and evidence that injury is bound to occur at values in excess of 50rad/s.

Impact velocity: this was included to identify the velocity that is most appropriate for helmet Standards. It is clear that a value between 7m/s and 12m/s should be considered.

GAMBIT: this is a criterion developed by Newman of Biokinetics and is a formula that combines peak linear and peak rotational acceleration. The results indicate that injury tends to occur between values of 1.5 and 2. Above 2 is almost certain to be injurious but the most severe injuries, AIS 3 to 5, occurred at less than 2.

It is clear that values of the above parameters that are likely to cause injury have been identified. In particular a limit of rotational acceleration of 5,000rad/s/s should be used a basis for Standards requirements, but this should be considered in combination with a limit for rotational velocity of 40rad/s.

HIC was less well defined but the research shows that a value of 1000, as used by the automotive industry, may be appropriate. Peak linear acceleration should be less than 250g. Gambit should be considered after further analysis.

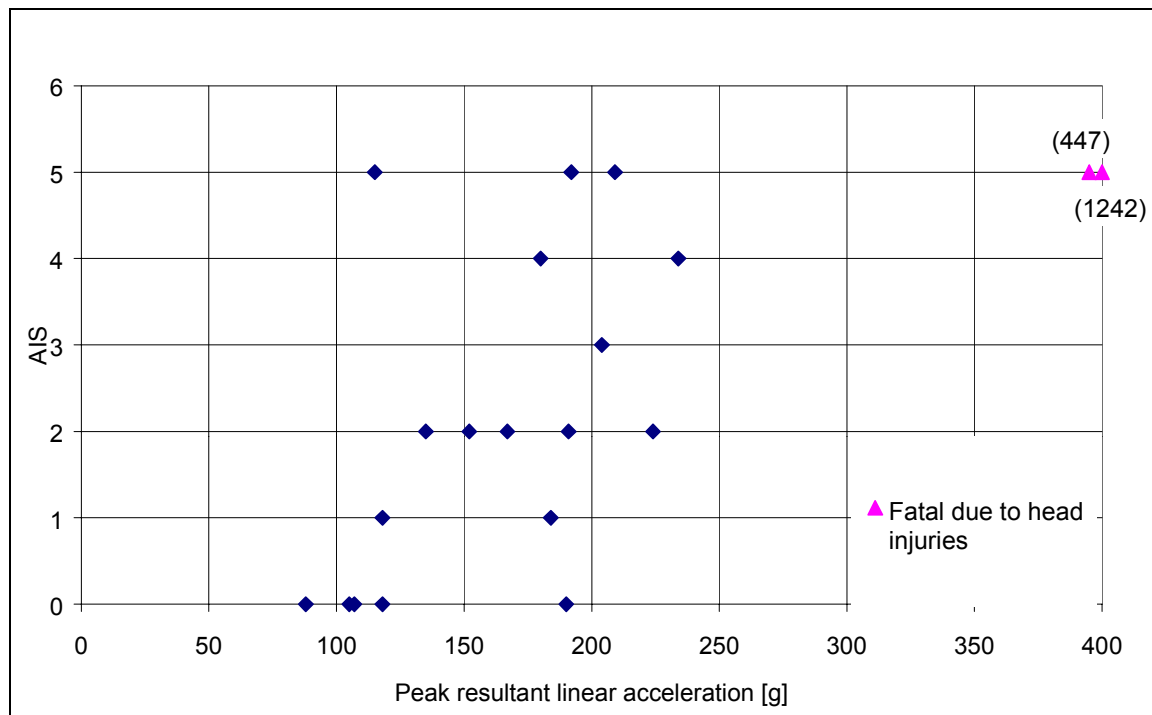


Figure 5.36. Peak resultant linear acceleration vs AIS

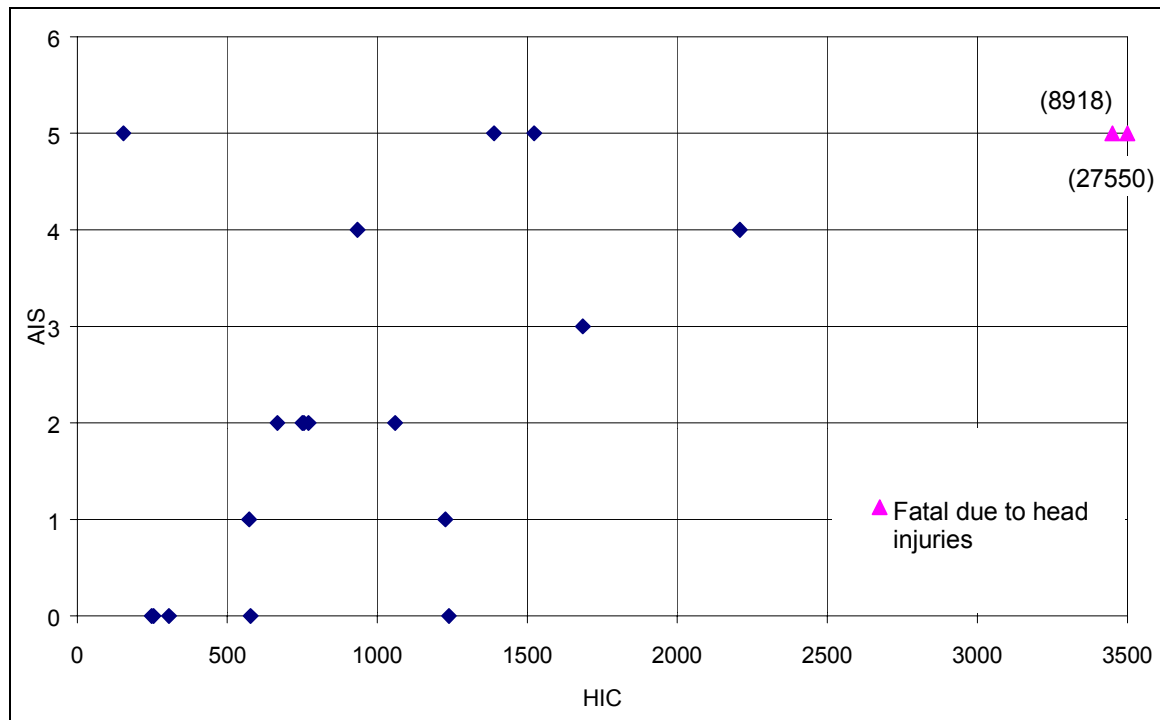


Figure 5.37. HIC vs AIS

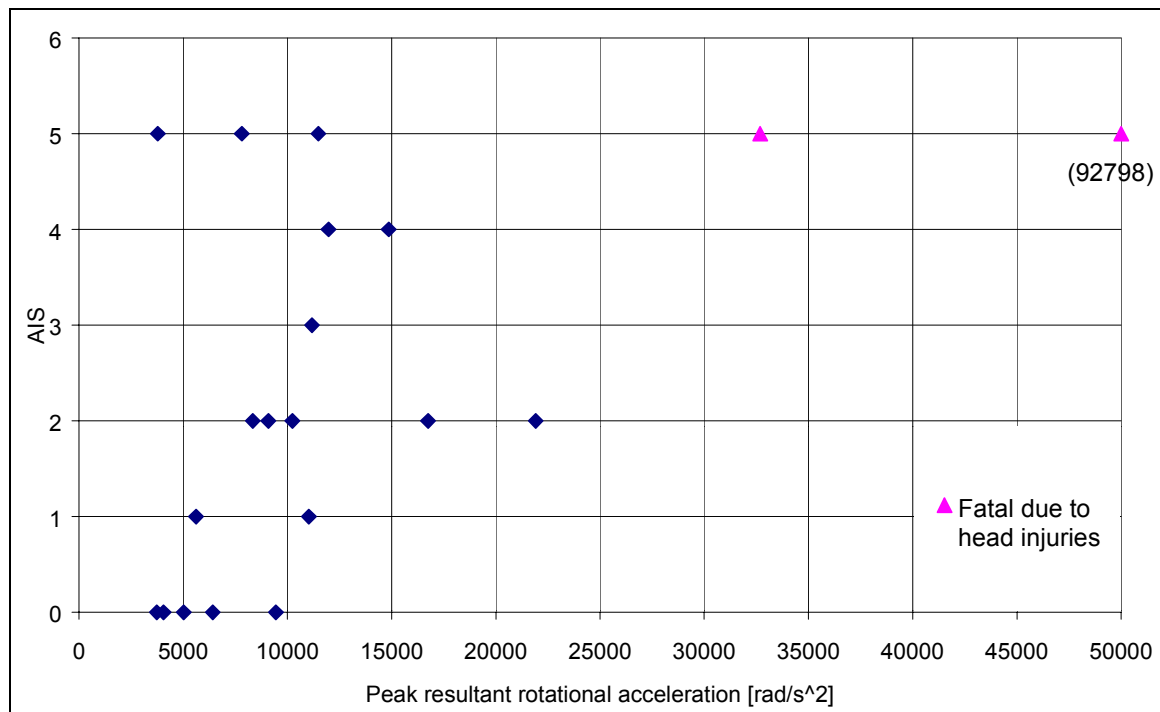


Figure 5.38. Peak resultant rotational acceleration vs AIS

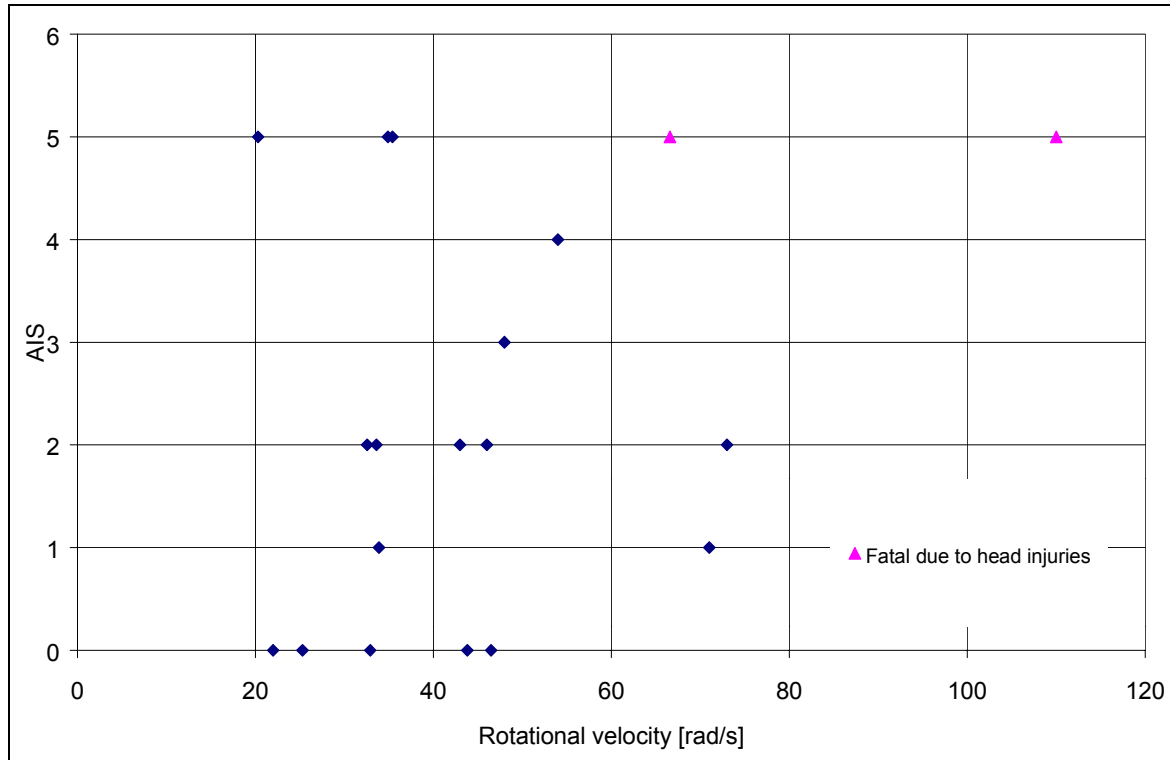


Figure 5.39. Rotational velocity vs. AIS

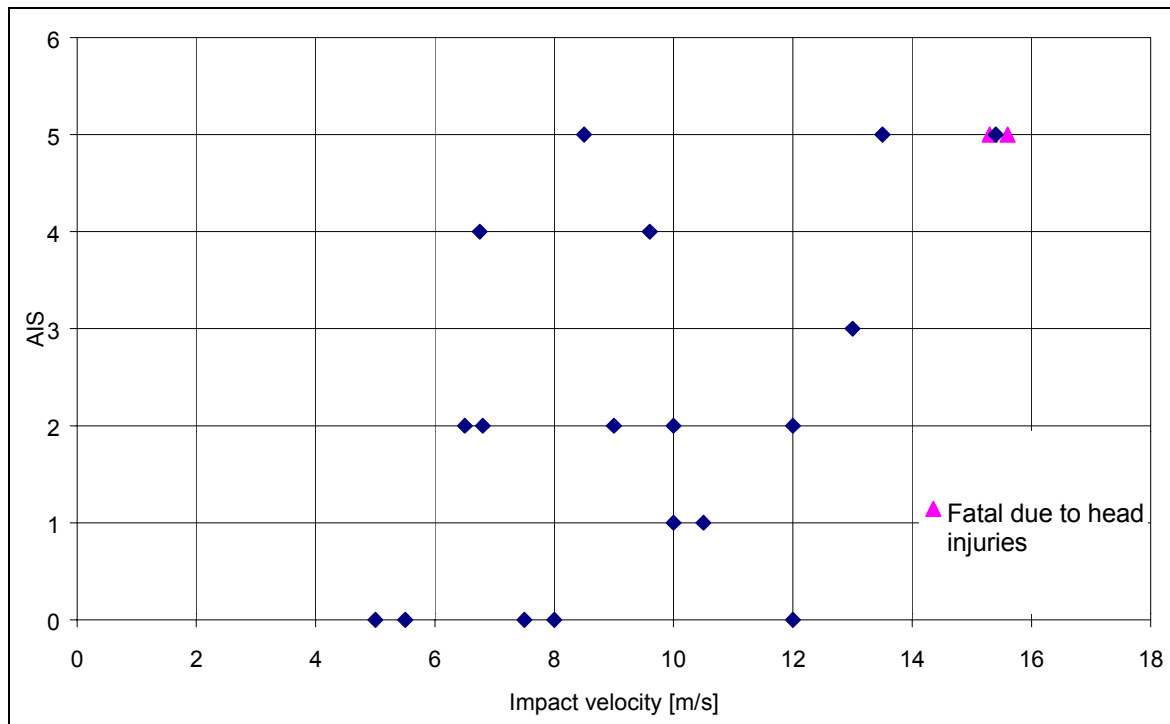


Figure 5.40. Impact velocity vs AIS

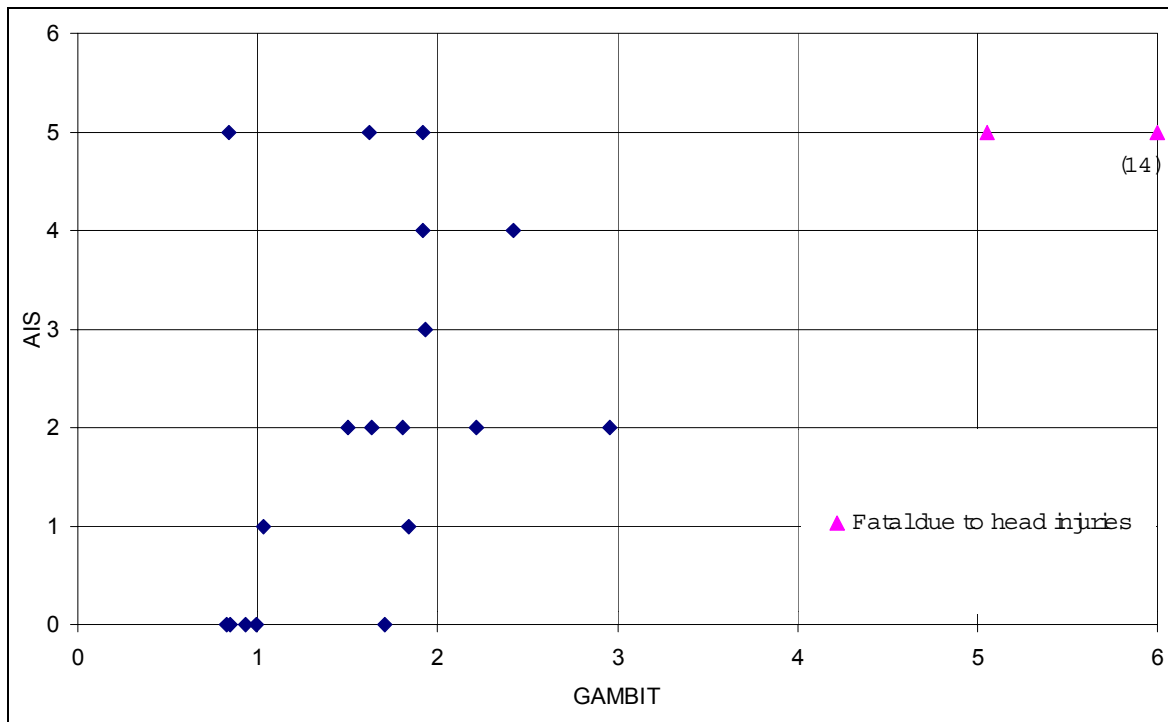


Figure 5.41. GAMBIT vs AIS

5.6. CONCLUSIONS

1 A computer model of a Hybrid III dummy rider and Norton Commander motorcycle, and a moving Ford Mondeo car has been developed in MADYMO and successfully validated. Much care was taken to ensure that the characteristics of the components of the dummy, the motorcycle and the car were accurately determined. This necessitated, for example, crush testing the wheels and forks of the motorcycle and the metal panels and sill of the car. Also examined were the suspension characteristics of the vehicles and the physical properties. The dummy and helmet material characteristics were similarly determined.

2 The above model has been successfully used to simulate motorcycle accidents of the type similar to the configuration of the full-scale impact test, 50km/h at 90° into the side of a stationary car, against which the model was validated. For example, in an accident where a motorcycle collided with the rear of a stationary van at 20km/h the rider sustained only minor leg abrasions from contact with the road. The peak linear acceleration predicted by the simulation, 70g, was similar to the 107g measured in the helmet damage replication tests. The rotational acceleration 8000 rad/s/s for the simulation was greater than the 5026 rad/s/s measured in the helmet damage replication tests, but of the same order of magnitude.

3 Accidents occur to a wide range of motorcycles in a wide range of circumstances and it is difficult to obtain information to validate the model for use across the range. Nevertheless, the model that has been developed is a sophisticated tool and there is extensive motorcycle impact test data available. Thus, with more research, the model could be validated against this data and a wide variety of motorcycle accident configurations and mechanisms may be investigated.

4 A neck developed to study the kinematic motion in slow speed rear car impacts was used as a replacement for the Hybrid III neck. The purpose of this was to examine the influence of the neck on the kinematic motion of the head in motorcycle accidents. The results showed that although the linear acceleration was similar, the rotational acceleration was somewhat greater for the modified neck, 9,000rad/s/s, compared with 6,000rad/s for the standard neck. This substantiates the belief that the Hybrid III neck is stiffer than a human neck and will lead to predictions of rotational acceleration that are too low.

5 Helmet damage seen in accident helmets was replicated in drop tests and the accelerations, rotational and linear, and external forces were measured. These measurements were compared with the injury severity, expressed as AIS, to establish "state of the art" information on human tolerance criteria. Twenty cases were investigated.

6 The replication tests have enabled values of measured parameters that are likely to cause injury to be identified. In particular, the work suggested that a limit of rotational acceleration of 5,000rad/s/s may be useful as a basis for Standards requirements, together with a limit of rotational velocity of 40rad/s. HIC was less well defined but the research showed that injuries up to AIS 5 occurred at a HIC of 1000 or less. Similarly injuries up to and including AIS 5 occurred at a peak linear acceleration of 250g or less.

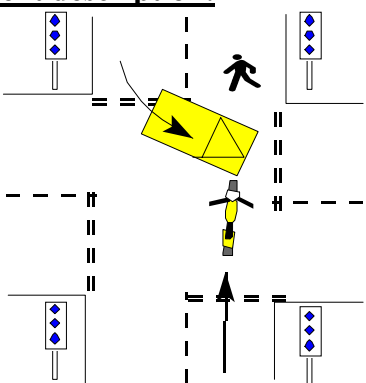
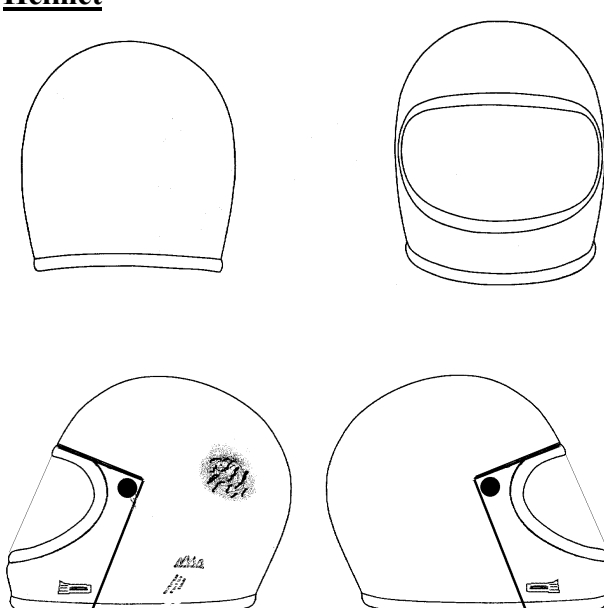
7. This research has produced a substantial amount of data and information relating to the human tolerance of the head that has previously not been available. This data has been used by the Computer Simulation Working Group and, in turn, the Head and Neck Tolerance Working Group to provide state of the art data on the tolerance of the human brain to injury.

APPENDIX 5I. MOTORCYCLE ACCIDENT REPLICATION RESULTS (2 EXAMPLES)

REPLICATION OF ACCIDENT G140

<p>Accident description:</p> <p>● = Rider final position</p> <p>V1</p> <p>Grassland</p>		V1	Yamaha FZR 1000	Speed	<96km/h
		<p>Rider approaches left hand bend and loses control on damp surface. The rider falls with bike onto left side and veers across carriageway and up embankment. The rider, still mounted, then collides heavily with the wire fencing and wooden posts along the embankment. The bike was reported to have been on its right side at the point of impact. The rider sustained fatal head injuries from the impact with a fence post. The motorcycle damage included a large dent in fuel tank, broken front forks and missing front wheel. The rider was assumed to have been riding below the signposted speed limit.</p>			
Casualty	Rider	Fatal:	Y	Male	Age: 35
Max head AIS:	4	Base of skull fracture			
Other sig. AIS:	1	Contusions left elbow			
Other head injuries:	Vault of skull fracture (AIS 3), Diffuse bilateral subarachnoid staining (AIS 3), Contusion left temporal pole (AIS 3), Contusion on undersurface of left frontal lobe (AIS 3), Laceration with underlying haematoma (deep) of right occipito-parietal scalp (AIS 2), Contusions of left eyelid and neck below right ear (AIS 1).				
		Make:	Shoei		
		Model:	GRV		
		Type:	Full face		
		Retained:	Y		
		Material:	GRP		
		Shell crack, 17cm long (including 5cm tear at base), running from behind right temporal region to base of helmet. Paint cracking and loss surround the shell crack forming an ellipse 10cm wide. Residual liner deformation adjacent to the shell crack with approximately 25% reduction in original 30mm liner thickness. Other minor scuffs and chips elsewhere on helmet, some pre-accident.			
Replication results	Target used: Wooden fence post				
Linear acceleration	Peak (HIC)	1242g (27550)			
Rotational acceleration	Peak (Integral)	92798 rad/s ² (110rad/s)			
Impact velocity	Resultant and Angle	15.6m/s @ 90 degrees			
Impact force	Normal and Tangential	38425N and 3410N			
	Coefficient of Friction	0.09			

REPLICATION OF ACCIDENT H14.130

<p>Accident description:</p> 		V1:	BMW K 100	Speed:	49km/h
		V2:	VW Golf Mk. 2	Speed:	7km/h
		<p>V2 failed to give way to an oncoming motorcycle and turned left in front of V1 who was going straight-ahead over the junction. The motorcycle was unable to avoid V2, and impacted the car in an upright position at an oblique angle. The impact caused severe crush damage to the car body and some frame damage to the bike. The rider was thrown over the car onto road surface.</p>			
Casualty	Rider	Fatal:	N	Male	Age: ?
Max head AIS:	2	Concussion			
Other sig. AIS:	1	Abrasion and contusions to thorax and limbs			
<p>Helmet</p> 		<p>Make: BMW</p> <p>Model: System 3</p> <p>Type: Full face</p> <p>Retained: Y</p> <p>Material: GRP with thermoplastic chin guard</p> <p>Damage: Abrasion damage to left side of helmet towards rear and crown. The abrasion is made up of irregular scratches and scuffs over a circular area of approximately 6cm diameter. The scuffs are generally deep and short. There are some additional abrasions and paint loss at helmet base due to secondary impact.</p>			
Replication results		Target used: Concrete slab			
Linear acceleration	Peak (HIC)	224g (1059)			
Rotational acceleration	Peak (Integral)	9088rad/s ² (33rad/s)			
Impact velocity	Resultant and Angle	6.5m/s @ 30degrees			
	Normal and Tangential	3.3m/s and 5.63m/s			
Impact force	Normal and Tangential	8179N and 2003N			
	Coefficient of friction	0.24			

CHAPTER 6. FINITE ELEMENT MODELLING AND SIMULATION OF HELMET, HEAD AND NECK

6.1. INTRODUCTION

Mathematical modelling was an important part of the Action and this section describes the construction and use of a finite element model of a skull, brain, neck and motorcycle helmet. Louis Pasteur University, Strasbourg and Polytecnico Milano developed the finite element models. The Transport Research Laboratory was responsible for helmets, much helmet data and supplying detailed brain injuries for some of the accident cases.

All of the models have been constructed in finite elements and Strasbourg University has constructed the brain, skull and helmet models in RADIOSS. Milano have constructed the neck, initially as a lumped mass multi-body model in VeDyAC, then as a finite element model in PAM CRASH. The multi-body model was used as a development tool to investigate the type of muscle control that may be needed to ensure a human-like response. It was important that the simulations were properly validated and a brief description of this process is included for each of the models. The brain was validated against published cadaver data, the neck against published human volunteer data and the helmet against data from test results at TRL and Strasbourg University. New and hitherto unpublished materials data, obtained by Strasbourg University, was used for the skull and also for the brain.

This report describes the construction and validation of the models and gives details of, and justification for, the material characteristics selected. Section 6.2 describes the brain and skull, section 6.3 the neck and section 6.4 the helmet. TRL was responsible for the study of head parameters to investigate the change in peak pressure and peak von Mises stress to variations in the bulk modulus and visco-elastic shear modulus of the brain, and Young's modulus of the cerebrospinal fluid. This was then followed by an investigation of the variation in the model output to changes in the mass and stiffness of an impactor striking the forehead.

The model was then used to investigate the behaviour of the brain in accident conditions specified from the range of accidents that were replicated by TRL as part of the process of the reconstruction of helmet damage.

6.2. HEAD MODELLING

6.2.1. Model development

The geometry of the inner and outer surfaces of the skull was digitised in the Strasbourg laboratory from a human skull and information given in an anatomical atlas by Ferner. This data was used to mesh the human head using the Hypermesh code. Figure 6.1 below shows the 3D skull surface obtained by digitising external and internal surfaces of a human skull and the meshed model.

Figure 6.2 shows a cross section of the model and illustrates the anatomical features of the skull and the brain and the position of the brain within the skull. The main anatomical features modelled were the skull, falx, tentorium, subarachnoid space, scalp, cerebrum, cerebellum, and the brain stem.

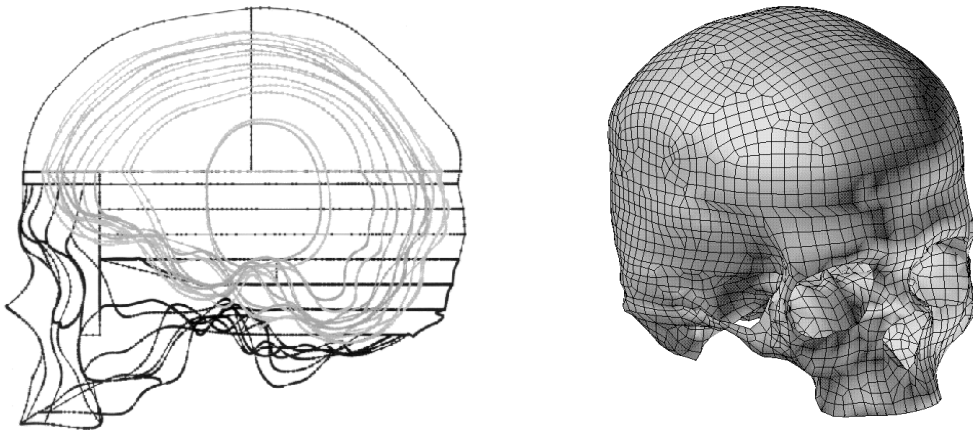


Figure 6.1. 3D skull surfaces used for the model construction and skull meshing.

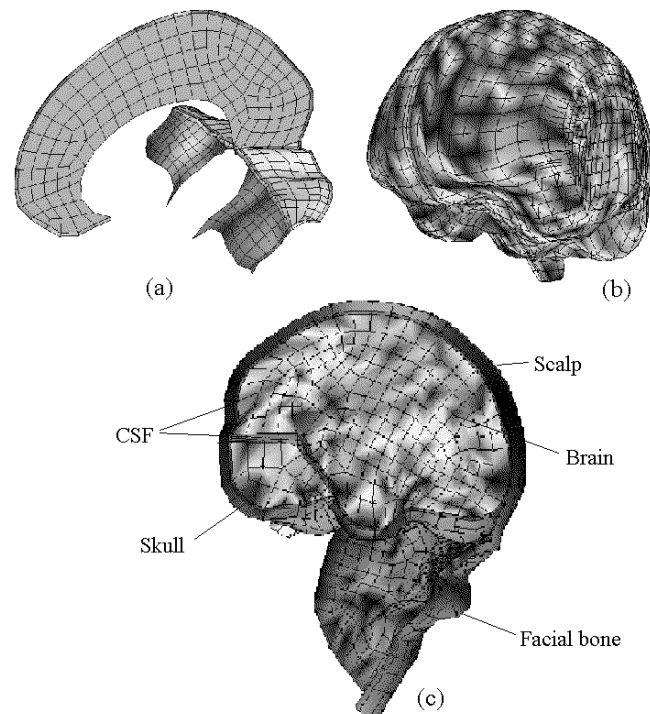


Figure 6.2. Three dimensional human head model

(falx and tentorium (a), brain (b) representations and overview (c))

The finite element mesh is continuous and represents an adult human head. The falx and tentorium were simulated with a layer of shell elements, the skull comprised a three layered composite shell and the remaining features were modelled with brick elements.

Of particular importance, and rarely modelled, is the subarachnoid space between the brain and the skull, which in this model was represented by a layer of brick elements to simulate the cerebral-spinal fluid. The tentorium separates the cerebrum and the cerebellum, and the falx separates the two hemispheres and brick elements were again

used to simulate the cerebral-spinal fluid that surrounds these membranes. The scalp, which surrounds the skull and facial bones was also modelled by a layer of brick elements. Overall, the current head model consists of 11939 nodes and 13208 elements divided in 10395 bricks and 2813 shells and it has total mass of 6.7 kg.

6.2.2. Material properties.

Material characteristics are very important to the success of a finite element model and Table 6.1 below lists the properties of the materials used in the model.

Table 6.1 Material properties of the head model

Part	Material property	Material parameter	Value	Element type	Shell thickness (mm)
Face	Elastic	Density	2.5E+03 Kg.m ⁻³	Shell	10.0
		Young's modulus	5.0E+03 MPa		
		Poisson's ratio	0.23		
Cranium (Cortical)	Elastic Plastic Orthotropic	Density	1.9 E+03 Kg.m ⁻³	Shell	2.0
		Young's modulus	1.5E+04 MPa		
		Poisson's ratio	0.21		
		Bulk modulus	6.2 E+03 MPa		
		UTS	90.0 MPa		
		UCS	145 MPa		
Cranium (Trabecular)	Elastic Plastic Orthotropic	Density	1.5E+03 Kg.m ⁻³	Shell	3.0
		Young's modulus	4.6E+03 MPa		
		Poisson's ratio	0.05		
		Bulk modulus	2.3E+03 MPa		
		UTS	35.0 MPa		
		UCS	28.0 MPa		
Scalp	Elastic	Density	1.0E+03 Kg.m ⁻³	Solid	-----
		Young's modulus	1.67E+01 MPa		
		Poisson's ratio	0.42		
Brain	Viscoelastic	Density	1.04E+03 Kg.m ⁻³	Solid	-----
		Bulk modulus	1.125E+03 MPa		
		Short time shear modulus	4.9E-02 MPa		
		Long time shear modulus	1.62E-02 MPa		
		Decay constant	1.45E-01		
CSF	Elastic	Density	1.04E+03 Kg.m ⁻³	Solid	-----
		Young's modulus	0.12E-01 MPa		
		Poisson's ratio	0.49		
Falx	Elastic	Density	1.14E+03 Kg.m ⁻³	Shell	1.0
		Young's modulus	3.15E+01 MPa		
		Poisson's ratio	0.45		
Tentorium	Elastic	Density	1.14E-09 Kg.m ⁻³	Shell	2.0
		Young's modulus	3.15E+01 MPa		
		Poisson's ratio	0.45		

Material properties of the cerebral spinal fluid, scalp, facial bones, tentorium and falx are all isotropic and homogenous. The viscoelastic properties assigned to the brain were scaled from Shuck et al 1972. The behaviour in shear was defined by:

$$G(t) = G_{\infty} + (G_0 - G_{\infty})\text{Exp}(-\beta t)$$

G_0 : Short term shear modulus

G_{∞} : Long term shear modulus

β : Decay constant

The Young's modulus of the subarachnoid space was determined by Willinger et al in 1994 using modal analysis. The material properties are similar to those used in a model by Wayne State University with the important exception that the skull in the Strasbourg University model was simulated by a three layered composite shell representing the inner table, the diploë and the external table of the human cranial bones. In order to reproduce the global compliance of the cranial bones, each layer was assigned a thickness in combination with an elastic brittle law. This skull modelling permitted simulating the bone fracture by introducing a material discontinuity and then analysing the effects on the head response in, for example, instances of head impacts resulting in skull fracture.

6.2.3. Model validation

The experimental data used for this work was published by Nahum et al. 1977 for a frontal blow to the head of a seated human cadaver. Table 6.2 presents the impact configuration for the Nahum test as used in this study to validate the model. The values of maximum linear head acceleration, impact force and the calculated HIC are also specified in this table.

Table 6.2 Impact conditions and test results for Nahum's test

Test	Impact area	Head/impactor interface	Force (N)	ACG (g) max.	HIC	Dt (HIC) (ms)
Nahum's Impact	frontal bone	rigid cylinder with padding	6900	198	744	2.4

In Nahum's test, intracranial pressures were recorded at five locations: behind the frontal bone adjacent to the impact area, in the parietal area immediately posterior to the coronal suture and superior to the squamosal suture, inferior to the lambdoidal suture in the occipital bone (one on each side), and at the posterior fossa in the occipital area. These measured pressure locations were named as frontal, parietal, occipital 1, occipital 2 and posterior fossa.

Since the neck was not included in this model, a free boundary condition was used to simulate Nahum's impact. This hypothesis was based on the justification that the time duration of the impact was too short (6 ms) for the neck to influence the kinematics of head response.

In order to reproduce the experimental impact conditions, the anatomical plane of the model was inclined at about 45°, as shown in figure 6.3, to be consistent with Nahum's experiment. Figure 6.3 presents the configuration of the Nahum's impact simulation. For modelling a direct head impact, the model was impacted frontally by a 5.6 kg rigid

cylindrical impactor launched freely with an initial velocity of 6.3 ms^{-1} . The impact force, head acceleration at the centre of gravity and five intracranial pressure time histories were calculated and compared with Nahum's experimental data. The finite element analysis was executed using the RADIOSS code and the method of one point integration was used for all analysis.

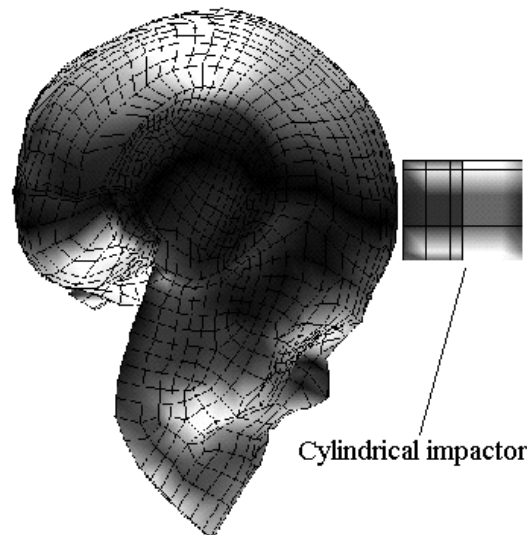


Figure 6.3. The 3D human head model in Nahum's frontal impact configuration

The forces and head accelerations for both the Nahum impact and the numerical analysis are shown in figures 6.4 and 6.5. Good agreement between the experiment and the simulation was obtained for the impact force and the head acceleration. The duration of the impact and the amplitudes were well matched as shown in figures 6.4 and 6.5. This result confirms that the free boundary assumption for the short pulse duration was justified.

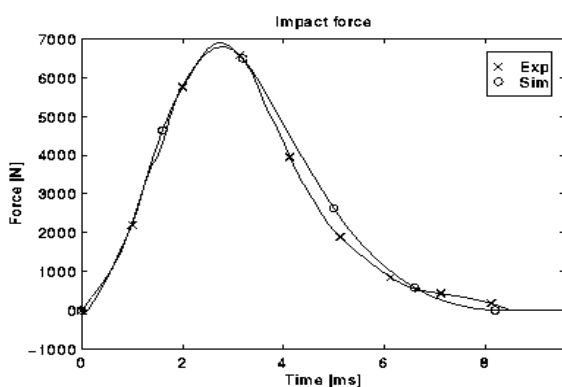


Figure 6.4. Impact force comparison for Nahum's impact

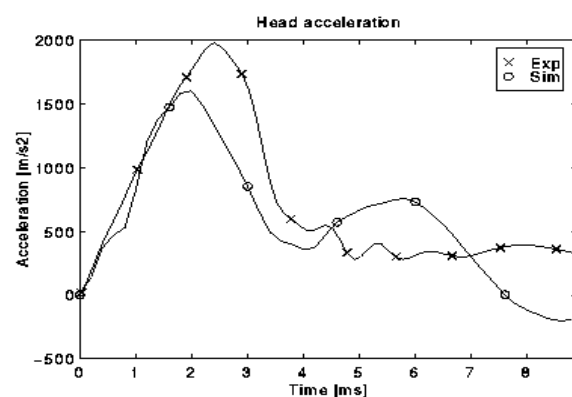


Figure 6.5. Head acceleration comparison for Nahum's impact

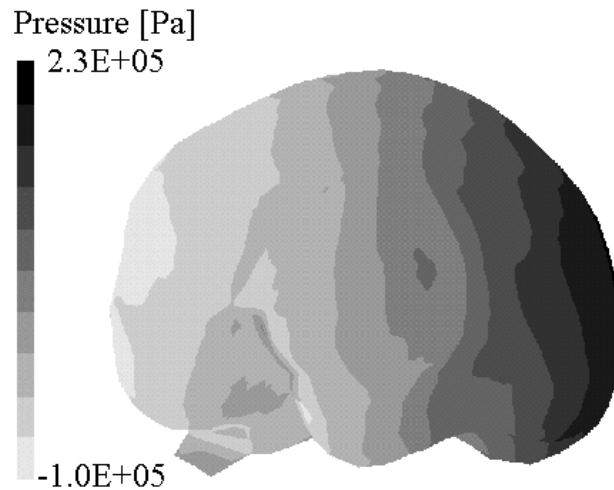


Figure 6.6. Intracranial pressure contour at 3 ms (Nahum's frontal impact)

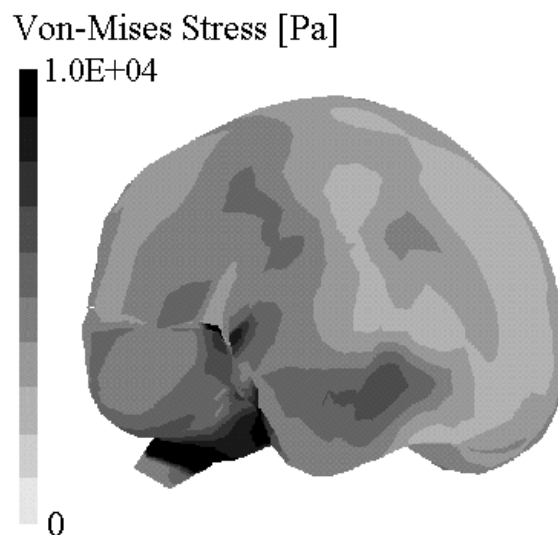


Figure 6.7. Intracranial von Mises stress contour at 4 ms (Nahum's frontal impact)

Intracranial pressure was uniformly distributed across the brain with compression in the frontal region and tension in the occipital region as shown in figure 6.6. This typical coup/contrecoup pressure pattern was also predicted by Ruan's and Zhou's models.

The model predicted a maximum compression of 0.24 MPa at impact point and a maximum tension of -1.15 MPa at the point opposite to the impact site. As shown in figure 6.7, the highest von Mises stress was in the brain stem and the lateral lobe and not in the frontal region located under impact point. This von Mises stress distribution was a similar response to that found with Zhou's model. However, this is contrary to what was predicted by Ruan's model, which was, that the maximum brain shear stress occurred in the frontal region and the brain stem.

The numerical (simulation) data and experimental data of the pressure time histories for all five of the sites at which Nahum measured pressure are presented in figures 6.8 to 6.12. These figures show that the five intracranial pressures from the model closely matched the

experimental data. This was particularly so for the peak pressure for which the maximum difference was less than 7%.

When pulse shape was compared, the model response was clearly more symmetrical than the equivalent head response data from Nahum's test and was particularly evident for the occipital pressures 1 and 2 as shown in figures 6.10 and 6.11. This symmetry occurred probably because the skull geometry and the head kinematics were more symmetrical in the simulation than in Nahum's experiment. However, these differences between the experimental and simulation data were considered to be inconsequential.

In the skull, the model predicted the highest von Mises stress to be at the impact site and then diminishing from the impact point throughout the rest of the skull. Skull fracture did not occur in this simulation, which is consistent with Nahum's observation in the autopsy. Overall, the results were very encouraging and gave confidence in the model sufficient to carry out head impact replications of real motorcycle accidents in order to investigate brain injury mechanisms.

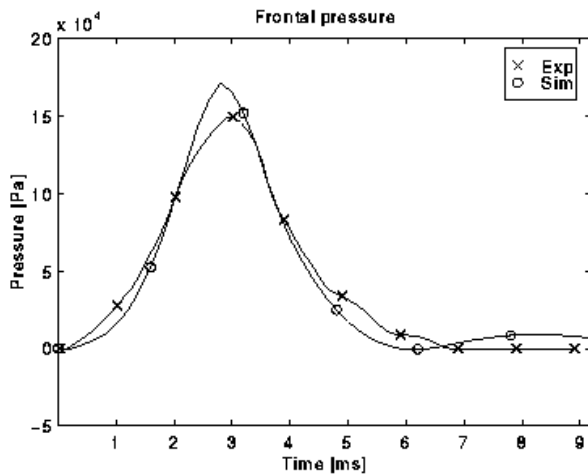


Figure 6.8. Frontal pressure (coup pressure) pressure comparison

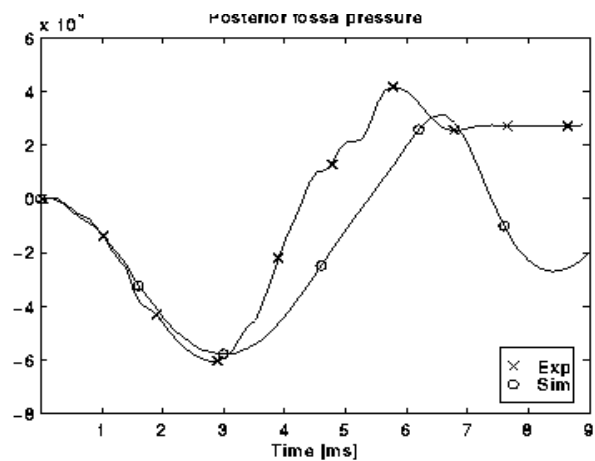


Figure 6.9. Posterior fossa (contrecoup pressure) comparison

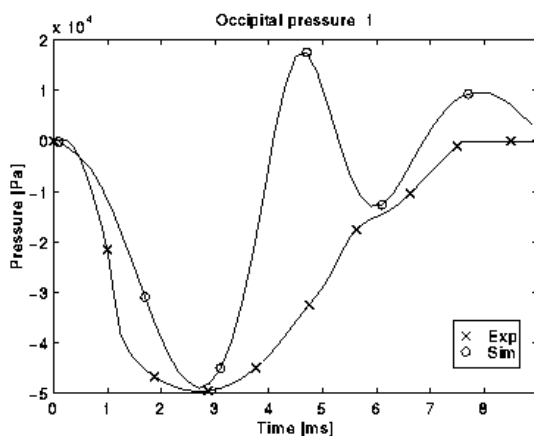


Figure 6.10. Occipital pressure 1 comparison

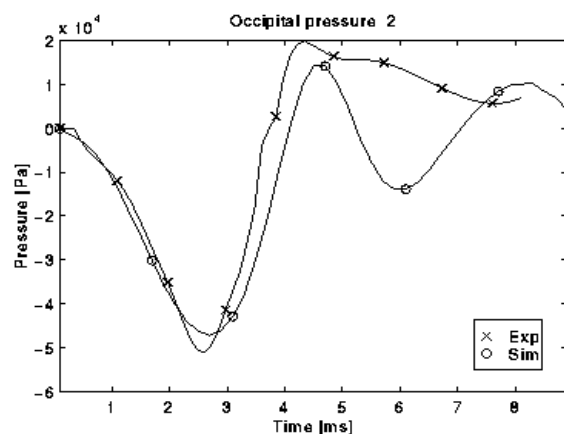


Figure 6.11. Occipital pressure 2 comparison

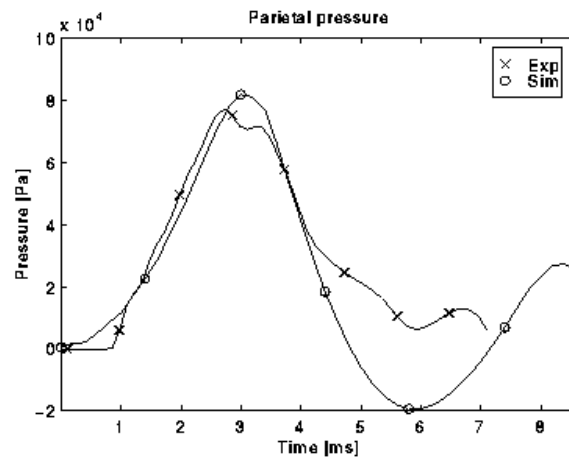


Figure 6.12. Parietal pressure comparison

6.3. DEVELOPMENT OF THE FINITE ELEMENT MODEL OF THE NECK

6.3.1. Description of the model

The model comprises 8 rigid vertebrae and a rigid head, 6 nonlinear viscoelastic intervertebral discs, 34 nonlinear viscoelastic ligaments, 17 nonlinear facet joints and 13 pairs of muscles. This model is made of 971 solid elements, 62 bar elements and 17 6-DOF Spring-Dashpot elements, figure 6.13.

The vertebrae and the head were considered as rigid bodies, since their deformation was insignificant compared with deformation of the soft tissues. Each vertebra in the range between C7 and C3 consists of 100 solid elements (bricks).

The axis, the T1 vertebra and the head, were represented by 97, 122, 18 and 18 solid elements, respectively. Each intervertebral disc consisted of 36 brick solid elements, arranged in three layers, linking the lower plate of the upper vertebral body to the upper plate of the lower vertebral body, figure 6.14.

All the ligaments, interspinous, flavium, anterior and posterior longitudinal, alar, apical, transverse ligaments and tectorial, anterior, posterior membranes were each simulated by one bar element joining the two adjacent vertebrae, figure 6.15; each muscle was also simulated by one bar element. The articular facets and the joint between the dens and the anterior arch of atlas were simulated each by 1 6-DOF Spring-Dashpot element joining the two adjacent articular surfaces.

6.3.2. Characteristics of the elements.

Data describing the mechanical characteristics of human neck tissue are incomplete, especially for dynamic loading. Therefore, the model response was compared with that of human response measured during experiments at the US Naval Biodynamics Laboratory (NBDL) when volunteers were subjected to 15g frontal and 7g lateral HYGE sled experiments. Mechanical properties of the elements were necessarily improved so that the model produced behaviour similar to that of NBDL volunteers in terms of kinematics and dynamics.

The mass and the inertial characteristics of the head were taken from studies performed at NBDL and includes correction for instrumentation with a mass of 0.53 kg: $M = 4.69$ kg,

$I_{xx} = 181 \text{ kg}\cdot\text{cm}^2$, $I_{yy} = 236 \text{ kg}\cdot\text{cm}^2$, $I_{zz} = 173 \text{ kg}\cdot\text{cm}^2$, $I_{xz} = 71 \text{ kg}\cdot\text{cm}^2$. A nonlinear viscoelastic material law was imposed on the solid elements simulating the intervertebral discs; elastic modulus for these elements is $7\cdot 10^7 \text{ N/m}^2$.

Ligament behaviour was modelled with elements producing viscoelastic force only in tension. This material model represents a generalised Kelvin mechanism which consists of a spring and a damper in parallel. The spring behaviour was prescribed by a nonlinear force-deflection curve simulating the sigmoidal shape of the biomechanical structures and the damper accounts for differences between dynamic and static ligament response.

The mechanical properties of the facet joints were simulated by a non linear viscoelastic material. This material model corresponds to a nonlinear spring-dashpot element connecting two nodes: the nonlinear spring force (moment) response was imposed on the 6-DOF Spring/Dashpot elements simulating the sliding movements of the facet joints and the laxity of the capsular ligaments. Viscous behaviour was represented by two constant damping coefficients that were set at 300 Ns/m for the translations and 1.5 Nms/rad for the rotations.

Only the stronger and the more superficial muscles were included in the model to study the effect of passive and active muscle behaviour on the head-neck impacts: longus colli, longus capitis, scalenus anterior, medius and posterior, trapezius, sternocleidomastoid, splenius capitis and cervicis, semispinalis capitis and cervicis, longissimus capitis and cervicis.

A simplified geometric representation was chosen in which each muscle force is directed along the straight line connecting origin and insertion. Passive muscle behaviour was modelled by a nonlinear force-elongation relation. Active muscles were represented by elements which reproduce passive and active muscle behaviour according with Hill muscle model.

6.3.3. Results

The model was tested in frontal and lateral impacts and compared with envelope curves that were obtained from NBDL tests. The model was loaded by imposing on vertebra T1 the same linear acceleration as those measured on the volunteers.

The results obtained with the model correspond well to the volunteer responses for both frontal and lateral directions. Better results were obtained in terms of kinematics responses of the head and neck running the model with muscle activation. This shows that muscle contraction has a large influence on the head-neck response.

Figure 6.16 and figure 6.17 shows the active and the passive response of the model compared with human volunteer response corridors for the frontal and lateral impact.

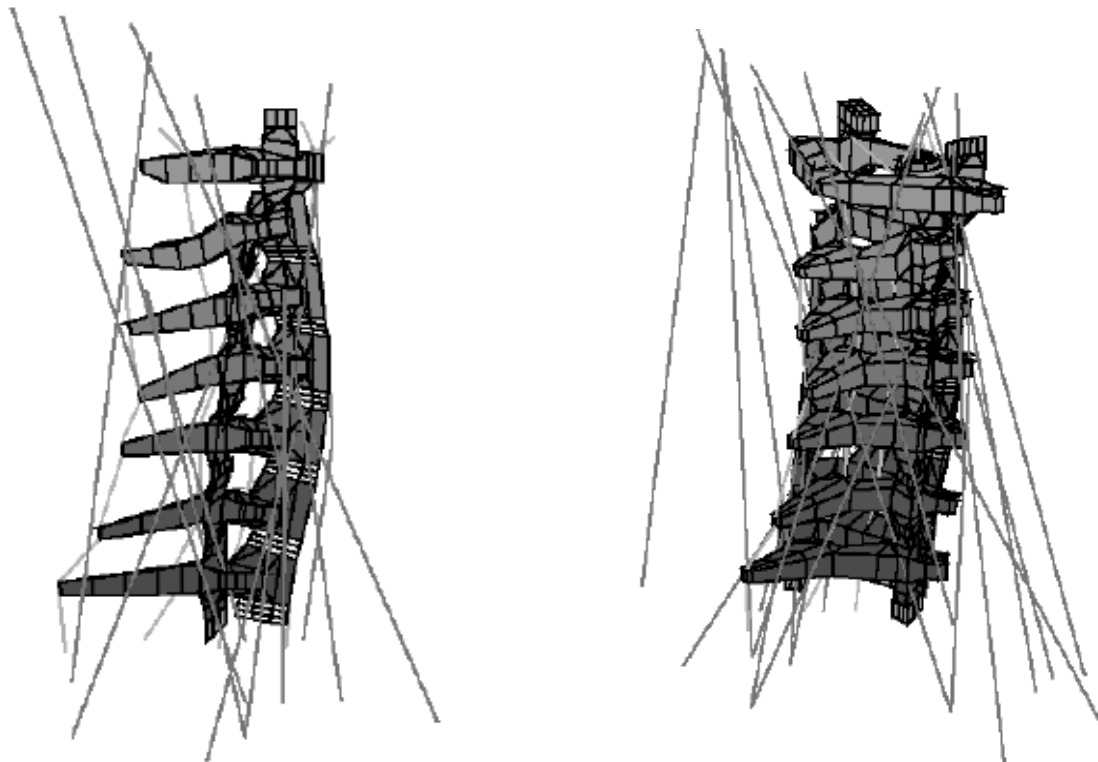


Figure 6.13. Lateral and oblique view of the finite element model

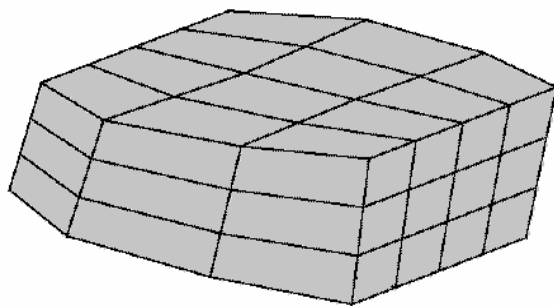


Figure 6.14. Oblique view of an intervertebral lower disc of the finite element model.

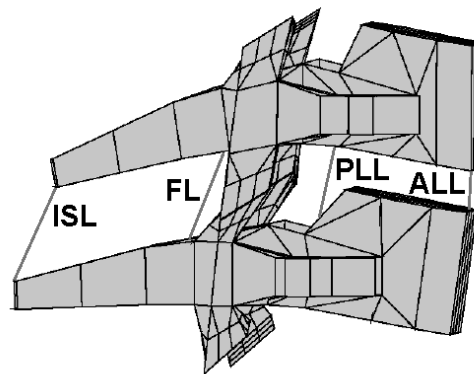


Figure 6.15. Lateral view of two cervical vertebrae with ligaments.

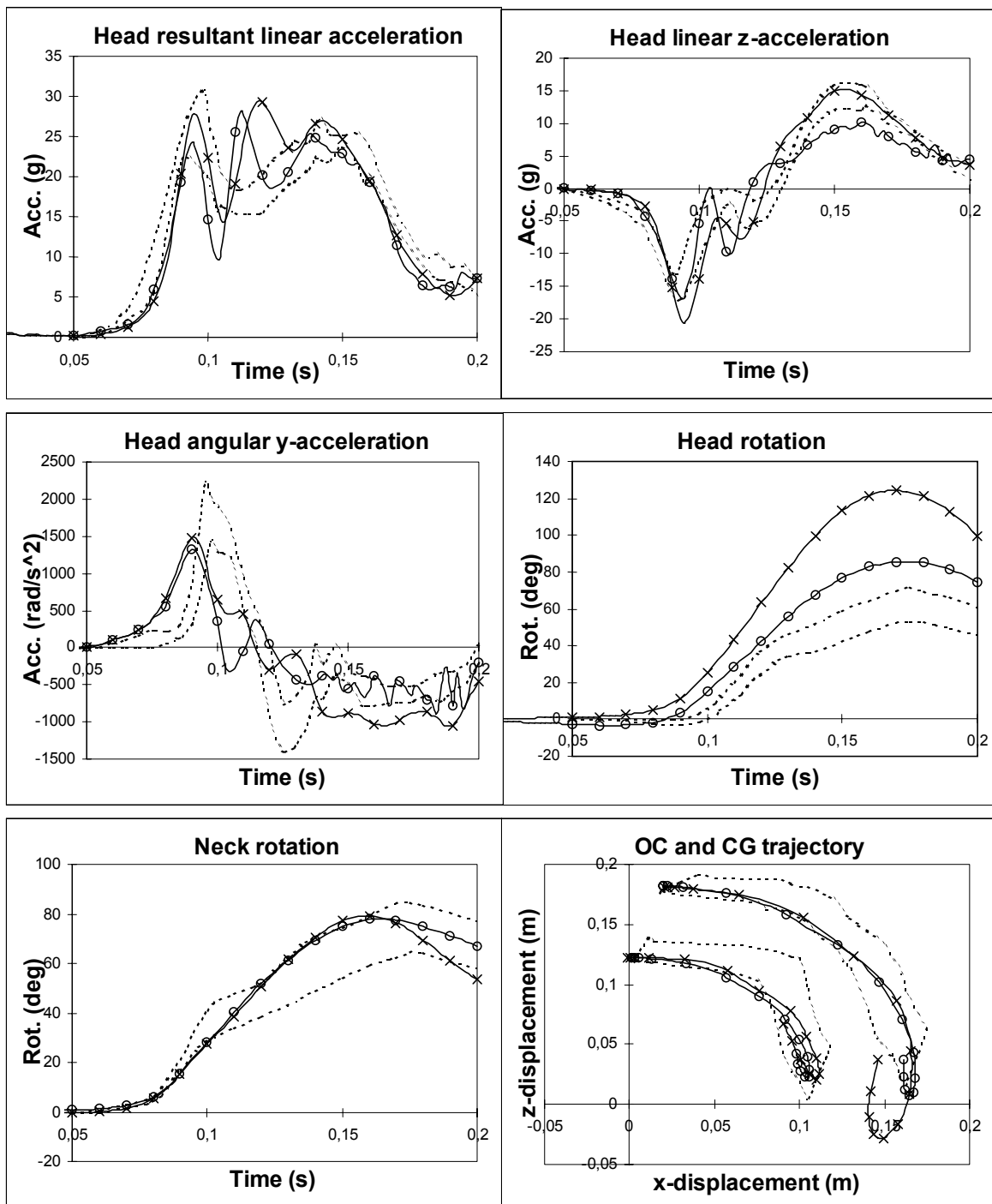


Figure 6.16. Response to frontal impact of the finite element model with active (o) and passive (x) muscle behaviour in comparison with the human volunteer response corridors (dotted lines). +x is forwards, +y is to left, +z is upwards.

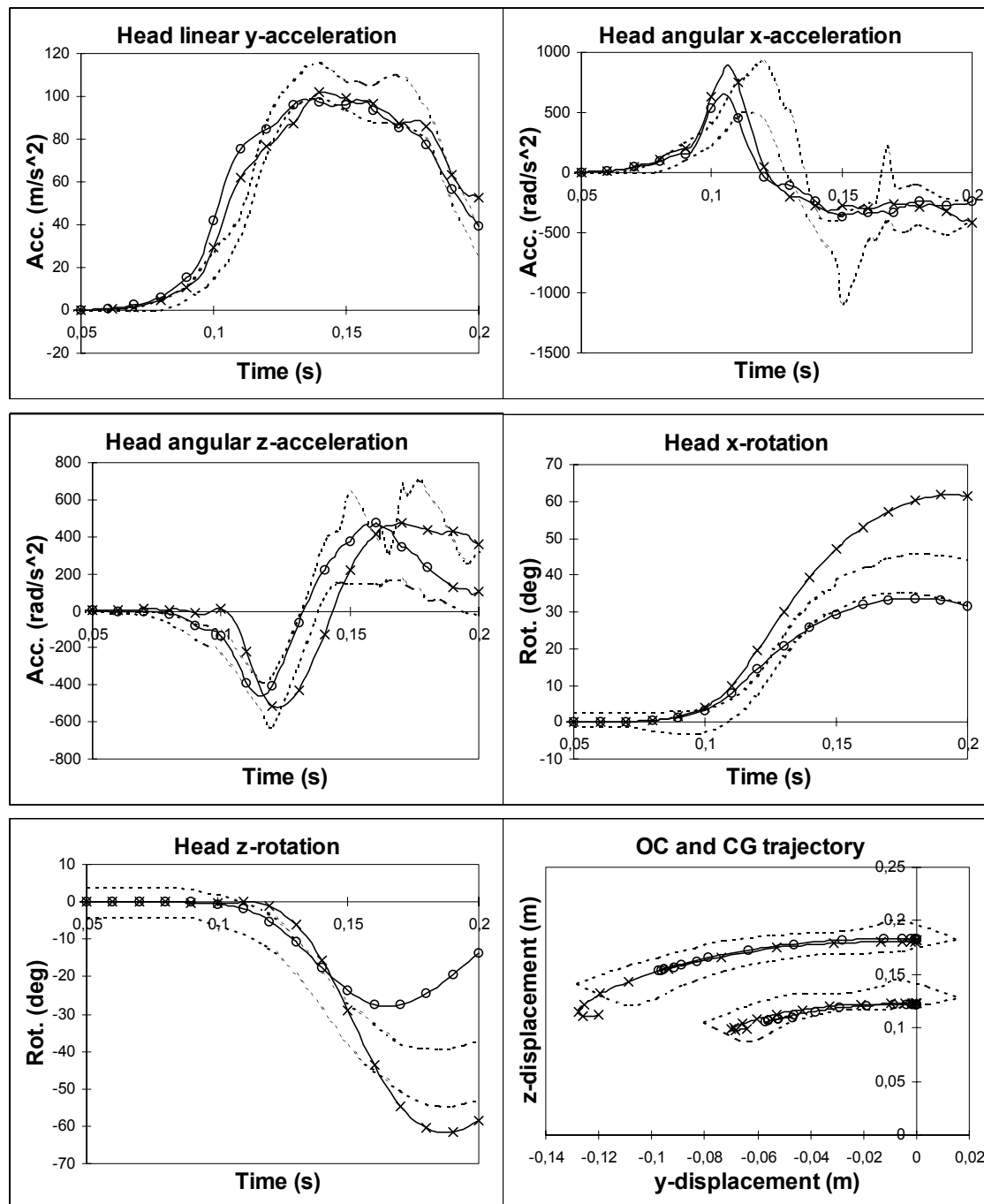


Figure 6.17. Response to lateral impact of the finite element model with active (o) and passive (x) muscle behaviour in comparison with the human volunteer response corridors (dotted lines). +x is forwards, +y is to left, +z is upwards.

6.4. HELMET MODELLING

6.4.1. Helmet profile measurements

The helmet chosen to be the basis of that used in the model was a Nimrod glass fibre helmet largely because this helmet had been the subject of many tests at TRL and, thus, much data on its performance was available. TRL agreed to supply the material

characteristics and these are given in the Reconstruction Working Group interim report. However, of prime importance was the outer profile and this needed to be determined accurately for the FE model.

The helmet was mounted upon a level platform and the geometry was recorded using a 3 dimensional arm linked to a computer. An ordinate system for defining the helmet geometry was based upon that used by ISO and adopted as EN 960 and incorporated into Regulation 22 (ECE Motor Vehicle Helmet Standard) for defining the geometry of headforms.

6.4.2. Helmet modeling and validation

The above described helmet has been meshed by shell elements for the shell and by brick elements for the protective foam. Constitutive equations for the different materials have been modelled after an experimental analysis of the helmet components. The Hybrid II dummy head has also been meshed and figure 6.18 shows the coupling of both models; the helmet model and the headform model. This global model has been validated against a standard impact on a flat anvil in terms of headform acceleration

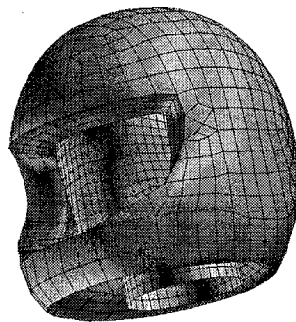


Figure 6.18. Finite element model of the helmet coupled with the headform for the helmet validation

The validation of the helmet FEM was in accordance with the impact test stipulated by the British Standard BS 6658A, and ECE-R022/04. The helmet was coupled with the headform, figure 6.18, and the comfort liner was modelled by a gap. The contact between the two parts was defined using a contact algorithm available in Radioss. A simulation of a frontal impact was used for the validation. The model was launched freely against a rigid anvil with an initial velocity of 7.5 m/s, experimentally at Transport Research Laboratory and numerically at ULP, Strasbourg. The linear acceleration and the force-displacement time histories produced by the headform model were used as the basis for the helmet validation. Figure 6.19 shows the headform acceleration time history for the impact from both the experiment and the simulation. The shape, the delay and the magnitude of the acceleration produced by the model agree very well with the experimental data.

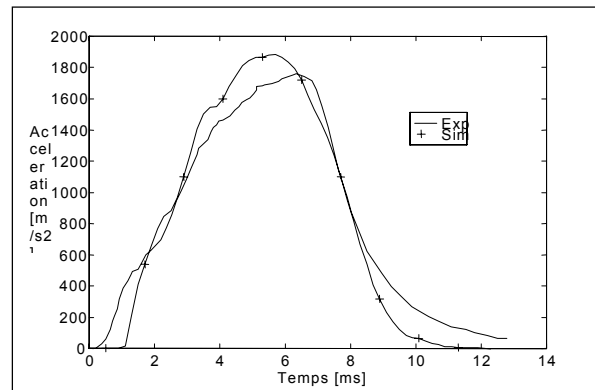


Figure 6.19. Comparison of experimental and numerical headform acceleration

6.5. AN ANALYSIS OF HEAD AND HEAD IMPACT PARAMETERS

6.5.1. Method

Following the validation of the head model it was concluded that further work should be completed on the model so that the output could be better understood. A study of head parameters was considered essential for this purpose. This section of the report describes the method and results of the analysis. It should be noted that to avoid unnecessary complications the cerebro-spinal fluid, in this research, was modelled as a material with the appropriate characteristics. Thus, the material was correctly assigned a Young's modulus as discussed below.

The parameter analysis investigated the change in the model response (pressure and von Mises stress) to variations in the bulk modulus and viscoelastic short time shear modulus of the brain. The change in the model response (pressure and von Mises stress) was also investigated for a range of values for the Young's modulus of the cerebrospinal fluid (CSF). These parameters were individually varied for 27 model runs. For all these runs, the model was configured to a specific set of experimental conditions. This consisted of propelling a padded cylindrical impactor at the forehead of the model at 6 m/s^{-1} .

Sixteen model runs were completed with the model configured to the same experimental conditions as the Parametric Analysis. For each run of the model, an isolated change was made either to the Young's modulus of the impactor padding (stiffness) or to the impactor mass. Thus, the sensitivity of the brain to variations in impact conditions, such as may be represented by changes to helmet materials, was investigated.

6.5.2. Results

Pressure and von Mises stress were monitored at specific elements spread throughout the brain of the model. These included elements positioned in the anterior, posterior and base of the brain, in addition to the brain stem. The peak pressures and von Mises stress were taken from the results and a Multiple Regression Analysis (MRA) performed to establish the relative importance and sensitivity of each parameter on the model's peak responses. MRA is a statistical method for fitting a mathematical relationship between a dependent variable and two or more independent variables. The results from the MRA were used to summarise and support the visual observations of the peak responses.

Overall, the response of the model to changes in its parameters and inputs did match what was expected. The brain bulk modulus was shown to have a direct influence on the peak brain pressure, and, in addition to the short time shear modulus, an inverse affect on the

peak von Mises stress of the brain. In general, increasing the mass of the impactor had a direct and inverse affect on the peak pressure and peak von Mises stress of the brain. However, in some cases the output from the model deviated from that which was expected, with progressive changes in the model parameters and inputs.

The direct influence of brain bulk modulus on the brain peak pressure was disrupted in elements experiencing large positive peak pressures close to the point of impact. For example, figure 6.20 shows that for runs with Young's modulus set high for the CSF, a direct relationship exists between brain bulk modulus and the peak pressure, for example runs 19,20,21 and 22,23 24. However, at lower values of the Young's modulus for the CSF there is no regular relationship between isolated changes made in brain bulk modulus and the peak pressure for example runs 1,2,3 and 4,5,6. It is postulated that this effect was caused by the load profile prescribed for the CSF, presented in figure 6.21. Visual inspection of the model revealed that the CSF elements, close to the point of impact, were crushed beyond 80% strain, leading to an increase in the stiffness of the elements. It is possible that this change, coupled with the designated changes in the model's chosen parameters could have upset the direct relationship between the brain bulk modulus and peak pressure.

Several observations provide supporting evidence for this theory. First, the Young's Modulus of the CSF only had a significant influence on the peak pressure response of elements experiencing large peak pressures at the anterior of the brain. The direct relationship between brain bulk modulus and the brain peak pressure was disrupted for these same elements. Second, in the results on the peak von Mises stress, where the Young's modulus of the CSF did not affect the results, disruptions were not observed in the relationship between peak von Mises stress and the brain bulk modulus. Third, the disruption to the relationship between the brain bulk modulus and peak pressure generally arose only in the runs where the Young's modulus of the CSF was at its lowest. This was when the elements of the CSF were more susceptible to strains above 80%. These comments are postulated and can be proved only with additional runs of the model, possibly with the Young's modulus of the CSF raised to higher values including a value to represent a rigid structure.

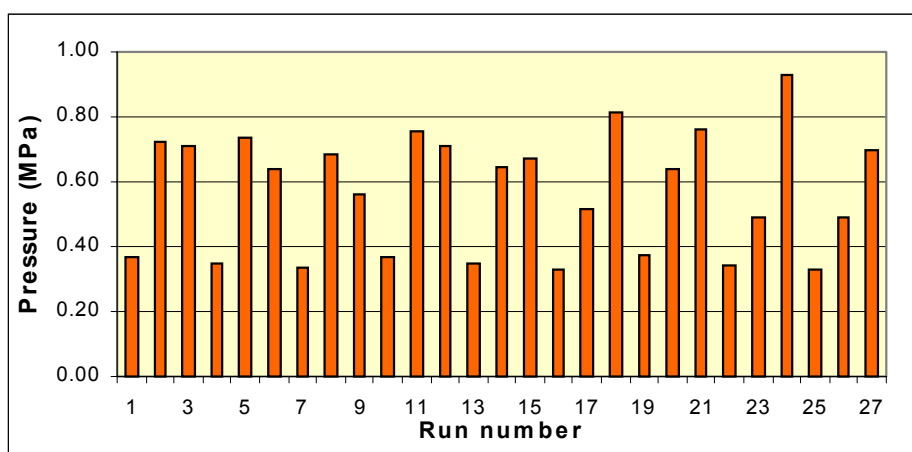


Figure 6.20. Peak pressures recorded in element 5503 for changes to the brain characteristics

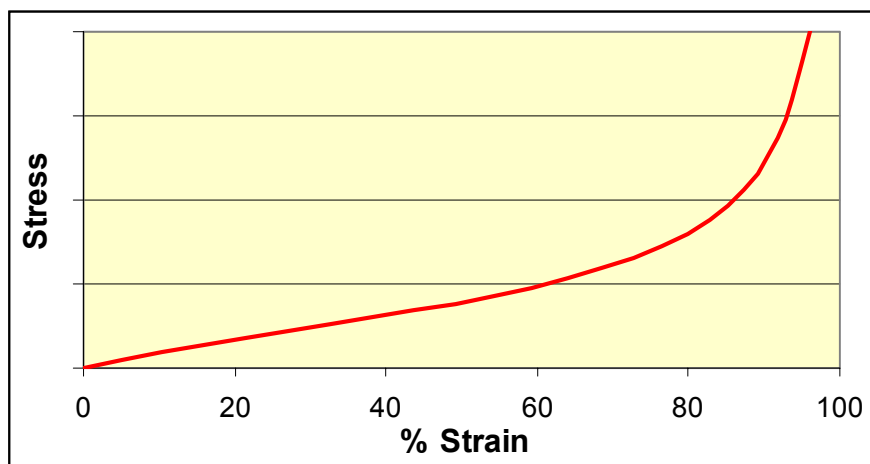


Figure 6.21. Stress strain characteristic for the Young's modulus of the CSF for the impactor analysis.

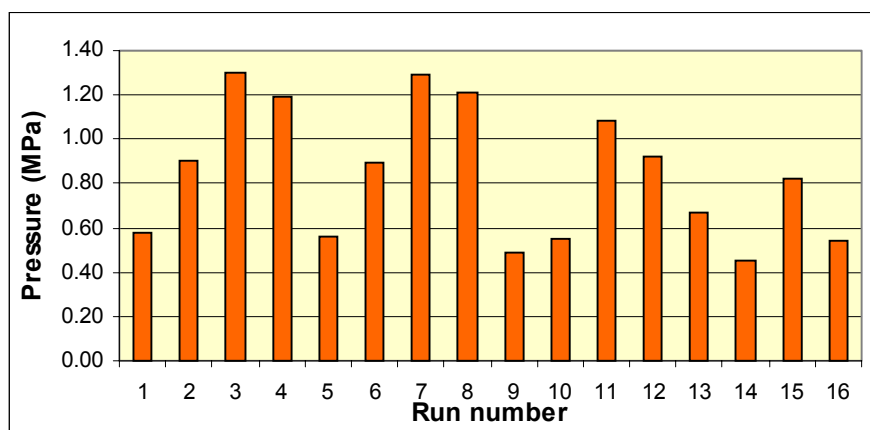


Figure 6.22. Peak pressure recorded in element 6327 for the impactor analysis.

Similar disruptions were observed when the impactor mass and padding stiffness were varied. Peak brain pressure was inversely affected by changes to the Young's modulus of the padding. Thus, contradicting the positive influence that this was expected to have on this model response. Furthermore, the effect of impactor mass on the brain peak pressure was expected to be direct but, when measured, was found to be erratic, especially in the elements experiencing large peak pressures close to the point of impact; figure 6.22 provides an example of this. It shows that with an isolated increase in the mass of the impactor, for example runs 1,2,3 and 5,6,7, there was an increase in the peak pressure. However, when the mass of the impactor was increased further, runs 4 and 8, the peak pressure was lower than it was at the lower impact mass.

Again, it is postulated that the load curve defined for the CSF (figure 6.21) may have been responsible for these effects observed in the impactor analysis. In addition, the Young's modulus of the impactor also changes at strains above 80%, and this may also have contributed to the irregular pattern and contradictory relationships observed between impactor mass, impactor stiffness and the output from the model. With hindsight it is considered that the Young's modulus of the impactor or its depth should have been increased to prevent the stiffness of the impactor from varying during the impact. This may have provided a more regular array of results to interpret. However, what the results do show is what may potentially occur in reality: that using a material with a low stiffness

or thickness to protect the head from injury could potentially lead to higher brain responses depending on the magnitude of the impact to the head.

Erratic results were achieved from the MRA performed to establish the relative importance and sensitivity of each parameter investigated. For many of the outputs, mainly peak pressure, weak relationships were achieved from the linear MRA. This result was more common for the elements positioned close to the impact site, where, for peak brain pressure, the magnitude of the response was at its greatest. In general, the analysis of the MRA results gave a good insight into the model response to parameter changes.

The results indicate that the bulk modulus of the brain and the short time shear modulus of the CSF have a significant influence on the peak pressure and von Mises stress in the brain. However, large changes are needed in the bulk modulus of the brain to produce significant change in the model's response. The Young's modulus of the CSF was generally found to have little effect on the response of the model. However, it was found to influence the peak pressure in elements positioned close to the point of impact. It is uncertain if these results provide a true reflection of how the CSF influences the brain's response. The observed effect could be caused by the use of a soft, elastic, solid body to represent what is in reality a fluid. Consequently, it is recommended that the material characteristics of the CSF be further developed to be more accurate.

It was found that impactor mass and impactor stiffness influenced the peak pressure and von Mises stress observed in the brain of the model. However, both the peak pressure and von Mises stress was found to be over a thousand times as sensitive to a unit change in the mass of the model (Kg) as to a unit change in the stiffness of the impactor (KPa).

6.6. NUMERICAL SIMULATION OF ACCIDENTS

6.6.1. Method

Part of the process of accident investigation was to collect the accident helmet. The damage was examined and then TRL replicated the damage by drop testing a helmeted Hybrid III dummy head fitted with a new helmet of the same type as was worn in the accident until the damage was accurately reproduced. Linear and rotational motion and external force was measured during the tests and Strasbourg University used this information as part of the investigation into the mechanism of brain injuries.

However, before accidents could be simulated, it was necessary to couple the human head model with the helmet model and then develop a simulation method that described the best input for a given accident. The coupling of the head with the helmet is illustrated in figure 6.23 below.

For the input analysis a parametric study was performed for a particular accident, G168. This showed that calculated intracerebral stresses are sensitive to the kind of inputs chosen for this specific accident.

It was possible, using the data supplied by TRL, to simulate the accident in two ways: use the velocity and helmet orientation measured by TRL at the point of impact as initial conditions for the simulation or use the linear and rotational acceleration time histories supplied by TRL as inputs to the skull. Both methods were applied to two accidents and there were no significant differences observed in the skull acceleration and intracerebral stress level. It was, therefore, decided to apply the 3D linear and angular acceleration recorded on the headform to the skull of the human head FEM. Only in case of skull fracture was velocity used as the input.

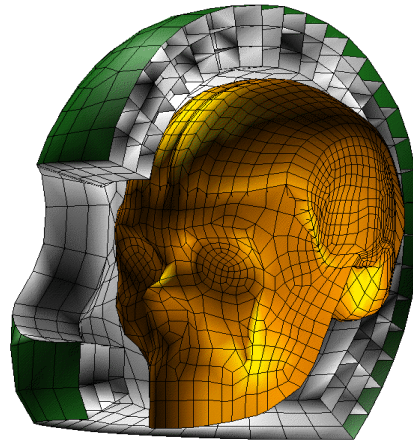


Figure 6.23. Coupling of the human head FEM with the helmet model

6.6.2. Head impact simulation

For the selected accident cases, reconstructed experimentally at TRL, the reconstruction report was transferred to ULP, Strasbourg. In addition ULP was provided with an electronic copy of the results of the 3D linear and angular acceleration of the dummy head. From this 3D-acceleration field, the velocity was calculated at three points on the skull FEM and this was used as the input to the FE accident simulation. Intracranial response was then computed with the RADIOSS code in order to calculate intracerebral stress and strain fields as well as brain-skull relative motion as a function of time. An example of a results sheet is shown in figure 6.24 for accident G165-1. It gives loading curves, maximum values and field parameter descriptions.

Table 6.3 presents the cases selected for the numerical accident reconstruction and it can be seen that AIS values vary from zero to five. This table also gives values for the peak input accelerations, the computed HIC value, and the maximum values of the outputs such as pressure, tensile and von Mises stress in the brain and intra-cerebral strain energy. As an example figures 6.25a and 6.25b show the linear and angular input data for case no.G174. Figures 6.25c to 6.25d show the variation of pressure with time and the von Mises stress and strain energy at the point where the pressure was a maximum. Figures 6.26a and 6.26b illustrate the distribution of these parameters through the brain.



NUMERICAL REPLICATION OF ACCIDENT G165_1

MEDICAL REPORT

MAIS 2
<i>Head injuries</i> : Obtunded on admission
<i>Neck injuries</i> :

EXPERIMENTAL REPLICATION

[m/s ²]	$\ddot{\omega}$ [rad/s ²]	HIC	Impact Velocity [m /s]@angle[degrès]
1	11447	669	12 @ 30 ⁰

NUMERICAL REPLICATION

Pressure [kPa] Min and max	V. Mises stress [kPa][Skull vM stress [kPa]	Skull-brain relative displacement [mm]
81 and 116	20		0.4

Numerical replication detail

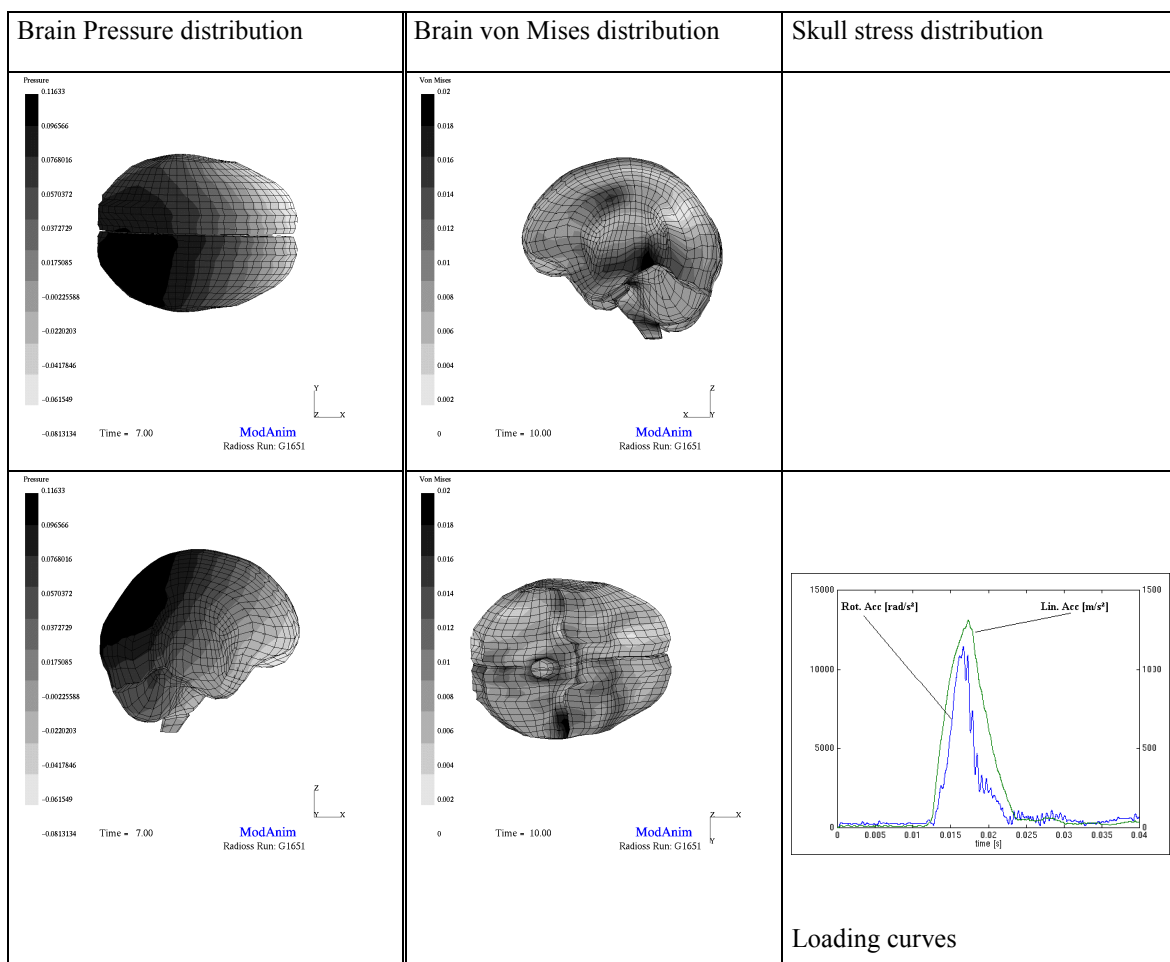


Figure 6.24. Result sheet relative to the numerical accident reconstruction

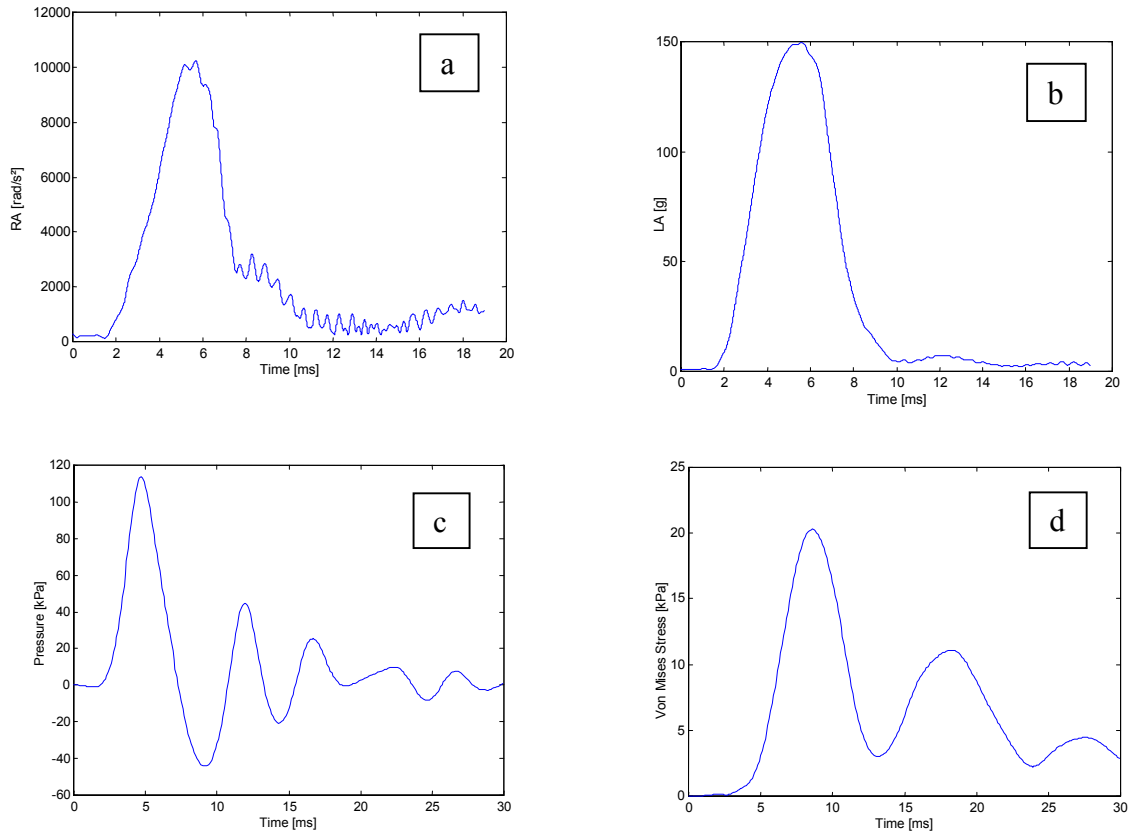


Figure 6.25. Time evolution of input and output parameters for accident simulation case G174 :

**6.25a) linear acceleration and
6.25c) maximum pressure and**

**6.25b) rotational acceleration for the inputs
6.25d) maximum von Mises brain stress
for the output.**

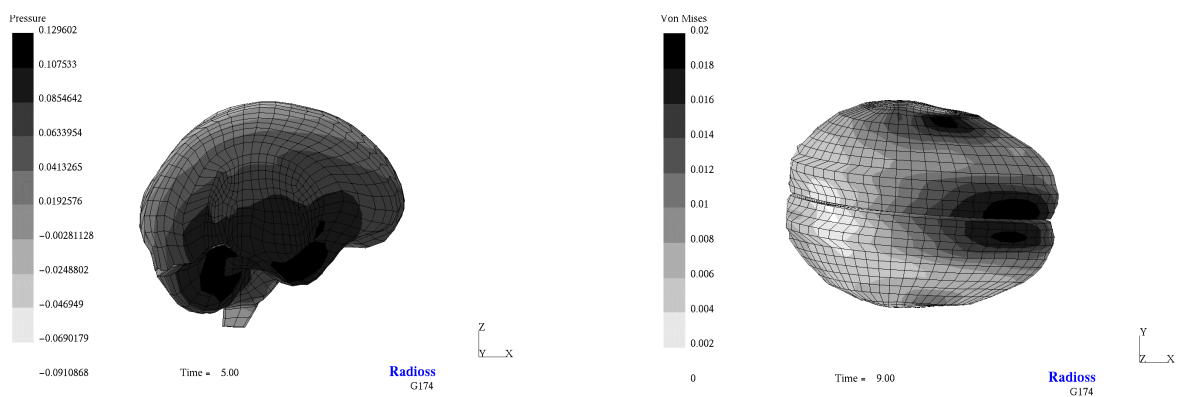


Figure 6.26. Intracerebral field parameters calculated for accident simulation case 174

6.26a) Pressure and

6.26b) von Mises stresses

Table 6.3 Details of the 13 accident cases selected for numerical replication

Case	AIS	Lesions	Group	PLA [g]	PRA [rad/s ²]	HIC	Pmax [KPa]	vMmax [kPa]	CSFIE [mJ]
G196	0	None	1	105	4056	306	130	15	2751
G313	0	None	1	88	6421	254	224	20	4077
G325_1	0	None	1	118	375	578	110	14	1955
G327	0	None	1	107	5026	248	115	15	1592
G165_1	2	Obtunded on admission	2	134	11447	669	80	20	1249
G174	2	Amnesiac for incident	2	152	10234	751	129	20	1698
G197_1	2	Obtunded with post traumatic amnesia	2	167	8341	771	190	20	1924
G345_1	2	Concussion	2	191	21910	667	151	22	1169
G107	5	Subdural and subarachnoid haematoma - unconscious on admission	3	192	11482	1389	186	13.5	3904
G411	4	Subdural and small subarachnoid haematoma - unconscious on admission	3	234	14860	2208	210	40	5221
G157	5	Base of skull and parietal bone fracture - extradural haematoma - unconscious	4	115	3780	154	220	26	4254
G154_2	3	Base of skull fracture - amnesiac for event	4	204	11173	1685	260	23	7365
G193	5	Base of skull fracture - contusions - brain swelling	4	447	32684	8918	760	45	23062

6.6.3. Results

Currently accident analysis attempts to correlate head injury with a value of AIS and, in turn, with measurements such as maximum linear or rotational acceleration and criteria derived from these measurements such as HIC and GAMBIT. The purpose of this research was to attempt to correlate the injury with the mechanism and explore the deficiencies in the AIS system through the investigation of ten cases.

Initially, the maximum pressure and the maximum von Mises stress was plotted against AIS for the 13 cases as shown in figure 6.27. Again, simple AIS values do not correlate well with either pressure or with shearing stresses. Case G196 (AIS 0) sustained a pressure similar to that of G174 (AIS 2) and G345 (AIS 2) sustained a shear force similar to that of G157 (AIS 3) and G154 (AIS 4).

However, when the type of lesion, rather than AIS, was used for comparison, then four distinct groups emerged: group 1, uninjured; group 2, concussed; group 3, sub-dural haematoma; and group 4, skull fracture. In order to analyse intra-cranial response in more detail, histograms were plotted of maximum intra-cerebral pressure, maximum von Mises stress, maximum strain energy and the maximum shearing force in the CSF layer. After examination it was found that the value of a given parameter for a specific group of

accident victims was found to be valid as a means of estimating a tolerance limit for the injury sustained by that group. For example, the histogram given in figure 6.28a shows that pressure, because of the wide variation was not responsible for the injury in groups 1 to 3. Only group four shows a correlation of injury with pressure.

The maximum von Mises stress and strain energy, see figures 6.28b and 6.28c, are of greater interest and show better correlation. group 1, uninjured, sustained low values whereas group 2, concussed, sustained values typically twice that of group one. However, for groups 3 and 4, haematoma and fracture, the von Mises stress and strain energy varied greatly. The third histogram figure 6.28c shows a further correlation.

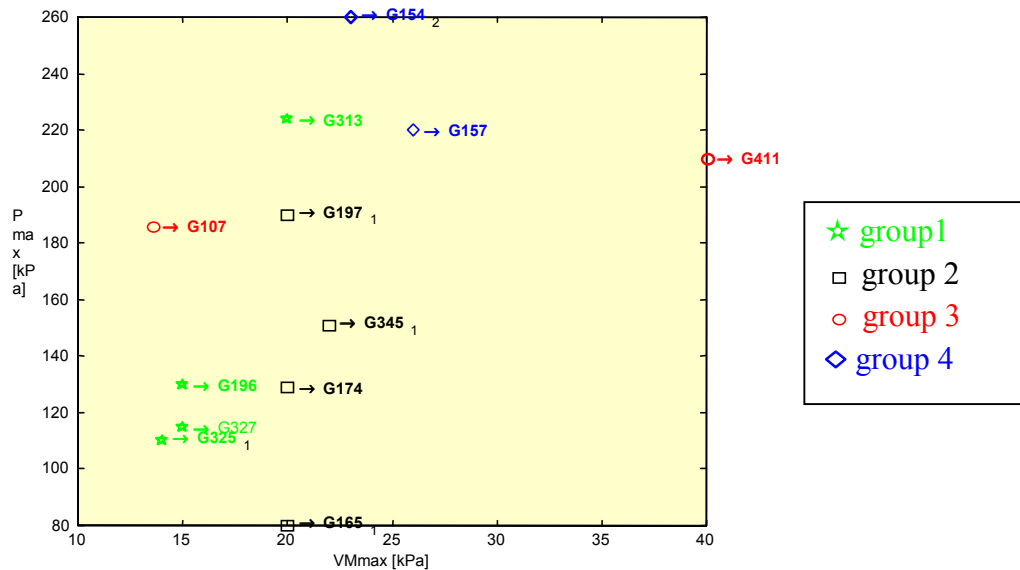
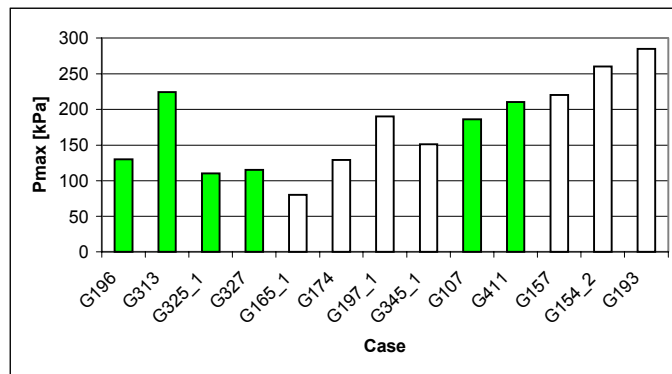


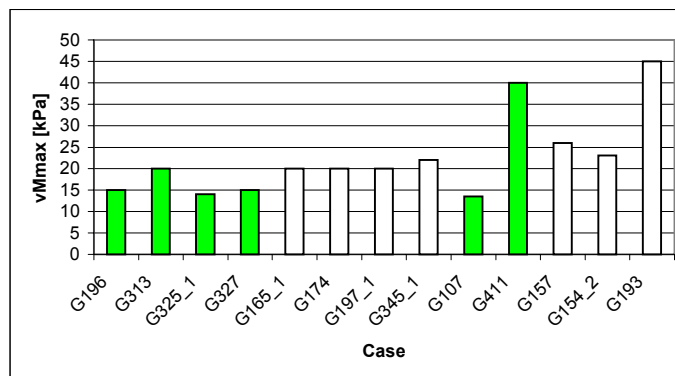
Figure 6.27. Results of the 13 simulated accident cases in the “maximum pressure-maximum von Mises plan”: (group 4 - case G193 is out of the figure)

The above analysis lead to the following conclusions. Intra-cerebral von Mises stresses and strain energy are indicators of concussion, group two, with values of 10kPa for short duration concussion and 20kPa for long duration. SDH, group 3 may be related to brain – skull relative motion which, in the above analysis, is expressed in terms of strain energy. Figure 6.28c shows that there is an upper limit of this parameter of the order of 4J. Finally, the skull fracture cases from group 4 are obviously due to skull stresses which were not calculated in this study.

a)



b)



c)

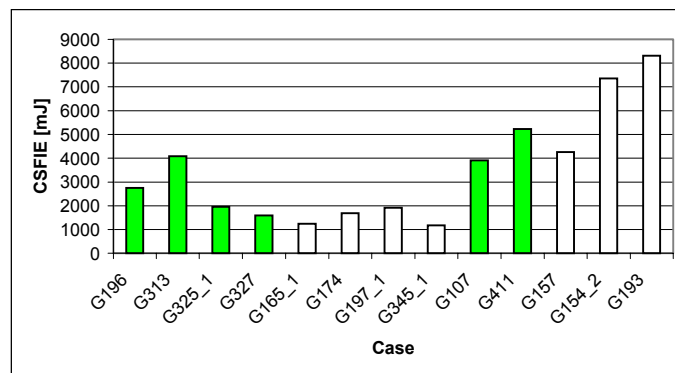


Figure 6.28. Histograms of intra-cranial parameters relative to the 13 accident simulations : a) Maximum brain pressure, b) maximum von Mises stress in the brain and c) maximum strain energy in the CSF layer.

6.7. CONCLUSIONS

1. A finite element model of a human skull and brain has been developed in RADIOSS by Strasbourg University. The skull model was meshed using data obtained by digitising, in detail, the inner and outer profiles of a human skull. The model is unique in the extent to which the various parts of the head and brain are defined. Of particular note is the representation of the subarachnoid space between the brain and skull with brick elements which, in this model, were used to simulate the cerebral-spinal fluid.

2. The head model has been successfully calibrated against the well known Nahum cadaver data and was shown to give accurate predictions at all the five sites within the brain, as examined by Nahum. Impact force, pressure at the impact site and opposite to it and the distribution of von Mises stresses were simulated sufficiently accurately to give confidence that the model may be used, as intended, for the investigation of head injury mechanisms over a wide range of input parameters.

3. The helmet model was developed by meshing, from three dimensional data supplied by TRL, of the outer profile of a typical UK helmet. The model was calibrated against data from impact tests of the helmet on a headform, supplied by TRL and Strasbourg University.

4. A neck model has been developed by Polytecnico Milano, first as a multi-body lumped mass model and then as a finite element model, in PAM CRASH, that can be linked with the model of the skull, brain and helmet. The neck comprises eight rigid vertebrae, six non-linear viscoelastic intervertebral discs, 34 non-linear viscoelastic ligaments, 17 nonlinear facet joints and 13 pairs of muscles. The model has been successfully calibrated against published human volunteer data obtained from sled tests. Particularly good agreement was obtained for the head acceleration and neck rotation. It should be noted that the inclusion of non-linear visco-elastic ligaments was essential to obtain good agreement of the head rotation with time.

5. An analysis of head and head impact parameters of the finite element model of the skull and brain showed that:

1) The brain bulk modulus has a significant influence on the peak pressure and von Mises stress of the brain, although large changes in the bulk modulus of the brain are needed to arouse significant changes in these model responses,

2) the short time shear modulus of the brain has a significant impact on the peak von Mises stress of the model, but an insignificant influence on the peak pressure,

3) In general the Young's modulus of the CSF has an insignificant influence on the peak pressure and von Mises stress of the brain in the head model,

4) The peak von Mises stress of the brain is around five orders of magnitude more sensitive to a unit change (KPa) in the brain short time shear modulus than it is to a unit change (KPa) in the bulk modulus of the brain,

5) Both the mass and stiffness of an impactor have an important impact on the peak pressure and von Mises stress in the brain,

6) Both the peak pressure and von Mises stress of the brain are around a thousand times as sensitive to a unit change (Kg) in the mass of an impactor striking the forehead, as they are to a unit change (KPa) in the stiffness of the impactor.

6. An FE mesh of the motorcycle helmet was added to the model, which was then used to simulate 13 motorcycle accidents selected from the COST 327 Action database. The damage to the accident helmets had been replicated by drop tests at TRL during which rotational and linear acceleration and external forces were measured. The output from the model was compared with the head injuries recorded for each case. It was concluded that AIS does not correlate well with the conventional test criteria such as linear acceleration, HIC and GAMBIT. However, when brain behaviour was examined the four distinct groups emerged: uninjured, concussion, sub-dural haematoma and skull fracture.

7. The foregoing analysis led to tentative proposals for brain injury criteria as follows;

- 1) Intra-cerebral von Mises stress of 10kpa for short duration concussion
 - 2) Intra-cerebral von Mises stress of 20kpa for long duration concussion
 - 3) Strain energy in the cerebral spinal fluid of approximately 4J for sub-dural haematoma
 - 4) Skull fracture was identified but not assessed in this study but should be included in future research.
8. It is believed, with good supporting evidence, that this overall model represents the state of the art for a finite element model of the skull, brain, neck and helmet.

CHAPTER 7. TOLERANCE OF THE HEAD AND NECK TO INJURY

7.1. INTRODUCTION

The objective of the Head and Neck Tolerance Working Group was to evaluate the tolerance of the head and neck to injuries sustained in motorcycle accidents and to present the results in terms of injury probability and injury prediction. The Head and Neck Tolerance Working Group was linked very closely to the Accident Investigation, the Reconstruction, and the Computer Simulation Working Groups which were responsible for accident data collection and experimental and numerical replication of selected accidents.

Part of the accident data collection process was to collect and examine the helmets and to record the extent and location of the damage. Also recorded was an estimate of the head impact speed, an estimate of the direction of the impact force to the head, and an estimate of the motorcyclist's trajectory during the accident. Detailed injury information was recorded and for the serious and fatal cases this included neuropathological data of the brain injuries. The Accident Investigation Working Group used such information, together with an extensive range of other data, to determine which accidents were likely to be suitable for replication. This information was then given to the Reconstruction Working Group.

The purpose of reconstruction was to examine the accident case file and the helmet, and then to attempt to reproduce the same damage, by drop testing equivalent new helmets. The test method was to drop a helmeted headform at different velocities onto a surface similar to what was impacted during the accident and at the angle identified by the accident data collection team. The headform was equipped with extensive instrumentation such that both the linear and rotational acceleration could be recorded. These measurements were then compared with the type and severity of head injuries that had been determined by clinical experts and, in particular, the neuropathological analysis provides detailed brain injuries for the fatal and serious cases.

The ULP numerical replication was performed on cases replicated experimentally by TRL. Finite element (FE) modelling was used to simulate the impact force, pressure at the impact site and opposite to it, and the distribution of von Mises stresses. The Bimass headform model was used to calculate linear and rotational acceleration of the skull and brain and also the linear and rotational acceleration of the skull relative to the brain.

7.2. PRINCIPLES OF HEAD INJURY SEVERITY PREDICTION, PROBABILITY, TOLERANCE

The severity of head injury was classified according to the well known Abbreviated Injury Scale (AIS) consisting of 6 discrete categories, AIS 1 minor, AIS 2 moderate, AIS 3 serious, AIS 4 severe, AIS 5 critical, and AIS 6 maximum; AIS 0 is uninjured. In the following analyses the AIS severity of head injury of the cases considered is plotted against specific physical parameters, which have been estimated by accident reconstruction, measured or calculated by experimental or numerical replication. For example, these parameters are head(form) impact speed, linear and rotational acceleration, and HIC etc. Statistical methods were used and a regression equation was applied to calculate the best possible correlation indicated by a maximum coefficient of precision r^2 .

In the present analyses this was normally a logarithmic function; a representative example is given in figure 7.1.

Except at points of intersection with AIS horizontals, such a regression function calculates undefined continuous “AIS-values” but not discrete integer AIS categories 0 – 6. Therefore, all non-integer results need to be transposed into integer values as is demonstrated for the example in figure 7.1.

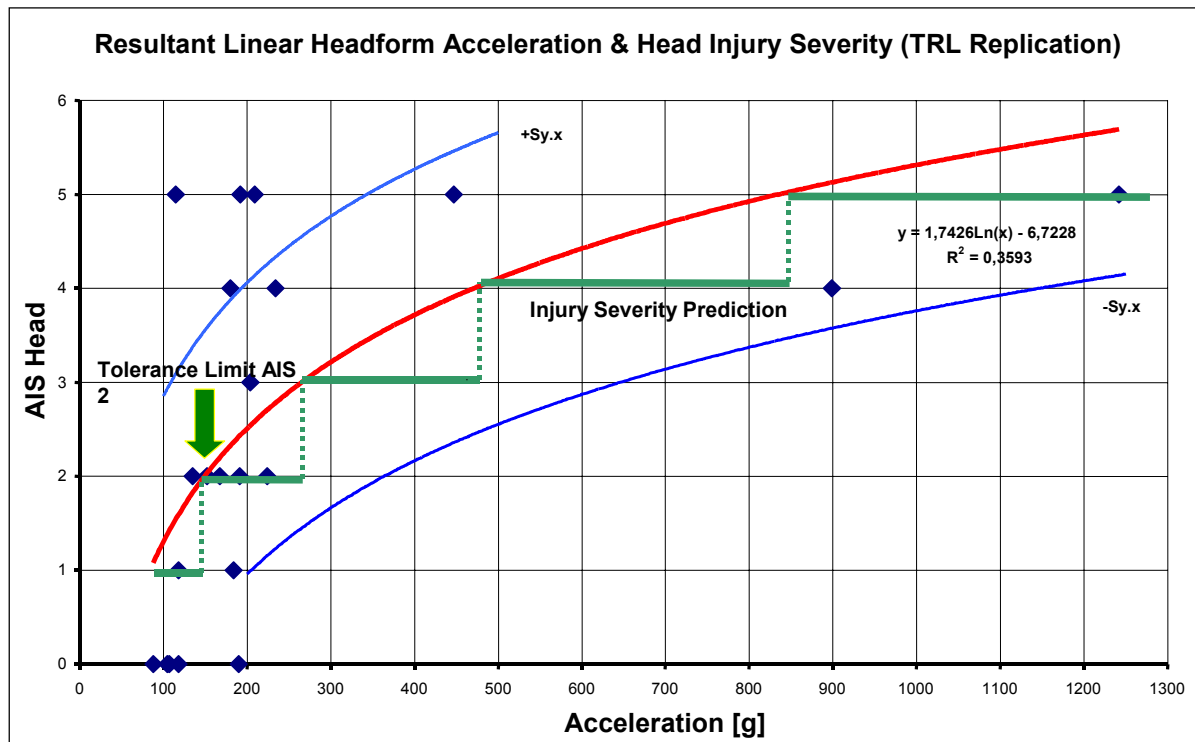


Figure 7.1. TRL replication showing resultant linear headform acceleration and head injury severity

When the equation $y = 1.7426 \ln(x) - 6.7228$ was applied for $x = 200$ g the result was “AIS = 2.51”. However, the best results for predicting AIS head injury severity were achieved by applying the mathematical integer function $\text{Int}(\text{“AIS”})$ in a strict sense, for example, $\text{Int}(2.y) = 2$ for all y , and values $y > .50$ were not rounded up to $y+1$. Thus, for instance, if $x = 200$ g is put in the equation $y = 1.7426 \ln(x) - 6.7228$ as shown figure 7.1 then $y = 2.51$ and the AIS head injury severity level predicted is $\text{Int}(2.51) = 2$. The best possible prediction of AIS levels was considered to be achieved if the percentage of AIS levels predicted accurately was highest in the samples examined. Therefore, the equations presented in the following sections were applied like transfer functions, the results of which needed to be transposed into integer AIS categories, as necessary.

The probability functions were approximated to a normal distribution of AIS values. As an example, figure 7.2 illustrates the approximate normal distribution of AIS levels in a selected headform acceleration range of 150 – 250 g, and for comparison the standard normal distribution is given. Of course, in intervals with very few data points, the normal distribution is not always as statistically significant as is shown in the example.

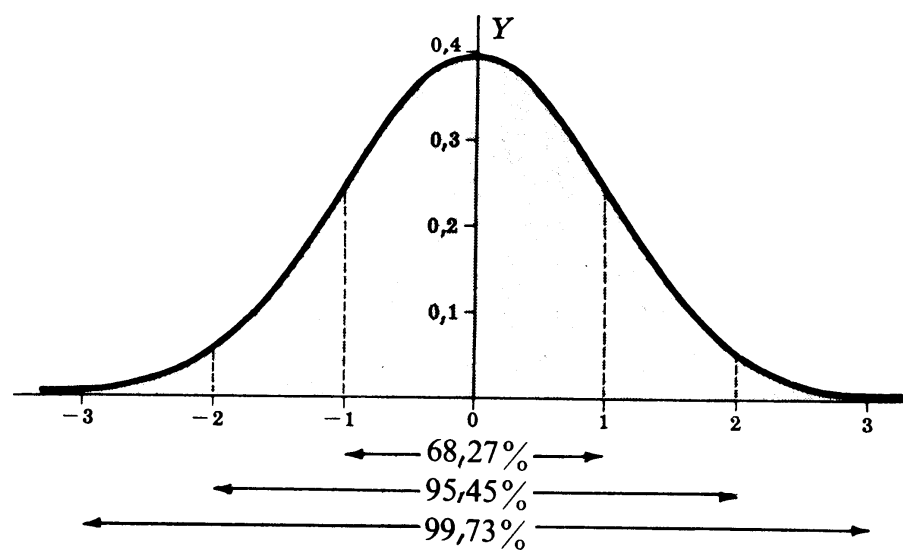
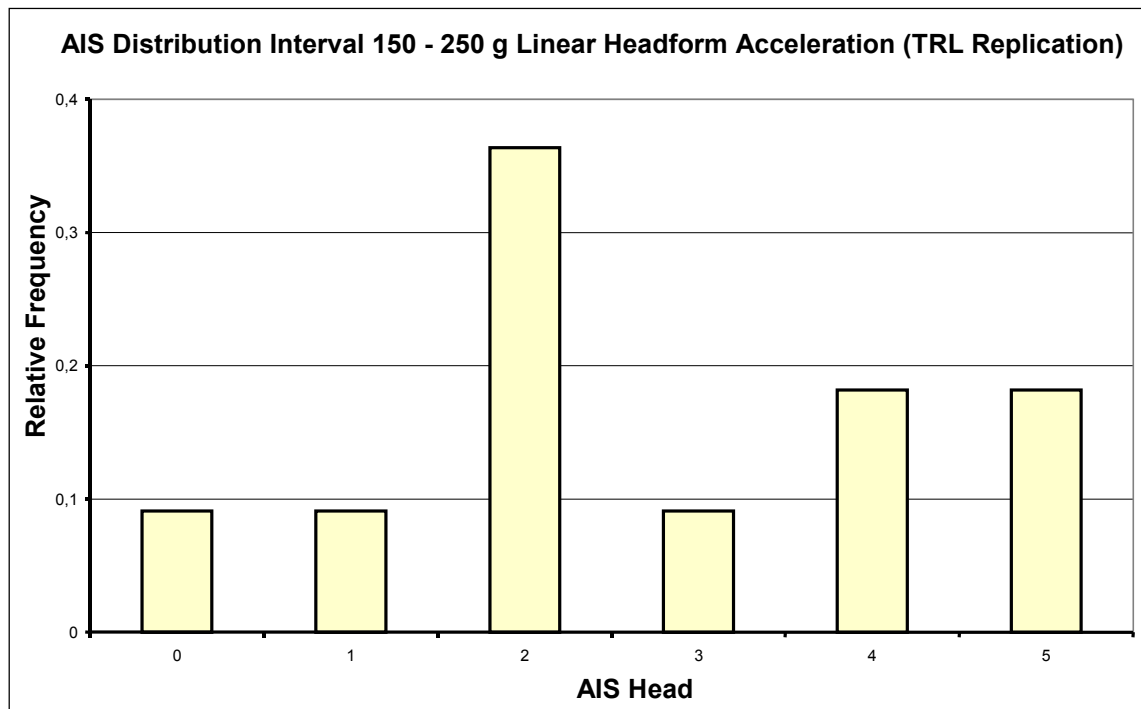


Figure 7.2. AIS distribution interval 150 - 250g linear headform acceleration (TRL replication) compared with normal distribution

The standard deviation of estimation for AIS levels $s_{y,x} = s_y (1 - r^2)^{1/2}$ permits the probability of AIS levels to be calculated for a given value of the physical parameter considered. The probability P is given by the ordinate of the standard normal distribution (Gauss Function, s_y is the standard deviation of all data points).

As shown in figure 7.1 the limits for one standard deviation, $\pm 1 s_{y,x}$, are included in the following diagrams and indicate an injury severity probability of approximately 24%. The regression curves (red centre lines) indicate a probability of about 40% (c.f. standard normal distribution).

Considering the example presented in figure 7.1. and the normal distribution as shown in figure 7.2 the probabilities of injury for 200 g headform peak linear acceleration are as follows:

AIS 1: P = 24% (cumulative 76%),

AIS 2: P = 38% (cumulative 62%),

AIS 3: P = 38% (cumulative 38%),

AIS 4: P = 24% (cumulative 24%),

AIS 5: P = 11% (cumulative 11%).

The points of intersection of the regression curves with the AIS horizontal lines are considered to define the tolerance limit for this particular AIS head injury level (c.f. figure 7.1). As shown, this definition correlates to a probability of about 40% but a lower limit, e.g. 24%, could be selected as well, then indicating higher tolerance limits.

7.3. ESTIMATED HEAD IMPACT SPEED AND HEAD INJURY SEVERITY

In the vast majority of the motorcycle accidents investigated the helmeted head struck rigid objects, for example, a car structure, tree, lamppost, kerbstone, road surface etc. It was considered that, in each case, the mechanical loading of the head associated with the impact caused the head injury. Therefore, the severity of the head injury should be related to the impact speed. However, in real world accidents, estimation of the head impact speed is very difficult because of the complexity of the impact kinematics. Nevertheless, the head impact speed was estimated for 161 cases for which figure 7.3 illustrates the estimated head impact speeds related to AIS head injury severity.

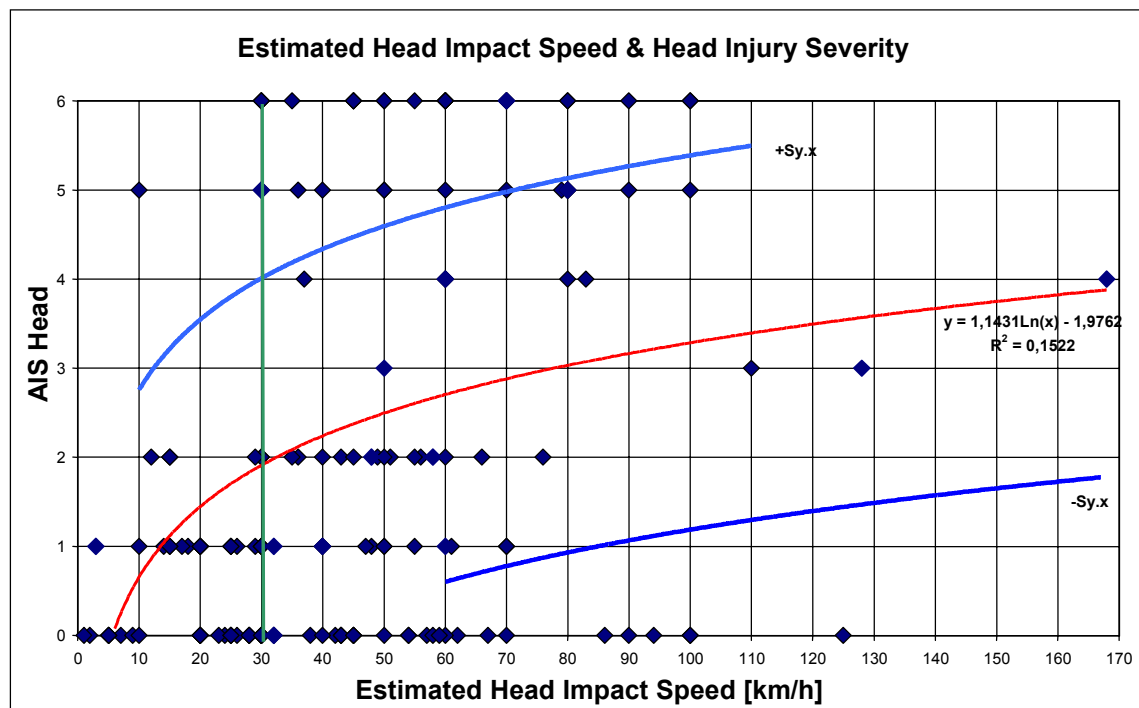


Figure 7.3. Estimated head impact speed and head injury severity

The distribution of data points in figure 7.3 indicates that, except for one case, serious head injury (AIS > 2) occurred at impact speeds of 30 km/h and higher. The majority of moderate head injuries are also related to impact speeds above 30 km/h. However, more

than 50% of the cases without head injury (AIS 0) were exposed to impact speeds between 30 km/h and 125 km/h, a distribution similar to critical and fatal head injury of AIS 5 and AIS 6. It can be concluded, therefore, that head impact speed v_{est} does not correlate well with AIS head injury severity.

The logarithmic regression shown in figure 7.3 shows that the best possible correlation is a very low coefficient of $r = 0.39$.

The equation

$$\text{AIS Head} = | 1.1431 \ln (v_{est}) - 1.9762 | \quad (7.1)$$

predicts the AIS severity of head injury accurately in only in 25% of cases and, in particular, this does not include the higher levels, AIS 5 and AIS 6.

The accident data suggests that a moderate head injury of AIS 2 is the most likely outcome at 30km/h.

7.4. EXPERIMENTAL REPLICATION AND HEAD INJURY SEVERITY

Experimental replication was performed at TRL for 21 accident cases, 1 case from Finland, 3 cases from Hannover and 17 cases from Glasgow. The laboratory test method and the replication data determined is described in Chapter 5.4. The following analyses are based upon this data and relate to the physical parameters obtained in the laboratory experiments in which helmet accident damage was replicated.

7.4.1. Headform impact speed

Figure 7.4 presents the headform impact speeds measured in the laboratory drop tests at TRL.

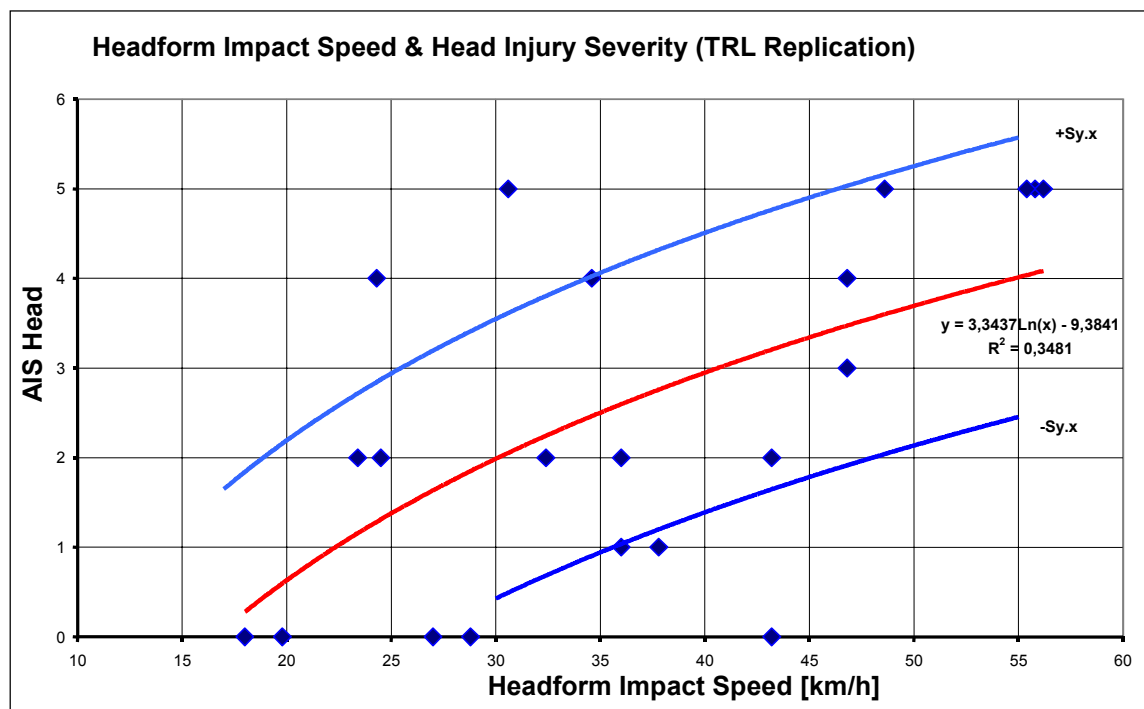


Figure 7.4. Headform impact speeds in laboratory drop tests at TRL

The logarithmic regression shown in figure 7.4 gives $r=0.59$ as the best possible correlation, which is much better than the 0.39 given in section 7.3 for the speed estimated from accident data.

The equation

$$\text{AIS Head} = | 3.3437 \ln (v_{hf}) - 9.3841 | \quad (7.2)$$

predicts the AIS value accurately in 24% of cases and furthermore, predicts that the head injury severity will be AIS 2, moderate, at 30 km/h and AIS 3, serious, at 40 km/h.

7.4.2. Linear headform acceleration

Figure 7.5 presents the values of the peak resultant linear headform acceleration recorded in the drop tests at TRL.

The logarithmic regression shown in figure 7.5 gives $r=0.60$ as the best possible correlation, which is similar to the 0.59 given in section 7.4.1 for the headform impact speed.

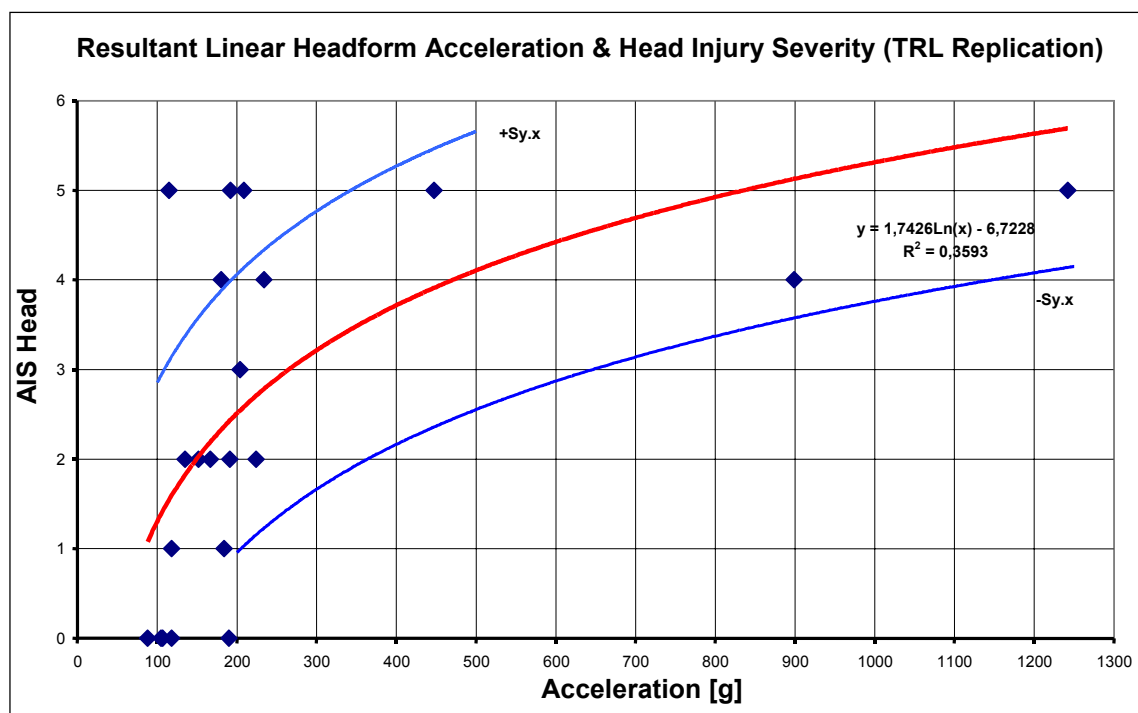


Figure 7.5. Peak resultant linear headform acceleration from laboratory drop tests

The equation

$$\text{AIS Head} = | 1.7426 \ln (a_{lin}) - 6.7228 | \quad (7.3)$$

predicts the AIS value accurately in 29% of cases and furthermore, this includes AIS 5 and AIS 6, which is an improvement over the previous analysis. The head injury severity is predicted to be AIS 2, moderate at 150g and AIS 3, severe, at 260g.

Figure 7.6 illustrates that head impact test data published in the literature are similar to those of this investigation. The logarithmic regression shown in figure 7.6 gives $r=0.58$ as the best possible correlation, the same as for the headform linear acceleration.

The equation

$$\text{AIS Head} = | 1.7967 \ln (a_{\text{lin}}) - 7.1333 | \quad (7.4)$$

predicts the AIS value accurately in 20% of cases and this includes AIS 5 and AIS 6.

From the literature data the head injury severity is predicted to be AIS 2 at 160g and AIS 3 at 280g.

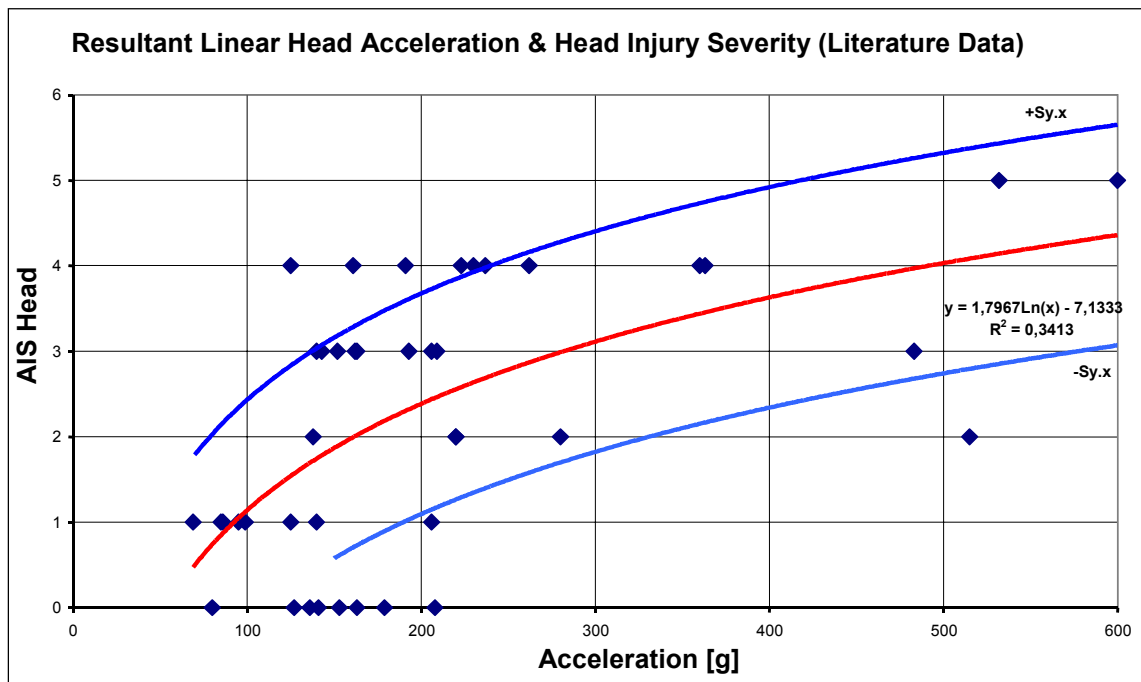


Figure 7.6. Head impact test data obtained from the literature data

7.4.3. Head Injury Criterion (HIC)

The Head Injury Criterion (HIC) is defined as follows:

$$HIC = \left[\left(\frac{1}{t_2 - t_1} \cdot \int_{t_1}^{t_2} a_{res} dt \right)^{2,5} \cdot (t_2 - t_1) \right]_{\max}$$

Linear acceleration and impact duration is considered in this well known head injury criterion, and it is generally considered that HIC 1000 relates to AIS 2 and HIC 1500 relates to AIS 3.

The logarithmic regression shown in figure 7.7 gives $r=0.80$ as the best possible correlation, and much better than for any of the previous analyses.

The equation

$$\text{AIS Head} = | 1.182 \ln (\text{HIC}) - 5.8364 | \quad (7.5)$$

predicts the AIS value accurately in 33% of cases and this includes AIS 5 and AIS 6. Figure 7.8 shows that HIC 1000 corresponds to a head injury severity of AIS 2 and HIC 1500 to a severity of AIS 3.

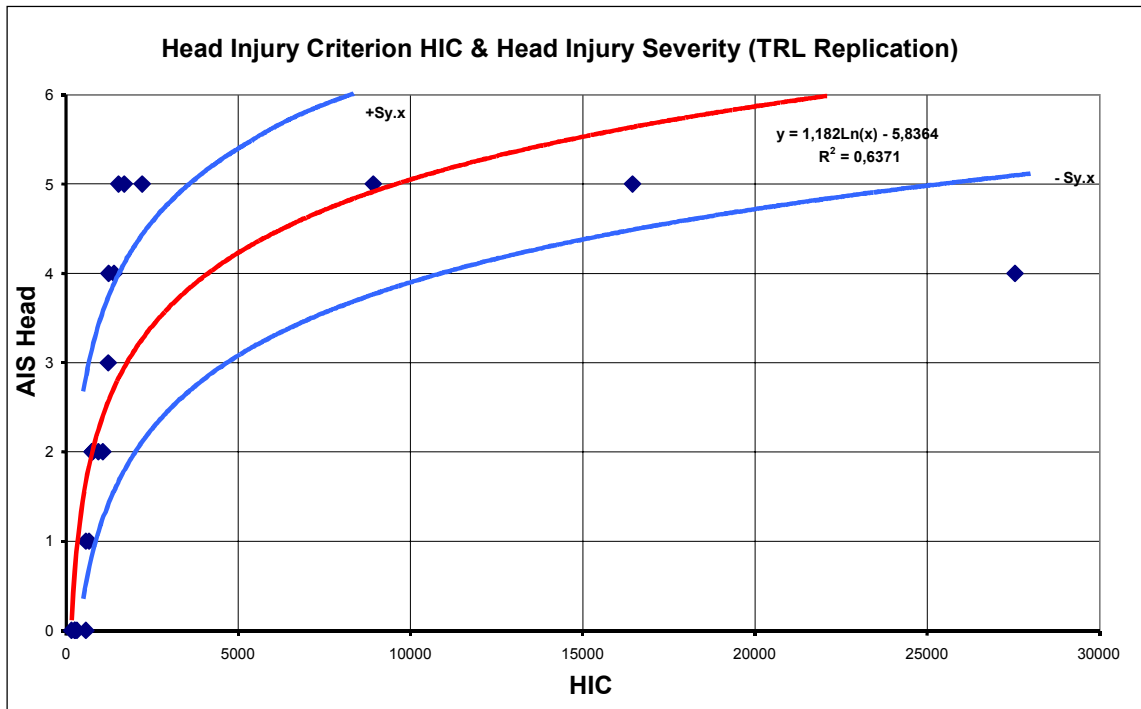


Figure 7.7. HIC and head injury severity from TRL replication

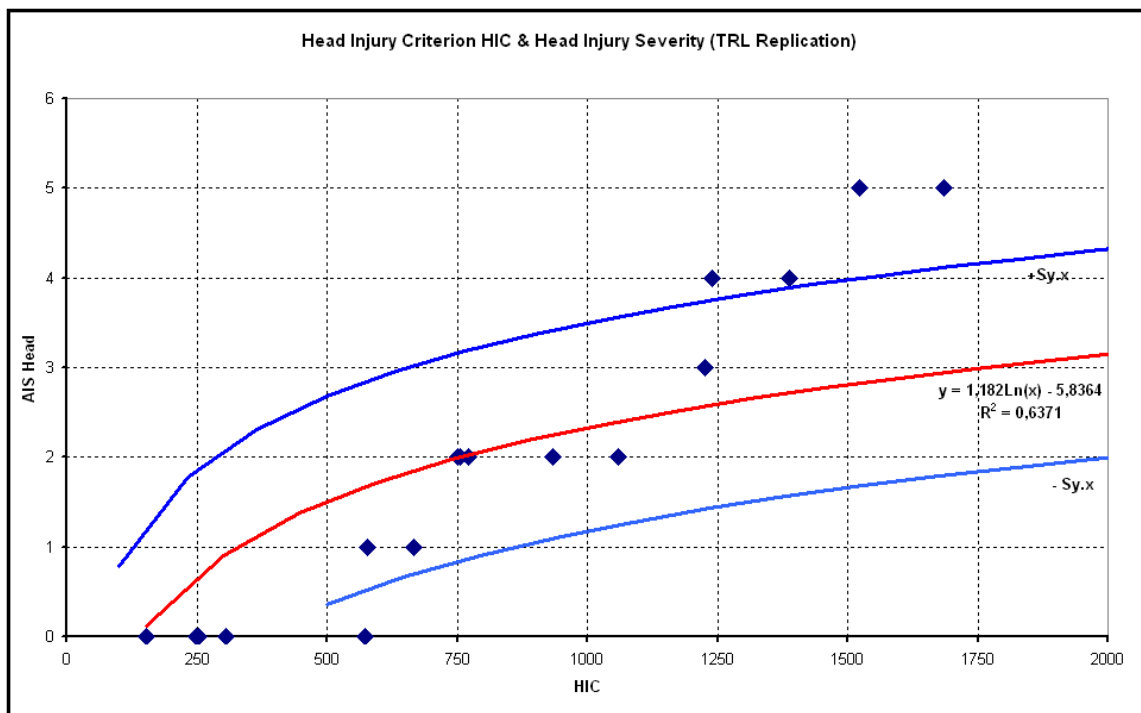


Figure 7.8. HIC and head injury severity from TRL replication

7.4.4. Rotational impact velocity

Figure 7.9 shows the peak values of the rotational headform velocities recorded in the drop tests at TRL.

In figure 7.9 it is evident that critical head injuries AIS 5 are related to lower rotational velocities than cases without head injury, AIS 0. Thus, it is not surprising to find that there is no correlation between rotational velocity and head injury severity ($r=0.007$).

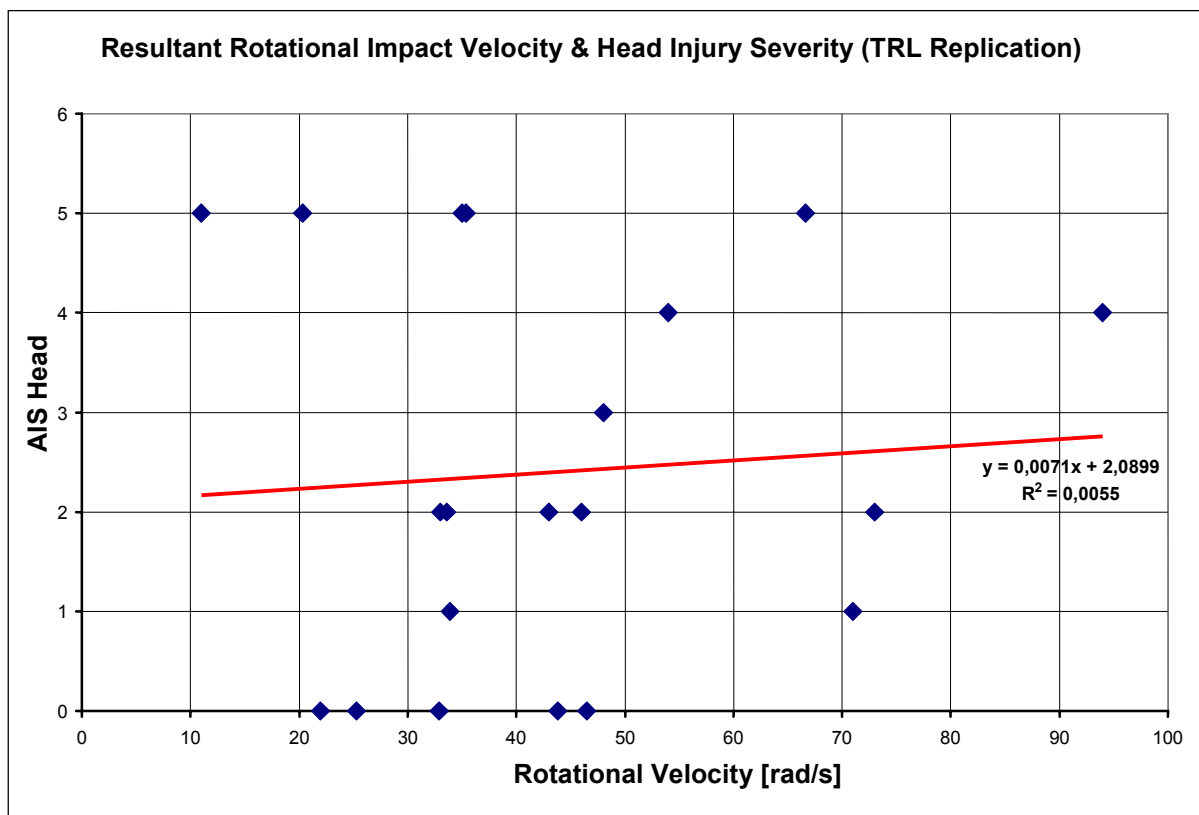


Figure 7.9. Peak values of the rotational headform velocities recorded in the drop tests at TRL

7.4.5. Rotational headform acceleration

Figure 7.10 presents the peak values of the resultant rotational headform accelerations recorded in the drop tests at TRL.

The logarithmic regression shown in Figure 7.10 gives $r=0.50$ as the best possible correlation, and lower than the 0.58 given in 7.4.2 for linear acceleration.

The equation

$$\text{AIS Head} = | 1.1485 \ln(\alpha) - 8.2818 | \quad (7.6)$$

predicts the AIS value accurately in 25% of cases and also predicts that predicts that the head injury severity will be AIS 2, moderate, at 8000 rad/s^2 and AIS 3, serious, at 19000 rad/s^2 .

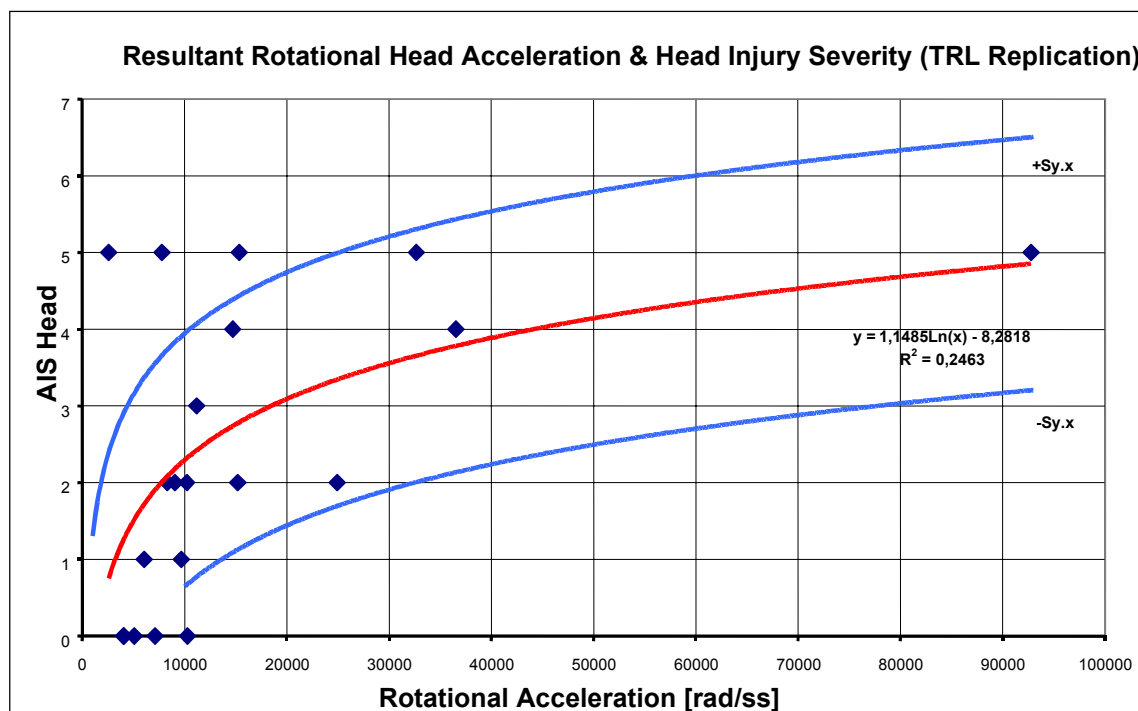


Figure 7.10. Peak values of the resultant rotational headform accelerations recorded in the drop tests at TRL

Figure 7.11 illustrates that the head impact test data published in the literature are similar to those of this investigation.

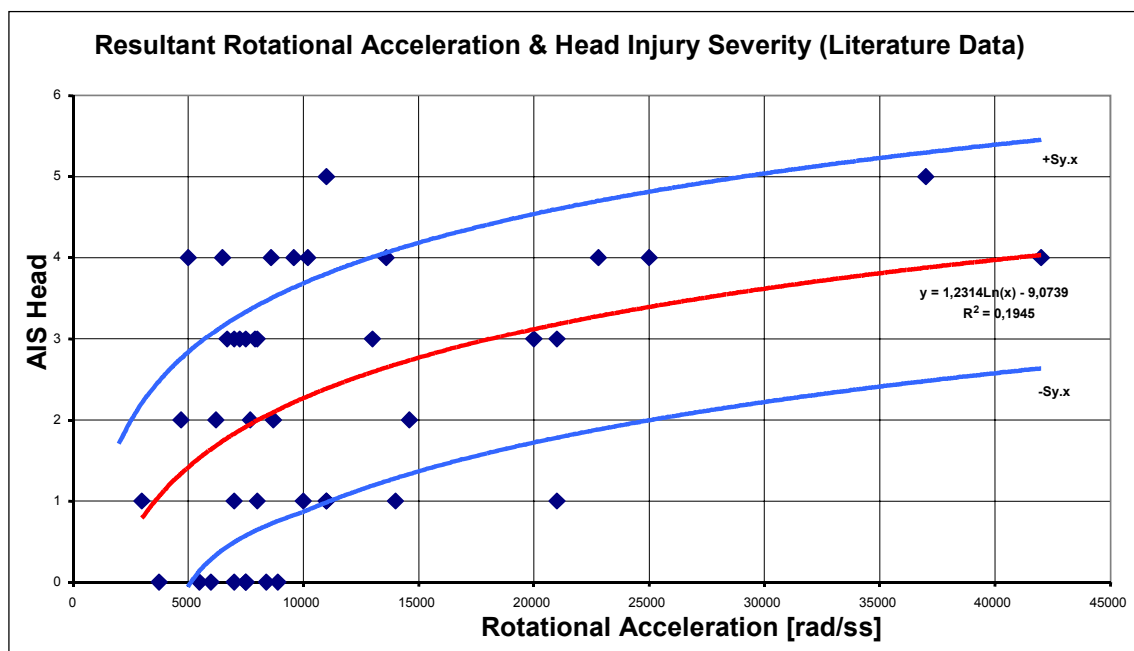


Figure 7.11. Head impact test data published in the literature

The logarithmic regression shown in Figure 7.11 gives the best possible correlation coefficient as $r = 0.44$, similar, though slightly less than, the 0.5 for the TRL drop tests.

The equation

$$\text{AIS Head} = | 1.2314 \ln(\alpha) - 9.0739 | \quad (7.7)$$

accurately predicts the AIS severity of head injury in 15% of cases: a far worse prediction than for all previous analyses.

Analysis from literature data predicts that the head injury severity will be AIS 2, moderate, at 8000 rad/s² and AIS 3, serious, at 18000 rad/s²; almost identical results those for the TRL drop tests.

7.4.6. Generalised Head Acceleration Model for Brain Injury Threshold (GAMBIT)

The Generalised Head Acceleration Model for Brain Injury Threshold, GAMBIT, is defined as follows (Newman 1986):

$$G(t) = \left[\left(\frac{a(t)}{a_c} \right)^n + \left(\frac{\alpha(t)}{\alpha_c} \right)^m \right]^{\frac{1}{s}}$$

Linear and rotational acceleration is considered in this head injury criterion. $G(t) = 1$ is considered to be the value at which head injury severity of AIS 3 occurs. The following analysis uses the parameters $n=m=s=2$ and the reference values $a_c = 250 \text{ g}$ and $\alpha_c = 10,000 \text{ rad/s}^2$.

The logarithmic regression shown in figure 7.12 gives best possible correlation coefficient as $r = 0.27$, a very low value.

The equation

$$\text{AIS Head} = | 0.7088 \ln(\alpha) + 2.1648 | \quad (7.8)$$

accurately predicts the AIS severity of head injury in only 10% of cases, a very poor result.

The regression curve in figure 7.12 confirms, approximately, that a value of GAMBIT = 1 corresponds to a moderate head injury of AIS 2.

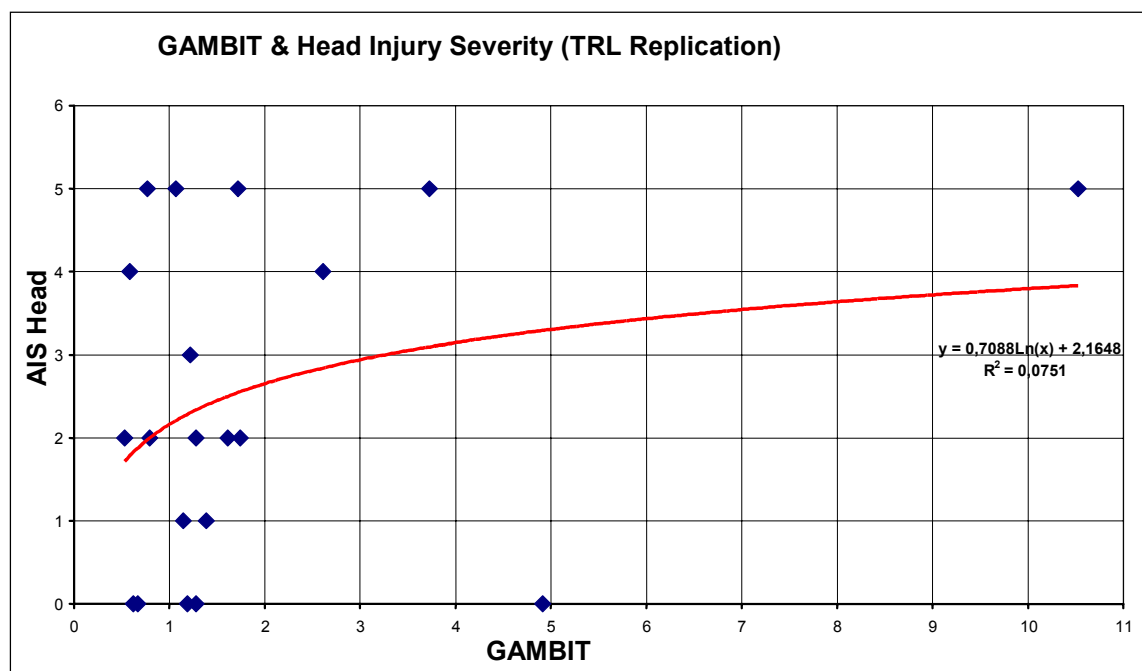


Figure 7.12. GAMBIT and HIC

7.4.7. External forces (normal and tangential)

Figure 7.13 presents the peak values of the external normal helmet forces recorded in the drop tests at TRL. The external normal force should correlate with linear headform acceleration.

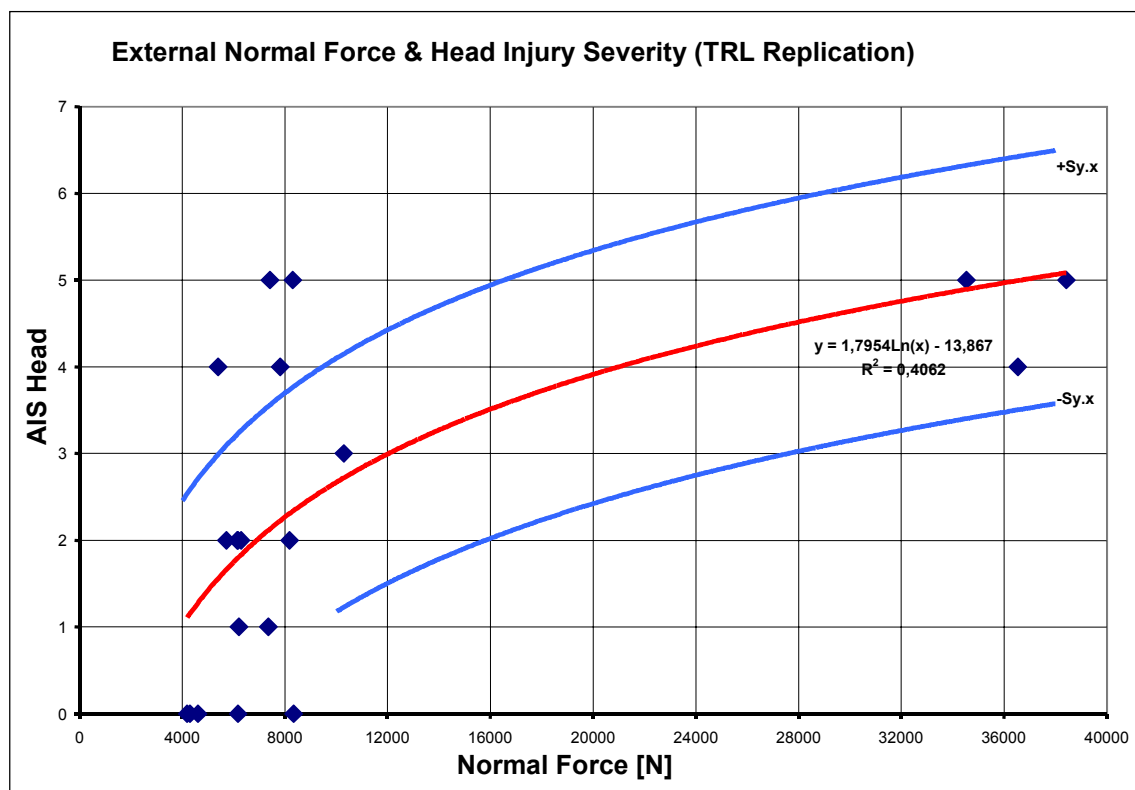


Figure 7.13. Peak values of the external normal helmet forces from drop tests at TRL

The logarithmic regression shown in figure 7.13 gives best possible correlation coefficient as $r = 0.64$ higher than the 0.58 for linear acceleration given in section 7.4.2. As expected the distribution of linear acceleration and normal force are similar.

The equation

$$\text{AIS Head} = | 1.7954 \ln (f_n) - 13,867 | \quad (7.9)$$

predicts the AIS severity of head injury in only 15% of cases and predicts that a head injury of severity AIS 2 will occur at 6500N and AIS 3 at 12,000N, normal force.

Figure 7.14 presents the peak values of the external tangential helmet forces recorded in the drop tests at TRL. The external tangential force should correlated with rotational headform acceleration.

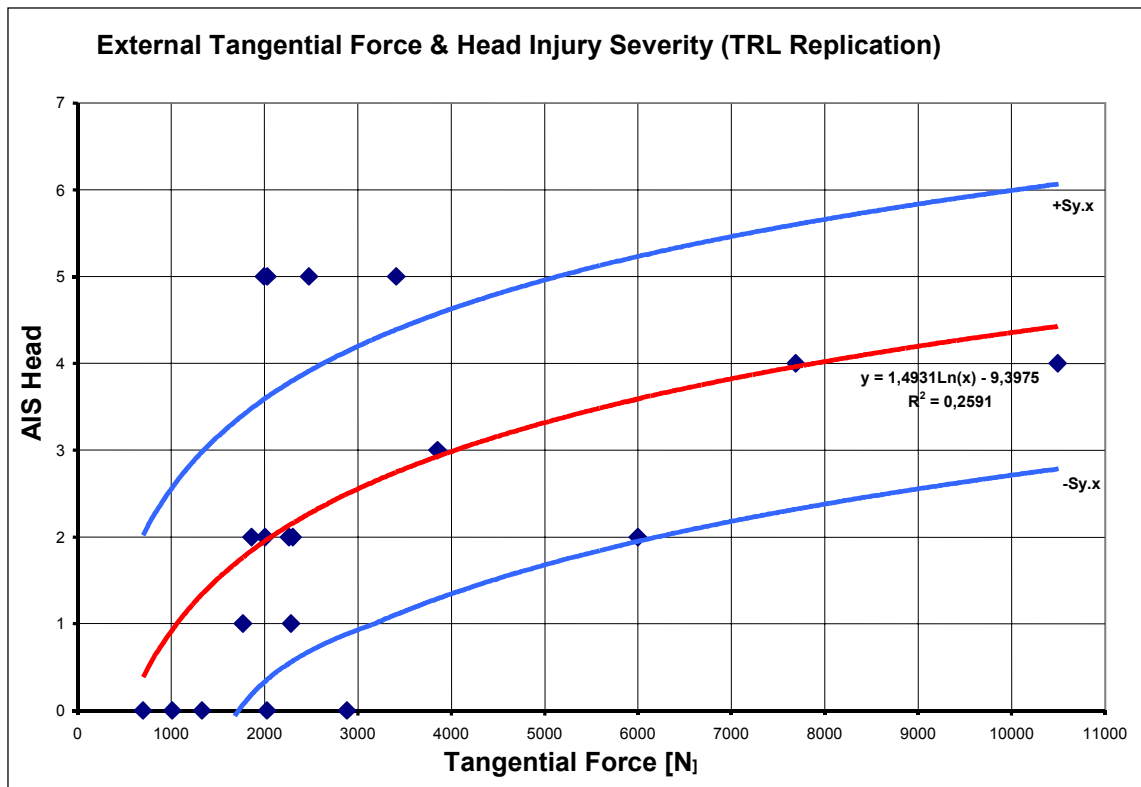


Figure 7.14. Peak values of the external tangential helmet forces from drop tests at TRL

The logarithmic regression shown in figure 7.14 gives the best possible correlation coefficient as $r = 0.51$, very similar to the 0.50 for the rotational acceleration presented in section 7.4.5. As expected, the distribution of rotational acceleration and tangential force are similar.

The equation

$$\text{AIS Head} = | 1.9431 \ln (f_i) - 9.3975 | \quad (7.10)$$

accurately predicts the AIS severity of head injury in 27 % of cases and predicts that a head injury of severity AIS 2 will occur 2000N and AIS 3 at 4000N tangential force.

7.5. NUMERICAL REPLICATION AND HEAD INJURY SEVERITY

The numerical replication was performed at ULP (Université Louis Pasteur de Strasbourg) for 20 accident cases (3 cases from Hannover and 17 cases from Glasgow). The mathematical models used and the replication data determined is described in Chapter 6.

7.5.1. Linear acceleration of Bimass headform

Figure 7.15 presents the peak values of the linear accelerations calculated for the skull of the Bimass headform model developed at ULP.

The logarithmic regression shown in figure 7.15 gives the best possible correlation coefficient as $r = 0.64$, better than the 0.58 for the solid headform linear acceleration presented in section 7.4.2.

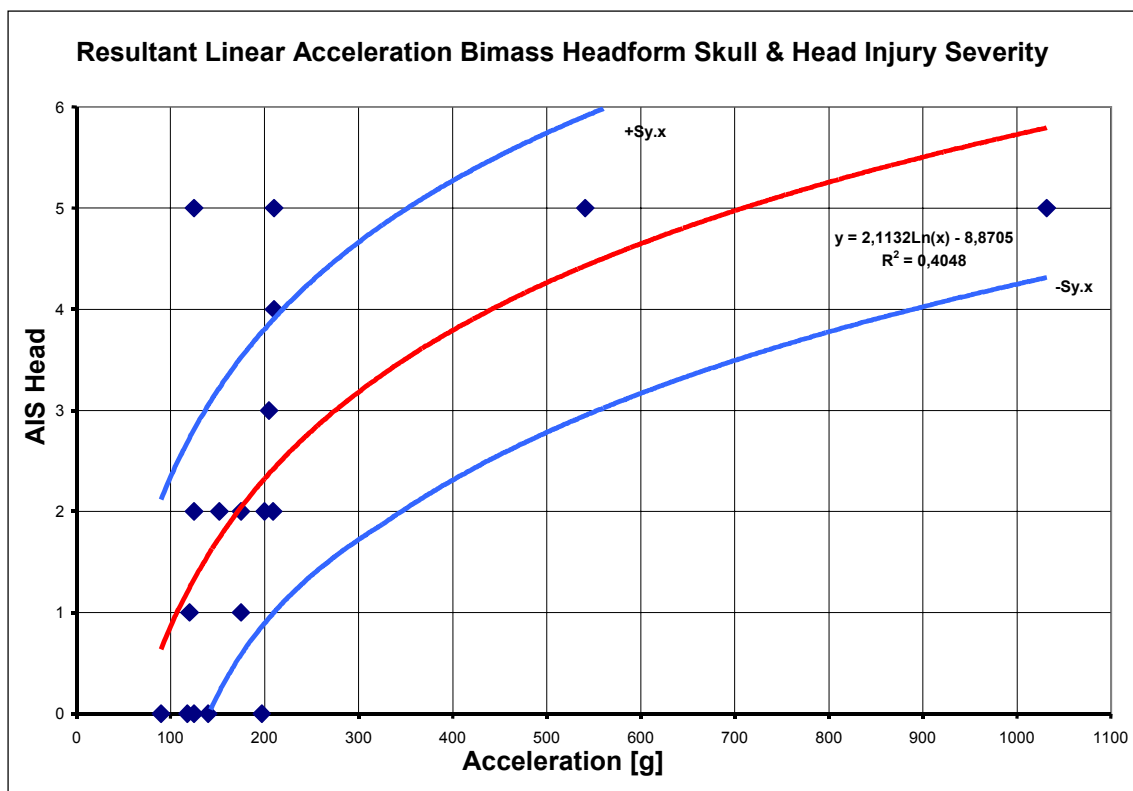


Figure 7.15. Peak values of the linear accelerations calculated for the skull of the Bimass headform model developed at ULP

The equation

$$\text{AIS Head} = | 2.1132 \ln (a_{lin}) - 8.8705 | \quad (7.11)$$

accurately predicts the AIS severity of head injury in 28% of cases and also predicts that a head injury of AIS 2 will be sustained at 160g and serious, AIS 3, at 280g.

Figure 7.16 presents the values of peak linear acceleration calculated for the brain of the Bimass headform model developed at ULP.

The logarithmic regression shown in figure 7.16 gives the best possible correlation coefficient as $r = 0.67$, better than the 0.58 for linear acceleration of the skull presented above.

The equation

$$\text{AIS Head} = | 2.1847 \ln (a_{lin}) - 9.2676 | \quad (7.12)$$

accurately predicts the AIS severity of head injury in 22% of cases and also predicts that a head injury of AIS 2 will be sustained at 180g and AIS 3 at 270g.

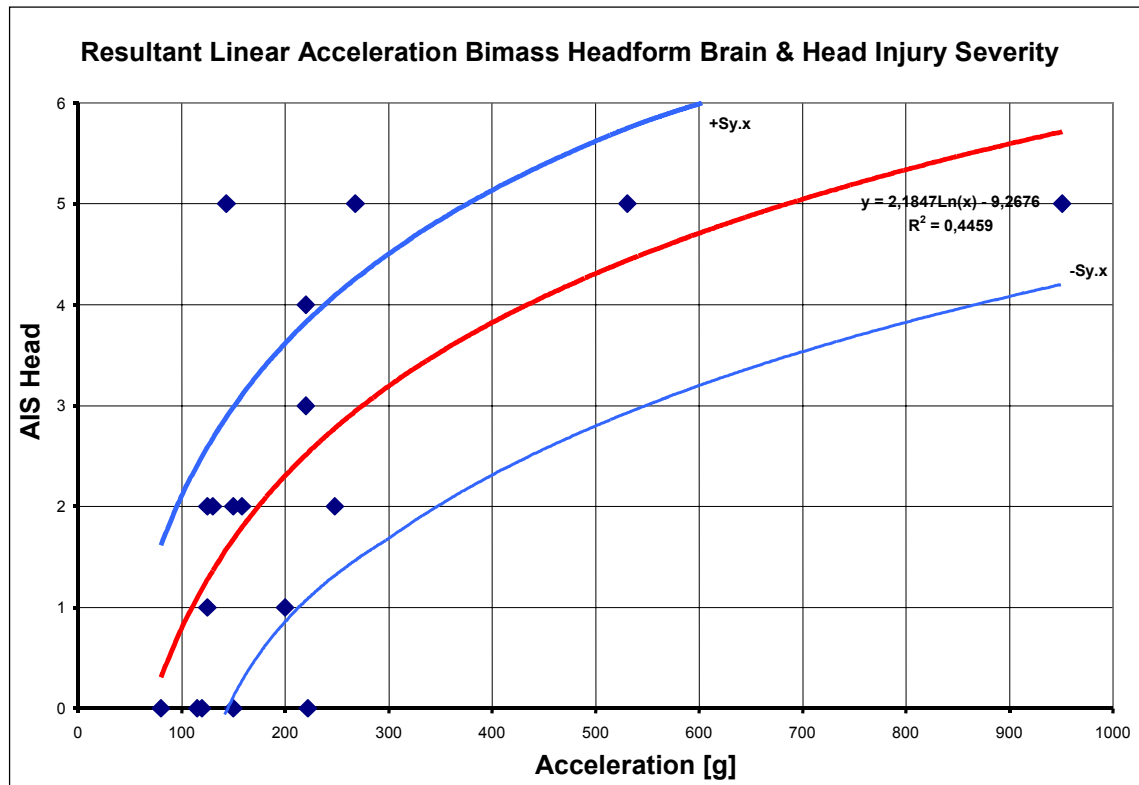


Figure 7.16. Values of peak linear acceleration calculated for the brain of the Bimass headform model developed at ULP

Figure 7.17 presents the peak values of the relative linear accelerations of skull and brain calculated for the Bimass headform model developed at ULP.

The logarithmic regression shown in figure 7.17 gives the best possible correlation coefficient as $r = 0.72$, better than for the skull and brain alone as presented above.

The equation

$$\text{AIS Head} = | 1.6733 \ln (a_{lin}) - 5.2672 | \quad (7.13)$$

accurately predicts the AIS severity of head injury in 50% of cases and also predicts that a head injury of AIS 2 will be sustained at 80g and AIS 3 at 150g .

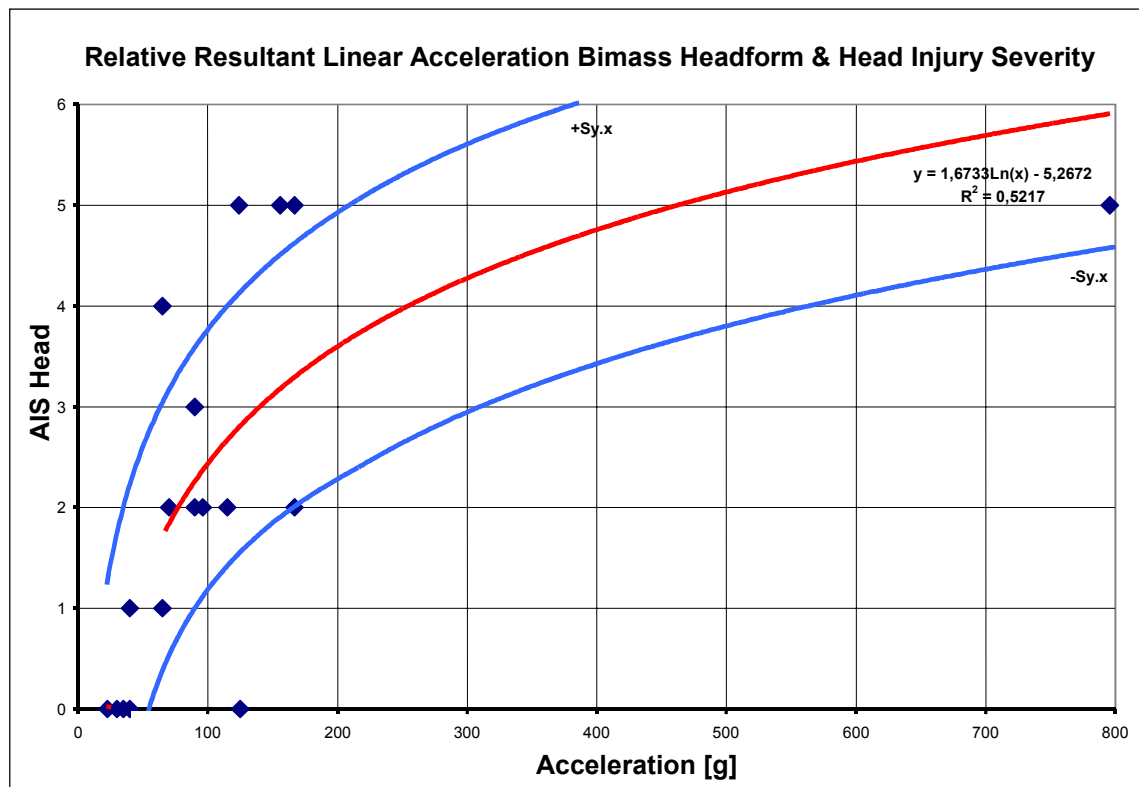


Figure 7.17. Relative linear accelerations of skull and brain calculated for the Bimass

7.5.2. Rotational acceleration of Bimass headform

Figure 7.18 presents the peak values of the rotational accelerations of the skull calculated for the Bimass headform model developed at ULP.

The logarithmic regression shown in figure 7.18 gives the best possible correlation coefficient as $r = 0.55$, better than the 0.50, for headform rotational acceleration presented in 7.4.5

The equation

$$\text{AIS Head} = | 1.2553 \ln(\alpha) - 9.1978 | \quad (7.14)$$

accurately predicts the AIS severity of head injury in 27% of cases and also predicts that a head injury of AIS 2 will be sustained at 8000 rad/s² and AIS 3 at 16000 rad/s².

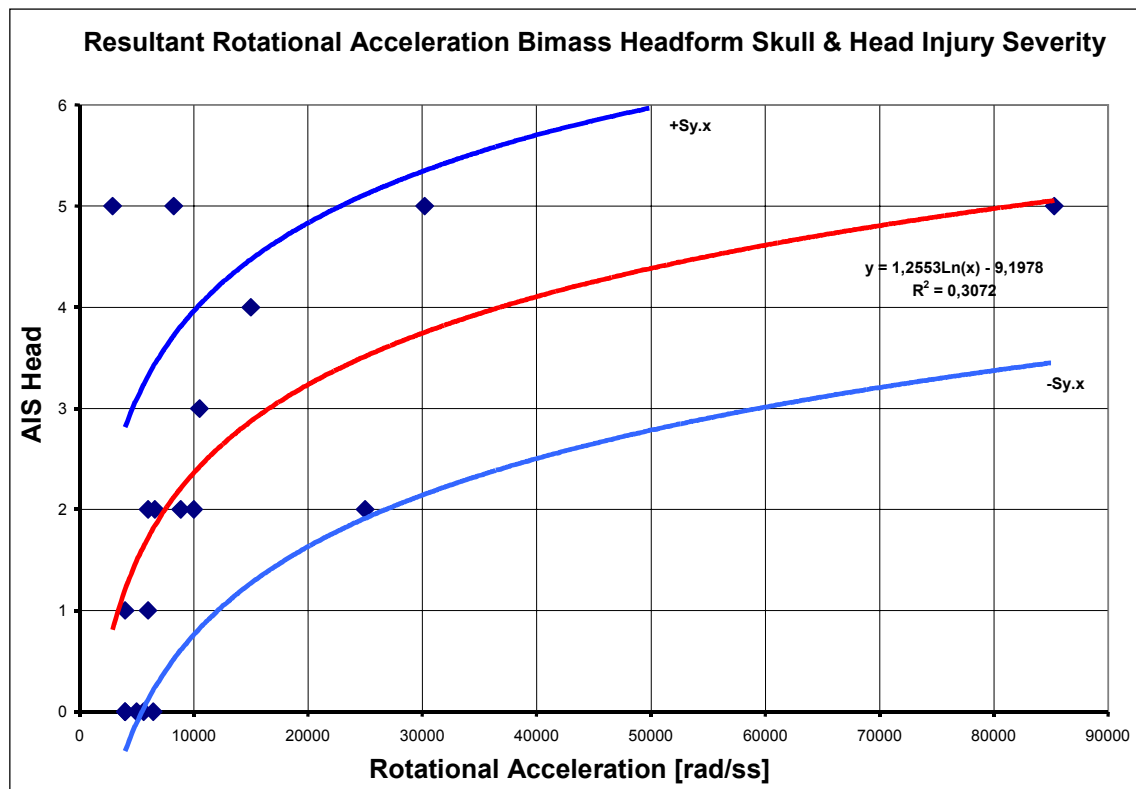


Figure 7.18. Peak values of the rotational accelerations of the skull calculated for the Bimass headform model developed at ULP

Figure 7.19 presents the peak values of the rotational accelerations of the brain calculated for the Bimass headform model developed at ULP.

The logarithmic regression shown in figure 7.19 gives the best possible correlation coefficient as $r = 0.73$ and better than the 0.51 for headform rotational acceleration presented in 7.4.5.

The equation

$$\text{AIS Head} = | 1.7301 \ln(\alpha) - 16.257 | \quad (7.15)$$

accurately predicts the AIS severity of head injury in 44% of cases and also predicts that a head injury of AIS 2 will be sustained at 36,000 rad/s^2 and AIS 3 at 70,000 rad/s^2 . It should be noted that these values cannot be related to values measured in a solid headform and should not be compared when considering tolerance to injury.

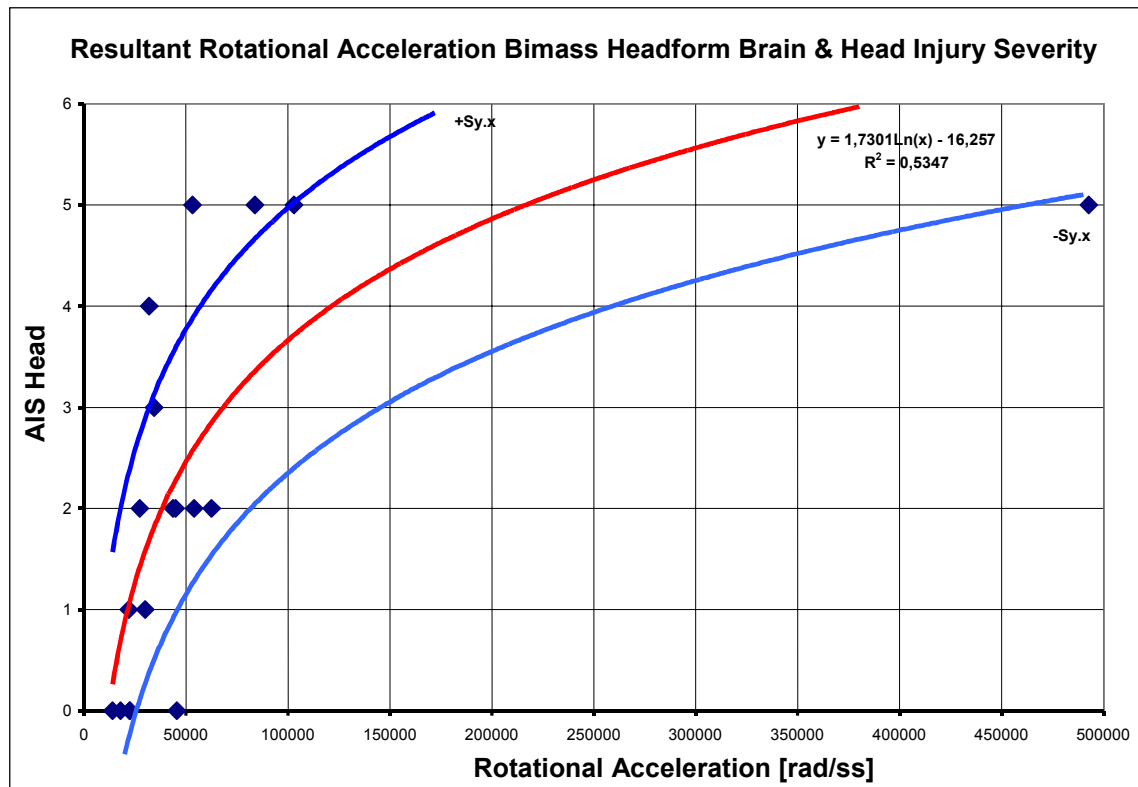


Figure 7.19. Peak values of the rotational accelerations of the brain calculated for the Bimass headform model developed at ULP

Figure 7.20 presents the peak values of the relative rotational accelerations of skull and brain calculated for the Bimass headform model developed at ULP.

The logarithmic regression shown in figure 7.20 gives the best possible correlation as coefficient $r = 0.74$ and slightly better than the value for the rotational acceleration of the skull and brain presented above.

The equation

$$\text{AIS Head} = | 1.6512 \ln(\alpha) - 15.321 | \quad (7.16)$$

accurately predicts the AIS severity of head injury in 44% of cases and also predicts that a head injury severity of AIS 2 will be sustained at 35,000 rad/s² and AIS 3 at 65,000 rad/s². It should be noted that these values cannot be related to values measured in a solid headform and should not be compared when considering tolerance to injury.

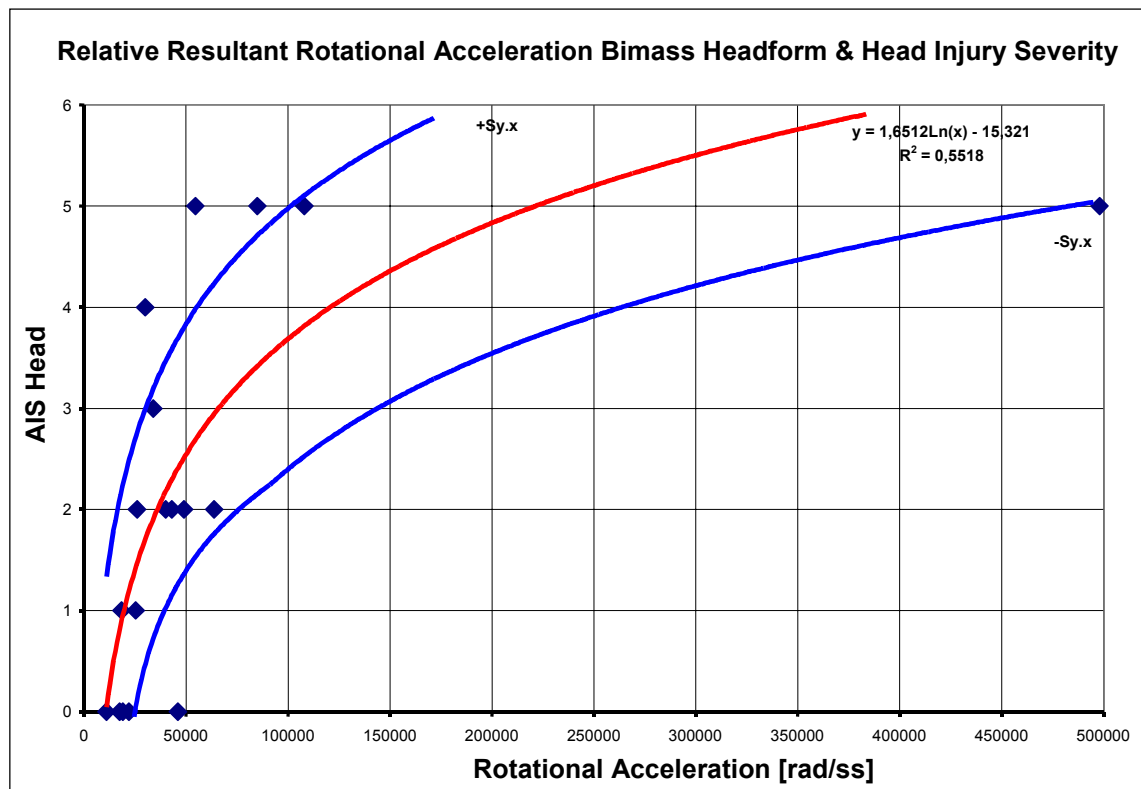


Figure 7.20. Peak values of the relative rotational accelerations of skull and brain calculated for the Bimass headform model developed at ULP

7.5.3. Finite element replication

Figure 7.21 presents the von Mises stress σ in the brain calculated in 16 cases by finite element (FE) modelling at ULP.

The logarithmic regression shown in figure 7.21 gives the best possible correlation coefficient as $r = 0.59$, similar to the 0.6 for headform linear acceleration given in 7.4.2.

The equation

$$\text{AIS Head} = | 2.4962 \ln(\sigma) - 5.5882 | \quad (7.17)$$

accurately predicts the AIS severity of head injury in 25% of cases and also predicts that head injury of severity AIS 2 will be sustained at 20 kPa and AIS 3 at 30 kPa.

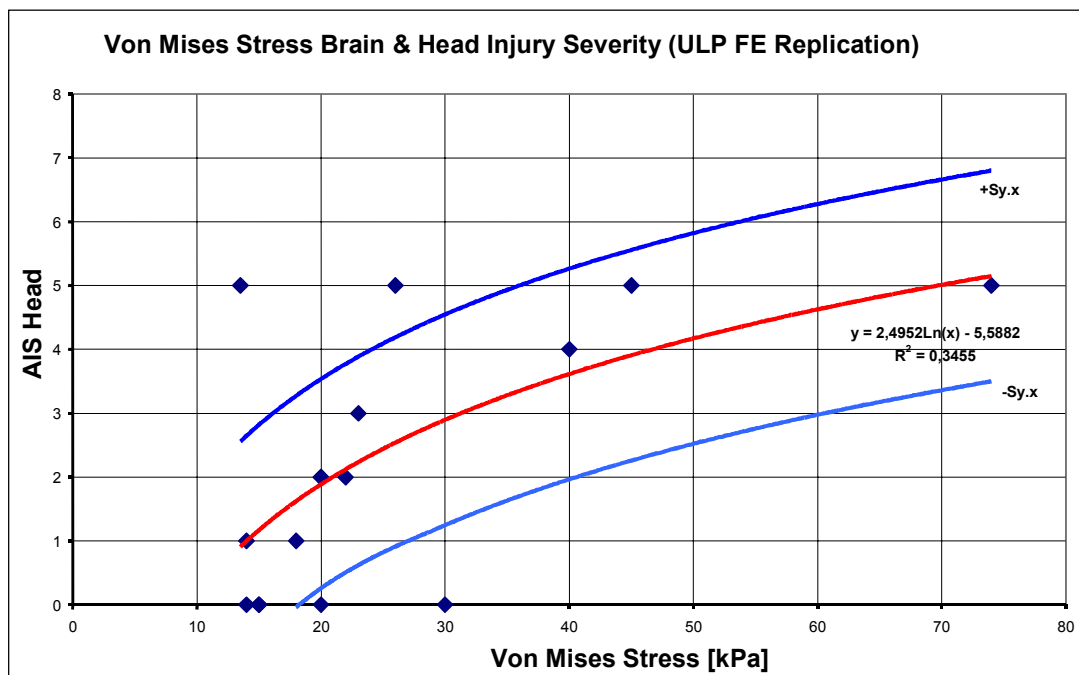


Figure 7.21. Von Mises stress σ in the brain calculated by FE modelling at ULP

Figure 7.22 presents the intracerebral tensile stress τ calculated by finite element (FE) modelling at ULP.

The logarithmic regression shown in figure 7.22 gives the best possible correlation coefficient as $r = 0.59$, the same as for the von Mises as given above.

The equation

$$\text{AIS Head} = | 5.7615 \ln(\tau) - 24.86 | \quad (7.18)$$

accurately predicts the AIS head injury severity in 19% of cases and also predicts that a head injury of severity AIS 2 will be sustained at -106 kPa and AIS 3 at -126 kPa.

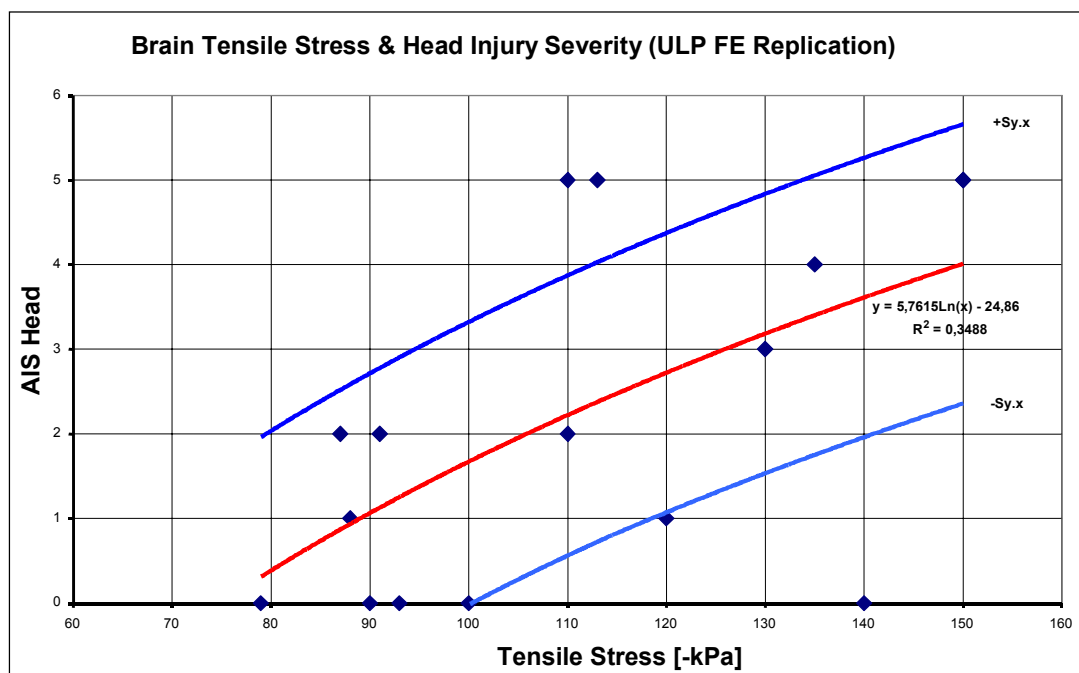


Figure 7.22. Intracerebral tensile stress τ calculated by finite element (FE) modelling at ULP

Figure 7.23 presents the intracerebral pressure δ in the brain calculated by finite element (FE) modelling at ULP.

The logarithmic regression shown in figure 7.23 gives the best possible correlation coefficient as $r = 0.61$, similar to that for the von Mises and tensile stress given above.

The equation

$$\text{AIS Head} = |1.9649 \ln(\delta) - 8.3424| \quad (7.19)$$

accurately predicts the AIS severity of head injury in 19% of cases and also predicts that a head injury of severity AIS 2 will be sustained at 200 kPa and AIS 3 at 320 kPa.

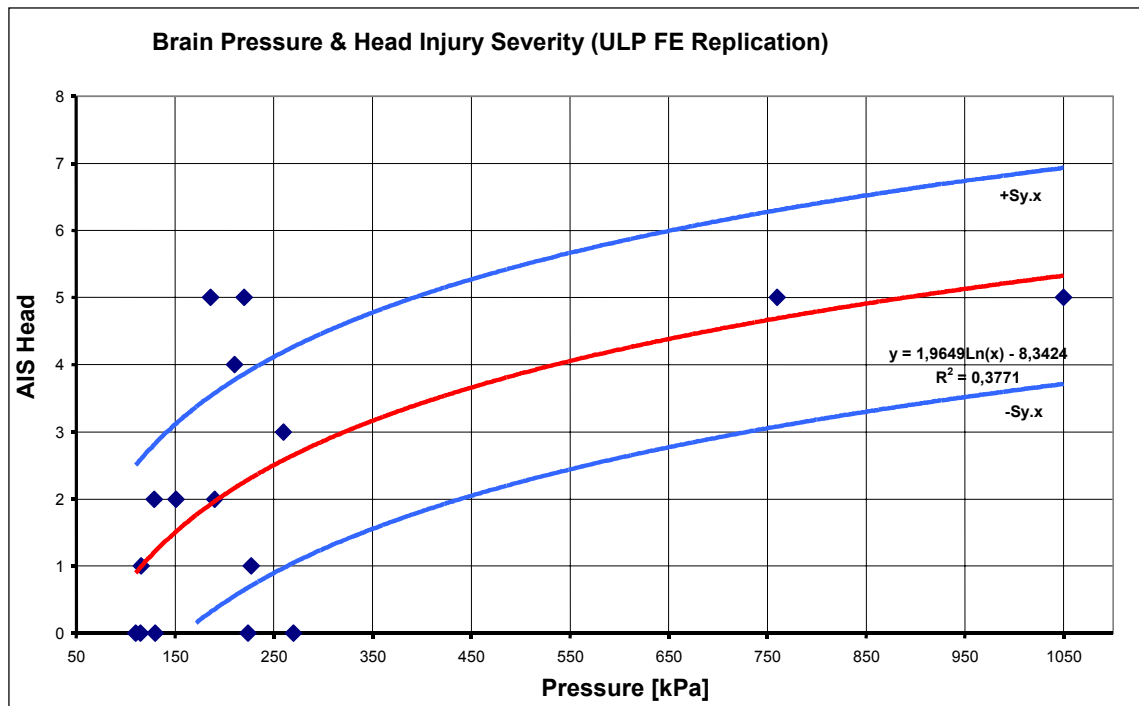


Figure 7.23. Intracerebral pressure δ in the brain calculated by finite element (FE) modelling at ULP

7.6. NECK INJURY SEVERITY

Neck injuries were analysed in order to identify loading parameters that could be applied to predict neck injury severity. Figure 7.24 shows the results of the analysis of impact speed estimated from the accident data and although there is a trend indicating that that neck injury potential increases with head impact speed the correlation is very poor with $r = 0.24$. Very serious neck injury can occur at low speed head impacts and even up to very high impact speeds, neck injury does not necessarily occur or may be minor.

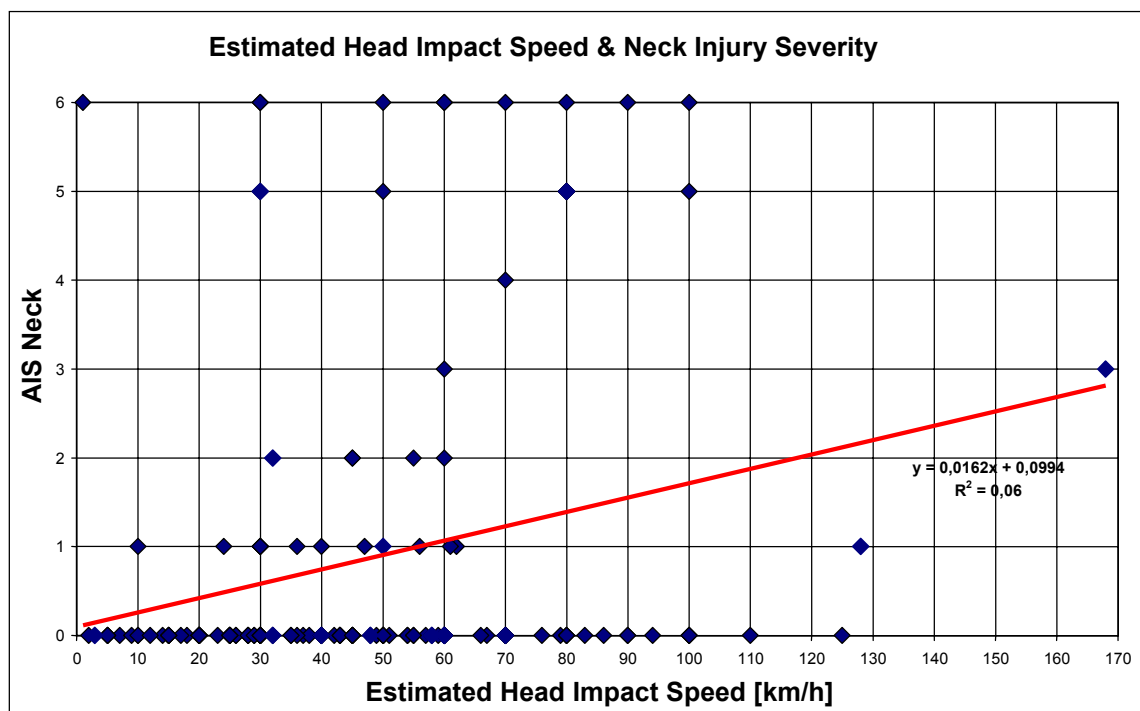


Figure 7.24. Analysis of impact speed estimated from accident data

Figure 7.25 shows that severe neck injuries are in general associated with severe head injury. Except in one case with fatal neck injury and no head injury, neck injury AIS 3 is always combined with a head injury of AIS ≥ 4 .

The cases selected for experimental and numerical replication included only one rider with moderate neck injury AIS 2. Therefore, it was not possible to determine the probability of injury from statistical analysis for which, more cases would need to be replicated.

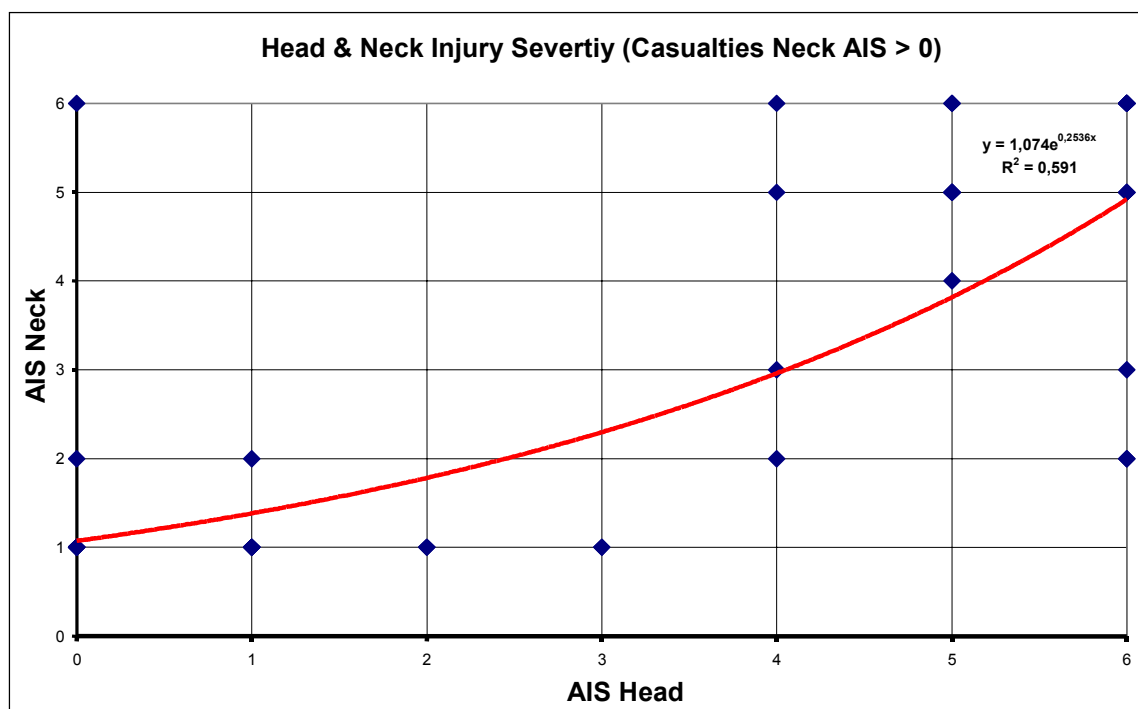


Figure 7.25. Head and neck injury severity

7.7. RISK OF AIS ≥ 3 HEAD INJURY ESTIMATED BY LOGISTIC REGRESSION

The foregoing analysis has attempted to identify the risk of injury severity for a range of physical parameters that can be measured in tests or computed. However, it can also be useful to know the probability of a particular injury severity for a range of values of a given parameter. Such an analysis can be estimated by logistic regression (Versace 1971)

$$P = 1 / (1 + \exp(a + bx)) \quad 0 \leq P \leq 1 \quad (7.20)$$

P is the probability of a certain injury type or severity related to the loading parameter x. The coefficients a and b must be approximated to the injury data considered. The best approximation is given at a maximum of the likelihood-function

$$L = \prod y_i * \prod (1 - y_j) \quad (7.21)$$

y_i is the probability of an injury occurring, y_j the probability of not being injured, n the total number of events.

Unfortunately, the logistic regression can be applied only for two dependant variables, yes or no, thus, it is common to calculate the injury risk curves for high severity levels AIS ≥ 3

The head injury risk curves for AIS ≥ 3 (AIS ≥ 2 for HIC and GAMBIT) are presented in the following figures. The results show that in general the 50% probability of the risk of AIS ≥ 3 head injury obtained by logistic regression is similar to value for AIS 3 (AIS 2 for HIC and GAMBIT) estimated by logarithmic regression in the forgoing analysis.

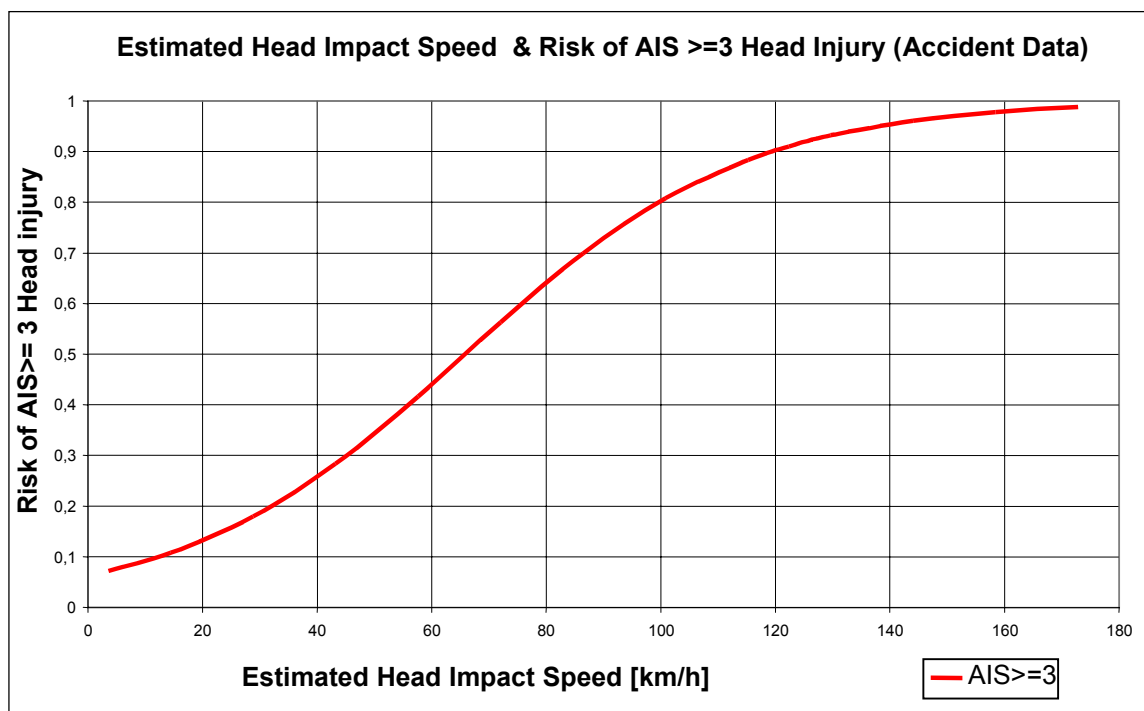


Figure 7.26. Estimated head impact speed (accident data).

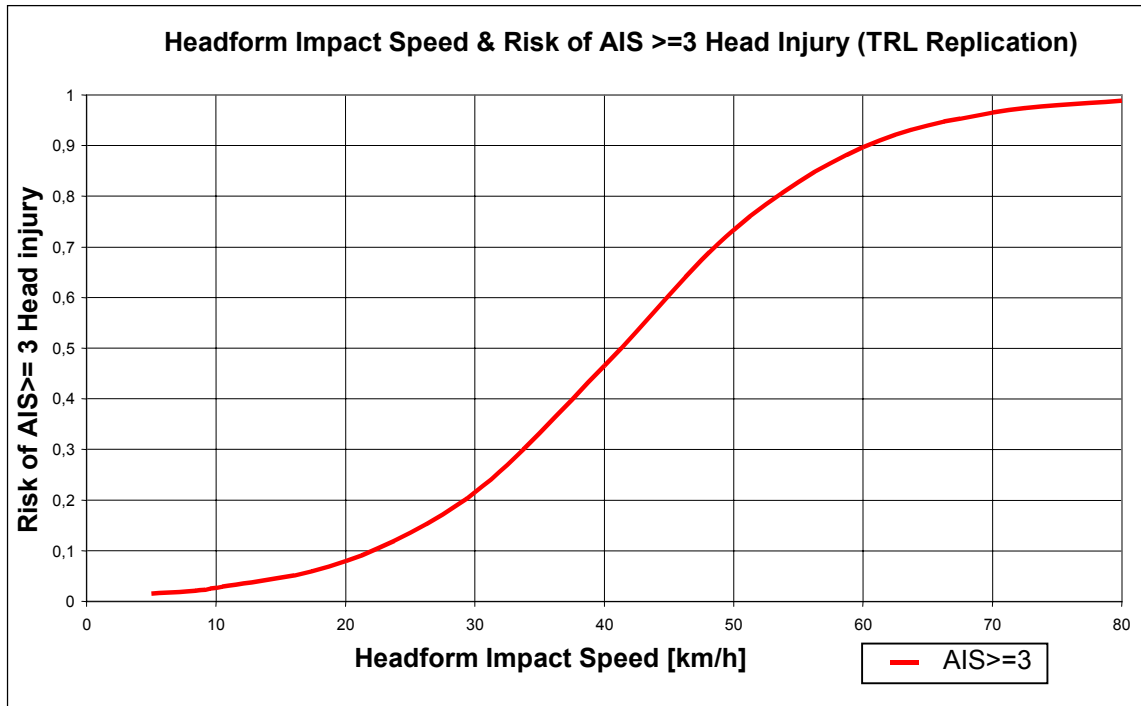


Figure 7.27. Headform impact speed (TRL Replication)

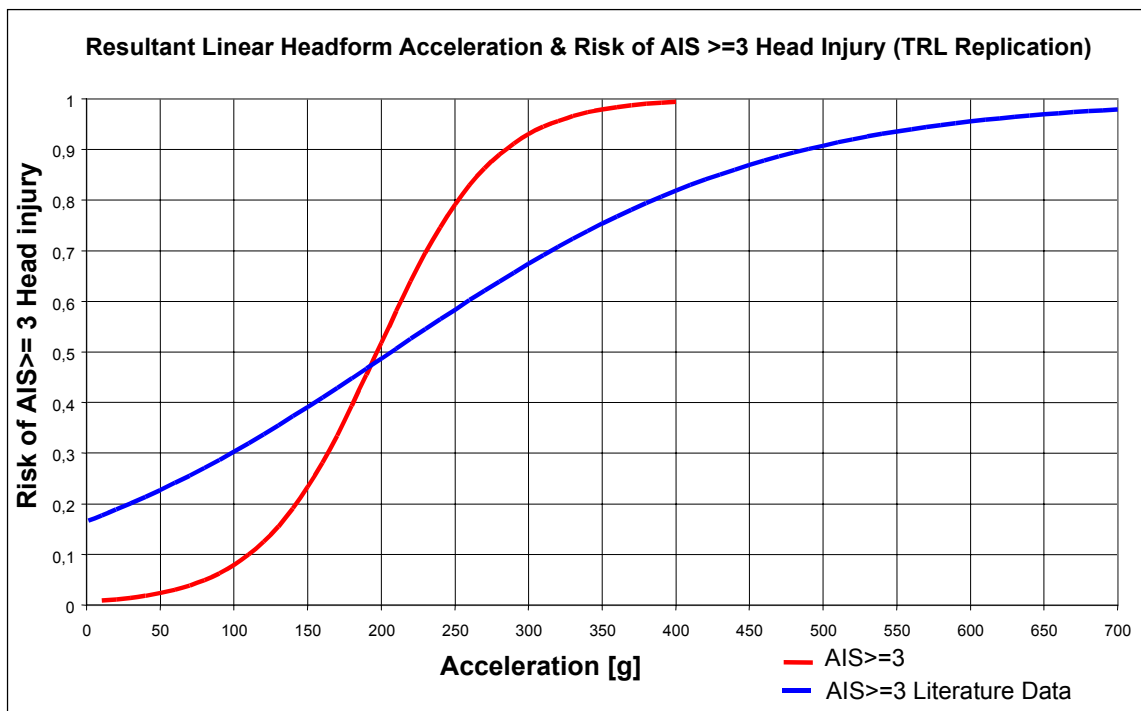


Figure 7.28. Linear headform acceleration (TRL replication and literature data)

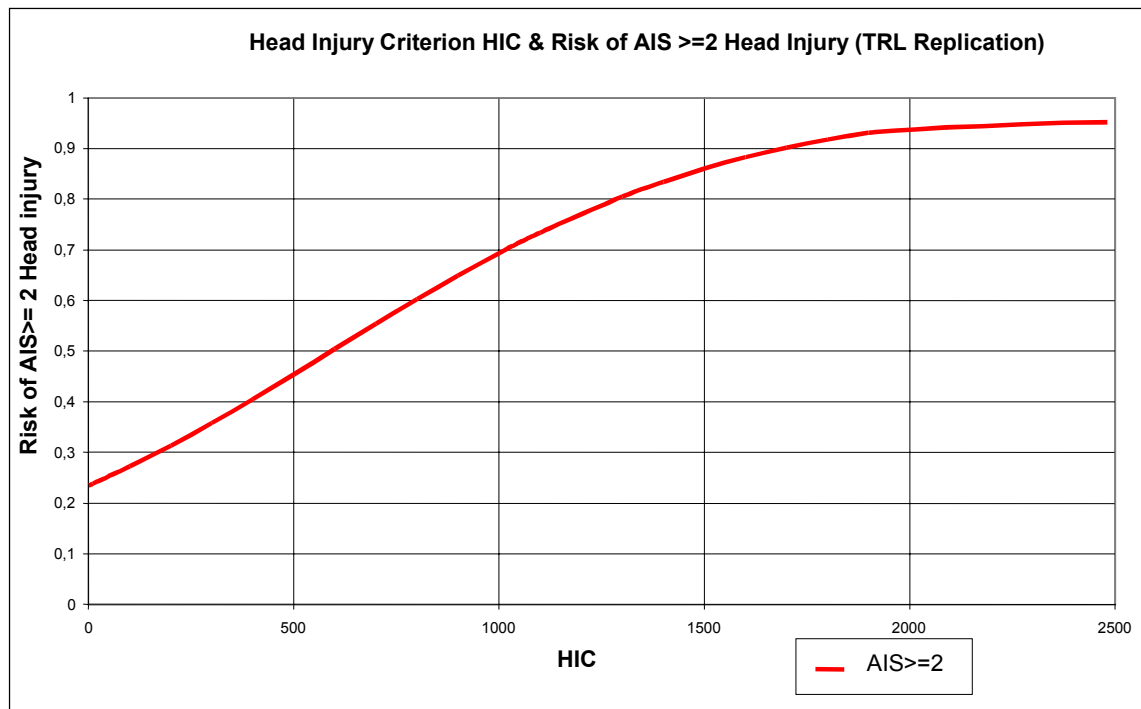


Figure 7.29. Head Injury Criterion (TRL replication)

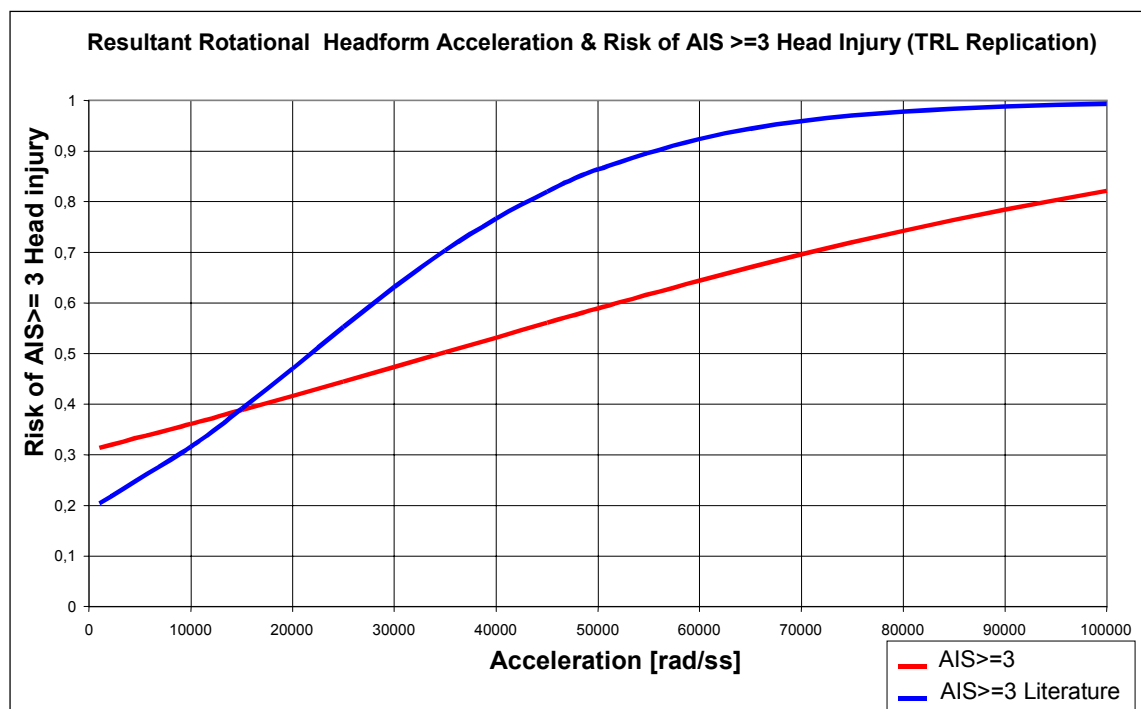


Figure 7.30. Rotational headform acceleration (TRL replication and literature data)

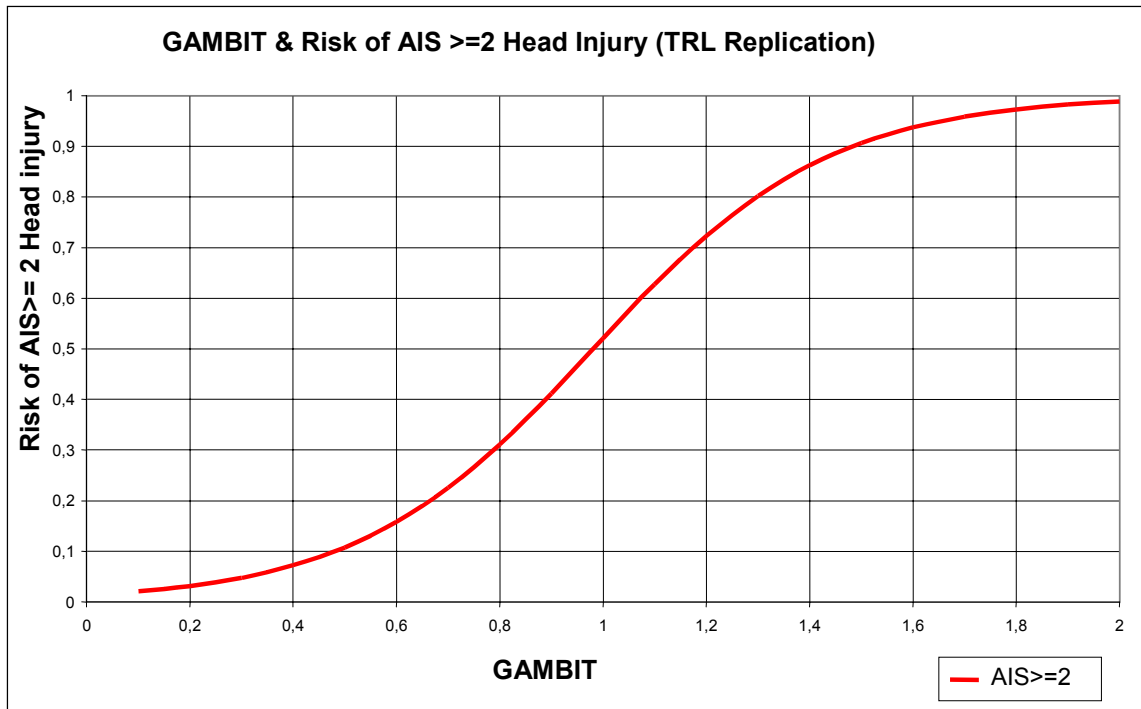


Figure 7.31. GAMBIT (TRL replication)

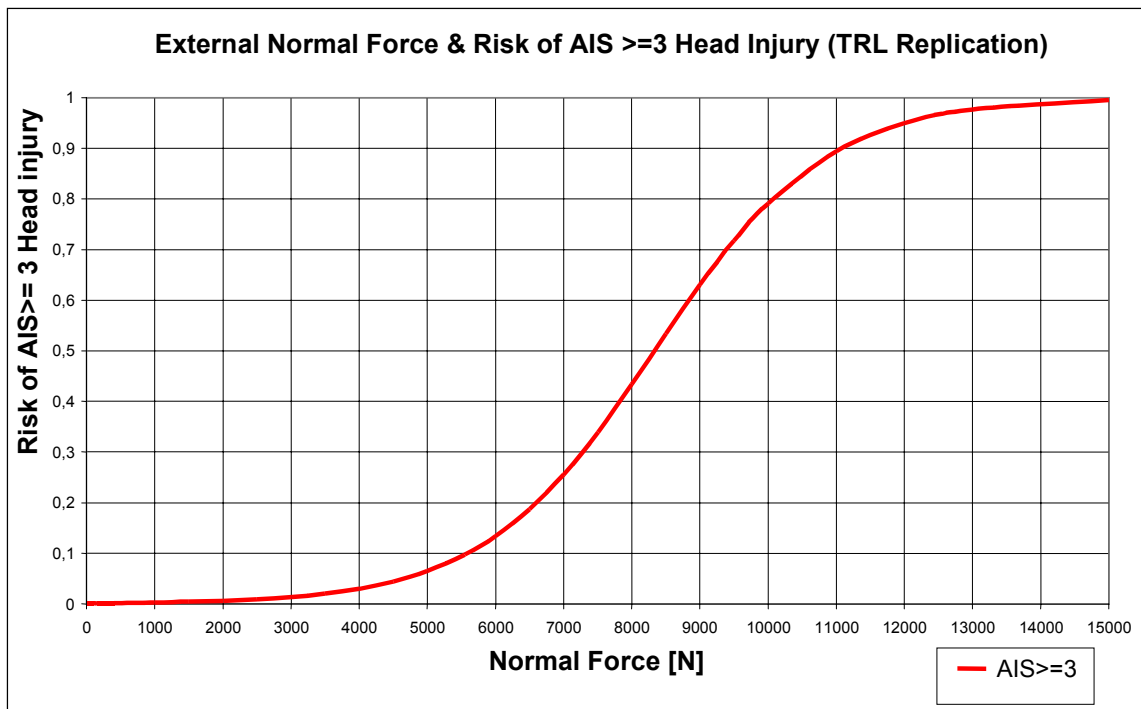


Figure 7.32. External normal force (TRL replication)

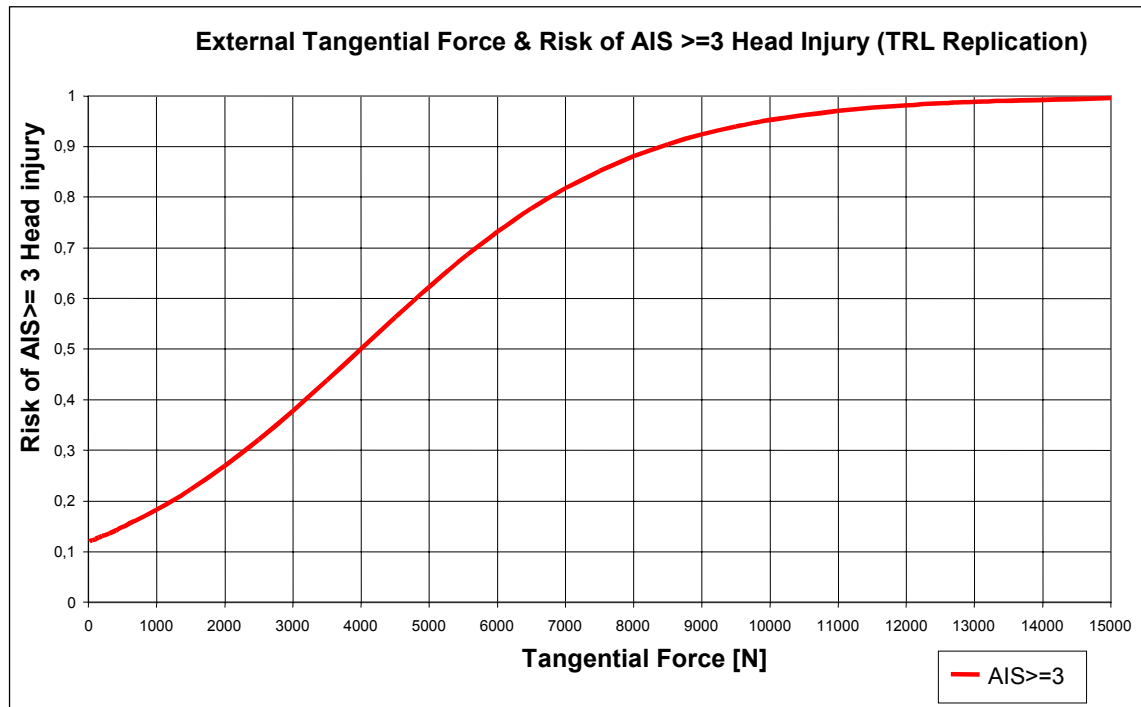


Figure 7.33. External tangential force (TRL replication)

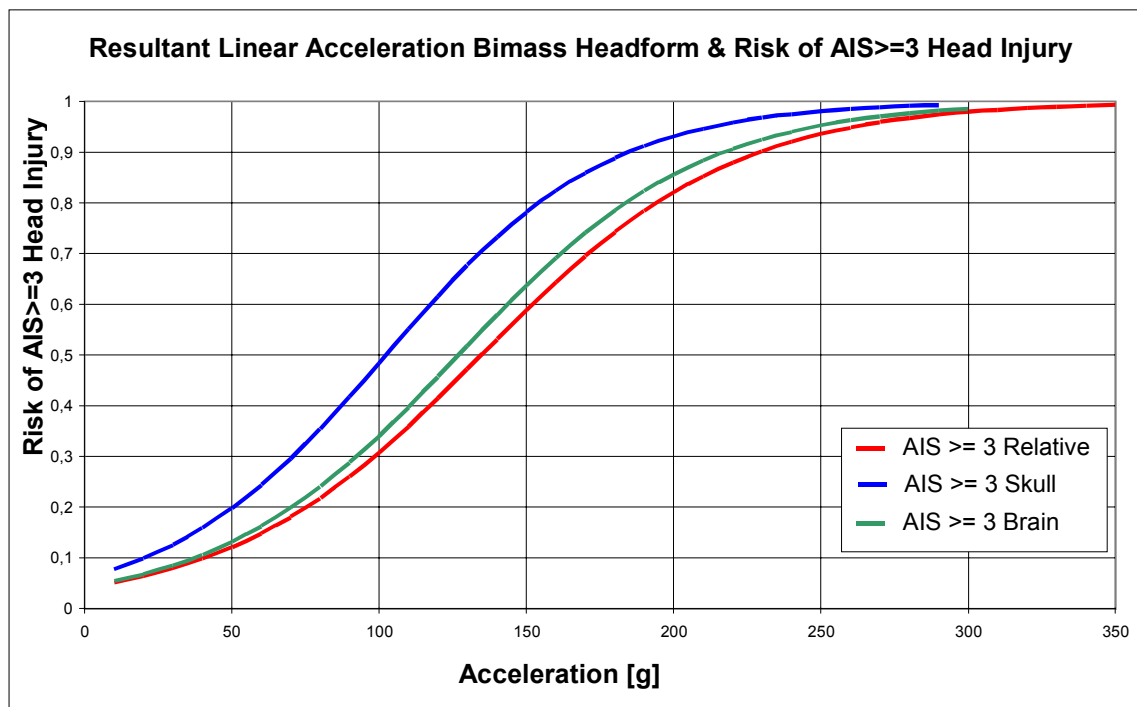


Figure 7.34. Linear acceleration of Bimass headform (ULP replication)

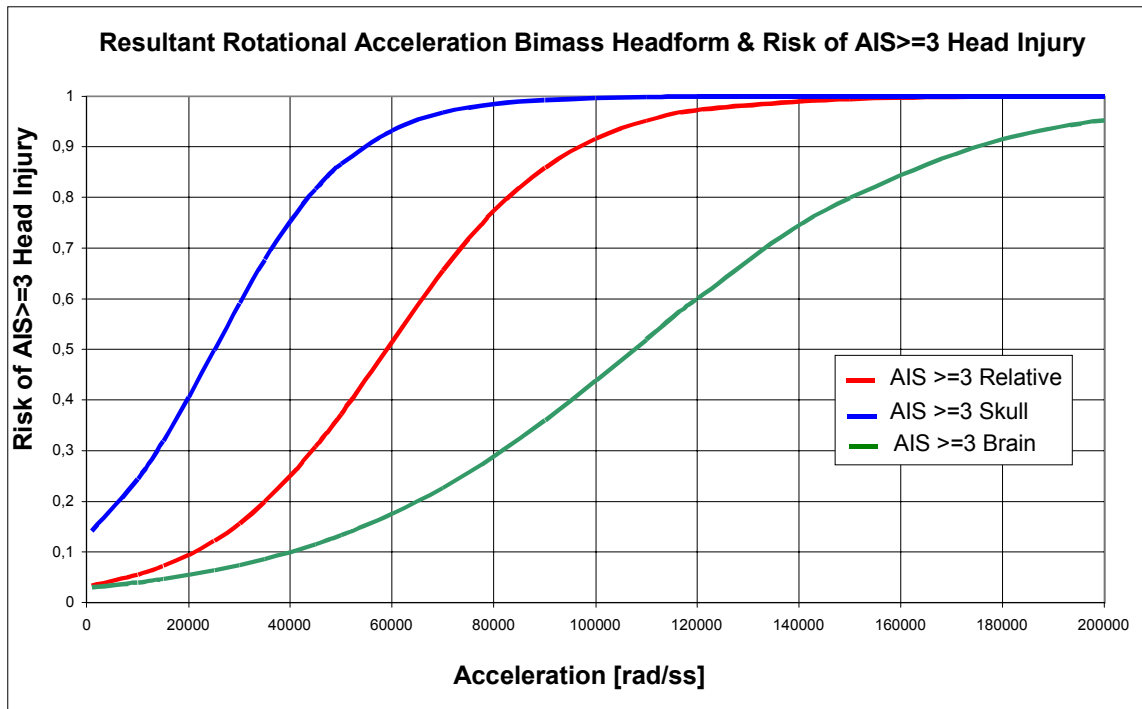


Figure 7.35. Rotational acceleration of Bimass headform (ULP replication)

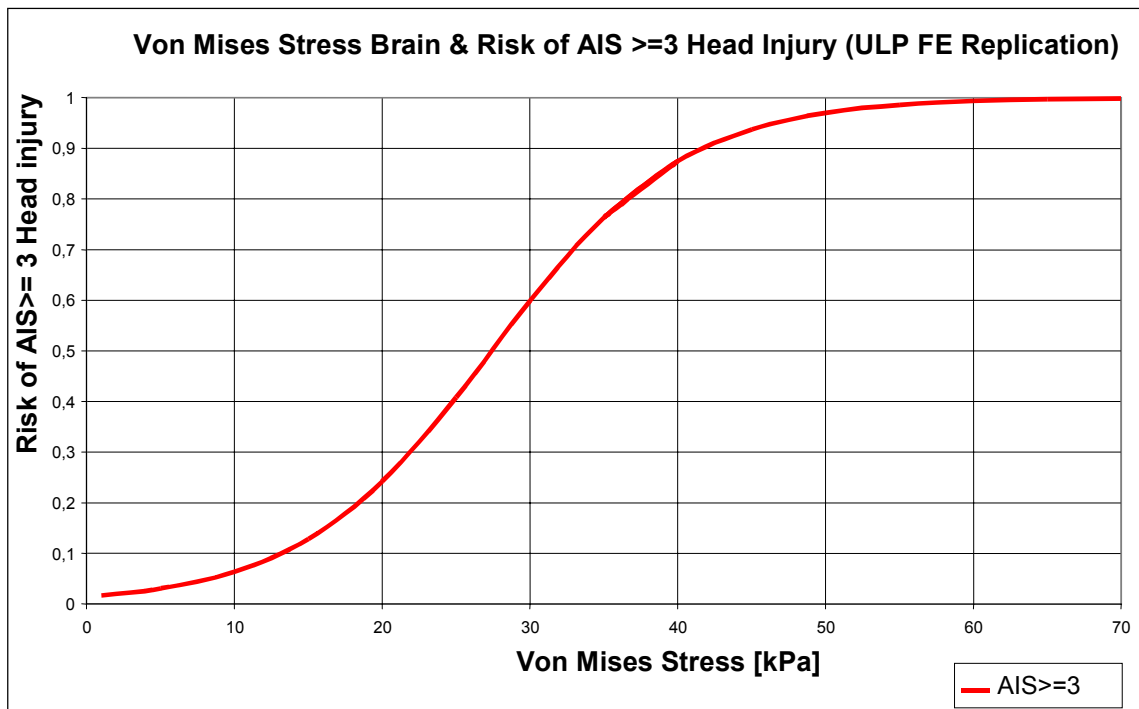


Figure 7.36. Finite element replication: von Mises stress (ULP replication)

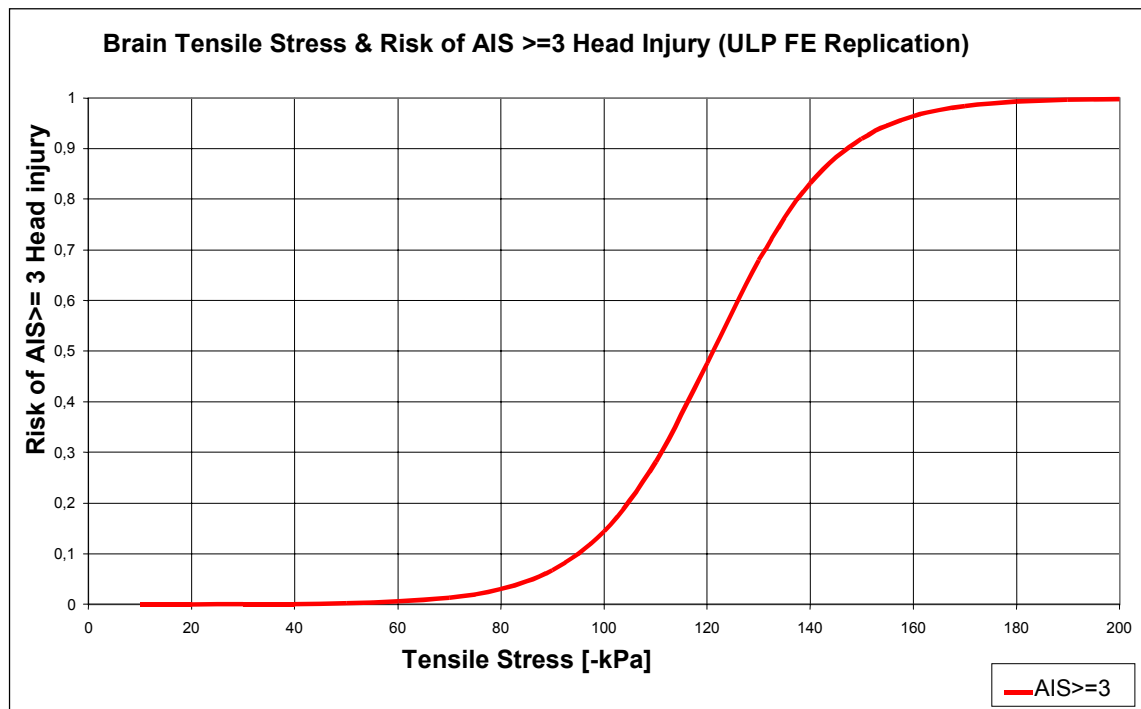


Figure 7.37. Finite element replication: tensile stress (ULP replication)

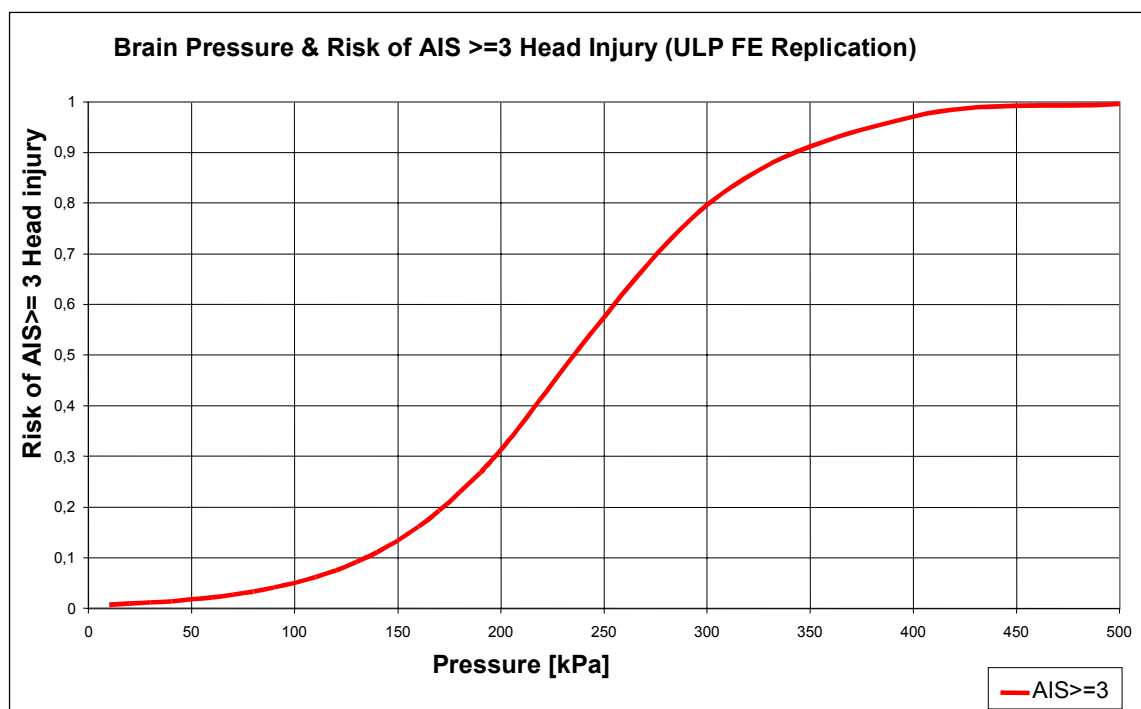


Figure 7.38. Finite element replication: brain pressure (ULP replication)

7.8. CONCLUSIONS

1 The head loading parameters determined by accident reconstruction, experimental and numerical replications have been analysed. The purpose was to improve the knowledge of human tolerance to head impact mechanisms and thus develop a means of predicting the probability of head injury severity for a range of impact parameters. Additionally, the frequency of occurrence and severity of neck injury was investigated.

2 Of the parameters analysed, the Head Injury Criterion (HIC) gave the best head injury severity prediction with a correlation coefficient $r = 0.80$. The analysis predicted that a moderate brain injury of AIS 2, for example cerebral concussion, would be sustained at a HIC of 1000 and that a brain injury of AIS 3 at a HIC of 1500.

3 The relative linear and rotational accelerations of skull and brain calculated for the Bimass headform model were the second most effective parameters for predicting head injury severity with correlation coefficients of $r = 0.72$ and $r = 0.74$. The analysis predicted that a brain injury of severity AIS 2 will be sustained at 80g peak relative linear acceleration and 35 krad/s² peak relative rotational acceleration and AIS 3 at 150 g and 65 krad/s². It should be noted that these values cannot be related to values measured in a solid headform and should not be compared when considering tolerance to injury.

4 The following table gives the values for all of the other parameters for which it was predicted that moderate, AIS 2, and serious, AIS 3, brain injury would be sustained.

Table 7.1 Parameter values for brain injury

Head Loading Parameter	AIS 2	AIS 3	AIS ≥ 3 *
Head Impact Speed (Accident Data)	30 km/h	80 km/h	65 km/h
Head Impact Speed (TRL Replication)	30 km/h	40 km/h	40 km/h
Linear Acceleration Headform	150 g	260 g	200 g
Linear Acceleration Literature Data	160 g	280 g	200 g
Rotational Acceleration Headform	8 krad/s ²	19 krad/s ²	35 krad/s ²
Rotational Acceleration Literature Data	8 krad/s ²	18 krad/s ²	22 krad/s ²
GAMBIT	1		1 (AIS ≥ 2)
Normal Force	6.5 kN	12 kN	8.3 kN
Tangential Force	2 kN	4 kN	4 kN
Linear Acceleration Bimass Headform Skull	160 g	280 g	100 g
Linear Acceleration Bimass Headform Brain	180 g	270 g	130 g
Rotational Acceleration Bimass Headform Skull	8 krad/s ²	16 krad/s ²	25 krad/s ²
Rotational Acceleration Bimass Headform Brain	36 krad/s ²	70 krad/s ²	108 krad/s ²
Peak Relative Linear Acceleration Bimass	80g	150g	135g
Peak Relative Rotational Acceleration Bimass	35 krad/s ²	65 krad/s ²	60 krad/s ²
Intracerebral von Mises Stress	20 kPa	30 kPa	28 kPa
Intracerebral Tensile Stress	-106 kPa	-126 kPa	-120 kPa
Intracerebral Pressure	200 kPa	320 kPa	230 kPa

*Logistic Regression 50% injury risk

5 Neck injury did not correlate well with head impact speed estimated from accident data, although there was a trend for neck injury severity to increase with speed. However, it was very evident that serious neck injury occurred in combination with serious head injury irrespective of the impact speed. Probability functions and tolerance levels for neck injury could not be evaluated from replication data, because only one case with moderate neck injury was included in the sample investigated.

CHAPTER 8. DEVELOPMENT OF TEST PROCEDURES

8.1. INTRODUCTION

In order to optimise the protection offered by motorcycle helmets, test procedures need to be improved to assess helmets as reliably, realistically and comprehensively as possible. This chapter presents the research undertaken by the Test Procedures Working Group at EMPA (Swiss Federal Laboratories for Materials Testing and Research) and AD Engineering (Italy), which began in 1996 and was completed in 2000. Helmet test methods were examined and new, more appropriate test procedures were developed using the outputs of the other COST 327 Working Groups as a basis.

A specific literature study on test principles and techniques was carried out based on information in the COST 327 Literature Review. The information gathered was thoroughly discussed and various possibilities for the development of helmet tests were derived. Table 8.1 summarises the most important head injury risks to motorcyclists, the related helmet properties and associated test procedures. The last column indicates the procedures investigated by the Test Procedures Working Group.

The mechanical behaviour of motorcycle helmets in impacts is directly related to head injury risks such as linear and rotational acceleration of the brain. In accidents rotational and linear acceleration usually occur together and both cause injury (Chapter 2.3). Current helmet Standards require shock absorption tests measuring linear acceleration using a falling headform, however a universally accepted method to assess the potential risk from rotational acceleration has yet to be developed.

A detached headform may not simulate adequately the dynamics of the head for all accidents. Particularly, the effect of the body mass on the linear and rotational acceleration experienced by an impacting head is not fully understood (Chapter 5.1). Test methods to assess the linear and rotational acceleration of the head were, therefore, investigated. The laboratory experiments included drop tests using a falling headform which were compared with the results of tests using a falling crash test dummy.

The results of the Accident Investigation Working Group showed that some 13% of helmets were lost during motorcycle accidents and that there is a need to improve the retention during an impact (Chapter 3.6.2). The stability of a helmet on the head was, therefore, investigated by means of a new chin-strap effectiveness test. Impacts against the chin are another important cause of severe head injuries (Chapter 2 and 3), but because a chin guard test was recently introduced in ECE Regulation 22-05, this was not investigated. The friction of a helmet shell affects the tangential impact forces and thus the resulting rotational acceleration of the head. As an alternative to oblique impact tests, a mechanical test method was used to study the frictional properties of helmets.

From an analysis of direct and indirect injury risks and of related helmet properties it was concluded that helmet physiology and ergonomics are very important factors for the safety of motorcyclists (Table 8.1). Improved physiological properties of helmets, such as sufficient ventilation and removal of heat and moisture from the inside of the helmet could help to keep the rider alert and prevent accidents in critical situations. Within the extension of COST 327 the work on test procedures concentrated on the development of concepts and test methods concerning ergonomic and physiological helmet properties for example a ventilation test. Table 8.1 shows that these aspects are not properly assessed by current European motorcycle helmet Standards.

Table 8.1 Direct and indirect injury risks for motorcyclists and related test procedures. The last column indicates procedures investigated by the Test Procedures Working Group.

Direct injury risk	Related helmet properties	Test procedure	European standards	COST 327 Test Procedures
linear acceleration	shock absorption capacity	falling headform test	ECE, BS	yes
rotational acceleration	shell material, friction	- friction test - oblique impact test onto abrasive anvil	- ECE - BS	yes
	shell design, projections	oblique impact test at projections (bar anvil)	BS	no
	peak, additional systems	Swedish test procedure	Swedish standard	no
combination of linear and rotational acceleration	as for linear and rotational acceleration	drop test using a dummy or a head/neck/torso-unit	no	yes
impact to the chin	impact protection of the chin guard	- falling mass drop test - falling headform test	- BS - ECE	no
loss or displacement of helmet during impact	stability of the helmet on the head	retention system tests (roll-off test, dynamic test, tests for chin-strap and buckle)	ECE, BS	yes
impact to sharp objects	resistance to penetration	penetration test	(ECE), BS	no
compression of the head	rigidity of the helmet shell	rigidity test	ECE	no
neck injury	helmet mass, helmet shape, chin-strap	- drop test using a dummy or a head/neck/torso-unit - retention system test	no	no
Indirect injury risk	Related helmet properties	Test procedure	European standards	COST 327 Test Procedures
reduction of vision	field of vision	peripheral vision test	ECE, BS	no
	optical properties of visor	optical tests	ECE	no
reduction of hearing	helmet materials and padding	?	no	no
heat production of the head	head ventilation, comfort	sweating and heated headform	no	yes
heat and moisture production of the face, CO ₂ -concentration inside the helmet	face ventilation	sweating and heated headform	no	yes

8.2. OBLIQUE IMPACT TESTS

8.2.1. Introduction

Rotational acceleration of the head may be the main cause of diffuse axonal injury in the white matter of the brain (COST 327 Literature Review, 1997). In real accidents, linear and rotational acceleration normally occurs in combination. Newman (1986) proposed a brain injury criterion and threshold for the combined effects of linear and rotational accelerations. At present there is not a helmet Standard that contains a specific rotational acceleration test, but the British Standard BS 6658 requires an oblique impact test to measure tangential forces. In order to investigate rotational acceleration resulting in drop tests according to this standard, Hybrid II headform impacts with an oblique abrasive anvil were carried out at EMPA.

The experiments concentrated on the analysis of the correlation between the rotational acceleration of the headform and the tangential force exerted on the anvil. In addition, the repeatability of oblique impact tests and the influence of different parameters, for example impact velocity and helmet characteristics, on rotational acceleration, were investigated. Forty-two full-face AGV helmets of four different types and size 58 were available for the test series which consisted of 84 impacts. Mr. F Frattini of AGV and ANCMA supplied the helmet samples for these tests.

8.2.2. Equipment

In the final report of the Headforms Working Group it was concluded that the Hybrid II headform has the best repeatability and response compared with aluminium and wood headforms (Chapter 4.4). A Hybrid II headform (50th percentile adult male) was, therefore, used for the experiments. The chin and the neck of this headform allow a good fit of the chin-strap.

The headform was equipped with nine accelerometers (Endevco 7264B-2000) positioned on a mounting block in a 3-2-2-2 array following the recommendations of Padgaonkar et al. (1975). The total mass of the Hybrid II headform, including mounting block and the accelerometers was 4.77 kg. The accelerometer signals were amplified by three voltage amplifiers (Endevco Model 136) and recorded at a sampling rate of 100 kHz using two Nicolet BE490XE transient recorder boards.

The drop tests were performed onto an anvil inclined at 15° to the vertical and fitted to a steel block fixed on a concrete block with a total weight of 1 tonne. The anvil corresponded to the specifications of BS 6658 and was equipped with a tri-axial Kistler type 9366AB force transducer, fixed on a mounting plate (230×300 mm), allowing the measurement of both normal and tangential force components. The impact area was covered with a sheet of abrasive paper (grade 80 closed-coat aluminium oxide) according to BS 6658, which was replaced after each impact.

A computer program was developed for data acquisition and processing. Forces were measured directly, whereas resultant linear and rotational accelerations, as well as additional parameters had to be computed; rotational acceleration was calculated according to Padgaonkar et al., 1975. Accelerometer and force transducer signals were electronically filtered according to CFC600 throughout this study. This filter eliminated most of the noise and high frequency oscillations from the data and provided the correct peak values. Force and acceleration data were recorded over periods of 25 ms.

The standard EMPA helmet test facility (satisfying ECE Regulation 22-04, 1995) consists of a drop test rig where the impact velocity can be changed by varying the drop height, see figure 8.1. The helmeted headform was positioned exactly on the desired impact point by the use of a support ring sustained by a carriage and a mirror under the ring. A guidance system lifts the helmeted headform to the selected height. After being released the helmeted headform falls in a guided free fall. The impact speed is measured using a light beam sensor shortly before the impact. For the impacts onto the oblique abrasive anvil, the drop test rig was adapted to satisfy the requirements of BS 6658, figure 8.2. The dynamic behaviour of the helmet and the headform during the impact was filmed with a high-speed video camera at 4500 frames per second.

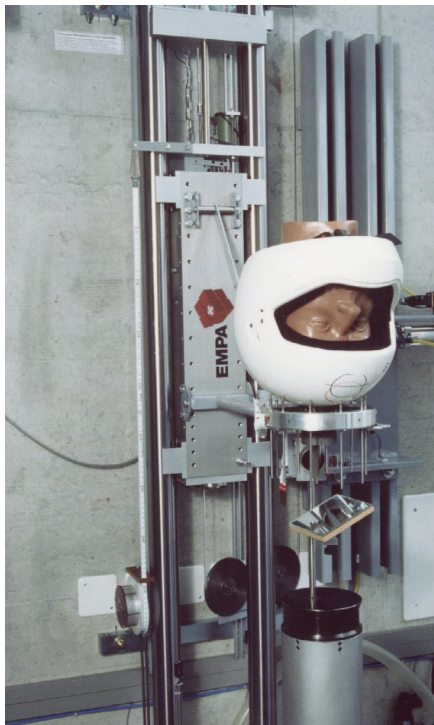


Figure 8.1. Standard helmet test facility.

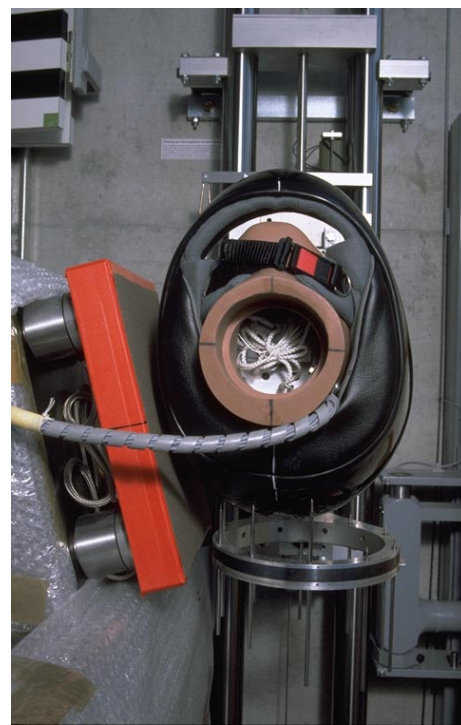


Figure 8.2. Oblique abrasive anvil and helmet positioning.

8.2.3. Test procedure

To investigate the effect of the impact velocity the helmeted headform was dropped from five different heights in order to achieve the selected velocities: 6.0 m/s, 7.5 m/s, 8.5 m/s, 10.0 m/s and 12.0 m/s. The kinetic energy of an impact at 12.0 m/s is four times as great as that for an impact at 6.0 m/s. This ensured that the calculated mean values, the correlation coefficients and the regression lines were meaningful and thus it was possible to determine if there was a significant relationship between the measured parameters. Each helmet was impacted twice: on the left and on the right lateral side. The helmet was positioned such that the central vertical axis of the headform was horizontal and the vertical median plane was vertical, figure 8.2. The distance between the headform eye line and the helmet rim was 40 mm. Between the first and the second impact the headform was repositioned and the retention system firmly re-fastened.

The characteristics of the helmets investigated are given in Table 8.2. The helmet types 1 and 2 are characterised by thermoplastic shells and differ only in the liner density. The types 3 and 4, both with a glassfibre shell, differ in the shell stratification. For each helmet type four oblique impact tests were performed at each of the velocities, 6.0, 7.5, 8.5, 10.0 and 12.0 m/s. To ensure a better comparability of the different helmet types, the visors and the visor mounts were removed from all helmet samples.

Table 8.2 Characteristics of the helmets investigated.

No. of Tests	Helmet Type (full-face)	Shell Material	Liner Density [g/l]	Mean Mass [g] (without visor)
22	AGV ARC EPS (Type 1)	ABS	40 (soft)	1280
20	AGV ARC EPS (Type 2)	ABS	55 (hard)	1329
20	AGV R3/R4 (Type 3)	Glassfibre (ECE stratification, soft)	45	1384
22	AGV R3/R4 (Type 4)	Glassfibre (SNELL 95 stratification, stiff)	45	1629

8.2.4. Results and discussion

Figure 8.3 shows mean time histories of the resultant linear and rotational accelerations of the headform and of the tangential forces measured on the oblique abrasive anvil. The signals are qualitatively similar for all impact velocities, but become narrow and rise with increasing velocity. The impact duration decreases with increasing impact velocity from about 20 ms at 6.0 m/s to about 15 ms at 12.0 m/s.

The plots in figure 8.3 show that the force signal rises about 1 ms earlier than the signals of linear and rotational acceleration, indicating the first contact between the helmet shell and the abrasive anvil. The headform is thus accelerated with a short time delay relative to the first contact. All three curves reach their peaks roughly at the same time. The maximum external force thus coincides with peak linear and rotational acceleration.

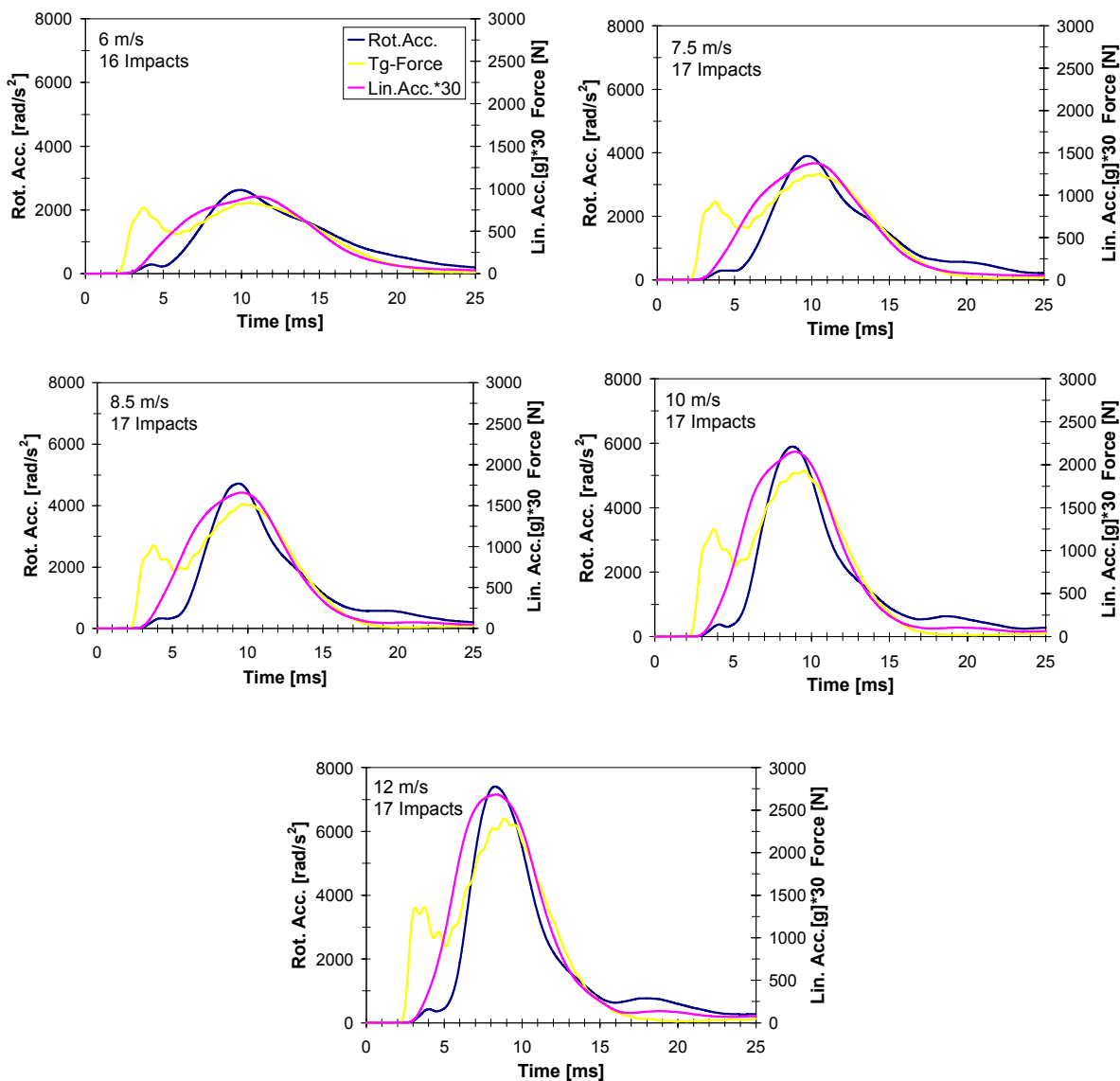


Figure 8.3. Mean time histories for drop tests onto the oblique abrasive anvil. It should be noted that, linear acceleration values on the right axis are multiplied by a factor of 30 to give a clearer comparison. The mean values were calculated using all available measurements and the number is indicated in the plots.

8.2.4.1. Statistical analysis

The effect of varying the impact velocity and the helmet type can be seen in Table 8.3. For the four or five drop tests performed with identical helmets and test parameters, the mean values, standard deviations, sd , and coefficients of variation v (standard deviation expressed as a percentage of the mean: $v = 100 \cdot sd / \text{mean}$) are given for the peak values of rotational acceleration, tangential force, rotational velocity and tangential impulse.

The mean values of peak rotational acceleration varied between about 2500 rad/s^2 and 8500 rad/s^2 and those of the rotational velocity between about 20 rad/s and 41 rad/s . Average peak tangential forces ranged from about 800 N to 2500 N , and the tangential impulses varied between about 9 Ns and 20 Ns . The values of all four parameters increased with the impact velocity for the same helmet type. As expected, impacts at 12.0 m/s thus represent the worst case of headform rotation.

The scatter of the measured data does not depend on the impact velocity or on the helmet type. Most of the coefficients of variation lie below 11 % and for a few impact configurations they vary between 11 % and 18 %. Thus, the repeatability is good for all impact velocities and helmet types and the calculated mean values are representative for the headform drop tests onto the oblique abrasive anvil.

The greatest rotational accelerations measured were with helmet types 1 and 2 (Table 8.3). These helmets are characterised by a thermoplastic shell and lower masses (mean mass 1280 g and 1329 g), whereas type 3 and 4 have a glassfibre shell and are heavier (mean mass 1384 g and 1629 g; see Table 8.2). For all impact velocities, helmets of type 2 experienced the greatest rotational accelerations, followed by type 1. The lowest values were found for the helmet types 3 and 4. The highest tangential forces were also recorded for helmets of type 2, but for the other types the ranking is different for every impact velocity.

The average peak rotational accelerations were between 17% and 26% greater for helmets with a thermoplastic shell than for helmets with a glassfibre shell. The special selection of test helmets, two helmet types with the same thermoplastic shell but different liner densities (type 1: 40 g/l; type 2: 55 g/l) and two helmet types with the same liner density (45 g/l) but different glassfibre shells (type 3: soft ECE stratification; type 4: stiff SNELL 95 stratification), enabled a separate comparison of the effects of the liner density and the shell stratification.

Table 8.3 Mean values of helmet mass, peak rotational acceleration, tangential force, rotational velocity and tangential impulse resulting from oblique impact tests onto an abrasive anvil.

Imp. Vel. [m/s]/ Helmet Type	No. of Tests	Mass [g]	Rot. Acc. [rad/s ²]	sd [rad/s ²]	v [%]	Tg-F. [N]	Sd [N]	v [%]	Rot. Vel. [rad/s]	Sd [rad/s]	v [%]	Tg-Imp. [Ns]	Sd [Ns]	v [%]	
6.0	1	4	1292	2716	263	9.7	799	86	10.	23.4	0.9	4.0	9.2	0.8	8.4
	2	4	1301	3095	169	5.5	1036	93	9.0	23.1	0.3	1.4	10.6	0.4	3.5
	3	4	1387	2488	158	6.3	801	86	10.0	23.9	2.7	11.3	9.8	0.8	8.4
	4	4	1641	2493	413	16.6	895	82	9.2	19.5	0.9	4.8	9.7	0.1	0.8
7.5	1	5	1274	4446	517	11.6	1361	250	18.4	28.8	3.0	10.5	13.3	1.8	13.4
	2	4	1361	4473	332	7.4	1439	78	5.4	27.2	1.2	4.4	13.2	0.2	1.3
	3	4	1401	3393	289	8.5	1238	79	6.4	26.6	4.3	16.1	12.6	1.7	13.6
	4	4	1658	3695	302	8.2	1237	38	3.0	22.2	2.0	9.0	11.0	0.4	3.7
8.5	1	4	1280	4870	362	7.4	1509	110	7.3	28.3	1.9	6.6	13.6	0.3	2.2
	2	4	1328	5389	530	9.8	1661	23	1.4	28.5	1.6	5.8	13.7	0.5	3.7
	3	4	1353	4386	193	4.4	1560	111	7.1	30.8	3.9	12.6	13.9	1.2	8.3
	4	5	1606	4354	688	15.8	1506	115	7.6	26.1	2.9	10.9	12.8	0.8	6.5
10.0	1	5	1282	6116	509	8.3	1888	157	8.3	30.8	2.2	7.1	15.4	1.3	8.1
	2	4	1349	6920	712	10.3	2045	153	7.5	32.6	1.6	5.0	15.7	0.6	4.1
	3	4	1381	5528	443	8.0	2058	86	4.2	34.0	2.9	8.4	16.2	0.8	5.2
	4	4	1633	5675	582	10.3	1909	140	7.4	27.4	2.6	9.7	14.3	1.1	7.7
12.0	1	4	1275	7870	283	3.6	2391	139	5.8	40.7	3.9	9.7	19.7	1.8	9.1
	2	4	1306	8551	898	10.5	2546	170	6.7	37.0	3.1	8.5	18.2	1.0	5.6
	3	4	1401	6817	547	8.0	2383	149	6.2	37.1	2.7	7.3	18.1	1.3	7.4
	4	5	1618	7186	633	8.8	2384	216	9.1	29.9	2.6	8.5	15.7	1.1	7.0

Table 8.4 shows the differences between type 1 and type 2 helmets in the mean values of rotational acceleration and tangential force, differing only in the liner density (see also Table 8.3). Thermoplastic helmets with a hard liner (type 2, 55 g/l) show systematically greater rotational accelerations than those with a soft liner (type 1, 40 g/l). The average difference was 9.4 %. Similar results were found for the tangential force where the mean difference was 12.1 %. The difference in helmet mass was only 49 g, which is less than 4 % (1 % if the mass of the headform is taken into account). The two helmet types are practically identical, therefore, it can be concluded that the differences observed in rotational acceleration and tangential force are due mainly to the different liner densities. The soft liner might allow a deeper penetration of the headform during the impact. This assumption is supported by the fact that the average linear acceleration (see figure 8.7) is also 13.6 % greater in the case of the hard liner.

Table 8.4 Differences in mean rotational acceleration and tangential force between the helmet types 1 and 2 with the same thermoplastic shell but different liner densities.

Impact Velocity [m/s]	Mean Rotational Acceleration [rad/s ²]		Mean Tangential Force [N]	
	Type 2 – Type 1	% (Type 1)	Type 2 – Type 1	% (Type 1)
6.0	379	13.9	238	29.7
7.5	27	0.6	78	5.7
8.5	519	10.7	152	10.1
10.0	804	13.2	156	8.3
12.0	681	8.6	155	6.5
Mean		9.4		12.1

The glassfibre helmets of type 3 and 4 appear identical, but differ in mass and shell stiffness (ECE stratification, SNELL 95 stratification). Differences in mean rotational acceleration and tangential force are given in Table 8.5 (see also Table 8.3). The differences between these two glassfibre helmets are not large and no clear tendency can be derived. The average mass difference of 245 g corresponds to 17.7 % of the lighter helmet, but taking the mass of the headform into account, this percentage reduces to 4 %. Neither the helmet mass nor the shell stiffness seems to affect significantly the rotational accelerations and tangential forces in oblique impacts with glassfibre helmets.

Table 8.5 Differences in mean rotational acceleration and tangential force between the helmet types 3 and 4 with different stratification's of the glassfibre shell.

Impact Velocity [m/s]	Mean Rotational Acceleration [rad/s ²]		Mean Tangential Force [N]	
	Type 4 – Type 3	% (Type 3)	Type 4 – Type 3	% (Type 3)
6.0	5	0.2	95	11.8
7.5	302	8.9	-1	-0.1
8.5	-32	-0.7	-54	-3.5
10.0	146	2.6	-150	-7.3
12.0	369	5.4	1	0.0
Mean		3.3		0.2

8.2.4.2. Headform rotation

In figure 8.4 rotational accelerations are plotted against tangential forces obtained from 84 headform drop tests onto the oblique abrasive anvil. The calculated linear regression and the correlation coefficient ($r = 0.97$) indicate a significant linear relationship between the peak values of rotational acceleration and tangential force.

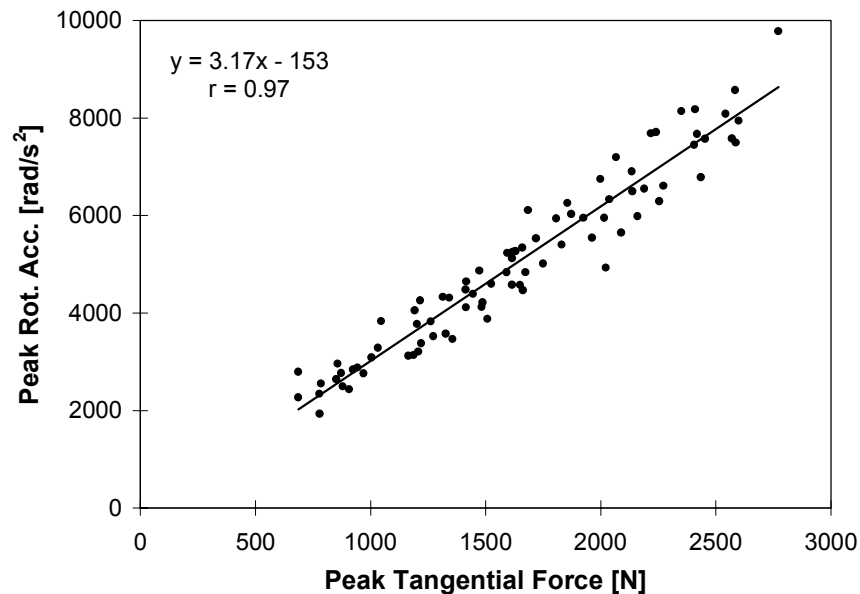


Figure 8.4. Peak rotational acceleration versus peak tangential force for impacts onto the oblique abrasive anvil.

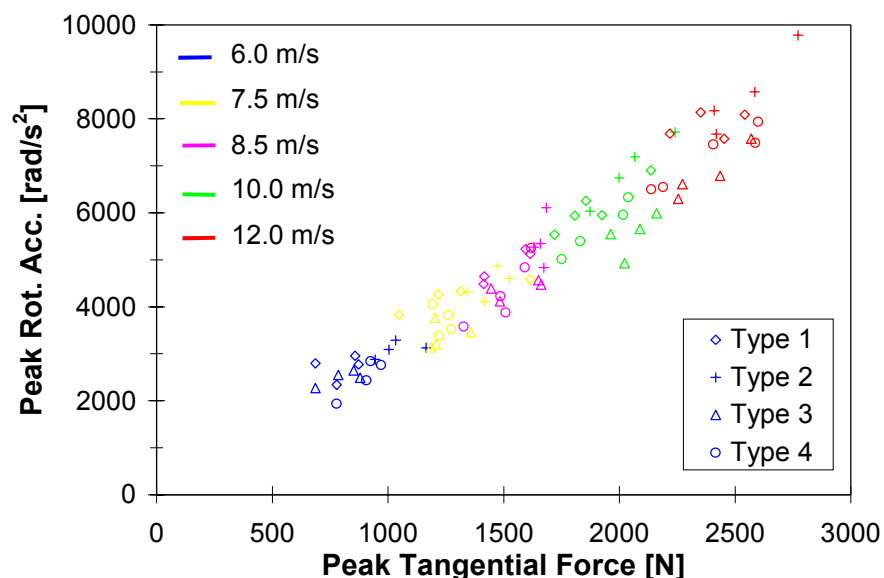


Figure 8.5. Peak rotational acceleration versus peak tangential force for four different helmet types and five impact velocities (same data as in figure 8.4).

In order to illustrate the effect of different impact velocities and helmet types the same results are plotted in figure 8.5 using different colours for the velocities and different

symbols for the helmet types. As already observed in Table 8.3, the measured rotational accelerations and tangential forces increased with the impact velocity. The data points for the five velocities are found in separate areas of the plot, except for a few impacts at 7.5 m/s and 8.5 m/s, where the difference in the kinetic energy is only about 20% for an identical helmet mass. The data for different helmet types is distinguished by symbol rather than colour and the trends are more difficult to observe.

Additional parameters describing the rotation of the headform and the force history, peak rotational velocities and anvil tangential impulses are plotted in figure 8.6. The rotational velocities ranged from 18.1 rad/s to 45.5 rad/s and the tangential impulses from 8.1 Ns to 21.6 Ns. The linear correlation between the two parameters ($r = 0.95$) is nearly as high as between peak rotational acceleration and peak tangential force.

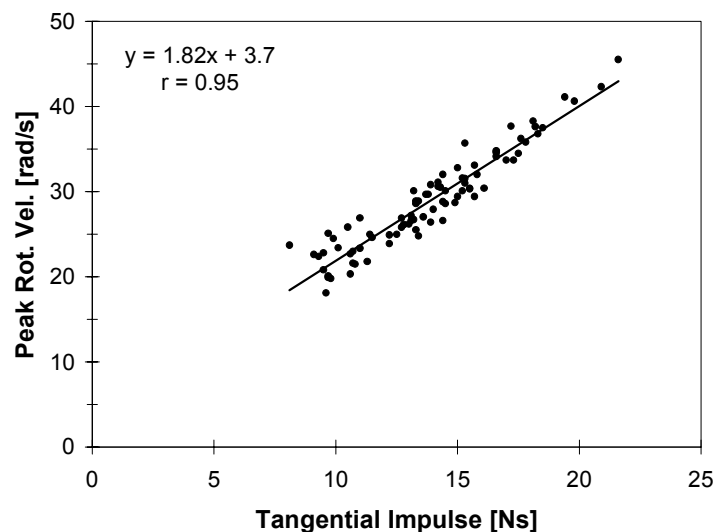


Figure 8.6. Peak rotational velocity versus peak tangential impulse for impacts onto the oblique abrasive anvil.

8.2.4.3. Linear and rotational acceleration

As expected, the measured peak linear accelerations were low and ranged from 22 g to 104 g depending on the impact velocity. In figure 8.7 rotational accelerations are plotted against linear accelerations for all impacts onto the oblique abrasive anvil. A significant linear correlation ($r = 0.91$) was found between the two types of acceleration. The effect of varying impact velocities is shown in figure 8.8. A clear increase of rotational and linear acceleration with increasing impact velocity can be seen, as already observed in Table 8.3.

The linear GAMBIT function is also drawn in figure 8.8 because, in real accidents, usually a combination of translational and rotational acceleration occurs. The GAMBIT line ($G = 1$), based on 250 g for pure linear and 10,000 rad/s² for pure rotational acceleration, is a brain injury threshold that takes into account the combined effect of both types of head accelerations (Newman, 1986; see also Chapters 5.5 and 7.3.3). Most of the data points in figure 8.8 lie below the GAMBIT line ($G < 1$) and can thus be considered as non critical with respect to severe head injuries. Nevertheless, impact velocities of 12 m/s lead to results above the line ($G > 1$) and can therefore be interpreted as critical and indicative of the onset of brain injury. It is interesting to note that for most of the oblique impacts the

peak linear accelerations do not exceed 100 g and thus lie far below the ECE R22-04 limit of 275 g.

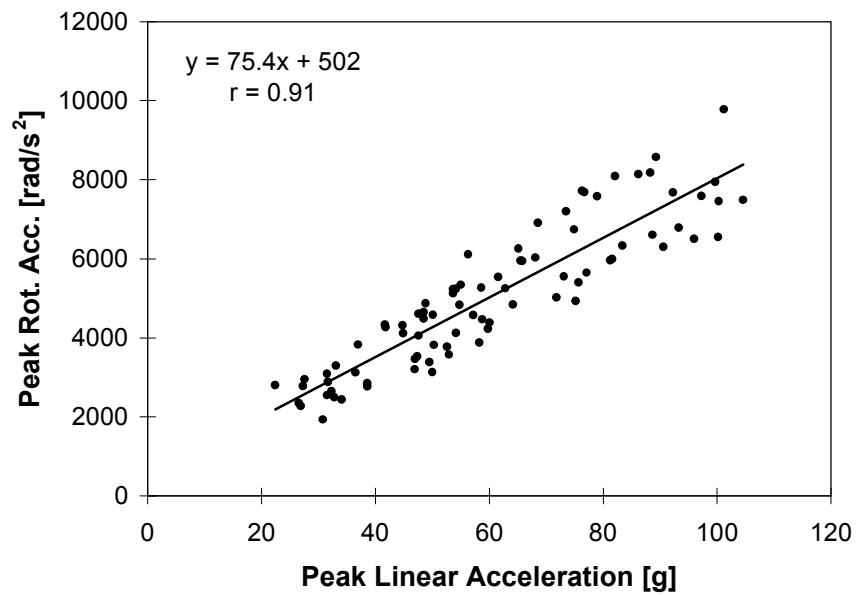


Figure 8.7. Peak rotational acceleration versus peak linear acceleration for all impacts onto the oblique abrasive anvil.

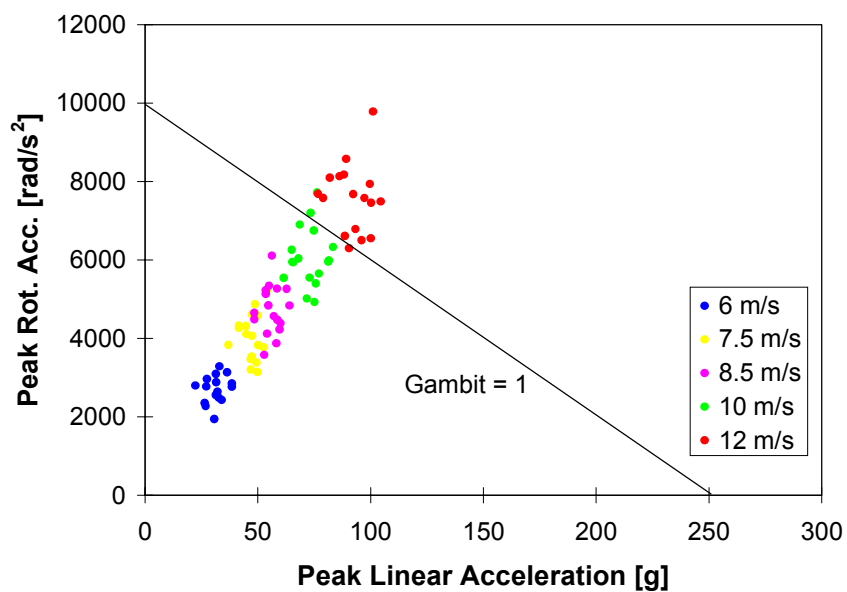


Figure 8.8. Peak rotational acceleration versus peak linear acceleration for impacts onto the oblique abrasive anvil. The linear GAMBIT function is plotted.

8.3. DUMMY DROP TESTS

8.3.1. Introduction

Falling headform tests take no account of the rider's body. In order to investigate the influence of the body mass on the dynamics of the head, drop tests using a complete helmeted Hybrid III dummy were carried out under various impact conditions. The Reconstruction Working Group analysed full scale crash tests impacting a complete helmeted dummy riding a motorcycle into the side of a car. These experiments, performed at TRL, showed much greater peak rotational accelerations and lower peak linear accelerations than observed in replication tests using a detached headform in the laboratory (Chapter 5.4.6.4). The different results were interpreted as a consequence of the interaction between the dummy's body and the head through the neck during impact. It was concluded that the dynamic behaviour of a human head in an impact would be between that of a free headform and that of a headform attached to a body via a stiff dummy neck (Dixon et al., 1997).

Full scale crash tests, impacting a dummy riding a motorcycle, are the most realistic reproduction of an accident, however, they are very time consuming and expensive. Thus, as a link between standard falling headform tests and full scale crash tests, a complete dummy was used for drop tests in the laboratory. The dummy with helmeted head was impacted onto a flat and an oblique anvil in two separate series of tests. It was expected that the complex dynamics of the human head and neck in an accident could be simulated more realistically with a dummy. The results were compared with those obtained in an identical test configuration but using a detached headform.

The aim of this study was to determine the influence of the neck and the body on the linear and rotational acceleration experienced by the dummy headform in comparison with the detached headform. Furthermore, EMPA investigated to what extent falling headform tests, as used in current helmet standards, could replace dummy drop tests if appropriate test parameters are defined. The following test programme was carried out at EMPA:

- Hybrid III dummy drop tests onto the flat anvil and onto the oblique abrasive anvil
- Hybrid III headform drop tests onto the flat anvil

Only a few experiments similar to those described here have been reported in the literature. Aldman et al. (1978a) dropped a helmeted Ogle-Opat dummy onto an impact surface made of asphalt concrete, using a test car to release the dummy and, at the same time, to define a vertical and a horizontal velocity component. Peak values of angular acceleration between 4.8 and 12.4 krad/s² were measured in the head. The results were similar to those obtained by dropping the same helmeted headform, which was attached to a rail-guided carriage, onto a simulated road surface mounted on a rotating disc (Aldman et al., 1976). No other experiments of a dummy being dropped onto an oblique abrasive anvil could be found in the published literature.

8.3.2. Equipment

The Hybrid II and the Hybrid III headform are built with the same technology and it was expected that both will have a similar response to impacts (Chapter 4.4). Therefore, it was decided to use a complete 50th-percentile adult male Hybrid III pedestrian dummy equipped with a standard neck and a standard headform for the drop tests. The Hybrid III dummy head was equipped with the same nine accelerometer array used in the preceding falling headform tests and also the rest of the electrical instrumentation was identical (see

section 8.2.2). The total mass of the Hybrid III dummy was 83 kg and the mass of the instrumented headform was 4.62 kg. Unfortunately it was not possible to measure the upper and lower neck forces. Force and acceleration data were recorded over periods of 25 ms. This recording time was long enough to measure the first and primary head impact. Secondary head impacts are considerably less violent (Aldman et al., 1978a).

All dummy tests were performed at ambient room temperature in the EMPA helmet test laboratory. The experimental set-up is shown in figure 8.9. It consisted of a suspended, helmeted dummy, an anvil equipped with the force transducer and shock absorbing material placed around the anvil to protect the dummy from damage. The dummy was suspended using a four-chain device with an automatic quick-release mechanism. Its orientation could be adjusted by changing the length of the chains. The vertical drop height and thus the impact velocity was selected using a crane. After being released the dummy fell in a free fall without horizontal displacement. The dynamic behaviour of the dummy head during the impact was filmed with a high-speed video camera at 2250 frames per second. An additional video camera recorded the impact of the whole dummy.

The test configurations were selected such that the helmet contacted the anvil at a defined impact point. After the first contact between the helmet and the anvil, the body of the dummy continued to move for several milliseconds before being stopped by shock absorbing materials. This allowed the head impact to be observed without any effects caused by contact of other parts of the body.

All joints of the dummy were preloaded with a force equivalent to that of gravity and the neck was fixed in the 0° position. Prior to the experiments, the dummy was calibrated at the DTC (Dynamic Test Centre, Biel, Switzerland).

For comparison, falling headform tests were performed onto the flat anvil using a detached Hybrid III headform (50th-percentile adult male). Apart from the flat anvil, which was equipped with a Kistler type 9361B force transducer, the same instrumentation was used as for the dummy tests. These experiments were performed at the standard EMPA helmet test facility, figure 8.1.

8.3.3. Test programme and procedure

The dummy test programme consisted of 31 drop tests onto the flat anvil and 18 impacts onto the oblique abrasive anvil. Eighteen new helmet samples were available for the test series. Three different body angles and four locations on the helmet were investigated, see Table 8.6. The body impact angle is defined as the angle between the longitudinal axis of the dummy and the horizontal, in accordance with the COST 327 Accident Investigation Working Group, Chapter 3.4.4. The results of this Working Group showed that about 50% of the motorcyclists impacted with a body angle between 0° and 10° during an accident. About 20% collided at angles around 30° and another 13% impacted at an angle around 90° (D. Otte, personal communication, 1999). These findings were combined with the statistical distribution of the head impact angles in accidents in order to define the geometrical configurations of the laboratory drop tests, see Table 8.6.

In addition, the impacts needed to be as reproducible as possible to obtain a high repeatability of the measurements. Vertical velocities of 4.4 m/s, 5.2 m/s and 6.0 m/s were defined to simulate realistic impact conditions and to limit the risk of severe damage to the dummy. The test programme of the falling headform experiments is shown in Table 8.7.

Table 8.6 Summary of the Hybrid III dummy test programme.

No. of Tests	Impact velocity [m/s]	Anvil	Body impact angle	Head impact point
9	4.4, 5.2, 6.0	flat	30°	frontal (B, ECE R22-04)
11	4.4, 5.2, 6.0	flat	90°	parietal (P, ECE R22-04)
11	4.4, 5.2, 6.0	flat	0°	occipital (R, ECE R22-04)
18	4.4, 5.2, 6.0	oblique abrasive (15°)	0°	lateral left and right (BS 6658)

Table 8.7 Summary of the Hybrid III headform test programme.

No. of Tests	Impact velocity [m/s]	Anvil	Head impact point
9	4.4, 5.2, 6.0	flat	frontal (B, ECE R22-04)
4	4.4, 6.0	flat	parietal (P, ECE R22-04)
6	4.4, 5.2	flat	occipital (R, ECE R22-04)

The same impact points on the helmet as specified in ECE R22-04, i.e. B (frontal), P (parietal) and R (occipital), were defined for dummy impacts onto the flat anvil. For each impact point the dummy was positioned with a defined body angle and released from the selected drop height when it was completely motionless. The corresponding test configurations are shown in the figures 8.9 and 8.10. In the impacts with the oblique abrasive anvil, the dummy was dropped with a body angle of 0°, figure 8.10 right. The left and right lateral impact points, as well as the positioning of the helmets, were in accordance with BS 6658 for oblique impact tests using a headform, figure 8.2.

Helmet samples of the same size 58 and of the same type 3, Table 8.2 were used in all experiments to provide a good comparability between the results. Each helmet was impacted at the points B, P and R onto the flat anvil and on the left and right lateral side onto the oblique anvil. The visors as well as the visor mounts were removed from all helmets. Before each drop test a helmet was positioned on the headform with a fixed distance, 40 mm, between the eye line and the helmet rim, and the retention system was fastened tightly. Body, legs and arms of the dummy were arranged in the correct position.



Figure 8.9. Experimental set-up for dummy drop tests: configuration for R/0°-impacts (left) and for P/90°-impacts (right).

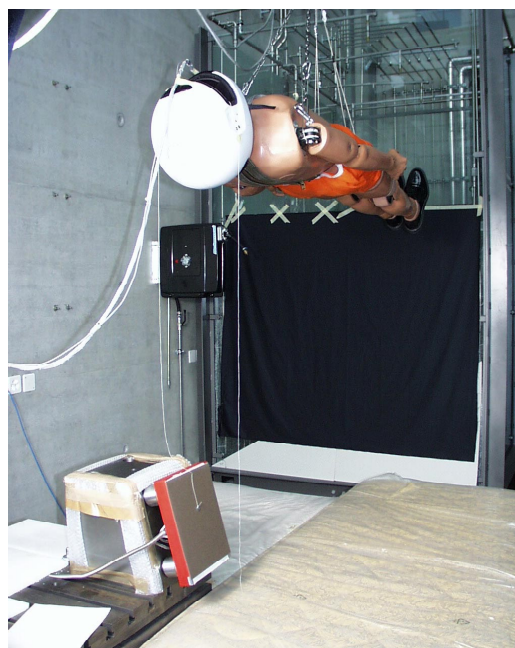


Figure 8.10. Drop test configuration for B/30°-impacts (left) and lateral/0°-impacts onto the oblique abrasive anvil (right).

8.3.4. Oblique impact tests using a dummy: results and discussion

Figure 8.11 shows mean time histories of the resultant linear and rotational accelerations of the headform and of the tangential forces measured on the anvil for oblique impacts of the dummy and the headform (below, right) at impact velocities of 4.4 m/s, 5.2 m/s and 6.0 m/s. Very similar curves were found for all three impact velocities, but the peak values increased with velocity.

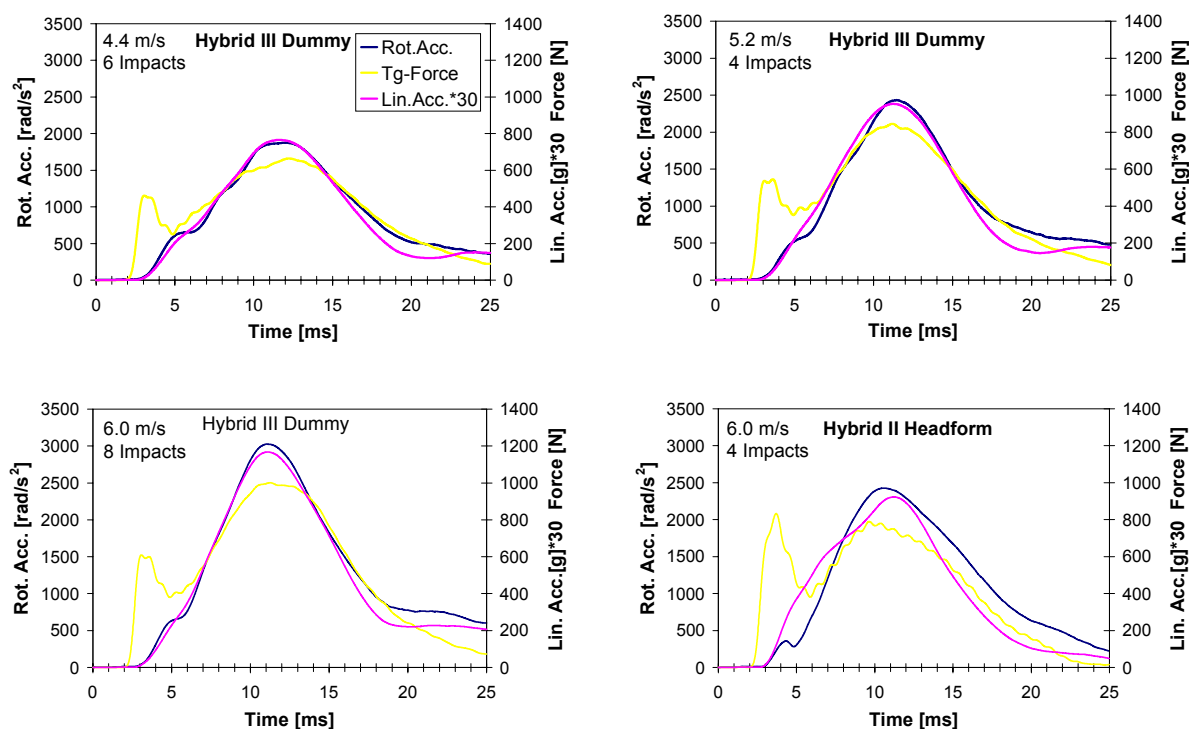


Figure 8.11. Mean time histories for drop tests onto the oblique abrasive anvil. For a better representation linear acceleration values on the right axis are multiplied by a factor of 30. The mean values were calculated using all available measurements; the number is indicated in the plots.

The plots in figure 8.11 show that the force rises about 1 ms earlier than the acceleration signals, indicating the first contact between the helmet shell and the abrasive anvil. Acceleration and rotation of the dummy headform follow with a short time delay. The curves for linear and rotational acceleration are qualitatively similar and reach their maximum at the same time; the correspondence is better for dummy tests. The broad peaks of the tangential forces also coincide with the peaks of linear and rotational acceleration. The signal forms of all three plotted parameters are comparable for dummy and headform tests, although the peak values are somewhat greater using the dummy. The time histories of the tangential forces show narrow peaks during the first phase of the contact. As high-speed videos confirm, these peaks are associated with the onset of considerable helmet shell deformation.

The analysis of high-speed video reveals that the trajectory and the orientation of the dummy body, figure 8.10 right, are barely influenced by the contact between the head and the oblique abrasive anvil. The great body mass and the stiffness of the neck are probably the main reason for this. In contrast, the contact between the helmet shell and the anvil induces a strong rotation of the head and the neck about the vertical dummy axis. The

dynamics resembles that observed for a detached headform colliding with the oblique anvil.

8.3.4.1. Statistical analysis

Table 8.8 shows mean values, standard deviations (sd) and coefficients of variation, (v); see section 8.2.4.1, for the peak values of rotational and linear acceleration, tangential force and rotational velocity resulting in dummy drop tests and falling headform tests on similar helmets. The peak tangential force was determined from the broad maximum of the force signal, which is closely related to the headform rotation, see figure 8.11.

Table 8.8 Results for oblique impact tests onto an abrasive anvil using a Hybrid III dummy and a Hybrid II headform (#).

Imp. Vel. [m/s]	No. of Tests	Rot. Acc. [rad/s ²]	Sd [rad/s ²]	v [%]	Tg-F. [N]	Sd [N]	v [%]	Rot. Vel. [rad/s]	Sd [rad/s]	v [%]	Lin. Acc. [g]	Sd [Ns]	v [%]
4.4	6	1939	226	11.7	712	53	7.4	18.8	1.6	8.5	26.7	1.3	5.0
5.2	4	2468	418	17.0	895	47	5.2	21.4	0.8	3.7	33.3	2.0	6.1
6.0	8	3087	451	14.6	1080	57	5.2	25.3	1.6	6.4	41.2	2.2	5.4
6.0 (#)	4	2488	158	6.3	801	86	10.7	23.9	2.7	11.3	30.9	2.7	8.8
7.5 (#)	4	3393	289	8.5	1238	79	6.4	26.6	4.3	16.1	49.1	2.7	5.6

In the dummy tests the mean peak values of linear acceleration were relatively low and ranged from 27 g to 41 g and the mean peak values of rotational acceleration from about 1900 rad/s² to 3100 rad/s². The rotational velocities varied between 19 rad/s and 25 rad/s and the mean peak values of the tangential forces between about 700 N and 1100 N. The scatter of the measured data does not appear to depend on the impact velocity; the coefficients of variation are below 10 %, except for the rotational acceleration measurements. Thus, the repeatability is good for all impact velocities and the calculated mean values are representative for the experiments.

The results of all four parameters increased with the impact velocity - for both dummy and headform tests. Comparisons between the mean values in Table 8.8 show that the dummy drop test results for an impact velocity of 5.2 m/s correspond approximately to those found for headform impacts at 6.0 m/s. The results of the Hybrid III dummy measurements at an impact velocity of 6.0 m/s lie between those of the Hybrid II headform measurements at 6.0 m/s and at 7.5 m/s, respectively. Consequently, for the same impact velocity the values of the measured parameters are greater for dummy drop tests than for falling headform tests. The differences may be due to the inertial effects of the body mass acting on the head through the neck.

The motion of the dummy body was practically unaffected by the impact, therefore the vertical velocity of the body slightly exceeded that of the head after the contact with the anvil. Thus, the body momentum forced the head to rotate about an axis in the neck area parallel to that passing through the ears. The corresponding contribution to the resultant rotational acceleration can clearly be identified in the data measured in dummy drop tests, whereas it is not found in headform tests. Although this component is considerably smaller than the rotation about the longitudinal axis of the headform, it accounts for the most of the differences between the dummy and headform experiments.

8.3.4.2. Dummy headform rotation

In figure 8.12 rotational accelerations are plotted against tangential forces measured in 18 dummy drop tests onto the oblique abrasive anvil. The results of impacts on the right and on the left helmet side at impact velocities of 4.4 m/s, 5.2 m/s and 6.0 m/s are shown. The calculated linear regression and the correlation coefficient ($r = 0.90$) indicate a significant linear relationship between the peak values of rotational acceleration and tangential force. If the results of the dummy tests are compared with those obtained with a detached Hybrid II headform (figure 8.4), a similar relationship between rotational acceleration and tangential force is found. The correlation coefficient is slightly lower when using a dummy, which could be caused by the relatively small data range.

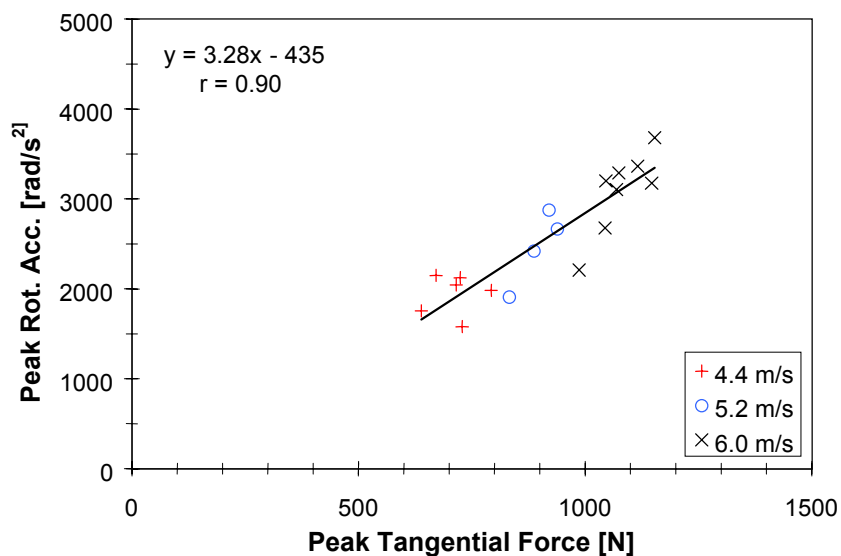


Figure 8.12. Peak rotational acceleration versus peak tangential force for dummy impacts onto the oblique abrasive anvil.

Figure 8.13 shows a direct comparison of the dummy drop test results, figure 8.12, with the results of falling headform tests, both performed using helmet samples of type 3. For both test series, rotational accelerations and tangential forces increased with the impact velocity. The results of the dummy tests are similar to those of the headform experiments, indicating a common relationship between rotational acceleration and tangential force. However, for the same impact velocity the values of the data points for the dummy drop tests were greater, see Table 8.8 and the related text above. It can be concluded that, in order to assess rotational acceleration, falling headform tests should be at a slightly greater velocity than the equivalent dummy drop tests.

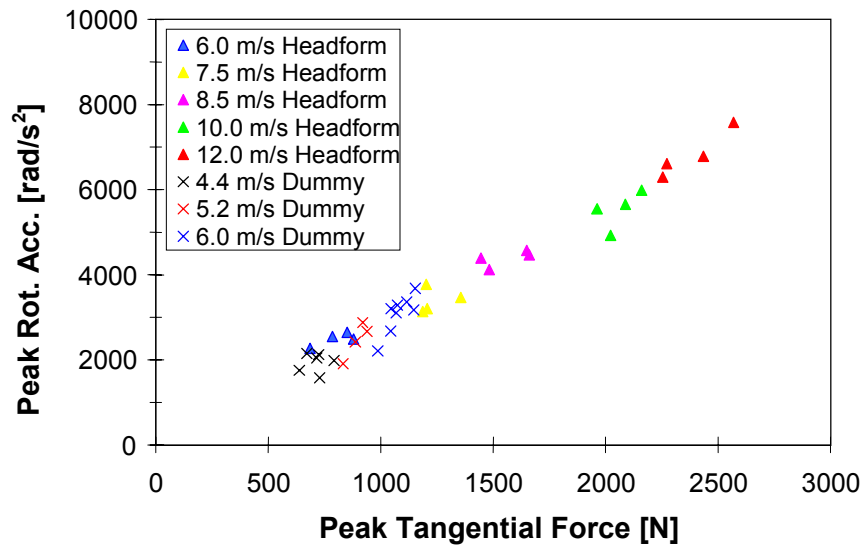


Figure 8.13. Peak rotational acceleration versus peak tangential force for dummy and headform impacts onto the oblique abrasive anvil.

8.3.4.3. Linear and rotational acceleration

In figure 8.14 the measured peak rotational accelerations are plotted against the peak linear accelerations. The linear correlation coefficient ($r = 0.93$) indicates a significant relationship between the two parameters. The regression line and the correlation coefficient are similar to those observed using a detached headform (figure 8.7).

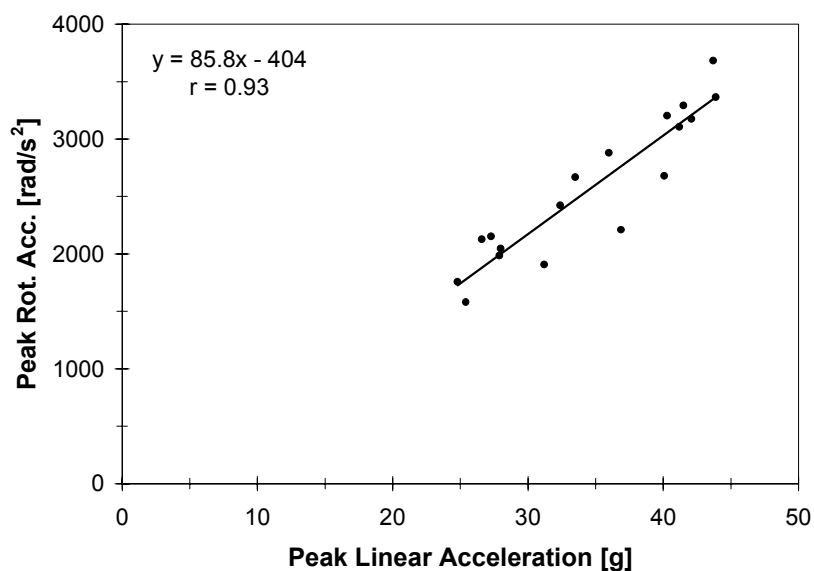


Figure 8.14. Peak rotational acceleration versus peak linear acceleration for dummy impacts onto the oblique abrasive anvil (all impact velocities).

Figure 8.15 shows a direct comparison between dummy drop tests and falling headform tests. Different colours were used for different impact velocities. For both dummy drop tests and falling headform tests the peak rotational and linear acceleration increase with

the impact velocity. The results of the dummy drop tests for rotational acceleration and tangential force are similar to those obtained for the detached headform, as was evident from figure 8.13. For the same impact velocity, peak linear and rotational accelerations occurring in dummy impact tests are somewhat greater than those measured using a detached headform. Relatively low impact velocities were used in the dummy drop tests, therefore, the corresponding data points in figure 8.15 are located clearly below the GAMBIT line ($G < 1$) and should thus not lead to severe head injuries.

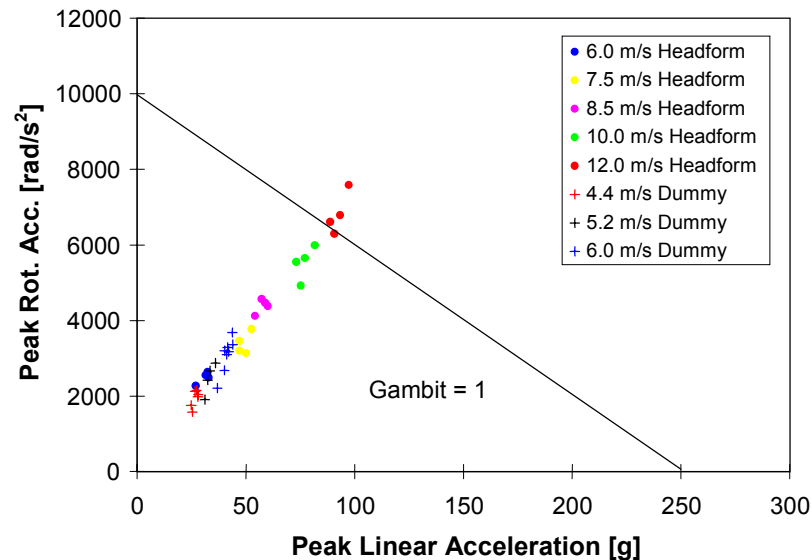


Figure 8.15. Peak rotational acceleration versus peak linear acceleration for dummy and headform impacts onto the oblique abrasive anvil; the linear GAMBIT function is plotted.

8.3.5. Dummy drop tests onto a flat anvil: results and discussion

Figure 8.16, left side, shows examples of mean time histories of the resultant linear and rotational accelerations and normal forces for the different dummy drop test configurations. The results of the corresponding headform tests are plotted on the right side. The signals of all three parameters were more complicated in the dummy tests than in headform tests. This was especially so for the measured rotational accelerations which showed important differences, indicating that both linear and rotational motion of a headform connected to a dummy are more complex than for a detached headform. Conversely, similar linear accelerations were measured in the dummy and headform experiments if the peak values are compared at comparable times.

At a given impact point, the average values of rotational and linear acceleration and normal force are similar for all the impact velocities investigated (not shown in figure 8.16). The dummy headform was accelerated with a time delay of about 1 ms after the first contact between helmet shell and anvil, regardless of whether or not it was attached to the dummy.

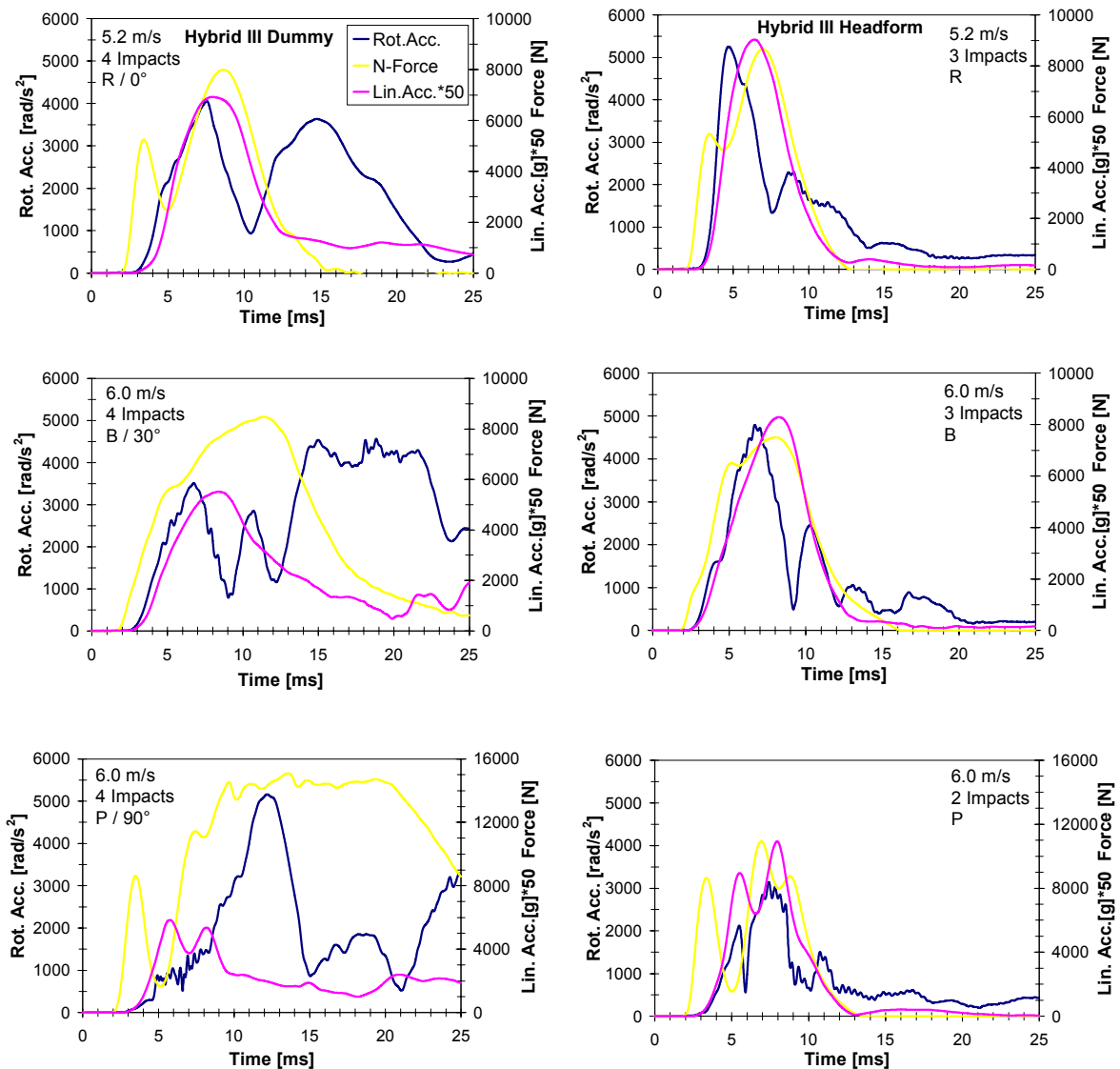


Figure 8.16. Mean time histories for dummy (left) and headform (right) for impacts onto the flat anvil for different impact configurations. B/30°- and P/90°-impacts are shown for the velocity of 6.0 m/s. R/0°-impacts are shown for the velocity of 5.2 m/s because headform impacts at 6.0 m/s are not available. Linear acceleration values on the right axes are multiplied by a factor of 50 for a better representation. The mean values were calculated using all available measurements (the number is indicated in the plots).

The high-speed videos of R/0°-impacts, figure 8.9 left, show that the dummy headform continued to move downwards during the first phase of the contact between helmet shell and anvil. After a contact time of about 8 ms the headform seems to rotate inside the helmet, while the helmet itself remains in the same position. This instance coincides with a local minimum of the rotational acceleration, figure 8.16 left. About 12 ms after the first contact the helmet also began to rotate in the direction of the chin about an axis passing through a point in the neck area rather than through the centre of gravity, as did occur with

the detached headform. The first peak of the rotational acceleration signal coincides with a substantial external force and is, therefore, directly related to the impact. Conversely, the second peak corresponds to a period with very low external force and is probably a consequence of the elastic properties of the neck. Presumably, the neck releases the energy accumulated in the first phase of the impact by rotation, compression or flexion.

This behaviour of the neck does not exactly simulate a human neck, which is more flaccid than the Hybrid III neck. The detached headform signals for the normal force and the linear acceleration were similar, see figure 8.16 right. However, a second peak did not occur for rotational acceleration and this confirms that this second peak is a consequence of the combined effects of the body dynamics and the neck properties in dummy tests. Thus, for the data analysis, the first peak of rotational acceleration was interpreted as the relevant maximum. The behaviour of a human head in a motorcycle accident would probably be between that of a detached headform and a headform attached to a body through a stiff neck. Whereas the measured peak normal forces are comparable in headform and dummy drop tests, greater peak values of linear and rotational acceleration were measured in the headform tests.

The analysis of the impacts at point B with a body angle of 30°, figure 8.10 left, shows that the motion of the dummy headform was not affected during the first phase of the contact between the helmet and anvil. Film analysis and the force measurement, see figure 8.16 left, indicated that the helmet contacted the anvil without rebound during this period. About 7 ms after the first contact, the helmet began to slide forward and then to rotate backwards until the chin guard touched the anvil. The rotational acceleration showed two small peaks followed by a broad and high maximum. This large maximum corresponded to a period with low external force and seems to be a consequence of the elastic behaviour of the neck; an analogous observation was made for impacts at point R. The maximum for rotational acceleration was thus determined from the first two peaks.

The results of the falling headform tests differ from the dummy measurements, although rotational acceleration was similar for the first two peaks, in figure 8.16. In the headform tests, greater peak values were measured for linear and rotational acceleration, but lower peak values for the normal force. In the dummy tests, the normal force reached a peak value later than in the falling headform tests, indicating the effect of the dummy body.

The most complex signals were measured in the impacts at point P with a body angle of 90°, see figure 8.9 right. The high-speed video shows that the helmet remains practically in the same position after the first contact with the anvil while the body and the neck of the dummy continue to move downwards. A rebound of the helmet was observed during which the helmet seemed to lose contact with the anvil for a short time. The rebound motion reversed about 3 ms after the first contact when the normal force assumed a local minimum, see figure 8.16 left. At a contact time of 8 ms the helmet began to rotate backwards and then to slide forwards onto the anvil while the legs and the body of the dummy followed in the opposite direction. Throughout this period, very high and approximately constant normal forces were exerted on the anvil. The rotational acceleration peak occurred during this phase when the linear acceleration fell to relatively low values following a double peak.

In most COST 327 accidents, the injuries sustained were a consequence of the combined effect of linear and rotational acceleration, Chapter 2.3. The two types of acceleration can also occur sequentially. Thus for the data analysis, the rotational acceleration peak at the centre of the measuring time was considered to be the relevant maximum. The linear accelerations were similar in shape, although the peak values were much greater than in

the falling headform tests. The rotational acceleration peaks were greater and occurred later in the dummy tests. The measured signals demonstrate that in the case of the impact configuration P/90°, the dynamic behaviour of the dummy head was influenced by the forces which were transmitted to the head through the neck.

Dummy impacts onto the flat anvil reflect the effect of the body mass, but they also show the importance of the mechanical properties of the Hybrid III standard neck, which is stiffer than a human neck. As for impacts onto the oblique anvil, the rotation of the dummy headform was determined by the combined effects of the body dynamics and the neck properties.

8.3.5.1. Statistical analysis

Table 8.9 contains mean values, standard deviations (sd) and coefficients of variation (v) for the peak values of rotational acceleration, normal force, linear acceleration and HIC, which were calculated for the dummy and the headform drop tests. The listed values represent the results of two, three or four drop tests with the same configuration.

Table 8.9 Results for Hybrid III dummy tests and Hybrid III headform (#) drop tests onto the flat anvil.

Imp. Point /Velocity	No. of Tests	Rot. Acc. [rad/s ²]	Sd [rad/s ²]	v [%]	N-F. [N]	Sd [N]	v [%]	Lin. Acc. [g]	Sd [g]	v [%]	HIC	sd	v [%]	
B/30°	4.4	2	2897	31	1.1	6507	56	0.9	85	1.9	2.2	251	8.1	3.2
	5.2	3	3551	355	10.0	7736	319	4.1	99	3.2	3.3	368	27.6	7.5
	6.0	4	3735	654	17.5	8758	561	6.4	111	4.6	4.1	510	53.2	10.4
R/0°	4.4	4	3677	370	10.1	7013	307	4.4	122	4.2	3.5	568	43.6	7.7
	5.2	4	4338	409	9.4	8071	196	2.4	142	5.8	4.1	820	41.8	5.1
	6.0	3	4789	427	8.9	8940	425	4.8	165	6.3	3.8	1106	75.1	6.8
P/90°	4.4	3	4172	548	13.1	11243	511	4.5	102	24.5	24.1	218	50.1	23.0
	5.2	4	4616	307	6.7	12936	864	6.7	113	13.6	12.1	320	37.8	11.8
	6.0	4	5304	559	10.5	15560	1430	9.2	134	10.3	7.7	387	34.4	8.9
B (#)	4.4	3	3905	642	16.5	5601	322	5.8	120	6.7	5.6	505	28.5	5.6
	5.2	3	4941	271	5.5	6119	459	7.5	126	11.3	9.0	635	84.2	13.3
	6.0	3	4814	66	1.4	7505	462	6.2	166	3.7	2.2	1074	59.0	5.5
R (#)	4.4	3	5504	519	9.4	7109	436	6.1	138	5.1	3.7	689	39.0	5.7
	5.2	3	5557	117	2.1	8715	265	3.0	182	8.7	4.8	1198	66.2	5.5
	6.0	n.a.	n.a.	n.a.	n.a.	n.a.	n.a.	n.a.	n.a.	n.a.	n.a.	n.a.	n.a.	n.a.
P (#)	4.4	2	1574	47	3.0	6908	673	9.7	136	10.5	7.7	535	82.8	15.5
	5.2	n.a.	n.a.	n.a.	n.a.	n.a.	n.a.	n.a.	n.a.	n.a.	n.a.	n.a.	n.a.	n.a.
	6.0	2	3390	244	7.2	10951	41	0.4	219	8.0	3.7	1515	88.5	5.8

n.a.: not available

The mean peak values of rotational acceleration varied between about 2900 rad/s² and 5300 rad/s² in the dummy tests. The peak values of linear acceleration ranged from 85 g to 165 g and those of the normal force from about 6500 N to 15600 N. At a given impact point, the results of all four parameters considered in Table 8.9 clearly increased with the

impact velocity. The results of the headform drop tests show an analogous behaviour, except for rotational acceleration. As expected, impacts at 6.0 m/s represent the worst case of linear and rotational acceleration of the dummy head. For dummy tests most of the coefficients of variation in Table 8.9 are below 12 %, at a given impact point and velocity, and only a few vary between 13 % and 24 %. It seems that the scatter of the data does not depend on the impact velocity or on the impact point and that it is of the same order of magnitude for the dummy and headform tests. Despite the complexity of the Hybrid III dummy drop tests, in comparison with headform tests, it can be concluded that the repeatability of these results is good and that the calculated mean values are representative.

For a given impact velocity, the mean values systematically depend on the impact point and the test configuration. The greatest normal forces result in impacts at point P with a body angle of 90°. This is not surprising because the dummy is dropped perpendicularly to the impact surface. The measured forces are much greater than for the other test configurations. Also the greatest rotational accelerations are measured in P/90°-impacts, although the differences are less significant. Considering linear acceleration and HIC, the greatest values are found for impacts at point R.

Table 8.9 shows that, for the same impact velocity, the normal forces for B/30° and P/90°-impacts are greater when using a dummy instead of a headform. For impacts at point R, the normal forces are similar in both cases. These findings are not surprising because the mean time histories of the normal forces in figure 8.16 are most similar for R-impacts, indicating that the body mass had very little effect. In contrast, the effect in the B/30°-impacts was substantial and even greater in the P/90°-impacts. Rotational acceleration was much greater using a complete dummy in P/90°-impacts than a detached headform. Conversely B/30° and R/0° impacts gave lower rotational acceleration peaks when using a dummy.

For the same impact point and velocity, the linear accelerations and HIC values were lower for dummy drop tests than for falling headform tests, see Table 8.9. The greatest differences found were for impacts at point P, followed by impacts at B, whereas the differences were small for impacts at R.

During an impact, the force acting on the head is a function of the effective mass of the head. Thus, for the same force, the linear acceleration will be inversely proportional to the effective mass. With a dummy, the head is connected to the body by the neck, thus the effective mass of the head is likely to be greater than for the head alone and this will give a lower linear acceleration. This would explain why the head linear accelerations were lower in the dummy tests than in the tests with the head alone. Dixon et al. (1997) found lower linear acceleration in a full scale crash test than in falling headform tests in which equivalent helmet damage was replicated.

In this study, the information on forces and linear accelerations is available for both dummy and headform tests, so that impacts at the same point with a similar value of normal force can be compared by means of the equation:

$$m_e \cdot a_e = m_h \cdot a_h$$

where:

m_e : effective mass of the helmeted dummy head

a_e : linear acceleration of the helmeted dummy head

m_h : mass of the detached helmeted headform

a_h : linear acceleration of the detached helmeted headform

The assumption that the same kinetic energy is required to produce equivalent helmet damage in falling headform tests and dummy drop tests provides a second equation:

$$\frac{1}{2} m_e \cdot v_d^2 = \frac{1}{2} m_h \cdot v_h^2$$

where:

v_d : impact velocity of the dummy head

v_h : impact velocity of the detached headform

The mass of the Hybrid III headform is 4.6 kg and the mean helmet mass about 1.4 kg, thus 6 kg was used as the mass of the detached helmeted headform. Table 8.9 shows that comparable normal forces are measured on the anvil in B/30°-impacts at 5.2 m/s, dummy, and 6.0 m/s, headform, in R/0°-impacts at 4.4 m/s (both) and in P/90°-impacts at 4.4 m/s, dummy and 6.0 m/s, headform. With the known velocities and the measured linear accelerations, the following effective masses of the helmeted dummy headform were calculated from the energy/force equations:

B/30°: 8 kg / 10 kg; R/0°: 6 kg / 7 kg; P/90°: 11 kg / 13 kg

These results confirm that an increased effective mass of the dummy headform reduces the linear acceleration of the head. The greatest effective mass and thus the greatest difference between dummy and headform tests occurred in P/90°-impacts, whereas R/0°-impacts increase the effective mass only slightly. The greater the body impact angle the greater the coincidence of the longitudinal neck axis with the direction of the normal impact force and, in turn, the greater the effect of the dummy body through the neck.

8.3.5.2. Comparison with results from the literature

Only a few experiments similar to this study have been reported in the literature. In the following, the results of this study are compared with the measurements carried out by Aldman et al. (1976, 1978a, 1978b) using an Ogle-Opat dummy fitted with a polycarbonate open face helmet. The main difference was the use of a test car to release the dummy, imposing an additional horizontal velocity component, typically 8-9 m/s, which caused an oblique impact with a flat surface made of asphalt concrete. Vertical impact velocities of 4.4 m/s and 5.2 m/s were used in the drop tests.

Considering similar test configurations, there is a good correspondence between Aldman's results and the results of this study with regard to linear acceleration see Table 8.10. This is explained by the fact that linear acceleration depends mainly on the vertical impact velocity which is dependent on the drop height. Conversely, Aldman measured rotational accelerations up to two or three times as great as the results of this study. Despite differences in the impact surfaces and in the neck and headform characteristics, the differing horizontal impact velocities may explain these large discrepancies. This is confirmed by extrapolation of the results of dummy drop tests onto the oblique abrasive anvil to higher impact velocities where the vertical and horizontal velocity components allow a direct comparison with the R/0°-configuration of Aldman, see Table 8.8. The extrapolated rotational accelerations are of the same order of magnitude as Aldman's results.

Table 8.10 Selection of the dummy drop test results from Aldman et al. (1978a) and mean values from this study (#) (see Table 8.9). Helmet impact points and body impact angles reported in the table are estimates from the figures reported by Aldman.

Impact Point / Body angle	Vertical Velocity [m/s]	Horizontal Velocity [m/s]	Peak Linear Acceleration [g]	Peak Rotational Acceleration [rad/s ²]	No. of Tests
R / 25°	5.2	8.1-8.4	120-150	5500-11400	4
R / 0°	5.2	8.2-8.3	138-162	6000-12300	3
R / 25°	4.4	8.4	120	7200	1
R / 25°	5.2	4.0-4.2	134	7000-7400	2
R / 25°	5.2	11.4-14.0	130-135	10000-10200	2
R / 25°	5.2	7.8	140	7700	1
R / 25°	5.2	8.4	120	12400	1
B / 25°	5.2	8.3	105	4800	1
B / 30° (#)	5.2	0.0	99	3551	3
R / 0° (#)	4.4	0.0	122	3677	4
R / 0° (#)	5.2	0.0	142	4338	4

8.3.5.3. Linear and rotational acceleration

In figure 8.17 peak values of rotational acceleration are plotted against peak values of linear acceleration for dummy drop tests onto the flat anvil. The regression lines for the different impact configurations can clearly be distinguished. Impacts at point R show the strongest linear relationship between linear and rotational acceleration, $r = 0.85$, whereas the correlation is weaker for B/30°-impacts, $r = 0.64$, and not significant for impacts at point P, $r = 0.33$. A higher correlation coefficient is found, if peak linear and rotational accelerations occur approximately simultaneously, as was the case for impacts at point R, and can be observed in figure 8.16 (left). This did not occur with impacts at point P because the peak rotational acceleration arose much later than that of the linear acceleration. The correlation between linear and rotational acceleration is decreased by the influence of the neck and the body on the dynamics of the dummy head.

Most of the data points in figure 8.17 are located below the GAMBIT line ($G < 1$), but a few points are located above the line ($G > 1$), of which some result from impacts at a velocity of only 5.2 m/s. Thus, even at the low impact velocities chosen for the dummy drop tests, some of the measured values, according to Newman, indicated the potential for brain injury.

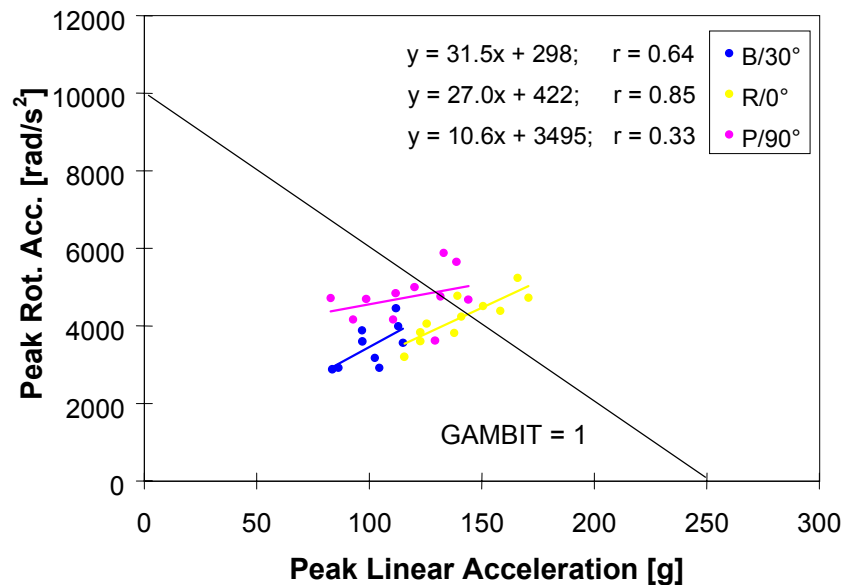


Figure 8.17. Peak rotational acceleration versus peak linear acceleration for dummy impacts onto the flat anvil at 4.4 m/s, 5.2 m/s and 6.0 m/s; the function $\text{GAMBIT} = 1$ is plotted.

8.4. MECHANICAL HELMET TESTS

8.4.1. Chin-strap effectiveness test

Chapter 3.6.2 indicates that, in the COST 327 accident sample, 14% of helmets came off the head during the impact phase and mainly after the first or the second impact of the head (Chapter 3.6.2). The Accident Investigation Working Group stated that there is a need to improve the retention during an impact. The stability of a helmet on the head was therefore investigated by means of a new chin-strap effectiveness test.

8.4.1.1. Method

The test method combined some of the elements found in retention system tests according to BS 6658:1985 and ECE R22-04 but, in addition, permitted the forces transmitted to the chin to be measured during dynamic loads to the chin-strap. The main component of the experimental set-up is an aluminium headform, which was developed and constructed by AD Engineering. This ISO size 57 headform is characterised by a modified chin equipped with a piezo-resistive load cell for the measurement of both static and dynamic forces exerted on the chin. In order to obtain a high sensitivity of the force measurement for typical retention system geometries, the axis of the load cell was inclined by an angle of 37° to the vertical axis of the headform. Figure 8.18 shows the design of the new headform. The response of the load cell was sampled by a transient recorder and analysed by a computer.

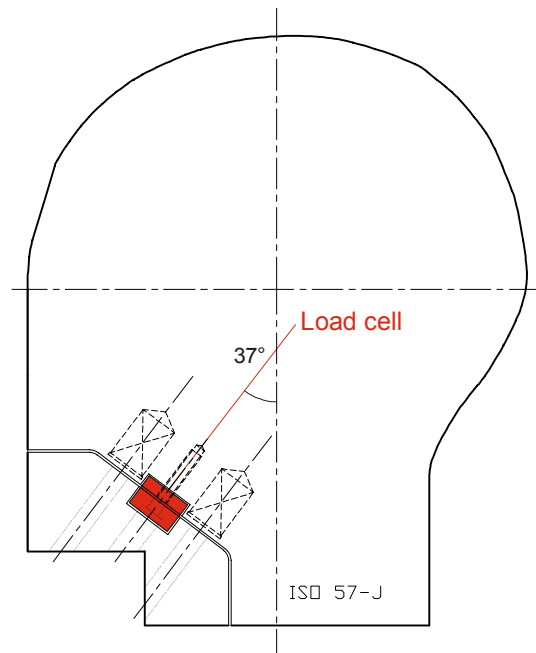


Figure 8.18. Headform developed for chin-strap effectiveness tests. A built-in load cell allows the measurement of static and dynamic forces exerted to the chin.

8.4.1.2. Test programme

The test device was used as a component in the experimental set-up for a retention test according to the ECE R22 roll-off test. Four test series were carried out in which the test parameters were chosen either in accordance with ECE R22 or changed slightly. A summary of the test programme is given in Table 8.11.

Although the test parameters of the second test series corresponded to the standard roll-off test, the helmets were positioned with a displacement of 25 mm towards the front of the headform in the first test series. For the third test series, the smooth aluminium headform was covered with a rubber skin to increase friction and to simulate the human head more realistically (note that a wig is specified in BS 6658). Eighteen helmet samples, 9 pairs of the same type, were available for the first three test series in which the same helmet samples were tested three times. Three additional helmet samples were investigated in the fourth test series.

The objectives of the experiments were to investigate the order of magnitude of the forces which are transmitted to the chin when the retention system is fastened and loaded dynamically. It is considered that the fastening of the chin-strap causes a static pre-load to the chin which influences the outcome of a roll-off test, i.e. the angle of helmet rotation. If so, the initial load should be specified in a test procedure. The maximum force onto the chin during a dynamic retention system effectiveness test is also of interest because high loads could be accompanied by neck injury risk.

Table 8.11 Test programme concerning the stability of a helmet on the head using a headform with a built-in load cell.

Test series	Tested helmets	Helmet positioning	Attachment of the retention system	Headform surface
1	18 (2×9)	displacement of 25 mm towards the front of the headform	normal (tight)	smooth aluminium surface
2	18 (2×9)	according to ECE R 22-04	normal (tight)	smooth aluminium surface
3	18 (2×9)	according to ECE R 22-04	normal (tight)	headform covered with a rubber skin
4	3 (2+1)	according to ECE R 22-04	varying initial loads	aluminium and rubber surface

8.4.1.3. Results and discussion

The forces transmitted to the chin were recorded over the whole duration of a roll-off test, from the fastening procedure until the end of the experiment. It was found that three force values are important to the evaluation of the measured signal, namely the initial load caused by the tightened chin-strap, the peak force during a roll-off test and the final load after the test. Preliminary tests showed that the static force measured 1 s before the peak value was an appropriate measure of the initial load and the static force measured 3 s after the peak value appropriate for the final load.

Table 8.12 shows the results of three series of chin-strap effectiveness tests using two surface conditions of the headform, aluminium and rubber. The measured forces varied over a wide range because of the different designs of the retention systems investigated, however, similar results were obtained for two helmets of the same type in all of the test series.

Table 8.12 Chin-strap effectiveness test results (18 helmets of 9 different types)

Test parameters	Initial force [N]				Peak force [N]				Final force [N]			
	min.	max.	mean	sd	min.	max.	mean	sd	min.	max.	mean	sd
Al/displaced	25	156	57	34	112	427	312	81	78	240	183	49
Al/normal	19	132	66	32	153	408	336	74	98	266	197	49
Rubber/normal	12*	96*	42*	22*	34*	310*	155*	89*	7*	257*	117*	77*

* One result ignored because of uncertain values.

Comparable results were also found for the two test series in which the helmets were positioned with and without a displacement on the aluminium headform. Slightly greater forces were measured for the normal positioning, nevertheless, the effect of initial orientation was small and did not affect the results overall, as can be seen from figure 8.19. The initial forces measured were between 19 and 156 N, the peak forces were between 112 and 427 N and the final forces were between 78 and 266 N. The peak forces

correlated more closely with the final loads, with linear correlation coefficients of 0.88 and 0.87, than with the initial loads, correlation coefficients 0.57 and 0.60. It is not known if forces of up to 400 N carry an injury risk to the neck or to the throat.

When the headform was covered with a rubber skin, the measurements were less reproducible. Presumably, the sliding of a helmet on the rubber surface was erratic because of a tendency to stick and slip alternately. Generally, lower forces were measured on the rubber surface, see figure 8.19. A linear correlation coefficient of 0.67 was found between the peak forces and the final forces and one of 0.61 between the peak forces and the initial forces, respectively. Although the rubber skin might simulate the friction characteristics of a human head more realistically, the smooth aluminium surface has to be preferred for better reproducibility.

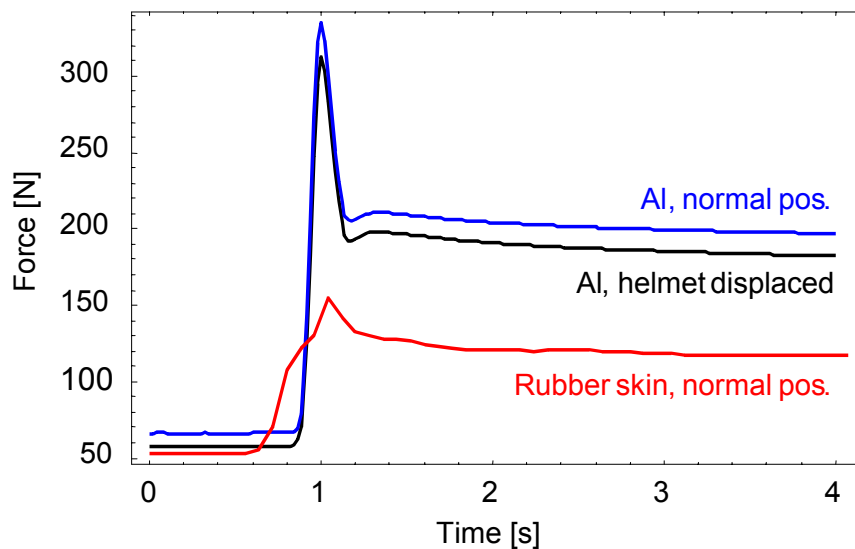


Figure 8.19. Average forces measured in chin-strap effectiveness tests (18 helmets). **Blue curve:** tests on the aluminium headform, normal positioning of the helmets. **Black curve:** tests on the aluminium headform, helmets displaced towards the front of the headform. **Red curve:** tests using a rubber skin on the headform, normal positioning of the helmets.

In figure 8.20 the angles by which the helmets rotated in the roll-off tests are plotted against the initial forces exerted to the chin via the retention system, test series 2 and 3, see Table 8.11. The initial forces, as well as the measured angles, tended to lower values when the headform was covered with a rubber skin. In the tests using the aluminium headform the angles decreased with increasing pre-loads. Part of the data scatter in figure 8.20 can be explained by the fact that the results comprise nine different types of retention systems.

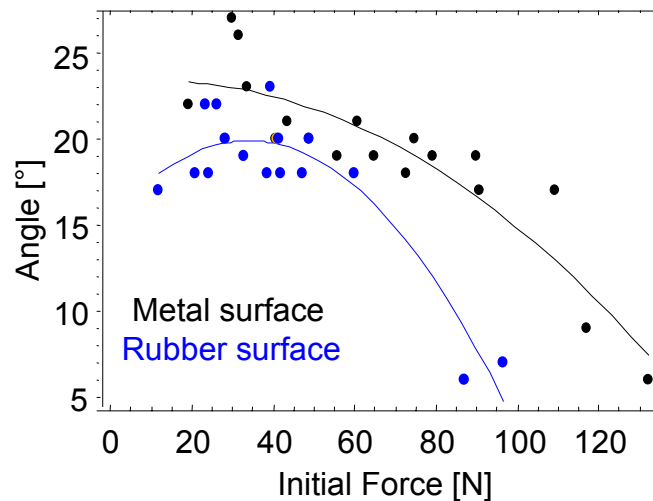


Figure 8.20. Relationship between the initial force to the chin and the angle by which the helmet rotated in roll-off tests (results for 17 helmets). Black curve: results for the aluminium headform (test series 2, see Table 8.11). Orange curve: results for the headform covered with a rubber skin (test series 3).

In order to study the dependence of angles resulting in roll-off tests on the initial loads in more detail, additional experiments were carried out in which helmets were investigated repeatedly using various pre-loads in the retention systems which were adjusted in a random order. Two helmets of the same type were tested on the aluminium headform (J1) and on the headform covered with the rubber skin (J2), respectively. A third helmet of a different type was tested on the aluminium headform only (K1); results are shown in figure 8.21.

For helmets of the same type (J1, J2) slightly smaller angles were observed when the headform was covered with the rubber skin, see figure 8.21, left. The differences were greater for small initial forces to the chin. The other helmet with a different retention system (K1) rotated by greater angles on the aluminium headform, indicating that the design of the retention system rather than the surface condition of the headform determines the test results. If the headform was used without the rubber skin the resulting angles clearly decreased with increasing initial loads for both helmet types investigated (J1, K1). At comparable initial loads the peak forces in roll-off tests were reduced by the rubber skin, see figure 8.21, right.

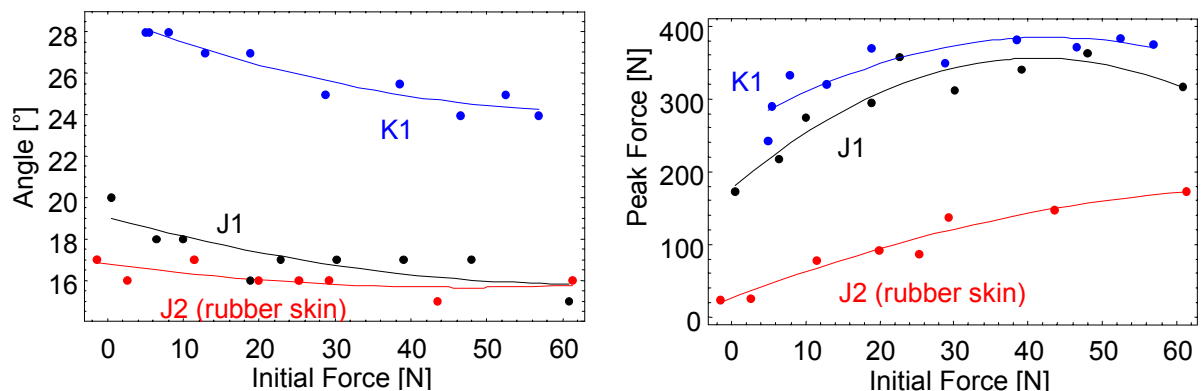


Figure 8.21. Angle by which a helmet rotates (left) and peak force in a roll-off test (right) versus the initial force against the chin.

The chin-strap effectiveness tests, using the new headform, showed that the angle achieved in a roll-off test depends on the pre-load exerted to the chin via the retention system. Thus, the outcome of a test is a function of the force applied when the chin-strap is tightened. It is, therefore, recommended that the initial load is specified in a future test procedure to examine chin-strap effectiveness.

In some experiments a rubber skin was used to increase the friction between the headform and the helmet. This reduced the measured forces as well as the angles by which the helmets rotated in the roll-off tests. However, the test results with a rubber skin were less reproducible.

The headform as developed, is an interesting new approach to the testing of chin-strap effectiveness. In the current form, the headform allows the measurement of a resultant force to the chin in one direction. The incorporation of two load cells could be a possible future improvement of the test device, by which the direction of the forces transmitted to the chin could be investigated in detail.

8.4.2. Friction test

8.4.2.1. Friction of the helmet shell

The friction of the helmet shell affects the tangential contact forces in an oblique impact and thus the resulting rotational acceleration of the head. In the case of an impacting rigid sphere with radius r and mass m , the following equation between rotational acceleration and normal force can be derived from the laws of rotational motion:

$\dot{\omega} = \frac{5}{2} \frac{\mu}{mr} F_N$, where $\mu = F_T / F_N$ denotes the ratio between the tangential and the normal force component and can be interpreted as a coefficient of friction.

The equation above allows the determination of coefficients of friction for the different types of helmet shells by linear regression of the oblique impact test results $\dot{\omega}(F_N)$, see figure 8.22. Using the data described in Chapter 8.2, the known helmet masses and a constant effective radius of 130 ± 6 mm (based on measured helmet dimensions and estimated radial deformations during oblique impacts), the coefficients of friction shown in the first line of Table 8.13 were calculated for the four helmet types. It can be seen that ABS shells (types 1 and 2) show significantly higher coefficients of friction under impact conditions than glassfibre helmets (types 3 and 4).

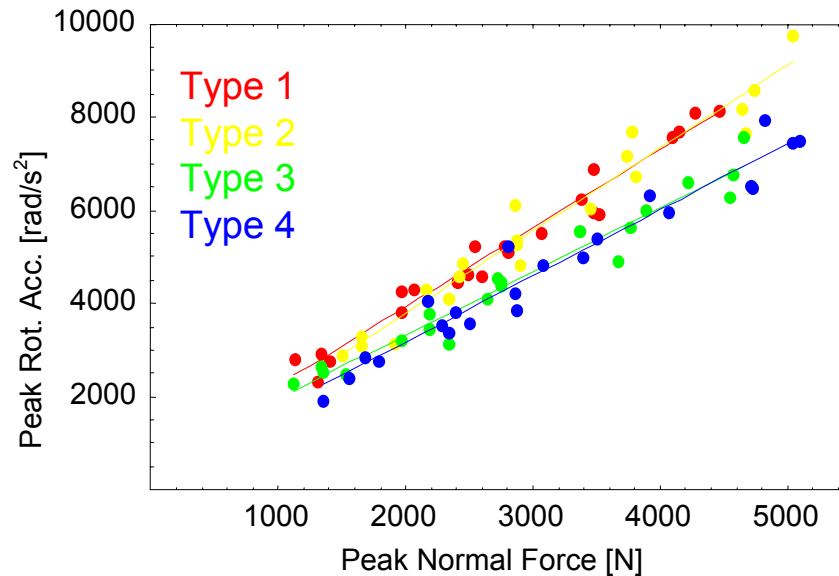


Figure 8.22. Peak rotational acceleration versus peak normal force measured for impacts onto the oblique abrasive anvil (results discussed in chapter 8.2). Linear regression lines were calculated for each helmet type.

Coefficients of friction between the helmet shells and the abrasive anvil can be calculated directly from the impact forces measured at the anvil. An analysis shows that for each oblique impact, the ratio of the tangential to the normal force component stays roughly constant over a period of at least 5 ms, indicating a steady sliding of the helmet on the abrasive paper. By averaging sliding phases of 5 ms duration, dynamic coefficients of friction were obtained on which statistical information is given in the second line of Table 8.13. Taking the standard deviations into account, the results are comparable with those of the linear regressions, except for the helmet type 3. The shells of type 3 are considerably less stiff than those of type 4 so that more significant radial deformations, greater contact areas and different pressures occur in impacts. This is confirmed by the abrasion marks.

Figure 8.22 implies a close relationship between the frictional properties of the helmet shells made of the same material (types 1 and 2 and types 3 and 4, respectively). In helmet types 3 and 4 the analysis, of the contact forces further indicates that the dynamic coefficients of friction are not only determined by the shell material but also affected by the dynamic behaviour of the shell during the impact. Whereas the dynamic behaviour seems to be very similar for helmets of types 1 and 2, it differs for helmets of types 3 and 4.

Table 8.13 Statistical results concerning the frictional properties of helmets.

Method	Determination of μ	Type 1 (22)	Type 2 (20)	Type 3 (20)	Type 4 (22)
Oblique Impact Tests	Linear regression	0.531 ± 0.032	0.562 ± 0.039	0.436 ± 0.029	0.472 ± 0.033
	$\mu = F_T/F_N$ (5ms)	0.586 ± 0.036	0.579 ± 0.034	0.570 ± 0.042	0.521 ± 0.040
		Type 1 (6)	Type 2 (6)	Type 3 (5)	Type 4 (6)
Friction Tests	μ static	0.613 ± 0.022	0.623 ± 0.037	0.690 ± 0.020	0.647 ± 0.018
	μ at 0.25 m/s	0.586 ± 0.013	0.587 ± 0.040	0.670 ± 0.013	0.626 ± 0.010

The first two lines show average coefficients of friction (μ) which were determined from oblique impact test results. Average static coefficients of friction and average coefficients of friction at a sliding velocity of 0.25 m/s, measured by an alternative friction test method, are given in the second part of the table. The numbers given in brackets indicate the number of tests.

8.4.2.2. Alternative friction test

The measurement of tangential and normal contact forces provides information on the friction of a helmet shell under impact conditions. However, an oblique impact test is complex and not appropriate as a friction test method. The frictional properties of helmets were, therefore, investigated by means of an alternative test method. It was also important to determine if a simple mechanical friction test can reproduce the results of oblique impact tests (chapter 8.4.2.1). The principle of the alternative friction test is shown in figure 8.23.

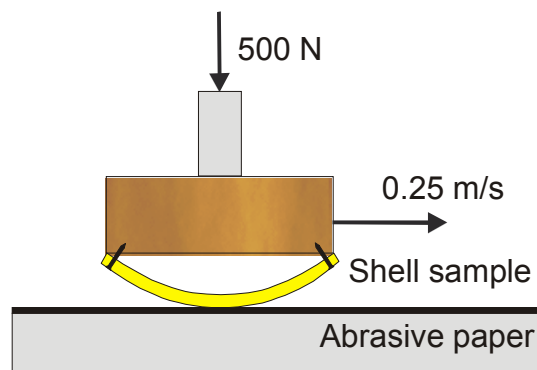


Figure 8.23. Principle of the alternative friction test. A sample cut from the helmet shell is horizontally displaced on abrasive paper while the force of friction is measured.

In contrast to the friction test method specified in ECE R 22-05, parts of the helmet shell are investigated instead of complete helmets. For each helmet type, samples 9 cm \times 14 cm were cut from the top and the rear of a helmet shell. Each sample was attached to a mounting block and tested on a friction test apparatus. A test consisted of three sliding

cycles, each displacing the sample about 20 cm on a horizontal plate covered with abrasive paper (grade 80 closed-coat aluminium oxide, according to BS 6658). The sliding velocity corresponded to a half sine function with a maximum of 0.25 m/s. Throughout a sliding motion the sample was loaded by a constant vertical force of 500 N. The resulting forces of sliding friction were measured by a force transducer. From the recorded force signal the static coefficient of friction (onset of sliding) as well as the coefficient of sliding friction at maximum speed, were determined. The results are summarised in Table 8.13.

Despite several essential differences in the two test methods, the friction coefficients measured at a sliding velocity of 0.25 m/s are comparable to the oblique impact test results for ABS shells (types 1 and 2). However, this did not occur with glassfibre helmets (types 3 and 4) which showed systematically greater coefficients of friction in the mechanical tests. Generally, the static coefficients of friction were higher than the dynamic coefficients of friction.

As in oblique impact tests, the friction test results depend on material and surface properties as well as deformation of the samples. Lower rigidity, greater compression and a greater contact area was observed for ABS shells than for glassfibre shells. The influence of parameters such as abrasion resistance on sliding friction could not be ascertained on the basis of the available data. Only two different shell materials were tested, therefore, further investigations should include a greater variety of materials.

Various physical parameters of the friction tests and oblique impact tests were quite different. For example, sliding velocities of 0-0.25 m/s compared with 6-12 m/s, mean normal forces of 500 N compared with 900-4200 N, contact areas of 7-11 cm² compared with 7-44 cm². Therefore, comparable results between the two methods cannot generally be expected. The frictional coefficients of plastics often decrease with increasing sliding velocities if values of 0.5-1.0 m/s are exceeded (Birley et al., 1991). The observation that the frictional coefficients measured at low sliding velocities tended to higher values than the oblique impact test results is consistent with the findings of Birley. Additionally, the ratios of the tangential to the normal force components, in oblique impact tests, decreased with increasing impact velocities between 6 m/s and 12 m/s.

Because greater frictional coefficients of helmet shells would imply higher rotational accelerations of the head, mechanical friction tests at low sliding velocities could be used to estimate the worst case of rotational acceleration in oblique impacts. Based on a tolerance level for rotational acceleration of the human head and, secondly, on a simple theoretical model, such as the impact of a rigid sphere as given by the equation in Chapter 8.4.2.1, it is likely that appropriate limits could be established for the coefficients of friction measured for helmet shells.

8.5. HELMET PHYSIOLOGY

8.5.1. Introduction

Physiological and ergonomic properties of helmets are very important factors for the safety of motorcyclists, Table 8.1. Heat, moisture and carbon dioxide produced within a helmet could reduce the ability of a motorcyclist to concentrate. In combination with inadequate physiological properties, for example poor helmet ventilation, factors such as the heat production of the head represent indirect injury risks (Rodahl et al., 1992). Apart from visor tests, tests relating to indirect injury risks and helmet physiology are not included in current helmet Standards. Consequently, motorcycle helmets with poor ventilation and insufficient heat dissipation that result in high humidity can be found on

the market. Discussions with different helmet manufacturers showed that the implementation of good ventilation properties is difficult and that an objective test method for the assessment of helmet ventilation would be of great interest.

At EMPA, a project on the physiological aspects of helmets began 1998. A first prototype of a heated and sweating headform was developed to simulate the essential physiological characteristics of a human head. A helmet is fitted to the headform and the helmeted headform is placed in a climatic chamber equipped with a wind tunnel in order to simulate a variety of riding conditions from typical to critical. The physiological performance of a helmet such as face or head ventilation can be evaluated in a test by measuring temperature and humidity with various sensors distributed over the headform.

The objectives of this study, which was part of the COST 327 extension, were:

- to gather information on the physiological and ergonomic properties of helmets
- to develop a concept of a future objective ventilation test for motorcycle helmets in order to optimise the physiological properties
- to perform the comparative tests of the ventilation properties of current helmets

The development of the first prototype of the sweating thermal headform is presented in section 8.5.2. The results of the first comparative ventilation tests of current helmets are given in section 8.5.5.

8.5.2. Development of a sweating thermal headform

A new sweating and heated headform was built at EMPA, adapting the technologies developed and used during several years for the testing of protective and physiological properties of clothing systems and complete garments, figure 8.24. The head is based on a shop window manikin made of polyester reinforced with glass fibre. The shape of the headform corresponds approximately to an average human male head of size 58. The headform is divided into three different areas: the skull, with zones defined by different colours in figure 8.24, the face, comprising also the forehead and the ears, and the neck. For helmet tests the neck has the function of a shield to avoid a thermal transition from the helmeted part of the head through conduction and is thus always kept at the same temperature as the face area. The heating system is divided into three independent heating circuits for the three head areas. Heating foils are stuck to the inside of the skull and neck zone and heating wiring to the inner side of the face. The temperature is measured by applying independent wiring covered with an epoxy resin layer onto the outer surface of each head area. This allows the measurement of a representative mean surface temperature at all three areas. A computerised control system is used to measure the surface temperature and to regulate the heating power continuously according to the selected values, in order to simulate the skin temperature of the human head under different strains.

In hot environments, the human thermal balance also depends on the evaporative heat loss from sweating. Therefore, it was decided to investigate the effect of sweating on thermal comfort. The sweating of the human head is simulated by 25 sweating nozzles distributed over the face (10) and the skull (15) of the manikin, see figure 8.24. The amount of sweat, distilled water, on the head surface is regulated by the control system through individual opening intervals of seven valves, each supplying a group of three or four nozzles. Each group can be activated separately, allowing a precise control of the water flow. The sweat rate can be changed from no sweat up to more than 70 g/h for the whole head,

corresponding to substantial sweating. The distilled water is supplied from a reservoir located approximately 1 m above the head through a tube to the valve unit, shown on the left in figure 8.24, and from there through 25 Teflon tubes to the sweating nozzles. The water reservoir is placed on a precision scale measuring the total amount of sweat supplied. For helmet testing, the headform is covered with a polyester stocking which distributes the sweat water from the 25 nozzles evenly over a larger area and allows a vaporised or liquid sweat rate to be produced.

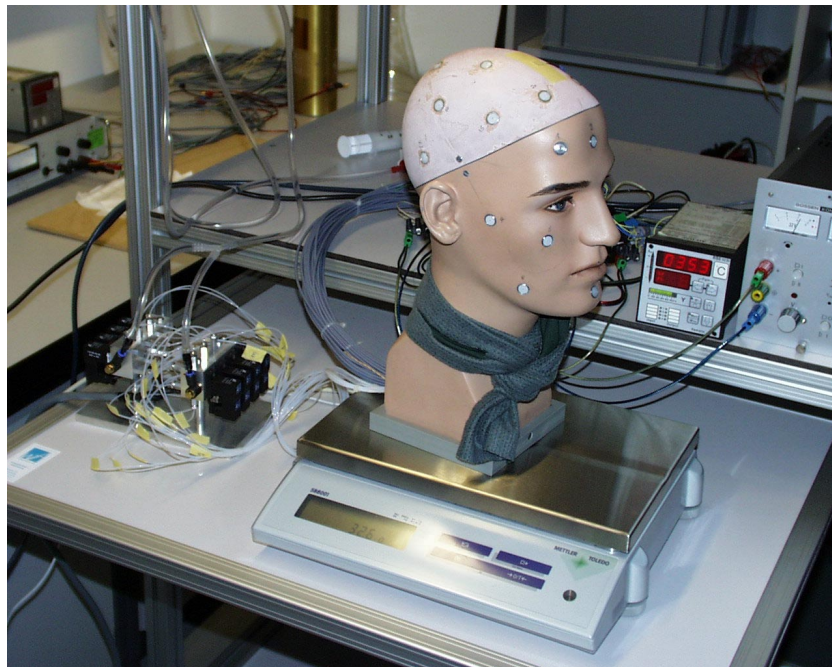


Figure 8.24. The novel sweating and heated headform.

The helmeted headform is placed on an additional precision scale in order to assess the amount of condensation inside the helmet. The headform can be operated at a constant surface, skin temperature, or it can be heated with a constant heating power, simulating metabolic heat. Skin temperature, heating power and sweat rate can be regulated by the PC-program from the control system to represent the behaviour of the human head. Different sweating and heating profiles can be selected.

The experiments are in a climatic chamber where typical ambient conditions can be simulated according to the required riding situation. Temperatures between sub zero and +35°C can be selected and ambient relative humidity ranges from 20% to 95%. The chamber is equipped with a wind tunnel providing an evenly distributed air flow and the velocity can be changed continuously between 0.3 m/s and 30 m/s. During the experiments the helmeted headform is placed in front of the wind tunnel with the helmet centred on the outlet of the air stream, figure 8.25.

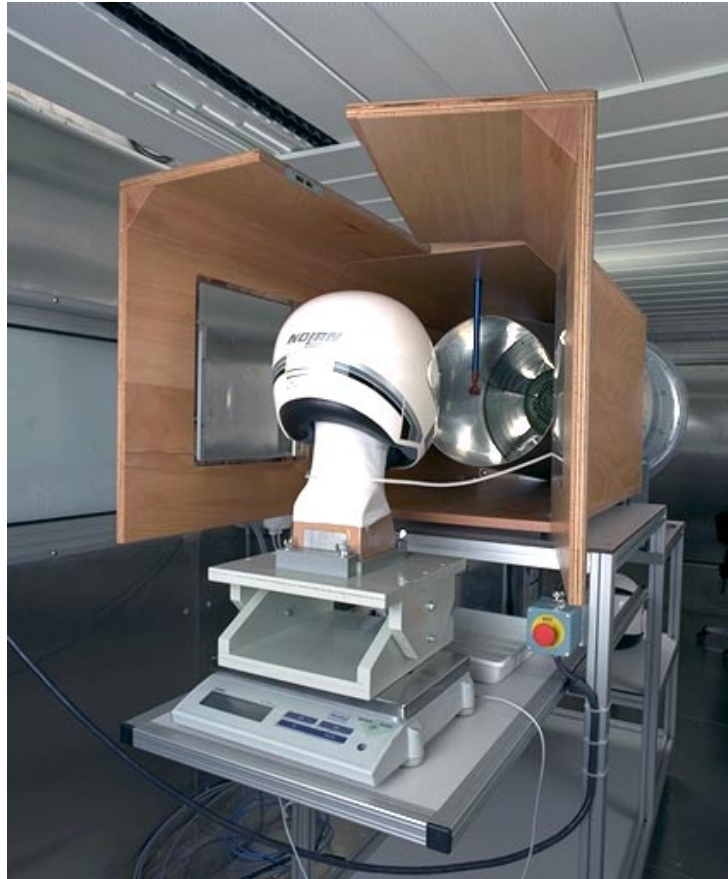


Figure 8.25. The experimental set-up in the climatic chamber with the wind tunnel.

8.5.3. Interpretation of the measured data

A human being is a homo isothermal organism and strives, therefore, to maintain the body core temperature at 37°C . When the body is in thermal equilibrium, only a relatively small amount of moisture, approximately 24 g/h over the body surface of 1.8 m^2 , is excreted from the sweat glands, *perspiratio insensibilis*. This moisture evaporates at the skin surface and is not felt as perspiration, subjectively. Only at higher body activities or temperatures or when the thermal insulation of the clothing worn is too high, is more sweat produced to cool the surface by evaporation and to prevent an increase of the body core temperature. However, the body can, during excessive temperature losses, considerably reduce the temperature of the extremities such as arms and legs to reduce the total emission of heat and to maintain the core temperature of the body. The head surface represents about 10% of the whole body, 1.8 m^2 . The emissivity can be very different for a range of individuals. Over the relatively large surface of the torso, for example, the body can obviously release larger amounts of sweat than at the extremities. Large quantities, approx. $1.5\text{ l/m}^2\text{h}$, of moisture can be released from the face, the largest release of sweat being found on the forehead. How much sweat is released from the part of the head covered with hair is not known precisely. Only sparse information on the distribution of sweat glands in the head area was found in the literature.

Blood can transport heat from one area of the human body to another and can be cooled by evaporation cooling, for example at the torso. The new headform is not heated by means of a fluid such as blood, but it is brought to a certain temperature by means of heated

wires. Usually, the head is brought to a surface temperature similar to the human skin temperature of 35 °C, while using an ordinary helmet. By changing only certain parameters such as opening or closing the ventilation openings of the helmet, small differences in the skin temperature have been observed. Even very small amounts of moisture, which evaporate from the skin, cause cooling of the head. One gram of sweating water is sufficient to withdraw 0.67 Watt hours of energy from the head.

The more efficient the ventilation of a helmet, the more energy will be withdrawn and the greater the temperature reduction of the face or skull for a given heating power. Polystyrene is used for efficient shock absorption, thus, thermal insulation is generally too great. For physiological reasons it is, therefore, very important to have good ventilation in the helmet which enables the heat to be dissipated from the head both by convection and by evaporation of sweat on the skin. The most critical situation is driving at a low speed, because the ventilation in the helmet is very low. At greater speeds, even helmets with a poor ventilation will probably have sufficient ventilation. All of these parameters can be investigated and quantified with the new headform. Furthermore, those types of ventilation systems that lead to a better sensation of comfort for the motorcyclists can be identified and, therefore, reduce the accident risk by improving the ability to concentrate.

8.5.4. Test procedure

The experimental set-up in the climatic chamber is shown in figure 8.25. For this first test series the following test conditions were defined:

- Climatic chamber temperature: 20 °C
- Climatic chamber humidity: 65%
- Constant surface temperature of the headform: 35 °C
- Constant heating power of the headform: face: 10 W; skull: 1.7 W; neck: 8 W
- Headform sweating rate: 6 g/h (low sweating rate)
- Wind speed: 10 m/s
- Duration of the tests: 15 h
- Measured data: Heating power (face, skull, neck)
Temperature (face, skull, neck)
Amount of sweat

The chosen climatic conditions were realistic values according to the results of the Accident Investigation Working Group in Chapter 3.8 and the wind speed represents an urban situation. Four different full-face helmet types (A, B, C, and D) were tested. Three of them were medium price helmets, whereas one was an expensive model.

The total duration of the test programme for each helmet was 15 h. The measurement for one helmet consisted of two phases which were repeated five times with different ventilation positions, as given in Table 8.14.

During the first phase, with a duration of 1 h, the headform was run, without sweat, at a constant surface temperature of 35 °C; the heating power automatically adapted to maintain this temperature. All ventilation openings, as well as the visor, were closed. This

was the acclimatisation phase, which allowed the headform to reach a steady state condition, and to be at an identical dry condition before the measuring phase began.

The second phase was the actual measuring phase with a duration of 2 h. The helmeted headform was at an initial surface temperature of 35 °C and was run at a constant low sweating rate. During this phase the headform was operated at a constant heating power which was selected to be slightly lower than the power required to maintain a temperature of 35 °C. This allowed measurement of the decrease in the surface temperature of the headform from the effect of the helmet ventilation openings and the evaporation of sweat.

After the first two phases, a third phase, identical to the first, was added to re-establish a steady state dry condition at 35 °C. The following measuring phase, phase 4, was identical to phase two but with an open chin ventilation, see Table 8.14. In the last phase, phase 10, the visor was in the first fixed position with an opening of about 1-2 cm depending on the helmet type. During all ten phases the wind tunnel provided a constant air flow of 10 m/s.

Table 8.14 Sweating headform test programme carried out for each helmet.

Phase (duration)	Sweating rate [g/h]	Fixed temperature (T) or power (P)	Ventilation position forehead	Ventilation position chin	Visor position
1 (1h)	0	T	Closed	closed	closed
2 (2h)	6	P	closed	closed	closed
3 (1h)	0	T	closed	closed	closed
4 (2h)	6	P	closed	open	closed
5 (1h)	0	T	closed	closed	closed
6 (2h)	6	P	open	closed	closed
7 (1h)	0	T	closed	closed	closed
8 (2h)	6	P	open	open	closed
9 (1h)	0	T	closed	closed	closed
10 (2h)	6	P	closed	closed	1. fixed open

8.5.5. Results and discussion

The temperature of the face and the skull of a ten-phase sequence is illustrated in figure 8.26. The odd phases are characterised by an identical final surface temperature of 35 °C for the face and the skull area. In the first phase, this temperature was reached quickly because the headform was dry, whereas in the other odd phases, accumulated sweat water needed time to evaporate and to obtain the initial temperature of 35 °C, which was selected for all phases. The temperature decrease recorded during a measuring phase was used as the criterion to assess the ventilation effect. It was a function of only the ventilation openings of the helmet when the other test parameters were identical. In order to compare different helmet models and different ventilation positions for the same helmet, it was important to use the same constant heating power in all measuring phases. The absolute temperatures observed in the experiments also depended on the construction of the helmet, the thickness of the liner, the comfort padding and the fit on the headform.

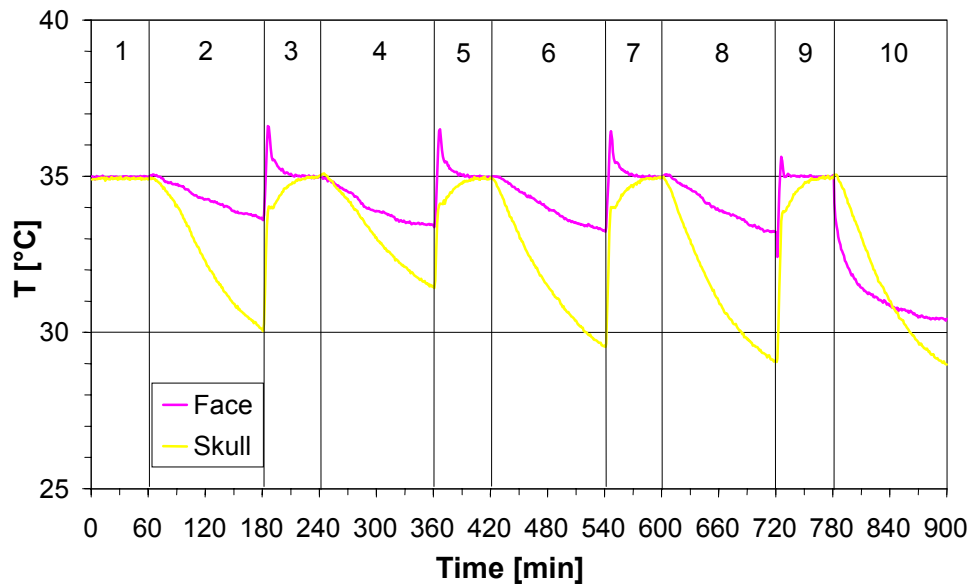


Figure 8.26. Time history of the face and the skull temperature for all ten phases (helmet D).

Figure 8.27 illustrates the importance of the sweat for a realistic simulation of the human skin temperature. In the acclimatisation phases, 1 and 3, the headform was run without sweat at a surface temperature of 35 °C. In the first measuring phase, 2, the headform was again run without sweat and with a constant heating power, whereas, in the second measuring phase 4, sweat water was supplied at a constant rate of 6 g/h. Even such a low sweat rate had a large effect on the surface temperature of the face and the skull area. Therefore, sweating must be simulated if the physiological properties of a human head are to be reproduced realistically.

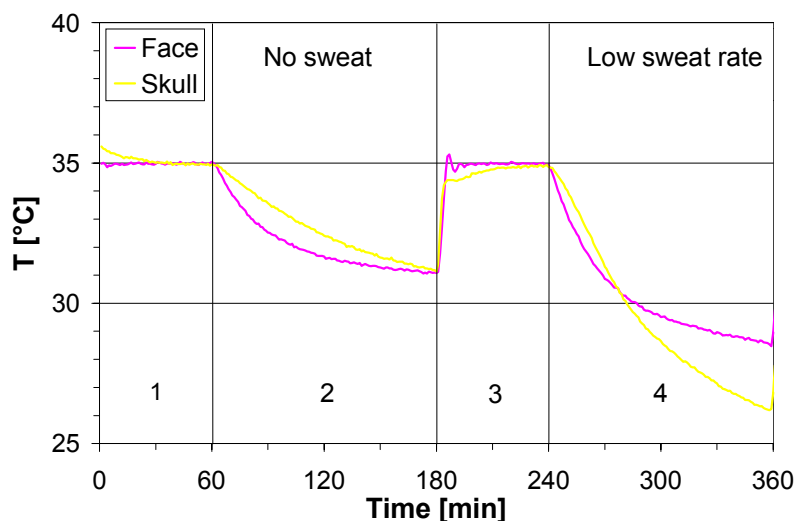


Figure 8.27. Time history of the face and the skull temperature with and without sweating.

The effect of the different ventilation openings for the same helmet and for all helmet types can be compared in figures 8.28 and 8.29. For this purpose, the second halves of the acclimatisation phases and the measuring phases are plotted on the same time scale for the face area, figure 8.28, and the skull area, figure 8.29. In the case of helmet C, a slight temperature increase was observed in the measuring phase for both head areas, whereas the other helmets showed a temperature decrease, as expected. The increase was caused by the greater thermal insulation of helmet C. The selection of a lower heating power would also have led to a temperature decrease for this helmet.

For all helmets, the greatest temperature decrease at the face area was found with the visor opened in the first fixed position, figure 8.28. When all the ventilation openings were closed, the temperature reductions were between 1°C and 4°C less. The ventilation openings of helmet A were not very efficient. The chin opening resulted in a maximum cooling of about 0.5°C. Helmet B provided better ventilation of the face. Simultaneously opening the forehead and the chin ventilation reduced the temperature by about 0.8°C at the end of the measuring period.

Helmet C was also equipped with poor ventilation, for example a slight increase in the face temperature was observed when the chin vent was opened. The reason for this behaviour is not yet clear, and additional measurements are necessary to investigate this effect in more detail. Helmet D showed relatively small temperature reductions of less than 0.5°C for the different openings. In general, although there were differences between the helmets investigated, the experiments with the wind speed of 10 m/s showed that the temperature in the face area was not substantially less when the chin vents were open than when they were closed. Opening of the visor to the first fixed position was found to be the most efficient way to achieve a temperature reduction in the face area.

In the skull area of the head, the effect of the different helmet openings was more complex, figure 8.29. The ventilation openings of helmet A were not very efficient in this area with almost no difference in temperature noted between the closed position and open positions after a two hour measuring phase. Helmets B and D were similar and for both helmets opening the chin vent led to an increase in the skull temperature. A tentative explanation could be that the opening of the chin ventilation changes the air pressure distribution around the helmet such that the Venturi effect, which extracts part of the warm air from inside the skull area of the helmet, is diminished.

Temperature measurements in the skull area were not available for helmets A and B with the visor opened in the first fixed position. Helmet C showed the largest ventilation effect at the skull area. The forehead opening, as well as the simultaneous opening of the forehead and the chin ventilation, reduced the skull temperature by more than 2°C. As expected, the chin ventilation did not cool the skull area very efficiently. For helmet D, the forehead opening reduced the skull temperature by about 0.5°C and the simultaneous opening of the forehead and chin ventilation led to a reduction of 1°C. In contrast to helmet C, opening the visor to the first position did not influence the skull temperature substantially for helmet D.

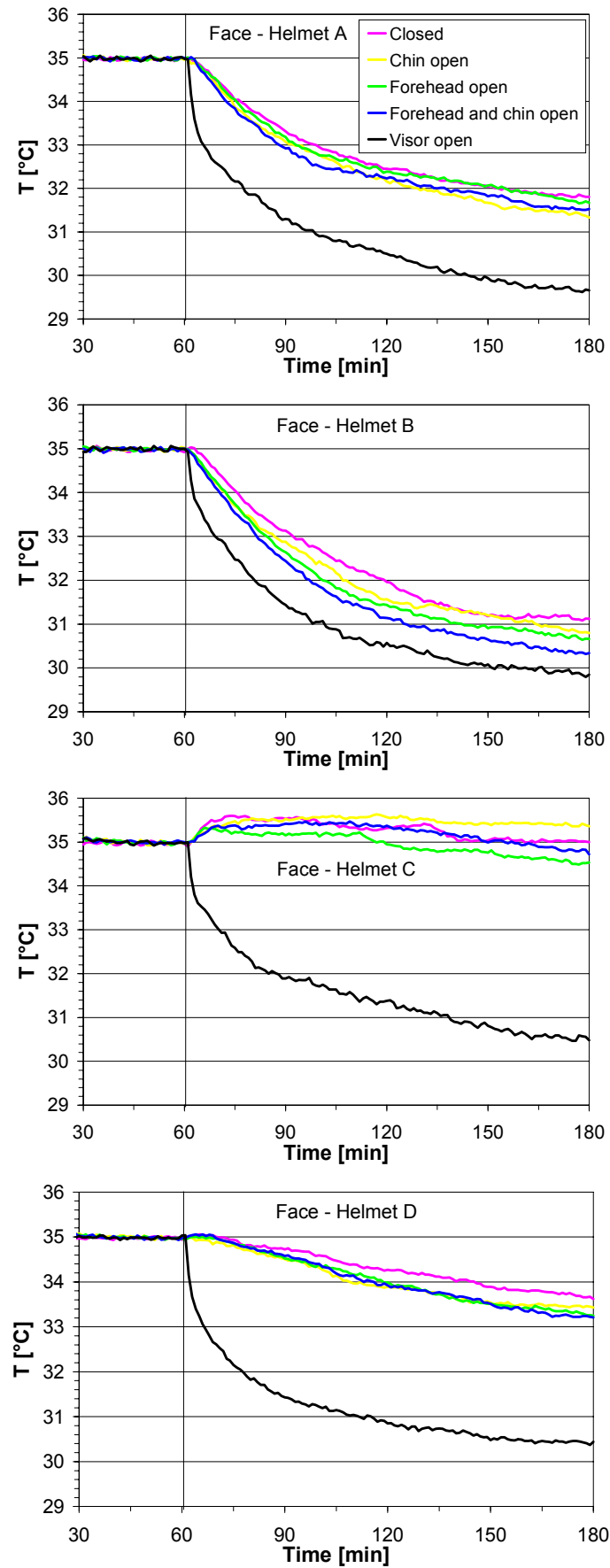


Figure 8.28. Face temperature for different ventilation openings and four helmet types.

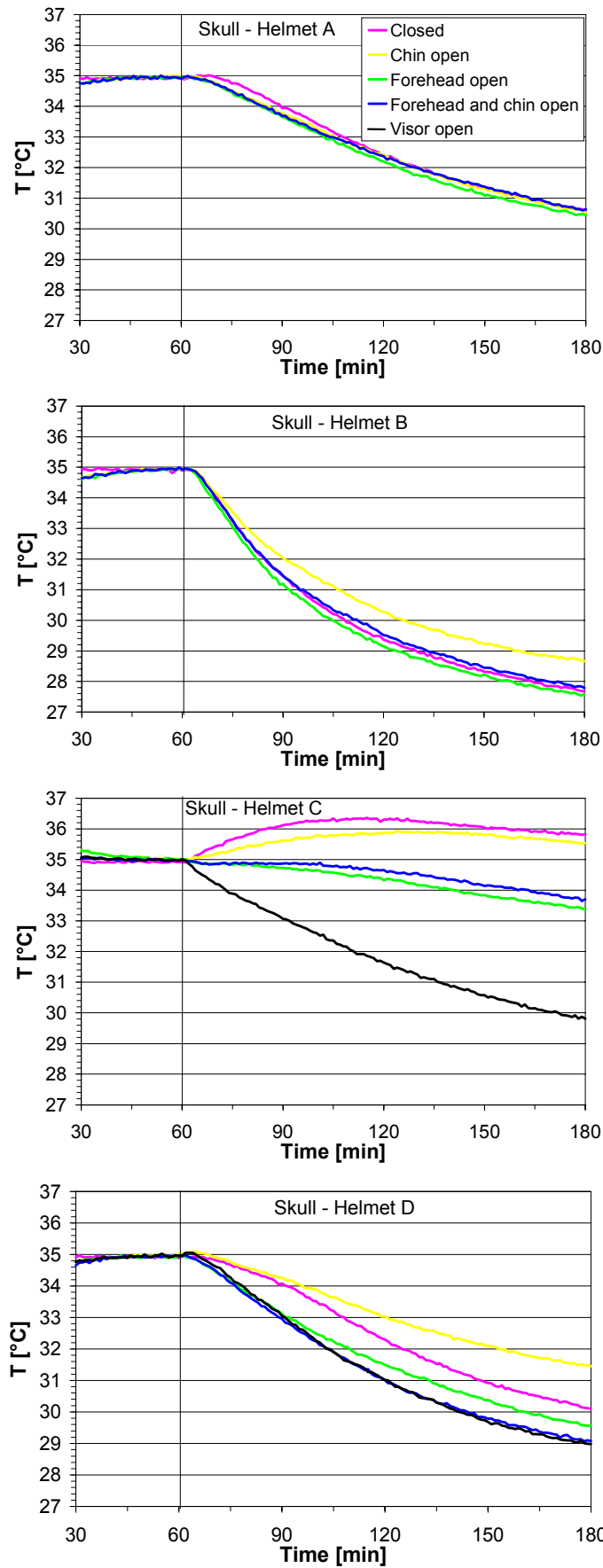


Figure 8.29. Skull temperature for different ventilation openings and four helmet types.

The helmet ventilation test series using the new sweating and heated headform prototype shows that there are large differences in the effectiveness of the ventilation systems of different helmet types as well as for the same helmet between the different openings. Most of the ventilation openings are not able to reduce the air temperature in the face area inside the helmet substantially at a wind speed of 10 m/s. Only the visor opened in the first fixed position leads to a significant temperature reduction. For the skull area the situation is similar, except for one case with relatively efficient forehead ventilation opening. The opening of the visor does not affect the skull temperature as much as the face area temperature. Generally, helmet ventilation systems need substantial improvement. The above experiments demonstrate the need for an objective test method to assess the physiological properties of helmets and, in particular, to quantify the efficiency of ventilation systems.

The novel sweating thermal headform is the first available objective test method to assess the physiological and ergonomic properties of motorcycle helmets. Of critical importance is the provision of the sweating capability, which allows the physiological conditions of a human head within a helmet to be investigated very realistically. The headform is an interesting new approach, which should be validated, in further test series. Additional helmet models should be investigated in order to determine the most appropriate heating power values for comparison of a wide range of helmets.

The temperatures measured on the sweating thermal headform with the vents set to the open and closed positions may possibly provide the physiological criteria for future helmet Standards. Further research is necessary to develop the appropriate test specifications such as external temperature, humidity and wind speed, as well as sweating rate and heating power for the different head areas.

8.6. MOTORCYCLE AERODYNAMIC NOISE

Motorcycle helmets are not currently required to actively protect the rider from aural damage, despite the fact that research has shown that noise levels while motorcycling are sufficient to cause hearing damage. It is low-frequency aerodynamic noise, generally centred around 500Hz, created by the turbulent airflow over the rider's helmet that has been shown to be the major contributory factor to these hearing problems. Previous research has demonstrated that both short-term and long-term hearing damage can occur as a result of exposure to aerodynamic noise, because at speeds greater than 40mile/h (64km/h) approximately 90dB(A) of low-frequency wind noise is produced at the rider's ear, with this level rising to around 120dB(A) at 100mile/h (160km/h).

At 55mile/h (88km/h) a motorcyclist experiences approximately 96dB(A) of aerodynamic noise and an exposure of more than two hours would exceed the second action level of the Health and Safety at Work Act, Great Britain (GB) where the wearing of hearing protection equipment becomes compulsory¹. Therefore, noise attenuation, especially at low frequencies is an area of helmet design that has the potential for considerable improvement and would confer substantial benefits to motorcycle riders.

¹ Health and Safety at Work Act 1974 gives effect in Great Britain to provisions of Council Directive 86/118/EEC (OJ No. L137, 24.5.86, p28) on the protection of workers from risks related to exposure to noise at work.

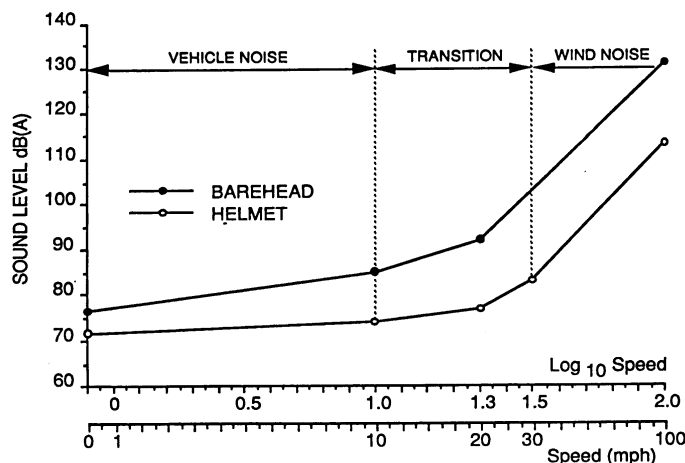


Figure 8.30. Aerodynamic noise generated at different motorcycle speeds

Exposure to this excessive low-frequency noise has the potential to cause hearing damage. Figure 8.30 shows that the levels of helmet noise rise to decibel values which, depending on the exposure time and the frequency of exposure, are capable of causing hearing damage at relatively low speeds.

Although the aerodynamic profile of the helmet has an effect on the level of wind noise generated, it has been demonstrated that the motorcycle design is also a major contributor to the noise levels experienced by the rider (Lower *et al* 1996). However, measures to limit the effect of the motorcycle design on helmet noise can be made by improving the fit of the helmet around the riders neck and by improving the visor fit relative to the helmet shell. Such simple modifications as these may reduce the sound pressure level at the rider's ear by between 5-8dB(A) (Lower *et al* 1996).

The overall problem of helmet noise is difficult to fully assess without testing the aerodynamic compatibility of motorcycle, helmet and rider. However, a test for the helmet has been proposed, since the design of the motorcycle, although strongly related to the generation of helmet noise, must be assessed separately. Similarly, the size of the rider, especially height, may have an effect on the level of aerodynamic noise experienced and a repeatable and objective method must be developed which is not influenced by such variables.

Exposure to excessive noise levels can cause temporary or permanent deterioration of the hearing thresholds. McCombe (1992) compared audiograms from riders recently exposed to high-speed motorcycling and those unexposed. The results showed a mean deterioration in hearing sensitivity of approximately 12dB(A) due to the effects of temporary threshold shift. Most of the deterioration occurred in the frequency range between 1kHz and 2kHz, therefore implicating the cause as wind noise with a frequency centred around 500Hz. Repeated exposure to noise levels sufficient to cause temporary threshold shift may lead to permanent threshold shift. McCombe and Binnington (1994) found that 45% of motorcycle Grand Prix riders had hearing losses greater than expected for age-matched controls. In addition, the degree of hearing damage was shown to exhibit a statistically significant increase with racing experience. Therefore, motorcyclists who are exposed to high noise levels, are at a greater risk of hearing damage.

Modern helmet designs are very similar in terms of their design and the shell and liner materials, since they are designed for protection and must meet the impact requirements of the relevant helmet standards. Consequently, McCombe *et al* (1994) stated that in general there are no "real world" differences between currently available motorcycle helmets with regard to noise levels. Lower *et al* (1996) stated that differences of between 7 and 10 dB(A) were measured using different helmets at the same air speed on the same motorcycle.

A helmet provides an improvement of 18-20dB(A) above wearing no helmet at all, because the helmet lifts the turbulent boundary layer 3-4cm away from the ear and reduces the degree of turbulence as a result of the smooth outer shell of the helmet. Binnington *et al* (1993). Tangorra and George (1991) showed that subtle alteration to a helmet's aerodynamics can significantly reduce the noise levels at the rider's ear. Particularly important features are the fit of the visor to the helmet and the protuberance of any other components of the helmet that break the aerodynamic profile of the helmet shell. This causes turbulence which creates aerodynamic noise.

McCombe *et al* (1992) found that earplugs provide some sound attenuation at lower frequencies, although a reduction in performance was noted at around 500Hz, probably as a result of resonance transferred from the helmet. However, past research has discovered that riders may be unenthusiastic about earplugs or improved ear padding because of fears that environmental and warning signals may be inaudible (McKnight and McKnight, 1994). Binnington *et al* (1993) found that a helmet improved signal detection of four common warning signals. At speeds below 35-40mile/h (56-64km/h) the detection of these signals was best without earplugs. However, at speeds greater than 40mile/h (64km/h), signal detection was improved with earplugs. The authors suggested that for higher speed journeys, where the risk of hearing damage is greater, wearing earplugs for the purpose of limiting aural damage would also improve the detection of warning signals. These results confirmed previous work in an industrial environment which found that signal and speech determination actually improved with increasing background noise (Wilkins and Martin, 1982).

8.6.1. Recommended test methods for measuring helmet noise

The problems associated with helmet designs and the effect on rider hearing have been outlined in the previous sections. It is recommended that any future helmet Standard include a test for the helmet's sound attenuation capabilities. There are two main areas that must be tested to ensure that aural damage is minimised. These are the aerodynamic design of the helmet and the degree to which the helmet attenuates the noise over a range of frequencies.

Two tests are proposed which will allow the noise qualities of different types of motorcycle helmet to be compared. Neither of these tests assesses the effect of the motorcycle on helmet noise. Although it is recognised that the motorcycle design can be an important factor in the generation of aerodynamic noise, it is considered that this is best assessed separately in relation to motorcycle design.

Two methods are necessary and are recommended. Test A aims to identify the noise dose at the rider's ear, whereas test B provides a more detailed breakdown of the sound attenuation capabilities of the helmet over a range of frequencies. The latter test, therefore, enables the performance of the helmet to be assessed over the important frequency ranges and ensures that concerns regarding hazard detection can be addressed.

8.6.1.1. Test A - Summary

Assessment of the 'equivalent continuous noise level' over a period of [5] minutes ($L_{Aeq,[5] \text{ minutes}}$) for a range of airflow speeds. The test limits have yet to be defined, but would be expressed as a maximum for each airflow speed. It is suggested that at 70 mile/h (112km/h) the maximum be set at a $L_{Aeq,[5] \text{ minutes}}$ of 90 dB(A).

8.6.1.1.1. Equipment requirements

The following equipment are necessary:

- A suitable sub-sonic wind tunnel, capable of airflow velocities up to 100 mile/h (160km/h), in which a helmeted headform may be positioned far enough away from the sides to avoid interference.
- A suitable dummy headform, either modified such that it has a representative human ear structure or an appropriate proprietary dummy supplied with the necessary microphone equipment within the ear.
- An appropriate miniature microphone (IEC 651 type 0 or 1)
- Appropriate analysis equipment of equivalent certified accuracy as that of the microphone capable of recording L_{Aeq} dB(A) and peak dB.

8.6.1.1.2. Test procedure

The miniature microphone shall be secured within the 'ear' of the headform and the helmeted headform placed inside the sub-sonic wind tunnel in a position such that the airflow around the helmet is unaffected by any structure other than the helmet under test.

The dB(A) over a period of [5] minutes and the peak dB level shall be recorded at every airflow velocity from 40 mile/h (64km/h) to 100 mile/h (160km/h), with airflow speed increasing in 10mile/h (16km/h) increments.

8.6.1.1.3. Test criteria and limits

The criteria of the test are $L_{Aeq,[5] \text{ minutes}}$ and peak dB (not A-weighted). The latter value is not A-weighted in order to allow compatibility with the GB Noise at Work Regulations of 1989.

The limits of these values is more difficult to define and require further research and testing before any figures are set. However, sensible limits based on what might be achievable and also to comply with the GB Noise at Work Regulations (1989), might be that $L_{Aeq,[5] \text{ minutes}}$ does not exceed 90dB(A) at 70mile/h (112km/h) and that at no speed must the peak dB level exceed 140dB.

The GB Noise at Work Regulations (1989) specify a first action level at an $L_{Aeq,8}$ of 85dB(A) for the entire working day and a second action level of 90dB(A). Since the exposure of a motorcyclist to noise is likely to be less than an average working day, it seems sensible to set the noise level for the maximum permissible speed limit (70mile/h, 112km/h) at the second action level of 90dB(A) level. In addition, the draft code of practice for noise exposure at discotheques (Noise Advisory Council, 1986) stated that the maximum permissible noise exposure level should be a $L_{Aeq,[5] \text{ minutes}}$ of 100dB (A) within an area directly adjacent to the speakers. Helmets for motorsport however require separate limits to be set since at high speeds even 100dB(A) will be exceeded. However, it is unlikely that the noise level may be retained below a fully 'safe' threshold even with the

use of technologies such as Active Noise Reduction (ANR). Therefore, a limit based on what may be achieved by current helmets would encourage manufacturers to design helmets with noise qualities in mind. Equivalent continuous noise levels ($L_{Aeq, [5]minutes}$) limits for speeds of 40 mile/h (64km/h), 50 mile/h (80km/h), 60 mile/h (96km/h), 70 mile/h (112km/h), 80 mile/h (128km/h), 90 mile/h (144km/h) and 100 mile/h (160km/h) should be defined so that a helmet would protect the rider sufficiently at a range of speeds. It is suggested that a ranking system be used to compare helmet performance. This would provide a simple and clear indication of the noise-reducing qualities of the helmet.

8.6.1.2. Test B - Summary

This test is an assessment of noise attenuation by sound frequency. This would enable determination of an audiogram for the entire frequency spectrum. The test criteria would be expressed in dB(A) and the attenuation limits are yet to be defined and would vary depending on the sound frequency.

8.6.1.2.1. Equipment requirements

The following equipment are necessary in order that this test may be performed.

- A suitable anechoic chamber conforming to BS 6655
- A suitable dummy headform, either one modified such that it has a representative human ear structure or an appropriate proprietary dummy which is supplied with the necessary microphone equipment within the ear
- An appropriate miniature microphone (IEC 651 type 0 or 1)
- Appropriate analysis equipment of equivalent certified accuracy as that of the microphone capable of recording dB(A).
- An appropriate speaker system capable of emitting pure tones of a specified frequency

8.6.1.2.2. Test procedure

The miniature microphone shall be secured within the 'ear' of the headform and the helmeted headform placed inside the anechoic chamber.

A series of pure tones between 100Hz and 6,000Hz shall be emitted from the speaker positioned exactly 1 metre from and at right-angles to, the in-ear microphone. The sound level dB(A) shall be recorded with and without the test helmet fitted and an audiogram determined to assess the noise attenuation qualities of the helmet over the entire frequency spectrum.

8.6.1.2.3. Test criteria and limits

The criteria of the test are proposed to be dB(A). The attenuation requirements are difficult to define. However tests with ANR fitted to a motorcycle helmet reliably achieved noise reductions of 3-8dB(A) and up to 11dB(A) under optimum conditions. Furthermore, past testing involving ANR fitted into flying helmets have resulted in reductions of up to 14dB(A), indicating that such reductions for motorcycle helmets are feasible. Even without ANR technology, improvements in visor fit, shell aerodynamics, ear padding, and the fit of the helmet at the neck have the potential to deliver significant noise reductions in the range 5-8dB(A). It is important that an optimum attenuation audiogram is identified so that the limits for noise attenuation over the frequency range influenced by aerodynamic noise can be identified without affecting safety by impairing hazard detection. Once this

has been determined, appropriate attenuation limits for each frequency range may be proposed.

However, limits such that attenuation of at least [6]dB(A) are achieved are suggested, since such a reduction in the range 500-1,000Hz would have the effect of reducing the sound pressure level reaching the ear by 75%.

8.7. CONCLUSIONS

1. A Hybrid II headform was drop tested onto an oblique abrasive anvil at impact velocities of 6.0 m/s, 7.5 m/s, 8.5 m/s, 10.0 m/s and 12.0 m/s, using four different helmet types (84 tests). The mean values of peak rotational acceleration varied between about 2500 rad/s² and 8500 rad/s² and the rotational velocity varied between about 20 rad/s and 41 rad/s. The mean peak tangential force varied from about 800 N to about 2500 N and the anvil tangential impulse varied between about 9 Ns and 20 Ns.

2. It was found that the linear correlation between peak rotational acceleration and peak tangential force was significant ($r = 0.97$), and similarly between peak rotational velocity and anvil tangential impulse ($r = 0.95$). A significant linear correlation ($r = 0.91$) between peak linear and rotational acceleration was also measured.

3. Most of the linear and rotational acceleration values measured in the oblique impact tests gave values for GAMBIT of less than 1 ($G < 1$) and were thus not critical for head injury. Nevertheless, impact velocities of 12 m/s gave values greater than 1 ($G > 1$) where the onset of brain injury is likely.

4. A detailed statistical analysis of the four helmet types (two thermoplastic and two glass fibre types) and different impact velocities showed that thermoplastic helmets induce values of rotational acceleration greater than those with a glass fibre shell. Mean values of peak rotational acceleration of both thermoplastic helmet types were between 17% and 26% greater than the corresponding values of both glass fibre helmet types. Thermoplastic helmets with a soft liner, 40 g/l, gave lower rotational acceleration values (average difference 9.4 %) and lower tangential forces (average difference 12.1 %) than identical helmets with a hard liner, 55 g/l. Linear acceleration values were on average 13.6% greater for the hard liner.

5. Different shell stiffness (ECE 22-04 type compared with SNELL 95 type) and different helmet mass (mean mass difference of 245 g) had little effect on the recorded peak rotational acceleration of otherwise similar glass fibre helmets.

6. The oblique impact drop test using a Hybrid II headform fitted with a nine accelerometer array is a suitable method to investigate rotational acceleration and to determine the performance of different helmet types. Reduction of rotational acceleration through factors such as shell material, liner density and helmet shape is identified by this method.

7. A helmeted Hybrid III dummy was drop tested in 31 tests, onto a flat anvil at three different impact velocities (4.4 m/s, 5.2 m/s and 6.0 m/s) at the helmet impact points and body impact angles R/0°, B/30° and P/90°. Mean peak linear accelerations measured were between about 85g and 165g, and rotational accelerations between about 2900 rad/s² and 5300 rad/s², depending on the impact velocity and the helmet impact point. Mean peak force normal to the anvil varied between about 6500 N and 15600 N. It should be noted that test repeatability was very good.

8. The helmeted Hybrid III dummy was also drop tested in 18 tests, onto an oblique abrasive anvil at 4.4 m/s, 5.2 m/s and 6 m/s. The mean peak rotational accelerations were low and varied between about 1900 rad/s² and 3100 rad/s². The mean peak linear acceleration values ranged from about 27g to 41g and the mean peak tangential forces varied between about 700 N and 1100 N depending on the impact velocity.

9. Results from the headform tests and dummy tests were compared. It was found that although the results for a given set of conditions were similar, in general the headform test needed to be at a slightly greater velocity to give the same results. More specifically, dummy impacts at 5.2 m/s corresponded, approximately, to headform impacts at 6 m/s. Dummy measurements at 6 m/s gave results that were between headform measurements at 6 m/s and at 7.5 m/s. The linear relationship between peak rotational acceleration and peak tangential force in the dummy tests was significant ($r = 0.90$) and was very similar to that obtained in detached headform tests (0.97). The differences between dummy and headform tests could be attributed to the inertial effects of the body mass acting on the head through the neck.

10. It was concluded from the above tests that a good replacement for dummy tests onto the oblique abrasive anvil is headform drop tests at a slightly greater velocity. However, this does not imply that the dummy tests accurately replicate a human rider in an accident. It is known that the Hybrid III standard neck is stiffer than a human neck, so that it is not clear how accurately the Hybrid III dummy drop tests replicate a rider in a motorcycle accident. Future experiments should be carried out with an improved neck model, in order to simulate the impact of a head more realistically.

11. Peak linear acceleration values for dummy tests onto a flat anvil were lower than the equivalent headform tests at the same velocity and impact point. This was attributed to the headform having a greater effective mass when attached to the dummy. The greatest effective mass occurred in P/90°-impacts, whereas R/0°-impacts showed only a small increase. The effect of the dummy body and the neck is thus a decrease of the measured linear acceleration values when compared with headform measurements.

12. To test for helmet retention, a novel headform was fitted with a transducer to measure the resultant force to the chin in one direction. Tests showed that the roll-off angle depended upon the pre-load exerted to the chin via the retention system. Thus, in part, the outcome of a test can be controlled by the force to which a chin-strap is tightened. It is recommended that the initial load should be specified in a future test procedure for chin-strap effectiveness. It is also recommended that two load cells should be added to the test device so that the direction of the chin force may be studied in detail.

13. The frictional properties of helmet shells were investigated by means of a simple mechanical friction test. Small shell samples were abraded at sliding velocities between 0 and 0.25 m/s on a plate which was covered with the same abrasive paper as used in oblique impact tests. For thermoplastic shells, the measured coefficients of friction were comparable to those calculated from the impact forces exerted to the oblique abrasive anvil. Significant differences were found for glass fibre shells. It was concluded that the frictional behaviour of helmet shells, either observed in a friction test or in an oblique impact test, depends on material and surface properties as well as deformation of the samples. Two different shell materials were tested, further investigations should include a greater variety of materials.

14. A novel sweating thermal headform prototype was developed to assess the physiological and ergonomic properties of motorcycle helmets, including the simulation of

sweat. A comparative helmet ventilation test series showed that there are large differences in the effectiveness of the ventilation openings of different helmet types and also for the same helmet between the different openings. Generally, helmet ventilation systems need substantial improvement. The experiments have demonstrated the need for an objective test method to assess the physiological properties of helmets and, in particular, to quantify the efficiency of ventilation systems.

15. The temperatures measured on the sweating thermal headform with the vents set to the open and closed positions may provide the physiological criteria for future helmet Standards.

16. Aerodynamic noise is caused by the turbulent airflow around the motorcyclist's helmet and reaches sound pressure levels corresponding to around 90dB(A) at 40mile/h (64km/h), rising to around 120dB(A) at 100mile/h (160km/h). Noise levels in this range are capable of causing hearing damage, although the risk of damage is dependent on the exposure time. At 55 mile/h(88km/h), 2 hours is equivalent to the second action level of the GB Health and Safety at Work Act (1989) at which point hearing protection becomes compulsory. Two separate tests have been proposed, one which assesses the aerodynamic noise at the rider's ear and one which assesses the attenuation qualities of the helmet over the entire frequency spectrum.

CHAPTER 9. CONCLUSIONS

1. The COST 327 Action has provided the first European database compiled from a detailed study of motorcycle accidents. Cases were drawn from Glasgow UK, Hannover and Munich, Germany and Helsinki and Lapland, Finland. From the national statistics of these countries, it was found that overall only 20% of riders admitted to hospital suffered a head injury. This indicated that current helmets offer good protection. However, 16% overall sustained a head injury of AIS 2-4 and this indicated that improvements to helmets would offer a worthwhile saving in injuries.

2. Location of helmet damage was distributed evenly with 26.9% lateral right, 26.3% lateral left, 23.6% frontal and 21.0% to the rear. Other locations frequently damaged were the forehead 16.1% and the chinguard, 15.4%. Impacts to the crown at 2.2% were less frequent.

3. It was found that head injury severity increased with head impact speed quite remarkably. The median was 18km/h for AIS 1, 50km/h for AIS 2-4 and 57km/h for AIS 5/6. Thus, it was estimated that an increase in helmet energy absorbing characteristics of some 30% would reduce 50% of the AIS 5/6 casualties to AIS 2-4. Further analysis showed that 20% of AIS 5-6 casualties could be reduced to AIS 2-4 if the energy absorbed by the helmet could be increased by some 24%.

4. Of particular interest is the median speed at which brain injury occurred, which may be assumed to be indicative of the sensitivity of the brain to a given impact severity at different locations. The median speed for concussion (considered separately to other brain injury types) at 43km/h was lower than that for brain injury, 60km/h. Injury to the brain was not particularly sensitive to the impact location as shown by the median speed. This was just below 60km/h for the rear, upper and lateral regions and just above 60km/h for the chinguard and forehead.

5. Neck fractures were found to occur primarily with impacts to the face whilst bending moments from low severity head impacts tended to be the main cause of neck strain, AIS 1. Eighty percent of AIS 1 neck injuries occurred at speeds of up to 60km/h and 80% of injuries AIS 2 or greater occurred at speeds above 45km. Severe neck injuries, AIS 4 and greater, were always associated with severe head injuries. Analysis showed that there was a 30% probability of an AIS4 or greater neck injury for head injuries of AIS 5/6.

6. The effect of climatic conditions on accident risk was investigated as part of the extension to COST 327. Trends were difficult to identify because this was a retrospective study and only regional climatic data was available and not for the location of each accident. However, of the 111 accidents investigated climatic conditions were estimated to have been the prime cause of 10 accidents, 9%. Of these, 6 (5%) occurred when the temperature was low, less than 10°C, and at high humidity, greater than 80%. Thus, the tentative link between high humidity at low temperature and accident risk should be further investigated.

7. Different headforms, wooden, metal, Hybrid II and III and Bimass were evaluated for use in impact tests to assess the safety performance of helmets. The headforms could be selected according to three main criteria:

- the anthropometric characteristics
- a capability to predict injuries
- repeatability of the test results.

8. The Bimass, as developed in a Hybrid III headform, allows the risk of injuries related to the relative motion between the brain and skull to be predicted. This is a substantial and important improvement over a conventional headform

9. The conclusion of the Headforms Working Group was that the dummy headform gave the best repeatability, the Bimass gave the most realistic injury prediction and the rigid headforms are available in a suitable range of sizes. Thus, helmets of the appropriate size should be tested using a Bimass dummy headform and a rigid headform should be used to evaluate other sizes.

10. A computer model of a Hybrid III dummy rider and Norton Commander motorcycle and a Ford Mondeo moving car has been developed in MADYMO and successfully validated. Much care was taken to ensure that the characteristics of the components of the dummy, the motorcycle and the car were accurately determined. This necessitated, for example, crush testing the wheels and forks of the motorcycle and the metal panels and sill of the car. Also examined were the suspension characteristics of the vehicles and the physical properties. The dummy and helmet material characteristics were similarly determined.

11. The above model has been successfully used to simulate motorcycle accidents of the type similar to the configuration of the full-scale impact test, 50km/h at 90° into the side of a stationary car, against which the model was validated. For example, in an accident where a motorcycle collided with the rear of a stationary van at 20km/h the rider sustained only minor leg abrasions from contact with the road. The peak linear acceleration predicted by the simulation, 70g, was similar to the 107g measured in the helmet damage replication tests. The rotational acceleration 8000 rad/s/s for the simulation was greater than the 5026 rad/s/s measured in the helmet damage replication tests, but of the same order of magnitude.

12. Helmet damage seen in accident helmets was replicated in drop tests and the accelerations, rotational and linear, and external forces were measured. These measurements were compared with the injury severity, expressed as AIS, to establish "state of the art" information on human tolerance criteria. Twenty cases were investigated.

13. The replication tests have identified values of measured parameters that are likely to cause injury. In particular, the work suggested that a limit of rotational acceleration of 5,000rad/s/s may be useful as a basis for Standards requirements, together with a limit for rotational velocity of 40rad/s. HIC was less well defined but the research showed that injuries up to AIS5 occurred at a HIC of 1000 or less. Similarly, injuries up to and including AIS5 occurred at a peak linear acceleration of 250g or less.

14. This research by the Reconstruction Working Group has produced a substantial amount of data and information relating to the tolerance of the human head that has previously not been available. This data has been used by the Computer Simulation Working Group and, in turn, the Head and Neck Tolerance Working Group to provide state of the art data on the tolerance of the human brain to injury.

15. A finite element model of a human skull and brain has been developed in RADIOSS by Strasbourg University. The skull model was meshed using data obtained by digitising, in detail, the inner and outer profiles of a human skull. The model is unique in the extent to which the various parts of the head and brain are defined. Of particular note is the representation of the subarachnoid space between the brain and skull with brick elements which, in this model, were used to simulate the cerebral-spinal fluid.

16. The head model has been successfully calibrated against the well known Nahum cadaver data and was shown to give accurate predictions at all the five sites within the brain as examined by Nahum. Impact force, pressure at the impact site and opposite to it and the distribution of von Mises stresses were simulated sufficiently accurately to give confidence that the model may be used, as intended, for the investigation of head injury mechanisms over a wide range of input parameters.

17. The helmet model was developed by meshing from three dimensional data, supplied by TRL, of the outer profile of a typical UK helmet. The model was calibrated against data from impact tests of the helmet on a headform, supplied by TRL and Strasbourg University.

18. A FE mesh of the motorcycle helmet was added to the model, which was then used to simulate 13 motorcycle accidents selected from the COST 327 Action database. The damage to the accident helmets had been replicated by drop tests at TRL during which rotational and linear acceleration and external forces were measured. The output from the model was compared with the head injuries recorded for each case. It was concluded that AIS does not correlate well with the conventional test criteria such as linear acceleration, HIC and GAMBIT. However, when brain behaviour was examined, four distinct groups emerged: uninjured, concussion, sub-dural haematoma and skull fracture.

19. The foregoing analysis led to tentative proposals for brain injury criteria as follows;

- 1) Intra-cerebral von Mises stress of 10kpa for short duration concussion
- 2) Intra-cerebral von Mises stress of 20kpa for long duration concussion
- 3) Strain energy in the cerebro-spinal fluid of approximately 4J for sub-dural haematoma
- 4) Skull fracture was identified but not assessed in this study although it should be included in future research.

20. It is believed, with good supporting evidence, that this model represents the state of the art for a finite element model of the skull, brain, neck and helmet.

21. The head loading parameters, determined by accident reconstruction, experimental and numerical replications, have been analysed. The purpose was to improve the knowledge of human tolerance to head impact mechanisms and thus develop a means of predicting the probability of head injury severity for a range of impact parameters. Additionally, the frequency of occurrence and severity of neck injury was also investigated.

22. Of the parameters analysed, the Head Injury Criterion (HIC) gave the best head injury severity prediction with a correlation coefficient $r = 0.80$. The analysis predicted that a moderate brain injury of AIS 2, for example cerebral concussion, would be sustained at a HIC of 1000.

23. The relative linear and rotational accelerations of skull and brain, calculated for the Bimass headform model, were the second most effective parameters for predicting head injury severity with correlation coefficients of $r = 0.72$ and $r = 0.74$. The analysis predicted that a brain injury of severity AIS 2 will be sustained at 80g peak relative linear acceleration and 35 krad/s² peak relative rotational acceleration and AIS 3 at 150 g and 65 krad/s². It should be noted that these values cannot be related to values measured in a solid headform and should not be compared when considering tolerance to injury. However, at 150g peak linear acceleration in a metal headform was found to correspond to AIS 2.

24. Neck injury did not correlate well with head impact speed estimated from accident data, although there was a trend for neck injury severity to increase with speed. However, it was very evident that serious neck injury occurred in combination with serious head injury irrespective of the impact speed. Probability functions and tolerance levels for neck injury could not be evaluated from replication data, because only one case with moderate neck injury was included in the sample investigated.

25. A Hybrid II headform was drop tested onto an oblique abrasive anvil at impact velocities of 6.0 m/s, 7.5 m/s, 8.5 m/s, 10.0 m/s and 12.0 m/s, using four different helmet types. The mean values of peak rotational acceleration varied between about 2500 rad/s² and 8500 rad/s² and the rotational velocity varied between about 20 rad/s and 41 rad/s. The mean tangential force varied from about 800 N to about 2500 N and the anvil tangential impulse varied between about 9 Ns and 20 Ns.

26. It was found, in the oblique tests, that the correlation between peak rotational acceleration and peak tangential force was significantly linear ($r = 0.97$), and similarly between peak rotational velocity and anvil tangential impulse ($r = 0.95$). A significant linear correlation ($r = 0.91$) between peak linear acceleration and rotational acceleration was also measured.

27. The oblique impact drop test is therefore a suitable method with which to determine the differences in rotational acceleration and thus performance of different helmet types that may be caused for example, by different shell material, liner density and helmet shape.

28. A helmeted Hybrid III dummy was drop tested in 31 tests, onto a flat anvil at three different impact velocities (4.4 m/s, 5.2 m/s and 6.0 m/s) at the helmet impact points and body impact angles R/0°, B/30° and P/90°. Mean peak linear accelerations were between about 85g and 165g depending on the impact velocity and the helmet impact point. Mean peak force, normal to the anvil, varied between about 6500 N and 15600 N. It should be noted that the test repeatability was very good.

29. The helmeted Hybrid III dummy was also drop tested in 18 tests, onto an oblique abrasive at 4.4 m/s, 5.2 m/s and 6 m/s. The mean peak rotational accelerations were low and varied between about 1900 rad/s² and 3100 rad/s². The mean peak linear acceleration values ranged from about 27g to 41g and the mean peak tangential forces varied between about 700 N and 1100 N depending on the impact velocity.

30. Results from the headform tests and dummy tests were compared. It was found that, although the results for a given set of conditions were similar, in general, the headform test needed to be at a slightly greater velocity to give the same results. More specifically, dummy impacts at 5.2 m/s corresponded approximately to headform impacts at 6 m/s. Dummy measurements at 6 m/s gave results that were between headform measurements at 6 m/s and at 7.5 m/s. The linear relationship between peak rotational acceleration and peak tangential force in the dummy tests was significant ($r = 0.90$) and was very similar to that obtained in detached headform tests (0.97). It was concluded from these tests that a good replacement for dummy tests onto the oblique abrasive anvil is headform drop tests at a slightly greater velocity. However, this does not imply that the dummy tests accurately replicate a human rider in an accident.

31. To test for helmet retention, a novel headform was fitted with a transducer to measure the resultant force to the chin in one direction. Tests showed that the roll-off angle depended upon the pre-load exerted to the chin via the retention system. Thus, in part, the outcome of a test can be controlled by the force to which a chin-strap is tightened. It is

recommended that the initial load should be specified in a future test procedure for chin-strap effectiveness. It is also recommended that two load cells should be added to the test device so that the direction of the chin force may be studied in detail.

32. A novel sweating thermal headform prototype was developed to assess the physiological and ergonomic properties of motorcycle helmets, including the simulation of sweat. A comparative helmet ventilation test series showed that there are large differences in the effectiveness of the ventilation openings of different helmet types and also for the same helmet between the different openings. Generally, helmet ventilation systems need substantial improvement. The experiments have demonstrated the need for an objective test method to assess the physiological properties of helmets and, in particular, to quantify the efficiency of ventilation systems.

33. The temperatures measured on the sweating thermal headform with the vents set to the open and closed positions may provide the physiological criteria for future helmet Standards.

34. Aerodynamic noise is caused by the turbulent airflow around the motorcyclist's helmet and reaches sound pressure levels corresponding to around 90dB(A) at 40mile/h (64km/h), rising to around 120dB(A) at 100mile/h (160km/h). Noise levels in this range are capable of causing hearing damage, although the risk of damage is dependent on the exposure time. At 55 mile/h(88km/h), 2 hours is equivalent to the second action level of the GB Health and Safety at Work Act (1989) at which point hearing protection becomes compulsory. Two separate tests have been proposed, one which assesses the aerodynamic noise at the rider's ear and one which assesses the attenuation qualities of the helmet over the entire frequency spectrum

CHAPTER 10. HELMET TEST SPECIFICATION

The research detailed in this report has identified many factors that affect the incidence and severity of head injury in motorcycle accidents. One of the main objectives was to use the findings to propose a specification for the future testing of motorcycle helmets in Europe.

Protection against linear and rotational motion with clearly defined limits based upon the research will best be achieved with the test criteria given in Table 10.1. Standards currently prescribe solid headforms. This research has shown that a Bimass headform better represents the motion of the brain within the skull and thus is a more accurate predictor of potential brain injury; this headform has been included for size J only, because other sizes have yet to be developed. For all other sizes, a metal headform, of the type currently used, is specified.

The accident data analysis, Chapter 3, clearly identified relationships between speed and the accumulative occurrence of casualties for a range of head injury severity defined by values of AIS. From this data it was shown that a 24% increase in impact energy at the median speed for AIS 2/4 corresponded to an increase in injury severity from AIS2/4 to AIS 5/6. This increase is equivalent to what was estimated would be needed by way of increased helmet energy absorption to reduce 20% of all AIS 5/6 head injury casualties to AIS 2/4.

Research by the Human Tolerance Working Group has indicated values relating to measurements from test apparatus, including the Bimass headform, that correspond clearly to AIS2 and AIS3, moderate injury. Values for AIS 5/6 were not clearly identified for the Bimass, hence the need to use the metal headform for size J at 8.5m/s (see below). To achieve the casualty reductions, indicated above, it was necessary to propose two test speeds, one for the injury values corresponding to AIS 2 and the other for the existing Regulation 22-05 test criteria that correspond approximately to AIS 5/6 very serious and fatal injury. The Literature Review indicated that HIC 2000 corresponds to some 50% probability of a fatal injury, 2400 is in excess of this and Newman (1986) indicated that 250g -300g corresponded to AIS 5 and >300g to AIS6.

A test speed corresponding to an increase of 24% in energy would be 8.4m/s and this will give the increase in energy absorption required to achieve the predicted injury reductions. However, it will be necessary to test at speeds corresponding to AIS 2/3 to ensure that the helmet stiffness is not increased to an extent that may increase injuries at lower impact severities. Current helmets are known to give test measurements corresponding to AIS 2 at a test speed of approximately 5m/s (based partly upon replication data in the Reconstruction Working Group Final Report). A notional increase of 1m/s represents approximately 24% of the energy at 7.5m/s. Hence Table 10.1 includes tests at a speed of 6m/s with limits corresponding to AIS 2 as indicated by the Human Tolerance Working Group.

The test limits corresponding to the metal headform given in Table 10.1 for tests at 8.5m/s are those of Reg.22-05 and the limits given for the Bimass and the metal headform at 6.0m/s, equate to an AIS 2 head injury potential. It is believed that, with modern technology, helmets can be made to absorb some 24% greater energy at the current test speed of 7.5 m/s and give values corresponding to AIS 2 at a new test speed of 6.0m/s. It is confidently expected that the Test Specification given in Table 10.1 will lead to a reduction of 20% of all AIS 5/6 head injury casualties to AIS 2-4. In addition it is likely that many AIS 2-4 casualties would be reduced to AIS 1 although it is not possible to quantify this. It should be noted that 8.5m/s was chosen for the high speed linear test, rather than 8.4m/s, to be consistent with the oblique impact test speed.

Table 10.1 COST 327 Helmet Test Specification

Cost 327 Helmet Test Specification	Test Anvil	Headform Type and Size		Test Sites on Helmet ²					
		Metal	Bimass ¹	B	X	R	P	S	Projections
Impact Velocity ³ (m/s)	F (flat)	A E J M O		8.5	8.5	8.5	8.5	5.5 ³	-
		A E M O	J	6.0	6.0	6.0	6.0	5.5	
	K (kerbstone)	A E J M O		8.5	8.5	8.5	8.5	5.5 ³	-
		A E M O	J	6.0	6.0	6.0	6.0	5.5	
A (abrasive)	-	J	8.5	8.5	8.5	8.5	8.5	-	
B (bar)	-	J	-	-	-	-	-	8.5	
Test Limits ^{4,5}	HIC			1000 at 6.0m/s and 2400 at 5.5m/s (S) and 8.5m/s					metal headform only
	Peak Linear Acceleration			180g at 6.0m/s and 5.5m/s (S) 180g at 6.0m/s and 275g at 8.5m/s and 5.5m/s(S)					brain for Bimass, resultant for metal headform
	Peak Relative Linear Acceleration			80g at 6.0m/s and 5.5m/s(S)					Bimass headform o only
	Peak Relative Rotational Acceleration			35 000 rad/s ² ,					Bimass headform only

¹based on Hybrid III Motorcycle Anthropometric Test Dummy headform

²as defined in UN ECE R22.05, paragraphs 7.3.4.2, 7.4.1.3 and 7.4.2.3 Helmet test sites: front - B
side - X
rear - R
crown - P
chin - S

³as defined in UN ECE R22.05.

⁴ metal headform commensurate with AIS 2 and AIS 5/6

⁵Bimass commensurate with AIS2

CHAPTER 11. RECOMMENDATIONS

11.1. ACCIDENT INVESTIGATION

- Motorcycle accident studies should be undertaken to investigate the effect of climate on accident outcome, more fully than has been possible with this study, preferably using "On The Spot" methods.

11.2. NUMERICAL MODELLING

- The MADYMO model should be validated against a variety of accident configurations.
- The finite element model of the neck should be developed further using data from the COST 327 accident database to investigate the causative mechanisms of neck injuries and methods to minimise or prevent them.
- The FE model of the head and neck should be used to simulate a greater number of COST 327 accident cases. This will help to refine the model and to study the injury outcome for a wide range of impact conditions.
- Consideration should be given to simulating airflow through and around helmets to investigate physiological properties such as noise and ventilation.

11.3. TEST PROCEDURES

- Work should be undertaken to improve the retention test so that the chin-strap tightening force and direction are measured in helmet Standards. A force transducer will need to be developed.
- Test houses should be given the opportunity to assess the Bimass headform as a tool for use in helmet Standards. The Commission and Member States should consider funding headform(s) for circulation to test houses. The work should include a study of skull fractures and attempt to improve confidence in the value used for the short time shear modulus.
- Test laboratories should consider the Bimass headform for use on anthropometric dummies used in full scale impact testing.
- Collaborative research, such as a Framework Programme or a new COST Action, should be initiated to develop further the EMPA headform and test methods so that helmet physiological properties such as head and face ventilation, comfort, misting and fogging, and noise may be examined in Standards.

11.4. ADVANCED HELMETS

- Steps should be taken to assess "state of the art" helmet designs in accordance with the specification proposed by COST 327.
- If the "state of the art" is such that the performance proposed by the COST 327 test specification cannot yet be met then consideration should be given to collaborative European Research, such as a Framework Programme, to develop the necessary materials and technologies.

- To aid the development of new helmet concepts, manufacturers should be made aware of the modelling techniques used in COST 327.

11.5. IMPLEMENTATION

- The Commission and Member States should put in place a mechanism whereby helmets become available to consumers, that are capable of meeting the test specification given in the COST 327 Final Report.
- Those responsible for national and international helmet Standards, such as the UNECE Expert Group GRSP, should be asked by the Commission and Member States to consider the COST 327 Test Specification as a basis for a revision to the relevant helmet Standards such as Regulation 22.
- The information contained in this report should be considered for use as a basis for developing a test programme designed to inform consumers about the performance of helmets.
- International motor sport organisations such as FIM and FIA and national motor sport bodies should be encouraged to use the information contained within the report to ensure that participants are well protected.

CHAPTER 12. BENEFITS TO DIFFERENT USERS

12.1. BIOMECHANICS EXPERTS

Of particular benefit to biomechanics experts are the accident data, replication data and validated FE model outputs that were used to develop a much better understanding of the human tolerance to skull and brain injuries. This data was correlated with the output from tests with the Bimass headform, a revolutionary new headform developed as part of this Action and which has the potential to imitate brain and skull injuries to an extent not possible with conventional headforms.

The validation methods and the use of the FE model of the helmet, skull and brain should be of great benefit to others. This included a parametric study to evaluate the sensitivity of the model to changes of mass and stiffness of impactor.

12.2. DUMMY DEVELOPERS

Extensive testing to compare the output from a comprehensively instrumented, helmeted headform and target with equivalent drop tests on a helmeted headform alone has provided valuable information on the influence of the dummy mass and neck stiffness on the head during various types of impact. Furthermore, the extensive investigation of the behaviour of the Bimass headform, by way of finite element modelling and laboratory tests, could be deployed to help improve the representivity of current dummies.

12.3. CRASHWORTHINESS EXPERTS

It is recognised that current dummies lack bio-fidelity, particularly in the head and the chest. Thus, the judgements of crashworthiness experts are tempered by this inadequacy. The development of the Bimass headform and the potential that this can give in providing relevant data that can be related directly to skull and brain injuries should be of great benefit.

Furthermore, crashworthiness experts are frequently required to develop test procedures for regulatory purposes that are much less expensive but remain representative of full scale tests. The information relating headform performance on a dummy to equivalent tests on a headform alone should greatly assist tests designed to use only a simple headform.

Recent road accident analysis has shown that serious and fatal brain injuries occur in car side impacts. Use of the Bimass headform attached to an appropriate anthropometric dummy such as EUROSID or its successor ES2 may lead to more readily identifiable solutions. Frontal impact research may also benefit from the use of the Bimass headform attached to, for example, a Hybrid III dummy.

Better information could be provided to consumers from testing programmes such as EuroNCAP. If the Bimass headform was attached to the test dummies. Additional information on potential brain damage would be available, for example to refine EuroNCAP data.

12.4. HELMET MANUFACTURERS

It can sometimes be difficult for manufacturers to implement the findings of research. The modelling techniques described in this research could be of great benefit in helmet development whereby the performance of new helmet designs can be investigated in simulation before expensive prototypes need be produced and tested.

12.5. STANDARDS AUTHORITIES

Standards authorities are frequently seeking information to assist in defining test methods criteria and limit values, such that procedures accurately relate to accident mechanisms and human tolerance. Much of what is contained in this report will greatly assist helmet Standards authorities. Moreover, the new helmet test specification is an indication of how research information can be used to derive an improved Standard.

12.6. END USERS

12.6.1. Motorcyclists

A 20% reduction in motorcycle casualties with fatal and very serious head injuries is confidently expected if all motorcyclists in the EU were to wear helmets that satisfied the criteria defined by the COST 327 test specification. Around 1000 lives could be saved each year.

12.6.2. Other users of protective helmets.

Knowledge gained from this research could be used to benefit users of protective helmets other than motorcyclists. For example, cyclists, horse riders, motor sport participants, those engaged in dangerous leisure activities such as skiing, snow boarding and hang gliding and team sports such as American football, rugby and cricket, where the hazard is violent body contact or a hard, fast-travelling object, could all benefit from a helmet Standard improved through use of the COST 327 knowledge.

12.7. NATIONAL GOVERNMENTS

Any reduction in the severity of injury accidents would help preserve the contribution to society of those who would otherwise have been injured, decrease the burden on health services and help to achieve national safety targets. The burden of injury accidents would also be reduced if Standards for helmets used in the workplace were improved through the use of this research.

CHAPTER 13. BIBLIOGRAPHY

13.1. LITERATURE REVIEW REFERENCES

A.R.U. (1994). State of accident data and possibility of information at Accident Research Unit (ARU) Medical University Hannover. Brussels 1994.

ABEL, J.M., GENNARELLI, T.A., et al. (1978). Incidence and severity of cerebral concussion in the rhesus monkey following sagittal plane angular acceleration. Proceedings of the Twenty-Second Stapp Car Crash Conference, p. 35-53.

ADAMS, J.H. (1975). The neuropathology of head injuries, in: Handbook of Clinical Neurology 23: Injuries of the Brain and Skull; Part I, Chapter 3. P.J. Vinken and G.W. Bruyn (Ed.), Amsterdam, North-Holland Publishing Company. p. 35-65.

ADAMS, J.H., DOYLE, D., et al. (1986). Gliding contusions in non-missile head injury in humans. Archives of Pathology & Laboratory Medicine 110 (6), p. 485-8.

ADAMS, J.H., MITCHELL, D.E., et al. (1977). Diffuse brain damage of immediate impact type. Brain 100, p. 489-502.

ADAMS, J.H., et al. (1980). Brain damage in fatal non-missile head injury. Journal of Clinical Pathology 33, p. 1132-45.

ADAMS, J.H., et al. (1981). Acceleration induced head injury in the monkey: II. Neuropathology. Acta Neuropathologica Supplement VII, p. 26-8.

ADAMS, J.H., et al. (1982a). Brain damage in non-missile head injury: Observations in man and subhuman primates, in: Recent Advances in Neuropathology. W.T. Smith and J.B. Cavanagh (Eds.), Edinburgh, Churchill Livingstone. p. 165-90

ADAMS, J.H., et al. (1982b). Diffuse axonal injury due to non-missile head injury in humans: An analysis of 45 cases. Annals of Neurology 12, p. 564-74.

ALDMAN, B and THOMGREN, L (1979). The protective effect of crash helmets. A study of 96 motorcycle accidents. 4th International IRCOBI Conference, Göteborg, Sweden. pp63-74

ALDMAN, B., MELLANDER, H., et al. (1983). The structure of European research into the biomechanics of impacts. Proceedings of the 27th Stapp Car Crash Conference, p. 129-36.

ALEM, N.M., NUSHOLTZ, G.S., et al. (1984). Head and neck response to axial impacts. Proceedings of the 28th Stapp Car Crash Conference, p. 275-88.

ALEM, N.M., MELVIN, J.W., et al. (1978). Whole body human surrogate response to three-point harness restraint. Proceedings of the 22nd Stapp Car Crash Conference, p. 359-400.

ANDERSON, T.E. (1985). Physical parameters of cord contusion differentiate between neural and vascular injury. *Journal of Neurosurgery* 62, p. 115-9.

ANZELIUS, A. (1943). The effect of the impact of a spherical liquid mass. *Acta Pathol. Microbiol Scand.* 1943, 48, pp153-159.

AOKI, N. and MASUZAWA, H. (1984). Infantile acute subdural haematoma - clinical analysis of 26 cases. *Journal of Neurosurgery* 61, p. 273-80

BAKAY, L. and GLASAUER, F.E. (1980). *Head injury*. Boston: Little, Brown and Company.

BANDAK, F A and EPPINGER, R.H. (1994). A 3D finite element analysis of the human brain under combined rotational and translational accelerations. 38th Stapp Car Crash Conference. SAE Paper 942215. pp145-163.

BELYTSCHKO, T.B. and PRIVITZER, E.(1979). A three-dimensional discrete element dynamic model of the spine head and torso. In AGARD Conference Proceedings - Models and analogues for the evaluation of human biodynamic response, performance and protection. CP-253, A9, pp.1-15.

BELYTSCHKO, T.B. , SCHWER, L , and SCHULTZ, A.B.(1976). A model for analytic investigation of three-dimensional head-spine dynamics. University of Illinois at Chicago, Report to Aerospace Medical Research Laboratory, Wright-Patterson Air Force Base, AMRL-TR-76-10.

BEUSENBERG, M. (1991). *Hoofdletselbiomechanica*, Eindhoven University of Technology, The Netherlands. Report No. 4J610 Overhead sheets for the Injury Biomechanics course, 08-04-1991.

BEUSENBERG, M.C.(1992). Modules for the inclusion of safety requirements in (sport) helmet standards. January, 1992. Amsterdam: Consumer Safety Institute.

BLUMBERGS, P.C. (1985). Neuropathological aspects of head injury. Symposium on Head and Neck Injury in Road Accidents held at University of Adelaide. pp. 79-85.

BRINN, J. and STAFFELD, S.E. (1970). Evaluation of impact test accelerations: a damage index for the head and torso. Proceedings of the 14th Stapp Car Crash Conference, p. 188-220.

BRIT, R.H., HERRICK, M.K., et al. (1980). Traumatic lesions of the pontomedullary junction. *Neurosurgery* 6 (6), p. 623-30.

BYCROFT, G.N.(1973). Mathematical model of a head subjected to an angular acceleration. *J. of Biomech.* 1973, pp.487-497.

CAPRA, N.F. and ANDERSON, K.V. (1984). Anatomy of the cerebral venous system, in: *The Cerebral Venous System and its Disorders*. J.P. Kapp and H.H. Schmidek (eds.), Orlando, Grune & Stratton. p. 1-36.

- CHAMOULARD, F., et al. (1986). Relationship between some biomechanical and dimensional characteristics of skull and risk of cerebral injuries. International IRCOBI Conference on the Biomechanics of Impacts: Zurich, September, 1986. pp. 133-152.
- CHAPMAN, P.J. (1985). Biomechanics and sequelae of impacts to the mid and lower facial region in relation to the road accident situation. Symposium on Head and Neck Injury in Road Accidents, p. 41-7. Road Accident Research Unit, University of Adelaide.
- CHAPON, A., et al. (1983). Research on brain vulnerability from real accidents. Commission of the European Communities Seminar on the Biomechanics of Impacts in Road Accidents, p. 170-81.
- CHAPON, A., et al. (1985). Clinical study of head injuries in patients with traumatic unconsciousness. 1985 International IRCOBI/AAAM Conference on the Biomechanics of Impacts, pp. 33-54
- CHENG, L.Y, et al. (1990). Finite element analysis of diffuse axonal injury. Vehicle Crashworthiness and Occupant protection in Frontal Collisions: International Congress and Exposition, Detroit, Feb 26-Mar 2. pp141-154. SP-807. SAE
- CHINN, B P, HOPES, P.D. and FINNIS, M.P.(1989). Leg protection and its effect on motorcycle rider trajectory. 12th International Technical Conference on Experimental Safety Vehicles, May 29-June 1, Göteborg, Sweden. Vol. 2.
- CHU, C.S and LEE, M.C. (1991). Finite element analysis of cerebral contusion. Advances in Bioeng. ASME-BED, v20, pp601-604
- CHU, C.S, et al. (1994). Finite element analysis of cerebral contusion. J. Biomech. v27, n2 pp187-194.
- CLARK, J.M. (1974). Distribution of microglial clusters in the brain after head injury. Journal of Neurology, Neurosurgery and Psychiatry 37, p. 463-74.
- CLEMENS, H.J. and BUROW, K. (1972). Experimentelle untersuchungen zurverletzungsmechanik der halswirbersaule beim frontal- und hekaufprall. Arch. Orthop. Unfall-Chir. 74, p. 116-45.
- COOPER, P.R. (1982). Post-traumatic intracranial mass lesions, in: Head Injury. P.R. Cooper (Ed.), Baltimore/London, Williams and Wilkins. pp. 185-232.
- COURVILLE, C.B. (1942). Archives of Surgery 45, p. 19.
- DE JAGER, M.(1993). Mathematical modelling of the human cervical spine: a survey of the literature. International IRCOBI Conference on Biomechanics of Impacts, Eindhoven. pp. 213-227.
- DE WOLF, V.A.(1986). The effect of helmet law repeal on motorcycle fatalities. NHTSA Technical Report DOT HS807065. (NHTSA, Washington DC)
- DENG, Y.C. and GOLDSMITH, W.(1987). Response of a human head/neck/upper-torso replica to dynamic loading - II. analytical/numerical model. J. Biomechanics, v 20, n 5, pp. 487-497.

DENNY-BROWN, D. (1945). Cerebral concussion. *Physiology Review* 25, pp. 296-325.

DENNY-BROWN, D. and RUSSELL, W.R. (1941). Experimental cerebral concussion. *Brain* 64, pp 93-164 (cited by Denny-Brown, 1945).

DEPARTMENT OF PUBLIC SAFETY AND THE TEXAS DEPARTMENT OF HEALTH (1988). The costs of treating head injured unhelmeted motorcyclists in Texas (June 1987 - November 1988).

DEPARTMENT OF TRANSPORT, (1989). Road Accidents Great Britain. HMSO, London.

DIMASI, F, et al. (1991). 3D anatomic brain model for relating cortical strains to automobile crash loading. Proc. of the 13th International Technical Conference on Experimental Safety Vehicles, v2 pp 916-923. National Highway Traffic Safety Administration, US DOT.

DOUGLASS, J.M., et al. (1968). Applications of experimental head injury research. Proceedings of the 12th Stapp Car Crash Conference, pp. 317-37.

DOWDELL, B, et al. (1988). A study of helmet damage and rider head/neck injuries for crash involved motorcyclists. Research Note 5/88, Australian Road Safety Bureau *Crashlab*.

DUFFY, E.M. and BLAIR, A.(1991). Motorcycle accidents: the leg injury problem in perspective. International IRCOBI Conference on Biomechanics of Impacts, Berlin. pp 231-47.

EIBAND, A.(1959). Human tolerance to rapidly applied accelerations: a summary of the literature. NASA Memorandum. Report No. 5-19-59E, June 1959.

ENGEL, A. (1992). Airbag fur motorisierte zweirader. Forschungsbericht zum Projekt 1.8903 des Bundesministers fur Verkehr, Bergisch Gladbach, 1992. Technical University of Darmstadt.

ENGIN, A.E. (1969). The axisymmetric response to a fluid filled spherical shell to a local radial impulse. *J. of Biomechanics*, v2, pp325-341.

EUROPEAN EXPERIMENTAL VEHICLES COMMITTEE (EEVC) AD-HOC GROUP (1993). Report on motorcycle safety. December 1993.

EVANS, F.G., LEBOW M. and LISSNER, H.R. (1960). Experimental studies on the relation between acceleration and intracranial pressure changes in man. *Surgery, Gynaecology, and Obstetrics* v113, pp. 329-38.

EWING, C.L. and THOMAS, D.H.(1972). Human head and neck response to impact acceleration. NAMRL Monograph 21, Naval Aerospace Medical Research Laboratory.

EWING, C.L. et al. (1977). Dynamic response of the human head and neck to +Gy acceleration. Proc. 21st Stapp Car Crash Conf. pp. 549-586.

- FAN, W.R.S. (1971). Internal head injury assessment. Proceedings of the 15th Stapp Car Crash Conference, pp. 645-65.
- FRUIN, A.H., JUHL, G.L., et al. (1984). Interhemispheric subdural haematoma. *Journal of Neurosurgery* 60, pp. 1300-2.
- FULLER, P.M. and SNIDER, J.N. (1987). Injury mechanisms in motorcycle accidents. International IRCOBI Conference on Biomechanics of Impacts, September Birmingham UK. pp33-42
- GADD, C.W. (1962). Criteria for injury potential. National Academy of Science/National Research Council Publication No. 997
- GADD, C.W. (1966). Use of a weighted-impulse criterion for estimating injury hazard. Proceedings of the 10th Stapp Car Crash Conference, pp. 164-74.
- GADD, C.W. (1971). Tolerable Severity Index in whole-head non-mechanical impact. Proceedings of the 15th Stapp Car Crash Conference, p. 809-16.
- GARDNER, E.D., GRAY, D.J., et al. (1986). Anatomy: a regional study of human structure. R. O'Rahilly (Ed.), 5th ed. Philadelphia, W.B. Saunders Company.
- GENNARELLI, T.A. (1982). Cerebral concussion and diffuse brain injuries, in: Management of Head Injury. P. Cooper (Ed.), Baltimore, Williams and Wilkins. pp. 83-98.
- GENNARELLI, T.A. (1985). The state of the art of head injury biomechanics - A review. Twenty-Ninth Conference of the Association for Advancement of Automotive Medicine, p. 447-63.
- GENNARELLI, T.A. (1987). Head injury biomechanics: a review. Head Injury Mechanisms Symposium, pp. 9-21.
- GENNARELLI, T.A. and THIBAUT, L.E. (1982). Biomechanics of acute subdural haematoma. *Journal of Trauma* v22 n8, pp. 680-6.
- GENNARELLI, T.A., et al. (1971). Comparison of translational and rotational head motions in experimental cerebral concussion. 15th Stapp Car Crash Conference, pp. 797-803.
- GENNARELLI, T.A., et al. (1972). Patho-physiologic responses to rotational and translational accelerations of the head. 16th Stapp Car Crash Conference, pp. 296-308.
- GENNARELLI, T.A., et al. (1979). Differential tolerance of frontal and temporal lobes to contusion induced by angular acceleration. 23rd Stapp Car Crash Conference, pp. 563-86.
- GENNARELLI, T.A. et al. (1981). Acceleration induced head injury in the monkey: the model, its mechanical and physiological correlates. *Acta Neuropathologica Supplement VII*, p. 23-5.
- GENNARELLI, T.A. et al. (1982a). Influence of the type of intracranial lesion on outcome from severe head injury. *Journal of Neurosurgery* 56, pp. 26-36.

GENNARELLI, T.A. et al. (1982b). Diffuse axonal injury and traumatic coma in the primate. *Annals of Neurology* v12 n6, pp. 564-74.

GENNARELLI, T.A., et al. (1987). Directional dependence of axonal brain injury due to centroidal and non-centroidal acceleration. 31st Stapp Car Crash Conference, p. 49-53.

GILCHRIST, A. and MILLS, N.J. (1987). Improvements in the design and performance of motorcycle helmets. International IRCOBI Conference on the Biomechanics of Impacts, Birmingham, UK, September. pp 19-32.

GOSCH, H.H., et al. (1969). Distortion and displacement of the brain in experimental head injuries. *Surgical Forum* 20, p. 425-6

GOSCH, H.H., et al. (1970). The lexan calvarium for the study of cerebral response to acute trauma. *Journal of Trauma* v10, pp. 370-6.

GOT, C. et al. (1983). Morphological and biomechanical study of 146 human skulls used in experimental impacts, in relation with the observed injuries. 27th Stapp Car Crash Conference, pp. 241-59.

GRANDEL, J. (1987). Verbesserung der passiven sicherheit durch unfallforschung. In: VDI - Bericht Nr. 657, Dusseldorf.

GRANDEL, J, and SCHAPER, D (1984). Impact dynamic, head impact severity and helmet's energy absorption in motorcycle/passenger car accident Tests. International IRCOBI Conference on Biomechanics of Impacts, Delft. pp 129-40.

GRECEVIK, N. and JACOB, H. (1965). Some observations on pathology and correlative neuroanatomy of cerebral trauma. 8th International Congress of Neurology, v1, pp. 369-73.

GROSS, G A (1958). A new theory on the dynamics of brain concussion and brain injury. *J. Neurosurgery*. v15 pp548-561.

GURDJIAN, E.S. (1966). Mechanisms of head injury. *Clinical Neurosurgery* v12, pp. 112-128.

GURDJIAN, E.S. (1975). Impact head injury: mechanistic, clinical, and preventive correlations. Gurdjian, E.S., Illinois, Springfield.

GURDJIAN, E.S. and GURDJIAN, E.S. (1976). Cerebral contusions: re-evaluation of the mechanism of their development. *Journal of Trauma* v16 n1, pp. 35-51.

GURDJIAN, E.S. and LISSNER, H.R. (1961). Photoelastic confirmation on the presence of shear strains at the craniospinal junction in closed head injury. *Journal of Neurosurgery* v18, pp. 58-60.

GURDJIAN, E.S., et al. (1949). Studies on skull fracture with particular reference to engineering factors. *American Journal of Surgery* 57 / 78, pp. 736-42

- GURDJIAN, E.S., et al. (1950). The mechanism of skull fracture. *Radiology* 54, pp. 313-39.
- GURDJIAN, E.S., et al. (1953a). Quantitative determination of acceleration and intracranial pressure in experimental head injury. *Neurology* 3, pp. 417-23.
- GURDJIAN, E.S., et al. (1955). Observations on the mechanisms of brain concussion, contusion and laceration. *Surgery, Gynaecology & Obstetrics* 101, pp. 680-90
- GURDJIAN, E.S., et al. (1961). Intracranial pressure and acceleration accompanying head impacts in human cadavers. *Surgery, Gynaecology, and Obstetrics* v113, pp. 185.
- GURDJIAN, E.S., et al. (1964). Tolerance curves of acceleration and intercranial pressure and protective index in experimental head injury. *Journal of Trauma* p. 600
- GURDJIAN, E.S., WEBSTER, J.E. et al. (1953). Observations on prediction of fracture site in head injury. *Journal of Radiology* 60, pp. 226-35
- HARMS, P.L.(1981). Injury patterns of motorcyclists involved in accidents. TRRL Supplementary report SR 651. Crowthorne:TRRL.
- HARMS, P.L. (1984). A study of motorcyclist casualties with particular reference to head injuries. International IRCOBI Conference on Biomechanics of Impacts, Delft. pp 1408-13
- HARMS, P.L.(1989). Leg injuries and mechanisms in motorcycling accidents. Twelfth International Conference on Experimental Safety Vehicles, Gothenburg May 1989.
- HARMS, P. L. (1993). Crash injury investigation and injury mechanisms in road traffic accidents. TRL State of the Art Review. London: HMSO.
- HARVEY, F.H. and JONES, A.M. (1980). Typical basilar skull fracture of both petrous bones: an unreliable indicator of head impact site. *Journal of Forensic Sciences* 25, pp. 280-6.
- HAYNES, L. and LISSNER, H. (1962). Experimental head impact studies. 5th Stapp Car Crash Conference.
- HIGHT, P.V., et al. (1986). An international review of motorcycle crashworthiness. International IRCOBI Conference on Biomechanics of Impacts, Zurich, 1986. pp 261-76.
- HIRAKAWA, K., HASHIZUME, K., et al. (1972). Statistical analysis of chronic subdural haematoma in 309 adult cases. *Neurologia, Medica-Chirurgica* 12. pp. 71-83.
- HODGSON, V.R. and GURDJIAN, E.S. (1967). The response characteristics of the head with emphasis on mechanical impedance.. 11th Stapp Car Crash Conference. pp 79-83.
- HODGSON, V.R. and PATRICK, L.M. (1968). Dynamic response of the human cadaver head compared to a simple mathematical model. 12th Stapp Car Crash Conference. pp. 280-301.

HODGSON, V.R. and THOMAS, L.M. (1971). Comparison of head acceleration injury indices in cadaver skull fracture. 15th Stapp Car Crash Conference. pp. 190-206

HODGSON, V.R. and THOMAS, L.M. (1972). Effect of long-duration impact on head. 16th Stapp Car Crash Conference. pp. 292-5.

HODGSON, V.R. and THOMAS, L.M. (1979). Acceleration induced shear strains in a monkey brain hemisection. 23rd Stapp Car Crash Conference. pp. 587-611.

HODGSON, V.R., et al. (1967). The determination of response characteristics of the head with emphasis on mechanical impedance techniques. 11th Stapp Car Crash Conference. pp. 125-38.

HODGSON, V.R., et al. (1970). Fracture behavior of the skull frontal bone against cylindrical surfaces. 14th Stapp Car Crash Conference. pp. 341-55

HODGSON, V.R., THOMAS, L.M., et al. (1983). The role of impact location in reversible cerebral concussion. 27th Stapp Car Crash Conference. pp. 225-40.

HOLBOURN, A.H.S. (1945). The mechanics of brain injury. British Medical Bulletin v3, pp. 147-49.

HOLBOURN, A.H.S. (1943). Mechanics of head injuries. The Lancet 2, pp. 438-41.

HOPES, P.D, and CHINN, B.P.(1989).Helmets: a new look at design and possible protection. IRCOBI Conference on Biomechanics of Impacts, Stockholm. pp 39-54.

HOPES, P.D, and CHINN, B.P. (1990). The correlation of damage to crash helmets with injury, and the implications for injury tolerance criteria. IRCOBI Conference on Biomechanics of Impacts. pp319-31.

HOSEY, R.R. and LIU, Y.C. (1982). A homeomorphic finite element model of the human head and neck. In R.H. Callagher, B.R. Simon, T.C. Johnson and J.F. Gross, editors, Finite Elements in Biomechanics, chap. 18, pp. 379-401. John Wiley & Sons.

HUELKE, D.F, et al. (1988). Basilar skull fracture produced by facial impacts - Case histories and a review of the literature. 32nd Stapp Car Crash Conference, pp. 35-44.

HURT, H.H. Jr, and THOM, D.R. (1992). Motorcyclist head injury mechanisms- with and without helmets. 36th Conference of the Association for the Advancement of Automotive Medicine. pp.235-250.

HURT, H. H.Jr, et al. (1981). Motorcycle accident cause factors and identification of counter-measures Vol. 1: Technical report, Cont. No. DOT HS-5-01160 US Department of Transportation NHTSA.

HURT, H.H. Jr., et al. (1986). Epidemiology of head and neck injuries in motorcycle fatalities. In: Mechanisms of Head and Spine Trauma by Sances, Thomas, Ewing, Larson and Unterharnscheidt. Aloray.

HUSTON, J.C. and ADVANI, S.H.(1976). Three dimensional model of the human head and neck for automobile crashes. In *Mathematical Modelling Biodynamic Response to Impact*, 1976, SAE Paper no. 760769. SAE SP 412.

INSURANCE INSTITUTE FOR HIGHWAY SAFETY (1992). Status report: motorcycle helmet laws. IIHS Status Report Vol. 27 n4.

INTERNATIONAL MOTORCYCLE MANUFACTURERS ASSOCIATION (1992). Leg protectors: do they work? Proceedings of the International Seminar on Leg Protectors, Chantilly, France, Nov. 1991. Paris: IMMA.

KALBE P, et al. (1981). Trauma assessment of injuries and their consequences in accidents with two-wheelers. 6th IRCOBI Conference on the Biomechanics of Impacts, Salon de Provence. pp166-75

KALLIERIS, D., SCHMIDT, G.& HAUSLER, E. (1980). Brain injuries under high speed loading: a study with models and cadaver heads. 5th IRCOBI Conference on Biomechanics of Impacts. pp229-240.

KESSLER, J.W. (1987). Developments of countermeasures to reduce pedestrian head injury. 11th ESV, Washington. pp 281-93

KHALIL, T.B. and HUBBARD, R.P. (1977) Parametric study of head response by finite element modelling. *J. of Biomec.* v10, 119-132.

KHALIL, T.B. and VIANO, D.C. (1982). Critical issues in finite element modelling of head impact. 26th Stapp Car Crash Conf. pp87-102.

KING, A.I. , NAKHLA, S.S. and MITAL, N.K.(1978). Simulation of head and neck response to -Gx and +Gz impacts. AGARD-CP-253, A7, pp.1-13.

KING, A.I., RUAN J.S. and KHALIL,T. (1991). Human head dynamic response to side impact by finite element modelling. *J. of Biomec.*, v113, pp276-283

KOMATSU, S., SATO, T., et al. (1979). Traumatic lesions of the corpus callosum. *Neurosurgery* v5, pp. 32-5.

KRABELL,G., et al. (1994) Finite element simulation of deformation characteristics of the human skull. International IRCOBI Conference on Biomechanics of Impacts. pp39-50.

KRANZ, K.P.G (1985). Head and neck injuries to motorcycle and moped riders - with special regard to the effect of protective helmets. *Injury* v16, pp 253-258.

KUIJPERS, A H.W.M., et al. (1996). The influence of different boundary conditions on the response of the head to impact: a 2D finite element study. In: *Traumatic brain injury bioscience and mechanics* ed. by F.A. Bandak, R.H. Eppinger and A.K. Ommaya. New York: Mary Ann Liebert Inc. pp 197-206

LABORATOIRE DE L'UNION TECHNIQUE DE L'AUTOMOBILE DU MOTOCYCLE ET DU CYCLE. Essais d'homologation de casques prélevés auprès des usagers - Ministère de l'industrie et de la Recherche. S.Q.U.A.L.P.I. (unpublished study).

LANDKOF, B., GOLDSMITH, W. and SACKMAN, J.L.(1976). Impact on a head-neck structure. *Journal of Biomechanics*, v 9, pp. 141-151.

LANGWEIDER, K (1977). Collision characteristics and injuries to motorcyclists and moped drivers. 21st Stapp Car Crash Conference, New Orleans. pp259-301.

LANGWEIDER, K, et al. (1986). Passive sicherheit am motorrad, Kritische Beurteilung der Einsatzmöglichkeiten von Airbags Vortrag: IfZ Workshop, Bochum, 1986.

LARDER, D (1984). Analysis of serious two-wheeled motor vehicle accidents. Department of Transport UK (Unpublished Contract Report).

LAU, I.V. and VIANO, D.C. (1986). The viscous criterion - bases and applications of an injury severity index for soft tissues. 30th Stapp Car Crash Conference. pp. 123-42.

LAU, I.V., VIANO, D.C., et al. (1987). Invalidity of speculated injury mechanism in autopsy reports. General Motors Research Laboratories. Report No. GMR-6026.

LEE, M.-C., MELVIN, J.W., et al. (1987). Finite element analysis of traumatic subdural haematoma. 31st Stapp Car Crash Conference. pp. 67-77.

LEE, Y.C. and ADVANI, S.H.(1970) Transient response of a sphere to torsional loading: a head injury model. *Math. Biosciences* v6. pp 473-486

LEESTMA, A.E., KALELKA, M.B., et al. (1983). Ponto-medullary avulsion associated with cervical hyperextension. *Acta Neurochirurgica Supplement* v32, pp. 69-73.

LIGHTHALL, J.W. (1988). Controlled cortical impact: a new model of mechanical brain injury. *Journal of Neurotrauma* v5 n1. pp. 1-12.

LINDENBERG, R. and FREYTAG, E. (1957). Morphology of cortical contusions. *Archives of Pathology* 63, p. 23-42

LINDENBERG, R. and FREYTAG, E. (1960). The mechanism of cerebral contusions. *Archives of Pathology & Laboratory Medicine* v69, pp. 440-69.

LINDENBERG, R. and FREYTAG, E. (1970). Brain stem lesions characteristic of traumatic hyperextension of the head. *Acta Neurochirurgica* 90, p. 509-15.

LISSNER, H.R. and GURDJIAN, E.S. (1961) Experimental cerebral concussion, ASME. Report No. 60-WA-273

LOFGREN, J. and ZWETNOW, N.N. (1973). Cranial and spinal components of the cerebrospinal fluid pressure-volume curve. *Acta Neurologica Scandinavica* v 49, pp. 575-85.

LOFGREN, J., VON ESSEN, C., et al. (1973). The pressure-volume curve of the cerebrospinal fluid space in dogs. *Acta Neurologica Scandinavica* v49, pp. 557-74.

LOW, T.C. and STALNAKER, R.L. (1987). A lumped parameter approach to simulate the rotational head motion. International IRCOBI Conference on the Biomechanics of Impacts, Birmingham, UK. pp. 203-15.

LÖWENHIELM, C.G.P. (1974a). Dynamic properties of the parasagittal bridging veins. *Zeitschrift für Rechtsmedizin* v74, p. 55-62

LÖWENHIELM, C.G.P. (1974b). Strain tolerance of the Vv. cerebri sup. (bridging veins) calculated from head-on collision tests with cadavers. *Zeitschrift für Rechtsmedizin* 75, p. 131-44.

LÖWENHIELM, C.G.P. (1975) Brain susceptibility to velocity changes, relative and absolute limits for brain tissue tolerance to trauma and their relation to actual traumatic situations. Proceedings of an International Interdisciplinary Symposium on Traffic Speed and Casualties held at G1 Aversaess, Funen, 22 - 24 April, 1975, Denmark

LUNA, G.D. et al. (1981). The role of helmets in reducing head injuries from motorcycle accidents: a political or medical issue? *The Western Journal of Medicine* 135, p. 89-92.

LYNN, P. (1990). Accident liability of motorcyclists - analysis of survey data. TRL Report CR146. Crowthorne: TRL.

MARGULIES, S.S. and THIBAUT, L.E.(1989) An analytical model of traumatic diffuse brain injury. *J. of Biomec. Eng.*, 1989, v.111, pp241-249

MARGULIES, S.S., et al. (1985). A study of scaling and head injury criteria using physical model experiments. International IRCOBI Conference on the Biomechanics of Impacts, pp. 223-34.

McELHANEY, J.H. et al. (1971). Door crashworthiness criteria. 15th Stapp Car Crash Conference, pp. 489-517.

McELHANEY, J.H. et al. (1972). Biomechanics of seat belt design. 16th Stapp Car Crash Conference, pp. 321-44

McELHANEY, J.H., STALNAKER, R.L., et al. (1973). Biomechanical aspects of head injury. Proceedings of the Symposium on Human Impact Response - Measurement and Simulation. pp. 85-112.

McKENZIE, J.A. and WILLIAMS, J.F.(1971). The dynamic behaviour of the head and cervical spine during 'whiplash'. *Journal of Biomechanics*, v 4, pp. 477-490.

McSWAIN, N.E Jr, BELLES, Anita and MAIER, R.V. (1990). Motorcycle helmets - medical costs and the law. *Journal of Trauma* v30, n10. pp1189-99.

McSWAIN, N.E., WILLEY, and JANKE (1985). The impact of re-enactment of the motorcycle helmet law in Louisiana. 28th Annual Conference of the Association for the Advancement of Automotive Medicine. pp425-46.

MELVIN, J.W. and EVANS, F.G. (1971). A strain energy approach to the mechanics of skull fracture. 15th Stapp Car Crash Conference, pp. 667-85.

MENDIS, K. (1992) Finite element modelling of the brain to establish diffuse axonal injury criteria. PhD dissert. Ohio State Univ. 1992

MERRIL, T.H. (1981). Three-dimensional lumped-parameter impact analysis of a head/neck system. M.S.Thesis, University of California, Berkeley, 1981.

MERRIL, T. ,GOLDSMITH, W. and DENG, Y.C. (1984).Three-dimensional response of a lumped parameter head-neck model due to impact and impulsive loading. J. Biomechanics, v 17, n2. pp. 81-95.

MILLER, J.D. and JENNETT, W.B. (1968). Complications of depressed skull fracture. Lancet 1, p. 991.

MITSUISHI, H, ONO, K., and NAKAMURA, N. (1994). Present and future performance levels of head injury protection for motorcycle helmets. International IRCOBI Conference of Biomechanics of Impacts. pp 259-70.

MOHAN, D., et al. (1984). Helmet and head injury study of crash involved motorcyclists in Delhi. International IRCOBI Conference on Biomechanics of Impacts, Delft. pp65-77..

NAHUM, A.M. and SMITH, R.W. (1976). An experimental model for closed head impact injury. 20th Stapp Car Crash Conference, pp. 785-814

NAHUM, A.M., et al. (1968). Impact tolerance of the skull and face. 12th Stapp Car Crash Conference, pp. 302-16.

NAHUM, A.M., et al. (1977) Intracranial pressure dynamics during head impact. 21st Stapp Car Crash Conference. pp339-366.

NEVIN, N.C. (1967). Neuropathological changes in the white matter following head injury. Journal of Neuropathology and Experimental Neurology v26, p. 77-84.

NEWMAN, J.A. (1975). On the use of the Head Injury Criterion (HIC) in protective headgear evaluation. Proc 19th Stapp Car Crash Conference. pp615-40.

NEWMAN, J.A. (1980). Head injury criteria in automotive crash testing. 24th Stapp Car Crash Conference, pp. 703-47.

NEWMAN, J.A.(1986). A Generalised Acceleration Model for Brain Injury Threshold (GAMBIT). International IRCOBI Conference on the Biomechanics of Impacts, Zurich, Switzerland.. pp.121 - 131

NHTSA (1972). Occupant crash protection -- Head Injury Criterion, U.S. Department of Transportation. Report No. FMVSS 208, Docket Number 69-7, Notice 17,

NITSCHKE, S. (n.d.). Validation of a finite element model of the human neck. Graduation Thesis, Technische Universität Berlin, Automobile Technical Institute.

NOÉL, G (1979). Etude sur de vieillissement naturel et artificiel des casques de protection - Centre d'Etudes sur le Bâtiment et les Travaux Publics. Etude publiée dans les annales de l'Institut Technique du Bâtiment et des Travaux Publics No 375, Septembre 1979.

NUSHOLTZ, G.S., et al. (1979a). Comparison of epidural pressure in live anaesthetised and postmortem primates. Seventh International Workshop on Human Subjects for Biomechanical Research. pp. 175-200.

NUSHOLTZ, G.S., et al. (1979b). Head impact response comparisons of human surrogates. 23rd Stapp Car Crash Conference, pp. 499-541

NUSHOLTZ, G.S. et al. (1984). Head impact response - skull deformation and angular accelerations. 28th Stapp Car Crash Conference, pp. 41-74.

O'CONNELL, J.E.A. (1934). Some observations on the cerebral veins. *Brain* 57, pp. 484-503.

OKA, K., RHOTON, A.L., et al. (1985). Microsurgical anatomy of the superficial veins of the cerebrum. *Neurosurgery* 17, pp. 711-48.

OLSSON, Y., RINDER, L., et al. (1971). Studies of vascular permeability changes in experimental brain concussion. III. A comparison between the effects of single and repeated sudden mechanical loading of the brain. *Acta Neuropathologica* 19, pp. 225-33.

OMMAYA, A.K. (1966). Experimental head injury in the monkey. IN: Head Injury Conference Proceedings. W.F. Caveness and E.E. Walker (Eds.). Ch. 23. pp260-75 Philadelphia: J.B. Lippincott Co.

OMMAYA, A.K. and CORRAO, P.G. (1968). Pathologic biomechanics of central nervous system injury in head impact and whiplash trauma. IN: Accident Pathology. Proceedings of the International Conference on Accident Pathology. K.M. Brinkhous. pp160-81 Washington, DC: Government Printing Office.

OMMAYA, A.K. and GENNARELLI, T.A. (1974). Cerebral concussion and traumatic unconsciousness. Correlation of experimental and clinical observations on blunt head injuries. *Brain* 97, pp. 633-54

OMMAYA, A.K., et al. (1964). Experimental concussion. *Journal of Neurosurgery* 21, pp. 249-64

OMMAYA, A.K., et al. (1966). The role of whiplash in cerebral concussion. 10th Stapp Car Crash Conference, pp. 314-24.

OMMAYA, A.K., et al. (1969). The lexan calvarium: an improved method for direct observation of the brain. *Journal of Neurosurgery* 30, pp. 25-9.

ONO, K. et al. (1980). Human head tolerance to sagittal impact reliable estimation deduced from experimental head injury using sub-human primates and human cadaver skulls. 24th Stapp Car Crash Conference. pp. 101-60.

ONSER (1983). Accidents impliqués des motocyclettes: (a) Revue Bibliographique, November 1983 Cahiers D'Etudes, ONSER 2 Avenue de General-Malleret-Joinville 94114 Arcueil Cedex.

OPPENHEIMER, D.R. (1968). Microscopic lesions in the brain following head injury. *Journal of Neurology, Neurosurgery and Psychiatry* v31 n4. pp. 299-306.

ORNE, D. and LIU, Y.K. (1971). A mathematical model of spinal response to impact. *Journal of Biomechanics*, v 4. pp. 49-71.

OTTE, D. (1980). A review of different kinematic forms in two-wheel accidents - their influence on effectiveness of protective measures. 24th Stapp Car Crash Conference, Detroit, USA. pp. 561-605

OTTE, D. (1989). Motorradunfälle mit sozios-situationsbericht von unfall und verletzungsmustern. In: VDI-Bericht Nr. 779, Dusseldorf

OTTE, D. (1991). Technical demands on safety in the design of crash helmets for biomechanical analysis of real accident situations. 35th Stapp Car Crash Conference. pp335-339

OTTE, D. and FELTEN, G. (1991). Requirements on chin protection in full-face helmets for motorcyclist impact and injury situations. *Forschunghefte Zweiradsicherheit* 7. (also Proceedings 1991 International Motorcycle Conference Bochum, Germany. pp229-64

OTTE, D. and SUREN, E.G. (1985). Schutzhelme für motorisierte zweiradfahrer. Band 2: Auswertung von Zweiradunfällen - Bergisch - Gladbach: Bundesanstalt für Straßenwesen, 1985. (Forschungsberichte der Bundesanstalt für Straßenwesen, 113).

OTTE, D. et al. (1981). Typical injuries to the soft body parts and fractures of the motorised 2-wheelers. 6th IRCOBI Conference on Biomechanics of Impacts, Salon de Provence, France.. pp148 - 165.

OTTE, D., et al. (1982). Erhebungen am unfallort; unfall- und sicherheitsforschung strassenverkehr. Heft 37, pp 7-10.

OTTE, D. et al. (1984). Impact points and resultant injuries to the head of motorcyclists involved in accidents, with and without crash helmets. International IRCOBI Conference on Biomechanics of Impacts, Delft. pp47-64.

PATEL, R. and MOHAN, D. (1993). An improved motorcycle helmet design for tropical climates. *Applied Ergonomics* 1993, v24n6. pp 427-43

PATRICK, L.M. et al. (1963). Survival by design - head protection. 7th Stapp Car Crash Conference,

PEDDER, J.B et al. (1979). A study of 93 fatal two-wheeled motor vehicle accidents. 4th IRCOBI Conference on Biomechanics of Trauma, Gotenburg.. pp24-38.

PEDDER, J B, et al. (1980). A study of two-wheeled vehicle casualties treated at a city hospital. 6th International IRCOBI Conference on Biomechanics of Impacts, Salon de Provence, France. pp111-27.

PEDDER, J B, et al. (1982). Head protection for road users with particular reference to Helmets for Motorcyclists. AGARD meeting on Impact Injury caused by Linear Acceleration, Cologne, 1982. AGARD-CP-322.

PEERLESS, S.J. and REWCASTLE, N.B. (1967). Shear injuries of the brain. *Canadian Medical Association Journal* v96 n10, pp. 577-82.

PINCEMAILLE et al. (1989). Some data related to human tolerance obtained from volunteer boxers . 33rd Stapp Car Crash Conference. pp177-90.

PLUCHE, R and KING, A.J.(1985) A finite element model. NHTSA Reports TASK E-F “Advanced Anthropomorphic Test Device Development Program”.

PRASAD, P., et al. (1985). Head. J.W. Melvin, K.W. Weber (Ed.). U.S. Department of Transportation. National Highway Traffic Safety Administration. Report No. DOT HS 807 042.

PRIVITZER, E. , HOSEY, R.R. , RYERSON, J.E.(1982). Validation of a biodynamic injury prediction model of the head-spine system. AGARD-CP-322, 30, pp.1-10.

PUDENZ, R.H. and SHELDEN, C.H. (1946). The lucite calvarium - a method for direct observation of the brain. *Journal of Neurosurgery* v3, pp. 487-505.

RADE, R.(1993). Aufbau eines dreidimensionalen Modells des menschlichen Halswirbelsäule mit Hilfe der FE-Methode. Diplomarbeit 11/93, Technische Universität Berlin, 1993.

RAMET, M., CESARI, D. and DEDOYAW, A. (1981). Two wheeler accidents. 6th IRCOBI Conference on Biomechanics of Impacts, Salon de Provence, France. pp.193-205.

ROAF, R. (1960). A study of the mechanics of spinal injuries. *The Journal of Bone and Joint Surgery*, v.42B, n 4.

ROJANAVANICH, V. and STALNAKER, R.L. (1991). A development of approximate impedance functions to estimate general human head impact response for off-axis impacts. International IRCOBI Conference on the Biomechanics of Impacts, Berlin. pp. 63-75.

RUAN, J.S., et al. (1991). Human head dynamic response to side impact by finite element modelling. *J. of Biomec. Eng.* v113. pp 276-283.

RUAN, J.S., et al. (1992). Finite element analysis of the human head to impact. *Advances in Bioeng.* v22, pp249-252

RUAN, J.S., et al. (1993). Finite element modelling of direct head impact. 37th Stapp Car Crash Conference. pp69-81.

RUAN, J.S., et al. (1994). Dynamic response of the human head to impact by three dimensional finite element analysis. *J. of Biomec. Eng.* v116, pp44-50.

RUTLEDGE, R and STUTTS, J. (1993). The association of helmet use with the outcome of motorcycle crash injury when controlling for crash/injury severity. *Accident Analysis and Prevention*, v. 25n3. pp347-53

RYAN, G., et al. (1989) Head impacts and brain injury in fatally injured pedestrians. International IRCOBI Conference on Biomechanics of Impacts, Stockholm. pp27-38

SAE (1968). Human tolerance to impact conditions as related to motor vehicle design. New York: Society of Automotive Engineers, Inc. Report No. SAE J885a..

SANCES, A. and MYKLEBUST, J.(1982). Head and spine injuries. AGARD-CP-322, 13, pp.1-34.

SCHMIDT, G. (1973). Die belastbarkeit des halses und der schadelbasis bei indirektem trauma. International IRCOBI Conference on the Biokinetics of Impacts. pp. 339-44.

SCHULLER, E. and BEIER, G. (1981) Safety helmets shell material and head injury incidence in motorcycle accidents. 6th IRCOBI Conference on Biomechanics of Impacts, Salon-de-Provence. France. pp 184-92

SCHULLER, E, et al. (1985) Assessment of the effectiveness of safety measures - conclusions drawn from the Munich area seat belt and motorcycle studies. SAE technical paper 850091.

SELLIER, K. and UNTERHARNSCHEIDT, F. (1963). Mechanik und pathomorphologie der hirnschäden nach stumpfer gewalteinwirkung auf den schädel. Hefte zur Unfallheilkunde 76. pp. 1-140. Berlin: Springer Verlag

SHANKAR, B.S et al (1992). Helmet use, patterns of injury, medical outcome, and costs among motorcycle drivers in Maryland. *Accid. Anal. and Prev.* v24,n4. pp385-96.

SHATSKY, S.A. et al. (1974a). Traumatic distortions of the primate head and chest: Correlation of biomechanical, radiological and pathological data. 18th Stapp Car Crash Conference. pp. 351-81.

SHATSKY, S.A. et al. (1974b). High-speed angiography of experimental head injury. *Journal of Neurosurgery* v 41, pp. 523-30.

SHELDEN, C.H., PUDENZ, R.H., et al. (1944). The lucite calvarium. A method for direct observation of the brain. I. The surgical and lucite processing techniques. *Journal of Neurosurgery* 1, p. 67-75 (cited by Denny-Brown (1945)).

SHEPPARD, D.B, HESTER, A.K., GATFIELD, S. and MARTIN, M. (1985). Motorcyclists' use of their front brakes. Research Report No.RR20. Crowthorne: TRRL.

SHUCK, L.Z. and ADVANI, S.H. (1972). Rheological response of human brain tissue in shear. *Journal of Basic Engineering.* pp. 905-911.

SHUGAR, T.A. (1977). A finite element head injury model. Report No. DOT HS 289-3-550-TA, vol. I.

SIMPSON, D.A., et al. (1989). Pontomedullary tears and other gross brain stem injuries after vehicular accidents. *Journal of Trauma* v29 n11, pp. 1519-25.

SKOLD, G. and VOIGT, G.E. (1977). Spinal injuries in belt-wearing car occupants killed by head-on collisions. *Injury* v9 n2, pp. 151-61.

SLATTENSCHKEK, A. and TAUFFKIRCHEN, W. (1970). Critical evaluation of assessment methods for head impact applied in appraisal of brain injury hazard, in particular in head impact on windshields. 1970 International Automobile Safety Conference Compendium. pp. 1084-1112.

- SMITH, B.H. and DEHNER, L.P. (1969). Fatal motorcycle accidents of military personnel. *Military Medicine* v 134 n13, p. 1477-87.
- SNELL (1985). Standard for protective headgear. Snell Memorial Foundation. Wakefield, USA.
- SPORNER, A., et al (1987). Development of a safety concept for motorcycles: results of accident analysis and of crash tests. Edinburgh: Jim Clarke Foundation.
- SPORNER, A., et al. (1989) Risk of leg injuries of motorcyclists - present situation and countermeasures. 12th ESV Conference, Gotenberg, May 1989.
- SPORNER, A., et al. (1990). Passive safety for motorcyclists - From the leg protector to the airbag. SAE International Congress and Exposition, Detroit. pp197-206.
- STALNAKER, R.L. et al. (1971a). Driving point impedance characteristics of the head. *Journal of Biomechanics* v. 4, pp. 127-139
- STALNAKER, R.L. et al. (1971b). MSC tolerance curve for human head impacts. *American Society of Mechanical Engineers* p. 1-10.
- STALNAKER, R.L. et al.(1977). Head impact response. 21st Stapp Car Crash Conference, pp305-335
- STALNAKER, R.L., et al. (1985). Application of the new mean strain criterion. *International IRCOBI Conference on Biomechanics of Impacts*. pp191-209.
- STALNAKER, R.L., et al. (1987). Translational energy criteria and its correlation with head injury in the sub-human primate. *International IRCOBI Conference on the Biomechanics of Impacts*, Birmingham, UK. pp. 223-38.
- STÖCKER, U. and LÖFFELHOLZ, H. (1984) Investigation into the protective effects of helmets on users of powered two-wheelers. *International IRCOBI Conference on Biomechanics of Impacts*, Delft. pp79-90.
- STRICH, S.J. (1956). Diffuse degeneration of the cerebral white matter in severe dementia following head injury. *Journal of Neurology, Neurosurgery and Psychiatry* v19, p. 163-85.
- STRICH, S.J. (1961). Shearing of nerve fibres as a cause of brain damage due to head injury - a pathological study of twenty cases. *Lancet* 2, p. 443-8.
- STRICH, S.J. (1969). The pathology of brain damage due to blunt head injuries .IN: *The Late Effects of Head Injury*. A.E. Walker, W.F. Caveness and M. Critchley (Eds.), Springfield, Thomas. pp. 501-24.
- STRICH, S.J. (1970). Lesions in the cerebral hemispheres after blunt head injuries. *Journal of Clinical Pathology* 23, Supplement 4, pp. 154-65
- SUH, C.H.(1977). Dynamic simulation of the cervical spine with use of the differential displacement matrix. *International IRCOBI Conference on Biomechanics of Impacts*.

SWEARINGEN, J.J. (1965). Tolerances of the human face to crash impact. Oklahoma: Office of Aviation Medicine, FAA, Civil Aeromedical Research Institute.

SYMONDS, C.P. (1962). Concussion and its sequelae. *Lancet* i, p. 1-5.

TANGORRA, J. and GEORGE, A.R. (1991). Wind noise of motorcycle helmets. *Forschungshefte Zweiradsicherheit* 7. 1991 International Motorcycle Conference.

THOM, D.R. and HURT, H.H. (1993). Basilar skull fractures in fatal motorcycle crashes. 37th Annual Conference of the Association for the Advancement of Automotive Medicine, pp. 61-76.

THOMAS, D.R., HODGSON, V.R., et al. (1973). Skull fracture and management of open head injury. IN: *Neurological Surgery*. J.R. Youmans (Ed.), Philadelphia: Saunders. pp. 969-77.

TIEN, C.S. and HUSTON, R.L.(1985). Biodynamic modelling of the head/neck system. IN: *Field Accidents Data Collection Analysis, Methodologies and Crash Injury Reconstruction*. SAE Paper no. 850438

TIEN, C.S. and HUSTON, R.L.(1987). Numerical advances in gross-motion simulations of head/neck dynamics. *J. Biomech. Eng.*, v. 109, pp. 163-168.

TOMLINSON, B.E. (1970). Brain-stem lesions after head injury. *Journal of Clinical Pathology* 23, Supplement 4, p. 154-65.

TROTTER, W. (1924). Certain minor injuries of the brain. *Lancet* 1, p. 935-9 (cited by Denny-Brown (1945)).

UENO, K and MELVIN, J.W. (1995) FE model of head impact based on a Hybrid III head acceleration. The effects of rotation and translational acceleration. *J. Biomed. Engineering*, V117, p39.

UNTERHARNSCHEIDT, F. and HIGGINS, L.S. (1969). Pathomorphology of experimental head injury due to rotational acceleration. *Acta Neuropathology* 12, p. 200-4.

VALLÉE, H. et al (1981). Characteristics of objects struck by the head of moped riders or motorcyclists. 6th IRCOBI Conference of Biomechanics of Impacts, Salon de Provence, France. pp 176-83.

VALLÉE, H. et al. (1984). The fracturing of helmet shells. International IRCOBI Conference on Biomechanics of Impacts, Delft. pp99-109.

VAUGHAN, .R. G. (1977). Motorcycle helmets and facial injuries. *Medical Journal of Australia*, v1, n5. pp125-7.

VERSACE, J. (1971). A review of the Severity Index. 15th Stapp Car Crash Conference, pp. 771-96. Also (MVSS208).

VIANO, D.C. (1985). Perspectives on head injury research. International IRCOBI Conference on the Biomechanics of Impacts. pp. 1-27.

- VIANO, D.C. (1988). Biomechanics of head injury: toward a theory linking head dynamic motion, brain tissue deformation and neural trauma. 32nd Stapp Car Crash Conference. pp. 1-20.
- VIANO, D.C. (1995). Personal communication
- VIANO, D.C. and LAU, I.V. (1988). A viscous tolerance criterion for soft tissue injury assessment. *Journal of Biomechanics* v21 n5, pp. 387-99.
- VIANO, D.C., et al. (1986). Measurement of head dynamics and facial contact forces in the Hybrid III dummy. 30th Stapp Car Crash Conference. pp. 269-89.
- VIANO, D.C., et al. (1989). Injury biomechanics research : an essential element in the prevention of trauma. *J. of Biomec.* v 22, pp 403-417
- VICENTINI, C. and GIAVOTTO, V (1995). Modelli ad elementi finiti per lo studio della meccanica dei traumi cerebrali. Tesi di Politecnico di Milano, 1995.
- VOIGHT, G.E. and LÖWENHIELM, C.G.P. (1974). "Gliding Contusions" des grosshirns. *Hefte zur Unfallheilkunde* 117, pp. 329-35
- VOIGHT, G.E. and SKOLD, G. (1974). Ring fractures of the base of the skull. *Journal of Trauma* v14 n6, pp. 494-505.
- WALKER, A.E. (1973). Mechanisms of cerebral trauma and the impairment of consciousness. *Neurological Surgery* 2, p. 936-49.
- WALZ, F, NIEDERER, P. and KOSIK, D. (1976). The influence of protection helmets in motorcycle accidents. Meeting on Biomechanics of Injury to pedestrians, cyclists and motorcyclists, Amsterdam. IRCOBI, pp 301-10.
- WARD, C.C. and THOMPSON, R.B.(1975). The development of a finite element brain model. 19th Stapp Car Crash Conference, San Diego.
- WATSON, P.M.F and LANDER, F.T.(1973). Motorcycle accidents and injuries. Conference on Vehicle Safety Legislation - its Engineering and Social Implications. London: IMechE.
- WHITAKER, J. (1980). A survey of motorcycle accidents. TRRL Laboratory Report LR 913. Crowthorne: TRRL.
- WILLIAMS, J.L. and BELYTSCHKO, T.B.(1983). A three-dimensional model of the human cervical spine for impact simulation. *J. Biomech. Eng.*, v.105, pp. 321-33.
- WILLINGER, R. and CESARI, D. (1990). Determination of cerebral motion at impact through mechanical impedance measurement. International IRCOBI Conference on the Biomechanics of Impacts, p. 203-13.
- WILLINGER, R., et al. (1991). Cerebral motion and head tolerance. 35th Conference of the Association for the Advancement of Automotive Medicine. pp. 387-404.

WILLINGER, R., et al. (1992). New concept of contrecoup lesions: modal analysis of a finite element head model. International IRCOBI Conference of Biomechanics of Impacts. pp283 - 297.

WILLINGER, R. et al. (1994) Mechanisms of brain injury derived from mathematical modelling and epidemiological data. *Accid. Anal. and Prev.*, v26 n6, pp767-779

WILLINGER, R. et al. (1995a). Modal and temporal analysis of head mathematical models. *J. of Neurotrauma* 1995, v12, no 4, pp743-754.

WILLINGER, R., et al. (1995b). Head biomechanics : from the finite element model to the physical model. International IRCOBI Conference on Biomechanics of Impacts. pp245-260.

WISMANS, J. (1991). Introduction in injury biomechanics. Eindhoven University of Technology, The Netherlands. Report No. 4J610 Lecture notes of the Injury Biomechanics course, 26-03-1991.

WISMANS, J, et al. (1992). Airbag - systeme fur motorrader. Tagungsunterlagen des 2. AKZO Syposiums fur Fahrzeuginsassen-Ruckhaltesysteme "Bag and Belt", Cologne, 1992.

YETRAM, A. L, GODFREY, N.P.M. and CHINN, B.P.(1994). Materials for motorcycle crash helmets - a finite element parametric study. *Plastics, Rubber and Composites Processing and Applications* 21 (1994).

YOGANANDAN, N., et al.(1990). Injury biomechanics of the human cervical column. *Spine*, v 15, pp. 1031-1039.

YOGANANDAN, N et al. (1991). Strength and kinematic response of dynamic cervical spine injuries. *Spine*, v16, pp. S511-S517.

ZELLMER, H. (1993). Investigation of the performance of motorcycle helmets under impact conditions. Stapp Car Crash Conference.

ZIMMERMAN, R.A. and BILANIUK, L.T. (1978). Computed tomography of shearing injuries of the cerebral white matter. *Radiology* 127, p. 393-6.

13.2. CHAPTER REFERENCES

Chapter 3.

AMERICAN ASSOCIATION FOR AUTOMOTIVE MEDICINE (1990). The Abbreviated Injury Scale - Revision 90. American Association of. Automotive Medicine.

COST 327 (1999). Accident description and analysis of motorcycle safety helmets" (March 1999).

COST 327 (1999). Data gathering analysis study on motorcycle safety helmets" (September 1999)

KOCH, H.(1986). Der Motorradunfall Beschreibung, Analyse, Prävention Forschungshefte Zweiradsicherheit Nr. 3. Institut für Zweiradsicherheit e.V. Bochum 1986

OTTE, D (1994a). The Accident Research Unit Hannover as example for importance and benefit of existing in depth investigations SAE-Paper No. 940712. Proc. International SAE Congress, Detroit/USA, 1994

OTTE,D (1994b). Improvements of optimal passive safety of motorcycles in traffic accidents with integrated leg protector. *VDI Berichte* Nr. 1159, p. 241-262, 1994

OTTE, D. KALBE, P. and APPEL,.(1994) Difference of injury patterns and accident kinematic of motorised and non-motorised two-wheelers. Proc. 29th American Association for Automotive Medicine, p. 335-352

OTTE, D. (1995). Injury scaling: from lesion assessment to passive safety improvement. Vortrag Round Table, Institute of Legal Medicine, University of Verona, June 1995

Chapter 4.

BS 6658: (1985), "British Standard Specification for Protective Helmets for Vehicle Users"

EN960 headforms for use in the testing of protective helmets, December 1994

FMVSS 208, Part 572

McELHANEY J.H., ROBERTS V.L., HILYARD J.F (1976). Handbook of human tolerance. Japan Automobile Research Institute, Tokyo 1976.

MELLOR, A N. (1995). Motorcycle helmet oblique impact tests using a Hybrid II headform. TRL Report.

NEWMAN, J.A.(1986). A Generalised Acceleration Model for Brain Injury Threshold (GAMBIT). International IRCOBI Conference on the Biomechanics of Impacts, Zurich, Switzerland.. pp.121 - 131

SCHULLER E, BEIER G und SPANN W(1993). Kriterien für die prüfung von motorrad-schutzhelmen, Teil B. Berichte der Bundesanstalt für Straßenwesen (BAST) Heft F2 (1993).

STALNAKER, R.L. Application of the new mean strain criterion. IRCOBI Conference. 1985, 191-211.

UNECE regulation 22

WILLINGER R., TALEB L., PRADOURA, P. (1995). Head biomechanics : from the finite element model to the physical model. Proceedings of IRCOBI 1995, pp245-260.

WILLINGER R., GUIMBERTEAU T., McLEAN AJ., ANDERSON R., FARMER M. (1996). Expérimental and theoretical modelling of head impact - Influence of head modelling. Proceedings of the International Research Council on Biokinetics of Impacts. Dublin 1996, pp 21, 34.

Chapter 5.

CHINN, BP, HAPPIAN-SMITH, J and MACAULAY, MA. (1989). The effect of leg protecting fairings on the overall motion of a motorcycle in a glancing impact. *Int. Journal of Impact Engng*, Vol. 8 No. 3, pp. 265-279, 1989.

COST 327 (2000). Accident Reconstruction Working Group, Final Report.

DIXON PR (1995). Physical properties of a Hybrid III motorcycle dummy and a Ford Mondeo. Project report PR/VE/178/95. TRL, Crowthorne, 1995.

HAPPIAN-SMITH, J, MACAULAY, MA and CHINN, BP (1987). Motorcycle impact simulation and practical verification. International Conference on Experimental Safety Vehicles, pp. 858-896, 1987.

HAPPIAN-SMITH, J (1988). Motorcycle and rider dynamics in frontal collision, simulation and verification, Thesis at Brunel University.

HAPPIAN-SMITH, J et al. (1994). Computer simulation of motorcycle crash tests, International Conference on Experimental Safety Vehicles, Paper No. 94-S7-O-10.

HAPPIAN-SMITH, J, MACAULAY, MA and CHINN, BP (1990). Computer simulation of a simple motorcycle in glancing impacts with a rigid barrier", , , in "Rider Passenger Protection in Motorcycle Collisions" , SAE SP-827, 900754.

KALEPS, I et al. (1988). Measurement of Hybrid III dummy properties and analytical simulation database development, Aerospace Medical Research Laboratory Report AAAMLT-TR-88-005.

McDONOUGH, PJ (1993). Opat dummy and Norton Commander motorcycle: determination of physical properties for impact simulation. TRL Project report PR/VE/10/93, 1993.

MACINNIS, DD, CLIFF, WE and ISING, KW, (1997). A comparison of moment of inertia estimation techniques for vehicle dynamics simulation. SAE Paper No. 970951. Pp99-116, 1997.

NIEBOER, J.J, WISMANS, J, VERSMISSEN, ACM, SLAGMAAT, MTP VAN, KURAWAKI, I and OHARA, N (1993). Motorcycle crash test modelling. SAE Paper No. 933133, pp 273-288, 1993.

OTTE, D et al. (1999). Accident description and analysis of motorcycle safety helmets, Task Group Accident Data COST 327.

PREUSER, DF et al. (1997). Analysis of fatal motorcycle crashes. Pergamon Press..

TNO (1997). Madymo database manual, version 5.3, TNO Road Vehicles Research Institute, Delft NL 1997.

YETTRAM, AL, HAPPIAN-SMITH, J, MO, LSM, MACAULAY, MA and CHINN, BP (1994). Computer simulation of motorcycle crash tests. International Conference on Experimental Safety Vehicles", Paper No. 94-S7-O-10, pp. 1227-1240, 1994.

ZELLNER, JW et al. (1991). Motorcycle leg protectors: an analysis of overall effectiveness via computer simulation. Proc. International Motorcycle Conference, Bochum.

ZELLNER, JW, KEBSCHULL, SA AND WILEY, KD (1991). Motorcycle leg protectors: an analysis of overall effectiveness via computer simulation. Proc. International Motorcycle Conference, Bochum, 1991.

Chapter 6.

FERNER H. and STAUBESAND J.(1985). Atlas d'anatomie humaine-tête, cou, membre thoracique. Edition Médicales Internationales Paris, 1985

SHUCK L.Z. and ADVANI S.H. (1972). Rheological response of human brain tissue in shearing, *Journal of Basic Eng.*, Dec.1972, pp 905-911.

WILLINGER, R., RYAN, G.A., MCCLEAN, A.J. and KOPP, C.M. (1994). Mechanisms of brain injury derived from mathematical modelling and epidemiological data. *Accid. Anal. and Prev.*, 1994, v26 n6, pp 767-779.

Chapter 7.

NEWMAN, J.A.(1986). A Generalised Acceleration Model for Brain Injury Threshold (GAMBIT). International IRCOBI Conference on the Biomechanics of Impacts, Zurich, Switzerland.. pp.121 - 131

VERSACE, J. (1971). A review of the Severity Index. 15th Stapp Car Crash Conference, pp. 771-96. Also (MVSS208).

Chapter 8.

ALDMAN A., LUNDELL B., and THORNGREN L., (1976). Non-perpendicular impacts, an experimental study on crash helmets. Proceedings of the 1976 IRCOBI conference, pp. 322-331.

ALDMAN A., LUNDELL B., and THORNGREN L., (1978a). Helmet attenuation of the head response in oblique impacts to the ground. Proceedings of the 1978 IRCOBI conference, pp. 118-128.

ALDMAN A., LUNDELL B., and THORNGREN L., (1978b). Oblique impacts, a parametric study in crash helmets. Proceedings of the 1978 IRCOBI conference, pp. 129-141.

BINNINGTON J.D., McCOMBE A.W. and HARRIS, M. (1993). Warning signal detection and the acoustic environment of the motorcyclist. *British Journal of Audiology* 27:415-422.

BIRLEY A. W., HAWORTH B., BATCHELOR J., (1991). Physics of plastics, Oxford University Press, New York.

BS 6658: (1985). British Standard Institution: Specification for protective helmets for vehicle users.

COST 327 (1997). Motorcycle safety helmets: literature review final report. TRL, Crowthorne, UK, 1997.

DIXON P. R., KARIMI H., and MELLOR A. N., (1997). Replication of test 10P. TRL Report, Crowthorne, UK.

ECE Regulation 22-04, (1995). United Nations Agreement. Uniform provisions concerning the approval of protective helmets for drivers and passengers of motorcycles and mopeds.

LOWER M.C., HURST D.W and THOMAS A. (1996). Noise levels and noise reduction under motorcyclist's helmets. Proceedings of Internoise '96, Book 2, pp979-982.

McCOMBE A.W. (1992). Wind noise, hearing loss and motorcyclists. Otolaryngology Dept, Bristol Royal Infirmary, Bristol.

McCOMBE A.W. and BINNINGTON J. (1994). Hearing loss in Grand Prix motorcyclists: occupational hazard or sports injury? *Br. J. Sp. Med.* 28(1):35-37.

McCOMBE A.W., BINNINGTON J.A. and. NASH D. (1994). Wind noise and motorcycle crash helmets. *Journal of Low Frequency and Vibration*, 13(2).

McKNIGHT A.J. and McKNIGHT A.S. 1995. The effects of motorcycle helmets upon seeing and hearing. *Accident Analysis and Prevention* 27(4): 493-501.

NEWMAN J. A., (1986). A generalised acceleration model for brain injury threshold (GAMBIT). Proceedings of the 1986 IRCOBi conference, pp. 121-131.

NOISE ADVISORY COUNCIL(1986). Draft Code of Practice on sound levels in discotheques. HMSO, 1986.

NOISE AT WORK REGULATIONS (1989). Statutory Instrument no. 1790. HMSO.

OTTE, D (1999). Personal communication

PADGAONKAR A. J., KRIEGER K. W., and KING A. I., (1975). Measurement of angular acceleration of a rigid body using linear accelerometers. *J. Appl. Mech.*, pp. 552-556.

RODAHL K., BJØRKLUND R. A., KULSRUD A.-H., KLÜWER L. D., and GUTHE T., (1992). Effects of protective Helmets on body temperature and psycho-motor performance. Proceedings of The Fifth Int. Conf. on Environmental Ergonomics, Maastrich, The Netherlands, pp. 98-99.

TANGORRA J. and GEORGE A.R. (1991). Wind noise of motorcycle helmets. Proceedings of the 1991 International Motorcycle Conference.

WILKINS, PA and MARTIN, AM (1982). The effects of hearing protection on the perception of warning sounds. In: Personal hearing protection in industry by P W Alberti. Raven Press. Pp 339-369

13.3. PUBLICATIONS RESULTING FROM THE ACTION

CANAPLE, B RUNGEN, P, MARKIEWICZ, E, RAVALARD, Y, DRAZETIC, P HAPPIAN-SMITH, J and CHINN, B.P.(2000). Simulation model for motorcycle. car impact in a lateral collision configuration. Presented at Forum SCGM 2000, Bureau des Congrès Universitaires, Canada, May 2000

CHINN, BP, DOYLE, D, OTTE, D and SCHULLER, E (1999). Motorcyclists head injuries: mechanisms identified from accident reconstruction and helmet damage replication. 1999 IRCOBI Conference on the Biomechanics of Impact, September 23-24 1999, Sitges (Barcelona, Spain)

CHINN, BP., WILLINGER, R, OTTE, D and SCHULLER, E (1999). COST 327: Motorcycle Safety Helmets: Injuries, analysis and simulation. Paper presented at the 2nd European Road Research Conference, 1999

COST 327. Accident description and analysis of motorcycle safety helmets. Final Report.

COST 327. Accident Reconstruction Working Group. Final report

COST 327. Data gathering analysis study on motorcycle safety helmets. September 1999

COST 327. Working Group on Computer Modelling of the Head, Neck and Helmet. Final report.

COST 327. Working Group on Headforms. Final report. 1999.

COST 327 Motorcycle safety helmets. Literature Review. 1997

COST 327: Motor Safety Helmets: accident description and analysis of motorcycle safety helmets - Task Group Accident Data Final Report

DI AW, BM, WILLINGER, R, GUIMBERTEAU, T CHINN, BP. (1999). Validation of a full face protective helmet finite element model and coupling with a human head model

DIXON, PR and MELLOR, AM (1998). Comparison of the variability in oblique anvil test results from four European laboratories. TRL unpublished Project Report PR/SE 460/98

DIXON, PR, KARIMI H and MELLOR, AM(1998). Replication of test 10P, 19th August 1997 Unpublished Project Report PR/SE/459/98

MELLOR, A, (2000). Analysis of head impacts during motorcycle accidents (2000). . Presented at Conference for Medical and Engineering Aspects of Dynamic Head and Neck Injuries, Cranfield University and Cranfield Impact centre, October 2000.

NEALE, M (1999). Report on a Scientific Mission to the Institut de Mecanique des Fluides (IMF), Strasbourg, France.. TRL unpublished Project Report PR/SE/585/99.

WILLINGER,R, BAUMGARTNER, D, CHINN, BP, NEALE, M (2000). Head tolerance limits derived from numerical replication of real world accidents. Paper presented at IRCOBI, 2000

WILLINGER, R, BAUMGARTNER, D, CHINN, B, SCHULLER, E (2001) New dummy head prototype: development, validation and injury criteria. International J. of Crashworthiness, 2001, v6. n3., p281-93

CHAPTER 14. MEDICAL TERMINOLOGY

Scalp (The hair bearing part of the coverings of the skull)

Abrasions. Areas of incomplete loss of skin caused by friction. Abrasions vary from the most superficial where the keratinised layer of the skin is removed, to deeper abrasions where deeper, vascular parts of the epidermis are damaged.

Abrasions may cover areas of the surface of the body and may be linear, as in superficial scratches.

Lacerations. The integrity of the skin is broken by a sufficiently sharp object. A sharp object such as a knife or metal projection may cause a clean cut. Lacerations may also occur when the skin is torn across a blunt object. Sharp and blunt lacerations with differing causes have differing healing properties.

Contusions. Contusions or bruises occur when the scalp strikes an object which compresses the tissues, causing damage to small blood vessels and other tissue components. Contusions may occur independently or with abrasions or lacerations. Contusions may occur at the edges of sharp lacerations or involve areas in which abrasions or lacerations have occurred. Very recent contusions may show only localised swelling and pallor of the tissues before much blood has leaked from small vessels. Contusions become blue bruises when blood has leaked into the tissues and, as days pass, haemoglobin is changed to substances with a greenish or brownish colour. Most bruises disappear completely but some leave discoloured areas when pigments remain.

Flap Wounds. When the continuity of the scalp is broken and undermined, the tissues can be raised as a flap. The construction of the scalp makes it possible for the entire scalp to be raised from the skull. At its extreme, the entire hair bearing scalp can be separated from the skull as lacerations may penetrate through all layers of the scalp and interactions with objects may cause the scalp to be torn from surrounding tissues.

Avulsion. In flap wounds, there is retention of some continuity with the skin of the face or neck. In avulsion a portion of the scalp may be completely separated from the body leaving areas completely uncovered.

Burns. Burns may occur in traffic injuries. Burns may be very superficial when the high temperature exposure has been short. If only the outer layers of the skin have been damaged there may be regeneration of the outer layers of the skin from the surviving deeper, intact tissue. Full thickness burns of the scalp occur most frequently in fatal situations and may be accompanied by burning of the skull and intracranial haemorrhages.

General Considerations of Scalp Wounds

Information may be obtained from scalp wounds about the direction and severity of the injuring forces by observing trends in linear wounds or abrasions and the retention of small fragments of tissue which show the relative direction of travel between the scalp and the injuring object.

Dimensions and patterns of surface wounds may allow assessment of the injuring objects as imprints or approximate imprints may be found on the surface of body.

Severe haemorrhage may occur because of the amount of blood which passes through the scalp's blood vessels and also because of the anatomical arrangement which prevents retraction and closure of scalp blood vessels.

Depths of scalp wounds may give information about the object which has caused the injury.

Face

The face is divisible into the following components:

The forehead - between the hairline and the eyebrows; eyelids, upper and lower; nose; upper and lower lips, maxillary and mandibular regions

Injuries which have been described for the scalp also occur in the face.

Ears

Anatomically, the external ear, tympanic membrane, the middle ear, the auditory ossicles, and the inner ear. (Also discussed under skull and cranial nerves).

External Ears. The injuries described under scalp occur. External ears may be torn, penetrated or avulsed.

Tympanic Membranes. These may be damaged by penetrating wounds or by pressure effects in impacts which cause occlusion of the external auditory meatus. Baro-trauma may cause rupture, in extreme situations.

Auditory Ossicles. May be dislocated in baro-trauma or penetrating injuries.

Neck

The larynx and trachea may be damaged by direct contact and the laryngeal skeleton may be fractured or distorted. Penetration of the larynx and trachea may occur with penetrating wounds or deep lacerations.

Major blood vessels in the neck are vulnerable in penetrating or deep lacerating wounds. The external carotid artery and its facial branches are particularly vulnerable and may cause severe external haemorrhage. The jugular veins and the common and internal carotid arteries may be penetrated or severed, usually in fatal cases as the haemorrhage from these veins and arteries is so severe that death may occur from blood loss as well as from interruption of blood flow to the brain.

Eyes

Cornea. Abrasions of variable depths may occur as contact injuries.

Penetration of the cornea may allow fluid from the anterior chamber to escape or allow structures such as the iris to pass through the cornea.

Foreign bodies and fragments generated in accidents may become embedded in the cornea or pass through the cornea into the chambers of the eye.

Conjunctival Sac. This is the space behind the eyelids which allows movement of the eyes. Material may enter the conjunctival sac, such as glass, fabric fragments or road dirt.

The conjunctival sac may be damaged by abrasions or penetrating wounds. Penetrating, long objects may pass into the orbit and may penetrate into the cranial cavity and the brain.

Globe. Non-penetrating injuries occur as the globe is distorted and bruised. These injuries may damage structures within the eye. Penetrating wounds allow loss of intra-ocular fluids and tissue.

Haemorrhages into the components of the eye may occur in conjunction with non-penetrating or penetrating injuries. Haemorrhage into the anterior chamber is often visible without special apparatus whereas haemorrhage into the posterior chamber of the eye may only be detectable with special equipment.

Retinal and choroid haemorrhages, with any of the above injuries, cause damage to the retina and nerve networks of the retina and damage vision. Retinal haemorrhages may also occur when severe acceleration influences and pressure imbalances have been generated through impact conditions or compression of major vessels such as cervical vessels.

Scleral Haemorrhages re haemorrhages in the firm outer layer of the globe, beneath the conjunctiva. These may result from compression or contusional injuries and may exist with or without haemorrhages in other parts of the eye.

Retro-orbital Haemorrhages are haemorrhages behind the globe of the eye, usually associated with the optic nerve and extra-ocular muscles. Haemorrhages in this area may be in continuity with haemorrhages around the optic nerve within the skull. They are caused by compression forces affecting the eye and also occur in association with distortion and/or fracturing of the walls of the orbit.

Optic Nerve may be injured through penetrating trauma or in fractures of the skull where bone fragments penetrate the coverings of the nerve and sever it completely or incompletely.

Mouth

Lips. Injuries can be of any of the types mentioned under scalp. Penetration of the lips may, however, be from within due to protrusion of teeth through to the lips.

Tearing of the angles of the mouth may occur with extreme distortion of the face in frictional and penetrating types of wounds.

Teeth. Teeth may be lost through injuring forces applied either directly to the teeth or through the lips or gums. From upper right and left three, backwards, tooth loss is often associated with maxillary fractures. From lower right and left three, backwards, tooth damage may be associated with fractures of the mandible.

Fracturing of teeth may occur where part or all of the crown may be separated from the root usually with direct trauma.

Tongue. The tongue may be bruised or lacerated through crushing between the teeth, through penetrating injuries or in association with fractures of the mandible, maxillae or palatal bones.

Skull

Subgaleal Haemorrhage. The galea aponeurotica is a firm sheet of tissue which covers the greater part of the outer surface of the vault of the skull. Haemorrhage may occur beneath this sheet of tissue and elevate it to a greater or lesser extent. These haemorrhages may occur with or without skull fractures.

Burns of the skull occur, with extreme heat, which may be transmitted through the skull to the underlying tissues. Large or small extradural haemorrhages may occur, with skull burns, without there being any skull fracture and without preceding impact.

Distortion. The skull is not rigid. The bones of the skull are joined together by suture lines which, in the very young, may be membranous, incomplete junctions, capable of considerable displacement. After 20 years all of the junctional areas are usually completely ossified so that distortion occurs by bending of bones rather than bending of bones with movement at the or suture lines. Distortion of the skull and displacement of skull bones may occur to a considerable extent before fractures occur. Distortion of the skull through impact in particular areas e.g. the back or the sides of the head, may cause characteristic patterns and types of fractures. Skull distortion may also cause transient cerebral, cerebellar or brain stem distortion.

Skull Fractures. The vault of the skull is the rounded upper part of the skull extending from the eyebrows to the junction of scalp and neck at the back of the head and from one ear to the other. This rounded vault comprises of frontal, parietal, squamous occipital and squamous temporal bones. The frontal, parietal and occipital bones have more distinct outer and inner tables or layers than do the temporal bones. The outer and inner tables are firm sheets of bone connected by a spongy layer of bone which contains blood vessels and bone marrow.

The architecture of the vault of the skull is complex, there being broader, stronger areas over the forehead, at the outer limits of the forehead, and at the occiput.

The base of the skull comprises the petrous temporal bones, the sphenoid and the basi-occiput. These strong bones form the floor of the cranial cavity and the foramen magnum, the large hole which allows the brain stem and upper spinal cord to be in continuity. The under aspect articulates with the spinal column and the bones at the base of the skull have channels in them through which the carotid arteries enter and jugular veins leave the skull. There are also numerous holes or foramina through which cranial nerves pass to the nose, eyes and orbit, face, mouth and the tissues around the skull. Some of these foramina may be involved in fractures of the base of the skull.

Orbit. The orbit comprises of a floor a roof and walls. The floor lies above the maxillae and the maxillary sinuses. The roof is also the floor of the anterior fossa of the skull. The bones of the orbital walls are very fragile and of egg shell thickness in places. Within the cavity of the orbit there are structures which attach and support the eyes and there is a small circular space which forms a pulley or trochlea for one of the muscles which move the eye. It is rarely directly affected in injuries but may be implicated in fractures.

The ethmoid and sphenoid air sinuses lie centrally in the anterior parts of the skull. They have very thin walls and are liable to fracturing in association with skull distortion or fractures of other parts of the skull. The ethmoid bone has small

channels which allow the olfactory nerves to pass through from the nasal cavity to the intracranial cavity.

The maxillae are the bones of the cheeks. These have firm parts and also very thin parts. They contain large air sinuses which communicate, as do frontal, ethmoidal and sphenoidal air sinuses, with the nasal spaces. The maxillae may also be affected by penetrating injuries, there being insufficient firm bone to deflect impinging objects.

Nose. The bones of the nose form the upper parts of the external contours of the nose while the lower parts are formed from thick plates of cartilage. Fractures of the nasal bones occur from direct trauma and rarely follow indirect injuries.

Mandible. The mandible comprises an upper condyle and ramus as well as a body, on each side. The bodies join together in the mid line at the chin at the symphysis. This is a firm, bony union in older people but may be more membranous in the very young. It is possible to separate the two halves of the mandible, by direct trauma, at the symphysis. Fracture of the body and ramus may occur on one side or on both sides. These generally result from direct trauma or impact to the mandible. Forces generated at the joint between the mandible and temporal bone, may cause base of skull fractures.

Facial Fractures. These are classified by the La Fort classification and its updates.

Types of Fractures

Impact site fractures occur when a concentrated force is applied to a vulnerable area. A blow to the face, mandible, or the vault of the skull may cause fractures at the point of impact. Over the vault of the skull, impact fractures may cause fracturing and displacement of bone fragments, pressing them towards the brain. These are depressed fractures. Some impacting objects may pass through the skull and cause penetrating injuries.

Transmitted force fractures occur when the fractures are at a site other than the position of a main impact. A severe impact on the back of the head may cause a fracture from the foramen magnum running into the occipital bone but not necessarily reaching the impact site. Some fractures of the base of the skull may be transmitted from the mandible upwards into the skull. A single impact may be responsible for a particular pattern of fractures to the vault of the skull and the base of the skull. Fractures may occur when these have been multiple impacts and elucidation of patterns of skull damage is difficult in these circumstances.

Growing fractures - fractures which increase in size - usually in children - are usually linear fractures of the vault of the skull. They may be associated with extradural haemorrhages and/or subgaleal haemorrhages.

Crush injuries of the skull cause distortion of the vault and base of the skull without necessarily damaging the intracranial contents. Where the crushing is insufficient to damage the intracranial contents, multiple fractures of the vault and base may occur with damage to cranial nerves.

Suture Diastasis (sprung suture). This is the term used to describe the separation of the bones of the skull, usually over the vault of the skull, in people (usually below the age of twenty) who have had severe skull distortion with or without fracturing of other sites. Suture diastasis is a form of fracture in that continuity or security of

the joints is lost. It implies severe distortion. In some situations the diastasis of the sutures leaves the bones in their normal anatomical position.

Closed fractures are fractures in which the bones are fractured but the scalp and other coverings remain intact.

Complicated fractures may involve several bones or involve numerous skull foramina. One particular type is the “hinge fracture” which passes from side to side across the base of the skull. This separation and loss of integrity can usually be more readily appreciated at post mortem when the front and the back halves of the base of the skull can be seen to move independently, as if hinged.

In comminuted fractures, there are numerous fragments of bone. This usually occurs in vault fractures and facial fractures and occasionally involves mandibular regions and other bones.

Compound fractures are in continuity with the outer surfaces of the body either through a scalp defect overlying a vault fracture or a base of skull fracture in communication with the nasal cavity, middle ear or air sinuses. These fractures are liable to infection as bacteria can enter the damaged tissue. Compound fractures may also allow cerebro-spinal fluid to pass out of the skull when the dura mater, lining the skull, is also torn.

Linear fractures more or less run in straight lines across bones such as the bones of the vault of the skull or the maxillae.

Depressed fractures have been mentioned above where the outer and/or inner tables are fractured and the fragments are pressed downwards towards the brain.

Pneumocephalus occurs when fractures pass through the sinuses or middle ear and allow air to enter through torn dura. Air enters the cranial cavity only in compound fractures.

Age Relationships. In the very young, the bones of all parts of the skull are softer and more compliant and the joints are less secure. During childhood the amount of bone increases in the developing skull components and the joints between the bones gradually close until, around the age of twenty, all of the sutures and junctions between the bones are united. In the younger ages when the bones are more compliant and have less substance to them, distortion is easier to induce and fractures are less easy to induce. In later years the reverse is true but distortion is still a major feature in the causation of intracranial and skull damage.

Intracranial haemorrhages

Extradural Haemorrhages are important because of the positions in which they form and their volumes. The largest extradural haemorrhages are around 300 ml, is usually fatal. Quantities of less than 25mls produce mild or no symptoms while volumes between 25 and 50 mls usually produce signs of distortion and compression of the brain.

Volumes between 75 and 100 mls produce symptoms and are life threatening.

Extradural haemorrhages accumulate between the skull and the dura. The dura mater is a firm sheet of tissue closely applied to the inner aspect of the skull and intimately associated with the periosteum of the skull. The skull is supplied with arterial blood, externally, from arteries in the scalp and face but, internally, it is supplied with blood through the middle meningeal artery. Extradural means

outside the dura and that means between the dura and the skull. A characteristic of this type of haematoma is that it is confined by the dura and its attachments to the skull at the junctions between the skull bones. The rates of accumulation of blood in the haematomas is variable. Some extradural haematomas accumulate very slowly while others appear to accumulate very rapidly. Some information is available on some haemorrhages through sequential x-ray studies. Information based on the progression of clinical signs may suggest that a haematoma has accumulated slowly but it is possible, in some cases, that the changes in brain function may have come on slowly, although the haematoma could have developed rapidly.

Acute Extradural Haemorrhages. The sites of formation of acute extradural haemorrhages usually relate to the position of branches of the middle meningeal artery. These enter the skull deep in the temporal region and pass upwards across the side of the head, spreading outwards in principal anterior and posterior branches. This artery is very thin walled and lies in a narrow channel on the inner aspect of the skull after it has passed through a small foramen at the base of the skull. Either at the foramen or the inner aspect of the skull, the artery is vulnerable if the bone is fractured. The artery can be torn across at the position of a fracture. Distortion of the bed of the artery, without fracturing, may occur and an extradural haemorrhage can accumulate without a fracture having occurred.

Burns related extradural haemorrhages have been noted above.

Abnormalities of blood coagulation may predispose to extradural haemorrhages if small branches of the vessels are torn across and coagulation does not occur to seal these vessels.

Torn veins or sinuses rarely cause extradural haemorrhage.

Chronic Extradural Haemorrhages are extremely rare but result from the accumulation of extradural blood in situations where the distortion of the underlying brain does not cause symptoms. Chronic extradural haemorrhages usually become walled off by tissue reactions it and may continue to occupy a small amount of space within the skull for many years or permanently.

Extradural haemorrhages may occur at the same time as acute subdural haemorrhages and subarachnoid haemorrhages where the cerebral distortion caused by the head injury mechanism is sufficiently severe. Many extradural haemorrhages, however, occur without damage to underlying structures, thereby giving the possibility of complete recovery without any sequelae after surgical removal of an extradural haemorrhage.

Subdural Haemorrhages occur on the deep or brainward aspect of the dura. The dura mater need not be damaged at all. Blood accumulating in the subdural space does not have the anatomical confines that an extradural haemorrhage has and the blood may flow over entire surfaces of the cerebral hemispheres.

Subdural haemorrhages are acute if they are less than 3 days old, subacute between 3 and 21 days or chronic if they have been present for at least 21 days.

Subdural haemorrhages are caused by the passage of blood into the subdural space. Bridging veins pass between the cerebral surface and the collecting venous sinuses of the skull. Over the upper part of the head, in the mid line, running from front to back, is the sagittal sinus which collects thin walled bridging veins from the

surface of the brain. There are also bridging veins between vessels on the surfaces of the temporal lobes and the lateral sinuses which run around the margins of the tentorium. Movement of the brain within the skull is thought to stretch the bridging veins which, because of their thin walls, are liable to be torn or ruptured. Bridging vein rupture occurs in head injuries where the brain movement is most likely to occur.

When a cerebral contusion occurs with disruption of surface blood vessels, blood may flow into the subdural space to cause a subdural haematoma.

Penetrating injuries may damage cerebral surface vessels and cause bleeding into the subdural space.

Cerebral arterial aneurysms may rupture and cause not only a subarachnoid haemorrhage but also a subdural haemorrhage if the jet of blood from the damaged aneurysm bursts through the arachnoid.

Age relationships in subdural haemorrhages are important. In the very young they occur through skull distortion and may also occur in non-impact situations such as the shaken baby syndrome. Where cerebral atrophy has occurred as an ageing or disease process, the increased intracranial fluid volume is thought to allow greater movement of the brain within the skull and rupture of stretched veins.

Intracerebral Haemorrhages are usually considered to be the result of impact injury to vessels of varying sizes within the substance of the brain. Tiny haemorrhages occur with the rupture of very small vessels in several parts of the brain but intracerebral haemorrhage or haematomas occur more commonly in the central white matter of the cerebral hemispheres or in relation to the components of the basal ganglia. It is presumed that medium sized blood vessels are damaged to allow the escape of a volume of blood sufficient to cause deep, small haematomas. Sometimes the haematomas are sufficiently large to be fatal or potentially fatal.

Acute, delayed haematomas arise several days after the impact and after early CT scans or other imaging may have shown no haemorrhage to have been present.

Intraventricular Haemorrhage. Blood entering the spaces within the brain - ventricles - is very common. Small amounts can be seen in imaging techniques to be mixed with the cerebro-spinal fluid. In some situations, the amount of blood within the ventricles is very large and may obstruct the passage of fluid from the cerebral hemispheres to the exit foraminae of the fourth ventricle. This may cause acute hydrocephalus by enlargement of the ventricular system through the accumulation of blood and cerebro-spinal fluid which cannot be released.

Structures within the ventricles and in their walls may be damaged, as impact phenomena, and allow bleeding of variable amounts into the ventricular system.

Ventricular angle rupture occurs at the angular parts of the bodies and temporal horns of the ventricles. This can be more easily appreciated in the lateral ventricles where the ventricular wall ruptures below the corpus callosum at the outer angle of the lateral ventricle. This may occur in a single focus or along the entire undersurface of the corpus callosum. Small amounts of blood may leak for a short time into the ventricles. The tissue damage at the ventricular angles may amount to disruption of the ependyma in a small focus or damage extending in to the cerebral substance causing rupture of the wall of the ventricle rather than just

an angle rupture. More extensive dissection into the components of the basal ganglia has been seen in severe head injuries.

The septum lucidum separates the lateral ventricles. This thin, transparent sheet, which has small blood vessels running in it, is attached to the undersurface of the corpus callosum in the mid line. The fornix bundles are attached to the lower aspect of the septum lucidum. Varying degrees of rupture of the septum lucidum occur as well as varying degrees of dislocation of the septum from the under aspect of the corpus callosum. The fornix bundles may also be separated from the septum lucidum or may be ruptured in severe cases. These injuries can cause haemorrhage into the ventricular system.

Subarachnoid Haemorrhage. The arachnoid is a very thin membrane which closely covers the surfaces of the brain. It is kept apart from the brain by cerebro-spinal fluid and the fluid is contained within a space which has a fine, spiders web-like attachments to the surface of the brain - hence the name arachnoid membrane. Beneath the arachnoid, the brain is covered by a thin limiting sheet of tissue, the pia mater. Pia means weak or soft in distinction to the dura mater lining the skull which is tough and hard.

Usually any bleeding from vessels on the surface of the brain will be contained by the arachnoid. If there is a contusion of the surface of the brain which damages the small blood vessels, subarachnoid haemorrhage may be found around the area of the contusion.

Subarachnoid haemorrhage is extremely common in head injuries of all magnitudes, usually over the convex surfaces of the cerebral hemispheres and may relate to impact sites and reflection sites of pressure waves from the opposite side of the brain. This pattern of distribution of subarachnoid haemorrhages may be the result of a mechanism usually described as coup and contre-coup in which damage may occur at the impact site and diametrically opposite.

Major blood vessel damage may also cause subarachnoid haemorrhage either through rupture of single vessels or numerous vessels through head injury mechanisms or penetrating injury mechanisms.

Arterial aneurysm rupture can cause subarachnoid haemorrhage. Occasionally an aneurysm ruptures in relationship to trauma but the exact timing and relationship may be difficult to prove. It is thought that shock pressure waves may rupture these vessels.

Contusions are haemorrhagic areas either on the surface of the brain or close beneath the surface of the brain.

Contusions vary from a millimetre in diameter up to several centimetres in diameter. The radial dimensions of damaged areas vary. Some are limited to part of the thickness of the cerebral cortex. Some are limited to the white matter beneath the cortex. Some involve the cerebral cortex from its pial surface through its full thickness into the subjacent white matter. It is assumed, that the area and depth of the contusion is a measure of its severity and may relate to the severity of the injuring forces. The volume of damaged tissue cannot be measured accurately.

The contusion index was devised to give some measure in simple, practical terms, of the severity of the contusions.

Contusions are caused by bleeding which may be continuous for at least a number of hours after an impact so that a contusion may develop into a significant mass of damaged brain and blood clot.

Spatial effects of impacts are difficult to ascertain. An impact to one side of the head may be associated with contusions on that side or the other. An impact to one side of the head may be associated with damage to both sides of the brain. This is the concept of coup and contre-coup injuries but the relationships are, as already stated, usually very difficult to substantiate. Blows to all parts of the head are most likely to cause contusions over the frontal poles, the orbital surfaces, the temporal poles and the lateral aspects of the temporal lobes. Contusions rarely occur in the occipital regions.

Fracture contusions lie immediately beneath the fractures and may be limited and circumscribed to the area beneath a fracture either of a linear, depressed or comminuted type.

Tentorial contusions occur where the temporal lobes and the tentorium collide. Small haemorrhagic zones are found along this line on one or other side. These contusions may occur because the brain is forced against the tentorium or, if skull distortion occurs, the components of the tentorium being stretched, thereby contacting the under aspects of the temporal lobes.

Falcine contusions occur on the medial aspects of the cerebral hemispheres - usually only on one side - the mechanism for these is thought to be similar to that of the tentorial contusion where the brain may be forced against the sharp margin of the tentorium or where distortion of the skull causes the sharp margin of the falx to become stretched.

Herniation contusions occur at the foramen magnum and at the tentorial incisura when the cerebellum may be forced against the margins of these structures.

(Tentorial and falcine contusions as well as herniation contusions may be difficult to separate from the consequences of the raised intracranial pressure causing cerebral herniation or cerebellar herniation). They can, however, be distinguished when these contusions are present in the absence of brain swelling.

Gliding contusions are haemorrhages i.e. haemorrhages within the substance of the brain - usually white matter - at the supero medial angles of the hemispheres, in one hemisphere or both, usually in the anterior two thirds of the hemispheres. They may be related to brain movement and stretching of penetrating vessels.

Supracallosal Dissection. Above the corpus callosum and between it and the cingulate cortex and cingulum, small tears occur. This implies movement between the corpus callosum and the tissues above it. This dissection may be on one side or the other and be of variable severity.

Axonal Injuries. Axons are very narrow tubes which pass from the cell bodies of neurones for variable distances to synapse with other neurones or other structures. Many axons in the white matter are surrounded by a layer of myelin - a complex lipid. These structures - axons and myelin can readily be damaged.

Shear strains and tensile strains as well as localised anatomical features and pressure forces may damage these axons. The physical forces are established during accelerations which may be either linear or angular. Accelerations occur with the increase or decrease of velocity.

Numerous terms have been applied to the damage to axons which occurs in head injuries.

The term diffuse axonal injury was coined in Edinburgh in 1963 for injuries to axons which occur through accelerations.

The term became associated with the diffuse axonal injury syndrome in which an individual is rendered unconscious from the moment of the head injury and remain so until death. Macroscopic features in the brain were haemorrhages or tears in the corpus callosum and haemorrhagic lesions in the dorso-lateral quadrants of the upper pons and the mid brain. These injuries may occur without contusions or other injuries elsewhere in the brain. Microscopically, in such individuals, axonal disruption would be identifiable in many parts of the brain but, most notably, in the corpus callosum, medial lemnisci, cerebral peduncles and the white matter of the cerebral hemispheres.

The term diffuse axonal injury is now being used in its original sense without the clinical syndrome being complete. It is used to describe varying amounts of axonal damage.

Axonal injuries in the cerebral white matter is frequent in subcortical white matter of the medial parts of the hemispheres, the deep central white matter, the forceps minor and forceps major, the corona radiata, the capsules (internal, external and extreme), the cingulum, the corpus callosum, the commissures, the major intracerebral axonal bundles, the white matter overlying the hippocampi and the fornix system. Brain stem lesions are found in the dorso lateral quadrants of the pons and mid brain, the medial lemnisci, the medial longitudinal fasciculi, the peduncles - cerebral and cerebellar. In the cerebellum axonal injuries are found in the central white matter and in the cerebellar peduncles.

In the spinal cord, axonal injuries are found in relation to distortion and contusion and in degeneration of long tracts.

Diffuse Vascular Injury is the term applied to the disruption of continuity and alteration of the physiological properties of blood vessels throughout the cerebral hemispheres. This term was also coined in Edinburgh in 1963 when effects of acceleration were being considered. It is revealed by small haemorrhages in many situations and in the presence of the brain swelling through altered vascular properties. Small haemorrhages may be found in the cerebral cortex, in the absence of contusions, in the white matter, corpus callosum, basal ganglia and periaqueductal grey matter. In the brain stem, small haemorrhages are to be found in the tegmentum of the pons and mid brain and, to a lesser extent, in the white matter of structures such as the basis pontis. Small haemorrhages may also be found in the parts of the cerebellum and spinal cord without obvious anatomical localisation.

Microscopic Phenomena in Diffuse Vascular and Diffuse Axonal Injury. Axonal retraction balls or regeneration buds occur at the ends of the severed or broken axons. The axonal cytoplasm forms a ball, bud or bulb which can be displayed by a variety of microscopic and immunocytochemical techniques. Varicose axons also occur where the normal regular cylindrical outlines of the axons are lost.

Microglial clusters occur in the white matter in positions in which the vascular and axonal injuries occur. These are clusters of phagocytic cells which remove damaged tissue.

Long tract degeneration occurs when major tracts and groups of nerve cells have been damaged. The axons arising from these areas degenerate and can be shown to be degenerate by a variety of techniques. The techniques which are used include routine histological staining, silver impregnation of the membranes of axons, methods to show myelin degradation, immunocytochemistry of the surfaces and contents of axons, and immunocytochemistry for the reactive cells such as microglia.

Secondary or sequential events

Subdural hygroma (meningitis serosa traumatica, traumatic subdural effusion): is the accumulation of fluid within loculi over the surfaces of the cerebral hemispheres which may be in communication with the cerebro-spinal fluid in the subarachnoid space or may be external to the arachnoid. The causes may be different in the two instances. Where there is no communication with the subarachnoid space, the cerebro-spinal fluid in the hygroma may have originated in a subdural haematoma, the blood having been removed and fluid being left within the membrane which bounded the haematoma.

Infections: Organisms may be introduced to the interior of the skull in penetrating injuries, attached to the penetrating object. These may cause bacterial infection in any of the compartments within the skull, including within the brain (cerebritis). Organisms may also enter through compound fractures.

Bacteria may cause meningitis, infection of the coverings of the brain. Infection may involve the subdural space and pass to the subarachnoid space. When the infection is limited to the subdural space an accumulation of pus can arise, an empyaema.

An abscess can form when bacteria form a localised infection which is then circumscribed by tissue reaction. Abscesses can follow penetrating injuries or arise from infections in surrounding spaces such as a middle ear infection or infection of the paranasal sinuses.

Common bacteria involved in producing infections within the skull after head injuries include pneumococcae, staphylococcae, streptococcae, diphtheroids, E.coli, coliforms and, more rarely, clostridia. Clostridia may produce gas and compound the effects of infection by “gas gangrene” effects.

Brain swelling may be localised, diffuse or a combination of both.

The causes of brain swelling are a combination of damage to small blood vessels and damage to the tissues. Loss of the balanced fluid circulation from and to small blood vessels allows the accumulation of fluid within the brain. Alteration of the cells of the brain allows accumulation of intracellular fluid.

Oedema is the term used to describe the accumulation of extracellular fluid. Only a small proportion of post traumatic brain swelling is caused by extracellular fluid.

Brain swelling is the favoured term which implies that the swelling is not entirely extracellular fluid.

Brain swelling occurs after any type of head injury and may be localised to an injured area such as around a contusion. It may also diffusely affect a part of a hemisphere, a whole hemisphere or both hemispheres. The amount of force

required to generate brain swelling is small. It may become seriously life-threatening even after minor injuries such as simple falls. Brain swelling remains a major contributor to secondary brain damage and death.

Consequences of brain swelling.

As brain swelling increases, cerebro-spinal fluid is forced out of the subarachnoid space and out of the ventricles. The volume of the brain increases and, progressively, the pressure within the skull increases. Increasing pressure opposes the arterial pressure in supplying blood to the brain and also interferes with the outflow of venous blood.

Cerebral perfusion pressure is the difference between the mean arterial pressure and the intracranial pressure. As the perfusion pressure is reduced by brain swelling, the point may be reached when the cerebral circulation is critically impaired or may cease. As these points are reached the cerebral tissues have impairment of their oxygen and nutrient supplies with consequences of tissue damage contributing further to the brain swelling.

Cerebral herniations. The brain is contained within compartments in the skull. There are right and left supratentorial compartments, separated in the midline by the falx. The tentorium separates the posterior fossa from the supratentorial compartments. The tentorium is attached to the petrous temporal bones and the squamous occipital bone. It forms a tough diaphragm of tissue which has limited freedom to move in its central parts. Components of the tentorium become taut and rigid when stretched. The gap in the tentorium allows the midbrain to continue into the pons. The upper and medial parts of the cerebellum lie below this gap and the medial part of the temporal lobe lie above the gap in the tentorium. The free margin of the falx lies between the cerebral hemispheres in a variable relationship to the upper surface of the corpus callosum and the cingulate gyri.

The foramen magnum is the round hole at the bottom of the skull which allows the brain stem and spinal cord to be in continuity.

The falx, tentorium and foramen magnum are the major structures which figure in discussion of cerebral and cerebellar herniation.

Symmetrical swelling of the cerebral hemispheres causes them to push the tentorium downwards onto the upper surface of the cerebellum. This deforms and flattens the upper surfaces of the cerebellum.

Tentorial herniation occurs when the medial parts of the temporal lobes are forced across the unyielding structures in the medial parts of the tentorium. This herniation may occur on one side or on both sides. Herniation produces grooves on these structures and, if displacement and pressure is sufficiently great, necrosis of tissue will occur in and around the grooves.

Blood vessels are trapped across this margin and, in particular, the posterior cerebral vessels may be occluded.

Medial occipital infarction (death of tissue through failure of circulation) occurs either on one side or both when the swelling of the hemispheres causes tentorial herniation and compression of the posterior cerebral blood vessels. The visual cortex is compromised.

Sub-falcine herniation occurs when brain swelling is asymmetrical. The more swollen cerebral hemisphere may be forced through the gap below the falx and a groove or indentation has formed on the surface of the brain where it has been in contact with the free margin of the falx. Again this may cause necrosis in and adjacent to the groove and may compromise blood vessels to the extent that infarction may follow e.g. compression of supracallosal branches of the anterior cerebral artery may cause infarction on the medial parts of the hemispheres.

Reversed tentorial herniation occurs when swelling or increase in volume of the cerebellum (perhaps through a haematoma or abscess) causes the cerebellum to be forced upwards through the tentorial gap. This causes deep grooving of the upper surfaces of the cerebellum and localised tissue necrosis as branches of cerebellar vessels are compressed.

Foramen magnum herniation (foraminal impaction, tonsillar herniation, coning): occurs when the pressure within the skull is sufficient to force tissue out of the largest available foramen. The foramen magnum has smooth margins which cause indentations on the parts of the cerebellum forced down through the gap (the tonsils). As swelling progresses the cerebellum is forced against the brain stem and the cerebellar tonsils are increasingly closely applied to the medulla. As time and pressure continue the herniated tissue may become necrotic and haemorrhagic and the brain stem may be so compressed that death occurs.

Brain stem distortion occurs through the downward displacement of the brain stem and cerebellum. The lower medulla and upper cervical spinal cord are displaced and deformed into a shallow "S" bend which, along with the compression from the cerebellar tonsils, is a cause of death.

Impairment of cerebral circulation: Blood flow into the brain may be compromised by extracranial events such as reduction of blood pressure after haemorrhage or the results of cardiac trauma. The carotid arteries in the neck may be compressed during accidents by external features such as components of vehicles, abnormal positions of unconscious subjects or the effects of impingement against safety equipment.

Carotid artery dissection is a condition in which the layers of the walls of the vessels are split and blood passes from the normal channel within the artery into the wall of the artery. This causes the flow of blood in the artery to be reduced or completely interrupted.

Thrombosis or clotting within these vessels may occur after the vessel wall has been injured in a compressive incident.

Intracranial, arterial wall dissection occurs, rarely, and may be related to a traumatic event. A proportion of cases with this feature have a pre-existing disorder of the structure of the vessel walls.

Arterial territories are supplied by individual major arteries. The anterior cerebral arteries supply parts of the under surfaces (orbital surfaces) of the frontal lobes, the anterior and lower parts of the frontal poles and the medial aspects of both cerebral hemispheres. They also supply a narrow strip along the most medial parts of the convex aspects of both hemispheres.

The middle cerebral arteries supply the greater parts of the lateral aspects of both cerebral hemispheres and anterior and medial parts of the temporal lobes including

the anterior parts of the hippocampi. The posterior cerebral arteries supply the posterior parts of the medial aspects of the cerebral hemispheres including the visual cortex.

The cerebellum is supplied by superior cerebellar arteries on its upper surface and by the anterior and posterior, inferior cerebellar arteries on its lower surface.

The brain stem and upper cervical cord are supplied by the vertebral and basilar arteries and their branches.

The arterial supply to the intracranial structures is often divided into anterior and posterior circulations. The anterior circulation is supplied by the internal carotid arteries to the anterior and middle cerebral arteries. The posterior circulation is the territory of the posterior cerebral arteries and the circulation of the cerebellum and brain stem.

The Circle of Willis is a ring of blood vessels at the base of the brain which joins the posterior and anterior circulations. Communicating arteries run between the posterior cerebral arteries and the upper limits of the internal carotid arteries. An anterior communicating artery joins the two anterior cerebral arteries. The basilar artery and its division to form the two posterior cerebral arteries completes the circle. The communicating arteries are variable in diameter and may be absent in any part of the circle. This means that the circle is not always available to distribute blood evenly from supplying arteries or to redistribute blood after a major artery has been compressed or occluded by thrombosis or compression.

Infarction of arterial territories occurs when a major artery or a major branch within that territory is occluded by thrombosis, compression or other events.

Boundary zones: The arterial territories of the brain, brain stem and cerebellum are well defined. There is little flow from one territory to another so that, if a major artery is blocked, only fringes of that territory receive a supply from the adjacent arterial territories. The boundaries between the arterial territories are called boundary zones. It has been considered, perhaps erroneously, for many years, that the boundary zones are vulnerable areas which become damaged when the blood flow into the major arterial territories is reduced. If the blood flow into two adjacent arterial territories is reduced the tissues at the furthest ends of the arterial territories, in the boundary zones, are likely to have a reduced supply while areas closer to the origin of the artery retain a circulation. This theory of boundary zone damage or boundary zone ischaemia or boundary zone infarction has been used to explain damage which occurs in these territories after head injury, usually in association with brain swelling and increased intracranial pressure.

Neurocytotoxic damage has a similar distribution to boundary zone infarcts. Neurocytotoxic damage is a consequence of accumulation of toxic products or components of cells in these areas. There may be a combination of circumstances causing boundary zone damage in the neurocytotoxic and the ischaemic theories.

Causes of death from head injury - WHO classification

- ISD classification (to be completed)

Glasgow coma scale: This scale has been accepted in many centres as an easily used and reproducible method of assessing head injury. It is, of course, used in

conjunction with clinical experience. The Glasgow coma scale concentrates on three features in the unconscious patient, namely, eye opening, best motor response and best verbal response. Each component - E, M or V has several categories and each can be scored. The Glasgow coma scale is written as follows:-

Eye Opening:	Best Motor Response:	Best Verbal Response:
Spontaneous - 4	Obeys verbal commands - 6	Orientated - conversing - 5
To command - 3	Localises pain- 5	Disorientated - conversing- 4
To pain - 2	Flexion withdrawal- 4	Inappropriate words- 3
None - 1	Flexion decorticate- 3	Incomprehensible sounds- 2
	Extension decerebrate- 2	None- 1
	None - 1	

Whereas a patient who has no coma features will be E4, M6, V5 i.e. a total score of 15, a patient who is not responding in any way and may be moribund will have a total score of 3.

Spinal Injuries:

Neck Injuries: Neck injuries in association with spinal injuries may be abrasions, lacerations or contusions with or without associated damage to major blood vessels - lacerations, compressions, thrombosis and dissection. Skeletal muscle contusions and lacerations may also be present.

Brachial Plexus Injuries: The brachial plexus is the system of nerves which pass from the cervical spine to the arm and to some neck structures. In some accidents, more frequently in motor-cycling accidents, severe deformation of the shoulder region by an impact may damage the nerve roots either their dorsal, sensory components or ventral, motor components. These nerves may be damaged by direct trauma in association with impact against the neck but may be avulsed or pulled out of the spinal cord by the sudden, violent movement.

Less severe damage to these nerves may be seen in many autopsies in traffic situations and in other types of severe trauma where haemorrhage occurs into the nerves of the brachial plexus and into the dural pockets which surround the nerves as they pass out of the dura towards the arms.

Autonomic nerves may be damaged by focal injuries, most commonly the sympathetic chain and ganglia in the neck may be damaged by direct and local trauma.

Spinal cord damage may result from direct contusions in association with fractures of the spine, penetrating injuries or by damage to the major supplying blood vessels such as the D10 spinal artery. The spinal cord may be compressed when there is dislocation of the spine or dislocation of fragments of the spine.

Bruising or contusion of the cord may occur at the time of dislocation, transection of the cord may be incomplete or complete and may be caused by penetrating injuries or by dislocation of the spine.

Spinal cord injuries cause loss of sensation and loss of control of muscular activity. The patterns of disturbance of these functions depends on the level at which the spinal cord is injured and the parts of the spinal cord which are damaged.

Cauda equina injuries occur below the first lumbar vertebral body where the spinal nerve roots alone occupy the spinal cavity. Sensory loss may be similar to that which occurs in spinal cord damage but the motor nerve damage is comparable to that of peripheral nerve damage.

Syringomyelia may occur as a post traumatic phenomenon. A cavity develops within the spinal cord and enlarges, passing up and down the cord and interrupting axons. The exact clinical features depend on the particular anatomy of the damage.

Conditions increasing risk of Traffic Accidents

Sleep apnoea: This is a condition in which heavy snoring and interruption of normal breathing activity cause the subject to waken frequently at night thereby becoming sleep deprived. This causes the risk of sudden onset of periods of sleep, even while performing tasks such as driving vehicles.

Narcolepsy: Is a similar phenomenon in that individuals suddenly fall asleep while performing tasks. It may be related to sleep apnoea or have a different origin.

Alcohol: Alcohol consumption and its effects on driving performance, the security of pedestrians and in the causation of accidents, in general, is well described in many works.

Substance Abuse: The exposure of individuals to toxic substances may lead to altered perceptions of their abilities and competence.

Medication: Many drugs carry warnings about driving while taking these substances. Individuals should know this risk.

Previous Head Injuries: May alter perception or motor skills.

Seizure Disorders (Epilepsy): These conditions are subject to legislative restrictions on driving.

Mental Retardations: Mental retardation may increase a liability to pedestrian types of injuries or cycling injuries.

Psychiatric Disorders: Some are subject to legislative restrictions on driving.

Body Size: Abnormally small stature and slim build may increase the liability to risk of some types of injuries through driver positioning. Short stature may also increase risk of injuries from some types of safety equipment such as air bags.

Diabetes mellitus with hypoglycaemia or hyperglycaemic ketosis can be hazardous by causing failure of normal cerebral abilities or unconsciousness.

Clinical Conditions.

Concussion = commotio-cerebri. This is a temporary and reversible situation. The incident of trauma causes an immediate loss of consciousness.

Amnesias: Retrograde amnesia is a period of amnesia stretching back from the time of the injury for a variable period.

Post traumatic amnesia is a period of amnesia stretching forwards from the time of amnesia.

Peri-traumatic amnesia is a combination of retrograde and post traumatic amnesia.

Lucid Interval. This is period of time following an injury in which the individual may be conscious, may be talking, walking or performing tasks but following which unconsciousness ensues. A lucid interval may be of very short duration or of several hours. The implication is that after the injury the parts of the brains subserving the functions which were being performed had not been damaged. Subsequent interference with function usually follows distortion of the brain as a result of an accumulation of a intracranial haemorrhage such as extradural, subdural or intracerebral haemorrhages. Brain swelling may also develop to cause interference with function and cause unconsciousness.

Diffuse Axonal Injury Syndrome. In this situation the individual becomes unconscious from the moment of the injury and remains so until death. This implies damage to the cerebral white matter, the corpus callosum and to the upper brain stem. Other injuries may coexist with these.

Post Traumatic Dementia. The interference with normal cerebral functions including communicative functions and memory may follow primary or secondary cerebral damage, particularly if the hippocampi have become damaged.

Secondary Brain Damage. Among causes of secondary damage are raised intracranial pressure, brain swelling, ischaemia, arterial territory infarcts, boundary zone infarcts, hypoxia, meningitis and fat embolisation.

“Locked In” syndrome. This is a situation where the individual may appear to be unconscious or unable to respond. The failure to make any verbal or limb movement may result from an injury involving the descending motor pathways in the pons. The individuals may be fully aware and have little, if any, brain damage but are unable to indicate that they are aware of their surroundings except by movements such as eye movements.

Persistent Vegetative State. In this state the individual is immobile and, apparently, unconscious without appropriate movements with any part of the body, including eye muscles. The eyes may remain open for periods of time and random eye movements may occur. The individual requires to be fed by gastric intubation and requires constant nursing care. This is one of the outcomes of diffuse axonal injury.

Brain Stem Specific Injuries. Compression of the brain stem occurs, front-to-back as brain swelling forces the tentorium down on the cerebellum and swelling or displacement of the cerebellum presses the brain stem forward.

Lower brain stem distortion as the brain stem was pushed downwards by brain swelling the lower brain stem assumes a shallow “S” bend.

Kernohan lesions occur when asymmetrical tentorial herniation forces the upper brain stem to one side. The cerebral peduncle on the side away from the displacing herniation is pushed against the free margin of the tentorium which cuts into the cerebral peduncle. A consequence of this is compression of the descending axons

in the cerebral peduncles. The middle thirds of the peduncles contain the cortico-spinal tracts. These may be affected by compression, in which case loss of function is reversible, or it may be cut through with irreversible loss of the cortico-spinal fibres.

Ponto-medullary tears occur usually in association with fractures of the base of the skull. The pons and medulla become incompletely or completely separated from each other as a tear develops anteriorly, between the two structures. The tear is caused by the tissues pulling apart at this point either by bending of the brain stem or by the difference in consistency and direction of the principal components of the pons and medulla.

Ponto-mid brain tears occur above the pons. These are generally incomplete tears passing for a short distance into the medial parts of the cerebral peduncles above the basis pontis.

Miscellaneous Conditions.

Emboli are abnormal particles or fluid masses circulating in blood. Air may enter blood vessels through tears in vessel walls, most usually around the neck. Particulate material is less likely to enter the blood vessels in traffic situations. This may be introduced artificially during therapeutic procedures. Tissue fragments may, however, be liberated into the blood stream in massive injury situations. Fragments of bone marrow may circulate in this way and block blood vessels, usually in the lungs.

Fat emboli may enter the blood stream from damaged bones with fatty marrow but, in many cases in which fat is found, it may be that the large fat globules or masses derive from redistribution of normal components of the blood. This may be a basis for the diffuse intravascular coagulation syndrome.

In situations of severe trauma, brain emboli may enter major venous channels and reach other organs and tissues.

Hypothalamic and Pituitary Damage. Damage in this area may be direct through penetrating objects or as a result of complicated fractures of the sphenoid area.

Pituitary infarction may result from compression of the pituitary blood supply as a result of brain swelling. Raised intracranial pressure is associated with pituitary infarction.

Pituitary stalk damage may occur in direct trauma or may follow severely increased intracranial pressure. In either situation posterior lobe damage or malfunction may occur.

Respiratory Distress Syndrome. This is a condition of the lungs in which severe oedema occurs and in which a protein containing fluid is deposited on the walls of airways. The adult respiratory distress syndrome is microscopically similar to the respiratory distress syndrome of new born babies. The adult respiratory distress syndrome is associated with over transfusion.

Annex I. Members of the COST 327 Management Committee

SIGNATORY COUNTRIES

BELGIUM

Ir. Dirk BOSTEELS
 Institut Belge pour la Sécurité Routière
 Département véhicules et équipements
 Chaussée de Haecht 1405
 B-1130 BRUXELLES
 Tel : 32/2.244.1578
 Fax : 32/2.216.43.42

Mr Kris VAN DER PLAS
 HONDA Motor Europe Ltd
 Aalst Office
 Wijngaardveld, 1
 B-9300 AALST
 Tel : 32/53 725.355
 Fax : 32/53 725.350
 E-mail : k.vandepas@hme-a.be

FINLAND

Mr. Matti KOIVUROVA
 Vehicle Safety Engineer
 Central Organization for Traffic Safety in
 Finland
 P. O. Box 29
 FIN-00421 HELSINKI
 Tel : 358/9.
 Fax : 358/941.74.74.00

Mr Seppo MÄKITUPA
 Servinkuja, 1 A4
 FIN-02150 ESPOO
 Tel : 358/40 51 61 850
 Fax : 358/9 468 32 93
 E-mail : smakitup@cc.hut.fi

FRANCE

Dr. François BERMOND
 INRETS
 LCB
 Cedex Case 24
 F-69675 BRON

Tel : 33/4.72.14.23.78
 Fax : 33/4.72.14.23.60

Dr. Dominique CESARI
 INRETS
 Case 24
 F-69675 BRON Cedex
 Tel : 33/4.72.14.25.61
 Fax : 33/4.72.14.25.65
 E-mail : dominique.cesari@inrets.fr

Mr. François CHALEIL
 UTAC
 Autodrome de Linas - Monthéry
 BP 212
 F-91 311 MONTHERY CEDEX
 Tel : 33/1.69.80.17.00
 Fax : 33/1.69.80.17.07

Dr Remy WILLINGER
 Institut de Mécanique des Fluides
 Laboratoire de Biomécanique
 Rue Boussingault, 2
 F-67083 STRASBOURG Cedex
 Tel : 33/388.41.65.85
 Fax : 33/388.61.43.00
 E-mail : willi@imf.u-strasbg.fr

GERMANY

Mr. Friedrich BEISSWÄNGER
 MPA-Universität Stuttgart
 Pfaffenwaldring, 32
 D-70569 STUTTGART
 Tel : 49/711.685.25.89
 Fax : 49/711.685.26.35

Dipl.-Ing. Eberhard FAERBER
 Regierungsdirektor
 Bundesanstalt für Straßenwesen
 Brüderstraße 53
 Postfach 100150
 D-51401 BERGISCH GLADBACH
 Tel : 49/2204.436.20
 Fax : 49/2204.43.676

Dr. Rudolf KRUPP
Bundesanstalt für Straßenwesen
Brüderstraße 53
D-51 427 BERGISCH GLADBACH
Tel : 49/2204.43 310
Fax : 49/2204.43 673

PF 25
XI., Csóka u.9
H-1502 BUDAPEST
Tel : 36/1.203.76.33 /-5 or /-8
Fax : 36/1.203.76.33 /-5
E-mail : autokut.test@mail.matav.hu

Mr. H. NEUKIRCHEN
Bundesministerium für Verkehr
Robert-Schumann-Platz 1
D-53 BONN 2
Tel : 49/228.300.25.45
Fax : 49/228.300.34.28

ITALY

Mr Fabio FRATTINI
ReD Management
AGV spa
Zona Industriale D5
I-15047 SPINETTA MARENGO
(ALESSANDRIA)
Tel : 390/0131.21.32.11
Fax : 390/0131.61.71.94
E-mail : agvrsc@alessandria.alpacom.it

Mr. Dietmar OTTE
Project Manager
Medizinische Hochschule Hannover
Accident Research Unit
Carl-Neuberg-Str. 1
D-30625 HANNOVER
Tel : 49/511.532.64.10
Fax : 49/511.532.64.19
E-mail : Aru-mh@mh-hannover.de

Prof. Vittorio GIAVOTTO
Politecnico di Milano
Dipartimento di Ingegneria Aerospaziale
Via Golgi 40
I-20133 MILANO
Tel : 39/02.23.99 83 91 (his secretary)
Fax : 39/02.23.99.40.34 (not sure)
E-mail : giavotto@aero.polimi.it

Dr. Erich SCHULLER
University of Munich
IFR
Frauenlobstraße 7A
D-80337 MÜNCHEN
Tel : 49/89.51.60.51.23
Fax : 49/89.51.60.51.44
E-mail : schuller@rechts.med.uni-
muenchen.de

NETHERLANDS

Dr. ir. P.H.M. BOVENDEERD
Eindhoven University of Technology
Faculty of Mechanical Engineering
Department of Mechanics and Control
P. O. Box 513
NL-5600 MB EINDHOVEN
Tel : 31/40.247.40.87
Fax : 31/40.246.14.18
E-mail : Pebov@wfw.wtb.tue.nl

GREECE

Mr. Nissim BENMAYOR
Ministry of Transports and Communications
Direction of Road Safety
Syggrou Avenue, 23
GR-10780 ATHENS
Tel : 30.1.923.66.77
Fax : 30/1.923.33.30

Dr. A. A. H. J. SAUREN
Eindhoven University of Technology
Faculty of Mechanical Engineering
Department of Mechanics and Control
P. O. Box 513
NL-5600 MB EINDHOVEN
Tel : 31/40.247.27.92
Fax : 31/40.247.22.06
E-mail : a.a.h.j.sauren@wtb.tue.nl

HUNGARY

Dr. Sándor VINCZE-PAP
Head of Laboratory
AUTOKUT

SPAIN

Ing. Ind. Eudard FERNANDEZ ARDEVOL
 Institut d'Investigació Aplicada de
 l'Automòbil
 Empresa del Departament d'Indústria i
 Energia de la Generalitat de Catalunya
 L'Albornar - Apartat Correus 20
 E-43710 SANTA OLIVA (Tarragona)
 Tel : 34/7716.60.00 /-08
 Fax : 34/77.16.60.09

SWEDEN

Dr. Per LOVSUND
 Chalmers University of Technology
 Department of Injury Prevention
 S-41296 Göteborg
 Tel : 46/31.772.36.42
 Fax : 46/31.772.36.60
 E-mail : per@ip.chalmers.se

Mr. J. WENELL
 Swedish Road and Transport Research
 Group
 Crash Safety Group
 S-58195 LINKÖPING
 Tel : 46/13.20.43.73
 Fax : 46/13.20.40.33

SWITZERLAND

Dr Siegfried DERLER
 EMPA
 Safety Department
 Lerchenfeldstrasse 5
 CH-9014 ST. GALLEN
 Tel : 41/71.274.77.66
 Fax : 41/71.274.77.62
 E-mail : derler@empa.ch

Dr ROGERS
 IMMA
 CP 1838
 Route de Pré-Bois
 CH-1215 GENEVE 15

UNITED KINGDOM

Dr. Bryan CHINN
 Transport Research Laboratory
 Vehicle Safety
 Old Wokingham Road
 GB-RG45 6AU Crowthorne, Berkshire
 Tel : 44/1344.77.06.13
 Fax : 44/1344.77.03.56
 E-mail : bchinn@trl.co.uk

Dr. David DOYLE
 Head of Department
 Southern General Hospital - NHS Trust
 Neuropathology
 1345 Govan Road
 GB-G51 4TF GLASGOW
 Tel : 44/141.201.20.50
 Fax : 44/141.201.29.98
 E-mail : d.doyle@clinmed.gla.ac.uk

Mr. Steve GILLINGHAM
 Department for Transport, Local
 Government and the Regions
 Vehicle Standards and Engineering Division
 Zone 2/06, Great Minster House
 76, Marsham Street
 GB- LONDON, SW1P 4DR
 Tel : 44/20.7944.2084
 Fax : 44/20.7944.2069 or 2079
 E-mail : Steve_gillingham@detr.gsi.gov.uk

EUROPEAN COMMISSION

M. René BASTIAANS
 European Commission
 DG VII-E3
 DM 28 – 06/26
 Tel : 32.2.299.41.15
 Fax : 32.2.296.83.50
 E-mail : rene.bastiaans@cec.eu.int

M. André BRISAER
 European Commission
 DG VII-B3
 DM 28 – 03/14
 Tel : 32/2.296.82.36
 Fax : 32/2.296.83.54
 E-mail : andre.brisaer@cec.eu.int

M. J.-P. VAN GHELUWE
European Commission
DG III - D.1.
SC15 - 3/171
Tel : 32/2.296.09.64
Fax : 32/2.296.62.73
E-mail :

OBSERVERS

Scientific Secretary

Mr Martin KEMP
European Commission
BU31 05/34
Tel: 32 2 296.49.79
Fax: 32 2 296.37.65

Annex II. COST 327 Memorandum of Understanding



Brussels, 18 August 1995

COST/249/95

Note

Subject: Memorandum of Understanding for the implementation of a European Research Action on motorcycle safety helmets (COST Action 327)

Delegations will find attached hereto the text of the abovementioned Memorandum, signed in Brussels on 17 May 1995.

MEMORANDUM OF UNDERSTANDING
FOR THE IMPLEMENTATION OF A EUROPEAN RESEARCH ACTION
ON MOTORCYCLE SAFETY HELMETS
(COST ACTION 327)

The Signatories to this Memorandum of Understanding, declaring their common intention to participate in a European research Action on motorcycle safety helmets, have reached the following understanding:

SECTION 1

1. The Signatories intend to co-operate in an Action to promote research on motorcycle safety helmets (hereinafter referred to as the "Action").
2. The main objective of the Action is to establish the tolerance of the human head and neck to the main injuries sustained by motorcyclists and, based on this, to propose a specification for testing motorcycle helmets.
3. The Signatories hereby declare their intention of carrying out the Action jointly, in accordance with the general description given in Annex 11, adhering as far as possible to a timetable to be decided by the Management Committee referred to in Annex 1.
4. The Action will be carried out through concerted action in accordance with the provisions of Annex I.
5. The overall value of the activities of the Signatories under the Action is estimated at ECU 2 000 000 at 1992 prices.
6. The Signatories will make every effort to ensure that the necessary funds are made available under their internal financing procedures.

SECTION 2

The Signatories intend to take part in the Action in one or several of the following ways:

- (a) by carrying out studies and research in their technical services or public research establishments (hereinafter referred to as "public research establishments");
- (b) by concluding contracts for studies and research with other organisations (hereinafter referred to as "research contractors");
- (c) by contributing to the provision of a Secretariat and/or other co-ordinatory services or activities necessary for the aims of the Action to be achieved;
- (d) by making information on existing relevant research, including all necessary basic data, available to other Signatories;

- (e) by arranging for inter-laboratory visits and by co-operating in a small-scale exchange of staff in the later stages.

SECTION 3

1. This Memorandum of Understanding will take effect for four years and 6 months upon signature by at least five Signatories. This Memorandum of Understanding may expire on the entry into force of an agreement between the European Communities and the non Community COST member countries having the same aim as that of the present Memorandum of Understanding. This change in the rules governing the project is subject to the, prior agreement of the Management Committee referred to in Annex 1.
2. This Memorandum of Understanding may be amended in writing at any time by arrangement between the Signatories.
3. A Signatory which intends, for any reason whatsoever, to terminate its participation in the Action will notify the secretary-general of the Council of the European Communities of its intention as soon as possible, preferably not later than three months beforehand.
4. if at any time the number of Signatories falls below five, the Management Committee referred to in Annex 1 will examine the situation which has arisen and consider whether or not this Memorandum of Understanding should be terminated by decision of the Signatories.

SECTION 4

1. This Memorandum of Understanding will, for a period of six months from the date of the first signing, remain open for signing, by the Governments of the countries which are members of the COST framework and also by the European Communities.

The Governments referred to in the first subparagraph and the European Communities may take part in the Action on a provisional basis during the abovementioned period even though they may not have signed this Memorandum of Understanding.

2. After this period of six months has elapsed, application to sign this Memorandum of Understanding from the Governments referred to in paragraph 1 or from the European Communities will be decided upon by the Management Committee referred to in Annex 1, which may attach special conditions thereto.
3. Any Signatory may designate one or more competent public authorities or-bodies to act on its behalf, in respect of the implementation of the Action.

SECTION 5

This Memorandum of Understanding is of an exclusively recommendatory nature. It will not create any binding, legal effect in public international law.

SECTION 6

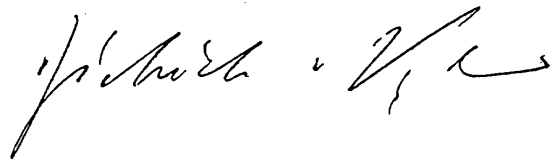
1. The secretary-general of the Council of the European Communities will inform all Signatories of the signing dates and the date of entry into effect of this Memorandum of Understanding, and will forward to them all notices which he has received under this Memorandum of Understanding.
2. This Memorandum of Understanding will be deposited with the General Secretariat of the Council of the European Communities. The secretary-general will transmit a certified copy to each of the Signatories.

Geschehen zu Brüssel am siebzehnten Mai neunzehnhundertfündundneunzig.

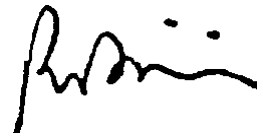
Done at Brussels on the seventeenth day of May in the year one thousand nine hundred and ninety-five.

Fait à Bruxelles, le dix-sept mai mil neuf cent quatre-vingt-quinze.

Für die Regierung der Bundesrepublik Deutschland



Pour le gouvernement de la République française



Pour le gouvernement de la République de Hongrie



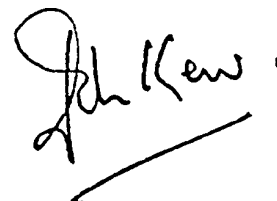
Für die Regierung der Schweizerischen Eidgenossenschaft

Pour le gouvernement de la Confédération suisse

Per il Governo della Confederazione svizzera



For the Government of the United Kingdom of Great Britain and Northern Ireland



CO-ORDINATION OF THE ACTION

CHAPTER 1

1. A Management Committee (hereinafter referred to as "the Committee") will be set up, composed of not more than two representatives of each Signatory. Each representative may be accompanied by such experts or advisers as he or she may need.

The Governments of the countries which are members of the COST framework and the European Communities may, in accordance with the second subparagraph of Section 40) of the Memorandum of Understanding, participate in the work of the Committee before becoming Signatories to the Memorandum, without however, having the right to vote.

When the European Communities are not a Signatory to the Memorandum of Understanding, a representative of the Commission of the European Communities may attend Committee meetings as an observer.

2. The Committee will be responsible for co-ordinating the Action and, in particular, for making the necessary arrangements for:
 - (a) the choice of research topics on the basis of those provided for in Annex 11 including any modifications submitted to Signatories by the competent public authorities or bodies; any proposed changes to the Action framework will be referred for an opinion to the COST Technical Committee on Transport;
 - (b) advising on the direction which work should take;
 - (c) drawing up detailed plans and defining methods for the different phases of execution of the Action;
 - (d) co-ordinating the contributions referred to in sub-paragraph (c) of Section 2 of the Memorandum of Understanding;
 - (e) keeping abreast of the research being done in the territory of the Signatories and in other countries;
 - (f) liaising with appropriate international bodies;

- (g) exchanging research results amongst the Signatories to the extent compatible with adequate safeguards for the interests of Signatories, their competent public authorities or bodies and research contractors in respect of industrial property rights and commercially confidential material;
 - (h) drawing up the annual interim reports and the final report to be submitted to the Signatories and circulated as appropriate;
 - (i) dealing with any problem which may arise out of the execution of the Action, including those relating to possible special conditions to be attached to accession to the Memorandum of Understanding in the case of applications submitted more than six months after the date of the first signing.
3. The Committee will establish its rules of procedure.
 4. The Secretariat of the Committee will be provided at the invitation of the Signatories by either the Commission of the European Communities or one of the Signatory States.

CHAPTER II

1. Signatories will invite public research establishments or research contractors in their territories to submit proposals for research work to their respective competent public authorities or bodies. Proposals accepted under this procedure will be submitted to the Committee.
2. Signatories will request public research establishments or research contractors, before the Committee takes any decision on a proposal, to submit to the public authorities or bodies referred to in paragraph 1 notification of previous commitments and industrial property rights which they consider might preclude or hinder the execution of the Actions of the Signatories.

CHAPTER III

1. Signatories will request their public research establishments or research contractors to submit periodical progress reports and a final report.
2. The progress reports will be distributed to the Signatories only through their representatives on the Committee. The Signatories will treat these progress reports

as confidential and will not use them for purposes other than research work. In order to assess better the final data on the Action, the Signatory States are invited, for the preparation of the final report, to state the approximate level of spending at national level arising from their involvement in the said Action. The final report on the results obtained will have much wider circulation, covering at least the Signatories' public research establishments or research contractors concerned.

CHAPTER IV

1. In order to facilitate the exchange of results referred to in Chapter 1, paragraph 2(g), and subject to national law, Signatories intend to ensure, through the inclusion of appropriate terms in research contracts, that the owners of industrial property rights and technical information resulting from work carried out in implementation of that part of the Action assigned to them under Annex 11 (hereinafter referred to as "the research results") will be under an obligation, if so requested by another Signatory (hereinafter referred to as the "applicant Signatory"), to supply the research results and to grant to the applicant Signatory or to a third party nominated by the applicant Signatory a licence to use the research results and such technical know-how incorporated therein as is necessary for such use if the applicant Signatory requires the granting of a licence for the execution of work in respect of the Action.

Such licences will be granted on fair and reasonable terms having regard to commercial usage.

2. Signatories will, by including appropriate clauses in contracts placed with research contractors, provide for the licence referred to in paragraph 1 to be extended on fair and reasonable terms, having regard to commercial usage, to previous industrial property rights and to prior technical know-how acquired by the research contractor insofar as the research results could not otherwise be used for the purpose referred to in paragraph 1.

Where a research contractor is unable or unwilling to agree to such extension, the Signatory will submit the case to the Committee, before the contract is concluded; thereafter the Committee will state its position on the case, if possible after having consulted the interested parties.

3. Signatories will take any steps necessary to ensure that the fulfilment of the

condition laid down in this Chapter will not be affected by any subsequent transfer of rights to ownership of the research results. Any such transfer will be notified to the Committee.

4. If a Signatory terminates its participation in the Action, any rights of use which it has granted, or is obliged to grant, to, or has obtained from, other Signatories in application of the Memorandum of Understanding and concerning work carried out up to the date on which the said Signatory terminates its participation will continue thereafter.
5. The provisions of paragraphs 1 to 4 will continue to apply after the period of operation of the Memorandum of Understanding has expired and will apply to industrial property rights as long as these remain valid, and to unprotected inventions and technical know-how until such time as they pass into the public domain other than through disclosure by the licensee.

GENERAL DESCRIPTION OF THE ACTION

1. Introduction

Motorcyclists are amongst the most vulnerable road users. Head injuries cause the largest proportion of fatalities to motorcyclists, while about one quarter of all injured riders suffered head injuries.

This action will investigate the causes and mechanisms of head injuries using accident data and mathematical modelling such that the design of motorcyclists' helmets can be optimised with regard to the protection offered to a motorcyclists' head and neck.

2. Objectives

- (i) To establish the distribution and severity of injuries experienced by motorcyclists, with particular reference to the head and neck.
- (ii) To establish the most significant injuries and injury mechanisms.
- (iii) To establish the tolerance of the human head, brain and neck to those injuries and injury mechanisms.
- (iv) To propose a specification for testing motorcycle helmets.

3. Research requirements

- (i) To analyse the available accident/medical data and determine the distribution and severity of impacts experienced and identify the injury mechanisms.
- (5) To consider all available documented information on brain injuries.
- (iii) To collect further accident/medical data if required.
- (iv) To develop a mathematical model of the human brain, head and neck, and a typical helmet to facilitate the study of brain injury mechanisms.
- (v) To determine test criteria and limits that will more accurately represent the tolerance of the human head, brain and neck to impact.
- (vi) To determine a test procedure to represent more accurately the risks of a type of impact taking place.

4. Benefits of the research Action

- (i) Increased understanding of the injury mechanisms to the human head, brain and neck.
- (ii) Increased understanding of the tolerance of the human head, brain and neck to impacts.
- (iii) Use of the information gained in (i) and (ii) such that motorcycle helmets can be improved and thereby offer better protection to the motorcycle rider.

5. Description of the research Action

- (i) Conduct an in-depth literature review/search of accident data, bio-mechanical research and the development of mathematical models of the human head, brain and neck. Produce a report.
- (ii) Collection of real life accident data - injuries, helmet damage, impact object, etc.
- (iii) Investigate and correlate the effect of using compliant and non-compliant headforms on the damage occurring to helmets, under similar impact conditions.
- (iv) Reconstruction of the impact to the helmet to replicate the helmet damage to ascertain impact energy. Consideration to be given to the effects of the headform being attached to a body.
- (v) Development of a mathematical model of a brain, skull, neck and helmet to emulate impacts and injury mechanisms.
- (vi) Establish the spectrum of tolerances of the human head to injury for specified injury mechanisms.
- (vii) Develop appropriate test procedures to ascertain and establish the total risk of head, brain and neck injury and to maximise the protection offered by helmets.

6. Work Programme

See attached Annex.

7. Duration of the Action

4 years and 6 months.

8. Estimate of Cost

ECU 2 million.

ACTION WORK PLAN

Project Number : COST 327
 Project Title : Motorcyclists' Helmets
 Issue Date : 2 July 1993

P = Planned A = Actual

Activity/Output		Year 1				Year 2				Year 3				Year 4				Year 5						
		1-3	4-6	7-9	10-12	1-3	4-6	7-9	10-12	1-3	4-6	7-9	10-12	1-3	4-6	7-9	10-12	1-3	4-6	7-9	10-12			
i) Literature Review	P	█																						
	A																							
ii) Accident Data Collection	P	█																						
	A																							
iii) Investigate headforms	P			█																				
	A																							
iv) Reconstruction of Helmet Impact & Damage	P			█																				
	A																							
v) Development of a Mathematical Model	P			█																				
	A																							
vi) Establish Human Head Tolerances	P			█																				
	A																							
vii) Develop Test Procedures	P																							
	A																							
Major/Project Module Reports	P																							
	A																							
Progress Reports	P			#			#		#			#			# #		#							
	A																							
Final Report	P			#			#		#			#			#						█			
	A																							
Critical		█		Non critical				█				Progress				█				Milestones				#

Annex III. COST Transport Overview

COST Transport is one of 17 domains existing in COST at the present time.

It was to be one of the seven areas seen as best suited for this new form of collaboration, which was officially set up by a Ministerial Conference in November 1971.

The Transport area lends itself particularly well to the COST framework, both because it combines aspects from a number of disciplines, and because of the need for harmonisation at European level. Liaison with the Transport Ministries and Administrations in the various countries is a key element of these COST Actions.

The COST Transport Secretariat is located within the Directorate General for Transport of the European Commission. The location with the staff managing the Fourth and Fifth Framework Transport RTD Programme, as well as the proximity with the Common Transport Policy Directorates, enables close collaboration between Transport Research activities and serves as a basis for further political action.

COST Transport Actions are authorised and supervised by the COST Technical Committee on Transport which, in turn, reports to the COST Committee of Senior Officials. Both of these decision-making bodies comprise representatives of the national governments of the COST countries.

By May 2000, the COST Transport domain comprised 13 ongoing Actions, with a total estimated cost of EURO 43 Million. 33 Actions have been completed, and a further 3 Actions have been selected and are under preparation.

Completed Actions

- COST 30: Electronic Traffic Aids on Major Roads
- COST 30 bis: Electronic Traffic Aids on Major Roads: Demonstration Project and Further Research
- COST 301: Shore Based Marine Navigation Systems
- COST 302: Technical and Economic Conditions for the Use of Electric Road Vehicles
- COST 303: Technical and Economic Evaluation of National Dual-mode Trolleybus Programmes
- COST 304: Use of Alternative Fuels in Road Vehicles
- COST 305: Data System for the Study of Demand for Interregional Passenger Transport
- COST 306: Automatic Transmission of Data Relating to Transport
- COST 307: Rational Use of Energy in Interregional Transport
- COST 308: Maintenance of Ships
- COST 309: Road Weather Conditions
- COST 310: Freight Transport Logistics
- COST 311: Simulation of Maritime Traffic
- COST 312: Evaluation of the Effects of the Channel Tunnel on Traffic Flows

- COST 313: Socio-economic Cost of Road Accidents
- COST 314: Express Delivery Services
- COST 315: Large Containers
- COST 317: Socio-economic Effects of the Channel Tunnel
- COST 318: Interactions between High-speed Rail and Air Passenger Transport
- COST 319: Estimation of Pollutant Emissions from Transport
- COST 320: The Impact of E.D.I. on Transport
- COST 321: Urban Goods Transport
- COST 322: Low Floor Buses
- COST 323: Weigh-in-Motion of Road Vehicles
- COST 324: Long Term Performance of Road Pavements
- COST 325: New Pavement Monitoring Equipment and Methods
- COST 326: Electronic Charts for Navigation
- COST 327: Motorcycle Safety Helmets
- COST 328: Integrated Strategic Transport Infrastructure Networks in Europe
- COST 329: Models for Traffic and Safety Development and Interventions
- COST 330: Teleinformatics Links between Ports and their Partners
- COST 331: Requirements for Horizontal Road Marking
- COST 332: Transport and Land-Use Policies
- COST 333: Development of New Bituminous Pavement Design Method
- COST 334: Effects of Wide Single Tyres and Dual Tyres
- COST 335: Passengers' Accessibility of Heavy Rail Systems
- COST 336: Use of Falling Weight Deflectometers in Pavement Evaluation
- COST 337: Unbound Granular Materials for Road Pavements

Actions Underway

- COST 339: Small Containers
- COST 340: Towards a European Intermodal Transport Network: Lessons from History
- COST 341: Habitat Fragmentation due to Transportation Infrastructure
- COST 342: Parking Policy Measures and their Effects on Mobility and the Economy
- COST 343: Reduction in Road Closures by Improved Maintenance Procedures
- COST 344: Improvements to Snow and Ice Control on European Roads and Bridges
- COST 345: Procedures Required for Assessing Highway Structures
- COST 346: Emissions and Fuel Consumption from Heavy Duty Vehicles
- COST 347: Pavement Research with Accelerated Loading Testing Facilities

Actions in preparation

COST 338: Drivers' Visual Information Overload

COST 348: Reinforcement of Pavements with Steel Meshes and Geosynthetics

Up-to-date information on COST Transport can be found on the World Wide Web, at the following address: <http://www.cordis.lu/cost-transport/home.html>.

European Commission

EUR xxxxx – COST 327 – Motorcycles Safety Helmets

Luxembourg: Office for Official Publications of the European Communities

1999 – xxx pp. – 17.6 x 25.0 cm

ISBN xx-xxx-xxxx-x

Price (excluding VAT) in Luxembourg : EURO xx.xx